atmosphere

Special Issue Reprint

Urban and Regional Nitrogen Cycle and Risk Management

Edited by
Chaofan Xian, Yu-Sheng Shen and Cheng Gong

mdpi.com/journal/atmosphere

MDPI

Urban and Regional Nitrogen Cycle and Risk Management

Urban and Regional Nitrogen Cycle and Risk Management

Guest Editors

Chaofan Xian
Yu-Sheng Shen
Cheng Gong

MDPI

Basel • Beijing • Wuhan • Barcelona • Belgrade • Novi Sad • Cluj • Manchester

Guest Editors

Chaofan Xian
State Key Laboratory of
Regional and Urban Ecology
Research Center for
Eco-Environmental Sciences
Chinese Academy of Sciences
Beijing
China

Yu-Sheng Shen
Institute of Urban
Environment
Chinese Academy of Sciences
Xiamen
China

Cheng Gong
State Key Laboratory of
Regional and Urban Ecology
Research Center for
Eco-Environmental Sciences
Chinese Academy of Sciences
Beijing
China

Editorial Office
MDPI AG
Grosspeteranlage 5
4052 Basel, Switzerland

This is a reprint of the Special Issue, published open access by the journal *Atmosphere* (ISSN 2073-4433), freely accessible at: https://www.mdpi.com/journal/atmosphere/special_issues/1V2W00M6BU.

For citation purposes, cite each article independently as indicated on the article page online and as indicated below:

Lastname, A.A.; Lastname, B.B. Article Title. *Journal Name* **Year**, *Volume Number*, Page Range.

ISBN 978-3-7258-3695-6 (Hbk)
ISBN 978-3-7258-3696-3 (PDF)
https://doi.org/10.3390/books978-3-7258-3696-3

Contents

atmosphere

MDPI

Editorial

Special Issue Editorial: Urban and Regional Nitrogen Cycle and Risk Management

Chaofan Xian [1,*], Yu-Sheng Shen [2] and Cheng Gong [1]

[1] Research Center for Eco-Environmental Sciences, Chinese Academy of Sciences, Beijing 100084, China; chenggong@rcees.ac.cn
[2] Institute of Urban Environment, Chinese Academy of Sciences, Xiamen 361021, China; ysshen@iue.ac.cn
* Correspondence: cfxian@rcees.ac.cn

Disturbance of urban and regional nitrogen cycles due to urbanization have resulted in the greenhouse effect, acid rain, eutrophication, and reductions in biodiversity. In light of this, the 'nitrogen cascade' effect induced by nitrogen cycle disruption has been recognized as the third most important global environmental problem after biodiversity loss and global warming. Possible risk managements to reduce reactive nitrogen being released into the environment include proper nitrogen management within the production and consumption cycles of essential resources, which could be supported by anthropogenic approaches (e.g., environmental pollution monitoring, environmentally friendly technology and residents' behavior) and natural-based approaches, including nitrogen retention within ecosystems. More importantly, from the perspective of synergizing the reduction in pollution and carbon emissions, the risk of nitrogen pollution is often accompanied by excessive emissions of greenhouse gases and atmospheric particles in the early stage. Progress in new areas of research will depend on relevant risk management. The reports presented in the Special Issue, 'Urban and Regional Nitrogen Cycle and Risk Management', are the result of collaborative work between researchers in an effort to reduce atmospheric emissions and mitigate the nitrogen risks, including both experimental and monitoring studies and mathematical/numerical modeling studies on the urban and regional scale. The publications of the issue (12 articles) cover the subjects of nitrogen and carbon coupling (5), ecological effects of nitrogen deposition (4), urban nitrogen flow analysis (1), and environmental monitoring and modeling (2). A brief overview of the main findings and conclusions of articles in the Special Issue will be presented below.

Received: 13 January 2025
Accepted: 14 February 2025
Published: 16 February 2025

Citation: Xian, C.; Shen, Y.-S.; Gong, C. Special Issue Editorial: Urban and Regional Nitrogen Cycle and Risk Management. *Atmosphere* **2025**, *16*, 223. https://doi.org/10.3390/atmos16020223

Wu and Shen [1] used bibliometric analysis and found that there are gaps between low-carbon policy and public awareness/behavior in the research hotspots of "Carbon Emission Reduction", which hinder research progress in synergizing the reduction of nitrogen (N) pollution and carbon emissions addressed by risk managements. Urbanization is a significant indicator of city progress, which may drive the growth of carbon emissions accompanied by N release, especially in urban agglomeration. Gao et al. [2] examined the spatial and temporal variations of carbon emissions in the Pearl River Delta (PRD) urban agglomeration in China, which is suffering from water N pollution. They found that total carbon emissions in the PRD region have been increasing over 2009–2019 with hotspots mainly distributed in Guangzhou, Shenzhen, and Dongguan cities. Liu et al. [3] comprehensively accounted for the greenhouse gas budgets of Beijing and Shenzhen cities from 2005 to 2020 and revealed that the energy activity sector was the greatest contributor to GHG emissions in this period, accounting for 82.5% and 76.0% of the total GHG emissions in Beijing and Shenzhen, respectively. The carbon sink provided by these two urban ecosystems could absorb only small parts of their emissions, and the neutralization rates

of sinks ranged from 1.7% to 2.3% in Beijing and from 0.3% to 1.5% in Shenzhen. This study found that household size had opposite effects on the two cities' emissions, i.e., a 1% increase in household size would increase GHG emissions by 0.487% in Shenzhen but reduce them by 2.083% in Beijing. Song et al. [4] also found that household size was the main diver influencing personal carbon emissions in the Sanjiangyuan region of the Qinghai–Tibet Plateau by interviewing more than 1000 herder households of 15 counties. The more people living in the household, the lower the per-capita carbon emissions. However, the effect size of potential carbon reductions was weakened when the number of family members rose to over three. They proposed that grazing prohibitions and low-carbon dietary shifts would contribute to low-carbon herder livelihoods, which also may contribute to lower N herder lifestyles with less fertilizer-N and livestock-N being released. Lama et al. [5] evaluated the conservation status and effectiveness of national parks, nature reserves, forest parks, geo-parks, and scenic spots on carbon sequestration within the Loess Plateau in China throughout 2000–2020. They found that all existing protected area types have good representation and conservation effectiveness on carbon sequestration. Nature reserves, where the natural N cycle is maintained, are the most representative form of carbon sequestration but are the least effective in protecting carbon sequestration. They proposed that implementing restoration measures in low carbon sequestration areas within grassland and wild plant nature reserves will help to achieve the goal of carbon neutrality early, which also can maximize the protection of the natural nitrogen cycles in these places from human interference.

In terms of modeling for synergizing the reduction in atmospheric pollution and carbon emissions, Yang et al. [6] develop a combination prediction model for atmospheric water vapor, which is an essential source of predicting global climate change, combined with the Zenith Tropospheric Delay (ZTD) data from 13 global navigation satellite system (GNSS) service stations in the United States. This regional/single station ZTD combination prediction model, based on the machine learning algorithms of radial basis function (RBF) neural networks, assisted by the K-means cluster algorithm (K-RBF) and long short-term memory of real-time parameter updating (R-LSTM), was proposed for online modeling to serve the response and feedback of the carbon, nitrogen, and water cycle to climate change. In addition, high resolution simulation of the concentration of atmospheric pollutants in urban areas can help to develop air pollution control policies. Wu et al. [7] takes the Wenhua Road block in Shenyang city, China, as the research object, and analyzes the spatial distribution characteristics of local climate zones (LCZ) and particulate matter (PM) in the block based on the ArcGIS platform. Their findings show that the spatial distribution characteristics of PM1, PM2.5, and PM10 under the same pollution level are relatively similar, while the spatial heterogeneity of the distribution of the same particulate matter under different pollution levels is higher. The built-up LCZ always has a larger average concentration of PM than that of the natural LCZ and building height and building density are the main factors causing the difference. It also provides theoretical and practical references for the simulation of nitrogen oxide concentration growth at an urban block scale, although there are few studies focusing on this research field in recent years.

Acid deposition is an important component of atmospheric pollution, N deposition has become a major ecological problem that endangers ecosystems and residents in cities. In the case study of Shenzhen city, China, Shu et al. [8] has drawn high-resolution spatial distribution maps of N retention in the city's ecological space, on the basis of a large number of soil sampling across the city, and they found that precipitation factors have the greatest impact on the spatial differentiation characteristics of N retention services provided by soil in three main types of land use (forested land, industrial land, and street town residential land). To examine the effects of atmospheric N deposition containing

different N components on the functional differences between invasive plants and native plants, Li et al. [9] conducted a study over a four-month period using a pot-competitive co-culture experiment to elucidate the effects of artificially simulated N deposition containing different N components, which was found to facilitate the growth performance of native monocultural *P. laciniata*, particularly in terms of the sunlight capture capacity and leaf photosynthetic area. Invasive Bidens pilosa exhibited a more pronounced competitive advantage than P. laciniata under artificially simulated N deposition containing different N components. Furthermore, Li et al. [10] conducted controlled experiments in a greenhouse to evaluate the functional differences and growth performance between the invasive plant *Amaranthus spinosus* L. and the native plant *A. tricolor* L. in mono- and mixed culture when exposed to an acid deposition with different sulfur–nitrogen ratios. They found that the lower pH acid deposition had imposed a greater reduction in the growth performance of both Amaranthus species than the higher pH acid deposition. Amaranthus spinosus was more competitive than *A. tricolor*, especially when exposed to acid deposition. From the perspective of microbiology, the soil N-fixing bacterial (NFB) community may facilitate the successful establishment and invasion of exotic non-nitrogen (N)-fixing plants. Invasive plants can negatively affect the NFB community by releasing N during litter decomposition, especially where N input from atmospheric N deposition is high. Li et al. [11] conducted an indoor litterbag experiment to quantitatively compare the effects of the invasive *Rhus typhina* L. and native Koelreuteria paniculata Laxm. trees on the litter mass loss and the NFB. They found that the litter mass loss of the two trees was mainly associated with the taxonomic richness of NFB. The form of N was not significantly associated with the litter mass loss in either species, the mixing effect intensity of the litter co-decomposition of the two species, and NFB alpha diversity. Litter mass loss of R. typhina was significantly higher than that of K. paniculata under urea. In view of the above research, although we all know that N-related acid deposition is harmful to plant growth, the negative impacts of which on the invasive plants are much smaller than those on native plants, this indicates that regional N pollution has a substantial negative effect on urban and regional biodiversity.

From the perspective of systemic metabolism for N risk assessment, Li et al. [12] used the material flow analysis method to estimate anthropogenic nitrogen emissions in Xiamen city, China, and found that the quantity of reactive N generated by human activities increased 3.5 times from 1995 to 2018. Specifically,, the total reactive N entering the water environment showed a general increase with fluctuations, resulting in N overload in the nearby sea with a threefold augmentation compared with surface waters and groundwater. Population and per capita GDP were major factors contributing to water N pollution, demonstrating that there is an urgent need for sustainable nitrogen management in coastal cities.

In summary, the 12 papers include in this Special Issue cover serval developments and applications related to the urban and regional N risk managements on multiple scales (indoor laboratory, city block, city, region), which highlight the potential benefits of using model simulation, spatial analysis, and controlled experiments in the research of N cycling, involving, for example, the characterization of nitrogen and carbon coupling in the atmosphere, and risk analyses and corresponding policies for synergizing the reduction in pollution and carbon emissions.

Author Contributions: Writing—original draft preparation, C.X.; writing—review and editing, C.X., Y.-S.S. and C.G. All authors have read and agreed to the published version of the manuscript.

Conflicts of Interest: The authors declare no conflict of interest.

References

1. Wu, X.; Shen, Y.-S. The Bibliometric Analysis of Low-Carbon Transition and Public Awareness. *Atmosphere* **2023**, *14*, 970. [CrossRef]
2. Gao, Z.; Wu, D.; Wu, Z.; Zeng, L. Investigation into Spatial and Temporal Differences in Carbon Emissions and Driving Factors in the Pearl River Delta: The Perspective of Urbanization. *Atmosphere* **2024**, *15*, 782. [CrossRef]
3. Liu, K.; Yang, S.; Huang, B.; Xian, C.; Han, B.; Xie, T.; Shu, C.; Chen, Z.; Wang, H.; Wang, H.; et al. Comparative Study on the Influencing Factors of the Greenhouse Gas Budget in Typical Cities: Case Studies of Beijing and Shenzhen. *Atmosphere* **2023**, *14*, 1158. [CrossRef]
4. Song, C.; Liu, L.; Xian, C.; Feng, F.; Ouyang, Z. Analysis of Carbon Emission Characteristics and Influencing Factors of Herder Households: A County-Scale Investigation of the Sanjiangyuan Region on the Qinghai–Tibet Plateau. *Atmosphere* **2023**, *14*, 1800. [CrossRef]
5. Lama, S.; Zhang, J.; Luan, X. Evaluating the Conservation Status and Effectiveness of Multi-Type Protected Areas for Carbon Sequestration in the Loess Plateau, China. *Atmosphere* **2024**, *15*, 764. [CrossRef]
6. Yang, X.; Li, Y.; Yu, X.; Tan, H.; Yuan, J.; Zhu, M. Regional/Single Station Zenith Tropospheric Delay Combination Prediction Model Based on Radial Basis Function Neural Network and Improved Long Short-Term Memory. *Atmosphere* **2023**, *14*, 303. [CrossRef]
7. Wu, W.; Liu, R.; Tang, Y. Study on Mapping and Identifying Risk Areas for Multiple Particulate Matter Pollution at the Block Scale Based on Local Climate Zones. *Atmosphere* **2024**, *15*, 794. [CrossRef]
8. Shu, C.; Du, K.; Han, B.; Chen, Z.; Wang, H.; Ouyang, Z. Driving Forces on the Distribution of Urban Ecosystem's Non-Point Pollution Reduction Service. *Atmosphere* **2023**, *14*, 873. [CrossRef]
9. Li, C.; Li, Y.; Liu, Y.; Zhong, S.; Zhang, H.; Xu, Z.; Xu, Z.; Du, D.; Wang, C. Does Atmospheric Nitrogen Deposition Confer a Competitive Advantage to Invasive *Bidens pilosa* L. over Native *Pterocypsela laciniata* (Houtt.) Shih? *Atmosphere* **2024**, *15*, 825. [CrossRef]
10. Li, Y.; Li, C.; Zhong, S.; Xu, Z.; Liu, J.; Xu, Z.; Zhu, M.; Wang, C.; Du, D. Is the Invasive Plant *Amaranthus spinosus* L. More Competitive than the Native Plant *A. tricolor* L. When Exposed to Acid Deposition with Different Sulfur–Nitrogen Ratios? *Atmosphere* **2024**, *15*, 29. [CrossRef]
11. Li, Y.; Li, C.; Cheng, H.; Xu, Z.; Zhong, S.; Zhu, M.; Wei, Y.; Xu, Z.; Du, D.; Wang, C.; et al. Litter Mass Loss of the Invasive *Rhus typhina* L. and Native *Koelreuteria paniculata* Laxm. Trees Alters Soil N-Fixing Bacterial Community Composition under Different N Forms. *Atmosphere* **2024**, *15*, 424. [CrossRef]
12. Li, Y.; Yang, X.; Wang, S.; Cui, S. Insight into Municipal Reactive Nitrogen Emissions and Their Influencing Factors: A Case Study of Xiamen City, China. *Atmosphere* **2023**, *14*, 1549. [CrossRef]

atmosphere

MDPI

Article

The Bibliometric Analysis of Low-Carbon Transition and Public Awareness

Xialu Wu [1,2,3,†] and Yu-Sheng Shen [1,2,3,*,†]

[1] Key Laboratory of Urban Environment and Health, Institute of Urban Environment, Chinese Academy of Sciences, Xiamen 361021, China
[2] Xiamen Key Laboratory of Urban Metabolism, Institute of Urban Environment, Chinese Academy of Sciences, Xiamen 361021, China
[3] University of Chinese Academy of Sciences, Beijing 101408, China
* Correspondence: ysshen@iue.ac.cn
† These authors contributed equally to this study.

Abstract: After the agreements of the Conference of the Parties, more and more countries announced plans to achieve net zero emissions over the coming decades and published new policies in response to the agreements. Public awareness is a crucial factor in achieving the goals of the agreements. Therefore, the study of public awareness/behavior toward the low-carbon transition is important. However, this topic lacks a comprehensive and systematic review. Thus, this study used bibliometric analysis, including performance analysis and scientific mapping analysis, to reveal research trends and clarify the status of studies in low-carbon transition and public awareness. We found that 95% of the literature on this topic was published from 2011 to 2022. Judging from keywords, the hotspots of this topic are "Sustainability", "Energy Transition", "Low-carbon Economy", and "Carbon Emission Reduction". Regarding the research field transition for this topic, environmental sciences have always been a core subject. Furthermore, economics, management, political science, and sociology have focused on this topic in recent years. Additionally, there are gaps between low-carbon policy and public awareness/behavior. Therefore, the frontier directions of low-carbon transition and public awareness include "low-carbon education", "policies with specific guidelines", and "worldwide collaboration".

Keywords: low-carbon transition; public awareness; low-carbon behavior

Citation: Wu, X.; Shen, Y.-S. The Bibliometric Analysis of Low-Carbon Transition and Public Awareness. *Atmosphere* **2023**, *14*, 970. https://doi.org/10.3390/atmos14060970

Academic Editor: Junwen Liu

Received: 24 April 2023
Revised: 27 May 2023
Accepted: 29 May 2023
Published: 1 June 2023

1. Introduction

Climate change is the defining issue of our time on a global scale. The influence of climate change includes threats to food production and security [1–4], rising sea levels [5–7], increasing the risk of catastrophic flooding [8–10], reducing the ice sheet and glacier mass [11–13], and causing droughts [14–16]. According to the report from the Intergovernmental Panel on Climate Change (IPCC (Intergovernmental Panel on Climate Change)) and previous studies, human-induced climate change is also responsible for storms and extinctions [7,17–21]. In this urgent situation, we must take action.

"United Nations Framework Convention on Climate Change", "Kyoto Protocol", and "Copenhagen Accord" were formulated to prevent the threat and risks generated by climate change [22]. In order to mitigate climate change worldwide, the Paris Agreement was adopted by 196 parties at the UN Climate Change Conference (COP21) in 2015, which is a legally binding international treaty on climate change [23]. Its overarching goal is to hold "the increase in the global average temperature to well below 2 °C above pre-industrial levels" and pursue efforts "to limit the temperature increase to 1.5 °C above pre-industrial levels" [23]. In order to limit global warming to 1.5 °C, greenhouse gas (GHG) emissions must decline by 43% by 2030 [23].

According to the UN (United Nations), carbon dioxide (CO_2) is the most abundant GHG, accounting for about two-thirds of all GHGs [15]. In recent years, many researchers have studied the possible options to reduce CO_2 emissions. Previous studies found that reducing CO_2 emissions is vital to mitigating climate change and achieving the low-carbon transition [24–32]. Studies found that CO_2 emissions from fossil fuel combustion are the main source of global climate change [33], and reducing demand for fossil fuels can directly contribute to the reduction of CO_2 emissions from waste disposal [34]. From an engineering point of view, CO_2 reduction options can be divided into three categories: (a) reduce energy intensity (energy saving) [35,36]; (b) reduce carbon intensity [37]; and (c) sequester carbon [37–41]. In addition, new energy is also a vital approach to achieving carbon neutrality [42]. Paustian et al. [43] found that reducing the frequency of bare fallow in crop rotations and increasing the use of perennial vegetation will increase the carbon stock of the soil. Lee et al. [44] found that green transportation and low-emission technology are the key aspects to balancing climate resilience and economic growth. Dietz et al. studied the influence of household low-carbon behaviors, and the results show that household actions can provide a behavioral wedge to reduce carbon emissions rapidly [45].

After the Paris Agreement, more and more countries announced their goal to achieve net zero emissions over the coming decades and also published new policies in response to the agreement. For example, the United Kingdom, Japan, and the Republic of Korea, along with 110 other countries, have pledged to reach carbon neutrality by 2050 [46–49], and China has pledged to achieve carbon neutrality by 2060 [50,51]. In order to achieve the carbon neutrality goal, the corresponding policies were formulated in many countries [52–54]. For example, China's energy policy promoted the social acceptance or public awareness of renewable energy [55,56].

As for the public's awareness/behavior response to policy, the "top-down" approach of telling the public "what to do" is confirmed to work ineffectively [57]. Although policy is a positive approach to encouraging low-carbon behavior, public awareness/behavior responses are also influenced by other factors [58,59]. That is to say, public awareness/behavior are variables that may delay the process of achieving the goal of the Paris agreement. In addition, there is a great gap between behavioral intention and actual actions [60]. A study found that awareness of climate change is widespread, but behavioral engagement is far lower [61]. Therefore, it is vital to study public awareness/behavior for the low-carbon transition.

Many studies have focused on the low-carbon transition and public awareness/behavior [62–70] However, this research topic lacks a comprehensive and systematic review. Therefore, this study analyzed the trends, progress, status, and hotspots of studies on low-carbon transition and public awareness/behavior through literature from the Web of Science (WoS) database, including countries/regions contribution analysis, institution contribution analysis, keyword analysis, and journal analysis. From the results of bibliometric analysis, this study obtains the countries/regions contributions, institution contributions, hot keywords, and highly productive journals of this research topic. Furthermore, this study indicated the gaps and future frontier directions for this research topic. These can contribute to comprehending the progress and content of this research topic and provide a guide, reference, and inspiration for low-carbon policies. Moreover, policymakers can formulate a suitable policy for low-carbon development based on the results of this study.

2. Data and Methods

2.1. Data

We collected the data for this study from the Web of Science Core Collection (WoSCC) database, which is one of the databases of the Web of Science (WoS). The WoSCC database includes Science Citation Index-Expanded (SCI-Expanded), Arts and Humanities Citation Index (AHCI), Emerging Sources Citation Index (ESCI), Social Sciences Citation Index (SSCI), Conference Proceedings Citation Index-Social Science and Humanities (CPCI-SSH), Book Citation Index-Science (BKCI-S), Book Citation Index-Social Sciences and Humanities

(BKCI-SSH), Conference Proceedings Citation Index-Science (CPCI-S), Emerging Sources Citation Index (ESCI), Current Chemical Reactions-Expanded (CCR-EXPANDED), and Index Chemicus (IC).

The literature data in this study were collected in February 2023. We selected and collected the literature data by using the following strategy: (a) The literature data was selected by the keywords that are related to "low-carbon transition" and "public awareness/behavior". The detailed search strategies were "TS = low-carbon AND awareness" OR "TS = low-carbon AND Lifestyle AND transition" OR "TS = low-carbon AND Lifestyle AND behavior" OR "TS = low-carbon AND behavior AND transition" OR "TS = low-carbon AND environmental education"; (b) only "Article" and "Review Article" literatures are included in this study; thus, only the literature data from peer-reviewed publications are collected; (c) only English literature publications were included in this study; and (d) this study obtained data from 1235 studies via the aforementioned process.

2.2. Methods

The bibliometric analysis in this study includes performance analysis and scientific mapping analysis, which can reveal research trends and clarify the current status of research. In this study, performance analysis evaluates the influence of studies from countries/regions, institutions, keywords, and journals. The scientific mapping analysis in this study encompasses the dynamics and relationships observed within the research. Therefore, this study conducted bibliometric analysis based on WoSCC data to evaluate publication trends, journal contributions, institutional contributions, and country contributions. Moreover, the frequency of specific keywords was analyzed through bibliometric analysis.

Microsoft Excel was used to analyze the general performance of publications. The results of the institution contribution analysis and highly productive journal analysis were obtained from the WoSCC. The analysis and visualization of keywords were conducted by Bibliometrix, which is an R-tool for comprehensive science mapping analysis. Countries/regions contribution analysis and visualization of the aforementioned studies were analyzed by CiteSpace 6.1 R3 (literature visual analysis software) Figure 1.

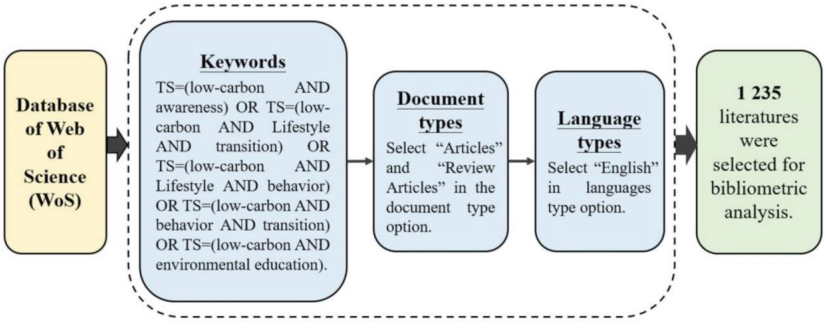

Figure 1. Flow chart of literature data collected for the study of low-carbon transition and public awareness/behavior. Note: TS means topic tag, which searches terms in title, abstract, author keywords, and keywords plus fields.

3. Results

3.1. General Performance of Publications

There were 1235 studies of low-carbon transition and public awareness/behavior collected from WoSCC. All the selected studies were cited 28,083 times in total. There were an average of 22.59 citations per piece of literature. Moreover, 33 studies were recorded as highly cited. The trend in the number of studies on the topics of low-carbon transition and public awareness/behavior can be seen in Figure 2.

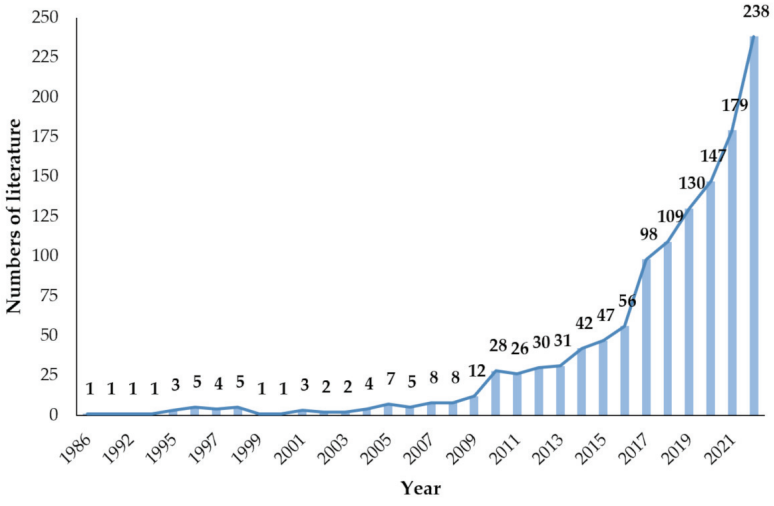

Figure 2. The trend of the number of annual publications for the study of low-carbon transition and public awareness/behavior.

As we can see in Figure 2, the study of low-carbon transition and public awareness/behavior drew a small amount of attention between 1994 and 1997 and 2000 and 2003. The number of publications has increased gradually since 2004. There has been a rapid growth trend in publications since 2016. In addition, there was the largest increase in the number of publications from 2021 to 2022. It is indicated that studies on the topics of low-carbon transition and public awareness/behavior have gradually become more popular since 2004. Since 2010, the study of low-carbon transition and public awareness/behavior has drawn high amounts of attention and become a popular research topic in the field of low-carbon.

3.2. High-Productivity Journal Analysis

Academic journals play an important role in the inheritance and dissemination of scientific achievements. Thus, they are essential for scientific research. There are 202 academic journals that published low-carbon transition and public awareness/behavior-related papers in this study. The top 10 journals on the study of low-carbon transition and public awareness/behavior are listed in Table 1, which includes the impact factors, SCImago journal rank, journal citation reports (JCR), and categories. Eight out of the top 10 journals were in JCR's first quarter.

Table 1. Top 10 journals for the study of low-carbon transition and public awareness/behavior.

Rank	Publications	Number of Publications	IF 2022	SJR 2022	JCR 2022	Categories
1	*Journal of Cleaner Production*	90	11.072	Q1	Q1	Environmental Science (SCIE)
2	*Sustainability*	74	3.889	Q2	Q1	Environmental Science (SSCI)
3	*Energy Policy*	52	7.576	Q1	Q1	Environmental Science (SCIE)
4	*Energies*	31	3.252	Q2	Q3	Energy and Fuels (SCIE)
5	*Materials Science and Engineering A: Structural Materials: Properties, Microstructure, and Processing*	29	6.044	Q1	Q1	Metallurgy and Metallurgical Engineering (SCIE)
6	*Energy Research and Social Science*	26	8.514	Q1	Q1	Environmental Science (SSCI)
7	*Metallurgical and Materials Transactions A: Physical Metallurgy and Materials Science*	25	2.726	Q1	Q2	Metallurgy and Metallurgical Engineering (SCIE)
8	*International Journal of Environmental Research and Public Health*	23	4.614	Q1	Q1	Public, Environment, and Occupational Health (SSCI)
9	*Renewable and Sustainable Energy Reviews*	21	16.799	Q1	Q1	Multidisciplinary Sciences (SCIE)
10	*Applied Energy*	18	11.466	Q1	Q1	Energy and Fuels (SCIE)

Note: IF: impact factors; SJR: SCImago journal rank; JCR: journal citation reports.

3.3. Keywords and Hotspot Analysis

The focus and content of the study of low-carbon transition and public awareness/behavior are analyzed through keyword analysis. The top 20 keywords for the study of low-carbon transition and public awareness/behavior can be seen in Figure 3. Additionally, Table 2 shows the top 20 keywords and their frequency, which is based on the study of low-carbon transition and public awareness/behavior. Moreover, Figure 4 illustrates the top 20 keywords with the strongest citation bursts and their popular periods.

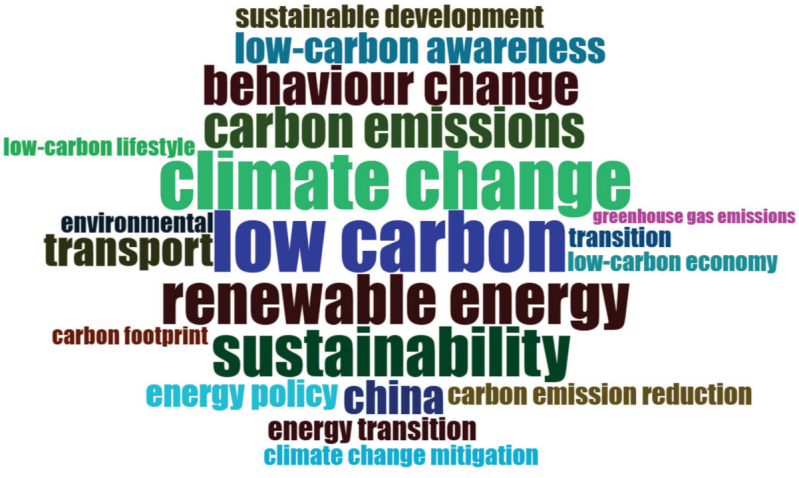

Figure 3. Word cloud of keywords for the study of low-carbon transition and public awareness/behavior. Note: the keyword font size in the diagram represents the frequency of the keywords during searches.

Table 2. Top 20 keywords for the study of low-carbon transition and public awareness/behavior.

Rank	Keywords	Frequency	Rank	Keywords	Frequency
1	Low Carbon	77	11	Energy Transition	29
2	Climate Change	73	12	Sustainable Development	29
3	Renewable Energy	62	13	Carbon Emission Reduction	27
4	Sustainability	62	14	Climate Change Mitigation	25
5	Carbon Emissions	51	15	Environmental	25
6	Behavior Change	50	16	Transition	25
7	China	43	17	Low-carbon Economy	24
8	Transport	43	18	Carbon Footprint	23
9	Low-carbon Awareness	39	19	Low-carbon Lifestyle	23
10	Energy Policy	34	20	Greenhouse Gas Emissions	18

The top 20 keywords on the study of low-carbon transition and public awareness/behavior include "Low Carbon", "Climate Change", "Sustainability", "Energy Transition", "Low-carbon Awareness", "Energy Policy", "Behavior change", "Low-carbon Economy", "Transport", "Environmental", "Renewable Energy", "Carbon Emission Reduction", "Sustainable Development", "Transition", "Climate Change Mitigation", "Carbon Footprint", "Carbon Emissions", "China", "Low-carbon Lifestyle", and "Greenhouse Gas Emissions".

According to the top 20 keywords, the focus of the study on low-carbon transition includes energy transition and economic transition, which should be guided by related policy. In order to decrease carbon emissions and mitigate climate change, researchers explored possible solutions, which include electric vehicles, introducing renewable energy, adapting to a low-carbon economy, and enhancing energy efficiency. In addition, researchers also focused on sustainability and biodiversity.

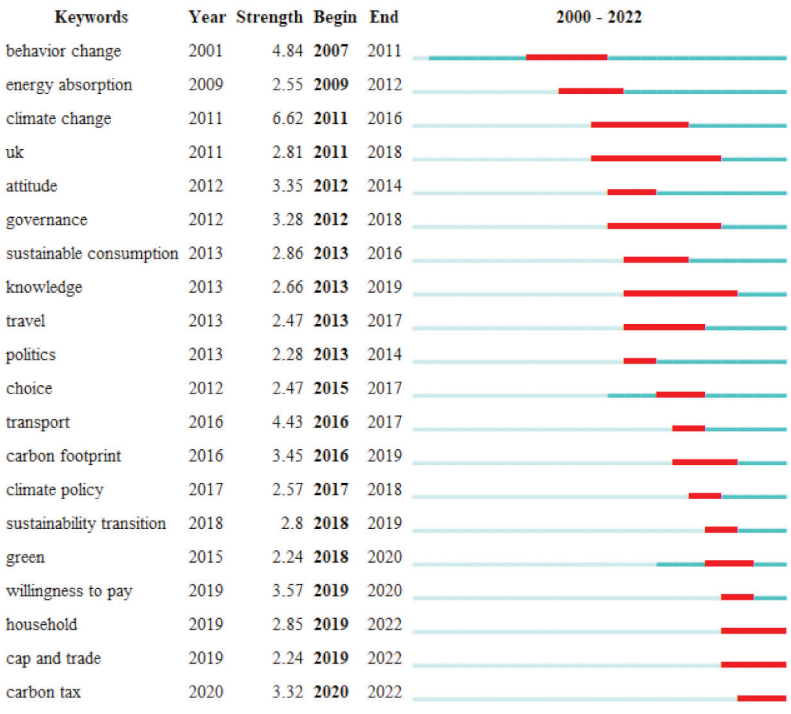

Figure 4. Top 20 keywords with the strongest citation bursts. Note: the year represents the starting year when keywords are mentioned.

3.4. Institution Contribution Analysis

Institutional contributions are critical to understanding the research intensity and composition of studies in specific fields. The performance of the top 10 institutions with the most publications on the study of low-carbon transition and public awareness/behavior is shown in Table 3. Research achievements in this field predominantly come from research institutes and universities. In addition, the top three institutions with high publications are as follows: the Chinese Academy of Sciences, the University of London, and Tianjin University.

Table 3. Performance of the top 10 institutions with the most publications within the study of low-carbon transition and public awareness/behavior.

Rank	Institution	Country	Number of Publications				Total
			1900–2005	2006–2010	2011–2015	2016–2022	
1	Chinese Academy of Sciences	China	0	4	6	30	38
2	University of London	UK	0	0	6	21	27
3	Tianjin University	China	0	0	8	19	27
4	Centre National de la Research Scienfique	Spain	2	3	1	17	23
5	Northeastern University	China	1	2	0	17	20
6	Tsinghua University	China	0	3	4	14	21
7	University College London	UK	0	1	4	14	19
8	United States Department of Energy	USA	4	0	5	10	19
9	Indian Institute of Technology System	India	0	2	3	13	18
10	University of Oxford	UK	0	0	4	14	18

3.5. Countries/Regions Contribution Analysis

The status of the low-carbon transition and public awareness/behavior were studied in various countries/regions. The geographical distribution and co-citation network for

the study of low-carbon transition and public awareness/behavior are illustrated, as seen in Figure 5. According to the result, the top three countries with the highest number of research publications are China, the United Kingdom (UK), and the United States (US). Moreover, as for research collaboration, China, the US, the UK, Australia, the Netherlands, and Germany have exhibited strong causal links with other countries. This shows that, on these research topics, researchers in these six countries collaborated closely with researchers in other countries, which further contributed to the increase in publications.

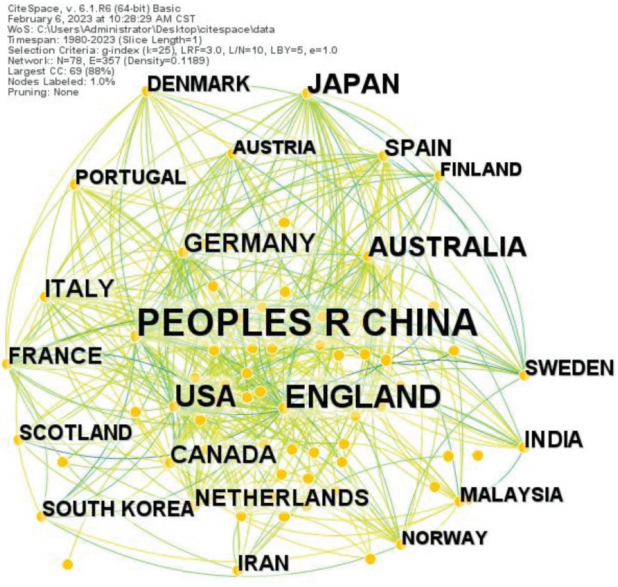

Figure 5. The geographical distribution and co-citation network for the study of low-carbon transition and public awareness/behavior. Note: the size of the label font in the figure represents the number of published documents, and the link between nodes represents the cooperative relationship between countries/regions.

The top 20 countries/regions with the most publications on the study of low-carbon transition and public awareness/behavior, as well as their whole and per capita publication numbers in 2022, are shown in Table 4. There were more than 100 publications each in China, the UK, and the US. Additionally, the top five countries with the highest number of publications are China, the UK, the US, Australia, and Japan. These results indicate that these countries have a wealth of high intensity focus on this research field and also have lots of publications. In addition, judging by the starting year of the research publications, the UK, the US, Japan, France, Spain, Denmark, and Finland all started the research on low-carbon transition and public awareness/behavior before 2000. This reflects the fact that these seven countries started research on this study topic much earlier than other countries. According to the per capita number of publications in 2022, the top three are Australia, the Netherlands, and the UK, which indicates that a relatively high percentage of researchers pay attention to this study topic in these countries.

Table 4. Top 20 countries/regions with the most publications surrounding the study of low-carbon transition and public awareness/behavior.

Rank	Country	Number of Publications	Starting Year	Number of Publications in 2022	Per Capita Number of Publications in 2022 (N/Million People)
1	China	499	2005	133	0.093
2	UK	195	1998	25	0.369
3	USA	142	1998	16	0.047
4	Australia	68	2008	13	0.492
5	Japan	66	1995	11	0.089
6	Germany	60	1998	7	0.084
7	Canada	42	2010	7	0.180
8	Italy	40	2008	6	0.102
9	France	38	1997	7	0.180
10	Netherlands	38	2001	8	0.454

Note: N represents the number of publications.

Figure 5 and Table 4 show the geographical distribution of publications for the study of the low-carbon transition and public awareness/behavior. According to the results, seven of the top ten countries/regions are located in North America and Europe, which indicates that this topic of study is conducted on these continents. Excepting the continents of North America and Europe, China (499), Australia (68), and Japan (66) are another three countries with a high number of publications on these research topics. Furthermore, within their respective continents, the quantity of research publications in China, Australia, and Japan is higher than in other countries.

4. Discussion

4.1. Research Trends, Development, and Hotspots

According to the bibliometric analysis results, studies on the topic of low-carbon transition and public awareness/behavior gradually became more popular in 2004, received high amounts of attention in 2016, and thereafter became a popular research topic in the fields of low-carbon. This may be because of the Paris Agreement in 2015, which drew strong attention to climate change worldwide, and then low-carbon became a popular topic in many fields.

According to the number of research publications, China, the UK, the US, Australia, and Japan have a wealth of high intensity focus on this research field. This may be in response to the Paris Agreement. For example, the United Kingdom, Japan, and many other countries have pledged to reach carbon neutrality by 2050 [46–49], and China has pledged to achieve carbon neutrality by 2060 [50,51]. In order to achieve the carbon neutrality goal, the corresponding policies were also formulated in many countries [52–54]. For example, China's energy policy promoted social acceptance or public awareness of renewable energy [55,56]. In addition, researchers are supported to study low-carbon transitions and public awareness/behavior in these countries. For example, researchers in China were encouraged and rewarded to study this topic and apply the findings to the policy-making process, which is a benefit to the low-carbon transition. Therefore, there are more publications than in any other country. However, publication numbers cannot represent the actual achievements of carbon emissions reduction in these countries since the benefits of low-carbon actions take time to be shown.

Additionally, according to the starting year of research publications, the UK, the US, Japan, France, Spain, Denmark, and Finland all started the research on low-carbon transition and public awareness/behavior earlier than other countries. According to the results of keyword analysis, energy transition and economic transition were the main study foci of the low-carbon transition.

According to Figure 4, behavior change was focused on by researchers in 2001, and it became a study hotspot between 2007 and 2011. In addition, researchers paid constant attention to behavior change from 2001 to the present day. Thus, behavior change should

be the key to achieving a low-carbon transition. As we can see, since climate change started becoming a popular study topic, researchers from the United Kingdom paid attention to it in the same year and studied the low-carbon transition and public awareness/behavior actively from 2011 to 2018. Since 2012, governments have been involved in this topic, and low-carbon policies have been formulated. Low-carbon technologies were studied soon after, such as low-carbon transport/travel, low-carbon education, carbon footprint reduction, and sustainability transition. Additionally, the public's willingness to pay for low-carbon products is also studied. From 2019 to 2022, household carbon emissions, carbon cap and trade, and carbon tax became the study hotspots.

Regarding the research filed for the study of low-carbon transition and public awareness/behavior (Figure 6), from 1900 to 2000, there were not many research fields paying attention to low-carbon transition and public awareness/behavior studies, just economics and environmental studies, and each only had one publication. From 2001 to 2010, the number of research fields increased, and environmental studies/sciences (19) ranked first. Some fields that did not appear in rankings from 1900 to 2000 were added to the ranking, including energy fuels, green sustainable science and technology, engineering environmental sciences, business, geography, management, and transportation. Thus, the main study focus of this period is new energy, carbon emissions reduction, low-carbon policy, and transportation footprint. From 2011 to 2022, environmental studies/sciences (638) still ranked the highest and have increased massively in number. Green sustainable science and technology ranked second (229); the following two are engineering environmental (111), and economics (90). Additionally, public environmental occupational health, urban studies, political science, sociology, educational research, communications, and development studies were added to the rankings. As we can see, the study of low-carbon transition and public awareness/behavior is getting more attention in environmental studies/sciences and has become a study topic in so many other fields in recent years.

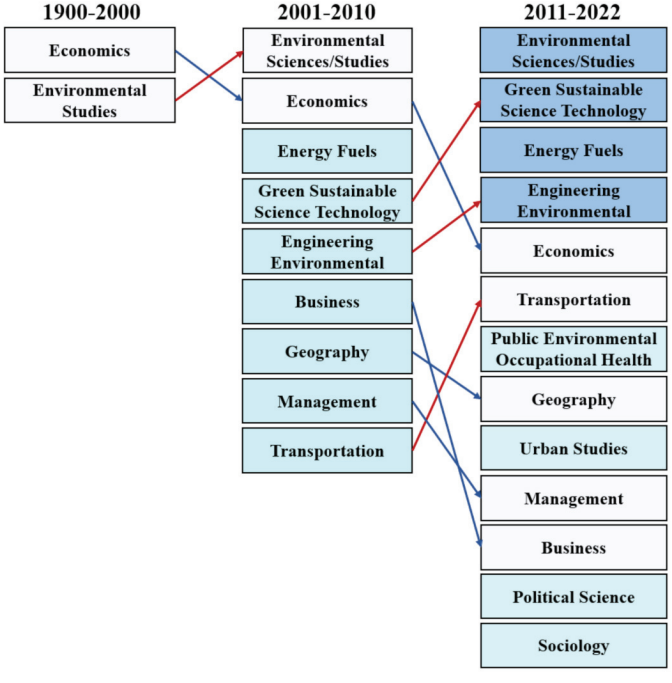

Figure 6. Research filed on transition for the study of low-carbon transition and public awareness/behavior.

A low-carbon energy transition is important to mitigate climate change impacts and temperature rises [62]. Adopting alternative technologies for fossil energy and improving energy efficiency are possible technical directions and options to reduce carbon emissions [33]. Previous studies found that 70% of CO_2 emissions (directly and indirectly) are from households; energy use at home, transportation options, and diets will have an effect on households' CO_2 footprint [63]. Peng et al. analyzed neighborhood residents' cognition of and participation in low-carbon behaviors. The results showed that neighborhood residents get involved in low-carbon behaviors through home energy conservation (HEC), efficient resource consumption (ERC), and recycling habits (RH) [64].

Environmental education has a positive impact on low-carbon behavior through pollution control and enhances green consumption intentions through residents' environmental awareness [65]. Previous studies found that the influence of awareness and personal/social norms is as important as monetary factors [63]. Hu et al. also found that attitude, perceived behavior control, environmental concern, and perceived moral obligation have a positive impact on low-carbon travel behavioral intention [66]. Thus, environmental education is a great approach to improving people's awareness of low-carbon behaviors. Additionally, personal and social norms have a significant influence on low-carbon behaviors. Niamire et al. found that behavioral factors (e.g., knowledge and awareness) have an effect on personal norms; a higher level of knowledge and awareness about environmental and climate issues comes along with a higher level of personal norms [63]. Chen and Li investigated the influence factors of low-carbon behavior and found that personal and social norms had a stronger impact on public low-carbon behavior than private low-carbon behavior [67]. Moreover, demographic factors (i.e., gender, education, and income) will impact low-carbon behavior [67]. Additionally, although some people have an awareness of low-carbon behavior, it is still hard for them to take proper action if they do not have knowledge of the carbon footprint of their behavior. Thus, there should be information provided to inform people of the carbon footprint of their decisions [71].

In sum, environmental education is a great way to improve society's awareness of low-carbon behavior [68,69]. Thus, there should be some environmental education projects conducted in the whole society and in such groups as neighborhoods and households.

4.2. Future Work and Frontier Directions

According to previous research, there are gaps between low-carbon-related policy and public awareness/behavior, which will postpone the progress of the low-carbon transition. First of all, there are many low-carbon policies formulated, but it is still a challenge to put them into action. For example, many policies are top-down demands within abstract and general concepts and usually aim for the benefits of the whole country or a larger range of populations, which seem remote from public personal life. Thus, it is difficult for the public to accept changes that are not closely related to their own interests. Therefore, low-carbon education needs to be invested in to let the public learn about their close relationship with the low-carbon transition and to explain the policy for guiding the public's low-carbon behavior. Additionally, policies are also expected to be more precise, such as providing specific carbon emission reduction measures and low-carbon behavior guidelines. Secondly, new low-carbon technologies should be introduced to the public more efficiently. For example, provide new low-carbon products with purchase discounts and reward the company for using low-carbon energy so as to guide the public to accept new energy or low-carbon technology products. Finally, the low-carbon transition needs collaboration worldwide. It is not the mission of one industry, country, or continent, but a human mission. Thus, the low-carbon transition is a revolution within the co-thinking, co-design, and co-action of every person, household, industry, country, and continent. In general, the frontier issues/directions of low-carbon transition and public awareness include "low-carbon education", "policies with specific guidelines", and "worldwide collaboration".

4.3. Strengths and Limitations

This study analyzed the trends and status of the research on low-carbon transition and public awareness/behavior through bibliometric analysis. In addition, this study systematically summarized the research progress on low-carbon transition and public awareness/behavior in previous studies, including factors that have an effect on low-carbon behavior, low-carbon transition mechanisms, and so on.

Finally, because English is the most widely used language for academic publications worldwide, this study only included publications in English. The limitation of this study is that it only analyzed English literature collected from the WoSCC database. Moreover, this study only considered peer-reviewed publications (i.e., "Article" and "Review Article") on low-carbon transition and public awareness/behavior. In addition, the search terms might have excluded other relevant literature.

5. Conclusions

After the Paris agreement, studies on low-carbon transition and public awareness/behavior became research hotspots in the low-carbon field. As a response, this study conducted bibliometric analysis to analyze the trends, progress, status, and hotspots of studies on low-carbon transition and public awareness/behavior, including country/region contribution analysis, institution contribution analysis, keyword analysis, and highly productive journal analysis.

This study analyzed the trends and status of the research on low-carbon transition and public awareness/behavior through bibliometric analysis. In addition, this study systematically summarized the research progress on low-carbon transition and public awareness/behavior in previous studies, including factors that have an effect on low-carbon behavior, low-carbon transition mechanisms, and so on. For example, researchers paid constant attention to behavior change from 2001 to the present day. Since 2012, governments have been involved in this topic, and low-carbon policies have been formulated. From 2019 to 2022, household carbon emissions, carbon cap and trade, and carbon tax became the study hotspots. From 1900 to 2000, there were not many research fields that paid attention to low-carbon and public awareness/behavior studies. From 2001 to 2010, there were publications in environmental studies/sciences, energy fuels, green sustainable science and technology, engineering environmental sciences, business, geography, management, and transportation fields. From 2011 to 2022, the publication numbers of low-carbon transition and public awareness/behavior studies have increased massively. Moreover, public environmental and occupational health, urban studies, political science, sociology, educational research, communications, and development studies were also focused on this topic.

Policymakers need to advocate for the carbon reduction benefits of urban forms and lifestyles and formulate implementable policies accordingly. A low-carbon society is feasible if widespread awareness is achieved. This is also in line with the trends in "public participation", "co-design", and "act locally". Regarding the frontier issues/directions of low-carbon transition and public awareness, low-carbon education needs to be invested in to let the public learn about their close relationship with low-carbon transition and to explain the policy for guiding the public's low-carbon behavior. Additionally, policies are also expected to be more precise, such as providing specific carbon emission reduction measures and low-carbon behavior guidelines. Moreover, new low-carbon technologies should be introduced to the public more efficiently. Finally, the low-carbon transition needs collaboration worldwide.

Author Contributions: Conceptualization, methodology, investigation/collection of data, data curation, analysis, writing—original draft, writing—review and editing, visualization, X.W.; conceptualization, methodology, writing—original draft, writing—review and editing, visualization, Y.-S.S. All authors have read and agreed to the published version of the manuscript.

Funding: This research was funded by the Chinese Academy of Sciences [grant numbers 2019TW2ZA0001] and the Ministry of Science and Technology of the People's Republic of China [grant number RW2019TW006].

Institutional Review Board Statement: Not applicable.

Informed Consent Statement: Not applicable.

Data Availability Statement: Not applicable.

Acknowledgments: We thank the funding support from the project of the Chinese Academy of Sciences and the project of the Ministry of Science and Technology of the People's Republic of China. The contents of this paper are solely the responsibility of the authors and do not represent the official views of the institutes and funding agencies.

Conflicts of Interest: The authors declare no conflict of interest.

References

1. Funk, C.C.; Brown, M.E. Declining global per capita agricultural production and warming oceans threaten food security. *Food Secur.* **2009**, *1*, 271–289. [CrossRef]
2. Gomez-Zavaglia, A.; Mejuto, J.C.; Simal-Gandara, J. Mitigation of emerging implications of climate change on food production systems. *Food Res. Int.* **2020**, *134*, 109256. [CrossRef] [PubMed]
3. Hendriks, S.L.; Montgomery, H.; Benton, T.; Badiane, O.; de la Mata, G.C.; Fanzo, J.; Guinto, R.R.; Soussana, J.-F. Global environmental climate change, COVID-19, and conflict threaten food security and nutrition. *BMJ-Brit. Med. J.* **2022**, *378*, e071534. [CrossRef]
4. Sundstrom, J.F.; Albihn, A.; Boqvist, S.; Ljungvall, K.; Marstorp, H.; Martiin, C.; Nyberg, K.; Vagsholm, I.; Yuen, J.; Magnusson, U. Future threats to agricultural food production posed by environmental degradation, climate change, and animal and plant diseases—A risk analysis in three economic and climate settings. *Food Secur.* **2014**, *6*, 201–215. [CrossRef]
5. Michener, W.K.; Blood, E.R.; Bildstein, K.L.; Brinson, M.M.; Gardner, L.R. Climate change, hurricanes and tropical storms, and rising sea level in coastal wetlands. *Ecol. Appl.* **1997**, *7*, 770–801. [CrossRef]
6. Nerem, R.S.; Beckley, B.D.; Fasullo, J.T.; Hamlington, B.D.; Masters, D.; Mitchum, G.T. Climate-change-driven accelerated sea-level rise detected in the altimeter era. *Proc. Natl. Acad. Sci. USA* **2018**, *115*, 2022–2025. [CrossRef]
7. Hallegatte, S.; Ranger, N.; Mestre, O.; Dumas, P.; Corfee-Morlot, J.; Herweijer, C.; Wood, R.M. Assessing climate change impacts, sea level rise and storm surge risk in port cities: A case study on Copenhagen. *Clim. Chang.* **2011**, *104*, 113–137. [CrossRef]
8. Miller, J.D.; Hutchins, M. The impacts of urbanisation and climate change on urban flooding and urban water quality: A review of the evidence concerning the United Kingdom. *J. Hydrol. Reg. Stud.* **2017**, *12*, 345–362. [CrossRef]
9. Arnell, N.W.; Lloyd-Hughes, B. The global-scale impacts of climate change on water resources and flooding under new climate and socio-economic scenarios. *Clim. Chang.* **2014**, *122*, 127–140. [CrossRef]
10. Huong, H.T.L.; Pathirana, A. Urbanization and climate change impacts on future urban flooding in Can Tho city, Vietnam. *Hydrol. Earth Syst. Sci.* **2013**, *17*, 379–394. [CrossRef]
11. Hanna, E.; Navarro, F.J.; Pattyn, F.; Domingues, C.M.; Fettweis, X.; Ivins, E.R.; Nicholls, R.J.; Ritz, C.; Smith, B.; Tulaczyk, S.; et al. Ice-sheet mass balance and climate change. *Nature* **2013**, *498*, 51–59. [CrossRef] [PubMed]
12. Bliss, A.; Hock, R.; Radic, V. Global response of glacier runoff to twenty-first century climate change. *J. Geophys. Res. Earth. Surf.* **2014**, *119*, 717–730. [CrossRef]
13. Dyurgerov, M.B.; Meier, M.F. Twentieth century climate change: Evidence from small glaciers. *Proc. Natl. Acad. Sci. USA* **2000**, *97*, 1406–1411. [CrossRef]
14. Leng, G.; Tang, Q.; Rayburg, S. Climate change impacts on meteorological, agricultural and hydrological droughts in China. *Glob. Planet. Chang.* **2015**, *126*, 23–34. [CrossRef]
15. UN. Available online: https://www.un.org/en/global-issues/climate-change (accessed on 30 December 2020).
16. Hanson, P.J.; Weltzin, J.F. Drought disturbance from climate change: Response of United States forests. *Sci. Total Environ.* **2000**, *262*, 205–220. [CrossRef]
17. Karim, M.F.; Mimura, N. Impacts of climate change and sea-level rise on cyclonic storm surge floods in Bangladesh. *Glob. Environ. Chang.* **2008**, *18*, 490–500. [CrossRef]
18. Bronstert, A.; Niehoff, D.; Burger, G. Effects of climate and land-use change on storm runoff generation: Present knowledge and modelling capabilities. *Hydrol. Process.* **2002**, *16*, 509–529. [CrossRef]
19. Day, J.W.; Christian, R.R.; Boesch, D.M.; Yanez-Arancibia, A.; Morris, J.; Twilley, R.R.; Naylor, L.; Schaffner, L.; Stevenson, C. Consequences of climate change on the ecogeomorphology of coastal wetlands. *Estuaries Coasts* **2008**, *31*, 477–491. [CrossRef]
20. Hellmann, J.J.; Byers, J.E.; Bierwagen, B.G.; Dukes, J.S. Five potential consequences of climate change for invasive species. *Conserv. Biol.* **2008**, *22*, 534–543. [CrossRef]
21. Bellard, C.; Bertelsmeier, C.; Leadley, P.; Thuiller, W.; Courchamp, F. Impacts of climate change on the future of biodiversity. *Ecol. Lett.* **2012**, *15*, 365–377. [CrossRef] [PubMed]

22. Shen, Y.-S.; Lin, Y.-C.; Cui, S.; Li, Y.; Zhai, X. Crucial factors of the built environment for mitigating carbon emissions. *Sci. Total Environ.* **2022**, *806*, 150864. [CrossRef] [PubMed]
23. UNFCCC. Available online: https://unfccc.int/process-and-meetings/the-paris-agreement (accessed on 25 September 2020).
24. Ohno, H.; Shigetomi, Y.; Chapman, A.; Fukushima, Y. Detailing the economy-wide carbon emission reduction potential of post-consumer recycling. *Resour. Conserv. Recycl.* **2021**, *166*, 105263. [CrossRef]
25. Zhang, J.; Zhang, L.; Qin, Y.; Wang, X.; Zheng, Z. Impact of Residential Self-Selection on Low-Carbon Behavior: Evidence from Zhengzhou, China. *Sustainability* **2019**, *11*, 6871. [CrossRef]
26. Zhang, L.; Yang, Z.; Liang, J.; Cai, Y. Spatial Variation and Distribution of Urban Energy Consumptions from Cities in China. *Energies* **2011**, *4*, 26–38. [CrossRef]
27. Kennedy, C.; Steinberger, J.; Gasson, B.; Hansen, Y.; Hillman, T.; Havranek, M.; Pataki, D.; Phdungsilp, A.; Ramaswami, A.; Villalba Mendez, G. Greenhouse Gas Emissions from Global Cities. *Environ. Sci. Technol.* **2009**, *43*, 7297–7302. [CrossRef]
28. Phdungsilp, A. Integrated energy and carbon modeling with a decision support system: Policy scenarios for low-carbon city development in Bangkok. *Energy Policy* **2010**, *38*, 4808–4817. [CrossRef]
29. Lin, J.; Cao, B.; Cui, S.; Wang, W.; Bai, X. Evaluating the effectiveness of urban energy conservation and GHG mitigation measures: The case of Xiamen city, China. *Energy Policy* **2010**, *38*, 5123–5132. [CrossRef]
30. Gurney, K.R.; Kilkis, S.; Seto, K.C.; Lwasa, S.; Moran, D.; Riahi, K.; Keller, M.; Rayner, P.; Luqman, M. Greenhouse gas emissions from global cities under SSP/RCP scenarios, 1990 to 2100. *Glob. Environ. Chang.* **2022**, *73*, 102478. [CrossRef]
31. Barthelmie, R.J.; Morris, S.D.; Schechter, P. Carbon neutral Biggar: Calculating the community carbon footprint and renewable energy options for footprint reduction. *Sustain. Sci.* **2008**, *3*, 267–282. [CrossRef]
32. Birge, D.; Berger, A.M. Transitioning to low-carbon suburbs in hot-arid regions: A case-study of Emirati villas in Abu Dhabi. *Build. Environ.* **2019**, *147*, 77–96. [CrossRef]
33. Liang, S.; Zhang, T. What is driving CO_2 emissions in a typical manufacturing center of South China? The case of Jiangsu Province. *Energy Policy* **2011**, *39*, 7078–7083. [CrossRef]
34. UN. Available online: https://www.un.org/en/academic-impact/how-mitigate-climate-change-key-facts-uns-2014-report (accessed on 28 April 2014).
35. Benhelal, E.; Zahedi, G.; Shamsaei, E.; Bahadori, A. Global strategies and potentials to curb CO_2 emissions in cement industry. *J. Clean. Prod.* **2013**, *51*, 142–161. [CrossRef]
36. Akbari, H. Shade trees reduce building energy use and CO_2 emissions from power plants. *Environ. Pollut.* **2002**, *116*, S119–S126. [CrossRef] [PubMed]
37. Wang, F.; Harindintwali, J.D.; Yuan, Z.; Wang, M.; Wang, F.; Li, S.; Yin, Z.; Huang, L.; Fu, Y.; Li, L.; et al. Technologies and perspectives for achieving carbon neutrality. *Innovation* **2021**, *2*, 100180. [CrossRef] [PubMed]
38. Yamasaki, A. An overview of CO_2 mitigation options for global warming—Emphasizing CO_2 sequestration options. *J. Chem. Eng. Jpn.* **2003**, *36*, 361–375. [CrossRef]
39. Brandao, M.; Levasseur, A.; Kirschbaum, M.U.F.; Weidema, B.P.; Cowie, A.L.; Jorgensen, S.V.; Hauschild, M.Z.; Pennington, D.W.; Chomkhamsri, K. Key issues and options in accounting for carbon sequestration and temporary storage in life cycle assessment and carbon footprinting. *Int. J. Life Cycle Assess.* **2013**, *18*, 230–240. [CrossRef]
40. Gattinger, A.; Muller, A.; Haeni, M.; Skinner, C.; Fliessbach, A.; Buchmann, N.; Maeder, P.; Stolze, M.; Smith, P.; Scialabba, N.E.-H.; et al. Enhanced top soil carbon stocks under organic farming. *Proc. Natl. Acad. Sci. USA* **2012**, *109*, 18226–18231. [CrossRef]
41. Ostle, N.J.; Levy, P.E.; Evans, C.D.; Smith, P. UK land use and soil carbon sequestration. *Land Use Policy* **2009**, *26*, S274–S283. [CrossRef]
42. Zou, C.; Xiong, B.; Xue, H.; Zheng, D.; Ge, Z.; Wang, Y.; Jiang, L.; Pan, S.; Wu, S. The role of new energy in carbon neutral. *Pet. Explor. Dev.* **2021**, *48*, 480–491. [CrossRef]
43. Paustian, K.; Six, J.; Elliott, E.T.; Hunt, H.W. Management options for reducing CO2 emissions from agricultural soils. *Biogeochemistry* **2000**, *48*, 147–163. [CrossRef]
44. Lee, C.T.; Hashim, H.; Ho, C.S.; Fan, Y.V.; Klemes, J.J. Sustaining the low-carbon emission development in Asia and beyond: Sustainable energy, water, transportation and low-carbon emission technology. *J. Clean. Prod.* **2017**, *146*, 1–13. [CrossRef]
45. Dietz, T.; Gardner, G.T.; Gilligan, J.; Stern, P.C.; Vandenbergh, M.P. Household actions can provide a behavioral wedge to rapidly reduce US carbon emissions. *Proc. Natl. Acad. Sci. USA* **2009**, *106*, 18452–18456. [CrossRef]
46. Davidson, M.; Karplus, V.J.; Zhang, D.; Zhang, X. Policies and Institutions to Support Carbon Neutrality in China by 2060. *Econ. Energy Environ. Policy* **2021**, *10*, 7–24. [CrossRef]
47. Williams, J.H.; Jones, R.A.; Haley, B.; Kwok, G.; Hargreaves, J.; Farbes, J.; Torn, M.S. Carbon-Neutral Pathways for the United States. *AGU Adv.* **2021**, *2*, e2020AV000284. [CrossRef]
48. Becker, S.; Bouzdine-Chameeva, T.; Jaegler, A. The carbon neutrality principle: A case study in the French spirits sector. *J. Clean. Prod.* **2020**, *274*, 122739. [CrossRef] [PubMed]
49. Perissi, I.; Jones, A. Investigating European Union Decarbonization Strategies: Evaluating the Pathway to Carbon Neutrality by 2050. *Sustainability* **2022**, *14*, 4728. [CrossRef]
50. Zhao, X.; Ma, X.; Chen, B.; Shang, Y.; Song, M. Challenges toward carbon neutrality in China: Strategies and countermeasures. *Resour. Conserv. Recycl.* **2022**, *176*, 105959. [CrossRef]

51. Li, J.; Ho, M.S.; Xie, C.; Stern, N. China's flexibility challenge in achieving carbon neutrality by 2060. *Renew. Sustain. Energy Rev.* **2022**, *158*, 112112. [CrossRef]
52. Owen, A.; Barrett, J. Reducing inequality resulting from UK low-carbon policy. *Clim. Policy* **2020**, *20*, 1193–1208. [CrossRef]
53. Corradini, M.; Costantini, V.; Markandya, A.; Paglialunga, E.; Sforna, G. A dynamic assessment of instrument interaction and timing alternatives in the EU low-carbon policy mix design. *Energy Policy* **2018**, *120*, 73–84. [CrossRef]
54. Cheng, B.; Dai, H.; Wang, P.; Xie, Y.; Chen, L.; Zhao, D.; Masui, T. Impacts of low-carbon power policy on carbon mitigation in Guangdong Province, China. *Energy Policy* **2016**, *88*, 515–527. [CrossRef]
55. Yuan, X.; Zuo, J. Transition to low carbon energy policies in China-from the Five-Year Plan perspective. *Energy Policy* **2011**, *39*, 3855–3859. [CrossRef]
56. Yuan, X.; Zuo, J.; Ma, C. Social acceptance of solar energy technologies in China-End users' perspective. *Energy Policy* **2011**, *39*, 1031–1036. [CrossRef]
57. Jiang, P.; Chen, Y.; Xu, B.; Dong, W.; Kennedy, E. Building low carbon communities in China: The role of individual's behaviour change and engagement. *Energy Policy* **2013**, *60*, 611–620. [CrossRef]
58. Liu, Y.; Yang, D.; Xu, H. Factors Influencing Consumer Willingness to Pay for Low-Carbon Products: A Simulation Study in China. *Bus. Strategy Environ.* **2017**, *26*, 972–984. [CrossRef]
59. Burch, S. In pursuit of resilient, low carbon communities: An examination of barriers to action in three Canadian cities. *Energy Policy* **2010**, *38*, 7575–7585. [CrossRef]
60. Jia, N.; Li, L.; Ling, S.; Ma, S.; Yao, W. Influence of attitudinal and low-carbon factors on behavioral intention of commuting mode choice—A cross-city study in China. *Transp. Res. Part A Policy Pract.* **2018**, *111*, 108–118. [CrossRef]
61. Whitmarsh, L.; Seyfang, G.; O'Neill, S. Public engagement with carbon and climate change: To what extent is the public 'carbon capable'? *Glob. Environ. Chang.* **2011**, *21*, 56–65. [CrossRef]
62. Chapman, A.; Okushima, S. Engendering an inclusive low-carbon energy transition in Japan: Considering the perspectives and awareness of the energy poor. *Energy Policy* **2019**, *135*, 111017. [CrossRef]
63. Niamir, L.; Ivanova, O.; Filatova, T.; Voinov, A.; Bressers, H. Demand-side solutions for climate mitigation: Bottom-up drivers of household energy behavior change in the Netherlands and Spain. *Energy Res. Soc. Sci.* **2020**, *62*, 1356. [CrossRef]
64. Peng, W.; Wang, X.; Guo, L. An Exploration of Neighborhood Residents' Cognition of and Participation in Low-Carbon Behaviors in Wuhan, China. *Adv. Civ. Eng.* **2018**, *2018*, 8764801. [CrossRef]
65. Wu, Y.; Wan, J.; Yu, W. Impact of environmental education on environmental quality under the background of low-carbon economy. *Front. Public Health* **2023**, *11*, 1128791. [CrossRef] [PubMed]
66. Hu, X.; Wu, N.; Chen, N. Young People's Behavioral Intentions towards Low-Carbon Travel: Extending the Theory of Planned Behavior. *Int. J. Environ. Res. Public Health* **2021**, *18*, 2327. [CrossRef] [PubMed]
67. Chen, W.; Li, J. Who are the low-carbon activists? Analysis of the influence mechanism and group characteristics of low-carbon behavior in Tianjin, China. *Sci. Total Environ.* **2019**, *683*, 729–736. [CrossRef] [PubMed]
68. Ye, H.; Ren, Q.; Hu, X.; Lin, T.; Xu, L.; Li, X.; Zhang, G.; Shi, L.; Pan, B. Low-carbon behavior approaches for reducing direct carbon emissions: Household energy use in a coastal city. *J. Clean. Prod.* **2017**, *141*, 128–136. [CrossRef]
69. Jiang, P.; Tovey, N.K. Opportunities for low carbon sustainability in large commercial buildings in China. *Energy Policy* **2009**, *37*, 4949–4958. [CrossRef]
70. Juvan, E.; Dolnicar, S. Can tourists easily choose a low carbon footprint vacation? *J. Sustain. Tour.* **2014**, *22*, 175–194. [CrossRef]
71. Liu, Z.; Ma, J.; Chai, Y. Neighborhood-scale urban form, travel behavior, and CO_2 emissions in Beijing: Implications for low-carbon urban planning. *Urban Geogr.* **2017**, *38*, 381–400. [CrossRef]

atmosphere

MDPI

Article

Investigation into Spatial and Temporal Differences in Carbon Emissions and Driving Factors in the Pearl River Delta: The Perspective of Urbanization

Ziya Gao [1], Dafang Wu [1,2,*], Zhaojun Wu [1,3] and Lechun Zeng [4]

[1] School of Geography and Remote Sensing, Guangzhou University, Guangzhou 510006, China; 2112301076@e.gzhu.edu.cn (Z.G.); 2112201066@e.gzhu.edu.cn (Z.W.)
[2] Laboratory for Earth Surface Processes, Peking University, Beijing 100871, China
[3] Guangzhou Institute of Geography, Guangdong Academy of Sciences, Guangzhou 510070, China
[4] Land Development and Regulation Center of Guangdong Province, Guangzhou 510620, China; zenglctd@163.com
* Correspondence: wudafang@gzhu.edu.cn

Abstract: Urbanization is a significant indicator of city progress, and as urbanization advances, carbon emissions exhibit an increasing trend that must not be disregarded. Therefore, it is imperative to thoroughly examine the spatial and temporal variations as well as the factors influencing carbon emissions during the urbanization process. In this paper, based on the 2009–2019 PRD region, carbon emissions are measured from energy consumption, industrial production process, solid waste, and wastewater according to the IPCC coefficients, and spatial and spatial differences in carbon emissions are combined with spatial analysis and the drivers analyzed using the gray correlation scale. The results show that: (1) The total carbon emissions in the PRD region have been increasing over the study period, and the distribution of total carbon emissions shows a pattern of "strong in the east and weak in the west", with energy consumption accounting for the highest proportion of carbon emissions. (2) The global Moran Index of carbon emissions in the PRD has been decreasing, with low and low clustering concentrated in Shaoguan and Zhaoqing, high and high clustering concentrated in Dongguan and Shenzhen, and low and high clustering concentrated in Shenzhen and Guangzhou, with cold spots mainly concentrated in Zhaoqing and hot spots mainly distributed in Guangzhou, Shenzhen, and Dongguan. (3) The degree of economic growth has a substantial influence on carbon emissions in the PRD cities, and the influence of technical advancement has intensified. Guangzhou City is propelled by low-carbon regulations that have a more equitable influence on all elements. Zhuhai City has a more significant influence on energy intensity, while Foshan City has a more noticeable decrease in the effect of foreign investment. To address the issue of carbon emissions, the government should establish appropriate rules to regulate carbon emissions in areas with high emissions, foster collaborative efforts across cities, and encourage the growth of environmentally friendly enterprises.

Keywords: carbon emissions; spatiotemporal differences; driving factors; the Pearl River Delta

Citation: Gao, Z.; Wu, D.; Wu, Z.; Zeng, L. Investigation into Spatial and Temporal Differences in Carbon Emissions and Driving Factors in the Pearl River Delta: The Perspective of Urbanization. *Atmosphere* **2024**, *15*, 782. https://doi.org/10.3390/atmos15070782

Academic Editors: Chaofan Xian, Yu-Sheng Shen and Cheng Gong

Received: 23 May 2024
Revised: 22 June 2024
Accepted: 25 June 2024
Published: 29 June 2024

1. Introduction

Cities are the primary sources of carbon emissions, and their coordinated role in driving socioeconomic transformation during urbanization is crucial for advancing energy efficiency and achieving China's goals of carbon peaking and carbon neutrality [1]. Cities, which are the primary hubs of human socioeconomic activity, cover about 3% of the Earth's surface area yet account for over 75% of the world's energy consumption and contribute to nearly 80% of global carbon emissions [2]. Consequently, achieving carbon peaking in cities has become a significant agenda for mitigating climate change [3]. Urbanization has caused a cascade of ecological and environmental problems, including scarcity of resources,

damage to the environment, and pollution [4]. Urbanization and carbon emissions have a very complicated connection. It is now critical and necessary to coordinate the interaction between urbanization and carbon emissions. Conducting research on carbon emissions, finely characterizing the spatiotemporal distribution patterns, and identifying influencing factors are of crucial importance. This research not only contributes to promoting regional coordinated development but also holds significant reference value for enhancing the scientific, targeted, and practical aspects of energy-saving and emission-reduction policies [5].

In recent years, both domestic and international scholars have undertaken comprehensive research on carbon emissions, examining diverse perspectives. Their investigations encompass the estimation of total emissions [6], performance metrics [7], and emission intensity [8] from various angles. Concurrently, these studies have delved into specific industries, including the financial sector [9], agriculture [6], industry [10], and tourism [11], in order to conduct in-depth analyses of carbon emissions. Li et al. (2015) conducted a thorough examination of carbon emissions at the county, municipal, and provincial levels; the findings revealed distinct patterns of regional distribution [12].

Zhao et al. (2018) observed distinct patterns of carbon emissions at the province level, characterized by a high concentration of emissions and a low amount of clustering [13]. When examining carbon emissions at the municipal level, Wu et al. (2023) identified clustering patterns. They noticed that per capita carbon emissions tend to rise from south to north and decrease from the eastern coastal regions towards the interior areas [14]. Wang et al. (2021) observed that at the county level, there is a clear spatial intensification associated with carbon emissions. They found a consistent geographic pattern of "higher in the north, lower in the south", in economically developed regions in China having more per capita carbon emissions compared to other areas [5]. Wang et al. (2015) discovered that the factors that affect carbon emissions are intricate and varied at the same time [15]. Li et al. (2015) investigated the geographical heterogeneity and spatial autocorrelation of carbon emissions using spatial panel econometric models and exploratory spatial data analysis (ESDA) techniques [12]. Liu et al. (2019) investigated the effects of production scale, the intensity of energy use, the structure of the industry, population size, and the structure of energy on carbon emissions consumption using the Logarithmic Mean Divisia Index (LMDI) model [16]. Geographic detectors were utilized to uncover the significant explanatory capability of economic urbanization in accounting for the variations in carbon emissions at the county level [17]. Using the STIRPAT model, Chen et al. (2018) found that a city's carbon emissions are greatly increased by population growth and the proportion of its output value that comes from secondary industries [18]. Song et al. (2023) applied geographic weighted regression and panel data regression models to identify varying levels of carbon emissions and major influencing factors among different types of counties [19].

Numerous academics have examined carbon emissions within the context of urbanization from the angles of drivers, geographical organization, and economic expansion. In terms of economic growth research, studies are usually conducted in two directions: economic growth in general or in a single sector. Among them, Wang et al. (2023) discovered a connection between economic development and the increase in CO_2 emissions when they examined carbon emissions from the perspective of general economic growth [20]. In their research, Dong et al. (2020) focused on six key sectors, including agriculture, industry, and construction, to examine the effects of carbon emissions. Their findings indicate that the transportation industry has the greatest influence [21]. Within the study of spatial structure, as the city size continues to expand, there is a growing trend of continuity and concentration of built-up regions, leading to an increase in carbon emissions [22]. The majority of studies employ the Geographically and Temporally Weighted Regression (GTWR) model, enabling an examination of urban agglomeration. It has been observed that the multifaceted structure of certain urban agglomerations fails to effectively reduce carbon emissions to a significant extent [23]. However, the GTWR model can analyze the urban change pattern by considering the factors that influence it, incorporating both temporal

and spatial dimensions. It reveals that the direction and strength of influence vary among different cities at different stages of development [24]. Ding et al. (2022) discovered that when urban agglomerations reach a more advanced stage of development, the degree of land use and land cover change (LUCE) increases, along with a greater concentration of districts and counties with a high level of carbon emissions [25]. China's energy sector produces carbon emissions that are typically greater than those of the rest of the world, and the country's growing economy is the main cause pushing up carbon emissions [26]. Yang et al. (2023) linked carbon emissions to urban high-quality development, demonstrating that advancements in technology, environmental governance, and economic growth are critical factors that may favorably impact both the moderate decrease in carbon emissions and the enhancement of environmental quality [27].

Based on the current study, there is still an opportunity for growth in this area even though studies on carbon emissions have been trending upward recently. The dominant techniques for measuring carbon emissions in metropolitan areas are largely concerned with emissions connected to energy consumption in the accounting process of carbon dioxide emissions [28]. This concentration leads to significant discrepancies between the calculated urban carbon emissions and the actual values. Second, the current research has mostly targeted provincial scales, with limited studies focusing on cities, and there is a scarcity of regional studies based on cities [5]. Third, there are very few studies on the spatiotemporal variations and driving forces of regional carbon emissions. Instead, research on carbon emission efficiency and productivity disparities has dominated the field.

Through experience summarization, this study seeks to provide a scientific reference for accomplishing the "dual carbon" objectives. Firstly, using economic and social data from the "Guangdong Statistical Yearbook", carbon emissions in four sectors—energy consumption, industrial production processes, solid waste, and wastewater—are calculated for the nine cities. Secondly, the total carbon emissions are determined by adding the emissions from these four sectors, and the spatiotemporal variations in carbon emissions are examined using spatial autocorrelation analysis. Lastly, the research assesses the influence of driving characteristics on the overall carbon emissions based on these computations.

Thus, this research specifically examines the Pearl River Delta area, investigating the spatial and temporal changes in carbon emissions that occur throughout the process of urbanization. The study identifies influential elements and examines their effect on carbon emissions in the Pearl River Delta. Ultimately, policy suggestions are provided based on the study findings. These results may be used as a benchmark for conserving energy and reducing carbon emissions throughout the process of urbanization.

2. Study Area and Data Source

2.1. Study Area

The Pearl River Delta (PRD) is situated in the central–southern region of Guangdong Province, including the middle and lower sections of the Pearl River, inside the subtropical zone. Adjacent to Hong Kong and Macau, it comprises nine prefecture-level cities: Guangzhou, Foshan, Zhaoqing, Shenzhen, Dongguan, Huizhou, Zhuhai, Zhongshan, and Jiangmen [29,30]. It makes up over one-third of Guangdong Province's entire land area, with a total size of around 54,767 square kilometers. With a high urbanization rate of 87%, the Pearl River Delta, despite its size, concentrates 81% of the province's entire economic output. The geographical location of the PRD is shown in Figure 1.

Analyzing the spatial distribution characteristics, temporal evolution, and driving forces of carbon emissions in highly urbanized regions can be facilitated by examining the spatiotemporal differentiation and driving factors of carbon emissions in the PRD urban cluster, one of China's three major urban agglomerations.

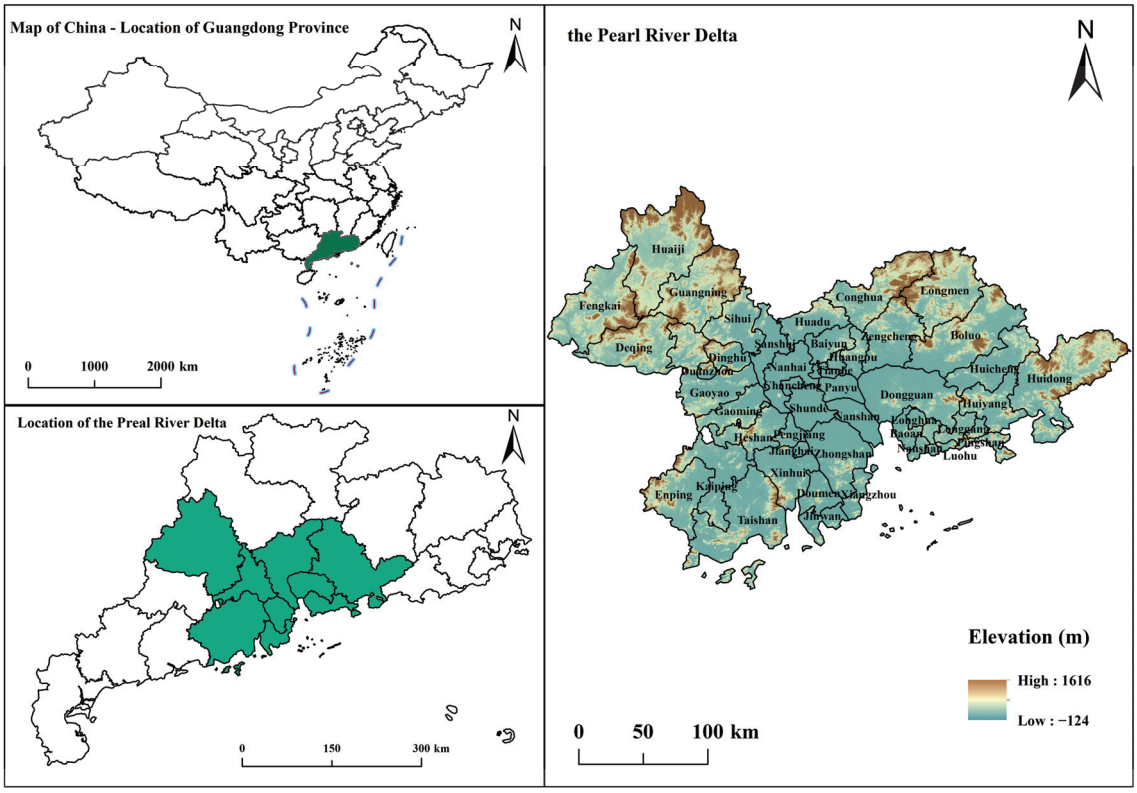

Figure 1. Study area.

2.2. Data Source

This research specifically examines the Pearl River Delta area and analyzes data on several carbon emission indicators, including raw coal, coke, domestic glass goods, pig iron, home waste emissions, household wastewater emissions, and industrial wastewater emissions. Indicators of economic development level, population size, urbanization level, energy intensity, and road network density are used as factors influencing urbanization-related carbon emissions. The Guangdong Statistics Yearbooks from 2009 to 2019 are the main source of the aforementioned statistics information. Linear interpolation and other sources like national economic and social development announcements and local statistics yearbooks are used to augment missing data [31]. Table 1 displays the specific information needed for this investigation.

Table 1. Details of each data.

Data Name	Data Description	Source
Fossil Fuel Consumption Data	Total annual energy consumption (raw coal, coke, crude oil, gasoline, kerosene, diesel, fuel oil, natural gas, etc.)	Guangdong Provincial Statistical Yearbook, China Energy Statistical Yearbook, and Municipal Statistical Yearbook, 2009–2019
Industrial Production Data	Total production of industrial products (daily glass products, pig iron, crude steel, finished steel, cement, flat glass, etc.)	
Solid Waste Discharge Data	Domestic waste emission	
Wastewater Discharge Data	Domestic wastewater discharge, industrial wastewater discharge	

Table 1. *Cont.*

Data Name	Data Description	Source
Socio-economic Data	Annual gross domestic product, permanent resident population at the end of the year, urban population, gross domestic product of the secondary industry, gross domestic product of the tertiary industry, energy intensity, number of kilometers opened to traffic, etc.	Guangdong Provincial Statistical Yearbook and Municipal Statistical Yearbook, 2009–2019
Administrative Boundary	Pearl River Delta city, county vector boundary	National Geographic Information Directory Service
Urban Area	Data redefined in 2016	

3. Research Methods

3.1. Calculation of Carbon Emissions

Urban areas bear a substantial burden of carbon emissions. Energy consumption, industrial production processes, solid waste, and waste-water carbon emissions are all factors that contribute to the environmental impact of cities in terms of their production and everyday activities. Carbon emissions stem from energy use in various industries. Additionally, energy consumption in industrial processes, such as the production of cement, lime, and glass, constitutes industrial production energy consumption, leading to carbon emissions from industrial production processes. Cities also handle a considerable amount of municipal and industrial waste, and the incineration, landfilling, and treatment of these wastes contribute significantly to carbon emissions.

This research assesses carbon emissions from four aspects: energy consumption, industrial production processes, solid waste, and wastewater, by using pertinent studies and employing the calculating methodologies specified by the Intergovernmental Panel on Climate Change (IPCC) [28,32,33]. This estimate does not take into account carbon emissions from agricultural production activities such as straw burning. The precise calculating procedure is as follows:

$$C_n = Q_{n\sim i} \times e_{n\sim i} \tag{1}$$

$$C_g = Q_{g\sim i} \times e_{g\sim i} \times 12 \div 44 \tag{2}$$

$$C_{wb} = Q_{wb} \times V_w \times P_w \times EF_w \tag{3}$$

$$C_{wf} = Q_{wf} \times 0.167 \times (1 - 75\%) \tag{4}$$

$$C_{g1} = N_p \times BOD \times SBF \times C_{BOD} \times FTA \times 365 \tag{5}$$

$$C_{g2} = Q_{wf} \times COD \times C_{COD} \tag{6}$$

In the formula, C_n shows the carbon emissions resulting from energy consumption, $Q_{n\sim i}$ denotes the energy type ith's usage, and $e_{n\sim i}$ shows the energy type ith's carbon emission coefficient. Class i industrial product consumption is denoted by $Q_{g\sim i}$, the carbon emission coefficient of Class i industrial goods is $e_{g\sim i}$, and C_g is the carbon emission of the industrial production process. The carbon emissions from waste incineration are denoted by C_{wb}, Q_{wb}, V_w, and P_w. The percentages of carbon content and mineral carbon in waste are 40% and 40%, respectively, and the total combustion efficiency of the waste combustion furnace is represented by EF_w, which is 95%. The landfill's water content is 71.5%, its carbon emission is C_{wf}, its quantity is Q_{wf}, and its CH_4 emission coefficient is 0.167. N_p is the population and C_{g1} is the carbon emissions from home wastewater. *BOD* stands for the organic matter content per capita, SBF for readily precipitable *BOD*, C_{BOD} for *BOD* emission factor, and *FTA* for *BOD* that degrades in wastewater without oxygen. The carbon dioxide (C_{g2}) emission of industrial wastewater is determined using the average *COD* value of different industrial wastewater reported by the IPCC. The maximal ability

to produce CH_4 is represented by C_{COD}. Q_{wf} is the volume of wastewater. COD is the chemical oxygen demand.

3.2. Spatial Autocorrelation

The first law of geography is that there is a higher likelihood of correlation between occurrences that are near each other. Within a certain geographical extent, the entire spatial dependency is reflected by global spatial autocorrelation [34]. This work computes the global geographical autocorrelation using Moran's I [35,36]. The exact method for calculating it is as follows:

$$I = \frac{n\sum_{i=1}^{n}\sum_{j=1}^{n} W_{ij}(x_i - \overline{x})(x_j - \overline{x})}{\sum_{i=1}^{n}\sum_{j=1}^{n} W_{ij}\sum_{i=1}^{n}(x_{i=1} - \overline{x})^2} \tag{7}$$

In the formula, variables x_i and x_j define the carbon emissions comprising unit i and unit j, respectively. W_{ij} represents the geographic weighting matrix of each unit i and unit j inside the research region. Moran's I is a statistical measure that ranges from -1 to 1. If the value is greater than zero, it shows a positive connection. When the value of I is less than 0, it indicates a negative correlation, with a greater magnitude indicating a greater amount of autocorrelation between spaces. When the value of I is equal to 0, it signifies an arbitrary distribution of space.

This article employs Getis-Ord G_i^* to examine the hot spots and cold spots in order to further investigate the accumulation regions of extreme and low values in space [37–39]. The precise computation procedure is as follows:

$$G_i^* = \frac{\sum_{i=1}^{n} W_{ij}x_i}{\sum_{i=1}^{n} x_i} \tag{8}$$

In the formula, the geographical weighting matrix, W_{ij}, represents the relationship across each unit i and unit j in the research region. When G_i^* exhibits strong regularity, it indicates that the region is a concentrated area of high value, sometimes referred to as a hot spot. If G_i^* is strongly negative, it suggests the region represents a low-value accumulation area, namely a cold spot area.

3.3. Grey Correlation Degree

The Grey Relational Analysis method utilizes the geometric similarity of sequence curves to determine whether different sequences are closely linked, which can make up for the deficiencies of combining statistical system analysis and has no special requirements on the required sample size [40]. Therefore, it can eliminate the errors caused by the limited sample size and has now become an effective tool for measuring the drivers of carbon emissions [41,42].

Based on the current research, the following nine elements that have an impact were chosen: The city's economic growth has a beneficial effect on carbon emissions inside its boundaries [43]. The yearly gross domestic product (GDP) serves as an index to gauge the economic status of each city. Urbanization results in growth in the urban population, but the focal point of urbanization is the concentrated makeup of people living in cities [44]. In this study, the year-end resident population and the proportion of the urban population to the total population are selected as indicators of population size and urbanization level. The secondary industry in China is responsible for 70% of the pollution generated by the production of goods [45]. Therefore, the scale of the secondary industry can be used as an indicator to examine the connection between urbanization and carbon emissions [46]. Additionally, the total economic output of the secondary industry is used as a measure of its size. The size of the tertiary industry scale is an indicator of the level of coordination during urban growth in the process of urbanization [47]. The gross domestic product of the tertiary industry is used to measure the size of the tertiary industry scale. The process of carbon emission is heavily influenced by energy intensity, making it the primary driving

factor [48]. Urbanization results in a larger land area being used [44] and the density of road networks is used as a measure of spatial urbanization. Foreign investment does not have a substantial impact on carbon emissions in China as a whole. However, it does have a major impact on carbon emissions in areas with varying energy intensities [49]. Therefore, this article considers foreign investment as a key factor. The role of science and technology in reducing carbon emissions has been generally acknowledged [50]. This article uses the number of patents as an indicator of the degree of technology in a certain region. Table 2 displays the elements that influence the variations in carbon emissions across different locations and time periods.

Table 2. Influences on the variations in carbon emissions in terms of distance and time.

Influence Factor	Unit	Indicator Specification	Symbol
Economic Development	10,000 yuan	Gross Annual Product	X_1
Population Size	10,000	Permanent Population at the end of the Year	X_2
Urbanization Level	%	Proportion of Permanent Urban Population in Total Population	X_3
Secondary Industry Scale	%	Proportion of the Gross Product of the Secondary Industry to the Gross Product	X_4
Tertiary Industry Scale	%	Proportion of the Gross Product of the Tertiary Industry to the Gross Product	X_5
Energy Intensity	Tons of standard coal/10,000 yuan	Ratio of Total Energy Consumption to Gross Domestic Product	X_6
Road Network Density	km/km^2	Traffic Mileage Per Square Kilometer	X_7
Foreign Investment	10,000 yuan	Cities Utilize Actual Foreign Investment	X_8
Technological Level	individual	Number of Patents Granted	X_9

Dimensionalization without meaning is used to standardize the data. To get the gray correlation coefficient, the following precise calculation method is used:

$$\xi_i(t) = \frac{min_i[\Delta_i(min)] + \rho max_i[\Delta_i(max)]}{|x_0(t) - x_i(t)| + \rho max_i[\Delta_i(max)]} \tag{9}$$

$$\Delta_i(min) = min_t|x_0(t) - x_i(t) \tag{10}$$

$$\Delta_i(max) = max_t|x_0(t) - x_i(t) \tag{11}$$

where t is year t and ρ is the resolution; this paper takes 0.5.

Grey relational degree r_i is obtained as:

$$r_i = \frac{1}{n}\sum_{t=1}^{n}\xi_i(t) \tag{12}$$

In the formula, the closer the correlation degree is to 1, the higher the correlation degree.

4. Results

4.1. Urban Carbon Emissions

It is evident from Figure 2 that the Pearl River Delta's carbon emissions measurement data indicate an overall rise in carbon emissions from energy use in the PRD between 2009 and 2019. Foshan witnessed the highest surge, adding 16.338 million tons, while Guangzhou experienced a reduction of 8.616 million tons in energy-related carbon emissions. The proportion of Foshan's energy-related carbon emissions in the PRD as a whole increased by 9.56% over time. In contrast, Guangzhou's share decreased from 28.74% to 15.42%.

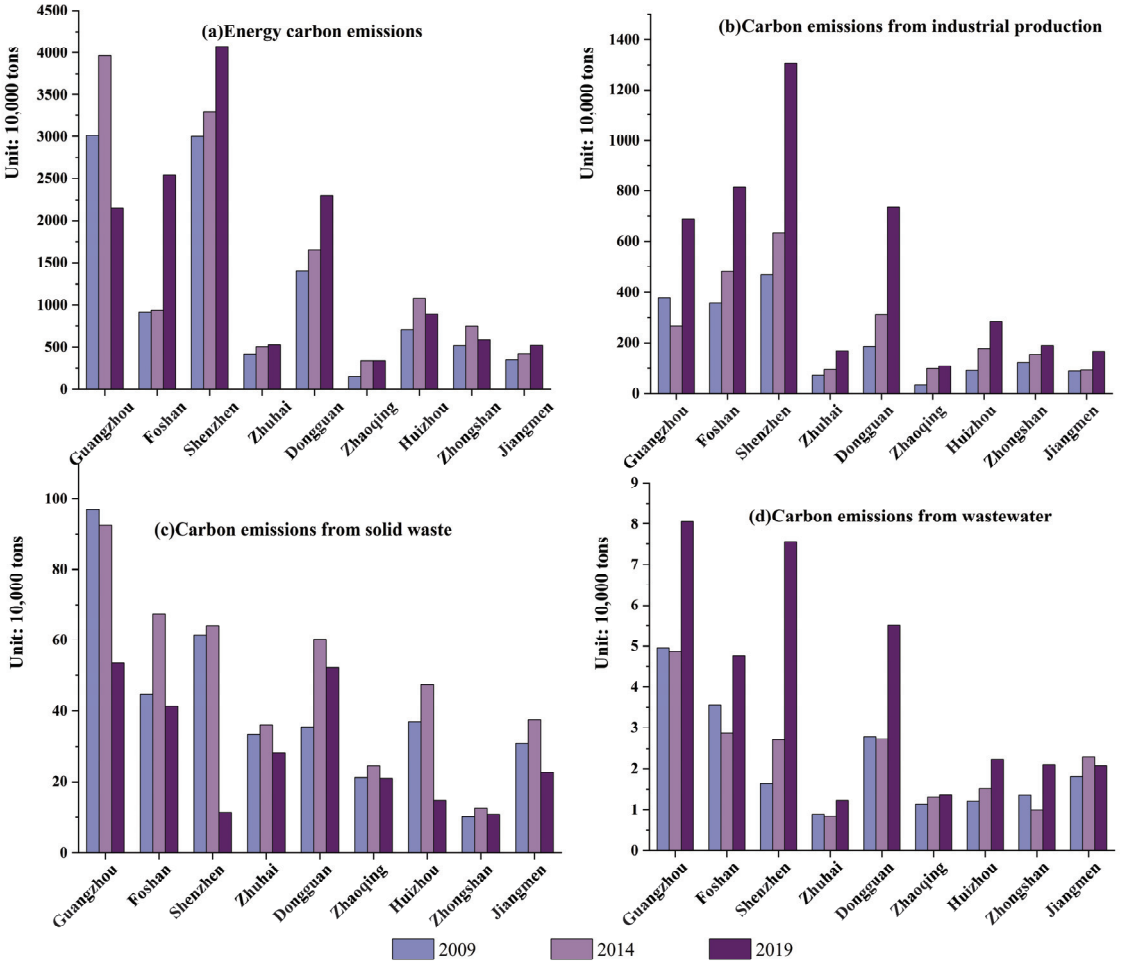

Figure 2. Carbon emissions from various sectors in the Pearl River Delta, 2009–2019.

For carbon emissions from industrial production, all the PRD cities recorded an overall increase, with Shenzhen leading the surge by 8.363 million tons and Zhaoqing having the smallest increase of 0.731 million tons. The proportion of industrial production carbon emissions for most cities showed a declining trend, with Guangzhou decreasing by 5.56%. However, Dongguan's proportion increased, rising from 10.25% to 16.49%.

Regarding carbon emissions from solid waste, an increase was observed from 2009 to 2014, followed by a decrease from 2014 to 2019. Carbon emissions from solid waste were significantly reduced in Shenzhen, Guangzhou, and Huizhou; they were down about 0.501 million tons, 0.436 million tons, and 0.221 million tons, respectively. Carbon emissions from solid waste in Dongguan increased to 0.204 million tons from 0.096 million tons. Dongguan also saw a 10.85% increase in the proportion of solid waste carbon emissions, while Shenzhen, Guangzhou, and Huizhou experienced decreases of 12.11%, 5.24%, and 4.15%, respectively.

Compared to carbon emissions from industrial production, wastewater carbon emissions generally showed an upward trend. Dongguan had the smallest increase, with carbon emissions rising about 0.021 million tons to 0.027 million tons, while Shenzhen and Guangzhou experienced the largest increases, adding 0.059 million tons and 0.031 mil-

lion tons, respectively. Wastewater carbon emissions represent the smallest portion of overall carbon emissions. Shenzhen's proportion increased from 8.45% to 21.72%. Although Guangzhou and Foshan saw significant increases in carbon emissions, their proportions decreased by 2.57% and 4.76%, respectively.

4.2. County Carbon Emissions

A geographical study of carbon emissions throughout the process of urbanization within the Pearl River Delta for major periods 2009, 2014, and 2019 was undertaken using ArcGIS 10.8 software. The purpose was to visually represent the variations in carbon emissions across different locations (Figure 3).

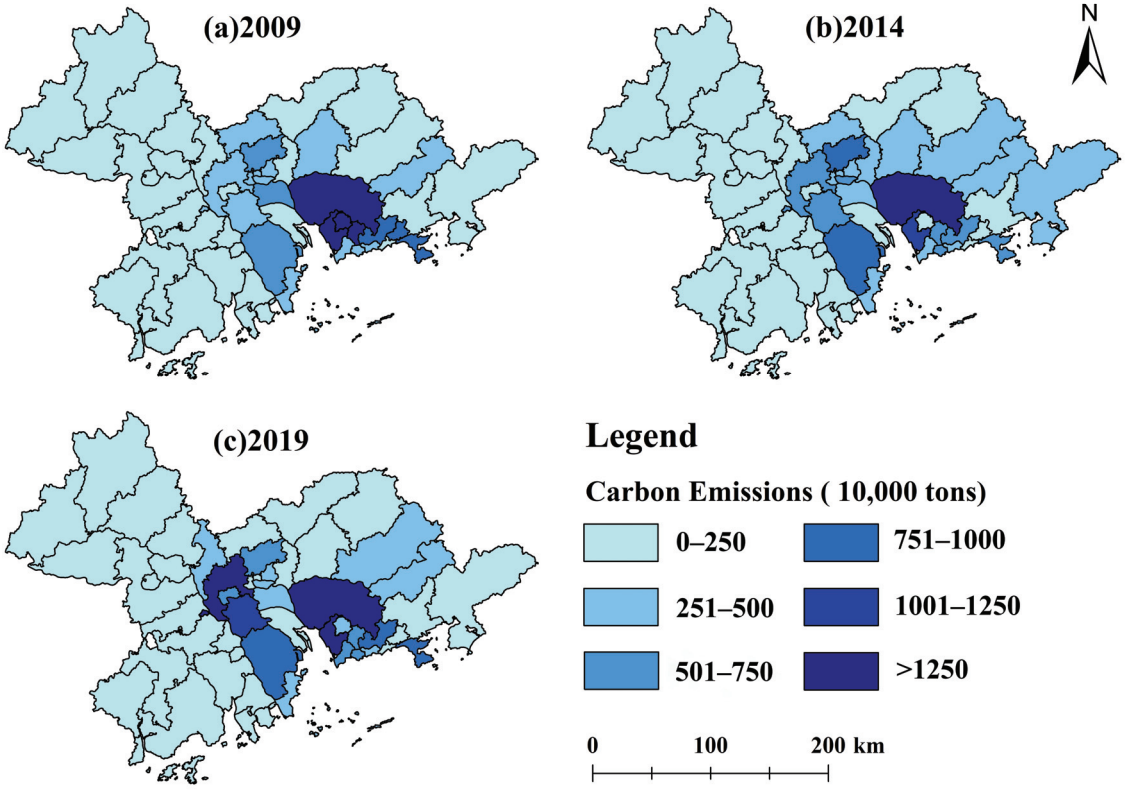

Figure 3. 2009–2019 carbon emissions in the Pearl River Delta counties.

The timeframe from 2009 to 2019 demonstrates an aggregate growing trajectory in carbon emissions throughout the PRD. In 2009, at the county level within the PRD, the majority of carbon emissions were below 5 million tons, with one-third even falling below 1 million tons. By 2019, most county-level carbon emissions exceeded 2 million tons, with an increasing number of counties surpassing 6 million tons.

From a geographical standpoint, the carbon emissions in the PRD region exhibit a pattern of being "high in the east and low in the west". The southern portion of the PRD Central Axis exhibits the highest levels of carbon emissions, primarily attributed to economic advancement, high population density, and frequent consumption. In 2009, carbon emissions were predominantly concentrated in Bao'an, Longgang, Zhongshan, Baiyun, and other regions. However, by 2019, the concentration shifted to Dongguan, Bao'an, Nanhai, Shunde, and Longgang. Notably, Nanhai and Shunde experienced significant growth in

carbon emissions between 2009 and 2019, while Shenzhen, Foshan, Dongguan, and Zhuhai exhibited the most substantial increase in emissions.

4.3. Spatial Aggregation Characteristics

The research investigated the geographical distribution of carbon emissions in Guangdong Province from 2009 to 2019, using global spatial autocorrelation analysis (Table 3). The findings showed a strong positive connection in carbon emissions, suggesting that emissions had a tendency to cluster. Areas with higher emissions were found to be next to other areas with higher emissions, while areas with lower emissions were next to each other. Regarding specific numerical values, Moran's *I* index exhibited a decreasing trend, declining from 0.329 to 0.168, indicating a reduction of 48.9%. This points towards a diminishing spatial interdependence and clustering of carbon emissions, primarily attributed to the gradual reduction in cold spots.

Table 3. Global carbon emissions index, Moran' *I* index, 2009–2019.

Year	2009	2014	2019
Moran's *I*	0.329	0.275	0.168
Z-score	3.911	3.836	2.443
p	0.000009	0.000125	0.00145

The Pearl River Delta region's carbon emissions are intricately clustered, with concentrated zones with high and low emissions mostly located in the northwest and western regions (Figure 4). In 2009, Kaifeng, Deqing, Guangning, Sihui, Dinghu, Duanzhou, and Gaoyao had a low–low clustering pattern, but western Dongguan and Shenzhen showed a high–high clustering pattern. In 2014, Gaoming, Kaiping, and Enping were added to the low domain. In 2019, low–low clusters were detected in Fengkai, Deqing, Sihui, Gaoyao, and Duanzhou, whereas low–high clusters were found in Guangming and Nansha. While the high–high cluster is mostly concentrated in Shenzhen and Dongguan, the low–low cluster resides primarily in the western and northwest parts of the PRD. However, there exist substantial geographical disparities within Guangzhou and Shenzhen, resulting in low and high clusters also being concentrated in these places. The time scale development reveals minor fluctuations in the clusters of high and low values, with the low clusters moving from the Northwest to the West and then returning to the Northwest. This suggests that carbon emissions in the Northwest are rising.

A study using the Getis-Ord G_i^* method was performed to detect the specific local correlation patterns of carbon emissions throughout the process of urbanization in Guangdong Province (Figure 5). The findings indicated that the areas with the highest concentrations of carbon emissions in the Pearl River Delta (PRD) region between 2009 and 2019 were mostly located in Shenzhen, Dongguan, and Guangzhou. In 2009, Zengcheng, Huangpu, Panyu, and Longgang had a hotspot confidence level of 95%, while Bao'an, Nanshan, Futian, Luohu, Nansha, and Dongguan had a higher confidence level of 99%. In 2014, the cities of Guangzhou, Shenzhen, and Dongguan exhibited the highest levels of confidence in terms of becoming hotspots. In 2019, the number of locations with a hotspot confidence level of 99% decreased, while Bao'an, Guangming, Longhua, Nanshan, Futian, and Luohu had confidence levels of 95%. This is due to both the increasing emissions from places with relatively lower carbon emissions and the elevated carbon emissions inside the PRD.

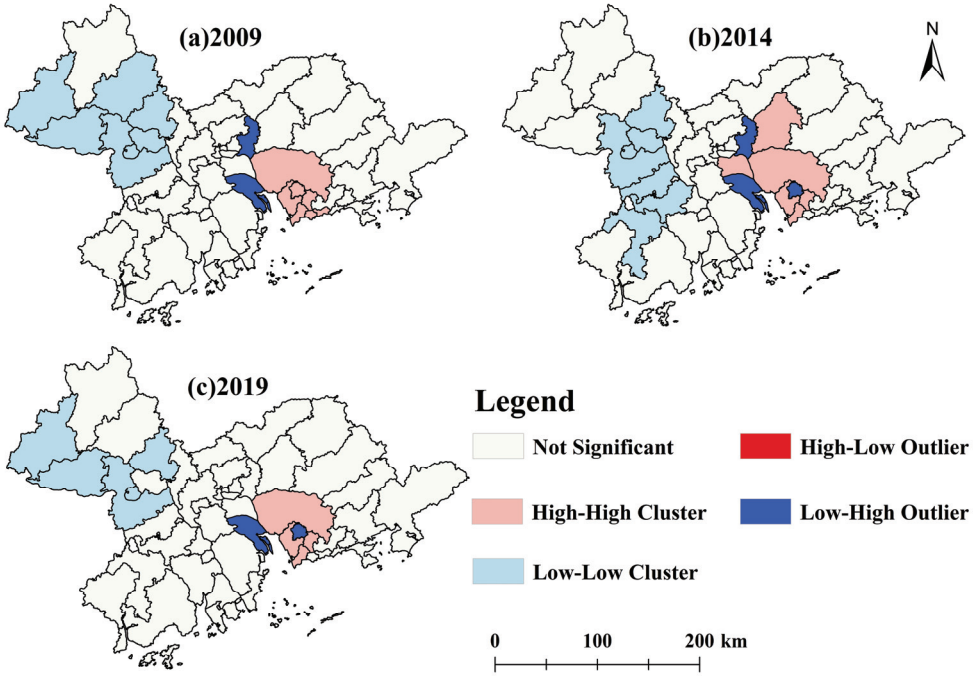

Figure 4. High and low carbon emissions in the Pearl River Delta are clustered, 2009–2019.

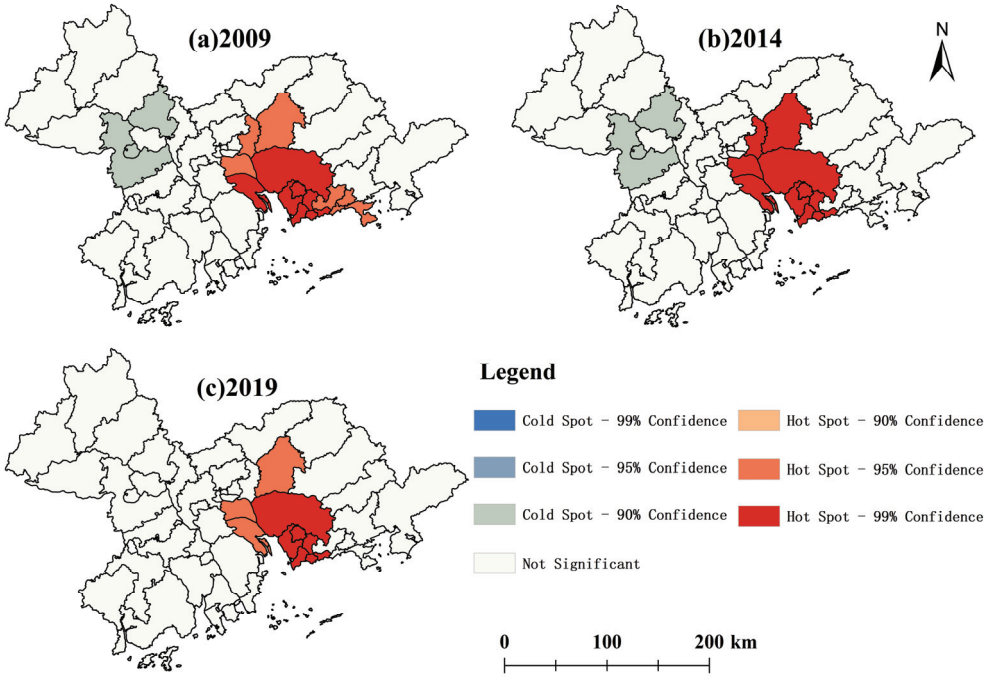

Figure 5. Pearl River Delta cold and hot spots in 2009–2019.

4.4. Analysis of Urban Carbon Emission Drivers

4.4.1. Gray Correlation Cross-Section Analysis Results

All relevant factors were accurately represented and analyzed using the results of the gray relational analysis (Figure 6). The research examined the relationship between the amount of urbanization, the structure of the secondary industry, and the density of the road network in Guangzhou and Shenzhen. It also investigated the variables that affect carbon emissions in Zhuhai and Shenzhen. The variables with stronger connections were urbanization level, secondary industry structure, and road network density, while the variables with weaker correlations were foreign investment and technology level.

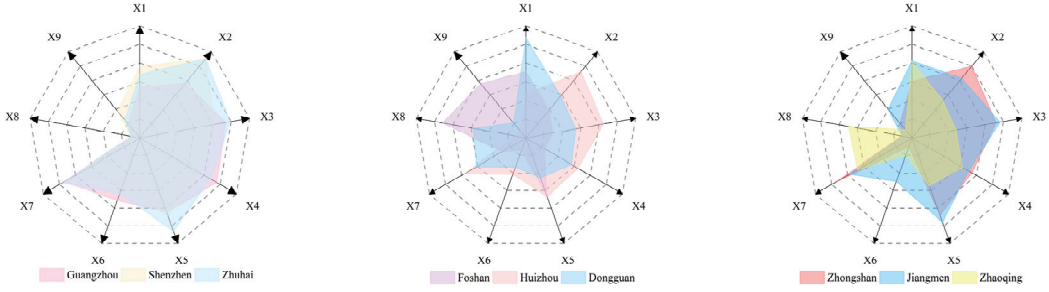

Figure 6. Grey correlation degree of carbon emission driver cross-section in the Pearl River Delta.

Zhuhai and Shenzhen have comparable sources of carbon emissions; however, Shenzhen's sources are more significant in terms of quantity. The determining variables in Zhuhai's impact are primarily its economic growth and the scale of its secondary sector, which is benchmarked against Shenzhen. The hierarchy of influencing variables in Zhuhai may be summarized as follows: population size, size of the tertiary industry, degree of urbanization, density of the road network, Shenzhen (replacing economic development and size of the secondary industry), energy intensity, level of research and technology, and foreign investment.

The correlation between Dongguan and Zhaoqing in terms of economic growth is 0.936 and 0.808, respectively. With correlations of 0.707 and 0.692, respectively, the relationship between the influencing factors of carbon emissions in Dongguan and the density of the road network and population size is also greater. The correlation between Zhaoqing's carbon-emission-influencing factors and energy intensity is 0.500, while the correlation between carbon-emission-influencing factors and technology level is 0.456.

In Foshan, foreign investment is the primary contributor to carbon emissions, with a value of 0.857, while energy intensity has the lowest impact, with a value of 0.471. The growth in carbon emissions in Jiangmen may be attributed to the high degree of urbanization and the significant amount of the tertiary sector, with coefficients of 0.882 and 0.880, respectively. The association between Jiangmen and carbon emissions is weakest in the case of foreign investment, with a coefficient of 0.456.

The rising population of Shenzhen, Zhuhai, Huizhou, and Zhongshan has a substantial impact on carbon emissions due to the process of urbanization. These cities have lower levels of impact from characteristics such as energy intensity and transportation network density.

4.4.2. Gray Correlation Time Series Analysis Results

The gray relational analysis indicates that the influence of economic growth, population size, and transportation network density on cities has changed over time (Table 4). In 2009, Guangzhou was mostly influenced by economic growth, whilst Zhongshan was primarily impacted by population size. Foshan was most significantly affected by foreign

investment, but both road network density and foreign investment had the greatest effect on Huizhou.

Table 4. The Pearl River Delta's carbon emissions driving elements have a grey correlation degree, 2009–2019.

Area										
Year	**Influence Factor**	**Guangzhou**	**Shenzhen**	**Zhuhai**	**Foshan**	**Huizhou**	**Dongguan**	**Zhongshan**	**Jiangmen**	**Zhaoqing**
2009	X_1	1.000	0.867	0.932	0.712	0.821	0.956	0.982	0.963	0.932
	X_2	0.624	0.520	0.914	0.836	0.871	0.861	0.997	0.677	0.622
	X_3	0.397	0.435	0.556	0.779	0.823	0.983	0.582	0.751	0.682
	X_4	0.346	0.368	0.583	0.753	0.642	0.863	0.576	0.550	0.631
	X_5	0.463	0.417	0.592	0.853	0.814	0.971	0.696	0.658	0.531
	X_6	0.340	0.336	0.704	0.654	0.600	0.741	0.341	0.587	0.486
	X_7	0.403	0.373	0.697	0.749	0.765	0.735	0.694	0.589	0.651
	X_8	0.627	0.719	0.802	0.981	0.889	0.869	0.940	0.864	0.755
	X_9	0.436	0.658	0.920	0.548	0.682	0.880	0.806	0.816	0.901
2014	X_1	0.882	0.822	0.922	0.736	0.757	0.798	0.924	0.984	0.988
	X_2	0.673	0.595	0.891	0.756	0.996	0.859	0.977	0.699	0.712
	X_3	0.390	0.465	0.551	0.732	0.922	0.952	0.610	0.652	0.763
	X_4	0.334	0.389	0.577	0.700	0.685	0.793	0.605	0.564	0.566
	X_5	0.457	0.460	0.585	0.930	0.943	0.993	0.700	0.609	0.632
	X_6	0.338	0.409	0.629	0.726	0.579	0.845	0.622	0.525	0.470
	X_7	0.386	0.363	0.727	0.755	0.917	0.623	0.566	0.615	0.650
	X_8	0.600	0.854	0.755	0.878	0.970	0.706	0.770	0.959	0.807
	X_9	0.500	0.564	0.927	0.737	0.701	0.822	0.733	1.000	0.829
2019	X_1	0.458	0.925	0.985	0.645	0.898	0.631	0.987	0.990	0.993
	X_2	0.570	0.567	0.934	0.657	0.901	0.774	0.921	0.759	0.729
	X_3	0.744	0.411	0.563	0.672	0.773	0.724	0.581	0.675	0.734
	X_4	0.550	0.362	0.567	0.713	0.624	0.701	0.582	0.572	0.640
	X_5	0.958	0.391	0.630	0.627	0.704	0.628	0.642	0.665	0.585
	X_6	0.577	0.360	0.626	0.450	0.462	0.623	0.581	0.559	0.486
	X_7	0.736	0.337	0.735	0.666	0.795	0.822	0.536	0.643	0.649
	X_8	0.439	0.540	0.584	0.420	0.871	0.509	0.876	0.984	0.861
	X_9	0.667	0.745	1.000	0.631	0.789	0.910	0.747	0.928	0.876

In 2014, Zhaoqing was mostly influenced by economic development, while Zhongshan was primarily impacted by population size. The effect on Dongguan was primarily influenced by the amount of urbanization, the structure of the secondary sector, the structure of the tertiary industry, and the intensity of energy use. Huizhou was most significantly influenced by road network density and foreign investment, whereas Jiangmen was most significantly influenced by the degree of research and technology.

In 2019, the economic factor had the most significant influence on Zhaoqing, while population size, energy intensity, and science and technology level had the most effect on Zhuhai. Shenzhen had the greatest fluctuation in its impact factor, with foreign investment playing the most prominent role. The most significant transformation in Zhuhai between 2009 and 2014 occurred in terms of energy intensity, but the most substantial shift between 2014 and 2019 was seen in foreign investment.

During the research period, Huizhou exhibited the highest population size, urbanization level, secondary industry structure, tertiary industry structure, road network density, and foreign investment. In Dongguan, the population size and foreign investment effect indices are consistently decreasing, while the impact indices of tertiary industrial size and energy intensity show an initial increase followed by a decrease. The foreign investment effect index in Jiangmen is on the rise, whereas the impact index of the scientific and technology level first climbs and then declines. Zhaoqing has very minor fluctuations in each of the impact variables but displays more pronounced variations in economic level, population size, and foreign investment.

5. Discussion

5.1. Discussion of the Research

This research presents three primary advancements. Firstly, it quantifies the amount of carbon dioxide released into the atmosphere as a result of urbanization. This is done by considering four specific sectors: energy consumption, industrial production processes, solid waste, and wastewater emissions. This broadens the range of carbon emissions that occur during urbanization, instead of just considering carbon emissions connected to energy. Furthermore, it examines the changing patterns of carbon emissions at the county level, providing a more in-depth comprehension of the characteristics of emission evolution at a very small scale. Finally, it scrutinizes the variables that have an impact on carbon emissions, assessing the specific roles played by each element. This analysis may serve as a realistic foundation for the government to develop policies aimed at reducing carbon emissions.

An attempt is put forward to confirm the dependability of the findings through contrasts of what is learned from this investigation with previous research results. Zhao et al. discovered that carbon emissions from land use within the study area follow a distribution pattern characterized by high values in the central region and lower values in the surrounding areas [51]. The geographic distribution pattern for urban carbon emissions has a resemblance with the observed pattern of "high in the east and low in the west" in this research.

Regarding the elements that influence carbon emissions, several researchers have extensively examined these aspects using the MEIC model. Their study reveals that economic urbanization has the greatest influence on carbon emissions [52]. Researchers have used the LMDI model to break down carbon emissions by industry and city in the Pearl River Delta area. Their analysis has shown that the rise in carbon emissions is mostly driven by economic expansion and population impact [53]. Researchers have analyzed carbon emissions in the context of urban agglomeration geography and discovered a notable polarization occurrence in the Pearl River Delta. This indicates an imbalance in regional development [23]. The results described above align closely with the outcomes of this investigation. Hence, it is essential to implement customized management and governance measures for carbon emissions, in addition to developing appropriate plans.

5.2. Carbon Emissions Optimization Policy

(1) Tailor-Made, Differentiated Carbon Emission Control Strategies.

In response to the spatial clustering and spatiotemporal differences of carbon emissions, regions with high carbon emissions should promote inter-city cooperation to foster the development of high-tech and innovative industries, forming collaborative emission reduction mechanisms across regions. For high-emission areas such as Guangzhou, Shenzhen, Foshan, and Dongguan, which are economically developed cities, emphasis should be placed on developing green industries, promoting clean and low-carbon energy, and optimizing industrial and energy structures [54–56]. Particularly in reducing carbon emission intensity, these cities should intensify efforts in research and application of new energy vehicles, renewable energy, and high-efficiency technologies. Meanwhile, economically weaker cities such as Zhaoqing, still in the industrialization phase, are expected to see an increase in carbon emissions [57,58]. Therefore, these cities need to prioritize reducing carbon emission intensity and promoting clean energy use as the core of clean production, driving the transformation of traditional industries towards green and low-carbon industries.

(2) Advancement of environmentally friendly technology, enhancement of energy infrastructure efficiency, and provision of policy direction.

To address the ongoing rise in carbon emissions in the Pearl River Delta region, policymakers ought to decrease the utilization of high-carbon energy sources like coal and coke. They should also limit the growth of energy-intensive industries and develop more logical regulations at the local government level to ensure the improvement of energy composition. It is important to actively promote the use of natural gas and renewable

energy and to stimulate the replacement of fossil fuels with low-carbon energy sources in order to decrease carbon emissions [59,60]. In addition, it is crucial to develop and enforce stringent carbon emission regulations and evaluation systems to encourage the adoption of environmentally friendly technology and renewable energy sources, enhance energy efficiency, and facilitate the widespread use and commercialization of eco-friendly and low-carbon technologies.

(3) People-Oriented Approach, Advancing Green Technology Innovation, and Low-Carbon Community Construction.

The Pearl River Delta, being a highly developed region economically, ought to concentrate on managing population size, enhancing population structure and quality, investigating the development of low-carbon homes and communities, and encouraging the adoption and popularization of low-carbon lifestyles [61,62]. The government must increase its support for green technology and alternative energy innovation, as well as set up suitable incentive systems and policy support in order to promote the development of new low-carbon industry types, optimize the industrial structure, and encourage the growth of green industries and technological innovation [63]. Through initiatives like the creation of green innovation funds, tax breaks, and fiscal subsidies, companies and academic institutions should be encouraged to carry out scientific investigations as well as the application of green technologies. They should also be encouraged to support the creation and growth of low-carbon cities, establish a supportive environment and policy framework, and advance the Pearl River Delta region's transition to a low-carbon economy.

5.3. Research Limitations and Perspectives

There are several further restrictions on this research. Firstly, regarding the method for calculating carbon emissions, although IPCC has become one of the most commonly used methods for carbon emission calculation, issues still exist due to its inherent limitations, leading to inaccuracies in carbon emission calculations. Secondly, climate and terrain factors were not considered in the carbon emission calculations. Lastly, the study used economic development and population size as driving factors, but the analysis may not be sufficiently in-depth. Therefore, future research could address these limitations by first considering factors such as climate and terrain in carbon emission calculations and validating the accuracy of the estimated data by fitting it with widely used techniques for estimating carbon emissions, such as data from evening lights. Second, using more specific social and economic variables to investigate the influence of variables like public attitudes, education level, and income distribution on environmental concerns in the study of population growth and economic development.

6. Conclusions

This research used the gray relational model and spatial analysis to examine the spatiotemporal distribution patterns of carbon dioxide throughout the urbanization process using data from nine cities in the PRD between 2009 and 2019. The present investigation also examined the impact of relevant influencing factors on carbon emissions. The following are the outcomes:

Firstly, there was an increase in the region's total carbon emissions from 2009 to 2019 in the Pearl River Delta. The biggest amount of carbon emissions came from energy-related sources, then the industrial output; the lowest percentage came from wastewater-related sources. Guangzhou showed a decrease in carbon emissions due to energy use, whereas Foshan and Shenzhen saw the largest increases in carbon emissions.

Secondly, there is an "east-high, west-low" trend in the geographical distribution of carbon emissions in the Pearl River Delta region. The majority of regions with comparatively large carbon emissions are found in places like Baiyun District, Zhongshan City, Longgang District, and Bao'an District. The carbon emissions in these regions rose even more in 2019, exhibiting a pronounced geographical clustering impact. The Pearl River Delta region's spatial autocorrelation of carbon emissions dropped from 0.329 to

0.168 between 2009 and 2019, according to global Moran's *I* analysis. This implies that the reduction in cold spot regions is the primary cause of the progressive weakening of the spatial linkages and clustering degree of carbon emissions.

Thirdly, gray relational analysis shows that while economic growth has a significant influence on carbon emissions, its impact is declining while the impact of technological level is increasing. When comparing the gray-related degrees of two cities, Zhaoqing and Jiangmen, the disparities in each carbon-emission-influencing factor were not more than 0.150. However, with variances of around 0.500 in each carbon-emission-influencing component, Guangzhou and Foshan showed greater fluctuations.

Author Contributions: Methodology, Z.G. and Z.W.; Investigation, Z.G.; Writing—original draft, Z.G.; Supervision, D.W. and L.Z. All authors have read and agreed to the published version of the manuscript.

Funding: This research was funded by the National Natural Science Foundation of China (41771096), the Open Fund Sponsored Project of Peking University, the Laboratory for Earth Surface Processes Ministry of Education (Serial No. 6), the Innovative Team Project of Guangdong Ordinary Colleges and Universities (Humanities and Social Sciences) (2023WCXTD019), the Guangdong Province Ordinary University characteristic innovation category Project (Humanities and Social Sciences category) (2022WTSCX087), the Tertiary Education Scientific research project of Guangzhou Municipal Education Bureau (No. 202235269), the Guangzhou University Graduate Students' "Civic Politics in the Curriculum" Demonstration Project (No. 6), and the Guangzhou University 2023 Exploratory Experimental Construction Project (No. SJ202310), the Teaching and Research Office of Real Estate Management Program, Teaching Quality and Teaching Reform Project for 2023 Undergraduate Colleges and Universities in Guangdong Province (Serial No. 269), the 2022 Guangzhou Higher Education Teaching Quality and Teaching Reform Project Teaching Team Program "Real Estate Management Teaching Team" (2022JXTD001), the 2022 Research Project of Guangdong Undergraduate Colleges and Universities Online Open Course Steering Committee: "Innovative Research on the Construction of First-class Courses Supported by Online Open Courses-Taking Real Estate Management as an Example" (2022ZXKC367), the Guangdong, Hong Kong and Macao Greater Bay Area Universities Online Open Course Consortium 2023 Education and Teaching Research and Reform Project "Exploration and Practice of Online-Offline Blended Teaching of Online Open Course "Real Estate Management" Based on the Consortium Platform" (WGKM2023139), the Guangzhou University Practice Base for Industry-Education Integration of Cultivated Land Protection (24CJRH13), the 2024 Guangzhou Higher Education Teaching Quality and Teaching Reform Project Section Industry-Teaching Integration Practice Teaching Base Project, Cultivated Land Protection Section Industry-Teaching Integration Practice Teaching Base (2024KCJJD002).

Institutional Review Board Statement: Not applicable.

Informed Consent Statement: Not applicable.

Data Availability Statement: The data in this study are available from the corresponding authors upon request. Due to the sensitivity of the study area, some data cannot be made public.

Conflicts of Interest: The authors declare no conflicts of interest.

References

1. Wang, S.; Wang, H.; Fang, C. Evolutionary characteristics and driving factors of carbon emission performance at the city level in China. *Sci. Sin.* **2022**, *52*, 1613–1626. [CrossRef]
2. Feng, X.; Li, Y.; Wang, S.; Yu, E.; Yang, J.; Wu, N. lmpacts of Urban Form on Carbon Emissions under the Goal of Carbon Emission Peak and Carbon Neutrality: A Case Study of the Yangtze River Economic Belt. *Environ. Sci.* **2023**, *45*, 3389–3401.
3. Wang, J.; Mo, H.; Fang, C. Carbon emissions dynamic simulation and its peak of cities in the Pearl River Delta Urban Agglomeration. *Chin. Sci. Bull.* **2022**, *67*, 670–684. [CrossRef]
4. Li, J.; Huang, X.; Chuai, X.; Sun, S. Spatial-temporal Pattern and Influencing Factors of Coupling Coordination Degree between Urbanization of Population and CO_2 Emissions of Energy Consumption in Jiangsu Province. *Econ. Geogr.* **2021**, *41*, 57–64.
5. Wang, S.; Xie, Z.; Wang, H. The spatiotemporal pattern evolution and influencing factors of CO_2 emissions at the level of China. *Acta Geogr. Sin.* **2021**, *76*, 3103–3118.
6. Jin, S.; Lin, Y.; Niu, K. Driving Green Transformation of Agriculture with Low Carbon: Characteristics of Agricultural Carbon Emissions and lts Emission Reduction Path in China. *Reform* **2021**, *5*, 29–37.

7. Shao, S.; Fan, M.; Yang, L. Economic Restructuring, Green Technical Progress, and Low-Carbon Transition Development in China: An Empirical Investigation Based on the Overall Technology Frontier and Spatial Spillover Effect. *J. Manag. World* **2022**, *38*, 46–69+44–10.
8. Ren, X.; Liu, Y.; Zhao, G. The impact and transmission mechanism of economic agglomeration on carbon intensity. *China Popul. Resour. Environ.* **2020**, *30*, 95–106.
9. Jiang, H.; Wang, W.; Wang, L.; Wu, J. The Effects of the Carbon Emission Reduction of China's Green Finance—An Analysis Based on Green Credit and Green Venture Investment. *Financ. Forum* **2020**, *25*, 39–48+80.
10. Wang, S.; Tian, S.; Cai, Q.; Wu, H.; Wu, C. Driving factors and carbon transfer of industrial carbon emissions in Guangdong province under the background of industrial transfer. *Geogr. Res.* **2021**, *40*, 2606–2622.
11. Huang, H.; Qiao, X.; Zhang, J.; Li, Y.; Zeng, Y. Spatio-Temporal Differentiation and Influencing Factors of Regional Tourism Carbon Emissions under the Background of Green Development: A Case Study of the Yangtze River Economic Belt. *Econ. Geogr.* **2019**, *39*, 214–224.
12. Li, J.; Huang, J.; Wu, C.; Zhou, Y.; Xu, G. Analysis of Spatial Heterogeneity impact Factors on Carbon Emissions in China. *Econ. Geogr.* **2015**, *35*, 21–28.
13. Zhao, Q.; Yan, Q.; Zhao, H. Research on Spatial Characteristics and Influencing Factors of Provincial Carbon Emissions in China. *J. Beijing Inst. Technol.* **2018**, *20*, 9–16.
14. Wu, J.; Jin, X.; Wang, H.; Feng, Z.; Zhang, D.; Li, X. Analysis of Carbon Emissions and Influencing Factors in China Based on City Scale. *Environ. Sci.* **2023**, *44*, 2974–2982.
15. Wang, S.; Liu, Y.; Fang, C. Review of energy-related CO_2 emission in response to climate change. *Prog. Geogr.* **2015**, *34*, 151–164.
16. Liu, Y.; Jin, S. Temporal and Spatial Evolution Characteristics and Influencing Factors of Energy Consumption Carbon Emissions in Six Provinces of Central China. *Econ. Geogr.* **2019**, *39*, 182–191.
17. Wang, R.; Zhang, H.; Qiang, W.; Li, F.; Peng, J. Spatial characteristics and influencing factors of carbon emissions in-level cities of China based on urbanization. *Prog. Geogr.* **2021**, *40*, 1999–2010. [CrossRef]
18. Chen, Z.; Wu, M.; Ma, W.; Liu, X.; Cai, B.; Liu, J.; Jia, X.; Zhang, M.; Chen, Y.; Xu, L.; et al. Driving forces of carbon dioxide emission for China's cities: Empirical analysis based on extended STIRPAT Model. *China Popul. Resour. Environ.* **2018**, *28*, 45–54.
19. Song, Y.; Zeng, J.; Wang, S.; Liang, C. Spatial-Temporal Evolution and Heterogeneity of Carbon Emissions at-Level in China. *Environ. Sci.* **2023**, *44*, 549–559.
20. Wang, Z.; Li, F.; Xie, Z.; Li, Q.; Zhang, Y.; Dai, M. Decoupling CO_2 Emissions from Economic Growth in China's Cities from 2000 to 2020: A Case Study of the Pearl River Delta Agglomeration. *Land* **2023**, *12*, 1804. [CrossRef]
21. Dong, B.; Ma, X.; Zhang, Z.; Zhang, H.; Chen, R.; Song, Y.; Shen, M.; Xiang, R. Carbon emissions, the industrial structure and economic growth: Evidence from heterogeneous industries in China. *Environ. Pollut.* **2020**, *262*, 114322. [CrossRef]
22. Luo, K.; Chen, S.; Cui, S.; Liao, Y.; He, Y.; Zhou, C.; Wang, S. Examining the Overall and Heterogeneous Impacts of Urban Spatial Structure on Carbon Emissions: A Case Study of Guangdong Province, China. *Land* **2023**, *12*, 1806. [CrossRef]
23. Yanan, W.; Yujia, N.; Meng, L.; Qianyu, Y.; Wei, C. Spatial structure and carbon emission of urban agglomerations: Spatiotemporal characteristics and driving forces. *Sustain. Cities Soc.* **2022**, *78*, 103600.
24. He, J.; Yang, J. Spatial–Temporal Characteristics and Influencing Factors of Land-Use Carbon Emissions: An Empirical Analysis Based on the GTWR Model. *Land* **2023**, *12*, 1506. [CrossRef]
25. Ding, Y.; Huang, Y.; Xie, L.; Lu, S.; Zhu, L.; Hu, C.; Chen, Y. Spatial Patterns Exploration and Impacts Modelling of Carbon Emissions: Evidence from Three Stages of Metropolitan Areas in the YREB, China. *Land* **2022**, *11*, 1835. [CrossRef]
26. Ma, X.; Wang, C.; Dong, B.; Gu, G.; Chen, R.; Li, Y.; Zou, H.; Zhang, W.; Li, Q. Carbon emissions from energy consumption in China: Its measurement and driving factors. *Sci. Total Environ.* **2019**, *648*, 1411–1420. [CrossRef]
27. Yang, X.; Liang, J.; Wang, S. Spatial–Temporal Evolution and Driving Factors of Coupling Coordination between High-Quality Urban Development and Carbon Emissions Intensity in Guangdong Province. *Land* **2023**, *12*, 2082. [CrossRef]
28. Zhang, M.; Huang, X.; Chuai, X. Research on China's Urban Carbon Emission Accounting and Influencing Factors. *Ecol. Econ.* **2019**, *35*, 13–19+74.
29. Chen, L.; Xu, L.; Yang, Z. Accounting carbon emission changes under regional industrial transfer in an urban agglomeration in China's Pearl River Delta. *J. Clean. Prod.* **2017**, *167*, 110–119. [CrossRef]
30. Chen, L.; Xu, L.; Yang, Z. Inequality of industrial carbon emissions of the urban agglomeration and its peripheral cities: A case in the Pearl River Delta, China. *Renew. Sustain. Energy Rev.* **2019**, *109*, 438–447. [CrossRef]
31. Liu, C.; Su, Y.; Li, L. The estimation and spatial distribution of the carbon emissions of units in China. *Environ. Pollut. Control* **2020**, *42*, 113–119. [CrossRef]
32. Xu, Q.; Yang, R.; Dong, Y.-X.; Liu, Y.-X.; Qiu, L.-R. The influence of rapid urbanization and land use changes on terrestrial carbon sources/sinks in Guangzhou, China. *Ecol. Indic.* **2016**, *70*, 304–316. [CrossRef]
33. Chuai, X.; Huang, X.; Wang, W.; Zhao, R.; Zhang, M.; Wu, C. Land use, total carbon emissions change and low carbon land management in Coastal Jiangsu, China. *J. Clean. Prod.* **2015**, *103*, 77–86. [CrossRef]
34. Zhang, C.; Zhao, L.; Zhang, H.; Chen, M.; Fang, R.; Yao, Y.; Zhang, Q.; Wang, Q. Spatial-temporal characteristics of carbon emissions from land use change in Yellow River Delta region, China. *Ecol. Indic.* **2022**, *136*, 108623. [CrossRef]

35. Lu, N.; Feng, S.; Liu, Z.; Wang, W.; Lu, H.; Wang, M. The Determinants of Carbon Emissions in the Chinese Construction Industry: A Spatial Analysis. *Sustainability* **2020**, *12*, 1428. [CrossRef]
36. Chen, J.; Wang, L.; Li, Y. Research on the impact of multi-dimensional urbanization on China's carbon emissions under the background of COP21. *J. Environ. Manag.* **2020**, *273*, 111123. [CrossRef]
37. Shi, T.; Si, S.; Chan, J.; Zhou, L. The Carbon Emission Reduction Effect of Technological Innovation on the Transportation Industry and Its Spatial Heterogeneity: Evidence from China. *Atmosphere* **2021**, *12*, 1169. [CrossRef]
38. Li, J.; Huang, X.; Yang, H.; Chuai, X.; Wu, C. Convergence of carbon intensity in the Yangtze River Delta, China. *Habitat Int.* **2017**, *60*, 58–68. [CrossRef] [PubMed]
39. Liu, H.; Nie, J.; Cai, B.; Cao, L.; Wu, P.; Pang, L.; Wang, X. CO_2 emissions patterns of 26 cities in the Yangtze River Delta in 2015: Evidence and implications. *Environ. Pollut.* **2019**, *252*, 1678–1686. [CrossRef]
40. Wang, M.; Wu, L.; Guo, X. Application of grey model in influencing factors analysis and trend prediction of carbon emission in Shanxi Province. *Environ. Monit. Assess.* **2022**, *194*, 542. [CrossRef]
41. Huang, M.; Wang, B. Factors influencing CO_2 emissions in China based on grey relational analysis. *Energy Sources Part A Recovery Util. Environ. Eff.* **2016**, *38*, 555–561.
42. Zhu, B.; Yuan, L.; Ye, S. Examining the multi-timescales of European carbon market with grey relational analysis and empirical mode decomposition. *Phys. A Stat. Mech. Appl.* **2019**, *517*, 392–399. [CrossRef]
43. Pei, J.; Niu, Z.; Wang, L.; Song, X.; Huang, N.; Geng, J.; Wu, Y.; Jiang, H.-H. Spatial-temporal dynamics of carbon emissions and carbon sinks in economically developed areas of China: A case study of Guangdong Province. *Sci. Rep.* **2018**, *8*, 13383. [CrossRef] [PubMed]
44. Wang, J.; Wang, S.; Li, S.; Feng, K. Coupling analysis of urbanization and energy-environment efficiency: Evidence from Guangdong province. *Appl. Energy* **2019**, *254*, 113650. [CrossRef]
45. Du, Y.; Wan, Q.; Liu, H.; Liu, H.; Kapsar, K.; Peng, J. How does urbanization influence PM2.5 concentrations? Perspective of spillover effect of multi-dimensional urbanization impact. *J. Clean. Prod.* **2019**, *220*, 974–983. [CrossRef]
46. Yue, W.; Liu, Z.; Su, M.; Gu, Z.; Xu, C. The impacts of multi-dimension urbanization on energy-environmental efficiency: Empirical evidence from Guangdong Province, China. *J. Clean. Prod.* **2021**, *296*, 126513. [CrossRef]
47. Gan, W.; Yao, W.; Huang, S. Evaluation of Green Logistics Efficiency in Jiangxi Province Based on Three-Stage DEA from the Perspective of High-Quality Development. *Sustainability* **2022**, *14*, 797. [CrossRef]
48. Wang, F.; Wang, C.; Su, Y.; Jin, L.; Wang, Y.; Zhang, X. Decomposition Analysis of Carbon Emission Factors from Energy Consumption in Guangdong Province from 1990 to 2014. *Sustainability* **2017**, *9*, 274. [CrossRef]
49. Song, W.; Mao, H.; Han, X. The two-sided effects of foreign direct investment on carbon emissions performance in China. *Sci. Total Environ.* **2021**, *791*, 148331. [CrossRef] [PubMed]
50. Huang, J.; Chen, X.; Yu, K.; Cai, X. Effect of technological progress on carbon emissions: New evidence from a decomposition and spatiotemporal perspective in China. *J. Environ. Manag.* **2020**, *274*, 110953.
51. Zhao, Y.; Ma, S.; Fan, J.; Cai, Y. Examining the Effects of Land Use on Carbon Emissions: Evidence from Pearl River Delta. *Int. J. Environ. Res. Public Health* **2021**, *18*, 3623. [CrossRef] [PubMed]
52. Xu, Q.; Dong, Y.; Yang, R.; Zhang, H.; Wang, C.; Du, Z. Temporal and spatial differences in carbon emissions in the Pearl River Delta based on multi-resolution emission inventory modeling. *J. Clean. Prod.* **2019**, *214*, 615–622. [CrossRef]
53. Ying, Y.; Yuqi, D.; Linyu, X.; Hanzhong, Z.; Wenhao, W.; Lei, C. A multi-level characteristic analysis of urban agglomeration energy-related carbon emission: A case study of the Pearl River Delta. *Energy* **2023**, *263*, 125651.
54. Hu, J.; Jiang, X. Study on the Influence of Urbanization on Carbon Emission under the Perspective of City Cluster. *J. China Univ. Geosci.* **2015**, *15*, 11–21.
55. Tan, R. FDI Intensity and Low-Carbon Development of Equipment Manufacturing Industries in Pearl River Delta Region: Empirical Analysis Based on Input-Output and Panel Data. *J. Int. Trade* **2012**, *2*, 81–91.
56. Zhong, W.; Gao, H.; Xu, W.; Yu, X. Exploring Carbon Peaking Pathways and Trends from a Multiclustering Perspective: Analysis Based on Panel Data of 21 Cities in Guangdong Province. *South China J. Econ.* **2021**, *12*, 58–79.
57. Zhang, H.; Huang, Y.; Wang, R.; Zhang, J.; Peng, J. Decoupling and spatiotemporal change of carbon emissions at the level in China. *Resour. Sci.* **2022**, *44*, 744–755. [CrossRef]
58. Su, Y.; Chen, X.; Ye, Y.; Wu, Q.; Zhang, H.; Huang, N.; Kuang, Y. The characteristics and mechanisms of carbon emissions from energyconsumption in China using DSP/OLS night light imageries. *Acta Geogr. Sin.* **2013**, *68*, 1513–1526.
59. Chandra Voumik, L.; Ridwan, M.; Hasanur Rahman, M.; Raihan, A. An investigation into the primary causes of carbon dioxide releases in Kenya: Does renewable energy matter to reduce carbon emission? *Renew. Energy Focus* **2023**, *47*, 100491. [CrossRef]
60. Adebayo, T.S.; Ullah, S.; Kartal, M.T.; Ali, K.; Pata, U.K.; Ağa, M. Endorsing sustainable development in BRICS: The role of technological innovation, renewable energy consumption, and natural resources in limiting carbon emission. *Sci. Total Environ.* **2023**, *859*, 160181. [CrossRef]
61. Waheed, R.; Sarwar, S.; Wei, C. The survey of economic growth, energy consumption and carbon emission. *Energy Rep.* **2019**, *5*, 1103–1115. [CrossRef]

62. Liu, X.; Cifuentes-Faura, J.; Zhao, S.; Wang, L. Government environmental attention and carbon emissions governance: Firm-level evidence from China. *Econ. Anal. Policy* **2023**, *80*, 121–142. [CrossRef]
63. Lin, B.; Li, Z. Spatial analysis of mainland cities' carbon emissions of and around Guangdong-Hong Kong-Macao Greater Bay area. *Sustain. Cities Soc.* **2020**, *61*, 102299. [CrossRef]

atmosphere

MDPI

Article

Comparative Study on the Influencing Factors of the Greenhouse Gas Budget in Typical Cities: Case Studies of Beijing and Shenzhen

Kuo Liu [1,2], Shishuai Yang [2], Binbin Huang [2], Chaofan Xian [2], Baolong Han [2], Tian Xie [2], Chengji Shu [2], Zhiwen Chen [2], Haoqi Wang [2], Haijun Wang [3,*] and Fei Lu [2,4,*]

[1] School of Ecology and Environmental Sciences, Yunnan University, Kunming 650504, China
[2] State Key Laboratory of Urban and Regional Ecology, Research Center for Eco-Environmental Sciences, Chinese Academy of Sciences, Beijing 100085, China
[3] Institute for Ecological Research and Pollution Control of Plateau Lakes, School of Ecology and Environmental Science, Yunnan University, Kunming 650504, China
[4] Beijing-Tianjin-Hebei Urban Megaregion National Observation and Research Station for EcoEnvironmental Change, Beijing 100085, China
* Correspondence: wanghaijun@ynu.edu.cn (H.W.); feilu@rcees.ac.cn (F.L.)

Abstract: Clarifying the pattern of the urban greenhouse gas (GHG) budget and its influencing factors is the basis of promoting urban low-carbon development. This paper takes Beijing and Shenzhen—the capital city and the most rapidly developing city in China, respectively—as case studies, comprehensively accounts their GHG budgets from 2005 to 2020, and investigates and compares the factors affecting their GHG budgets. The total GHG emissions in Beijing were lowest in 2005 (160.3 $TgCO_2$ equivalents) and peaked at 227.7 $TgCO_2$ equivalents in 2019, and then decreased to 209.1 $TgCO_2$ equivalents in 2020. Meanwhile, the total GHG emissions in Shenzhen gradually increased from 36.0 $TgCO_2$ equivalents in 2005 to 121.4 $TgCO_2$ equivalents in 2019, and then decreased to 119.1 $TgCO_2$ equivalents in 2020. The energy activity sector was the greatest contributor to GHG emissions in this period, accounting for 82.5% and 76.0% of the total GHG emissions in Beijing and Shenzhen, respectively. The carbon sink of the ecosystems of these two cities could absorb only small parts of their emissions, and the neutralization rates of sinks ranged from 1.7% to 2.3% in Beijing and from 0.3% to 1.5% in Shenzhen. The enhancement of population, economic product, and consumption increased the greenhouse gas emissions in both cities. A 1% increase in population size, per capita GD (gross domestic product), and residential consumption level would increase total GHG emissions by 0.181%, 0.019%, and 0.030% in Beijing, respectively. The corresponding increases in Shenzhen would be 0.180%, 0.243%, and 0.172%, respectively. The household size had opposite effects on the two cities, i.e., a 1% increase in household size would increase GHG emissions by 0.487% in Shenzhen but reduce them by 2.083% in Beijing. Each 1% increase in secondary industry and energy intensity would reduce GHG emissions by 0.553% and 0.110% in Shenzhen, respectively, which are more significant reductions than those in Beijing.

Keywords: Beijing; Shenzhen; greenhouse gas emissions; carbon sinks; influencing factors

Citation: Liu, K.; Yang, S.; Huang, B.; Xian, C.; Han, B.; Xie, T.; Shu, C.; Chen, Z.; Wang, H.; Wang, H.; et al. Comparative Study on the Influencing Factors of the Greenhouse Gas Budget in Typical Cities: Case Studies of Beijing and Shenzhen. *Atmosphere* **2023**, *14*, 1158. https://doi.org/10.3390/atmos14071158

Academic Editor: László Haszpra

Received: 16 April 2023
Revised: 20 June 2023
Accepted: 13 July 2023
Published: 17 July 2023

1. Introduction

1.1. Motivations

The global average temperature increased by 0.8 °C~1.3 °C from 1900 to 2019 [1], and human activities are the main cause of global warming. Significant increases in atmospheric greenhouse gas (GHG) concentrations (especially CO_2, CH_4, and N_2O) since the Industrial Revolution have been considered to be the main cause of global warming. Adaptation to global warming and mitigation of the warming rate are currently the main issues faced in the development of the international community [2,3]. China has proposed to strive to cap its CO_2 emissions by 2030 and to strive to achieve carbon neutrality by 2060. Concurrently, cities have become hotspots for GHG emissions [4]. Urban areas accounted for 61.8% of

global greenhouse gas emissions in 2015, and the proportion of urban emissions in overall global GHG emissions will gradually increase in the future, possibly exceeding 80%; this is related to rapid urban economic development and the increasing urban population. It has been further suggested that improving the energy-use efficiency and shifting consumption patterns will help reduce emissions, and slowing the rate of urban expansion and increasing urban green infrastructure will help protect carbon sinks [5]. Moreover, during urbanization, the constructed land area will expand, while the area of natural ecosystems such as forests will simultaneously shrink, resulting in a reduction in urban carbon sinks and an expansion of carbon sources; this change will aggravate the imbalance of urban GHG sinks and sources [6,7]. Therefore, cities are important carriers and key components for reducing greenhouse gas emissions. Establishing a scientific and systematic urban greenhouse gas budget accounting system, clarifying the patterns of urban GHG budgets, and analyzing their influencing factors are the foundation for regulating the urban greenhouse gas budget and promoting low-carbon development in cities.

1.2. Literature Review

Energy consumption has always been the sector with the highest greenhouse gas emissions in urban areas. According to a report released by the International Energy Agency (IEA), Paris, France, China is the world's largest greenhouse gas emitter, accounting for about one-quarter of global emissions, and approximately 85% of China's CO_2 emissions come from urban energy consumption [8]. Energy consumption was reported as accounting for the highest proportion of CO_2 emissions from Chinese cities between 2001 and 2015, ranging from 85.14% to 89.3% [9]. During this period, the GHG emissions from energy consumption increased by 188%. Some studies on the GHG emissions of single cities also indicated that energy consumption accounted for the highest proportion of emissions and had increased continuously in recent decades [10]. In recent years, with the continuous expansion of cities, the implicit GHG emissions caused by intercity power and heat inputs and outputs has drawn broad concern in academic circles. In Bursa, Turkey, the GHG emissions from electricity were found to have reached one-quarter of the total GHG emissions of the city in 2016 [11]. In addition, it was reported that GHG emissions from the external electricity industry had the highest dependency on external power transfers in Beijing and accounted for approximately 19.5% of the city's total emissions [12].

A series of studies focusing on GHG budgets outside the energy sector have also been conducted in recent years. For example, Markolf et al. estimated the GHG emissions of 100 US cities, of which industrial production processes contributed to 18% of total emissions and became the second-highest sector after energy consumption [13]. GHG emissions from the waste sector are also increasing in many countries around the world. For instance, GHG emissions from Mexico's waste sector increased by 180% from 1998 to 2012 [14], while GHG emissions from domestic waste in Tianjin increased by 65.9% from 2013 to 2018 [15]. At the urban level, along with socioeconomic development, cities are more often consumption centers rather than production entities. Therefore, the "hidden" GHG emissions from city commodities and services are enormous. Hachaichi et al. conducted a comparative study of the carbon footprints of 252 cities worldwide, which indicated that food consumption and commodity consumption accounted for approximately 25% and 9% of the total carbon footprint, respectively [16]. Guo studied the household carbon emissions in Beijing and found that durable goods, food, and clothing consumption accounted for 15%, 8%, and 2% of greenhouse gas emissions, respectively [17]. Previous studies have indicated that urban carbon sinks could offset a certain proportion of carbon sources. However, the urbanization process (especially the expansion of constructed area) would reduce both the area and carbon sink of the ecosystem and exacerbate the imbalance of sink and source in the urban area. For example, from 1995 to 2019, the urban area in the Monterrey metropolitan area of Mexico expanded by 2.6 times, and the regional carbon sink decreased by 38.6% [18]. Studies in China have also paid increasing attention to the offsetting or neutralization effect of urban carbon sinks. In 2020, the neutralization rates of green spaces in Beijing, Shenzhen,

and Tianjin on total GHG emissions were 0.99%, 0.15%, and 0.84%, respectively. Wang et al. found that the offset rate of CO_2 emissions from fossil fuel consumption through ecological restoration reached 9.9% in Beijing [19].

Currently, the main method for analyzing factors affecting urban GHG emissions is factor decomposition. This method decomposes the GHG emissions into different influencing factors and analyzes the main factors affecting GHG emissions in different types of cities by comparing their contribution values. The models used to study the influencing factors of GHG emissions are mainly the Kaya model, LMDI decomposition model (logarithmic mean Divisia index method), IPAT model (Impact = Population × Affluence × Technology), and STIRPAT model (stochastic impacts by regression on PAT) [20–22]. In 1990, the Japanese scholar Kaya first proposed the Kaya formula, which points out the relationship between CO_2 emissions and carbon emission coefficients, energy intensity, economic development, and population size. Based on this, different scholars have conducted related exploration and research. Ang et al. proposed the LMDI decomposition method, which decomposes the GHG budget into different factors and analyzes the degree to which each factor contributes to the GHG budget [23]. This method solves the problem of residual error and zero value existence in the decomposition results. In 1971, Ehrlich first proposed the IPAT model, which divides the influencing factors into population size, economic development, and technological factors [24]. Due to certain limitations of the IPAT model, Dietz et al. established the STIRPAT model based on the IPAT model in 1997. The STIRPAT model still maintains the original product structure of the IPAT model and still regards population, economy, and technology as determining factors, but it is more flexible and can add, modify, or decompose relevant influencing factors according to the research purposes. Subsequently, this model has been widely used in studies of influencing factor analysis [25].

To date, research on the influencing factors of urban GHG budgets has mainly decomposed changes in GHG emissions into the population scale, urbanization, economic development, energy intensity, and other influencing factors and then analyzed the degree of contribution of each factor to emissions.

Regarding the impact of population factors on the GHG budget, existing studies have focused mainly on the impacts of the urban population and its changes on GHG emissions. For example, in Shanghai, carbon emissions increase by 2.62% for every 1% increase in the permanent population [26]. A total of 23 cities in the Guangdong–Hong Kong–Macao Greater Bay Area and its surrounding areas were taken as the research area for analysis. The results showed that with a sharp increase in the urban population, the total emissions of the 23 cities increased by 43.19% from 2000 to 2016 [27]. Urban expansion leads to the transformation of natural ecosystems into urban ecosystems, and the transformation of ecosystems leads to changes in vegetation and soil carbon pools, affecting the urban GHG budget [28]. Taking Leipzig, Germany, as the research area, the carbon storages corresponding to different urbanization levels were calculated. The study found that the carbon storage of the central area with higher urbanization was lower, while the carbon storages of the areas with lower urbanization were the highest]. Based on an analysis of urbanization and changes in the soil and plant carbon cycles in North America, the soil organic carbon pool in Denver was found to have decreased by approximately 60% in 50 years [29].

Past studies show a close relationship between economic development and the greenhouse gas budget. Based on a dataset of 274 typical cities in the world, the multiple regression method was used to analyze the influencing factors of the urban GHG budget [30]. The results show that economic activities are most closely related to greenhouse gas emissions. A study on the economic development and GHG emissions of seven typical cities in the world, such as New York and London, showed that countries with high GDP per capita have higher greenhouse gas emissions [31]. In a Chinese study, the LMDI decomposition method was used to analyze the factors influencing greenhouse gas emissions from energy consumption in 11 typical Chinese cities, and the findings showed that economic development was the main contributing factor to the increase in CO_2 emissions

from urban energy consumption [32]. China's coal-based energy consumption structure is the main factor leading to its substantial growth of greenhouse gas emissions [33]. By analyzing the relationship between GHG emissions and the industrial structure in 30 major cities in China [34], the results showed that the industrial structure is positively correlated with GHG emissions, and with the upgrading and adjustment of the urban industrial structure, the impact of the industrial structure on GHG emissions is decreasing annually. Therefore, adjustment of the industrial structure and energy structure is critical for reducing GHG emissions.

These studies have made great progress in clarifying the pattern of the urban GHG budget and analyzing its influencing factors, thereby providing a basis for promoting urban low-carbon development and regulating the urban greenhouse gas budget. However, existing research on the influencing factors of GHG budgets has been based mostly on individual cities, while there is a lack of comparative research examining different cities to reveal the common laws and differences in GHG budgets among different cities.

This paper selects Beijing and Shenzhen—two low-carbon pilot cities in China—to comprehensively account for their urban greenhouse gas budgets by using the coefficient method, and then analyzes the influencing factors of these typical cities' greenhouse gas budgets from 2005 to 2020 based on the improved STIRPAT (stochastic impacts by regression on population, affluence, and technology) model and the ridge regression method to explore the dynamic patterns, influencing factors, and causes of differences in the two cities' GHG budgets.

2. Methods

2.1. Study Area

Beijing is the capital of China, the political and cultural center of the country, and a world-famous city with a history of over 3000 years. Located in the northern part of the North China Plain, Beijing has a warm, temperate, semi-humid (Table 1), semi-arid monsoon climate [35,36]. Unlike southern cities, Beijing provides all-day heating during winter. Beijing is strategically important in China and, as the capital and the world's first "dual-Olympic" city, it has a good foundation and conditions for green and low-carbon transformation. It is capable of and responsible for playing a leading role in the national dual-carbon action. Shenzhen, located in southern China, has a transitional oceanic climate from subtropical to tropical and abundant wetland resources. Shenzhen is the window and flag of China's reform and opening up, serving as a bridge connecting the inland region and Hong Kong, and was the first city in China to achieve comprehensive urbanization. Unlike Beijing's historical background, Shenzhen is a modern metropolis with more prominent modern entertainment facilities, such as the Window of the World. Moreover, as one of the first pilot cities promoting low-carbon development in China and an experimental demonstration zone for socialism with Chinese characteristics, Shenzhen leads the trend of institutional innovation and reform in China. Therefore, we chose Beijing and Shenzhen as research areas.

Table 1. Social and economic indicators in Beijing and Shenzhen.

	Beijing	**Shenzhen**
Administrative level	Municipality directly under the central government	Sub-provincial city
Geographical location	Northern China	Southern China
Land area	16,410.54 km^2	1997.47 km^2
Resident population in 2005	15.38 million	8.28 million
Resident population in 2020	21.89 million	17.63 million
Urban GDP in 2005	CNY 715.0 billion	CNY 503.6 billion
Urban GDP in 2020	CNY 3610.26 billion	CNY 2767.02 billion
GDP ratio of three industries in 2005	1.22:26.68:72.10	0.19:53.81:46.00
GDP ratio of three industries in 2020	0.30:15.83:83.87	0.09:37.78:62.13
Growth rate of the per-capita consumption expenditure from 2005 to 2020	192.74%	155.04%
Growth rate of the secondary industry output value from 2005 to 2020	199.70%	285.80%
Growth rate of the tertiary industry output value from 2005 to 2020	487.31%	642.14%

2.2. Data Sources

The sources of GHG budget accounting data and emission factors applied in this paper are shown in Table 2. Since the statistical concepts of China's cities are often divided according to administrative units rather than built-up areas, as well as due to data availability, it is difficult to separately account for activities such as energy consumption and residential consumption, so the emissions involved in agricultural activities within the administrative units of specific cities (Beijing and Shenzhen, in this study) are also included. Because the main industrial products in Shenzhen do not include cement or steel, this study calculated the GHG emissions only from industrial processes in Beijing.

Table 2. Sources of GHG activity data and emission factors.

	Sources of Activity Data	Sources of Emission Factors
Energy activities	China Energy Statistical Yearbook [34]; Guangdong Statistical Yearbook [35]; Shenzhen Statistical Yearbook [36].	Shan, et al., 2018 [37]; Provincial Greenhouse Gas Inventory Preparation Guidelines (Trial) [38].
Industrial processes	Beijing Statistical Yearbook [39].	Provincial Greenhouse Gas Inventory Preparation Guidelines (Trial); Liu, et al., 2016 [40].
Waste disposal	China Statistical Yearbook on Environment [41]; Information Announcement on Prevention and Control of Environmental Pollution by Solid Wastes Shenzhen [42].	Provincial Greenhouse Gas Inventory Preparation Guidelines (Trial).
Household consumption	Beijing Statistical Yearbook; Shenzhen Statistical Yearbook.	Liu, et al., 2018 [43].
Agricultural activities	Beijing Statistical Yearbook; Shenzhen Statistical Yearbook.	Provincial Greenhouse Gas Inventory Preparation Guidelines (Trial).
Carbon sinks	Land change survey in Beijing [44]; land change survey in Shenzhen [45].	Accounting Standards of Gross Ecosystem Product (Trial) [46]; Yu, et al., 2022 [47]; Zhang, et al., 2022 [48].
Analysis of influencing factors	Beijing Statistical Yearbook; Shenzhen Statistical Yearbook.	-

The energy activity data of Shenzhen are incomplete, so they were calculated according to the provincial activity data. By consulting the Shenzhen Statistical Yearbook, we found that the statistical energy consumption data include the energy consumption of raw coal, crude oil, gasoline, kerosene, diesel, fuel oil, liquefied petroleum gas, natural gas, and electricity in the industrial sector, and that the total energy consumption of each of these parts is less than the terminal consumption of Shenzhen. Therefore, the missing energy consumption data of Shenzhen can be calculated by combining the obtained energy consumption data with the consumption data of Guangdong Province. The specific accounting formula is shown in Equation (1) as follows:

$$E'_{ij} = E_{ij} \times \left(E'_{ia} - E'_{ib}\right) / \left(E_{ia} - E_{ib}\right) \quad (1)$$

where E'_{ij} is the energy consumption of category j in sector i of Shenzhen (Tgce), E_{ij} is the energy consumption of category j in sector i of Guangdong Province (Tgce), E'_{ia} is the terminal consumption of department i of Shenzhen (Tgce), E'_{ib} is the sum of all kinds of energy consumption available for sector i in the Shenzhen Statistical Yearbook (Tgce), E_{ia} is the terminal consumption of sector i in Guangdong Province (Tgce), and E_{ib} is the sum of the energy consumption of sector i in Guangdong Province corresponding to the energy contained in E'_{ib} (Tgce).

2.3. Accounting for Urban GHG Emissions

GHG emission sectors include urban energy activities, industrial processes, waste disposal, household consumption, and agricultural activities, and the main GHGs included are CO_2, CH_4, and N_2O.

2.3.1. GHG Emissions from Energy Activities

GHG emissions from energy activities include the direct emissions of GHGs from fossil fuel consumption and the indirect emissions of GHGs from the external transfer of power and heat. GHG emissions from fossil fuel consumption are accounted for with reference to the method provided by the IPCC [49], and the coefficient method is adopted to determine the GHG emissions from energy external transfer; this term is estimated according to Formula (2) as follows:

$$E = \sum_{i}\sum_{j}\left(E_{ij} \times NCV_i \times EF_i \times O_{ij} \times 44/12\right) \quad (2)$$

where the subscripts i and j in the equation refer to the fossil fuel types and sectors, respectively, E represents the CO_2 emissions ($GgCO_2$), E_{ij} represents fossil fuel consumption (Gg), NCV_i represents the net caloric value of fossil fuels (GJ/Gg), EF_i represents the carbon content (GgC/GJ), O_{ij} is the carbon oxidation factor (%), and 44/12 is the molecular weight ratio of CO_2 to C. These terms are listed in Table 3. The GHG emission coefficients of power and heat consumption are 0.604 ($kgCO_2$/kW·h) and 0.11 ($GgCO_2$/TJ), respectively [38]. The GHG emission parameters of external power transfer in Beijing and Shenzhen are 1.246 ($kgCO_2$/kW·h) and 0.714 ($kgCO_2$/kW·h), respectively, and the GHG emission parameter of heating is 0.11 ($GgCO_2$/TJ) [50].

Table 3. Accounting parameters of fossil fuel consumption.

Energy Type	NCV_i	EF_i	O_i
Raw coal	0.21	26.32	85
Cleaned coal	0.26	26.32	85
Other washed coal	0.15	26.32	85
Briquettes	0.18	26.32	90
Coke	0.28	31.38	93
Other gas	0.83	21.49	99
Other coking products	0.28	27.45	93
Crude oil	0.43	20.08	98
Gasoline	0.44	18.90	98
Kerosene	0.44	19.60	98
Diesel oil	0.43	20.20	98
Fuel oil	0.43	21.10	98
Liquefied petroleum gas	0.47	20.00	98
Refinery gas	0.43	20.20	98
Other petroleum products	0.51	17.20	98
Natural gas	3.89	15.32	99

2.3.2. GHG Emissions from Industrial Processes

GHG emissions from industrial processes refer to CO_2 emissions caused by physical and chemical reactions in production processes, rather than GHG emissions caused by industrial combustion. These emissions include the high-temperature decomposition process of ironmaking solvents and the decarbonization process in the production of steel, as well as the high-temperature calcination process of limestone in cement production [40,51].

The accounting formula of GHG emissions in the industrial production process (E, in $GgCO_2$) is shown in Formula (3) as follows:

$$E = \sum_i AD_i \times EF_i \quad (3)$$

where i refers to the ith industrial production process, AD refers to the product output (Gg), EF refers to the carbon emission factor ($GgCO_2/Gg$), and the emission factors of cement and steel are 0.538 and 0.265 ($GgCO_2/Gg$), respectively [40].

2.3.3. GHG Emissions from Waste Disposal

GHG emissions from waste disposal are calculated according to the methods recommended in the Provincial Greenhouse Gas Inventory Preparation Guidelines [38], including CH_4 and CO_2 emissions from solid waste landfill and incineration, as well as CH_4 and N_2O emissions from wastewater treatment.

GHG Emissions from Solid Waste Treatment

1. CH_4 emissions from landfill treatment

CH_4 emissions from landfill treatment (E_{CH_4}, in $GgCH_4$) were estimated using Formula (4):

$$E_{CH_4} = (MSW \times L_0) \times (1 - OX) \quad (4)$$

where MSW refers to the landfill treatment capacity (Gg/yr), L_0 represents the CH_4 generation potential ($GgCH_4/Gg$ waste), and OX refers to the oxidation factor (%). The accounting parameters are listed in Table 4.

Table 4. Accounting parameters of waste disposal.

Accounting Parameter	Unit	Value [38]
CH_4 generation potential (L_0)	$GgCH_4/Gg$ waste	0.03
Landfill oxidation factor (OX)	%	10
Total carbon content (CCW)	%	20
Fraction of fossil carbon in the total carbon (FCF)	%	39
Combustion efficiency of waste incinerator (EF)	%	95
Emission factor of domestic wastewater (EF)	$kgCH_4/kgBOD$	0.099
Values of BOD/COD in Beijing	—	0.45
Values of BOD/COD in Shenzhen	—	0.47
Emission factor of industrial wastewater (EF)	$kgCH_4/kgCOD$	0.025
Protein consumption per capita (Pr)	kg/person/year	35.22
N_2O emission factor for wastewater treatment (EF)	kgN_2O/kgN	0.0015

2. CO_2 emissions from incineration

CO_2 emissions from incineration (E_{CO_2}, in Gg) were estimated using Formula (5):

$$E_{CO_2} = \sum IW \times CCW \times FCF \times EF \times 44/12 \quad (5)$$

where IW refers to the waste incineration capacity ($GgCO_2/yr$), CCW is the total carbon content (%), FCF refers to the fraction of fossil carbon in the total carbon (%), EF is the combustion efficiency (%), and 44/12 is the conversion factor from C to CO_2; the accounting parameters are shown in Table 4.

GHG Emissions from Wastewater Treatment

1. Wastewater treatment CH_4 emissions

CH_4 emissions from wastewater treatment (E_{CH_4}, in $GgCH_4$) were estimated using Formula (6):

$$E_{CH_4} = \sum_i TOW_i \times EF_i \quad (6)$$

where i refers to domestic wastewater and industrial wastewater, E_{CH_4} refers to the total CH_4 emissions ($GgCH_4/yr$), TOW_i refers to organics in wastewater (kgBOD/yr; kgCOD/yr), and EF_i refers to the emission factor ($kgCH_4/kgBOD$; $kgCH_4/kgCOD$). The accounting parameters are shown in Table 4.

2. Wastewater Treatment N_2O Emissions

N_2O emissions from wastewater treatment (E_{N_2O}, in kgN_2O) were estimated using Formula (7):

$$E_{N_2O} = P \times P_r \times EF_E \times 44/28 \quad (7)$$

where P is the population, P_r is the annual per capita protein consumption (kg/person/year), EF_E is the N_2O emission factor (kgN_2O/kgN), and 44/28 is the transformation coefficient; the accounting parameters are shown in Table 4.

According to the global warming potential (GWP), CH_4 and N_2O were converted to CO_2 equivalents, and the GWP parameters of CH_4 and N_2O were 29 and 298, respectively.

2.3.4. GHG Emissions from Household Consumption

GHG emissions from household consumption can be divided into three categories: GHG emissions from clothing, from food, and from household articles [52,53]. To avoid repeat calculations, housing and transportation can be included in energy activities, waste disposal, and other sectors. GHG emissions from household consumption (E, in $GgCO_2$) were estimated using Formula (8):

$$E = \sum_i AD_i \times EF_i \quad (8)$$

where i represents clothing, food, and household articles and AD refers to the per capita expenditure on food, clothing, and household articles (CNY/year); these values are 0.120, 0.077, and 0.244 ($kgCO_2/CNY$), respectively [43].

2.3.5. GHG Emissions from Agricultural Activities

GHG emissions from agricultural activities are accounted for according to the methodology recommended by the provincial Greenhouse Gas Inventory Preparation Guidelines [38]; these emissions mainly include direct and indirect GHG emissions from cropland and CH_4 emissions from rice paddies, animal enteric fermentation, and animal manure management. According to the accounting results, CH_4 and N_2O emissions were converted into CO_2 equivalents.

GHG Emissions from Cropland

1. Direct emissions

The direct emissions come from the nitrogen fertilizer input, and the estimation formula for the direct emission sector (is E_{N_2O}, in GgN_2O) is shown in Formula (9):

$$E_{N_2O} = N_{N\ fertilizer} \times EF_{direct} \quad (9)$$

where $N_{N\ fertilizer}$ refers to the amount of nitrogen fertilizer applied (Gg) and EF is the emission factor of nitrogen input from cropland; the emission factors are 0.0057 and 0.0178 (kgN_2O/kgN) for Beijing and Shenzhen, respectively [38].

2. Indirect emissions

Indirect N_2O emissions come from atmospheric nitrogen deposition ($N_2O_{deposition}$, in GgN_2O) and leaching runoff ($N_2O_{leaching}$, in GgN_2O) [54], and the formulae are as follows:

$$N_2O_{deposition} = \left(N_{animal} \times 20\% + N_{input} \times 10\%\right) \times 0.01 \quad (10)$$

$$N_2O_{leaching} = N_{input} \times 20\% \times 0.0075 \quad (11)$$

$$N_{animal} = \sum_i \text{number of animals}_i \times \text{animal nitrogen excretion}_i \quad (12)$$

where N_{animal} represents animal manure emissions (Gg) and N_{input} represents cropland nitrogen inputs (Gg). According to the statistical yearbook data, Beijing's statistics include cattle, sheep, goats, pigs, and poultry, while the statistical data of Shenzhen include dairy cattle, other cattle, pigs, and poultry; all corresponding emission factors are shown in Table 5.

Table 5. Nitrogen excretion of animals.

Beijing animal	Poultry	Pig	Cattle	Sheep	Goat	Other
Nitrogen excretion (kg/head/year) [50]	0.6	16	50	12	2	40
Shenzhen animal	Poultry	Pig	Dairy cattle	Other cattle		
Nitrogen excretion (kg/head/year) [50]	0.6	16	60	40		

Methane (CH_4) Emissions from Rice Paddies

CH_4 emissions from rice paddies (E_{CH_4}, in $GgCH_4$) were estimated using Formula (13):

$$E_{CH_4} = AD \times EF \quad (13)$$

where AD is the sowing area (ha) and EF is the CH_4 emission factor ($kgCH_4\ ha^{-1}$); the EF values in Beijing and Shenzhen are 234 and 236.7 ($kgCH_4\ ha^{-1}$), respectively [38].

GHG Emissions from Animal Enteric Fermentation

CH_4 is produced as a byproduct in the process of animals' enteric digestion of feed, and CH_4 is excreted in the form of gas through the mouth, nose, and rectum of livestock. Ruminant livestock are the main emission sources of CH_4 produced by enteric fermentation, while non-ruminant livestock can be ignored because of their small CH_4 production. However, considering the large number of pigs in Beijing, the emission sources of CH_4 from enteric fermentation mainly include cattle, goats, sheep, and pigs [55]. CH_4 emissions from animal enteric fermentation (E_{CH_4}, in $kgCH_4$) were estimated using Formula (14):

$$E_{CH_4} = \sum_i EF_{CH_4} \times AP_i \times 10^{-7} \quad (14)$$

where i is the species of livestock, AP_i is the number of heads of livestock species (head), and EF_i is the CH_4 emission factor of the livestock population ($kgCH_4\ head^{-1}\ year^{-1}$); the values of each coefficient are shown in Table 6.

Table 6. CH_4 emission factors of animal enteric fermentation.

Beijing animal	Cattle	Sheep	Goat	Pig
Emission factors ($kgCH_4$ $head^{-1}$ $year^{-1}$) [38]	70.5	8.2	8.9	1
Shenzhen animal	Dairy cattle	Other cattle	Pig	
Emission factors ($kgCH_4$ $head^{-1}$ $year^{-1}$) [38]	88.1	52.9	1	

GHG Emissions from Animal Manure Management

Greenhouse gas emissions from animal manure management refer to the CH_4 and N_2O produced by the storage and treatment of animal manure prior to its application to the soil. GHG emissions from animal manure management (E_{CH_4}, in $kgCH_4$; E_{N_2O}, in kgN_2O) were estimated using Formula (15):

$$E_{CH_4(N_2O)} = \sum_i AP_i \times EF_i \quad (15)$$

where i refers to the livestock species, AP_i refers to the number of heads of livestock species (head), and EF_i is the CH_4 (N_2O) emission factor for the livestock population ($kgCH_4$ $head^{-1}year^{-1}$; kgN_2O $head^{-1}year^{-1}$). The values of each coefficient are shown in Table 7.

Table 7. Emission factors of CH_4 and N_2O from animal manure management.

Beijing animal	Cattle		Sheep		Goat		Pig		Poultry	
	CH_4	N_2O	CH_4	N_2O	CH_4	N_2O	CH_4	N_2O	CH_4	N_2O
Emission factors (kg $head^{-1}year^{-1}$) [38]	5.14	1.32	0.15	0.093	0.17	0.093	3.12	0.227	0.01	0.007
Shenzhen animal	Dairy cattle		Other cattle		Pig		Poultry			
	CH_4	N_2O	CH_4	N_2O	CH_4	N_2O	CH_4	N_2O		
Emission factors (kg $head^{-1}year^{-1}$) [38]	8.45	1.71	4.72	0.805	5.85	0.157	0.02	0.007		

2.4. Accounting for Carbon Sinks

The carbon sink mainly calculates the carbon sink of forest land, garden plots, cultivated land, grassland, and wetlands. According to the accounting standard of the Gross Ecosystem Product (Trial) and previous studies [46–48], the carbon sink rate method was adopted. Since grassland vegetation withers every year, and because fixed carbon is returned to the atmosphere or soil, only the soil carbon sink amount of grasslands is considered here. On the basis of the available data, the carbon emissions from cultivated land were calculated in the agricultural part. Therefore, to avoid repeated calculations, the carbon sink amount of cultivated lands was obtained mainly by calculating the soil carbon sink amount of agricultural fields applied with chemical fertilizer, and the formula is as follows:

2.4.1. Carbon Sink of Forestlands

The carbon sink of forestlands (Q, in $kgCO_2$ yr^{-1}) was estimated using Formula (16):

$$Q = (FVCSR + FSCSR) \times S \times 44/12 \quad (16)$$

where FVSCR is the carbon sink rate of forest vegetation (kgC ha^{-1} $year^{-1}$), FSCSR is the rate of soil carbon sink in forestlands (kgC ha^{-1} $year^{-1}$), and S is the area of forestlands (ha).

2.4.2. Carbon Sink of Garden Plots

The carbon sink of garden plots (Q, in $kgCO_2\ yr^{-1}$) was estimated using Formula (17):

$$Q = GCSR \times S \times 44/12 \quad (17)$$

where GSCR is the carbon sink rate of garden plots ((kgC ha^{-1} $year^{-1}$) and S is the area of garden plots (ha).

2.4.3. Carbon Sink of Cultivated Lands

The carbon sink of cultivated lands (Q, in $kgCO_2\ y^{r-1}$) was estimated using Formula (18):

$$Q = SCSR \times S \times 44/12 \quad (18)$$

$$\text{Beijing}: \ SCSR = 0.5286 \times TNF + 0.002 \quad (19)$$

$$\text{Shenzhen}: \ SCSR = 1.5339 \times TNF - 0.267 \quad (20)$$

$$TNF = NF/S \quad (21)$$

where SCSR is the carbon sink rate of cultivated lands (kgC ha^{-1} yr^{-1}), S is the area of cultivated lands (ha), TNF is the amount of chemical nitrogen fertilizer per unit area of cultivated lands (kg ha^{-1} $year^{-1}$), and NF is the amount of chemical nitrogen fertilizer applied (kg $year^{-1}$).

2.4.4. Carbon Sink of Grasslands

The carbon sink of grasslands (Q, in $kgCO_2\ year^{-1}$) was estimated using Formula (22):

$$Q = GSCSR \times S \times 44/12 \quad (22)$$

where GSCSR is the carbon sink rate of grasslands (kgC ha^{-1} $year^{-1}$) and S is the area of grasslands (ha).

2.4.5. Carbon Sink of Wetlands

The carbon sink of wetlands (Q, in $kgCO_2\ yr^{-1}$) was estimated using Formula (23):

$$Q = SCSR \times SW \times 10^{-2} \times 44/12 \quad (23)$$

where SCSR is the carbon sink rate of wetlands (kgC ha^{-1} $year^{-1}$) and SW is the area of wetlands (ha). Each parameter is shown in Table 8.

Table 8. Carbon sink rate (kgC ha^{-1} $year^{-1}$).

	Forest Vegetation [46]	Forest Soil [46]	Garden Plot [47]	Grassland [46]	Wetland [48]
Beijing	551	586	1274	30	477
Shenzhen	554	118	1274	18	3305

2.5. Accounting of Net GHG Emissions from Urban Ecosystems

Net GHG emissions refer to the difference between the total GHG emissions and total carbon sinks ($E_{Net\ emission}$, in $kgCO_2$), as estimated by Formula (24). According to the accounting, the net GHG emissions of Beijing and Shenzhen during 2005–2020 can be determined as follows:

$$E_{Net\ emission} = E_{total\ emission} - E_{carbon\ sink} \quad (24)$$

where $E_{\text{total emission}}$ is the GHG emissions from the energy sector, industrial processes, agricultural activities, waste disposal, and household consumption, while $E_{\text{Carbon sink}}$ is the carbon sink from forestlands, garden plots, cultivated lands, grasslands, and wetlands.

2.6. Analysis Method of Influencing Factors of the GHG Budget

The STIRPAT model was developed from the IPAT model to examine the impacts on the environment [25,56], where I represents the influence of the environment, P represents the population size, A represents the affluence, and T represents the technological level. Dietz et al. built the STIRPAT model on the basis of the IPAT model [25]; the STIRPAT model can be expressed as follows:

$$I = P^b \times A^c \times T^d \times a \times e \tag{25}$$

where b, c, and d represent the index of each variable, a is the constant term, and e is the residual error term.

Since the model can add or decompose relevant influencing factors, in this paper, in combination with the urban development situation of China, the population factor is divided into three variables: the total population, household size, and urbanization rate. The GDP per capita and resident consumption level are used to reflect economic development, and the technical level is divided into two variables (the proportion of secondary industry and the energy intensity), with the formula of influencing factors of the GHG budget (I) expressed as follows:

$$I = P_1^{X_1} \times P_2^{X_2} \times P_3^{X_3} \times A_1^{X_4} \times A_2^{X_5} \times T_1^{X_6} \times T_2^{X_7} \times a \times e \tag{26}$$

The description of each independent variable is shown in Table 9. After logarithmic processing, the expression is as follows:

$$\begin{aligned} \ln I = {} & X_1 \ln P_1 + X_2 \ln P_2 + X_3 \ln P_3 + X_4 \ln A_1 + X_5 \ln A_2 + X_6 \ln T_1 + X_7 \ln T_2 \\ & + \ln e + \ln aa \end{aligned} \tag{27}$$

Table 9. Variable description.

Variable	Symbol	Define	Unit
Greenhouse gas budget	I	Greenhouse gas budget	$TgCO_2$ equivalents
Population	P_1	Number of permanent residents	10,000 persons
Household size	P_2	The ratio of registered population to registered households	Persons/household
Urbanization rate	P_3	The proportion of urban population to total population	%
GDO per capita	A_1	Ratio of GDP to population	CNY 10,000/person
Resident consumption level	A_2	Monthly consumption expenditure per person	CNY 100
Proportion of secondary industry	T_1	The proportion of secondary industry to GDP	%
Energy intensity	T_2	Ratio of energy consumption to GDP	kgce/CNY 1000

In view of the urban development of Shenzhen, the two indicators of the population and household size reflecting the population size were selected for practical applications, while the impact of the urbanization rate on the GHG budget was not selected. With the help of SPSS (Statistical Product and Service Solutions) software (IBM SPSS Statistics 26), factors influencing the total GHG emissions, carbon sinks, GHG budget, sectoral GHG budget, and categorical GHG budget in Beijing and Shenzhen were analyzed. Based on the STIRPAT extended model, serious multicollinearity was found among the variables when using the least-squares method for regression analysis. To solve this multicollinearity, the ridge regression estimation method was used. Ridge regression adds a K value [57,58] to the least-squares estimation and changes its estimated value to make the estimation result stable. The K value of the ridge parameter was selected with the help of programming in SPSS software, and the selection principle was to ensure that the regression coefficients were essentially stable.

3. Results

3.1. Comparison of the Patterns and Dynamics of the GHG Budgets of Beijing and Shenzhen

3.1.1. Pattern and Dynamics of Total GHG Emissions

Beijing's GHG emissions were always higher than Shenzhen's in 2005–2020 (Figure 1). On the whole, the GHG emissions in Beijing showed a relatively stable range of change. The GHG emissions increased from 160.3 $TgCO_2$ equivalents in 2005 to 209.1 $TgCO_2$ equivalents in 2020, with a growth rate of 30.5%. The GHG emissions in Shenzhen showed a gradual increasing trend, from 36.0 $TgCO_2$ equivalents in 2005 to 119.1 $TgCO_2$ equivalents in 2020, with a growth rate of 231.1%. Figure 2 shows the per capita and per unit GDP GHG emissions of Beijing and Shenzhen in 2005–2020. Beijing's per capita GHG emissions show an overall decreasing and fluctuating trend (decrease–increase–decrease), with the lowest per capita GHG emissions of 9.3 tons of CO_2 equivalents per person in 2015, and a slight increase from 2016 to 2019. The change in per capita GHG emissions in Beijing is related to both the promotion of low-carbon-emission efforts and the changes in population size, which began to decrease slightly in 2016. As shown in Figure 2, the per capita GHG emissions in Beijing were higher than those in Shenzhen. However, the per capita GHG emissions in Beijing decreased from 10.4 tons of CO_2 equivalents per person in 2005 to 9.6 tons of CO_2 equivalents per person in 2020, while the per capita GHG emissions in Shenzhen increased from 4.3 tons of CO_2 equivalents per person in 2005 to 6.8 tons of CO_2 equivalents per person in 2020. This indicates that Beijing has achieved certain results in reducing GHG emissions, but its emissions are still higher than those of Shenzhen. It is necessary to continue implementing emission reduction measures. Shenzhen needs to further strengthen low-carbon publicity, raise public awareness of emissions reduction, and reduce per capita GHG emissions. The GHG emissions per unit GDP in Beijing and Shenzhen decreased significantly from 2005 to 2020, and the degree of decrease in Beijing was greater than that in Shenzhen. The GHG emissions per unit GDP in Beijing decreased by 74.2%, from 2.2 tCO_2 equivalents/10^4 CNY GDP in 2005 to 0.6 tCO_2 equivalents/10^4 CNY GDP. Meanwhile, the greenhouse gas emissions per unit GDP in Shenzhen decreased by 39.7%, from 0.7 t CO_2 equivalents/10^4 CNY GDP in 2005 to 0.4 t CO_2 equivalents/10^4 CNY GDP in 2020. Although the GHG emissions per unit GDP in Beijing were higher than those in Shenzhen, their reduction was greater, and the gap between the two cities has clearly narrowed. This proves Beijing's efforts in optimizing industrial production structures, adjusting energy structures, vigorously introducing natural energy sources, and improving energy efficiency.

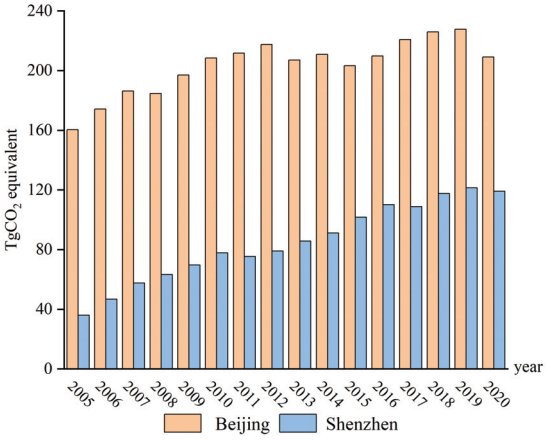

Figure 1. Total GHG emissions of Beijing and Shenzhen.

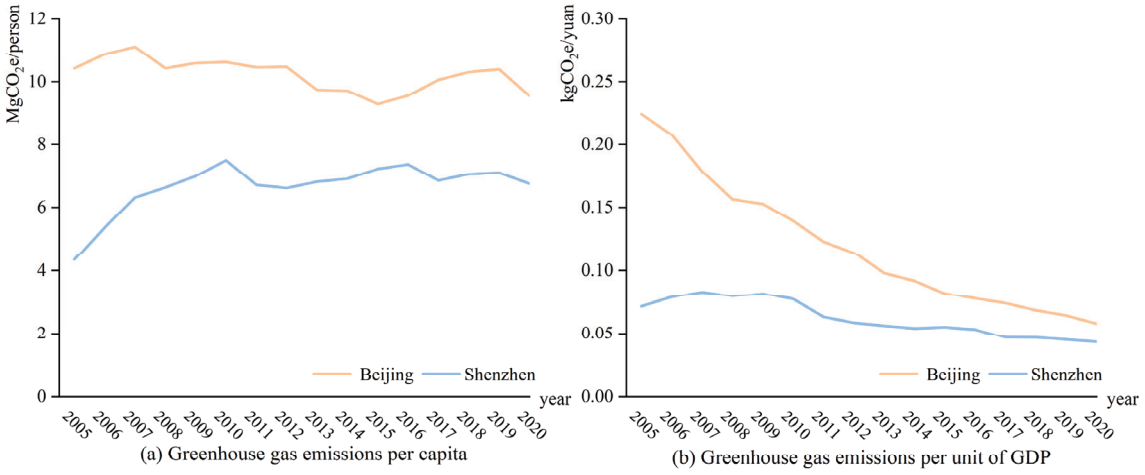

Figure 2. GHG emission intensities of Beijing and Shenzhen.

3.1.2. Characteristics of Sectoral GHG Emissions

Energy activities were still the main source of GHG emissions in Beijing and Shenzhen from 2005 to 2020 (Figures 3 and 4). Although the highest average proportion of GHG emissions from energy activities in Beijing was 82.5%, its emission structure changed significantly. The GHG emissions from energy consumption decreased by 4.0% (Figure 4a), while the GHG emissions from external energy transfer increased gradually, increasing by 93.8% in 2020 compared to 2005. Overall, the GHG emissions from energy activities in Shenzhen showed an increasing trend, increasing by 214.4% in 2020 compared to 2005, but the proportion of GHG emissions from energy activities in the total GHG emissions decreased slightly, from 75.9% in 2005 to 72.0% in 2020 (Figure 4b). In 2007, Shenzhen changed from energy transfer out to energy transfer in, and the amount of energy transfer in gradually increased; thus, the GHG emissions from energy transfer out increased from 710.2 $GgCO_2$ equivalents in 2007 to 11,778.8 $GgCO_2$ equivalents in 2020.

The greenhouse gas emissions from industrial production processes in Beijing have shown a significant downward trend, decreasing by 77.2% from 8.9 $TgCO_2$ equivalents in 2005 to 2.0 $TgCO_2$ equivalents in 2020 (Figure 4c); among these emissions, the GHG emissions from the cement and steel industries decreased by 75.8% and 80.9%, respectively.

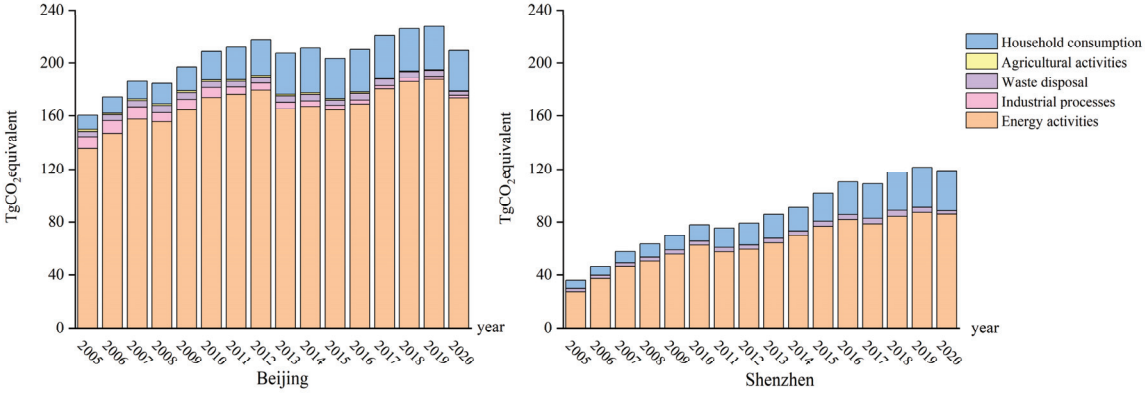

Figure 3. GHG emissions in Beijing and Shenzhen from 2005 to 2020.

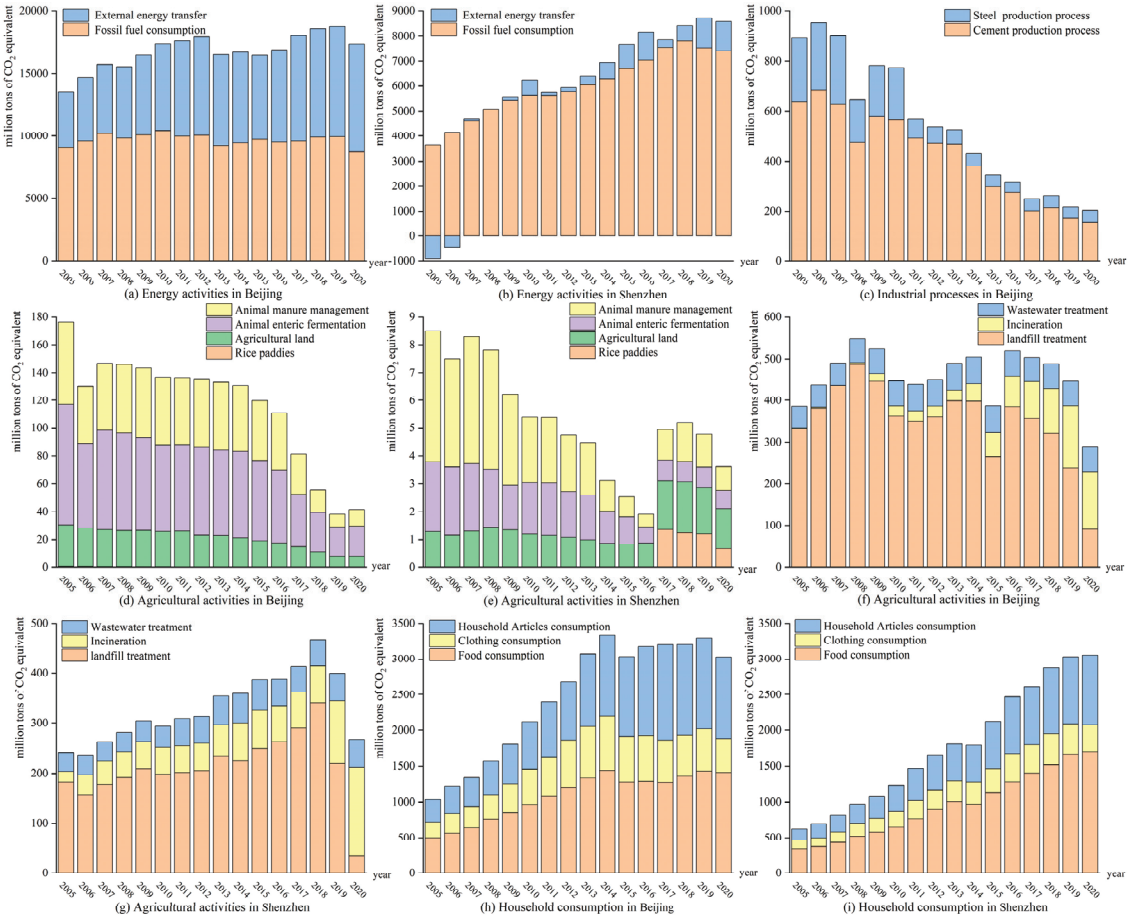

Figure 4. Sectoral GHG emissions in Beijing and Shenzhen from 2005 to 2020. Note: (**a**–**i**) refers to each department.

Overall, Beijing's waste disposal GHG emissions started to decrease gradually in 2008, increased slightly in 2013, and then gradually decreased again from 2016, with an overall decrease of 25.3% in 2020 compared to 2005 (Figure 4d). Shenzhen's waste disposal GHG emissions showed a trend of first increasing and then decreasing, with a 42.65% decrease in 2020 compared to 2018 (Figure 4e). The GHG emissions from waste disposal in Beijing and Shenzhen changed from the highest proportion corresponding to landfill disposal to the highest proportion corresponding to incineration disposal. The GHG emissions from incineration treatment in Beijing and Shenzhen increased from 20.1 and 213.5 $GgCO_2$ equivalents in 2005 to 1378 and 1759.9 $GgCO_2$ equivalents in 2020, respectively, and the GHG emissions from landfill treatment decreased from 3311.6 and 1825.5 $GgCO_2$ equivalents in 2005 to 907.8 and 356.0 $GgCO_2$ equivalents by 2020, respectively.

From 2005 to 2014, the GHG emissions from household consumption in Beijing significantly increased (Figure 4f), with an average annual growth rate of 13.9%. After 2016, the changes tended to flatten out, with an average annual growth rate of −1.57% in 2020 compared to 2016. The greenhouse gas emissions from household consumption in Shenzhen steadily increased (Figure 4g), with a growth rate of 394.3% in 2020 compared to 2005 and an average annual growth rate of 11.2%.

The GHG emissions from agricultural activities in Beijing generally showed a decreasing trend, with a decrease of 76.5% in 2020 compared to 2005 (Figure 4h). GHG emissions from agricultural activities in Shenzhen gradually decreased from 2005 to 2016 and increased significantly in 2017 (Figure 4i), mainly due to an increase in the area of rice paddies sown in Shenzhen in 2017, resulting in an increase in GHG emissions from agricultural activities.

3.1.3. Components of GHG Emissions

Both cities had the highest proportions of CO_2 emissions (Figures 5 and 6), at over 90%, followed by CH_4, and the lowest share of N_2O emissions, the GWP of which accounted for less than 1% of the GHG emissions; in addition, in both cities, the proportions of CO_2 gradually increased, while the proportions of CH_4 and N_2O showed decreasing trends year by year. The Beijing CO_2 emissions showed a fluctuating upward trend from 2005 to 2020, with an increase of 33.9% in 2020 compared to 2005, while the Shenzhen CO_2 emissions increased steadily during 2005–2020, with a growth rate of 250.7%.

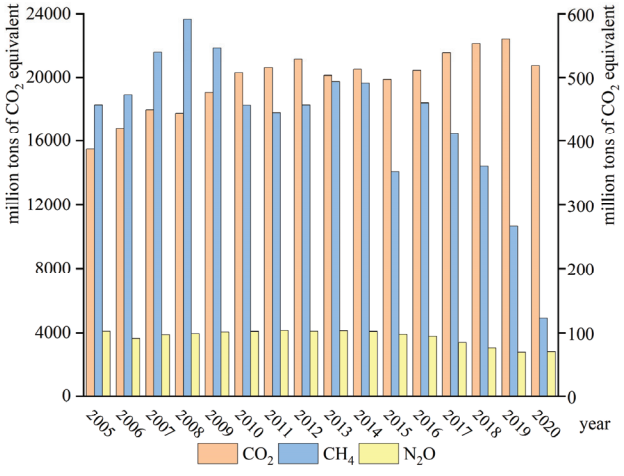

Figure 5. Emissions of CO_2, CH_4, and N_2O in Beijing from 2005 to 2020.

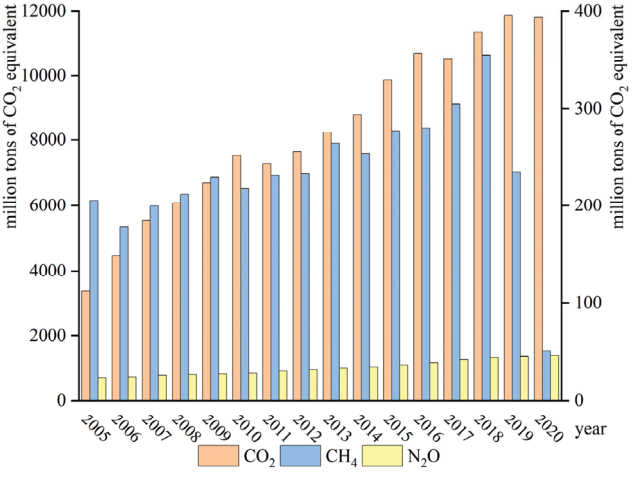

Figure 6. Emissions of CO_2, CH_4, and N_2O in Shenzhen from 2005 to 2020.

The CH_4 emissions in Beijing exhibited large changes, first decreasing by 28.4% in 2015 compared to 2014, and then rapidly decreasing from 2016. The Beijing People's Government introduced waste-treatment-related policies in 2013, requiring Beijing to reduce the amount of waste landfill disposal to less than 30% by the end of 2015 and, further, to build an industrial system of clean and circular development in the 13th Five-Year Plan period, thereby keeping the amount of disposed waste to a minimum and developing efficient and modern agriculture, through which CH_4 emissions could be gradually reduced. CH_4 emissions in Shenzhen showed a trend of first increasing and then decreasing. The increase was obvious in 2018, and the emissions decreased rapidly after 2018. The decrease in 2020 was 85.92% compared to 2018, possibly related to the waste disposal methods applied in Shenzhen, the increase in waste landfills in Shenzhen in 2018, and Shenzhen fully promoting the "waste-free city" construction pilot work in 2019 to achieve the full amount of domestic waste incineration and tend towards zero landfill, causing CH_4 emissions to be reduced.

The N_2O emission proportions of the two cities were the lowest, and their global warming potential was less than 1%. The average annual N_2O emissions in Beijing from 2005 to 2020 were 892.3 $GgCO_2$ equivalents, with a gradual decrease of 29.4%, and in Shenzhen from 2005 to 2020 they were 330.42 $GgCO_2$ equivalents, with an increasing trend of 96.2%. N_2O emissions were generated in the agricultural activity sector and the wastewater treatment sector. In recent years, Beijing has adopted measures such as fertilizer saving and pesticide saving to build new agricultural industries. The number of animal stocks in 2020 decreased by 74.6% compared to that in 2005, so the N_2O emissions decreased significantly. The N_2O emissions from agricultural activities in Shenzhen decreased by 35.9%, but overall, the N_2O emissions increased by 96.2%; the main reason for this is that the N_2O emissions from wastewater treatment in 2020 had increased by 113.0% compared to 2005.

3.1.4. Carbon Sinks in Beijing and Shenzhen

The carbon sink of Beijing increased from 3674.9 $GgCO_2$ in 2005 to 4698.1 $GgCO_2$ in 2020, among which the carbon sink of forestlands made the largest contribution to the GHG emission reduction (Figure 7), accounting for more than 77% of the total GHG absorption of the five land types, followed by the carbon sinks of garden plots, grasslands, cultivated lands, and wetlands, which contributed less to reducing the GHG emissions. The overall trend of the carbon sink of Shenzhen decreased and then increased, and it increased significantly in 2020, with a total carbon sink of 397.0~544.2 $GgCO_2$ equivalents, among which the carbon sinks of forestlands, wetlands, and garden plots in Shenzhen contributed the most to reducing the GHG emissions. The contributions of grasslands and cultivated lands to reducing the GHG emissions were small.

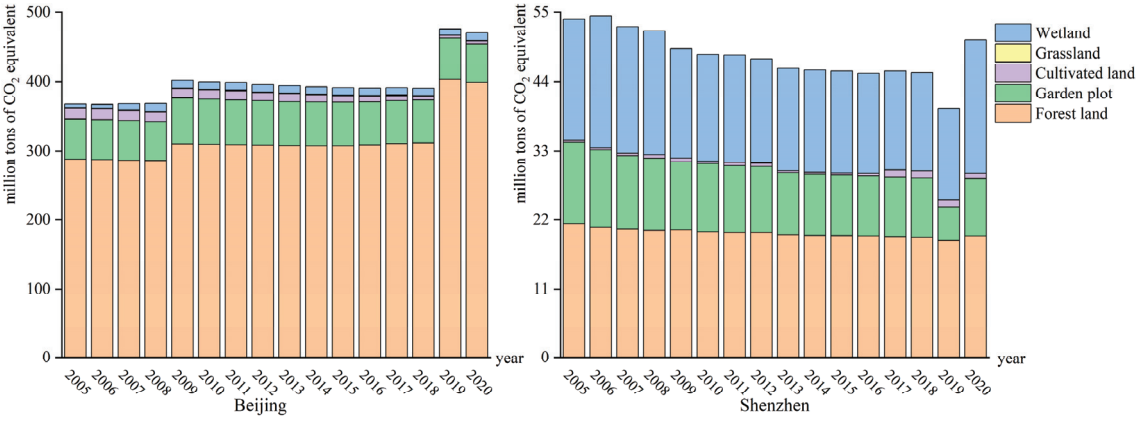

Figure 7. Carbon sinks in Beijing and Shenzhen from 2005 to 2020.

3.1.5. Net GHG Emissions in Beijing and Shenzhen

Net emissions are GHG emissions minus carbon sinks. The net emissions of GHGs in Beijing from 2005 to 2020 were 156.6~222.9 $TgCO_2$ equivalents, and the neutralization rates of carbon sinks to total GHG emissions ranged from 1.7% to 2.3% (Figure 8). Shenzhen's GHG emissions increased significantly from 2005 to 2020, but the growth rate showed a slowing trend. The net GHG emissions increased from 35.4 $TgCO_2$ equivalents in 2005 to 118.5 $TgCO_2$ equivalents in 2020—an increase of 234.7%. The neutralizing effect of carbon sinks on total GHG emissions declined overall, from 1.5% of GHG emissions in 2005 to 0.4% of GHG emissions in 2020.

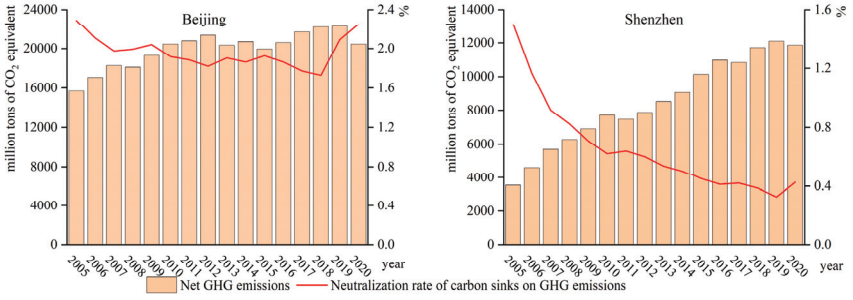

Figure 8. Net GHG emissions in Beijing and Shenzhen.

3.2. Influencing Factors on the GHG Budget in Beijing and Shenzhen

3.2.1. Multicollinearity Testing

A correlation analysis and ordinary least-squares (OLS) estimation were conducted based on the GHG emissions in Beijing and Shenzhen, and significant correlations were found between the emissions and a series of independent variables (Table 10). Secondly, multiple linear regression was performed using OLS, and the results showed that the variance inflation factor (VIF) for all independent variables was greater than 10 (Table 11). Based on these findings, it can be concluded that there was multicollinearity among the independent variables. Therefore, the analysis of the factors influencing greenhouse gas budgets adopted the ridge regression method.

Table 10. Correlation test results.

1. Beijing								
	lnI	lnP_1	lnP_2	lnP_3	lnA_1	lnA_2	lnT_1	lnT_2
lnI	1.000							
lnP_1	0.923 **	1.000						
lnP_2	−0.898 **	−0.850 **	1.000					
lnP_3	0.917 **	0.973 **	−0.892 **	1.000				
lnA_1	0.865 **	0.926 **	−0.891 **	0.970 **	1.000			
lnA_2	0.884 **	0.960 **	−0.864 **	0.979 **	0.987 **	1.000		
lnT_1	−0.845 **	−0.912 **	0.909 **	−0.950 **	−0.988 **	−0.970 **	1.000	
lnT_2	−0.795 **	−0.888 **	0.828 **	−0.941 **	−0.985 **	−0.973 **	0.962 **	1.000
2. Shenzhen								
	lnI	lnP_1	lnP_2	lnA_1	lnA_2	lnT_1	lnT_2	
lnI	1.000							
lnP_1	0.952 **	1.000						
lnP_2	0.938 **	0.979 **	1.000					
lnA_1	0.981 **	0.981 **	0.964 **	1.000				
lnA_2	0.966 **	0.995 **	0.978 **	0.986 **	1.000			
lnT_1	−0.970 **	−0.990 **	−0.977 **	−0.983 **	−0.993 **	1.000		
lnT_2	−0.937 **	−0.996 **	−0.969 **	−0.980 **	−0.988 **	0.981 **	1.000	

Notes: ** indicates significance at the 1% level.

Table 11. OLS results.

Variables	Unstandardized Coefficients	t-Statistic	Sig.	VIF
1. Beijing				
Constant	14.130	0.908	0.390	
$\ln P_1$	0.271	0.763	0.467	44.684
$\ln P_2$	−4.364	−2.252	0.054	10.617
$\ln P_3$	−1.479	−0.382	0.713	65.472
$\ln A_1$	0.623	2.013	0.079	349.091
$\ln A_2$	0.187	0.937	0.376	135.634
$\ln T_1$	0.951	2.750	0.025	67.323
$\ln T_2$	0.369	2.446	0.040	81.172
R^2	0.963			
F test	29.392			
Sig.	0.000			
2.Shenzhen				
Constant	−0.434	−0.061	0.953	
$\ln P_1$	2.074	2.337	0.044	528.617
$\ln P_2$	−1.134	−1.935	0.085	28.973
$\ln A_1$	1.481	6.915	0.000	45.535
$\ln A_2$	−0.128	−0.312	0.762	192.359
$\ln T_1$	−1.145	−1.400	0.195	90.131
$\ln T_2$	1.903	4.532	0.001	200.276
R^2	0.993			
F test	214.656			
Sig.	0.000			

3.2.2. Influencing Factors on the Total GHG Budget

In recent years, the land-use changes in Beijing and Shenzhen have been relatively small, resulting in relatively small changes in carbon sinks. The average annual growth rate of the carbon sinks in Beijing from 2005 to 2018 was 0.5%. The average annual decrease in the carbon sinks in Shenzhen from 2005 to 2020 was 0.4%, so the influence of various factors on the carbon sinks was not significant. Therefore, this paper analyzes the influence of each factor on the total and net GHG emissions in Beijing and Shenzhen (Table 12). The population promoted GHG emissions in both Beijing and Shenzhen, the urbanization rate promoted GHG emissions in Beijing, and the household size had opposing effects on GHG emissions in the two cities. The GDP per capita and resident consumption levels contributed to GHG emissions in Beijing and Shenzhen, with a greater impact observed in Shenzhen. The proportion of secondary industry and the energy intensity had more significant impacts in Shenzhen, where they were negatively correlated with GHG emissions.

Table 12. Results of the ridge regression analysis for Beijing and Shenzhen.

	Beijing		Shenzhen	
	Total GHG Emissions	Net GHG Emissions	Total GHG Emissions	Net GHG Emissions
$\ln P_1$ (population)	0.181 **	0.185 **	0.180 **	0.175 **
$\ln P_2$ (household size)	−2.083 **	−2.122 **	0.487 **	0.470 **
$\ln P_3$ (urbanization rate)	1.256 **	1.263 **	-	-
$\ln A_1$ (GDP per capita)	0.019 **	0.019 *	0.243 **	0.270 **
$\ln A_2$ (resident consumption level)	0.030 **	0.031 **	0.172 **	0.179 **
$\ln T_1$ (proportion of secondary industry)	−0.026	−0.025	−0.553 **	−0.591 **
$\ln T_2$ (energy intensity)	0.003	0.003	−0.110 **	−0.097 **
Constant	4.839	4.788	7.910	8.037
R^2	0.864	0.862	0.933	0.936
Sig	0.006	0.006	0.000	0.000

Note: ** and * indicate significance at the 5% and 10% levels, respectively.

3.2.3. Factors Influencing the Sectoral GHG Budget

In Beijing's energy activity sector, the population, urbanization rate, and household size had relatively great degrees of influence on GHG emissions, with the population and urbanization rate promoting GHG emissions and the household size playing a negative role (Table 13). In the industrial process sector, the urbanization rate, GDP per capita, residential consumption level, proportion of secondary industry, and energy intensity had relatively great influences on GHG emissions, with the increase in the urbanization rate, GDP per capita, and residential consumption level suppressing GHG emissions, while the proportion of secondary industry and the energy intensity played positive roles. In the household consumption sector, increases in the population, urbanization rate, GDP per capita, and residential consumption level promoted GHG emissions, while the proportion of secondary industry and the energy intensity played negative roles. In the agricultural activity sector, the population, proportion of secondary industry, and energy intensity promoted GHG emissions, the GDP per capita played a negative role in GHG emissions, and the household size, urbanization rate, and resident consumption level had less significant roles in affecting GHG emissions. The impact of each influencing factor on GHG emissions from the waste disposal sector in Beijing was not significant.

Table 13. Results of the analysis of influencing factors on GHG emissions by sector in Beijing.

	Energy Activities	Industrial Processes	Household Consumption	Agricultural Activities
$\ln P_1$ (population)	0.115 *	−0.127	0.837 **	1.054 **
$\ln P_2$ (household size)	−2.518 **	2.831	−1.934	6.119
$\ln P_3$ (urbanization rate)	1.074 **	−3.393 **	4.996 **	−1.834
$\ln A_1$ (GDP per capita)	0.018 *	−0.240 **	0.100 **	−0.296 **
$\ln A_2$ (resident consumption level)	0.019 *	−0.206 **	0.168 **	−0.107
$\ln T_1$ (proportion of secondary industry)	−0.028	0.636 **	−0.198 **	0.649 **
$\ln T_2$ (energy intensity)	0.007	0.290 **	−0.084 **	0.335 **
Constant	6.412	19.19	−19.296	−1.485
R^2	0.807	0.920	0.935	0.753
Sig	0.021	0.001	0.000	0.051

Note: ** and * indicate significance at the 5% and 10% levels, respectively.

In Shenzhen's energy activity sector, the population, GDP per capita, and residential consumption level had significant promoting effects on GHG emissions, while the proportion of secondary industry had a negative effect (Table 14). In the waste disposal sector, the population, GDP per capita, and residential consumption level played promoting roles, while the proportion of secondary industry and the energy intensity played negative roles. The GHG emissions of the household consumption sector increased with increasing population, household size, GDP per capita, and residential consumption level, while the proportion of secondary industry and the energy intensity had negative effects. The impact of each influencing factor on GHG emissions from the agricultural activity sector in Shenzhen was less significant.

Table 14. Results of the analysis of influencing factors on GHG emissions by sector in Shenzhen.

	Energy Activities	Waste Disposal	Household Consumption
$\ln P_1$ (population)	0.141 **	0.092 **	0.313 **
$\ln P_2$ (household size)	0.389 *	−0.053	0.840 **
$\ln A_1$ (GDP per capita)	0.264 **	0.137 **	0.313 **
$\ln A_2$ (resident consumption level)	0.158 **	0.126 **	0.259 **
$\ln T_1$ (proportion of secondary industry)	−0.564 **	−0.210 *	−0.734 **
$\ln T_2$ (energy intensity)	−0.063	−0.069 *	−0.237 **
Constant	8.143	5.174	4.945
R^2	0.888	0.633	0.988
Sig	0.001	0.096	0.000

Note: ** and * indicate significance at the 5% and 10% levels, respectively.

3.2.4. Influencing Factors of the Categorical GHG Budget

Ridge regression analysis showed that the influence of each factor on CH_4 emissions in Beijing and Shenzhen was not significant; therefore, this study analyzed the influence of each influencing factor on the CO_2 and N_2O budgets (Table 15).

Table 15. Influencing factors of the categorical GHG budgets in Beijing and Shenzhen.

	Beijing		**Shenzhen**	
	CO_2	**N_2O**	**CO_2**	**N_2O**
lnP_1 (population)	0.202 **	0.467 **	0.179 **	0.161 **
lnP_2 (household size)	−2.403 **	1.848	0.499 **	0.417 **
lnP_3 (urbanization rate)	1.471 **	0.274	-	-
lnA_1 (GDP per capita)	0.021 *	−0.087 **	0.278 **	0.090 **
lnA_2 (resident consumption level)	0.034 **	−0.018	0.181 **	0.112 **
lnT_1 (proportion of secondary industry)	−0.018	0.206	−0.610 **	−0.297 **
lnT_2 (energy intensity)	0.005	0.110 **	−0.098 **	−0.119 **
Constant	3.937	−2.253	7.986	2.191
R^2	0.890	0.637	0.934	0.987
Sig	0.003	0.174	0.000	0.000

Note: ** and * indicate significance at the 5% and 10% levels, respectively.

The analysis of the factors influencing the CO_2 budget in Beijing shows that the population, urbanization rate, GDP per capita, and resident consumption level played positive roles, the household size played a negative role, and the energy intensity and the proportion of secondary industry had no significant impact. The analysis results of the factors influencing N_2O emissions in Beijing indicate that the population and energy intensity played positive roles, the GDP per capita played a negative role, and the household size, urbanization rate, residential consumption level, and proportion of secondary industry were less significant.

The analysis of influencing factors in Shenzhen shows that each factor had a consistent effect on the CO_2 and N_2O emissions. The population, household size, GDP per capita, and residential consumption level all played roles in promoting the CO_2 budget and N_2O emissions, with the household size contributing most strongly. The proportion of secondary industry and the energy intensity both played negative roles in GHG emissions.

4. Discussion

4.1. Comparison of the Characteristics of the GHG Budgets in Beijing and Shenzhen

The main source of GHG emissions in both Beijing and Shenzhen is the energy activity sector. The GHG emissions from energy consumption in Beijing's energy activity sector decreased slightly over the study period, while the GHG emissions from external energy transfer gradually increased. This was due mainly to the various measures taken by Beijing in recent years, such as implementing the conversion of coal to electricity, vigorously introducing high-quality energy such as electricity and natural gas, and reducing residents' energy use [59]. At the same time, the traditional energy-consuming industries underwent a comprehensive transformation, resolutely eliminating high-energy-consuming production industries and introducing equipment with low consumption and lower emissions to high-tech industries to replace energy-intensive industries. This finding is consistent with the study by Xue et al. [58] on GHG emissions in Beijing.

GHG emissions from energy activities in Shenzhen showed an increasing trend overall. In 2007, the mode changed from energy transfer out to energy transfer in, and the amount of energy transfer gradually increased. Shenzhen has developed rapidly in recent years. On the one hand, due to its increasing urban population, energy consumption in transportation and energy consumption in life have increased significantly [60]; on the other hand, to cope with the air pollution problem in megacities, Shenzhen has carried out electrification reform of its manufacturing industry, and this has promoted the increasing demand for

electricity; these findings are consistent with the study results of Liao et al. [61] obtained in Shenzhen.

The GHG emissions from industrial processes in Beijing decreased gradually from 2006 to 2008, increased slightly in 2009 and 2010, and continued to decrease from 2011; this change trend is consistent with the findings of Liu [50].

In Beijing and Shenzhen, the greatest proportion of GHG emissions from waste disposal changed from the landfill source to the incineration source, mainly because the two cities adjusted their waste treatment structures in recent years, thereby increasing their incineration rates and reducing their landfill rates. Beijing has accelerated the construction of waste incineration treatment plants in recent years and increased the incineration rates of household waste to more than 70%. In 2019, Shenzhen comprehensively promoted the pilot construction of a "waste-free city" and achieved the total incineration of household waste and near-zero landfill. As a result, the landfill disposal of waste in Beijing and Shenzhen decreased significantly. The above results are similar to the findings of Zhang et al. [62,63].

Beijing's GHG emissions from household consumption increased gradually from 2005 to 2014, with smaller changes observed from 2016 to 2020; Shenzhen's GHG emissions from household consumption increased gradually from 2005 to 2020, and the highest percentage of GHG emissions from household consumption in both cities was from food consumption. Studies have shown that [64–66] GHG emissions from household consumption are related mainly to the population size and income level. Beijing's population showed a gradual increasing trend from 2005 to 2014, and the increase in the urban population increased the demands for food and other consumer goods as well as increasing GHG emissions. From 2016 to 2020, Beijing's population showed a slight decreasing trend, so the change range of GHG emissions was small. With the continuous increase in the population of Shenzhen, the demands for clothing, food, and household articles have increased, resulting in an increase in GHG emissions, and with their increased incomes, people now have increasingly higher requirements for food quality, resulting in increasing indirect emissions.

The scale of agriculture in Beijing and Shenzhen has been decreasing in recent years; the sown area of rice paddies in Beijing decreased by 73.3%, while the stock of major animals decreased by 74.6%, and the stock of major animals in Shenzhen decreased by 69.8%. In recent years, both cities have carried out pollution control measures on large-scale breeding farms, improved their agricultural production technology, and developed a conservation-oriented agriculture that is resource-saving and land-saving, so their agricultural-activities-related GHG budget has decreased. Shenzhen's agricultural activities increased significantly in 2017, mainly due to the increase in the area of rice paddies sown in Shenzhen in 2017, resulting in an increase in GHG emissions from agricultural activities.

The total carbon sink of Beijing was larger than that of Shenzhen, and the neutralization rate of the carbon sink to GHG emissions was also higher than that of Shenzhen, partly because of the abundance of forestlands and other land resources in Beijing [67], and partly because of the larger growth of GHG emissions in Shenzhen. Forestlands contributed the most to the carbon sink in Beijing, while forestlands and wetlands contributed the most to the carbon sink in Shenzhen; these differences are mainly related to the geographical locations of Beijing and Shenzhen. Shenzhen is a coastal city with abundant wetland resources [68], so the carbon sink of wetlands is larger there than in Beijing.

4.2. Differences in the Influencing Factors of the GHG Budget in Beijing and Shenzhen

4.2.1. Population Size

The increasing populations have played a role in increasing GHG emissions in both Beijing and Shenzhen, with population growth leading to increased demands for energy and urban household consumer goods, thereby generating more GHG emissions. The increased urbanization rate has promoted GHG emissions in Beijing, and the migration of the rural population into cities, the growth of urban construction lands, and changes in people's consumption patterns all produce more GHG emissions, as has been proven by a large number of studies [32,69].

The household size had opposite influences on GHG emissions in Beijing and Shenzhen. The number of households in Beijing increased by 23.4% from 2005 to 2020, while the growth rate of the registered population was 18.6%. The registered population was smaller than the increase in the number of households, resulting in a constant decrease in the household size in Beijing. Meanwhile, the number of households in Shenzhen increased by 104.60% from 2005 to 2020. The growth rate of the registered population was 172.0%, and the registered population number was greater than the increase in the number of households, causing the household size in Shenzhen to increase continuously. It has been shown that an increase in the number of urban households and a decrease in the household size can cause increased emissions in terms of household energy and other aspects [70], and the household size in Beijing has been decreasing in recent years; thus, CO_2 emissions are expected to increase as the household size decreases. Significant increases in the number of households and the registered population of Shenzhen will bring more demands for energy and other resources, so an increase in the household size will increase Shenzhen's greenhouse gas emissions.

4.2.2. Economic Development

Using the GDP per capita and residential consumption level to represent the changes in urban economic development, the regression results show that economic development influenced GHG emissions to different degrees in the two cities, and that the degree of influence was greater for Shenzhen than for Beijing. Therefore, this paper further explores the relationship between economic development and GHG emissions using the Tapio decoupling model [71,72]. The Tapio decoupling model divides the decoupling status into three major categories and eight subcategories according to the decoupling index T (Table 16). The decoupling indices were calculated separately for Beijing and Shenzhen (Table 17). Beijing was in a decoupling state between GHG emissions and economic development from 2005 to 2020, indicating that Beijing's economic development was no longer at the cost of high GHG emissions. However, the relationship between GHG emissions and economic development in Shenzhen was mostly expansionary negative decoupling from 2005 to 2010, meaning that the growth rate of GHG emissions far exceeded the growth rate of the economy. From 2010 to 2020, the decoupling state was unstable, with three strong decoupling periods, five weak decoupling periods, and two expanding connection periods. This means that with the increase in the GDP per capita and the residents' consumption level, GHG emissions are increasing. From this point of view, seeking a balance between economic development and emission reductions will remain an important goal of Shenzhen's development in the future.

Table 16. Classification of the decoupling state between GHG emissions and economic development.

ΔGDP	ΔGHG	Decoupling Index T	Decoupling State		
>0	>0	0 < T < 0.8	Weak decoupling	GHG emissions growth rate is lower than that of economic growth	Decoupling
>0	<0	T < 0	Strong decoupling	GHG emissions decrease while GDP increases	
<0	<0	T > 1.2	Recessionary decoupling	GHG emissions decrease faster than economic decline	
>0	>0	T > 1.2	Expansionary negative decoupling	GHG emissions growth rate is faster than economic growth	Negative decoupling
<0	>0	T < 0	Strong negative decoupling	GHG emissions increase while GDP decreases	
<0	<0	0 < T < 0.8	Weak negative decoupling	GHG emissions decrease at a slower pace than economic decline	
>0	>0	0.8 < T < 1.2	Expansionary coupling	GHG emissions growth rate is close to that of economic growth	Coupling
<0	<0	0.8 < T < 1.2	Recessionary coupling	GHG emissions reduction rate is close to that of economic decline	

Table 17. Decoupling between GHG emissions and economic development in Beijing and Shenzhen.

Year	Beijing		Shenzhen	
	Decoupling Index T	**Decoupling State**	**Decoupling Index T**	**Decoupling State**
2005–2006	0.50	Weak decoupling	1.70	Expansionary negative decoupling
2006–2007	0.29	Weak decoupling	1.37	Expansionary negative decoupling
2007–2008	−0.06	Strong decoupling	0.67	Weak decoupling
2008–2009	0.72	Weak decoupling	1.39	Expansionary negative decoupling
2009–2010	0.36	Weak decoupling	0.64	Weak decoupling
2010–2011	0.10	Weak decoupling	−0.17	Strong decoupling
2011–2012	0.26	Weak decoupling	0.37	Weak decoupling
2012–2013	−0.43	Strong decoupling	0.65	Weak decoupling
2013–2014	0.22	Weak decoupling	0.61	Weak decoupling
2014–2015	−0.45	Strong decoupling	1.20	Expansionary coupling
2015–2016	0.35	Weak decoupling	0.68	Weak decoupling
2016–2017	0.50	Weak decoupling	−0.10	Strong decoupling
2017–2018	0.22	Weak decoupling	0.94	Expansionary coupling
2018–2019	0.11	Weak decoupling	0.48	Weak decoupling
2019–2020	−4.39	Strong decoupling	−0.78	Strong decoupling

4.2.3. Technical Level

The effects of the proportion of secondary industry and the energy intensity on GHG emissions differed between the two cities. The effects of the proportion of secondary industry and the energy intensity on GHG emissions in Beijing were less significant, while the effect on GHG emissions from industrial processes in Beijing was more significant. With decreases in the proportion of secondary industry and the energy intensity, the GHG emissions in Beijing's industrial production process decreased. The proportion of secondary industry and the energy intensity negatively affected GHG emissions in Shenzhen.

Secondary industry is usually regarded as a high-GHG-emission sector. In recent years, Beijing has adjusted its industrial structure and changed into a low-consumption production mode, shifting the traditional high-GHG-emission secondary industry to a green and low-carbon tertiary industry. Therefore, the reductions in the proportion of secondary industry and the energy intensity played a role in reducing GHG emissions. The proportion of secondary industry in Shenzhen decreased from 53.8% in 2005 to 37.8% in 2020. Although secondary industry continued to decrease, the GHG emissions brought by secondary industry increased by 12.2%. Therefore, although Shenzhen has followed the "321" industrial economic pattern in recent years, it still needs to further optimize its industrial structure.

The energy intensity denotes the technical level and energy-use efficiency of a city. During the study period, the energy intensity of Beijing and Shenzhen decreased year by year, but the energy intensity had opposite effects on GHG emissions from industrial processes in Beijing and on total GHG emissions in Shenzhen. Beijing reduced its raw coal consumption by 95.8% from 2005 to 2020 by adjusting its energy structure. Therefore, although energy consumption is still increasing, the growth rate slowed down significantly, and the reduction in the energy intensity played a role in reducing the GHG emissions. The energy intensity of Shenzhen played a negative role—on the one hand, because of the rapid economic development of Shenzhen, and on the other hand, because of the continuous increase in energy consumption in Shenzhen. Therefore, although the energy intensity was reduced, the total energy consumption and economic scale expanded, resulting in an increase in GHG emissions. Therefore, the energy structure should be further adjusted.

5. Conclusions

This study comprehensively accounted for the GHG budgets in Beijing and Shenzhen from 2005 to 2020 and investigated the factors affecting the GHG budgets. We found that the total GHG emissions of both cities showed an increasing trend from 2005 and peaked in 2019 before decreasing in 2020. The GHG emissions of Beijing, which increased from 160.3 $TgCO_2$ equivalents in 2005 to 209.1 $TgCO_2$ equivalents in 2020, were always greater than those of Shenzhen (36.0 TgCO2 equivalents in 2005 and 119.1 $TgCO_2$ equivalents in 2020). However, the growth rate of GHG emissions from Shenzhen (231.1%) was almost seven times larger than that of Beijing (30.5%). Energy activities in Beijing and Shenzhen have always been the main emission sectors of GHGs from 2005 to 2020, accounting for more than 70% of the total GHG emissions. Among the three GHGs, CO_2 contributed over 90% to the total emissions, followed by CH_4, (2.2% in Beijing, 3.0% in Shenzhen), while N_2O contributed the lowest proportion of global warming effect (less than 1%). The neutralization rate of carbon sinks on GHG emissions was greater in Beijing (1.7% to 2.3%) than in Shenzhen (0.3% to 1.5%), and the carbon neutrality rate of the ecosystem carbon sink in Shenzhen showed a decreasing trend overall. Forest alone contributed about 79% of Beijing's ecosystem carbon sink, while in Shenzhen, the carbon sink effect of forest, garden, and wetlands contributed 41.3%, 21.2%, and 36.3% of the total urban carbon sink, respectively. Population size, GDP per capita, and residents' consumption level were positively correlated with GHG emissions in both Beijing and Shenzhen. Meanwhile, household size had opposite effects on the two cities, with a decrease in household size and an increase in GHG emissions in Beijing, while there was a positive correlation between household size and GHG emissions in Shenzhen. The increase in the proportion of secondary industry and the energy intensity had more significant impacts on GHG emissions in Shenzhen, where they were negatively correlated with greenhouse gas emissions. Based on the above analysis, the following suggestions and insights are proposed:

1. Promote the high-quality development of urbanization: The rapid development of urbanization is accompanied by population growth and urban expansion, which promote increased GHG emissions. The populations of Beijing and Shenzhen will increase further in the future, so we should focus on the quality of urban development and develop a concentrated and compact urban spatial structure to reduce GHG emissions. At the same time, to reduce the GHG emissions caused by increasing populations, governments should strengthen the publicity of low-carbon consumption and guide residents' awareness of low-carbon consumption to achieve their GHG emission reduction goals.
2. Optimize the industrial structure and adjust the energy structure: Although Beijing and Shenzhen have followed the "321" industrial model, in the process of adjusting their industrial structures and gradually building industrial systems dominated by tertiary industry, attention should also be paid to the internal structure of the tertiary industry; this industry should gradually be transformed into a knowledge-intensive industry with low consumption and low emissions. At the same time, technological upgrading should be strengthened, low-carbon technologies should be developed, the close integration of industry, academia, and research should be promoted, the energy-utilization efficiency should be improved, and GHG emissions should be reduced. Shenzhen should further adjust its energy structure, focus on optimizing its energy structure and layout, reduce its coal consumption, and increase its development and utilization of clean energy and new energy.
3. Increase carbon sinks: Forestry is the main carbon sink resource, and the main countermeasures used to increase the carbon sink capacity include increasing the carbon sequestration capacity, improving the quality of forestland resources, focusing on the conservation of forest trees, expanding the area of forestlands, encouraging the development of unused lands, and giving priority to the conversion of cultivated lands, grasslands, and forestlands, reducing the construction occupation and increasing the area of public green spaces to increase the carbon sink.

Since the relevant activity-level data of Beijing and Shenzhen are not complete, applying different methods to calculate the urban GHG budgets and selecting different GHG emission coefficients would lead to differences in the GHG accounting results. The carbon sink accounting performed in this paper was based on previous studies, so the accounting standard had a certain universality, but because the actual environment of each city has some differences, the calculated results showed some deviation. Moreover, the data used in this paper were obtained from statistical data. There is no more detailed division of land use and vegetation types, and unused land was not considered in the accounting process. As a result, the calculated values were small. Therefore, we hope that in future research the standards and parameter values used to establish an urban GHG budget inventory can be refined to fully conform to the characteristics of Chinese cities and accurately calculate the GHG budgets at different urban scales. The GHG income and expenditure process contains very complex influencing factors that are not only affected by the population size, economic development, and technical level but are also related to many unquantifiable factors, such as climate change, geographic spatial differences, and living habits. Therefore, in future work, multidisciplinary and cross-disciplinary research should be combined with the actual situations of different cities to propose emission reduction measures.

Author Contributions: Conceptualization, K.L. and S.Y.; methodology, K.L., S.Y. and B.H. (Binbin Huang); software, K.L., S.Y. and C.S.; validation, K.L. and S.Y.; formal analysis, K.L., S.Y. and H.W. (Haoqi Wang); investigation, K.L., S.Y. and Z.C.; resources, K.L. and S.Y.; data curation, K.L., S.Y. and T.X.; writing—original draft preparation, K.L. and S.Y.; writing—review and editing, K.L., S.Y., C.X., B.H. (Baolong Han), H.W. (Haijun Wang) and F.L.; visualization, K.L. and S.Y.; supervision, K.L., S.Y., H.W. (Haijun Wang) and F.L.; project administration, K.L., S.Y., H.W. (Haijun Wang) and F.L.; funding acquisition, K.L., S.Y., H.W. (Haijun Wang) and F.L.; K.L. and S.Y. contributed equally to this work. All authors have read and agreed to the published version of the manuscript.

Funding: This work was supported by the National Natural Science Foundation of China (Grant 72174192), the National Key Research and Development Program of China (Grant 2022YFB3903701), the Carbon Peak Carbon Neutrality Eco-Environmental Technology Project of the Research Center for Eco-Environmental Sciences, Chinese Academy of Sciences (Grants RCEES-TDZ-2021-8 and RCEES-TDZ-2021-16), the Major Research Program of Hebei Province (Grant 21373902D), and the Youth Innovation Promotion Association, Chinese Academy of Sciences (Grants 2013030 and 2014312).

Institutional Review Board Statement: Not applicable.

Informed Consent Statement: Not applicable.

Data Availability Statement: The data used to support the findings of this study are available from the author upon request.

Conflicts of Interest: The authors declare no conflict of interest.

References

1. IPCC. *Climate Change 2021: The Physical Science Basis*; Masson-Delmotte, V., Zhai, P., Pirani, A., Connors, S.L., Péan, C., Berger, S., Caud, N., Chen, Y., Goldfarb, L., Gomis, M.I., Eds.; Cambridge University Press: Cambridge, UK; New York, NY, USA, 2021.
2. Yang, T.; Fang, L.; Wang, H.L. Total Carbon Emission Accounting and the Determination of Carbon Peak at the District and County Scale. *J. Energy Conserv. Environ. Prot.* **2021**, *8*, 37–39.
3. Zhang, Y.; Lu, H.J.; Zheng, H.M. Progress in the study of nitrogen cycling and nitrogen metabolism under the influence of multi-scale human activities. *Chin. J. Popul. Resour. Environ.* **2016**, *26*, 417–422.
4. Cai, B.; Wang, J.; Yang, S.; Mao, X.; Cao, L. Carbon dioxide emissions from cities in China based on high resolution emission gridded data. *Chin. J. Popul. Resour. Environ.* **2017**, *15*, 58–70. [CrossRef]
5. Gurney, K.R.; Kılkış, Ş.; Seto, K.C.; Lwasa, S.; Moran, D.; Riahi, K.; Keller, M.; Rayner, P.; Luqman, M. Greenhouse gas emissions from global cities under SSP/RCP scenarios, 1990 to 2100. *Glob. Environ. Change* **2022**, *73*, 102478. [CrossRef]
6. Zhao, H.X. *Research on the Relationship between Chinese Urbanization Development and Carbon Emissions*; Jilin University: Changchun, China, 2015.
7. Cai, M.M.; Zhao, M.; Wu, K.Y. Impact of urbanization on carbon emission in Shanghai. *J. Anhui Agric. Univ.* **2017**, *44*, 81–86.
8. Shan, Y.; Guan, D.; Hubacek, K.; Zheng, B.; Davis, S.J.; Jia, L.; Liu, J.; Liu, Z.; Fromer, N.; Mi, Z.; et al. City-level climate change mitigation in China. *Sci. Adv.* **2018**, *4*, eaaq0390. [CrossRef] [PubMed]

9. Zhang, M.; Huang, X.J.; Chuai, X.W. Research on China's urban carbon emission accounting and influencing factors. *Ecol. Econ.* **2019**, *35*, 13–19+74.
10. Huang, R.Q.; Zeng, Q. Research on the dynamic evolution and grade assessment of carbon emission in Xi'an. *Environ. Sci. Sur.* **2023**, *42*, 1–8.
11. Mutlu, V.; Cindoruk, Y.O.; Cindoruk, S.S. Evaluation of Bursa metropolitan greenhouse Gas inventory and reduction targets. *Urban Clim.* **2020**, *34*, 100717. [CrossRef]
12. Liu, J.B.; Xu, X.Y.; Li, S.W. Lifecycle carbon footprint analysis of China's power industry. *Chin. J. Popul. Resour. Environ.* **2022**, *32*, 31–41.
13. Markolf, S.A.; Matthews, H.S.; Azevedo, I.L.; Hendrickson, C. An integrated approach for estimating greenhouse gas emissions from 100 U.S. metropolitan areas. *Environ. Res. Lett.* **2017**, *12*, 024003. [CrossRef]
14. Castrejón-Godínez, M.L.; Sánchez-Salinas, E.; Rodríguez, A.; Ortiz-Hernández, M.L. Analysis of solid waste management and greenhouse gas emissions in Mexico: A study case in the central region. *J. Environ. Prot.* **2015**, *6*, 146. [CrossRef]
15. Guo, Y.J.; Gong, Y.P.; Zou, Y.F.; Ying, Z.; Jiangdu, L.; Xinyi, Z. Temporal variation characterstics and influencing factors of carbon emissions from municipal solid waste treatment in Tianjin. *J. Environ. Engr. Technol.* **2022**, *12*, 834–842.
16. Hachaichi, M.; Baouni, T. Virtual carbon emissions in the big cities of middle-income countries. *Urban Clim.* **2021**, *40*, 100986. [CrossRef]
17. Guo, Z. *Analysis on the Characteristics and Influence Factors of Carbon Emission Urban Typical with Household Consumption in Beijing*; University of Chinese Academy of Sciences: Beijing, China, 2015.
18. Carpio, A.; Ponce-Lopez, R.; Lozano-García, D.F. Urban form, land use, and cover change and their impact on carbon emissions in the Monterrey Metropolitan area, Mexico. *Urban Clim.* **2021**, *39*, 100947. [CrossRef]
19. Wang, W.J.; Lu, F.; Ou Yang, Z.Y. Spatial identification of territory space ecological conservation and restoration: A case study of Beijing. *Acta Ecol. Sin.* **2022**, *42*, 2074–2085.
20. Zheng, Y.; Lu, F.; Liu, J.R.; Wang, X.K. Comparative study on CO_2 emissions from fossil energy consumption and its influencing factors in typical of China. *Acta ecol. Sin.* **2020**, *40*, 3315–3327.
21. Xu, G.Q.; Liu, Z.Y.; Jiang, Z.H. Decomposition model and empirical study of carbon emissions for China, 1995–2004. *Chin. J. Popul. Resour. Environ.* **2006**, *6*, 158–161.
22. Wang, Y.; Chen, W.; Kang, Y.; Li, W.; Guo, F. Spatial correlation of factors affecting CO_2 emission at provincial level in China: A geographically weighted regression approach. *J. Clean. Prod.* **2018**, *184*, 929–937. [CrossRef]
23. Ang, B.W.; Zhang, F.G.; Choi, K.-H. Factorizing changes in energy and environmental indicators through decomposition. *Energy* **1998**, *23*, 489–495. [CrossRef]
24. Ehrlich, P.; Holdren, J. Impact of population growth. *Popul. Resour. Environ.* **1972**, *3*, 365–377.
25. Dietz, T.; Rosa, E.A. Effects of population and affluence on CO_2 emissions. *Proc. Natl. Acad. Sci. USA* **1997**, *94*, 175–179. [CrossRef]
26. Zhou, Y.; Shan, Y.; Liu, G.; Guan, D. Emissions and low-carbon development in Guangdong-Hong Kong-Macao Greater Bay Area cities and their surroundings. *Appl. Energy* **2018**, *228*, 1683–1692. [CrossRef]
27. Svirejeva-Hopkins, A.; Schellnhuber, H.J. Urban expansion and its contribution to the regional carbon emissions: Using the model based on the population density distribution. *Ecol. Model.* **2008**, *216*, 208–216. [CrossRef]
28. Strohbach, M.W.; Haase, D. Above-ground carbon storage by urban trees in Leipzig, Germany: Analysis of patterns in a European city. *Landscape Urban Plan.* **2012**, *104*, 95–104. [CrossRef]
29. Pataki, D.E.; Alig, R.J.; Fung, A.S.; Golubiewski, N.E.; Kennedy, C.A.; McPherson, E.G.; Nowak, D.J.; Pouyat, R.V.; Romero Lankao, P. Urban ecosystems and the North American carbon cycle. *Glob. Chang. Biol.* **2006**, *12*, 2092–2102. [CrossRef]
30. Creutzig, F.; Baiocchi, G.; Bierkandt, R.; Pichler, P.P.; Seto, K.C. Global typology of urban energy use and potentials for an urbanization mitigation wedge. *Proc. Natl. Acad. Sci. USA* **2015**, *112*, 6283–6288. [CrossRef]
31. Croci, E.; Melandri, S.; Molteni, T. Determinants of cities' GHG emissions: A comparison of seven global cities. *Int. J. Clim. Chang Str.* **2011**, *3*, 275–300. [CrossRef]
32. Li, Z.; Deng, X.Z.; Peng, L. Uncovering trajectories and impact factors of CO_2 emissions: A sectoral and spatially disaggregated revisit in Beijing. *Technol. Forecast. Soc. Chang.* **2020**, *158*, 120124. [CrossRef]
33. Zhou, Y.; Li, Y.P.; Huang, G.H. Planning sustainable electric-power system with carbon emission abatement through CDM under uncertainty. *Appl. Energy* **2015**, *140*, 350–364. [CrossRef]
34. Energy Statistics Division, National Bureau of Statistics. *China Energy Statistical Yearbook*; China Statistics Press: Beijing, China, 2011.
35. Guangdong Provincial Bureau of Statistics, National Bureau of Statistics. *Guangdong Statistical Yearbook*; China Statistics Press: Beijing, China, 2006.
36. Shenzhen Municipal Bureau of Statistics. *Shenzhen Statistical Yearbook*; China Statistics Press: Beijing, China, 2006.
37. Shan, Y.; Guan, D.; Zheng, H.; Ou, J.; Li, Y.; Meng, J.; Mi, Z.; Liu, Z.; Zhang, Q. China CO_2 emission accounts 1997–2015. *Sci. Data.* **2018**, *5*, 170201. [CrossRef] [PubMed]
38. Department of Climate Change of the National Development and Reform Commission. *Provincial Greenhouse Gas Inventory Preparation Guidelines (Trial)*; Department of Climate Change of the National Development and Reform Commission: Beijing, China, 2011.
39. Beijing Municipal Bureau of Statistics. *Beijing Statistical Yearbook*; China Statistics Press: Beijing, China, 2006.

40. Liu, H.Q.; Fu, J.X.; Liu, S.Y.; Xie, X.Y.; Yang, X.Y. Calculation methods and application of carbon dioxide emission during steel-making process. *Iron Steel* **2016**, *51*, 74–82.
41. National Bureau of Statistics. *China Statistical Yearbook on Environment*; China Statistics Press: Beijing, China, 2006.
42. Shenzhen Municipal Bureau of Ecology and Environment. Information Announcement on Prevention and Control of Environmental Pollution by Solid Wastes Shenzhen. Available online: http://meeb.sz.gov.cn/xxgk/qt/tzgg/content/post_2085853.html (accessed on 5 January 2022).
43. Liu, L.; Qu, J.; Zhang, Z.; Zeng, J.; Wang, J.; Dong, L.; Pei, H.; Liao, Q. Assessment and determinants of per capita household CO_2 emissions (PHCEs) based on capital city level in China. *J. Geogr. Sci.* **2018**, *28*, 1467–1484. [CrossRef]
44. Beijing Municipal Commission of Planning and Natural Resources. Land change survey in Beijing. Available online: http://ghzrzyw.beijing.gov.cn/zhengwuxinxi/sjtj/tdbgdctj/201912/t20191213_1159087.html (accessed on 16 January 2022).
45. Shenzhen Municipal Bureau of Planning and Natural Resources. Bulletin of the Main Data Results of the Land Change Survey. Available online: http://pnr.sz.gov.cn/xxgk/sjfb/tjsj/index_17.html (accessed on 16 January 2022).
46. National Development and Reform Commission, National Bureau of Statistics. *Accounting Standards of Gross Ecosystem Product (Trial)*; Department of Climate Change of the National Development and Reform Commission: Beijing, China, 2022.
47. Yu, T.R.; Lu, F.; Yang, S.S. Greenhouse gas budget and net carbon sequestration of different afforestation types used in grain for green project—A case study in central south and east China. *Bull. Soil Water Conserv.* **2022**, *42*, 337–347+59.
48. Zhang, X.D.; Zu, J.H.; Kang, X.M. An overview of greenhouse gas inventory in the Chinese wetlands. *Acta Ecol. Sin.* **2022**, *42*, 9417–9430.
49. IPCC. *IPCC Guidelines for National Greenhouse Gas Inventories*; IPCC: Geneva, Switzerland, 2006.
50. Liu, R. *Research on Greenhouse Gas Emission in Beijing*; Beijing University of Civil Engineering and Architecture: Beijing, China, 2016.
51. Sun, Y.G. *Characteristics and Driving Forces of Carbon Emissions of 50 Chinese Cities During 2000–2015*; Nanjing University: Nanjing, China, 2019.
52. Long, Y.; Jiang, Y.; Chen, P.; Yoshida, Y.; Sharifi, A.; Gasparatos, A.; Wu, Y.; Kanemoto, K.; Shigetomi, Y.; Guan, D. Monthly direct and indirect greenhouse gases emissions from household consumption in the major Japanese cities. *Sci. Data* **2021**, *8*, 301. [CrossRef]
53. Wu, Y.; Wang, X.K.; Lu, F. The carbon footprint of food consumption in Beijing. *Acta Ecol. Sin.* **2012**, *32*, 1570–1577.
54. Xian, C.F.; Ouyang, Z.Y. Urban ecosystem nitrogen metabolism: Research progress. *Chin. J. Ecol.* **2014**, *33*, 2548–2557.
55. Li, N. *Study on Energy Consumption and GHG Emissions of Agriculture in China*; Dalian University of Technology: Dalian, China, 2014.
56. Shuai, C.; Chen, X.; Wu, Y.; Tan, Y.; Zhang, Y.; Shen, L. Identifying the key impact factors of carbon emission in China: Results from a largely expanded pool of potential impact factors. *J. Clean Prod.* **2018**, *175*, 612–623. [CrossRef]
57. Xiong, C.H.; Chen, S.; Huang, R. Extended STIRPAT model-based driving factor analysis of energy-related CO_2 emissions in Kazakhstan. Environ. *Sci. Pollut. Res.* **2019**, *26*, 15920–15930. [CrossRef]
58. Xue, Y.X.; Xie, J.C.; Huai, C.P. Decomposition Analysis of Influencing Factors of Energy Related Carbon Emission in Beijing. *J. Build. Energy Effic.* **2022**, *50*, 128–132.
59. Tang, B.J.; Zhou, B.J.; Feng, C. Analysis on influence factors of energy consumption and research on energy saving and emission reduction in Beijing: Based on the industrial perspective. *J. Chongqing Univ. Tech.* **2015**, *29*, 19–27+67.
60. Li, F.; Mao, H.W.; Lai, Y.P. Greenhouse Gas Inventory and Emission Accounting of Shenzhen. *Urban Dev. Stud.* **2013**, *20*, 136–139+43.
61. Liao, S.; Wang, D.; Ren, T.; Liu, X. Heterogeneity and Decomposition Analysis of Manufacturing Carbon Dioxide Emissions in China's Post-Industrial Innovative Megacity Shenzhen. *Int. J. Env. Res. Public Health* **2022**, *19*, 15529. [CrossRef] [PubMed]
62. Wang, A.; Zhao, T.Z. Greenhouse Gas Emission Characteristics of Municipal Waste Management in Beijing. *Environ. Monit. China* **2017**, *33*, 68–75. [CrossRef]
63. Zhang, J.F.; Fang, H.; Ma, B.F.; You, H. Study on Carbon Emissions from Municipal Solid Waste in Shenzhen. In Proceedings of the 2015 International Symposium on Energy Science and Chemical Engineering, Guangzhou, China, 12–13 December 2015; He, Y., Ed.; Atlantis Press: Paris, France, 2015; Volume 45, pp. 232–235.
64. Wang, Y.; Li, F.; Chen, X.C. Characteristics and influencing factors of carbon emission from typical community household consumption: A case of Beijing. *Acta Ecol. Sin.* **2019**, *39*, 7840–7853.
65. Li, W.L. *The Research of Driving Forces of CO_2 Emission from Household Consumption in Beijing*; Beijing Institute of Technology: Beijing, China, 2018.
66. Zhang, G.; Li, L.; Huang, C.; Huang, H.; Chen, M.; Chen, C.; Zhou, N. Carbon emissions of the household living in Shanghai using Urban-R AM model. *Acta Sci. Circumstantiae* **2014**, *34*, 457–465.
67. Liu, A.Y.; Ke, S.F.; Wang, Y. The Land Resources Endowment and Carbon Sinks Volume of Beijing. *For. Econ.* **2015**, *37*, 94–98+128.
68. Zeng, H.; Gao, Q.; Chen, X.; Li, G. Changes of the wetland landscape in Shenzhen city from 1988 to 2007 and the driving force analysis. *Acta Ecol. Sin.* **2010**, *30*, 2706–2714.
69. Su, K.; Wei, D.Z.; Lin, W.X. Influencing factors and spatial patterns of energy-related carbon emissions at the city-scale in Fujian province, Southeastern China. *J. Clean. Prod.* **2020**, *244*, 118840. [CrossRef]
70. Wen, L.; Zhang, Z.Q. Probing Energy-Related CO_2 Emissions in the Beijing-Tianjin-Hebei Region Based on Ridge Regression Considering Population Factors. *Pol. J. Environ. Stud.* **2020**, *29*, 2413–2427. [CrossRef]

71. Song, X.C.; Du, S.; Shen, P. Analysis of Decoupling Relationship Between Economy and CO_2 from Manufacturing Industry of China. *Environ. Sci. Technol.* **2022**, *45*, 201–208.
72. Su, M. *Decoupling Effect of Carbon Emissions and Economic Growth and Its Driving Forces in Shandong Province*; China University of Petroleum (East China): Qingdao, China, 2019.

atmosphere

MDPI

Article

Analysis of Carbon Emission Characteristics and Influencing Factors of Herder Households: A County-Scale Investigation of the Sanjiangyuan Region on the Qinghai–Tibet Plateau

Changsu Song [1,†], Lu Liu [2,†], Chaofan Xian [3,*], Fan Feng [4] and Zhiyun Ouyang [3]

[1] Department of Social & Ecological Studies, Chinese Academy of Governance, Beijing 100091, China; songcs@ccps.gov.cn
[2] Department of Economics, Chinese Academy of Governance, Beijing 100091, China; llyyazsq@163.com
[3] State Key Laboratory of Urban and Regional Ecology, Research Center for Eco-Environmental Sciences, Chinese Academy of Sciences, Beijing 100085, China; zyouyang@rcees.ac.cn
[4] School of Economics and Management, Nanjing University of Science and Technology, Nanjing 210094, China; ffyukitaco@njust.edu.cn
* Correspondence: cfxian@rcees.ac.cn
† These authors contributed equally to this work.

Abstract: With further urbanization, household consumption firmly plays a key role in China's national carbon emissions. However, current research concerning carbon issues has mainly focused on urban household consumption, and few studies have paid attention to herder households, leading to a research gap in the field of low-carbon shifting related to nomadic economies. In this study, we interviewed more than one-thousand herder households in the Sanjiangyuan region of the Qinghai–Tibet Plateau in China. The household carbon emissions and their influencing factors were investigated across the herder households of 15 counties. Our findings revealed the following: (1) There exist differences in the amounts of household carbon emissions and their compositions in the Sanjiangyuan region. From the perspective of spatial distribution, the emission hotspots are mainly concentrated in the eastern part of the Sanjiangyuan region. (2) At the prefecture level, average personal emissions were larger in the Hainan Prefecture (3.26 t ce/year), while they were approximately 1.36 times that of the Huangnan Prefecture (2.4 t ce/year), though with smaller personal emissions. The indirect carbon emissions of the four prefectures all occupied larger percentages of household carbon emissions that were mainly contributed by food consumption and housing. (3) Family type was the main diver influencing personal carbon emissions in the Huangnan Prefecture, Guoluo Prefecture, and Yushu Prefecture. The more people living in the household, the lower the per capita carbon emissions. However, the effect size of potential carbon reductions was weakened when the number of family members rose to over three. (4) We propose that grazing prohibitions and low-carbon dietary shifts would contribute to low-carbon herder livelihoods, especially for small-sized households that should be peer-to-peer targeted by regional government propaganda, which may help to strengthen the implementation of in-depth low-carbon promotions across the Sanjiangyuan region and even the overall Qinghai–Tibet Plateau.

Keywords: herder households; household consumption; carbon emissions; demographic effects; Sanjiangyuan region

Citation: Song, C.; Liu, L.; Xian, C.; Feng, F.; Ouyang, Z. Analysis of Carbon Emission Characteristics and Influencing Factors of Herder Households: A County-Scale Investigation of the Sanjiangyuan Region on the Qinghai–Tibet Plateau. *Atmosphere* **2023**, *14*, 1800. https://doi.org/10.3390/atmos14121800

Academic Editor: Dmitry Belikov

Received: 3 September 2023
Revised: 28 November 2023
Accepted: 6 December 2023
Published: 8 December 2023

1. Introduction

The era of global warming is not yet over, while the era of global boiling has already arrived. With rapid global industrialization and modernization, the excessive consumption of energy by humans has led to a dramatic increase in greenhouse gas emissions [1], thereby exacerbating the global warming situation. Urban areas are the hotspots of human energy consumption, accounting for over 70% of global carbon emissions. For developing

countries, residential energy consumption serves as a main engine for economic growth and a major source of regional carbon emissions [2,3]. For the rapidly urbanizing China, the direct and indirect carbon emissions caused by household consumption have driven the growth of carbon emissions over recent decades [4]. In view of China's current international commitments to achieve carbon peaking by 2030 and carbon neutrality by 2060, it is necessary to investigate the dynamics of carbon emissions from different types of consumption in Chinese households from a multi-scale perspective.

Recently, research concerning the energy-related carbon emissions of Chinese households has emerged. Su et al. (2023) [5] conducted a dynamic assessment of residential energy consumption and related carbon emissions in Chinese households. It indicated that the annual carbon emissions caused by different types of Chinese households would decrease at different levels. Chen et al. (2023) [6] studied the drivers of urban–rural disparities in household carbon emissions in China, and they found that the temporal and spatial characteristics in household carbon emissions between urban and rural areas were influenced by sociometric factors such as economic development levels, household consumption patterns, and demographic effects. Jiang et al. (2021) [7] proposed that carbon emissions from households in rural areas may be much higher than those from urban households due to the different energy types used by urban and rural households. Yuan et al. (2019) [8] revealed that the household carbon emissions in most coastal provinces and subordinate cities were mostly influenced by residents' income levels and their demographic effects, while the higher household carbon emissions were observed in some non-coastal industrial provinces were due to laggard carbon-control technologies. Concerning the regional carbon emissions from northern agricultural regions, Liang et al. (2013) [9] found that coal still was the main energy source resulting in the growth of greenhouse gas (GHG) emissions, and these results were based on an investigation of the structural changes in household energy use from 1980 to 2009 in Shandong Province, northern China. Most current research concerning household carbon emissions has focused on the carbon emission characteristics of urban household consumption and their influencing factors, and relevant studies related to rural household consumption, especially at the county scale, are fewer. Although the limited studies conducted by Jiang et al. (2021) [7] and Liang et al. (2013) [9] investigated the carbon emissions of rural households in typical agricultural regions, they focused on suburban regions within metropolitan areas. Compared with rural households, fewer researchers have paid attention to the carbon issues of herdsman livelihoods, which may present different stories about carbon issues due to the different cultures of these ethnic minorities and the special topographies of the plateau regions. Therefore, the mere selection of urban and rural households as case studies cannot provide a comprehensive mapping of carbon emissions from households' consumption in China.

Currently, there is no doubt that fewer in-site studies have concerned herdsman livelihoods in plateau regions with low urbanization levels, which may also be potentially affected by rapid urbanization in the future. The ecosystems of forests, grasslands, wetlands, and permafrost in the Qinghai–Tibet Plateau are the important carbon sinks which will play a long-term, crucial role in achieving global carbon neutrality. As a natural barrier, the unique environment of the Qinghai–Tibet Plateau requires the development of corresponding sustainable development strategies to achieve the United Nations' 17 Sustainable Development Goals (SDGs) [10]. However, it is not easy to develop such suitable and effective strategies for the Qinghai–Tibet Plateau due to its fragile environment as the "Third Pole" region in the world. The difference between this "Third Pole" and other polar regions on the earth is that this region is constantly threatened by urbanization [11]. The population of the Tibet Plateau is rapid rising along with the development of regional economies, and the related increasing exhaust gases emissions resulting from household energy combustion (such as heating, cooking, electricity, etc.) in this region not only threaten local air quality and human health, but also hinder progress in achieving the goal of carbon-peaking by 2030 and carbon neutrality by 2060 in Qinghai–Tibet. However, neither governance nor

academia have paid long-term attention to this carbon issue for plateau regions, resulting in less relevant research to date [10].

Rising carbon emissions have already threatened sustainable development in the Qinghai–Tibet Plateau. A household investigation in the Qinghai Province concluded that there is significant population aggregation and economic development within the Qinghai–Tibet Plateau. Previous studies found that household-related carbon emissions have increased at an average annual rate of 23% for the period 2002 to 2012. However, these studies only acquired an insights into carbon emissions related to urban households at the provincial level [12], and they failed to provide further information about herdsman livelihoods in typical plateau regions. The pastoral communities, especially those living in the higher altitude of Asia, are increasingly exposed to threats brought about by the aforementioned climactic and anthropogenic factors, and thus their livelihoods are more vulnerable to climate change compared with those in the urban and rural areas in lower altitudes. These herder households making up pastoral communities have largely been dependent on their local knowledge in managing their daily livelihoods [13]. In terms of energy consumption, over the past thousand years, local herders have preferred livestock manure (e.g., yak, sheep, etc.) and crop residues as their main energy sources [14], and they usually lack the means for adopting clean energy to reduce household carbon emissions. As for energy saving for climate change mitigation, their external dependency has been increased due to recent climatic anomalies and economic development, which should be addressed and guided by practitioners and policy makers to better reduce household carbon emissions for the adaptation of regional climate change. However, there exists a significant gap between the energy consumption per capita of herders and that of non-herders within Qinghai Province. The aforementioned factors might lead to different situations for the dynamic carbon emissions and their driving factors in herder households. To address this emerging question—whether the carbon emissions of herder households are high enough to form a significant carbon source that has a negative impact on the low-carbon development of the plateau—this study took the Sanjiangyuan region of the Qinghai Province as an example, and analyzed the characteristics of the carbon emissions of herder households though a door-to-door household survey across different counties, aiming to provide scientific support for the overall Qinghai–Tibet Plateau to achieve the relevant carbon goals and sustainable development goals.

2. Literature Review

In recent years, the research topic of household carbon emissions has gradually attracted more academic attention. The existing research has mainly focused on the accounting of household carbon emissions in urban and rural communities and analyzing the relevant factors impacting these carbon emissions. Most studies have highlighted the importance of families as the basic units of society in carbon emission reductions; however, in the plateau regions, the role of herder households in carbon emission reductions remains unclear. It is essential to investigate this issue to gain further insights, since there exist differences between the family lifestyles of herder households and those of urban and rural residents. Previously, Jiang et al. (2020) [3] studied the characteristics of household energy consumption levels in the agricultural and pastoral areas of the Qinghai Province, and they proposed that the limited data retrieved from official statistics were not enough to explain the regional differences [15] and that local surveys were needed to address this issue. Zhang et al. (2020) [16] studied the internal changes in household consumption levels and related carbon emissions based on a field survey, but they neglected herder families in the plateau regions. Further, the factors of household characteristics usually play an important role in explaining the dynamics of household carbon emissions. Zhang et al. (2023) [17] found that household sizes in China have significant negative impacts on per capita household carbon emissions, and the negative impact on indirect carbon emissions is much greater than that on direct carbon emissions. Zhou et al. (2023) [18] found that the impact of national population aging on carbon emissions presented an inverted U-shaped

relationship, which showed that aging first increased and then decreased the related carbon emissions. Zhou et al. (2016) [19] found that the impact of changing age structures on energy use was not statistically significant, but it led to an increase in emissions across the country, especially in eastern China. Xu et al. (2016) [20] found that food consumption was the second largest source of carbon emissions in China. Peng et al. (2023) [4] found that household income and consumption played important roles in promoting China's carbon emissions, and the proportion of income-based household emissions in the total emissions was higher than that of consumption-based emissions. Golley et al. (2012) [21] mentioned that rich households generated more emissions per capita than those emitted by poor households. Akrofi et al. (2023) [22] mentioned that the promotion of renewable energy technologies such as solar home systems (SHS) had great potential to reduce greenhouse gas emissions. The environmental satisfaction levels of households have also been proposed to have positive impacts on reducing carbon emissions [23–25].

In terms of a driving force analysis of household carbon emissions, statistical analysis techniques have been adopted to target this issue, including regression analysis and decomposition analysis [26]. However, these methods have been mainly used for variable analyses [27,28], predictions [29], and decompositions [8] and they performed weakly in addressing the multicollinearity problems that arise while handling non-normally distributed data, and so optimal scale regression analysis has been proposed to be more practical for analyzing questionnaire data. It can be used to perform integrated analyses for multiple types of questionnaire data sources, and it has the advantage of being able to gradually remove variables that fail the significance test with high collinearity [30–32]. As the "Third Pole" region in the world, the Qinghai–Tibet Plateau's ecosystems are relatively fragile and more sensitive to climate change. As mentioned, studies concerning carbon emission reductions in herder households in the Qinghai–Tibet Plateau are meaningful to this research field [3,33]. Currently, relevant research based on first-hand data retrieved from local surveys is limited, and therefore, an investigation based on large-scale household surveys would, indeed, help to further outline the carbon emissions related to herder livelihoods compared with previous work based on a limited number of questionnaires in the Qinghai–Tibet Plateau [7]. Further, through the acquisition of household scale micro-data, we could estimate regional household carbon emissions using the scaling-up method, and provide scientific support for the launch of regional low-carbon strategies, which could not be achieved by previous large-scale studies that relied on national and provincial statistics.

3. Research Methods

3.1. Region Selection

The Sanjiangyuan region (31°39′ N 89°45′ E–36°12′ N 102°23′ E) is located in the southern part of the Qinghai Province in China. It is the origin of the Yangtze River, Yellow River, and Lancang River. The average elevations in the Sanjiangyuan region range from 3500 to 4800 m. Autonomous prefectures for ethnic minorities are the prefecture-level administrative units in this plateau area, and they include several subordinate county-level administrative regions. The study area included sixteen counties in four Tibetan autonomous prefectures, including Yushu, Guoluo, Hainan, and Huangnan, which accounted for approximately 43% of the total area of the Qinghai Province and a total area of 302,500 square kilometers (Figure 1). The existing population was 556,000, with over 90% being Tibetans and other ethnic groups, including Hans, Huis, Salas, and Mongolians. The Sanjiangyuan region is a typical less-developed region. In 2021, its GDP was CNY 19,954,000,000 [34,35], accounting for only 5.96% of the Qinghai Province's GDP [13,36]. Due to the characteristics of the ground cover, as a frigid zone meadow vegetation area plateau, the primary economic industry in the Sanjiangyuan region is dominated by animal husbandry, causing it to be a typical area for herder households.

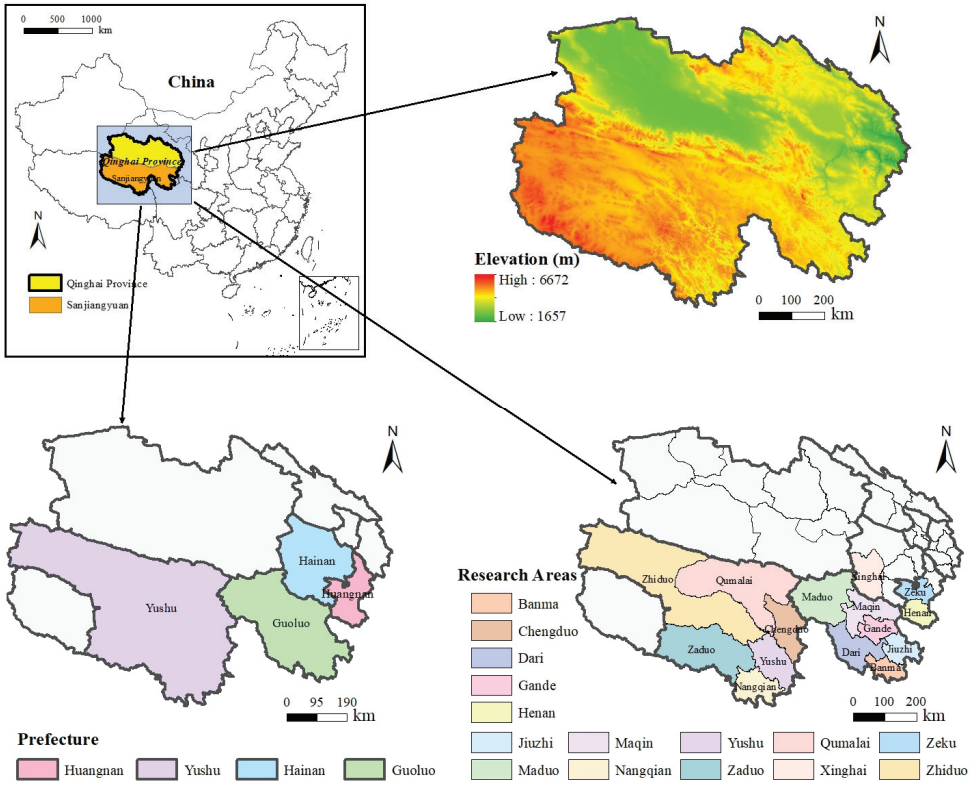

Figure 1. The location of the research area.

3.2. Data Resources

Based on the relevant literature and suggestions from experts [35–38], we designed a questionnaire named "Questionnaire on Households' Livelihoods and Ecological Compensation in Qinghai Province", which consisted of the following four sections: family member information, livelihood activities, livelihood capital, and ecological policies and perceptions. Considering the cultural issues induced by language barriers during the face-to-face surveys, each questionnaire was conducted with the help of local volunteers familiar with the local languages. Subsequently, the questionnaire contents were transferred to the form of a spreadsheet, and cross-validation was subsequently carried out among the sampled spreadsheet data to ensure the accuracy of the first-hand data for the statistical analysis. A total of 1100 questionnaires across 15 counties within 4 prefectures were conducted, with a final collection of 1027 questionnaires (the effective questionnaires occupied 93.36%).

3.3. Variable Settings

Taking the individual carbon emissions from the different counties as the dependent variable, the related socioeconomic factors are thereby regarded as the independent variables (Table A1). According to existing research [17,21,33,39–41], the socioeconomic factors influencing the individual carbon emissions (Y) included family type, age structure, education level, annual income, solar utilization, environmental satisfaction, and grazing prohibition. The definitions of each variable are shown in Table 1.

Table 1. The settings of the independent and dependent variables.

Variable Name	Variable Symbol	Variable Attribute	Variable Definition
Individual Carbon Emissions	Y	Numerical Variable	Carbon emissions from personal energy consumption (t ce/year)
Family Type	X_1	Ordinal Variable	Single family = 1, a family of two = 2, a family of three = 3, a family of four = 4, and a family with many members = 5
Age Structure	X_2	Ordinal Variable	Under 18 = 0, 18–65 = 1, and over 65 = 2
Education Level	X_3	Ordinal Variable	Illiteracy = 1, primary school = 2, junior high school = 3, high school/technical secondary school = 4, junior college = 5, bachelor's degree or above = 6, (monastic education: less than 6 years as primary school = 2 and 7 years and above as junior high school = 3)
Annual Income	X_4	Numerical Variable	Annual personal income (Yuan)
Solar Utilization	X_5	Nominal Variable	Yes = 1 and no = 2
Environmental Satisfaction	X_6	Ordinal Variable	Gets better = 1, stays the same = 2 and gets worse = 3
Grazing Prohibition	X_7	Ordinal Variable	Tighter = 1, unchanged = 2 and looser = 3

3.4. Carbon Emissions Accounting

3.4.1. Direct Carbon Emissions Accounting

Direct energy consumption by pastoral communities mainly consists of cooking and transportation, and it is divided into fossil energy and non-fossil energy [13]. Based on the survey, we calculated the main fossil energy used by the respondents including coal, natural gas, and related electricity, as well as the non-fossil energy referring to biofuels such as firewood, straw, and livestock manure [17,42] (Table A2). It is acknowledged that the quantification of carbon emissions generated by the use of electricity is usually complicated, especially residential electricity. Relevant processes do not burn fossil fuels directly, but their upstream production will consume numerous fossil fuels. Therefore, it has been recognized as one of the main energy sources. Except the electricity consumption, the downstream carbon emissions generated by other energies were considered. This study converted various energy consumptions into a unified unit of standard coal (kg ce) as follows:

$$Q_i = \sum q_i r_i \tag{1}$$

$$E_i = \sum Q_i c_e, \tag{2}$$

and

$$ME_i = \frac{E_i}{n}. \tag{3}$$

In the above equation, Q_i represents the original consumption of the i energy source, q_i represents the original consumption of the i energy source, and r_i is the conversion coefficient of the i energy source to standard coal. E_i represents the direct carbon emissions of households, c_e represents the carbon emission coefficient of coal, ME_i is the personal direct carbon emissions, and n is the number of household members. The energy conversion coefficient to standard coal was based on the coefficient published in the China Energy Statistical Yearbook [43]. The conversion coefficient [3,44] for livestock manure (per kilogram) was 0.5, and it was 0.7143 for coal (per kilogram), 1.214 for natural gas (per cubic meter), and 0.1229 for electricity (per kilowatt hour).

3.4.2. Indirect Carbon Emissions Accounting

The consumption expenditure for households was divided into eight categories, including food, clothing, household equipment, supplies and services, healthcare, transportation and communication, and cultural, educational, and recreational supplies, as well as services, living, and other goods and services [36]. Each category of consumption expenditure corresponded to one or more relevant industries. The industry sectors corresponding to the different consumption categories and their corresponding embedded emissions intensities are shown in Table 2. These embedded carbon emissions of residents' consumption could be therefore calculated based on the input–output analyses (IOA) method. IOA is an economic quantitative method to explore delineate the carbon emissions embedded in the interdependence of supply and consumption among different flows of goods and services across sectors within economic activities [12]. Typically, the input–output table is published every five years, and the recent input–output table for the Qinghai Province was available for 2017. This study investigated the indirect carbon emissions resulting from daily household consumption, which could be calculated through multiplying the survey data for household consumption levels (Table A2) by the cumulative carbon emissions intensities of the corresponding sectors. The relationships between consumption expenditure types and industry types in the input–output table were based on the classification suggested by Dong and Geng [45]. The calculation formulas used for the consumer lifestyle method are as follows:

$$C = FY = F'(I - A)^{-1}Y \tag{4}$$

and

$$MC = \frac{C}{n}. \tag{5}$$

Table 2. Industry sectors and the embedded carbon emission intensities corresponding to consumption category.

Consumption Category	Corresponding Industry	Embedded Emission Intensity (t ce/Ten Thousand Yuan *)
Food	Food and tobacco	2.3030
Clothing	Textiles, Clothing, Shoes, Hats, Leather, Down and associated products	1.7465
Household Equipment, Supplies and Services	Wood processing products and furniture + Electrical machinery and equipment	2.8267
Healthcare	Health and Social work + Public administration, Social security and social organization	1.6650
Transportation and Communication	Transportation equipment + Communication equipment, Computers and other electronic equipment + Transportation, warehousing and postal services + Information transmission, Software and information technology services	2.1963
Cultural, Educational and Entertainment Supplies and Services	Paper printing and cultural and educational sporting goods + Education + Culture, sports and entertainment	1.8771
Living	Building + Non-metallic mineral products + Metal products + Rental and business services	4.2978
Other Goods and Services	Wholesale and retail + Accommodation and catering + resident services, repairs and other services	1.8041

* Purchasing power in 2019 (1 USD = 6.8985 yuan).

In the above equations, C represents the indirect carbon emissions from household consumption, F is a 1×8 row vector representing the embedded carbon intensities of

sectors 1~8, F' is a 1×8 row vector representing the direct carbon intensities of sectors 1~8, A is the 8×8 matrix of the direct consumption coefficients from an input–output table, I represents an identity matrix of the same order as A, Y denotes a column vector representing the household expenditures based on eight consumption categories, $(I - A)^{-1}$ is the Leontiv inverse matrix (which shows the impacts of production technologies changing in one sector of the national economy on all the other sectors), and MC represents the per capita indirect carbon emissions.

3.4.3. Household Carbon Emissions Accounting

Based on the results of the direct and indirect carbon emissions accounting, the regional carbon emissions of the prefectures, as well as their per capita carbon emissions, could be estimated as follows:

$$MD = \frac{E_i + C}{n} \tag{6}$$

and

$$PMD_t = \frac{\sum MD_t}{N}. \tag{7}$$

In the above equations, MD represents the overall personal carbon emissions of specific household, PMD_t is the total per capita emissions of the households in each prefecture t, and the maximum value of t is four. MD_t represents the per capita emissions of each subordinate household within each prefecture t, and N represents the number of subordinate households in each prefecture t.

3.5. Factors Influencing Household Carbon Emissions

3.5.1. Optimal Scale Regression Analysis

We set the personal carbon emissions in the different counties as the dependent variable and the aforementioned influencing factors as the independent variables. As many variables as possible in the influencing factors were classified into variables (such as family type) rather than being used as numerical variables, which would cause significant uncertainty in the analysis by linear regression. Optimal scale regression analysis could quantify the different values of the categorical variables and convert them into numerical types for the statistical analysis. Previous studies have shown that some subjective factors such as consumer preferences [46] and the impact of land expansion on rural revitalization [47] can be set as categorical variables and then converted into numerical analyses. Therefore, the optimal scale regression analysis could be adopted to reveal the influencing factors of the household carbon emissions. This method firstly involved the calculation of the correlation coefficient R of the independent variable and the correction of the judgment coefficient R^2 to determine the fitting effect of the regression equation, and then the correlation parameter (the sum of the squares, degrees of freedom, F-values, etc.) of the regression residual was summarized to determine the significance level of the regression. Finally, we calculated the standardization coefficient of the independent variable and gradually removed variables with high collinearity that had not passed the significance test by determining the optimal solution after repeated iterations. In order to deeply analyze the main influencing factors of the personal carbon emissions in each county, the software suite Statistical Product and Service Solutions (SPSS 21.0) was used for the optimal scale regression analyses. The definition formula of the regression model is as follows:

$$\widehat{Y} = b_1\widehat{x_1} + b_2\widehat{x_2} + \cdots + b_n\widehat{x_n} + \varepsilon. \tag{8}$$

In the above formula, $\widehat{Y}$ represents the standardized dependent variable, while $\widehat{x_1}$, $\widehat{x_2}$, and $\cdots \widehat{x_n}$ represent the transformed independent variables and b_1, b_2, and $\cdots b_n$ represents the standardized regression coefficients of the independent variables; n represents the number of independent variables, and ε represents the error term.

3.5.2. Multiple Comparative Analysis

We selected the significant influencing factor with the highest importance among the independent variables, and we used the multiple comparison analysis with an LSD test (Fisher's least significant difference) in SPSS21.0 to further determine the degree of influence of the explanatory variable on the dependent variable at the different levels. We used *t*-tests to complete the paired comparisons between the mean values of each group. The minimum significant difference was the critical value at which the mean difference reached the level of a significant difference. When the mean difference was greater than or equal to this critical value, the difference was significant; When the mean deviation was less than the critical value, the difference was not significant. The higher sensitivity of this test, as well as the small differences in the mean values between the different levels, could also be detected. This was conducive to analyzing the differences in the independent variables at the different levels and their corresponding dependent variables, which could be used to compare the differences in the main influencing factors of the household carbon emissions in the different counties, aiming to identify the targeted groups with higher personal carbon emissions.

4. Results and Analysis

4.1. Characteristics of the Herdsman Households

Based on our large-scale household survey, the basic information about the herdsman households across 15 counties within 4 prefectures and the whole Sanjiangyuan region is shown in Tables 3 and 4. Overall, the average family size in the Sanjiangyuan region was over four members, with a mean age that ranged from 25 to 30 years old. The average educational level was mainly primary and middle school. The Hainan Prefecture had the largest average household size of approximately around 4.77 people, which was slightly higher than those of other three prefectures, and it had the lowest average age and the lowest average education level. In this region, the average annual income of the households was the second highest (CNY 6679.20) among the four prefectures, with the highest levels of environmental satisfaction and the strictest grazing prohibitions. The average age in the Huangnan Prefecture was 30.375, which was the oldest among the four prefectures in the Sanjiangyuan region. Although its average household size was smaller than that of Hainan Prefecture, its average annual income was the highest compared to other three prefectures, and its average education level was relatively high, though it was inferior to that of the Guoluo Prefecture (1.83). Overall, the per capita education level and average income level in the Huangnan Prefecture performed well. Although the average family size in the Guoluo Prefecture was only second to the Hainan Prefecture, the average family size level (4.87) of the subordinated Gande County within this prefecture was the highest among all counties in this study. The grazing prohibition situation of the Guoluo Prefecture was roughly the same as that of the Huangnan Prefecture, since the policies for grazing prohibition for these two areas were stricter. The Yushu Prefecture had the smallest average household size among the four prefectures in the Sanjiangyuan region, along with the lowest average annual income. It had the lowest environmental satisfaction and the most liberalizing policy of grazing prohibition policy compared to the other three prefectures. Overall, our study found that there existed significant differences among the herdsman households across the different prefectures of the Sanjiangyuan region in terms of their daily livelihoods, which provided valuable first-hand data for the calculation of carbon emissions and the analysis of driving forces.

Table 3. Basic information of herdsman households across Sanjiangyuan region.

Prefecture	County	Sample Size		Average Family Size		Average Age		Average Literacy		Average Annual Income/Yuan *		Environmental Satisfaction		Grazing Prohibition	
Hai nan	Xing hai	179	179	4.77	4.77	25.62	25.62	1.69	1.69	6678.20	6678.20	1.56	1.56	1.30	1.3
Huang nan	Ze ku	557	785	4.56	4.61	29.06	30.38	1.77	1.83	5071.73	7985.55	1.88	1.66	1.97	1.86
	He nan	228		4.66		31.69		1.89		10,899.36		1.44		1.75	
Guoluo	Ma qin	427	1426	4.43	4.66	29.90	26.67	2.07	1.88	7848.06	6153.10	1.76	1.83	1.79	1.86
	Gan de	180		4.87		25.81		1.77		3711.66		2.08		1.88	
	Jiu zhi	256		4.68		28.43		1.99		5215.31		2.36		1.97	
	Ban ma	234		4.80		26.13		1.88		5074.73		1.59		1.97	
	Da ri	163		4.83		23.82		1.79		7559.82		1.90		1.86	
	Ma duo	166		4.36		25.92		1.78		7509.04		1.27		1.69	
Yu shu	Cheng duo	103	819	4.44	4.50	29.26	27.88	1.83	1.73	4520.92	5883.37	2.02	2.21	1.98	1.93
	Yu shu	169		4.46		26.50		1.77		4513.28		2.05		1.90	
	Nang qian	234		4.85		27.10		1.69		5373.64		2.12		1.85	
	Za duo	162		4.79		28.81		1.75		9348.45		2.26		1.77	
	Zhi duo	14		4.14		25.86		1.50		3496.00		2.43		2.21	
	Qu malai	137		4.30		29.74		1.82		8047.92		2.38		1.88	

* Purchasing power in 2019 (1 USD = 6.8985 yuan).

Table 4. Descriptive statistics of herdsman households in the Sanjiangyuan region.

Variable Name	Min	Max	Mean	Standard Deviation
Family Size	1	5	4.58	0.732
Age	0.02	98	29.94	20.02
Literacy	1	6	1.94	1.25
Annual Income	0	300,000	7226.328	16,451.80647
Environmental Satisfaction	1	3	1.87	0.934
Grazing Prohibition	1	3	1.82	0.934

4.2. Household Carbon Emission Characteristics

In terms of direct regional carbon emissions, the Guoluo Prefecture had the highest direct carbon emissions, followed by the Yushu Prefecture and the Huangnan Prefecture, while the Hainan Prefecture had the lowest emissions. Further, the indirect regional carbon emissions also presented similar spatial distribution characteristics. In terms of counties, the highest direct carbon emissions were found in Zeku County, while the lowest emissions were found in Zhiduo County. In addition, the indirect carbon emissions were higher in Maqin County and lower in Zhiduo County. The overall household carbon emissions of the different regions are shown in Figure 2. The regional emissions were found to be the highest in Nangqian County and the lowest in Zhiduo County, and the hotspots with higher carbon emissions were concentrated in the eastern part of the Qinghai Province. In terms of the per capita household carbon emissions, the average direct personal carbon emissions in the Yushu Prefecture were higher than those of the Hainan Prefecture, and the average direct carbon emissions of individuals in the Guoluo Prefecture were the lowest (Figure 3), which was mainly due to the differences in the structures of domestic energy supplies. The indirect personal carbon emissions of the different prefectures are shown in Figure 4. The indirect personal carbon emissions of the Hainan Prefecture were 2.27 t ce CO_2/year, which was similar to those of the Yushu Prefecture. The lowest personal indirect carbon emissions (1.55 t ce CO_2/year) were observed in the Huangnan Prefecture.

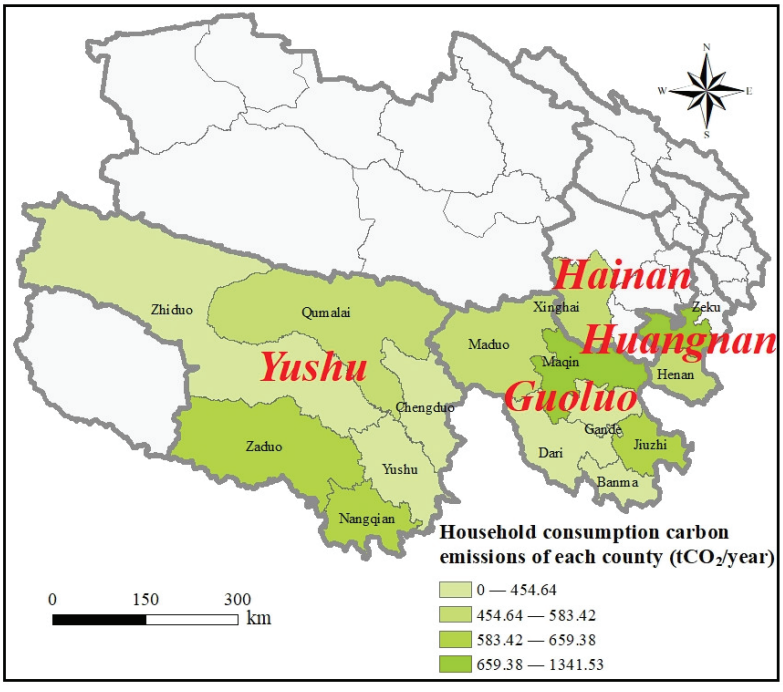

Figure 2. Household carbon emissions of different counties and prefectures.

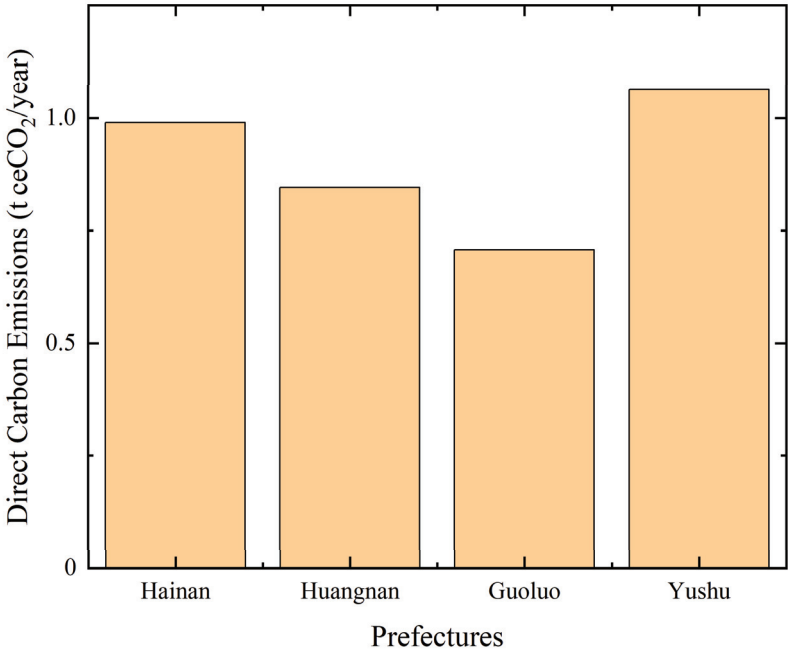

Figure 3. Direct personal carbon emissions among four prefectures in the Sanjiangyuan region.

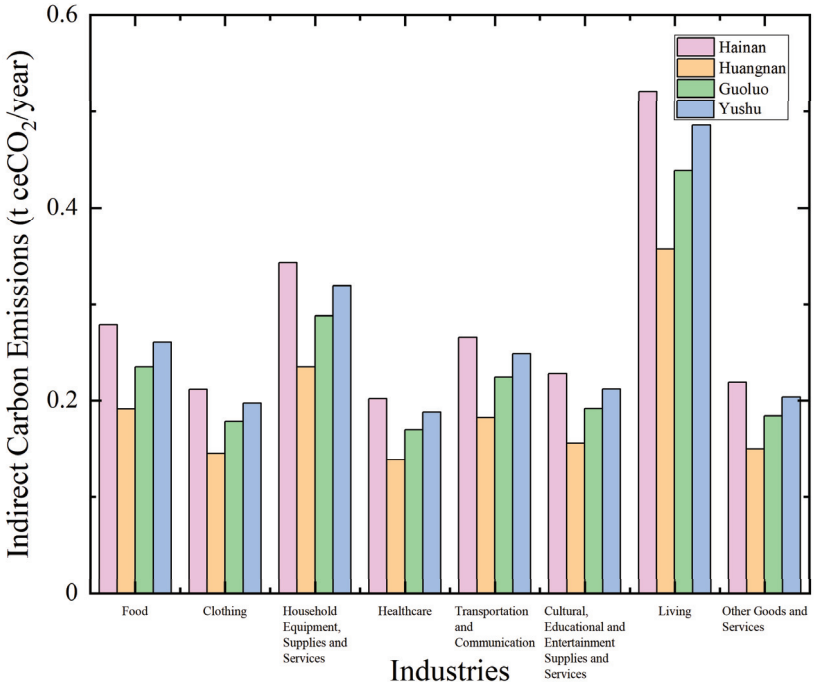

Figure 4. Indirect personal carbon emission embedded in eight industry sectors among four prefectures in the Sanjiangyuan region.

4.3. Personal Carbon Emissions and Their Influencing Factors

To explore the main influencing factors of personal carbon emissions (Y), the optimal scale regression was conducted by adopting X_1, X_2, X_3, X_4, X_5, X_6 and X_7 as the independent variables. The significance levels of the regression equations were mainly p values of less than 0.05, indicating that the model was statistically significant after the tests for autocorrelation and heteroscedasticity (Table 5). The tolerance values of each variable in the model were greater than 0.1 before and after transformation, indicating that the model did not have collinearity issues. Based on the parameter estimation results of the coefficient table (Table 6) retrieved from the optimal scale regression model, the independent variables with strong importance levels (p = 0.05) were selected for analysis. The impact of family type on personal carbon emissions in the four prefectures all passed the significance test at the 0.05 level, but the degrees of the impacts were different. The importance values for family type in the Huangnan Prefecture, the Guoluo Prefecture, and the Yushu Prefecture all exceeded 0.5. The use of solar energy was not significant in any of the prefectures. Annual income had significant impacts on personal carbon emissions in the Huangnan Prefecture, the Guoluo Prefecture, and the Yushu Prefecture. Individuals with different levels of environmental satisfaction in the Huangnan Prefecture, the Guoluo Prefecture, and the Yushu Prefecture showed significant differences for their personal carbon emissions. Although their contributions were not high, they still indicated that environmental satisfaction had an impact on their personal carbon emissions to some extent. According to relevant research [48], residents' perceptions of heat and air quality affected their behaviors in relation to energy consumption. Meanwhile, the grazing prohibitions in the Huangnan Prefecture, the Guoluo Prefecture, and the Yushu Prefecture Prefecture had significant impacts on their carbon emissions.

Table 5. Variance analysis for each model.

Prefecture	R^2	Adjusted R^2	F	P
Hainan	0.223	0.087	1.645	0.108
Huangnan	0.294	0.270	12.285	0.000
Guoluo	0.208	0.193	13.700	0.000
Yushu	0.192	0.170	8.609	0.000

Table 6. Parameter estimation results of the main influencing factors of personal emissions.

Prefecture	Variable	Standardized Coefficient		(Sig)	Correlation			Importance	Tolerance	
		Beta	Coefficient Standard Error		Zero-Order	Partial Correlation	Partial Correlation		After Conversion	Before Conversion
Hainan	Number of people in a family	−0.251	0.213	0.258	−0.244	−0.255	−0.233	0.275	0.86	0.85
	Age structure	0.022	0.069	0.749	0.135	0.024	0.021	0.013	0.898	0.902
	Education level	−0.335	0.229	0.105	0.025	−0.226	−0.205	−0.037	0.375	0.739
	Annual total income	0.468	0.234	0.05	0.213	0.298	0.276	0.448	0.346	0.685
	Environmental satisfaction	−0.175	0.125	0.15	−0.23	−0.179	−0.161	0.181	0.84	0.843
	Grazing prohibition	−0.2	0.136	0.122	−0.133	−0.204	−0.183	0.12	0.837	0.92
Huangnan	Number of people in a family	−0.46	0.047	0	−0.432	−0.476	−0.454	0.676	0.975	0.977
	Age structure	0.02	0.044	0.64	0.023	0.024	0.02	0.002	0.996	0.995
	Education level	0.207	0.047	0	0.162	0.233	0.202	0.114	0.951	0.968
	Annual total income	0.182	0.05	0	0.14	0.209	0.18	0.087	0.975	0.97
	Solar energy usage	0.056	0.04	0.166	0.085	0.065	0.055	0.016	0.957	0.978
	Environmental satisfaction	−0.104	0.052	0.019	−0.066	−0.118	−0.1	0.023	0.919	0.957
	Grazing prohibition	0.187	0.044	0	0.128	0.205	0.176	0.081	0.889	0.945
Guoluo	Number of people in a family	−0.346	0.039	0	−0.353	−0.359	−0.342	0.588	0.976	0.971
	Age structure	−0.092	0.042	0.027	−0.084	−0.102	−0.092	0.037	0.984	0.984
	Education level	−0.048	0.075	0.522	−0.064	−0.054	−0.048	0.015	0.993	0.993
	Annual total income	0.147	0.034	0	0.179	0.16	0.144	0.126	0.972	0.977
	Solar energy usage	0.045	0.034	0.185	0.082	0.05	0.045	0.018	0.976	0.976
	Environmental satisfaction	−0.124	0.041	0	−0.163	−0.136	−0.122	0.097	0.975	0.979
	Grazing prohibition	−0.146	0.051	0.005	−0.171	−0.158	−0.143	0.12	0.956	0.961
Yushu	Number of people in a family	−0.405	0.046	0	−0.399	−0.402	−0.394	0.842	0.948	0.979
	Age structure	0.052	0.043	0.223	0.056	0.055	0.05	0.015	0.901	0.887
	Education level	0.115	0.055	0.004	0.109	0.123	0.111	0.065	0.937	0.912
	Annual total income	0.105	0.049	0.03	0.042	0.11	0.1	0.023	0.898	0.876
	Solar energy usage	0.041	0.041	0.312	0.008	0.045	0.04	0.002	0.952	0.958
	Environmental satisfaction	−0.089	0.042	0.013	−0.114	−0.094	−0.085	0.053	0.921	0.934
	Grazing prohibition	−0.086	0.047	0.039	0	−0.092	−0.083	0	0.943	0.98

Based on the above parameter estimations of the main influencing factors, household type was the key factor that influenced the personal carbon emissions in the Huangnan Prefecture, the Guoluo Prefecture, and the Yushu Prefecture. In order to further explore the impact of household types on personal carbon emissions, we conducted an LSD test (Table 7) and found the average personal carbon emissions of single households with three family members in the Hainan Prefecture were 1.14 t ce higher than those of households with four family members. Further, individuals in a four-member family emitted 0.53 t ce more CO_2 annually than individuals in households with over four members. This indicated that when the household population exceeded three members, the effect size of the potential carbon reduction would be weakened when the number of family members rose. There existed significant differences among the different family types in the Guoluo Prefecture. The personal carbon emissions were 6.1 t ce CO_2/(per household) for two-member families, 3.76 t ce CO_2/(per household) for three-member families, 3.11 t ce CO_2/(per household) for four-member families, and 2.31 t ce CO_2/(per household) for the families with more than four members, respectively. Therefore, with increasing numbers of family members, the average personal carbon emissions of herder households could be reduced in the Huangnan Prefecture. Such impacts of demographic effects on household carbon reductions were also observed in the Guoluo Prefecture and partly in the Yushu Prefecture, where there were no significant differences in the personal carbon emissions between two-member and three-member families.

Table 7. LSD test results for household type.

Prefecture	Household Type (Number of Family Members)		Mean Difference(I-J)	Standard Error	Significance	95% Confidence Interval	
						Lower Bound	Upper Bound
Hainan	two	three	−2.057 *	0.673	0.003	−3.386	−0.729
		four	−0.916	0.647	0.158	−2.192	0.360
		five or more	−0.381	0.567	0.503	−1.501	0.738
	three	two	2.057 *	0.673	0.003	0.729	3.386
		four	1.141 *	0.494	0.022	0.166	2.116
		five or more	1.676 *	0.384	0.000	0.918	2.434
	four	two	0.916	0.647	0.158	−0.360	2.192
		three	−1.141 *	0.494	0.022	−2.116	−0.166
		five or more	0.535	0.336	0.113	−0.128	1.197
	five or more	two	0.381	0.567	0.503	−0.738	1.501
		three	−1.676 *	0.384	0.000	−2.434	−0.918
		four	−0.535	0.336	0.113	−1.197	0.128
Huangnan	two	three	−0.610	0.650	0.348	−1.885	0.666
		four	0.271	0.642	0.673	−0.989	1.530
		five or more	1.033	0.636	0.105	−0.216	2.281
	three	two	0.610	0.650	0.348	−0.666	1.885
		four	0.880 *	0.176	0.000	0.535	1.225
		five or more	1.643 *	0.153	0.000	1.341	1.944
	four	two	−0.271	0.642	0.673	−1.530	0.989
		three	−0.880 *	0.176	0.000	−1.225	−0.535
		five or more	0.762 *	0.115	0.000	0.536	0.988
	five or more	two	−1.033	0.636	0.105	−2.281	0.216
		three	−1.643 *	0.153	0.000	−1.944	−1.341
		four	−0.762 *	0.115	0.000	−0.988	−0.536
Guoluo	two	three	2.335 *	0.315	0.000	1.717	2.953
		four	2.986 *	0.300	0.000	2.398	3.574
		five or more	3.782 *	0.293	0.000	3.207	4.357
	three	two	−2.335 *	0.315	0.000	−2.953	−1.717
		four	0.651 *	0.143	0.000	0.370	0.932
		five or more	1.447 *	0.128	0.000	1.196	1.698

Table 7. *Cont.*

Prefecture	Household Type (Number of Family Members)		Mean Difference(I-J)	Standard Error	Significance	95% Confidence Interval	
						Lower Bound	Upper Bound
Guoluo	four	two	−2.986 *	0.300	0.000	−3.574	−2.398
		three	−0.651 *	0.143	0.000	−0.932	−0.370
		five or more	0.796 *	0.084	0.000	0.631	0.961
	five or more	two	−3.782 *	0.293	0.000	−4.357	−3.207
		three	−1.447 *	0.128	0.000	−1.698	−1.196
		four	−0.796 *	0.084	0.000	−0.961	−0.631
Yushu	one	two	−1.197	1.094	0.274	−3.345	0.951
		three	−1.270	1.061	0.231	−3.352	0.812
		four	−0.025	1.059	0.981	−2.104	2.054
		five or more	0.969	1.050	0.356	−1.091	3.030
	two	one	1.197	1.094	0.274	−0.951	3.345
		three	−0.073	0.356	0.837	−0.773	0.626
		four	1.172 *	0.352	0.001	0.482	1.863
		five or more	2.167 *	0.321	0.000	1.535	2.798
	three	family	1.270	1.061	0.231	−0.812	3.352
		two	0.073	0.356	0.837	−0.626	0.773
		four	1.246 *	0.226	0.000	0.803	1.689
		five or more	2.240 *	0.175	0.000	1.896	2.583
	four	one	0.025	1.059	0.981	−2.054	2.104
		two	−1.172 *	0.352	0.001	−1.863	−0.482
		three	−1.246*	0.226	0.000	−1.689	−0.803
		five or more	0.994 *	0.166	0.000	0.669	1.319
	five or more	one	−0.969	1.050	0.356	−3.030	1.091
		two	−2.167 *	0.321	0.000	−2.798	−1.535
		three	−2.240 *	0.175	0.000	−2.583	−1.896
		four	−0.994 *	0.166	0.000	−1.319	−0.669

* indicates $p < 0.05$.

5. Discussion

Compared with other studies that relied on modeling, this study carried out a widespread analysis of household carbon emissions based on local widespread surveys, which could provide further insight into the relationships between carbon emissions and herder households. After all, official statistics for herder households have not been developed as well as those for urban and rural households outside of the Qinghai–Tibet Plateau. Further, the carbon issues of herder households have attracted less attention from researchers. Zhang et al. (2023) [49] found that with improvements in living standards, the per capita carbon emissions of non-urban households nearly exceeded those of urban households, based on the differences between the carbon emissions of urban and rural households in thirty provinces in China. Qu et al. (2013) [50] investigated the household carbon emissions in the cold and arid regions of northwestern China, and their results indicated that herder households in high-altitude highlands potentially exhibited the higher personal carbon emissions. Further, Xian et al. (2019) [51] revealed that with advancements in the China Western Development Strategy policy, energy consumption in the Western plateau region was producing a more severe problem of high-intensity exhaust emissions than the Eastern coastal areas. Zhang et al. (2023) [16] found that the per capita carbon emissions of pastoral households in Tibetan areas still were lower than those of the whole country; however, they would be continuously increased with improvements in living standards, which could not be neglected. The aforementioned studies all proposed that the individual carbon emissions of urban and rural households were not consistently greater than those of herder households in some cases. The contributions of carbon emissions from herder households to regional carbon emissions cannot be ignored. This study substantially supported the abovementioned viewpoints based on wide-spread field investigations, and it provides a new perspective for understanding the impacts of herder households on climate change.

Concerning the differences between direct and indirect carbon emissions, we suggested that household carbon reductions should not merely focus on household energy savings, but also addresses the importance of shifting to low-carbon behaviors for herder households. For example, the carbon emissions generated by the life-cycles of food consumption accounted for the largest proportion of household emissions, and therefore, moderate reductions in meat consumption could reduce carbon footprints during household dining [52,53]. Despite this, may be difficult for the ethnic minorities of herder households to adopt lighter diets without the meat of yak and sheep, since the diets of Tibetans and other ethnic groups, including Huis, Salas, and Mongolians, have long relied on meat consumption. However, the waste production during meat consumption could be reduced, which, to some extent, would contribute to both direct and indirect carbon reductions. Our findings further confirmed that larger household sizes contributed to reductions in personal carbon emissions, which may be attributable to the positive impacts of larger families on food waste reductions. The relevant studies conducted by Song et al. [54], Song et al. [55], and Zhang et al. [56] directly or indirectly support this viewpoint. Meanwhile, this study found a negative correlation between grazing prohibitions and personal household emissions. On the one hand, the governmental promotions of grazing prohibitions have raised awareness about environmental protections, which have guided the herdsmen to embrace more greener lifestyles with less consumption of fertilizers, pesticides, and fossil energies during their residential livelihoods, therefore resulting in lower household carbon emissions. On the other hand, the scale and range of livestock grazing are limited by official grazing prohibitions, and the fossil and non-fossil energy consumption levels related to animal husbandry have been reduced.

It is undeniable that this study had limitations, and they limited our ability to further understand household carbon emissions in the Qinghai–Tibet Plateau. In future, the number of questionnaires during the on-site surveys could be increased to cover more counties located in other plateau regions within the Qinghai–Tibet Plateau. In addition, the frequency of the surveys could be appropriately increased to two or more times in one year, aiming to reveal the seasonal responses of household consumption to climate change. These elements would strengthen the objectivity of the statistical results and improve the ability of the relevant analyses to elucidate the roles of herder households in climate change mitigation.

6. Conclusions

Based on on-site questionnaire surveys, this study estimated direct and indirect household carbon emissions and explored their influencing factors by using an optimal scale regression analysis and multiple comparative analysis methods. Our findings indicated the following: (1) Spatial differences exist in the amounts of household carbon emissions and their compositions in the Sanjiangyuan region. The regional carbon emissions were found to be the highest in Nangqian County and the lowest in Zhiduo County, and the hotspots with higher regional carbon emissions were concentrated in the eastern part of the Sanjiangyuan region. (2) The direct personal carbon emissions were higher for the Yushu Prefecture, and those of the Guoluo Prefecture were the lowest. Indirect carbon emissions were higher than direct carbon emissions in all four prefectures, and the industry sectors of food and housing were the two main indirect emission sources. The Hainan Prefecture exhibited the highest per capita indirect carbon emissions. (3) Household type was the main factor influencing personal carbon emissions across the prefectures. The larger the household population, the lower the personal carbon emissions. However, the effect size of the potential carbon reduction was weakened when the number of family members rose to more than three. (4) We propose that proper grazing prohibitions and low-carbon dietary shifting would contribute to lower-carbon herder livelihoods, especially for small-sized households that should be peer-to-peer targeted by regional government propaganda. Given the limited financial resources in these less-developed regions, this may help to

strengthen the implementation of in-depth low-carbon promotions from door-to-door campaigns across the Sanjiangyuan region and even the overall Qinghai–Tibet Plateau.

Author Contributions: Conceptualization, C.S., L.L., C.X. and Z.O.; methodology, C.S., L.L. and C.X.; software, L.L. and F.F.; validation, C.S., L.L. and C.X.; formal analysis, C.S., L.L. and F.F.; investigation, C.S., L.L. and F.F.; data curation, C.S., L.L. and C.X.; writing—original draft preparation, C.S., L.L. and C.X.; writing—review and editing, C.S., C.X. and Z.O.; visualization, C.S. and L.L. All authors have read and agreed to the published version of the manuscript.

Funding: This research was funded by the Second Tibetan Plateau Scientific Expedition and Report, grant number 2019QZKK0308, the National Key Research and Development Program of China (2022YFB3903701), and the National Natural Science Foundation of China (No. 42101290).

Institutional Review Board Statement: Not applicable.

Informed Consent Statement: Not applicable.

Data Availability Statement: The data presented in this study are available from the corresponding author upon reasonable request. The data are not publicly available due to restrictions or privacy.

Conflicts of Interest: The authors declare no conflict of interest.

Appendix A

Table A1. The definitions of variables for household characteristics and their corresponding questions in the questionnaire.

Variable Name	Variable Definition	Corresponding Questionnaire Question
Family Type	Single family = 1, A family of two = 2, A family of three = 3, A family of four = 4, Family with many members = 5	How many people are there in the family? (Fill in the blanks)
Age structure	Under 18 = 0, 18-65 = 1, Over 65 = 2	In the first part of the questionnaire, the age of the family members was counted. (Fill in the blanks)
Education Level	Illiteracy = 1, Primary school = 2, Junior high school = 3, High school/Technical secondary school = 4, Junior college = 5, Bachelor's degree or above = 6, (Monastic education: less than 6 years as primary school = 2, 7 years and above as junior high school = 3)	In the first part of the questionnaire, the information table of family members is used to calculate the educational level. (Multiple choice) Options: Illiterate, primary school, junior high school, senior high school/technical secondary school, junior college, undergraduate and above, monastic education
Annual Income	Annual personal income (Yuan)	In the second part of the questionnaire, annual net income was measured for subsistence activities. (Fill in the blanks)
Solar Utilization	Yes = 1, No = 2	The third part of the questionnaire, living capital, counted the amount of solar energy. (Fill in the blanks)
Environmental Satisfaction	Gets better = 1, Stays the same = 2, Gets worse = 3	In the fourth part of the questionnaire, ecological policy and perception: do you think the surrounding grassland has become better in the past ten years? (multiple choice) Choice: Better, unchanged, worse
Grazing Prohibition	Tighter = 1, Unchanged = 2, Looser = 3	In the fourth part of the questionnaire, ecological policy and perception: do you think there has been any change in the prohibition of grazing in the surrounding pastures in the past ten years? (multiple choice) Choice: strict, unchanged, loose

Table A2. The definitions of variables for household carbon estimation and their corresponding questions in the questionnaire.

Variable Name	Variable Definition	Inclusion Variable	Corresponding Questionnaire Question
Individual Direct Carbon Emissions	Direct carbon emissions from personal energy consumption (t ce/year)	Animal Manure	In the third part of the questionnaire, the amount of cow manure and sheep manure used was counted. (Fill in the blanks)
		Coal	The third section of the questionnaire, livelihood capital, measured coal use. (Fill in the blanks)
		Natural Gas	The third part of the questionnaire, livelihood capital, counted natural gas or liquefied gas. (Fill in the blanks)
		Electricity	The third part of the questionnaire, living capital, calculates electricity consumption. (Fill in the blanks)
Individual Indirect Carbon Emissions	Direct and indirect emissions from personal energy consumption (t ce/year)	Food	In the third part of the questionnaire, the living capital is counted the monthly living expenses (food, oil, meat, vegetables, etc.). (Fill in the blanks)
		Clothing	The third part of the questionnaire, living capital, calculates the cost of buying clothes. (Fill in the blanks)
		Household Equipment, Supplies and Services	The third part of the questionnaire, living capital, statistics furniture, appliances, and other durable goods consumer spending. (Fill in the blanks)
		Healthcare	In the third section of the questionnaire, living capital, medical expenses were counted. (Fill in the blanks)
		Transportation and Communication	In the third part of the questionnaire, transportation cost and communication cost are counted, respectively. (Fill in the blanks)
		Cultural, Educational and Entertainment Supplies and Services	In the third part of the questionnaire, living capital, the expenditure on children's schooling was calculated. (Fill in the blanks)
		Living	In the third part of the questionnaire, living capital, the consumption of housing construction is counted. (Fill in the blanks)
		Other Goods and Services	In the third part of the questionnaire, living capital, counted the cost of human favors and gifts, weddings, and funerals, respectively. (Fill in the blanks)

References

1. Shen, Y.; Sun, X.; Fu, Y. The spatial network and its driving factors for sustainable total-factor ecology efficiency: The case of China. *Environ. Sci. Pollut. Res. Int.* **2021**, *28*, 68930–68945. [CrossRef] [PubMed]
2. Pang, Q.; Xiang, M.; Zhang, L.; Chiu, Y.-H. Indirect carbon emissions from household consumption of middle-income groups: Evidence from Yangtze River Economic Belt in China. *Energy Sustain. Dev.* **2023**, *76*, 101280. [CrossRef]
3. Jiang, L.; Xue, B.; Xing, R.; Chen, X.; Song, L.; Wang, Y.; Coffman, D.M.; Mi, Z. Rural household energy consumption of farmers and herders in the Qinghai-Tibet Plateau. *Energy* **2020**, *192*, 116649. [CrossRef]
4. Peng, S.; Wang, X.; Du, Q.; Wu, K.; Lv, T.; Tang, Z.; Wei, L.; Xue, J.; Wang, Z. Evolution of household carbon emissions and their drivers from both income and consumption perspectives in China during 2010–2017. *J. Environ. Manag.* **2023**, *326*, 116624. [CrossRef] [PubMed]

5. Su, S.; Ding, Y.; Li, G.; Li, X.; Li, H.; Skitmore, M.; Menadue, V. Temporal dynamic assessment of household energy consumption and carbon emissions in China: From the perspective of occupants. *Sustain. Prod. Consum.* **2023**, *37*, 142–155. [CrossRef]
6. Chen, Z.; Zhang, Z.; Feng, T.; Liu, D. What drives the temporal dynamics and spatial differences of urban and rural household emissions in China? *Energy Econ.* **2023**, *125*, 106849. [CrossRef]
7. Jiang, L.; Xing, R.; Chen, X.; Xue, B. A survey-based investigation of greenhouse gas and pollutant emissions from household energy consumption in the Qinghai—Tibet Plateau of China. *Energy Build.* **2021**, *235*, 110753. [CrossRef]
8. Yuan, R.; Rodrigues, J.F.D.; Behrens, P. Driving forces of household carbon emissions in China: A spatial decomposition analysis. *J. Clean. Prod.* **2019**, *233*, 932–945. [CrossRef]
9. Liang, L.; Wu, W.; Lal, R.; Guo, Y. Structural change and carbon emission of rural household energy consumption in Huantai, northern China. *Renew. Sustain. Energy Rev.* **2013**, *28*, 767–776. [CrossRef]
10. Zhou, Y.; Yuan, G.; Cong, Z.; Wang, X. Priorities for the sustainable development of the ecological environment on the Tibetan Plateau. *Fundam. Res.* **2021**, *1*, 329–333. [CrossRef]
11. Zhang, J.; Shi, Y.; Xian, C.; Zhang, L.; Zou, Z. How urbanization affect the ecosystem health of Tibet based on terrain gradients: A case study of Shannan, China. *Ecosyst. Health Sustain.* **2022**, *8*, 2097449. [CrossRef]
12. Fan, Y.; Fang, C. Insight into carbon emissions related to residential consumption in Tibetan Plateau—Case study of Qinghai. *Sustain. Cities Soc.* **2020**, *61*, 102310. [CrossRef]
13. Li, T.; Cai, S.; Singh, R.K.; Cui, L.; Fava, F.; Tang, L.; Xu, Z.; Li, C.; Cui, X.; Du, J.; et al. Livelihood resilience in pastoral communities: Methodological and field insights from Qinghai—Tibetan Plateau. *Sci. Total Environ.* **2022**, *838*, 155960. [CrossRef] [PubMed]
14. Ping, X.; Li, C.; Jiang, Z. Household energy consumption patterns in agricultural zone, pastoral zone and agro-pastoral transitional zone in eastern part of Qinghai—Tibet Plateau. *Biomass Bioenergy* **2013**, *58*, 1–9. [CrossRef]
15. Wei, Y.-M.; Liu, L.-C.; Fan, Y.; Wu, G. The impact of lifestyle on energy use and CO_2 emission: An empirical analysis of China's residents. *Energy Policy* **2007**, *35*, 247–257. [CrossRef]
16. Zhang, H.; Shi, X.; Wang, K.; Xue, J.; Song, L.; Sun, Y. Intertemporal lifestyle changes and carbon emissions: Evidence from a China household survey. *Energy Econ.* **2020**, *86*, 104655. [CrossRef]
17. Zhang, Y.; Wang, F.; Zhang, B. The impacts of household structure transitions on household carbon emissions in China. *Ecol. Econ.* **2023**, *206*, 107734. [CrossRef]
18. Zhou, Y.; Wang, H.; Qiu, H. Population aging reduces carbon emissions: Evidence from China's latest three censuses. *Appl. Energy* **2023**, *351*, 121799. [CrossRef]
19. Zhou, Y.; Liu, Y. Does population have a larger impact on carbon dioxide emissions than income? Evidence from a cross-regional panel analysis in China. *Appl. Energy* **2016**, *180*, 800–809. [CrossRef]
20. Xu, X.; Han, L.; Lv, X. Household carbon inequality in urban China, its sources and determinants. *Ecol. Econ.* **2016**, *128*, 77–86. [CrossRef]
21. Golley, J.; Meng, X. Income inequality and carbon dioxide emissions: The case of Chinese urban households. *Energy Econ.* **2012**, *34*, 1864–1872. [CrossRef]
22. Akrofi, M.M.; Okitasari, M.; Qudrat-Ullah, H. Are households willing to adopt solar home systems also likely to use electricity more efficiently? Empirical insights from Accra, Ghana. *Energy Rep.* **2023**, *10*, 4170–4182. [CrossRef]
23. Zhang, J.; Li, F.; Sun, M.; Sun, S.; Wang, H.; Zheng, P.; Wang, R. Household consumption characteristics and energy-related carbon emissions estimation at the community scale: A study of Zengcheng, China. *Clean. Responsible Consum.* **2021**, *2*, 100016. [CrossRef]
24. Zeng, M. Relationship between awareness and behavior of carbon emission reduction in household consumption and its influence path. *Bus. Econ.* **2023**, *7*, 5–13.
25. Li, Z.; Li, G.P.; Hu, Z. Xi'an household carbon emission characteristics. *Resour. Sci.* **2017**, *39*, 1394–1405.
26. Zhao, M.; Yuan, Z.; Chan, H.S. Housing wealth and household carbon emissions: The role of homeownership in China. *Ecol. Econ.* **2023**, *212*, 107908. [CrossRef]
27. Arachchi, J.I.; Managi, S. Social capital, household income and carbon dioxide emissions: A multicountry analysis. *Environ. Impact Assess. Rev.* **2022**, *96*, 106838.
28. Adua, L. Super polluters and carbon emissions: Spotlighting how higher-income and wealthier households disproportionately despoil our atmospheric commons. *Energy Policy* **2022**, *162*, 112768. [CrossRef]
29. Xia, Y.; Wang, H.; Liu, W. The indirect carbon emission from household consumption in China between 1995–2009 and 2010–2030: A decomposition and prediction analysis. *Comput. Ind. Eng.* **2019**, *128*, 264–276. [CrossRef]
30. Ruiping Wang, B.L. Application of optimal scale analysis and implementation of SPSS software. *Shanghai Pharm.* **2022**, *43*, 46–49.
31. Xun Xiao, X.Y.; Xin, X. Investigation and analysis for mathematical ability of middle school students with optimal scale regression analysis method. *Theory Pract. Contemp. Educ.* **2020**, *12*, 29–35.
32. Li Luo, F.L.; Haiqi, K.; Zhongwei, H. Analysis of factors affecting livestock and poultry disease control act of Beijing: Based on the optimal scaling regression. *Mark. Perspect.* **2016**, *52*, 8–13.
33. Büchs, M.; Schnepf, S.V. Who emits most? Associations between socio-economic factors and UK households' home energy, transport, indirect and total CO_2 emissions. *Ecol. Econ.* **2013**, *90*, 114–123. [CrossRef]
34. China National Bureau of Statistics. *China Statistical Year Book (County-Level) 2022*; China Statistics Press: Beijing, China, 2022.

35. China National Bureau of Statistics. *China Statistical Year Book 2022*; China Statistics Press: Beijing, China, 2022.
36. Liu, M.; Rao, D.; Yang, L.; Min, Q. Subsidy, training or material supply? The impact path of eco-compensation method on farmers' livelihood assets. *J. Environ. Manag.* **2021**, *287*, 112339. [CrossRef] [PubMed]
37. Zhu, D.; Niu, Q.; Wang, Y.; Peng, S.; Lu, X.; Zhou, H.; Zhang, F. The influence of psychological cognition and policy environment on the basin residents' behavior of ecological compensation under the background of carbon neutrality: A case study in upper Yellow River basin, China. *Ecol. Indic.* **2023**, *148*, 110031. [CrossRef]
38. Yang, Q.; Nan, Z.; Tang, Z. Influencing factors of the grassland ecological compensation policy to herdsmen's behavioral response: An empirical study in Hexi corridor. *Acta Ecol. Sin.* **2022**, *42*, 74–79. [CrossRef]
39. Li, Y.; Zhao, R.; Liu, T.; Zhao, J. Does urbanization lead to more direct and indirect household carbon dioxide emissions? Evidence from China during 1996–2012. *J. Clean. Prod.* **2015**, *102*, 103–114. [CrossRef]
40. Han, H.; Wu, S.; Zhang, Z. Factors underlying rural household energy transition: A case study of China. *Energy Policy* **2018**, *114*, 234–244. [CrossRef]
41. Liu, Y.; Xie, X.; Wang, M. Energy structure and carbon emission: Analysis against the background of the current energy crisis in the EU. *Energy* **2023**, *280*, 128129. [CrossRef]
42. Yu, M.; Meng, B.; Li, R. Analysis of China's urban household indirect carbon emissions drivers under the background of population aging. *Struct. Change Econ. Dyn.* **2022**, *60*, 114–125. [CrossRef]
43. China National Bureau of Statistics. *China Energy Statistical Year Book 2022*; China Statistics Press: Beijing, China, 2022.
44. The Intergovernmental Panel on Climate Change (IPCC). *IPCC Guidelines for National Greenhouse Gas Inventories*; IPCC WGI Technical Support Unit: Bracknell, UK, 2006.
45. Dong, H.; Geng, Y. Study on Carbon Footprint of the household consumption in Beijing based on Input-Output analysis. *Resour. Sci.* **2012**, *34*, 494–501.
46. Yang, Y.Z.; Dan, W.; Fei, X. Construction of cigarette consumer brand preference prediction model based on optional scale regression. *China J. Commer.* **2022**, 80–85.
47. Zheng Wang, W.Z. Relationship between land elements promotion mode and rural revitalization level in Shandong Province based on optional scaling analysis. *J. Hebei Agric. Sci.* **2021**, *25*, 20–24.
48. Chen, Y.; Liu, H.; Shi, L. Operation strategy of public building: Implications from trade-off between carbon emission and occupant satisfaction. *J. Clean. Prod.* **2018**, *205*, 629–644. [CrossRef]
49. Zhang, S.; Shi, B.; Ji, H. How to decouple income growth from household carbon emissions: A perspective based on urban-rural differences in China. *Energy Econ.* **2023**, *125*, 106816. [CrossRef]
50. Qu, J.; Zeng, J.; Li, Y.; Wang, Q.; Maraseni, T.; Zhang, L.; Zhang, Z.; Clarke-Sather, A. Household carbon dioxide emissions from peasants and herdsmen in northwestern arid-alpine regions, China. *Energy Policy* **2013**, *57*, 133–140. [CrossRef]
51. Xian, C.; Zhang, X.; Zhang, J.; Fan, Y.; Zheng, H.; Salzman, J.; Ouyang, Z. Recent patterns of anthropogenic reactive nitrogen emissions with urbanization in China: Dynamics, major problems, and potential solutions. *Sci. Total Environ.* **2018**, *656*, 1071–1081. [CrossRef]
52. González-García, S.; Esteve-Llorens, X.; Moreira, M.T.; Feijoo, G. Carbon footprint and nutritional quality of different human dietary choices. *Sci. Total Environ.* **2018**, *644*, 77–94. [CrossRef]
53. Xian, C.; Gong, C.; Lu, F.; Zhang, L.; Ouyang, Z. Linking dietary patterns to environmental degradation: The spatiotemporal analysis of rural food nitrogen footprints in China. *Front. Nutr.* **2021**, *8*, 717640. [CrossRef]
54. Song, G.; Li, M.; Semakula, H.M.; Zhang, S. Food consumption and waste and the embedded carbon, water and ecological footprints of households in China. *Sci. Total Environ.* **2015**, *529*, 191–197. [CrossRef]
55. Song, G.; Semakula, H.M.; Fullana-I-Palmer, P. Chinese household food waste and its' climatic burden driven by urbanization: A Bayesian Belief Network modelling for reduction possibilities in the context of global efforts. *J. Clean. Prod.* **2018**, *202*, 916–924. [CrossRef]
56. Zhang, H.; Duan, H.; Andric, J.M.; Song, M.; Yang, B. Characterization of household food waste and strategies for its reduction: A Shenzhen City case study. *Waste Manag.* **2018**, *78*, 426–433. [CrossRef] [PubMed]

atmosphere

MDPI

Article

Evaluating the Conservation Status and Effectiveness of Multi-Type Protected Areas for Carbon Sequestration in the Loess Plateau, China

Sony Lama, Jingjing Zhang * and Xiaofeng Luan

School of Ecology and Nature Conservation, Beijing Forestry University, Beijing 100083, China; sonylama@bjfu.edu.cn (S.L.); luanxiaofeng@bjfu.edu.cn (X.L.)
* Correspondence: jjzhang@bjfu.edu.cn

Abstract: Evaluating the conservation effectiveness of multiple types of protected areas (PAs) on carbon sequestration services can enhance the role of PAs in mitigating global warming. Here, we evaluated the conservation status and effectiveness of national parks, nature reserves, forest parks, geo-parks, and scenic spots on carbon sequestration within the Loess Plateau throughout 2000–2020. The results show that all existing PA types have good representation and conservation effectiveness on carbon sequestration. Nature reserves are the most representative of carbon sequestration but are the least effective in protecting carbon sequestration and are the only ones that are weekly effective in protecting critical carbon sequestration. The main factors influencing these results are PA size, 2000 precipitation, slope, change rate of evapotranspiration, PA rank, and 2000 evapotranspiration. We suggest upgrading the critical carbon sequestration distribution areas in scenic spots, forest parks and geo-parks to national parks or nature reserves in the future and implementing appropriate protection and restoration measures in low carbon sequestration areas within grassland and wild plant nature reserves to help achieve the goal of carbon neutrality early.

Keywords: type of protected areas; carbon sequestration services; conservation status; conservation effectiveness; Loess Plateau

Citation: Lama, S.; Zhang, J.; Luan, X. Evaluating the Conservation Status and Effectiveness of Multi-Type Protected Areas for Carbon Sequestration in the Loess Plateau, China. *Atmosphere* **2024**, *15*, 764. https://doi.org/10.3390/atmos15070764

Academic Editor: Dmitry Belikov

Received: 6 June 2024
Revised: 21 June 2024
Accepted: 25 June 2024
Published: 27 June 2024

1. Introduction

Human-induced climate change and biodiversity loss pose interconnected emergencies that threaten human well-being [1–3]. Policy frameworks such as the Sustainable Development Goals, United Nations Framework Convention on Climate Change, Convention on Biological Diversity, and others emphasise that ecological conservation and restoration should simultaneously contribute to biodiversity conservation and climate change mitigation [4–7]. Increasing concentrations of greenhouse gases like carbon dioxide (CO_2) are significant contributors to global warming [8,9], accelerated by increasing deforestation and vegetation degradation [10–12].

Establishing Protected areas (PAs) not only enhances biodiversity conservation [13–15] but also mitigates global warming by increasing vegetation's carbon sequestration services [16,17]. In response to global climate change, most countries are still planning to reach net-zero carbon emissions by 2050–2070 [18], and the Chinese government has proposed achieving carbon neutrality by 2060 [19]. Strengthening vegetation's carbon sequestration in PAs is a key strategy to achieve this goal [20,21]. China is building a PA system mainly composed of national parks to address issues of spatial overlap and multiple management of existing PA types [22]. Given global climate change and the opportunity to integrate and optimise PAs in China, it is necessary to scientifically assess the conservation effects of different PA types on carbon sequestration.

Current studies predominantly focus on analysing changes in total carbon sequestration within PAs. Melillo et al. [16] analysed the changes in carbon sequestration in over

150,000 PAs worldwide from 1700 to 2005, finding that global carbon sequestration in PAs was 0.5 PgC per year, accounting for about one-fifth of the annual carbon sequestration of all terrestrial ecosystems; Tian et al. [23] assessed changes in carbon sequestration in 8133 different types of terrestrial PAs in China from 1980 to 2020, showing that the amount of carbon sequestration in PAs over past 40 years had significantly increased, with nature reserves sequestering the enormous amount of carbon, and forest parks sequestering the highest amount of carbon per unit area, despite a clear downward trend.

Research on conservation effects is not uniform. Internationally, studies tend to analyse all PAs as a single type. For instance, Duncanson et al. [24] analysed the conservation effects of 260,000 PAs globally on carbon sequestration between 2000 and 2020 using the propensity score matching method (PSM), and the results showed that PAs are crucial for climate change mitigation globally, especially in areas with high carbon sequestration. In China, the focus is more on the conservation effects of nature reserves on carbon sequestration. For example, Cao [25] used PSM to analyse the conservation effect of 19 national nature reserves in the Qinling Mountains on carbon sequestration from 2010 to 2015, finding that carbon sequestration in national nature reserves increased more than that outside the reserves. However, Xu et al. [26] used the representativeness evaluation method to assess the protection status of carbon sequestration in 2412 nature reserves in China during 2010 and found that the representativeness of nature reserves on carbon sequestration was weak. More research on different PA types regarding conservation effectiveness assessment is needed, as various methods can yield different results. Exploring the conservation effectiveness of different PA types on carbon sequestration can help promote the effective management of carbon sequestration and thus mitigate climate change.

The Loess Plateau, with severe soil erosion and a fragile ecological environment, is one of the most concentrated regions in China in terms of population, resources, and environmental conflicts [27]. To curb soil erosion, the Chinese government launched the Grain for Green Project on the Loess Plateau in 1999, significantly changing the regional land use pattern [28]. This paper investigates the conservation status and effects of carbon sequestration in five significant PAs types (national parks, nature reserves, forest parks, geo-parks, and scenic spots) on the Loess Plateau from 2000 to 2020. The objectives of this study are (1) to clarify the conservation status and effects of different PA types on carbon sequestration, (2) to identify the critical factors affecting the conservation effects of carbon sequestration, and (3) to provide suggestions for subsequent conservation management, thereby offering scientific support for the integration and optimisation of China's PAs and contributing to global goals of carbon neutrality and climate change mitigation.

2. Materials and Methods

2.1. Study Area

The Loess Plateau is a temperate semi-moist and semi-arid transition zone in China that spans approximately 649,000 km^2, accounting for 6.76% of China's total land area [29]. The region's average annual rainfall is between 20 and 700 mm, and the vegetation (Figure 1) from southeast to northwest is warm-temperate deciduous broad-leaved forest, forest grassland, typical grassland, and desert grassland [30]. In addition, the Loess Plateau is the world's largest accumulation area of loess and an essential ecological function area in the middle reaches of the Yellow River [31]. In order to protect the regional ecological environment, more than 700 PAs of different types, accounting for 15.1% of the total area of the Loess Plateau, of which more than 160 are nature reserves, have been established.

2.2. Methods

In this study, we first selected PAs with carbon sequestration functions established within the Loess Plateau by 2020 and those established by 2000 and earlier. We then conducted a representative analysis and applied methods based on the strictness of PAs to evaluate their conservation status and effectiveness in carbon sequestration. Subsequently, we identified factors affecting conservation effectiveness based on the basic attributes of

the PAs, such as natural geography, socio-economic, and demographic aspects. Finally, we provided targeted recommendations to enhance the effectiveness of these conservation efforts. Figure 2 shows the research flowchart.

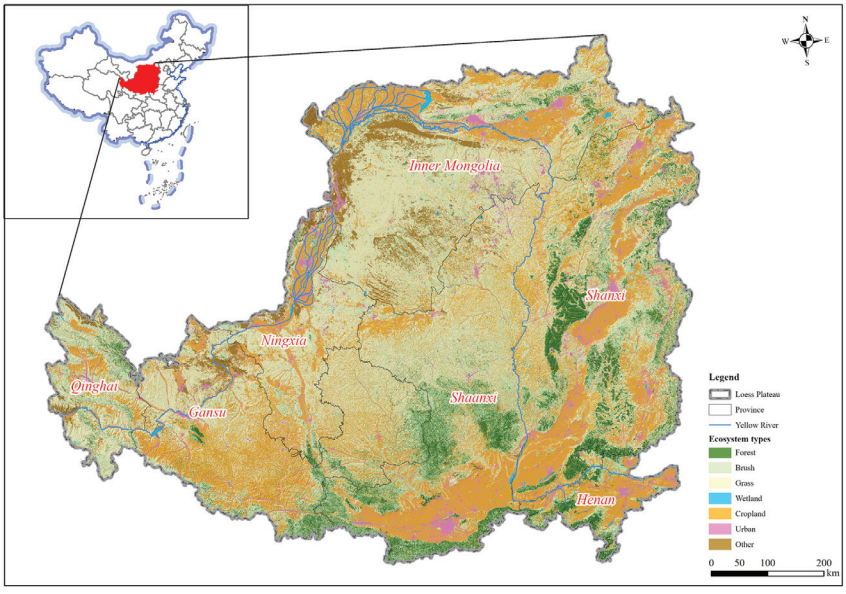

Figure 1. Map of the study area.

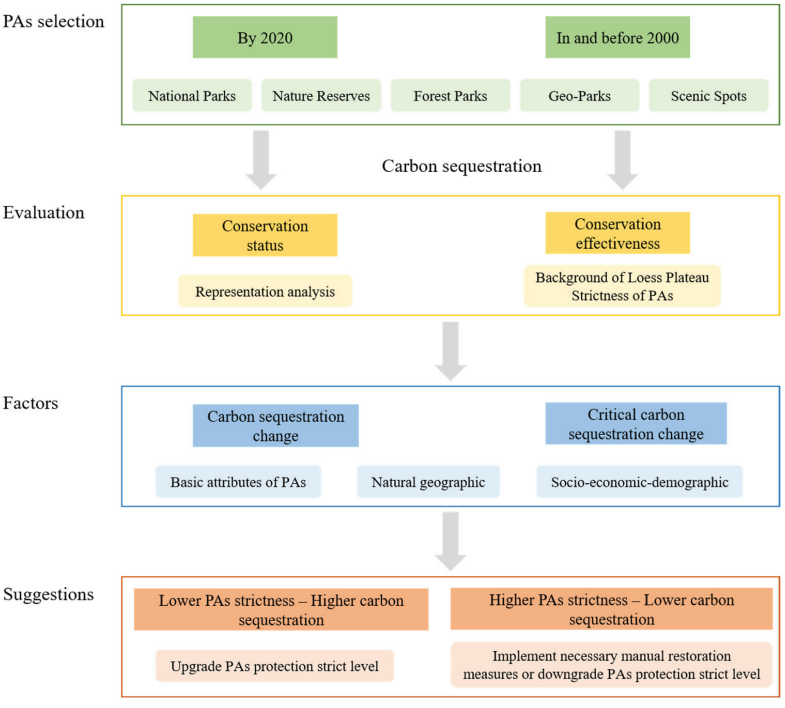

Figure 2. Research flowchart.

2.2.1. Data Sources

We obtained data on the spatial distribution and basic information of PAs on the Loess Plateau from the State Forestry and Grassland Administration. To evaluate the conservation status and effectiveness, we obtained carbon sequestration data from the 2000 to 2020 China Ecosystem Services Dataset of the Ecological Environment Research Centre of the Chinese Academy of Sciences, with a resolution of 250 m. Data on influencing factors, including precipitation, temperature, evapotranspiration, population density, GDP, soil texture, DEM, and slope, were obtained from the Resource Environmental Science Data Registry and Publishing System at a spatial resolution of 1 km. We used a spatial resolution of 250 m to assess the conservation effects of cs, and a spatial resolution of 1 km was used to analyse the impact factors, both in WGS 1984 Albers coordinates and calculated in ArcGIS 10.8.

2.2.2. Selected Protected Areas

In the current conservation situation analysis, we choose PAs with an area larger than 5 km^2 and with more vegetation distribution to remove those without carbon sequestration or lower carbon sequestration functions. Selected five types of PAs, including national park pilot areas, forest parks, geo-parks, scenic spots, and nature reserves (dominated by forests, grasslands, wild animal, and wild plant types), to assess the 2020 conservation status of carbon sequestration in 2020. We only selected the PAs established in 2000 and before for the dynamic analyses. Because we could not obtain the boundaries of the PAs in each period, we assumed that the boundaries of these PAs had not changed.

2.2.3. Carbon Sequestration

We used the fixed amount of CO_2 to evaluate the physical quantity of carbon sequestration in natural ecosystems, which was calculated by the carbon sequestration rate method [32].

$$Q_{tCO_2} = M_{CO_2}/M_C \times (VCSR + SCSR) \times S \quad (1)$$

where, Q_{tCO_2} means the total carbon sequestration (t CO_2/a), $\frac{M_{CO_2}}{M_C} = 44/12$, means the coefficient of conversion of C to CO_2, VCSR means the carbon sequestration rate of vegetation, SCSR means the carbon sequestration rate of soil, and S indicates the area of each ecosystem type.

The importance of ecosystem services indicates the significance of ecological protection for different ecological units. Based on the physical amount of carbon sequestration in the Loess Plateau region, we classified 50% of the area with the highest physical amount as critical [33].

2.2.4. Conservation Effectiveness

We used spatial overlay analysis and before-and-after comparisons to analyse the conservation effectiveness of carbon sequestration in PAs. For status quo conservation effectiveness, we only used the carbon sequestration data in 2020 by using representation analysis as follows [26]:

$$\frac{PA_{CS_{20}}}{LP_{CS_{20}}} \times 100\% \geq \frac{PA_{area_{20}}}{LP_{area}} \times 100\% \quad (2)$$

For dynamic protection effectiveness assessments, we used the rate of change in the physical amount of carbon sequestration from 2000 to 2020 as follows:

$$\frac{PA_{CS_{20}} - PA_{CS_{00}}}{PA_{CS_{00}}} \times 100\% \geq W_i \times \frac{LP_{CS_{20}} - LP_{CS_{00}}}{LP_{CS_{00}}} \times 100\% \quad (3)$$

where $PA_{CS_{20/00}}$ means the physical amount (critical amount) of carbon sequestration in the PAs in 2020/2000; $LP_{CS_{20/00}}$ means the physical amount (critical amount) of carbon

sequestration in the Loess Plateau in 2020/2000; $PA_{area_{20}}$ means the total area of PAs in the Loess Plateau in 2020; LP_{area} means the area of Loess Plateau.

W_i means the weights of different PA types were set according to their strictness rating in China [34]. Prior to the establishment of national parks in China, nature reserves were set as the strictest type of PAs [35], subdivided into three function zones (e.g., core, buffer, and experimental), three major categories (e.g., natural ecosystem, wildlife, and natural relics), and nine types. Only a partial of the experimental zones can be opened to the public with permission. Natural ecosystem types nature reserves contained representativeness, typicality, and completeness ecosystems; wildlife types nature reserves focused on rare wildlife species and their habitats. Other PA types, such as forest parks, geo-parks, and scenic spots, were less subdivided and relatively more open to the public. Based on that, the weight of nature reserves is set to 2/3 (when considering nature reserve types alone, the weight of nature reserves of natural ecosystem types is set to 2/3, the weight of nature reserves of wildlife types is set to 1/3), the weight of geo-parks, forest parks, and scenic spots is set to 1/3.

2.2.5. Impact Factors

Using the rate of change in the physical volume of carbon sequestration within PAs as the dependent variable, Spearman correlation analyses were conducted using SPSS software to reveal the drivers, such as differences in PAs (e.g., time, area, and area), natural factors (e.g., dem, slope, temperature, precipitation, evapotranspiration, and soil texture), and threatening factors (e.g., population density, GDP, and cropland). We define a correlation coefficient of less than 0.3 as a weak correlation, 0.3 and 0.6 as a moderate correlation, and greater than 0.6 as a strong correlation.

3. Results

3.1. Conservation Status

Regarding physical quantity, the total amount of carbon sequestration in the Loess Plateau in 2020 was 277.41 Tg, of which 138.71 Tg is critical. Regarding spatial distribution (Figure 3), the amount of carbon sequestration shows a pattern that is higher in the southeast and lower in the northwest. The areas with high carbon sequestration are mainly distributed in the southern part of the Lvliang Mountains, the southern part of the Taihang Mountains, the Zhongtiao Mountains, the Ziwu Ridge, the northern part of the Qinling Mountains, the southern part of the Liupan Mountains, and the Daban Mountains; the areas with low carbon sequestration mainly concentrated in the northern desert area.

Based on the screening method, a total of 430 PAs (including national park pilot areas, forest parks, geo-parks, scenic spots, and nature reserves) have been selected, with a total area of about 70,500 km^2, accounting for 10.85% of the total area of the Loess Plateau in 2020. Regarding spatial distribution (Figure 4a), there are fewer PAs in the central part of the Loess Plateau, and most of them are distributed in the eastern part. In terms of the number of PA types (Figure 4b), the number of forest parks is higher, accounting for 51.86% of the total, followed by nature reserves, which account for 27.21%, scenic spots and national parks account for a smaller proportion of the total, with 6.05% and 0.23%, respectively. In terms of the area of the types (Figure 4b), the nature reserves accounted for the largest proportion of the area of the Loess Plateau at 5.70%, followed by forest parks at 2.79%, scenic spots, and national parks accounted for a relatively small proportion of the area at 0.51% and 0.37% respectively.

In 2020, the total amount of carbon sequestration in the 430 PAs was 104.52 Tg. The total amount of critical carbon sequestration was 69.44 Tg, which accounted for 37.68% and 50.07% of the total amount of the Loess Plateau, respectively; this is much more than the proportion of the total area of the Loess Plateau accounted for by the PAs (10.85%). As can be seen from Figure 5, the conservation effect of carbon sequestration in the five types of PAs was better, with the proportion of forest parks, geo-parks, and scenic spots exceeding 40% of the proportion of the area. Although nature reserves are more effective in protecting

carbon sequestration, in terms of specific types, forest and wild animal types of nature reserves are more effective in safeguarding carbon sequestration. In contrast, grassland and wild plant types are relatively weaker.

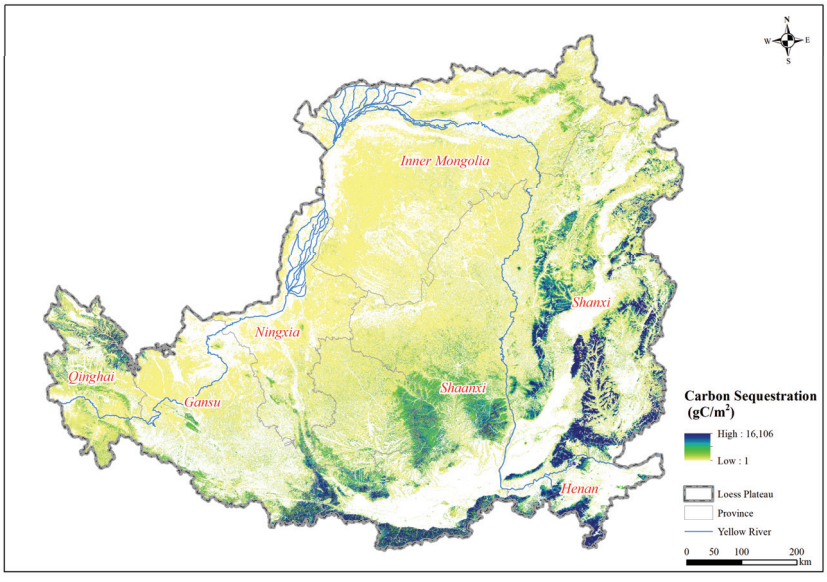

(**a**)

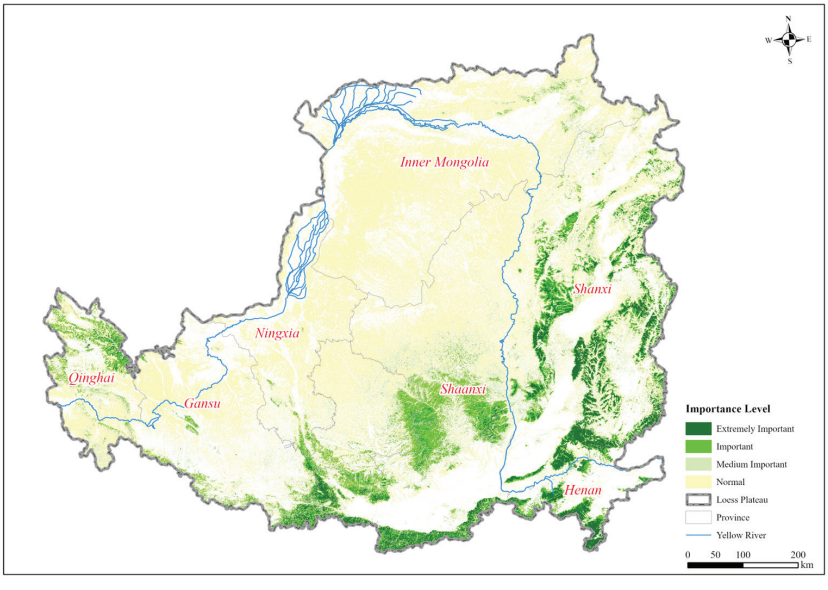

(**b**)

Figure 3. Spatial distribution of carbon sequestration in Loess Plateau (**a**) physical quantity; (**b**) Importance level.

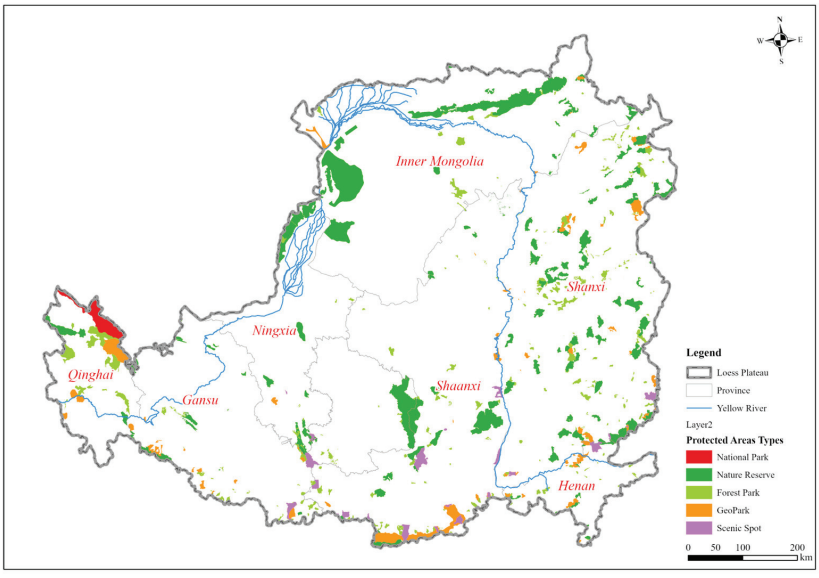

(**a**)

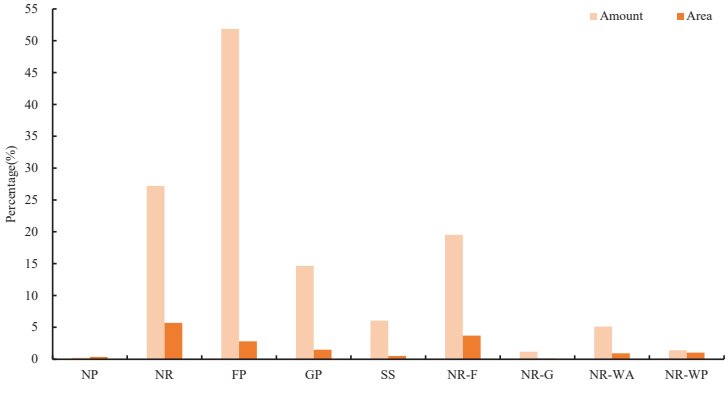

(**b**)

Figure 4. The situation of PAs in Loess Plateau in 2020. (**a**) spatial distribution; (**b**) amount and area, where NP: national park, NR: nature reserve, FP: forest park, GP: geo-park, SS: scenic spot; NR-F: forest NR, NR-G: grass NR, NR-WA: wild animal NR, NR-WP: wild plant NR.

In terms of specific quantities, about 100% of national parks, 88.46% of scenic spots, 75.21% of nature reserves, 72.65% of forest parks, and 60.32% of geo-parks are more effective in protecting the total amount of carbon sequestration. About 80.95% of forests, 77.27% of wild animals, 33.33% of wild plants, and 20% of grassland-type nature reserves are more effective in protecting the total carbon sequestration. About 100% of national parks, 91.30% of scenic spots, 84.62% of geo-parks, 80% of nature reserves, and 77.27% of forest parks protect critical carbon sequestration well; all wild animals and plants, and 75.38% of forest-type nature reserves protect critical carbon sequestration well.

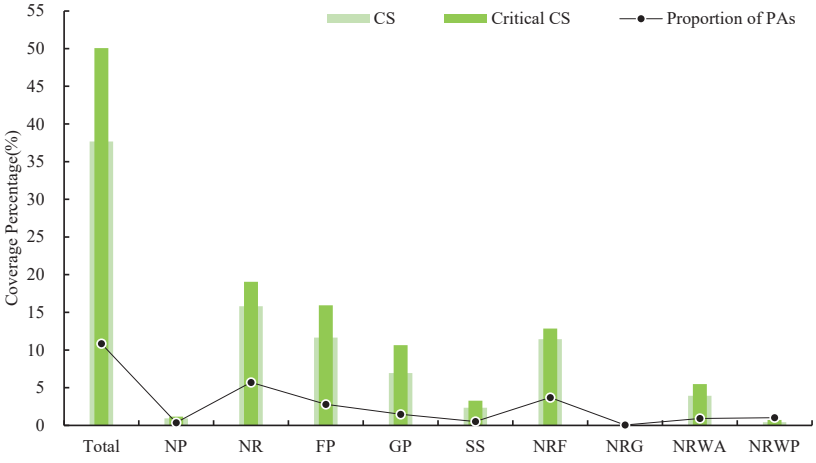

Figure 5. A coverage percentage of different PAs for carbon sequestration and Critical carbon sequestration in 2020.

3.2. Conservation Effectiveness

During the past 20 years, the total amount of carbon sequestration within the Loess Plateau increased from 152.48 Tg to 277.41 Tg, increasing about 81.93%. We selected 187 eligible PAs (Figure 6), with a total area of about 36,500 km^2, accounting for 5.62% of the total area of the Loess Plateau. Forest parks had the most significant number of sites, amounting to 93, followed by nature reserves with 53, scenic spots and geo-parks with 23 and 18 sites, respectively; nature reserves accounted for the largest share of the area, followed by forest parks, scenic spots, and geo-parks. In terms of the specific types of nature reserves, the number of forest and wild animal types of nature reserves is higher, the area of forest and wild plant types of nature reserves accounts for a higher proportion, and the area of grassland types of nature reserves accounts for a minor proportion.

Total carbon sequestration in the 187 PAs increased from 30.43 Tg to 46.99 Tg, increasing about 54.42%. In terms of specific types, the total amount of carbon sequestration in nature reserves increased the most during the 20 years, reaching 62.47%, followed by scenic spots and forest parks, with increases of 52.71% and 52.51%, respectively, and geo-parks with the smallest increase of 41.34%; despite the high increase in total carbon sequestration within nature reserves, in terms of specific types, forest and wild animal type nature reserves had the most considerable increase of 75.60% and 45.47%, respectively, followed by wild plant type nature reserves with a rise of 18.42%. However, grass-type nature reserves showed a certain degree of decline, with a decrease of 3.31%.

The total amount of critical carbon sequestration in the 187 PAs increased from 21.98 Tg to 31.95 Tg, an increase of about 45.36%. In terms of specific types, the total amount of critical carbon sequestration within forest parks increased the most during the 20 years, with 50.98%, followed by scenic spots and nature reserves, with 41.64% and 40.30%, respectively, and geo-parks with the smallest increase of 41.34%. In terms of specific types of nature reserves, the largest increase in the amount of critical carbon sequestration was in the forest-type nature reserves, followed by the wild animal-type nature reserves, and there was no distribution of critical carbon sequestration within the grass and wild plant type nature reserves.

The results show that during the past 20 years, all four types of PAs have a better protection effect on carbon sequestration, among which scenic spots and forest parks have a better protection effect, followed by geo-parks and nature reserves (Figure 7). Only forest and wild animal types of nature reserves had a better protection effect on carbon sequestration services. In contrast, grassland and wild plant types of nature reserves had

a lesser protective effect. For critical carbon sequestration, forest parks, scenic spots, and geo-parks all have a better protection effect. In comparison, nature reserves have a weaker protection effect. Regarding the specific types of nature reserves, only wild animal-type nature reserves have a better protection effect.

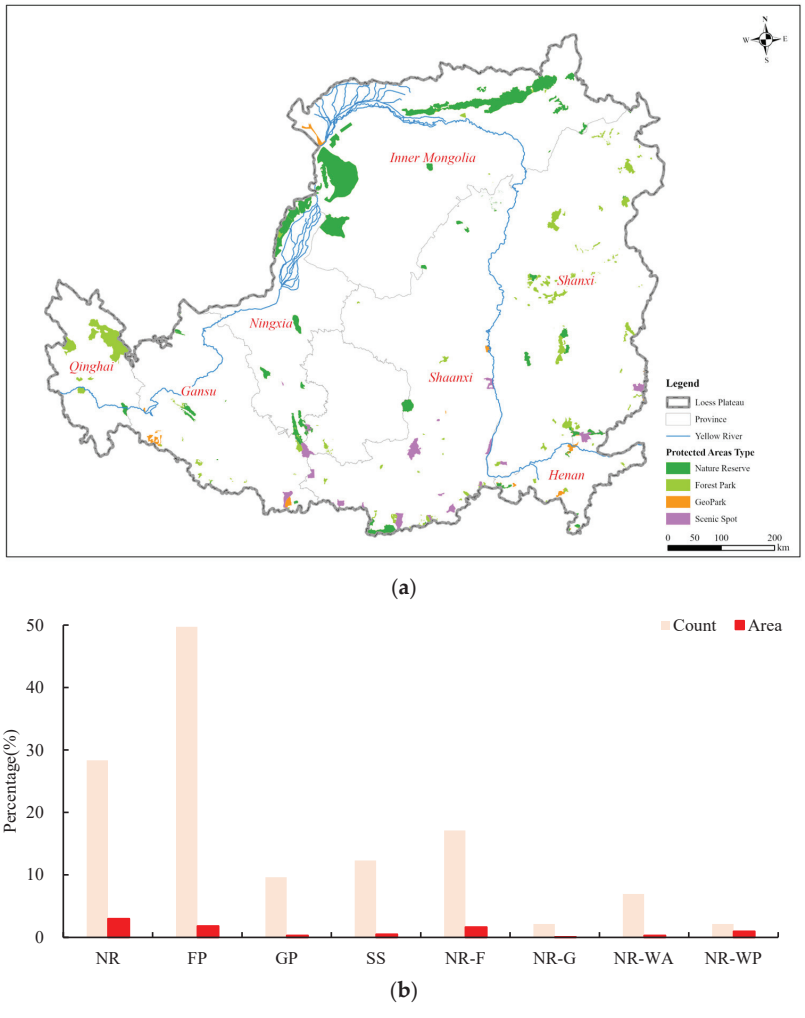

Figure 6. Situation of PAs in Loess Plateau in 2000. (**a**) spatial distribution; (**b**) amount and area, where NR: nature reserve, FP: forest park, GP: geopark, SS: scenic spot; NR-F: forest NR, NR-G: grass NR, NR-WA: wild animal NR, NR-WP: wild plant NR.

In terms of the number of specific PAs, about 91.30% of scenic spots, 83.87% of forest parks, 77.78% of geo-parks, and 54.72% of nature reserves are more effective in carbon sequestration; about 75% of wild plants, 69.23% of wild animals, 56.25% of forests, and 25% of grassland-type nature reserves are more effective in carbon sequestration. About 69.57% of scenic spots, 56.99% of forest parks, 44.44% of geo-parks, and 15.09% of nature reserves are more effective in protecting critical carbon sequestration; about 53.85% of wild animals and 15.63% of forest-type nature reserves are more effective in safeguarding critical carbon sequestration.

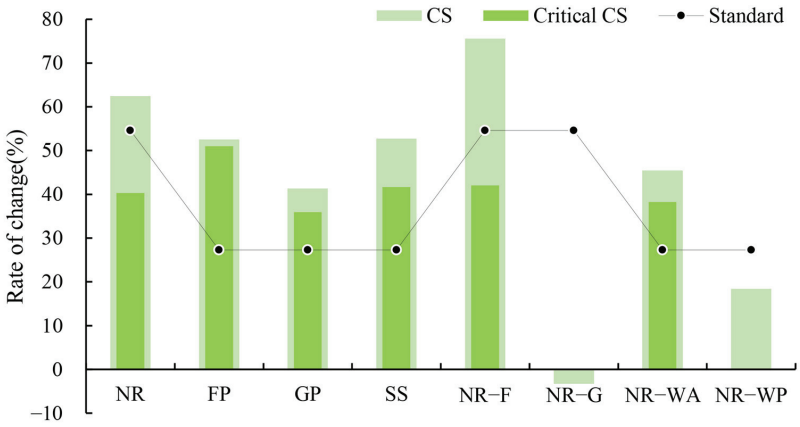

Figure 7. Rate of change in carbon sequestration and critical carbon sequestration by different PAs types from 2000 to 2020.

3.3. Main Factors

Spearman's correlation analysis showed (Table 1) that there were many factors affecting the rate of change of carbon sequestration, with highly significant strong positive correlation with the size of the PAs, highly significant moderate positive correlation with precipitation, slope, rate of change of evapotranspiration, and the grade of the PAs in 2000; highly significant moderate negative correlation with evapotranspiration in 2000; highly significant weak positive correlation with cropland area in 2000; and highly significant weak negative correlation with silt loam content.

Table 1. Correlation test results.

R	CS Change Rate	Critical CS Change Rate
PA establishment year	0.169 *	0.107
PA level	0.331 **	0.221 **
PA area	0.612 **	0.146 *
DEM	0.042	−0.264 **
Slope	0.380 **	0.345 **
Silt	−0.266 **	−0.453 **
Sand	0.106	0.246 **
Temperature in 2000	−0.03	0.278 **
Rate of temperature change	0.03	0.212 **
Precipitation in 2000	0.418 **	0.638 **
Rate of precipitation change	−0.14	−0.307 **
Evapotranspiration in 2000	−0.313 **	−0.369 **
Rate of evapotranspiration change	0.326 **	0.605 **
Population density in 2000	0.074	0.235 **
Rate of population density change	0.082	0.025
GDP in 2000	0.099	0.213 **
Rate of GDP change	0.047	0.069
Cropland in 2000	0.281 **	0.004
Rate of cropland change	−0.048	0.046

Notes: * indicates significance at the 0.05 level, ** indicates significance at the 0.01 level.

The factors that were highly significant and strongly positively correlated with the rate of change of critical carbon sequestration were precipitation in 2000 and evapotranspiration change rate; the only factors that were highly significant and moderately positively correlated was slope, but they were highly significant and moderately negatively correlated with evapotranspiration in 2000, silt, and precipitation change rate; and highly significant

and weakly positively correlated with the temperature in 2000, population density in 2000, the grade of PAs, GDP in 2000, and the temperature change rate, but highly significant and weakly negative with DEM; in addition, it was also highly significant and weakly positively correlated with the size of the PAs.

4. Discussion

This study analysed the conservation status of carbon sequestration in 430 PAs of five types on the Loess Plateau during 2020 using the representative evaluation method. We found that, without considering the spatial overlap of different PA types, directly adding up the areas of all PAs, the 430 PAs accounted for only 10.85% of the total area of the Loess Plateau but provided 37.68% and 50.07% of the total amount of carbon sequestration and critical carbon sequestration, which was much higher than the area share of the PAs; therefore, we believe that PAs on the Loess Plateau are better representative of the carbon sequestration and the critical sequestered carbon. However, the representativeness of different types of PAs for carbon sequestration services varies, with nature reserves having the best representativeness for carbon sequestration, followed by forest parks and geo-parks, which is consistent with the results of the national study [23], which may be because, nature reserves as the most stringent type of PAs in China, are established larger than other types to protect the integrity of the ecosystem [36]. In the case of the Loess Plateau, the area of nature reserves in the region exceeds that of forest parks by a factor of two and that of geo-parks by a factor of four. Larger areas generally provide more resources and habitats, thus supporting greater carbon sequestration [37]. Although nature reserves are better represented for carbon sequestration services, in terms of specific types, only forest and wild animal-type nature reserves are better represented for carbon sequestration. In contrast, grassland and wild plant-type nature reserves show lesser representativeness. The reason for this phenomenon is that the vegetation types of wild plant type nature reserves in the Loess Plateau region are dominated by grasslands, which in turn have a lower carbon sequestration capacity than that of forests [38,39], so overall grassland and wild plant type nature reserves are weakly represented for carbon sequestration services.

Based on the differences in the degree of protection stringency of different types of PAs [33], constructing the protection effect of multiple types of PAs on carbon sequestration services not only identifies the differences in the protection of each type of PAs but also proposes targeted protection advice which is conducive to the overall improvement of the protection effect. Until now, China has established more than 11,800 PAs [40], which can be classified into three types: strict protection, restricted use, and protected use [34,41]. According to the degree of strictness of protection, nature reserves are recognised as the strict type of reserve. They are divided into three categories and nine types [42]. While scenic spots, forest parks, and geo-parks can be classified as restricted use types. There are many nature reserves with complex classification systems, of which nearly 18% have spatial overlap and cross-cutting management authorities, resulting in ineffective management, especially in the Taihang Mountains region within the Loess Plateau [43]. Therefore, we constructed a method for assessing the conservation effect of multiple types of PAs on carbon sequestration services by setting reasonable weights, considering the variability of background conditions and the degree of protection stringency of PAs on the Loess Plateau. Our proposed method is, on the one hand, more scientific than determining the conservation effect or contribution based only on the increase or decrease of carbon sequestration in the before-and-after timeframe. On the other hand, it is more convenient to operate than the propensity score matching method. We have taken into account the strictness of the protection of different types of PAs, such as nature reserves being the most strict type; only the experimental area allows part of the scientific research activities, its management policies, measures, funds, personnel and other aspects of the investment are higher than other types of PAs, the primary purpose is to protect the main object from interference [44]. Forest parks, scenic spots, and geo-parks allow a certain degree of human activities, considering the functions of protection, landscape, recreation, and

popular science education [45], so there is a difference in the setting of weights. In addition, the PSM method needs to consider more environmental variables [46]. It even needs to take relevant policy factors into account. Still, it is difficult to maintain the consistency of the policy factors implemented inside and outside the PAs, so not all the PAs can be found in the periphery of the environmental factors of the same matching samples (such as the PAs of small size, the environmental factors do not match) [47]. The workload is heavier and not very operable. The reasonable weights we set based on the difference in protection strictness can quickly and scientifically assess the protection effect of different types of PAs on carbon sequestration services.

Based on the proposed conservation effectiveness assessment method, we assessed the conservation effectiveness of carbon sequestration services in 187 PAs established in 2000 and before of four categories in 2000–2020. We found that the total carbon sequestration within the Loess Plateau increased by about 81.93% during the 20 years, while the total carbon sequestration services within the 187 PAs increased by about 54.42%, which was lower than the increase in total carbon sequestration within the Loess Plateau. This phenomenon may be due to the unique soil conditions of the Loess Plateau itself, where soil erosion occurs from time to time in areas not covered by PAs [48]. To combat this ecological problem, China has dramatically increased the vegetation cover in the region by implementing long-term natural forest protection projects, grain for green, soil and water conservation, and other conservation and restoration measures [28,49]. At the same time, PAs are constrained by relevant policies and laws and cannot carry out too much artificial restoration [48], so the total increase in carbon sequestration services within the Loess Plateau was more extensive than that in PAs, but this does not indicate that PAs are less effective in protecting carbon sequestration. Combining the strict degree of protection of PAs and the background condition of the Loess Plateau and by setting reasonable weights [34], we found that all 187 PAs of the four categories have a better protective effect on carbon sequestration services. Still, scenic spots and forest parks have a better protective effect on carbon sequestration than geo-parks and nature reserves, forest and wild animal type nature reserves have a better protective effect on carbon sequestration, and grassland and wild plant type nature reserves have a weaker protective effect on carbon sequestration, suggests a need for targeted interventions to enhance their conservation outcomes [50]. The main reason for this result is that scenic spots, forest parks, forest and wild animals type nature reserves are mainly distributed in the eastern and southern parts of the Loess Plateau. In contrast, geo-parks, large nature reserves, grassland, and wild plant nature reserves are distributed primarily in the northern part of the Loess Plateau. The vegetation type of the eastern and southern parts of the Loess Plateau is dominated by forests, while grasslands dominate that of the northern part. In contrast, precipitation and slope in the southeastern part of the Plateau are higher than in the north, and evapotranspiration is lower than in the north. Evapotranspiration is a key indicator of water availability and plant health, directly affecting carbon uptake [51]. Related studies have also shown that high precipitation and low evapotranspiration are essential influences on the carbon sequestration capacity of vegetation [52]. For critical carbon sequestration, forest parks, scenic spots, and geo-parks all have a better protection effect on it. Only nature reserves have a weaker effect on it, but wild animal-type nature reserves have a better effect. The main reason for this phenomenon is that there is a spatial mismatch between most of the nature reserves and critical carbon sequestration [26], which is concentrated in the southeastern part of the Loess Plateau, but the distribution of nature reserves is more expansive and not focused enough.

Our findings underscore the crucial role of considering PA types and background conditions when evaluating conservation effectiveness. The outstanding performance of scenic spots, forest parks, and geo-parks indicates that these PA types may benefit from management practices prioritising carbon sequestration. Conversely, the relatively weaker performance of grassland and wild plant nature reserves suggests a need for targeted interventions to enhance their conservation outcomes, such as carrying out artificial restoration of degraded grasslands with a multi-species configuration of native grasses with a variety

of legumes [50,53]. Our results suggest that integrating and optimising the management of PAs should focus on upgrading the protection level of critical carbon sequestration areas within scenic spots, forest parks, and geo-parks [54]. Combined with the overlapping analysis of PAs [55], the area should be included in future national parks or nature reserves according to the actual situation. Implementing comprehensive protection and restoration measures in low-performing PAs, particularly grassland and wild plant nature reserves, can significantly enhance their carbon sequestration capacity. This approach aligns with China's broader goal of achieving carbon neutrality and emphasises the dual benefits of biodiversity conservation and climate change mitigation.

The IUCN classifies PAs into six categories, with category Ia representing strict PAs [56]. Countries around the world have further subdivided PA types based on this. Despite these differences, all are classified into certain levels of strict protection. Therefore, this study provides a methodological reference for evaluating the effectiveness of PAs with varying protection levels in different regions and countries, supporting related international research, and then mitigating global climate change.

5. Conclusions

This study analysed the conservation status and effects of different types of PAs on carbon sequestration services within the Loess Plateau from 2000 to 2020. The results found that: (1) The existing PAs demonstrate good representativeness and conservation effectiveness for carbon sequestration services, though these vary by type. While stricter PAs generally show better representativeness, this does not always translate to higher conservation effectiveness. For example, nature reserves exhibit the best representativeness for carbon sequestration, yet their conservation effectiveness is lower compared to other types of PAs. (2) Factors that positively and significantly affect the conservation effect of carbon sequestration include the size of the PAs area, precipitation in 2000, slope, rate of change of evapotranspiration, and PAs class. (3) It is recommended to appropriately upgrade the protection level of areas with low protection stringency but high carbon sequestration and to implement necessary restoration measures in areas with high protection stringency but low carbon sequestration. This approach will not only serve as a reference for the integration and optimisation of PAs in China but also provide guidance for other regions worldwide with similar classifications of PAs so that we can comprehensively enhance the carbon sequestration capacity and help achieve the goal of carbon neutrality.

Author Contributions: Conceptualization, J.Z., S.L. and X.L.; methodology, J.Z. and S.L.; software, S.L. and J.Z.; validation, S.L., J.Z. and X.L.; formal analysis, S.L.; investigation, S.L. and J.Z.; resources, J.Z.; data curation, S.L., J.Z. and X.L.; writing—original draft preparation, S.L. and J.Z.; writing—review and editing, S.L. and J.Z.; visualisation, J.Z. All authors have read and agreed to the published version of the manuscript.

Funding: This research was funded by the National Natural Science Foundation of China (No. 32101400) and the Scientific Research Projects of the School of Ecology and Nature Conservation, Beijing Forestry University (No. BH2022-09).

Institutional Review Board Statement: Not applicable.

Informed Consent Statement: Not applicable.

Data Availability Statement: The data presented in this study are available from the corresponding author upon reasonable request. The data are not publicly available due to restrictions or privacy.

Acknowledgments: We would like to thank all the authors and reviewers for their excellent guidance and help in writing this manuscript.

Conflicts of Interest: The authors declare no conflicts of interest.

References

1. Almond, R.; Grooten, M.; Juffe Bignoli, D.; Petersen, T. *Living Planet Report 2022: Building a Nature-Positive Society*; WWF: Gland, Switzerland, 2022.
2. Tong, S.; Bambrick, H.; Beggs, P.J.; Chen, L.; Hu, Y.; Ma, W.; Steffen, W.; Tan, J. Current and Future Threats to Human Health in the Anthropocene. *Environ. Int.* **2022**, *158*, 106892. [CrossRef]
3. Baste, I.A.; Watson, R.T. Tackling the Climate, Biodiversity and Pollution Emergencies by Making Peace with Nature 50 Years after the Stockholm Conference. *Glob. Environ. Change* **2022**, *73*, 102466. [CrossRef]
4. Convention on Biological Diversity. *Kunming-Montreal Global Biodiversity Framework*; Convention on Biological Diversity: Montreal, QC, Canada, 2022.
5. *Guidebook for the Preparation of Science, Technology and Innovation (STI) for SDGs Roadmaps*; United Nations Inter-Agency Task Team on Science, Technology and Innovation for the SDGs and European Coomission, Joint Research Centre: New York, NY, USA, 2021.
6. United Nations Environment Programme. *Global Climate Litigation Report: 2023 Status Review*; United Nations Environment Programme: Nairobi, Kenya, 2023.
7. Matocha, J.; Schroth, G.; Hills, T.; Hole, D. Integrating Climate Change Adaptation and Mitigation through Agroforestry and Ecosystem Conservation. In *Agroforestry—The Future of Global Land Use*; Nair, P.K.R., Garrity, D., Eds.; Springer: Dordrecht, The Netherlands, 2012; pp. 105–126. ISBN 978-94-007-4676-3.
8. Kabir, M.; Habiba, U.E.; Khan, W.; Shah, A.; Rahim, S.; los Rios-Escalante, P.R.D.; Farooqi, Z.-U.-R.; Ali, L.; Shafiq, M. Climate Change Due to Increasing Concentration of Carbon Dioxide and Its Impacts on Environment in 21st Century; A Mini Review. *J. King Saud Univ. Sci.* **2023**, *35*, 102693. [CrossRef]
9. Jones, M.W.; Peters, G.P.; Gasser, T.; Andrew, R.M.; Schwingshackl, C.; Gütschow, J.; Houghton, R.A.; Friedlingstein, P.; Pongratz, J.; Le Quéré, C. National Contributions to Climate Change Due to Historical Emissions of Carbon Dioxide, Methane, and Nitrous Oxide since 1850. *Sci. Data* **2023**, *10*, 155. [CrossRef]
10. Qin, Y.; Xiao, X.; Wigneron, J.-P.; Ciais, P.; Brandt, M.; Fan, L.; Li, X.; Crowell, S.; Wu, X.; Doughty, R.; et al. Carbon Loss from Forest Degradation Exceeds That from Deforestation in the Brazilian Amazon. *Nat. Clim. Change* **2021**, *11*, 442–448. [CrossRef]
11. Li, Y.; Brando, P.M.; Morton, D.C.; Lawrence, D.M.; Yang, H.; Randerson, J.T. Deforestation-Induced Climate Change Reduces Carbon Storage in Remaining Tropical Forests. *Nat. Commun.* **2022**, *13*, 1964. [CrossRef] [PubMed]
12. Zeng, Z.; Wang, D.; Yang, L.; Wu, J.; Ziegler, A.D.; Liu, M.; Ciais, P.; Searchinger, T.D.; Yang, Z.-L.; Chen, D.; et al. Deforestation-Induced Warming over Tropical Mountain Regions Regulated by Elevation. *Nat. Geosci.* **2021**, *14*, 23–29. [CrossRef]
13. Ivanova, I.M.; Cook, C.N. The Role of Privately Protected Areas in Achieving Biodiversity Representation within a National Protected Area Network. *Conserv. Sci. Pract.* **2020**, *2*, e307. [CrossRef]
14. Arneth, A.; Leadley, P.; Claudet, J.; Coll, M.; Rondinini, C.; Rounsevell, M.D.A.; Shin, Y.; Alexander, P.; Fuchs, R. Making Protected Areas Effective for Biodiversity, Climate and Food. *Glob. Change Biol.* **2023**, *29*, 3883–3894. [CrossRef]
15. Visconti, P.; Butchart, S.H.M.; Brooks, T.M.; Langhammer, P.F.; Marnewick, D.; Vergara, S.; Yanosky, A.; Watson, J.E.M. Protected Area Targets Post-2020. *Science* **2019**, *364*, 239–241. [CrossRef]
16. Xu, X.; Huang, A.; Belle, E.; de Frenne, P.; Jia, G. Protected Areas Provide Thermal Buffer against Climate Change. *Sci. Adv.* **2022**, *8*, eabo0119. [CrossRef] [PubMed]
17. Wu, H.; Yu, L.; Shen, X.; Hua, F.; Ma, K. Maximizing the Potential of Protected Areas for Biodiversity Conservation, Climate Refuge and Carbon Storage in the Face of Climate Change: A Case Study of Southwest China. *Biol. Conserv.* **2023**, *284*, 110213. [CrossRef]
18. Chen, L.; Msigwa, G.; Yang, M.; Osman, A.I.; Fawzy, S.; Rooney, D.W.; Yap, P.-S. Strategies to Achieve a Carbon Neutral Society: A Review. *Environ. Chem. Lett.* **2022**, *20*, 2277–2310. [CrossRef]
19. Zhao, W. China's Goal of Achieving Carbon Neutrality before 2060: Experts Explain How. *Natl. Sci. Rev.* **2022**, *9*, nwac115. [CrossRef]
20. Shi, H.; Li, X.; Liu, X.; Wang, S.; Liu, X.; Zhang, H.; Tang, D.; Li, T. Global Protected Areas Boost the Carbon Sequestration Capacity: Evidences from Econometric Causal Analysis. *Sci. Total Environ.* **2020**, *715*, 137001. [CrossRef] [PubMed]
21. Chen, Y.; Fiankor, D.-D.D.; Kang, K.; Zhang, Q. Assessing the Role of Institutional Effectiveness on Carbon Sequestration: The Case of China's Nature Reserve Policy. *China Agric. Econ. Rev.* **2023**, *15*, 777–794. [CrossRef]
22. Huang, B. Improve Governance System of National Parks, Build the World's Largest National Park System with High Quality. *Bull. Chin. Acad. Sci.* **2024**, *39*, 219–229.
23. Tian, J.; Feng, C.; Fu, G.; Fan, L.; Wang, W. Contribution of Different Types of Terrestrial Protected Areas to Carbon Sequestration Services in China: 1980–2020. *Front. Ecol. Evol.* **2023**, *11*, 1074410. [CrossRef]
24. Duncanson, L.; Liang, M.; Leitold, V.; Armston, J.; Krishna Moorthy, S.M.; Dubayah, R.; Costedoat, S.; Enquist, B.J.; Fatoyinbo, L.; Goetz, S.J.; et al. The Effectiveness of Global Protected Areas for Climate Change Mitigation. *Nat. Commun.* **2023**, *14*, 2908. [CrossRef]
25. Cao, M. Conservation Effectiveness Assessment and Influencing Factors Analysis of National Nature Reserves in Oinling Mountains. Master's Thesis, Chinese Research Academy of Environmental Sciences, Beijing, China, 2022.
26. Xu, W.; Xiao, Y.; Zhang, J.; Yang, W.; Zhang, L.; Hull, V.; Wang, Z.; Zheng, H.; Liu, J.; Polasky, S.; et al. Strengthening Protected Areas for Biodiversity and Ecosystem Services in China. *Proc. Natl. Acad. Sci. USA* **2017**, *114*, 1601–1606. [CrossRef]

27. Fu, B.; Liu, Y.; Lü, Y.; He, C.; Zeng, Y.; Wu, B. Assessing the Soil Erosion Control Service of Ecosystems Change in the Loess Plateau of China. *Ecol. Complex.* **2011**, *8*, 284–293. [CrossRef]
28. Chen, Y.; Feng, X.; Tian, H.; Wu, X.; Gao, Z.; Feng, Y.; Piao, S.; Lv, N.; Pan, N.; Fu, B. Accelerated Increase in Vegetation Carbon Sequestration in China after 2010: A Turning Point Resulting from Climate and Human Interaction. *Glob. Change Biol.* **2021**, *27*, 5848–5864. [CrossRef] [PubMed]
29. An, K.; Zhang, Y.; Liu, Y.; Huang, J.; Li, G. Construction of nature reserves and the effectiveness of habitat protection in the Loess Plateau. *Shaanxi For. Sci. Technol.* **2023**, *51*, 8–17.
30. Yang, Y.; Zhang, P.; Wu, F.; Zhou, Y.; Song, Y.; Wang, Y.; An, S. The significance and countermeasures of vegelalion constmuction on the Loess Plateauto carbon neutrality. *Acta Ecol. Sin.* **2023**, *43*, 9071–9081. [CrossRef]
31. Dang, X.; Wu, Y.; Liu, G.; Yang, Q.; Yu, X.; Jia, Y. Spatial-temporal changes of ecological footprint in the Loess Plateau after ecological construction between 1995 and 2010. *Geogr. Res.* **2018**, *37*, 761–771.
32. National Development and Reform Commission. *National Bureau of Statistics Accounting Specification of Total Value of Ecological Products*; National Development and Reform Commission: Beijing, China, 2022.
33. Fang, Z.; Xu, W.; Zhang, J.; Xiao, Y.; Zhang, L. Designing protected area systems in the Qinling Mountains based on biodiversity and ecosystem service evaluation. *Acta Ecol. Sin.* **2017**, *37*, 5334–5341.
34. Tang, X.; Luan, X. Developing a nature protected area system composed mainly of national parks. *For. Resour. Manag.* **2017**, *2017*, 1–8. [CrossRef]
35. Tang, X.; Liu, Z.; Ma, W. A study on integration and optimization rules and paths for natural protected areas in China. *For. Resour. Manag.* **2020**, 1–10. [CrossRef]
36. Wang, W.; Li, J. In-situ conservation of biodiversity in China: Advances and prospects. *Biodivers. Sci.* **2021**, *29*, 133–149. [CrossRef]
37. Weiskopf, S.R.; Isbell, F.; Arce-Plata, M.I.; di Marco, M.; Harfoot, M.; Johnson, J.; Lerman, S.B.; Miller, B.W.; Morelli, T.L.; Mori, A.S.; et al. Biodiversity Loss Reduces Global Terrestrial Carbon Storage. *Nat. Commun.* **2024**, *15*, 4354. [CrossRef]
38. Chen, W.; Li, H. Growth potential of carbon sequestration and carbon sinks increase in forest and grass ecosystem in China. *Sci. Technol. Rev.* **2024**, *42*, 93–102.
39. Zhang, X.; Jia, W.; Sun, Y.; Wang, F.; Miu, Y. Simulation of Spatial and Temporal Distribution of Forest Carbon Stocks in Long Time Series-Based on Remote Sensing and Deep Learning. *Forests* **2023**, *14*, 483. [CrossRef]
40. Li, B.V.; Pimm, S.L. How China Expanded Its Protected Areas to Conserve Biodiversity. *Curr. Biol.* **2020**, *30*, R1334–R1340. [CrossRef] [PubMed]
41. Chen, Y.; Jiao, M. Literature review and inspiration of the classification of Chinese natural reserves. *Planners* **2020**, *36*, 5–12.
42. Zhao, W.; Zong, L.; Wang, M. Spatial distribution of nature reserves in China. *Acta Ecol. Sin.* **2024**, *44*, 2786–2799. [CrossRef]
43. Ma, T.; Lv, C.; Lei, G. The spatial overlapping analysisi for China's natural protected area and countermeasures for the optimization and integration of protected area system. *Biodivers. Sci.* **2019**, *27*, 758–771. [CrossRef]
44. Wang, C.; Xie, M. Governance of nature reserves with national parks as the main body: History, challenges, and systemic optimization. *Chin. Rural Econ.* **2023**, *2023*, 139–162. [CrossRef]
45. Cui, G. Discussion and suggestions on serveral key issues in the integration and optimization of protected areas. *Biodivers. Sci.* **2023**, *31*, 180–187. [CrossRef]
46. Yang, H.; Viña, A.; Winkler, J.A.; Chung, M.G.; Huang, Q.; Dou, Y.; McShea, W.J.; Songer, M.; Zhang, J.; Liu, J. A Global Assessment of the Impact of Individual Protected Areas on Preventing Forest Loss. *Sci. Total Environ.* **2021**, *777*, 145995. [CrossRef]
47. Feng, C.; Cao, M.; Wang, W.; Wang, H.; Liu, F.; Zhang, L.; Du, J.; Zhou, Y.; Huang, W.; Li, J. Which Management Measures Lead to Better Performance of China's Protected Areas in Reducing Forest Loss? *Sci. Total Environ.* **2021**, *764*, 142895. [CrossRef]
48. Yan, Y. Trade-Offs of Ecosystem Services and Determination Ofconservation Priority Areas in the Loess Plateau. Master's Thesis, Chang'an University, Xi'an, China, 2023.
49. Feng, X.; Fu, B.; Lu, N.; Zeng, Y.; Wu, B. How Ecological Restoration Alters Ecosystem Services: An Analysis of Carbon Sequestration in China's Loess Plateau. *Sci. Rep.* **2013**, *3*, 2846. [CrossRef] [PubMed]
50. Asner, G.P.; Knapp, D.E.; Martin, R.E.; Tupayachi, R.; Anderson, C.B.; Mascaro, J.; Sinca, F.; Chadwick, K.D.; Higgins, M.; Farfan, W.; et al. Targeted Carbon Conservation at National Scales with High-Resolution Monitoring. *Proc. Natl. Acad. Sci. USA* **2014**, *111*, E5016–E5022. [CrossRef] [PubMed]
51. Zhang, L.; Xiao, J.; Zheng, Y.; Li, S.; Zhou, Y. Increased Carbon Uptake and Water Use Efficiency in Global Semi-Arid Ecosystems. *Environ. Res. Lett.* **2020**, *15*, 34022. [CrossRef]
52. Zhang, X.; Chen, Y.; Zhang, Q.; Xia, Z.; Hao, H.; Xia, Q. Potential Evapotranspiration Determines Changes in the Carbon Sequestration Capacity of Forest and Grass Ecosystems in Xinjiang, Northwest China. *Glob. Ecol. Conserv.* **2023**, *48*, e02737. [CrossRef]
53. Peng, Y.; Chang, J.; Zhao, X.; Shi, Y.; Bai, Y.; Li, Q.; Yao, S.; Ma, W.; Fang, J.; Yang, Y. Grassland Carbon Sink in China and its Promotion Strategies. *Bull. Natl. Nat. Sci. Found. China* **2023**, *37*, 587–602.
54. Tang, F.; Lv, X.; Cai, F.; Aun, H.; Luo, W. Reflections on integrated optimization schemes of protected areas. *Landsc. Archit.* **2020**, *27*, 8–13. [CrossRef]

55. Wu, R.; Hua, C.; Yu, G.; Ma, J.; Yang, F.; Wang, J.; Jin, T.; Long, Y.; Guo, Y.; Zhao, H. Assessing Protected Area Overlaps and Performance to Attain China's New National Park System. *Biol. Conserv.* **2020**, *241*, 108382. [CrossRef]
56. Vimal, R.; Navarro, L.M.; Jones, Y.; Wolf, F.; Le Moguédec, G.; Réjou-Méchain, M. The global distribution of protected areas management strategies and their complementarity for biodiversity conservation. *Biol. Conserv.* **2021**, *256*, 109014. [CrossRef]

atmosphere

MDPI

Article

Regional/Single Station Zenith Tropospheric Delay Combination Prediction Model Based on Radial Basis Function Neural Network and Improved Long Short-Term Memory

Xu Yang [1,2,3,4,*], Yanmin Li [1,3,4], Xuexiang Yu [1,3,4], Hao Tan [1,3,4], Jiajia Yuan [1,3,4] and Mingfei Zhu [1,3,4]

[1] Key Laboratory of Aviation-Aerospace-Ground Cooperative Monitoring and Early Warning of Coal Mining-Induced Disasters of Anhui Higher Education Institutes, Anhui University of Science and Technology, KLAHEI (KLAHEI18015), Huainan 232001, China
[2] The Key Laboratory of Universities in Anhui Province for Prevention of Mine Geological Disasters, Huainan 232001, China
[3] Coal Industry Engineering Research Center of Mining Area Environmental and Disaster Cooperative Monitoring, Anhui University of Science and Technology, Huainan 232001, China
[4] School of Geomatics, Anhui University of Science and Technology, Huainan 232001, China
* Correspondence: xyang@aust.edu.cn

Abstract: Atmospheric water vapor is an essential source of information that predicts global climate change, rainfall, and disaster-natured weather. It is also a vital source of error for Earth observation systems, such as the global navigation satellite system (GNSS). The Zenith Tropospheric Delay (ZTD) plays a crucial role in applications, such as atmospheric water vapor inversion and GNSS precision positioning. ZTD has specific temporal and spatial variation characteristics. Real-time ZTD modeling is widely used in modern society. The conventional back propagation (BP) neural network model has issues, such as local, optimal, and long short-term memory (LSTM) model needs, which help by relying on long historical data. A regional/single station ZTD combination prediction model with high precision, efficiency, and suitability for online modeling was proposed. The model, called K-RBF, is based on the machine learning algorithms of radial basis function (RBF) neural network, assisted by the K-means cluster algorithm (K-RBF) and LSTM of real-time parameter updating (R-LSTM). An online updating mechanism is adopted to improve the modeling efficiency of the traditional LSTM. Taking the ZTD data (5 min sampling interval) of 13 international GNSS service stations in southern California in the United States for 90 consecutive days, K-RBF, R-LSTM, and K-RBF were used for regions, single stations, and a combination of ZTD prediction models regarding research, respectively. Real-time/near real-time prediction results show that the root-mean-square error (RMSE), mean absolute error (MAE), coefficient of determination (R2), and training time consumption (TTC) of the K-RBF model with 13 station data are 8.35 mm, 6.89 mm, 0.61, and 4.78 s, respectively. The accuracy and efficiency of the K-RBF model are improved compared with those of the conventional BP model. The RMSE, MAE, R2, and TTC of the R-LSTM model with WHC1 station data are 6.74 mm, 5.92 mm, 0.98, and 0.18 s, which improved by 67.43%, 66.42%, 63.33%, and 97.70% compared with those of the LSTM model. The comparison experiments of different historical observation data in 24 groups show that the real-time update model has strong applicability and accuracy for the time prediction of small sample data. The RMSE and MAE of K-RBF with 13 station data are 4.37 mm and 3.64 mm, which improved by 47.70% and 47.20% compared to K-RBF and by 28.48% and 31.29% compared to R-LSTM, respectively. The changes in the temporospatial features of ZTD are considered, as well, in the combination model.

Keywords: regional troposphere delay modeling; RBF neural network; LSTM; combinatorial model

Citation: Yang, X.; Li, Y.; Yu, X.; Tan, H.; Yuan, J.; Zhu, M. Regional/Single Station Zenith Tropospheric Delay Combination Prediction Model Based on Radial Basis Function Neural Network and Improved Long Short-Term Memory. *Atmosphere* **2023**, *14*, 303. https://doi.org/10.3390/atmos14020303

Academic Editor: Martin Dameris

Received: 15 January 2023
Revised: 30 January 2023
Accepted: 31 January 2023
Published: 3 February 2023

1. Introduction

1.1. Motivations

Climate change and extreme weather are major threats to the sustainability of our society. As an important greenhouse gas, atmospheric water vapor plays a very important role in climate change research and weather forecasting, especially in extreme weather nowcasting [1,2]. The presence of water vapor can lead to tens of meter range measurement errors. Therefore, it is also an important source of error for earth observation systems, such as the Global Navigation Satellite System (GNSS) [3]. It also plays a crucial role in the global water cycle. The water vapor on the Earth mainly comes from the evaporation of the ocean's surface. The atmospheric flows transport the evaporated water vapor over the continent to form precipitation and then return to the ocean through rivers and underground runoff, thereby forming the atmospheric terrestrial marine water cycle [4–6]. Carbon, nitrogen, and water cycles in terrestrial ecosystems are connected and coupled with one another, jointly driving the key processes of the balance of carbon revenue and expenditure in the ecosystem [7]. Global climate change, rising atmospheric CO_2 concentration, increased deposition of atmospheric nitrogen, and changes in precipitation patterns affect the carbon revenue and expenditure balance and carbon exchange capacity of terrestrial ecosystems at various levels. However, as of now, the key processes of carbon–nitrogen–water coupling cycles and biological regulation mechanisms in terrestrial ecosystems must be strengthened to evaluate the carbon exchange function and spatial pattern of terrestrial ecosystems and their response and feedback to global changes in land ecosystems accurately. Therefore, exploring carbon–nitrogen–water coupling cycles in terrestrial ecosystems and their responses and adaptation mechanisms to climate change is urgent [8]. It can provide a scientific basis for the carbon–nitrogen–water coupling research in terrestrial ecosystems, increase carbon sinks, and reduce pollution emissions, thereby helping China achieve its "double carbon" goals.

Zenith tropospheric delay (ZTD) can be divided into zenith hydrostatic delay (ZHD) and zenith non-hydrostatic delay, which is always called zenith wet delay (ZWD) [9]. ZWD can be converted into precipitable water vapor, PWV. It is an important factor that affects GNSS navigation and positioning accuracy. In recent years, with the gradual improvement of the high spatiotemporal resolution of ZTD products and the more frequent occurrences of disastrous weather conditions, such as thunderstorms and typhoons, regional real-time/near real-time ZTD modeling has gradually become a hot issue in GNSS and other research fields [10]. This research has important research significance and economic benefits [11].

According to the different conditions of ZTD model application (mainly referring to whether meteorological parameters are needed), the ZTD model can be divided into two categories. The first kind of ZTD model needs measured meteorological parameters (e.g., atmospheric pressure, water vapor pressure, and temperature), which mainly include Hopfield, Saastamoinen, and Black models [12]. In the actual navigation and positioning, meteorological parameters cannot be obtained sometimes, or the obtained meteorological parameters are unstable, thereby causing inconvenience for navigation and positioning. Given this problem, many scholars have established a second type of empirical ZTD model without the use of measured meteorological parameters, which only relies on a large number of empirical data to establish the mapping among various influencing factors and ZTD. Considering that the participation of any meteorological parameters is not needed, the empirical ZTD model, which mainly includes the early UNB series and EGNOS models, as well as GPT2, GPT2w, and IGGtrop models proposed by some scholars in recent years, has made great progress [13].

In recent years, with the rapid development of numerical weather prediction (NWP) and the encryption of GNSS observation stations in the region, empirical models that are more suitable for a certain region are established by fusing the multi-source observation data using spatiotemporal analysis methods. Usually, the long-term linear trend of ZTD is obtained by least-squares [14] and maximum likelihood estimation. The nonlinear

characteristics of ZTD (e.g., trend features, short-period disturbances [15], and seasonal periodicities) are obtained by time series analysis methods, such as wavelet analysis [16], spectral analysis, and intelligent analysis. The relationship between ZTD and topography, station elevation, latitude, and longitude is analyzed by spatial structure function, iterative tropospheric decomposition, seasonal Gaussian function, and least-squares collocation methods [17]. For the alpine area of Switzerland, Wilgan and Geiger [18] presented high-resolution models of tropospheric total refractivity and ZTD. Different combinations of data sources, including NWP and GNSS data, were used in the models. Using least-squares collocation, the tropospheric parameters were interpolated to arbitrary locations. Chen et al. [19] analyzed the temporal and spatial characteristics of the ZTD data of GNSS stations of the Crustal Movement Observation Network of China (CMONOC), which was measured for six years. They also established the ZTD empirical model (SHAtrop) for mainland China by using the periodic and grid functions. The accuracy was better than the common empirical models (such as EGNOS, UNB3 m, and GPT2). Zhao et al. [20] established the high-precision ZTD model of altitude-related correction with China as the research area. The ZTD residuals were obtained based on the ZTD initial values determined by the GPT3 model and the GNSS-derived ZTD values. The annual, semi-annual, and seasonal cycles of the residual were analyzed. Moreover, the relationship between the residual and GNSS elevation was analyzed. To some extent, the model overcame the defect, in which the existing empirical ZTD model failed to consider the influence of height on ZTD well.

Owing to the spatial inhomogeneity and temporal variability of atmospheric density and the nonlinear relationship among different meteorological parameters [21], ZTD has the characteristics of dynamic variability, many influencing factors, and strong randomness. Studying the physical mechanism of ZTD [22,23] is difficult, especially for ZTD's high spatial and temporal resolution modeling in areas with rugged terrain and large meteorological contrast [17]. Without explicitly providing the physical mechanism, data-driven models that use machine learning (ML) approaches have become a hot research topic. The main tasks of ML include supervised learning (e.g., classification and regression), unsupervised learning (e.g., clustering and dimensionality reduction), and reinforcement learning (e.g., control and decision-making), which can deal with nonlinear problems better and are widely used in data interpolation, modeling, and forecasting. In recent years, ML technology has been widely used in several fields and has achieved certain achievements in ZTD modeling. Such models include multi-layer perceptron, adaptive network-based fuzzy inference system (ANFIS), artificial neural network (ANN), and least-squares support vector machine (LSSVM) [24]. The most widely used model is the regional tropospheric model, based on ANN, which realizes the interpolation, prediction, fusion, or improvement of tropospheric delay correction parameters by inputting different parameters in global or local areas. Taking the ZTD data of global positioning system (GPS) stations in the Southern California GPS network as the research object, Wang et al. [25] investigated the ZTD prediction model by using the backpropagation (BP) neural network algorithm and by taking the longitude, latitude, and altitude of the station as inputs. To overcome a large amount of computing volume, proneness to the "over-fitting" phenomenon, and the problem of model instability of the traditional BP neural network, Xiao et al. proposed an improved BP neural network to establish a regional ZTD model. The model takes the normalized geodetic longitude, latitude, and geodetic height as the model inputs, as well as ZTD as the output [26]. Based on the ZTD data of North America, Li conducted ZTD modeling using the BP neural network, LSSVM, and radial basis function (RBF) neural network and systematically evaluated the modeling accuracy, efficiency, and stability of different models. The results show that the RFB algorithm has the best effect in small-scale sample modeling, and the BP algorithm has evident advantages in large-scale sample modeling [27]. Shi et al. proposed a long short-term memory (LSTM) network ZTD prediction model based on Keras platform and compared it with the prediction effects of the BP neural network model. The experimental results show that the root mean square error (RMSE) of

the prediction results of the LSTM model reaches the mm level, and its mean absolute error (MAE) and mean absolute percentage error (MAPE) are lower than those of the BP model. The accuracy and stability of the LSTM model are significantly improved compared with those of the BP model [28]. With the comprehensive consideration of the spatiotemporal information of the GPS stations in West Antarctica, Zhang et al. conducted ZTD modeling through two blind source separation algorithms, namely, principal component analysis (PCA), independent component analysis (ICA), and BP neural network and performed high-precision ZTD prediction using the LSTM network [29]. Li et al. improved the ZTD correction performance of the GPT3 model in Antarctica using RBF and LSTM models in terms of space and time, respectively [30]. Zhang et al. proposed a new ZTD time-series forecasting method that used transformer-based machine-learning techniques [31]. For the investigation, analysis, and forecasting of ZTD, the global VMF stations provided by the global geodetic observing system (GGOS) during 2008–2020 were used. Results showed that forecasted ZTD results were more accurate than those of LSTM, RNN, convolutional neural network (CNN), and GPT3 series models. Zhang et al. [22] estimated the ZTD of seven GNSS monitoring stations in China for two consecutive years by using static precise point positioning (PPP) technology. The K-nearest neighbor (KNN) algorithm was used to interpolate the ZTD data gap. The ZTD difference values between KNN and periodic models were trained and predicted by LSTM. The predicted value, combined with the periodic model (ZTD), restored the final ZTD prediction result (LSTM-ZTD), which was better than BP neural network modeling. Static PPP verification experiments with the LSTM-ZTD showed that PPP convergence time was improved in summer, autumn, and winter compared with GPT2 ZTD. Shamshiri et al. [17] developed a new method based on ML Gaussian process (GP) regression approach using the combination of small-baseline interferograms and GNSS-derived ZTD values to mitigate phase delay caused by the troposphere in interferometric observations. On average, it reduced RMSE by 83%, compared to 50%, by using ERA-Interim to correct tropospheric data. Zheng et al. [32] developed a stacked ML model for mapping ZTD into PWV without meteorological parameters. The fifth-generation European Center for Medium-range Weather Forecast Reanalysis (ERA5) and radiosonde information were used to assess and validate the model's performance. The proposed model performed better than the physical model that used GPT3-derived meteorological parameters. Other techniques that can sense ZTD can benefit from this model for real-time PWV retrieval. Chkeir et al. [21] studied nowcasting extreme rain and extreme wind speed with 3 ML techniques, namely, ANN, LSTM, and LSTM Encoder Decoder (LSTM E/D), applied to different input datasets from ground-based weather sensors, GNSS receivers, C-band radars, and lightning detectors. The analysis showed that the LSTM E/D approach was suitable for the nowcasting of meteorological variables.

1.2. Contributions

Most of the aforementioned ML models focus on BP neural network and LSTM. BP neural network refers to an adaptive nonlinear dynamic system with strong learning and memory functions. However, it has the disadvantage of slow convergence speed and easily falls into local optimum. LSTM can remember long and short-term information and solves the problem of gradient disappearance and explosion during long sequence training; however, it cannot be parallelized and is time consuming [31]. The shortcomings of the two models limit their application ability in real-time high-precision regional ZTD modeling. With the continuous development of real-time precision positioning technologies (e.g., real-time kinematic positioning (RTK), regional continuously-operating reference station (CORS), real-time PPP (RT-PPP), and integer ambiguity resolution-enabled precise point positioning (PPP-RTK)) and the frequent occurrence of extreme weather, the use of the ZTD spatiotemporal information of regional GNSS monitoring stations for regional real-time ZTD high-precision modeling has become a key technology for real-time precision positioning and short-term strong convective weather forecasting. The model will exhibit high precision, spatiotemporal resolution, reliability, and timeliness. It can collect the current

ZTD data of some regional GNSS monitoring stations to carry out ZTD spatiotemporal modeling, provide regional atmospheric enhancement products for real-time precise positioning, offer short-term and imminent forecasting services for strong convective disaster weather for seconds to hours, and support data bases for the study of mutual conversion processes, such as condensation and evaporation of water vapor [33]. RBF has the characteristics of high stability, fast convergence speed, and global approximation, and LSTM has been widely used in ZTD modeling and short-term weather forecast. However, its algorithmic effectiveness and optimization research in regional real-time ZTD modeling applications are unsatisfactory. This paper attempts to improve them from the aspects of modeling efficiency and modeling accuracy.

1.3. Organization

Overall, the proposal of a high-precision ZTD model based on ML algorithms suitable for online modeling is expected, and the model accuracy is not affected by factors, such as elevation. The remainder of the paper is summarized as follows. Section 2 uses the ZTD data (5 min sampling interval) of 13 international GNSS service (IGS) stations in southern California in the United States for 90 consecutive days. Given that the real-time meteorological parameters do not need to be inputted based on the three-dimensional coordinates and time of the participating modeling stations as input, the RBF neural network assisted by the K-means cluster algorithm (K-RBF) is used to construct a regional ZTD prediction model. In addition, based on the single station ZTD non-full life cycle historical time series data (few epochs), the single station ZTD prediction model is established by using the LSTM of real-time parameter updating (R-LSTM). Finally, based on the two ZTD models, a regional/single-station ZTD prediction model combined with K-RBF and R-LSTM (KR-RBF-LSTM) is proposed. Section 3 presents the modeling results of the three different ZTD models. Section 4 discusses the modeling effect in terms of modeling efficiency and accuracy. Section 5 presents the conclusion and mentions the limitations of this work and future research direction.

2. Materials and Methods

2.1. Study Region and Datasets

The final ZTD data of 13 IGS monitoring stations in southern California are selected (ftp://igs.gnsswhu.cn/pub/gps/products/troposphere/new, accessed on 11 December 2022). The plane position of the station and its elevation distribution are shown in Figures 1 and 2, respectively. The data period is 90 days, that is, from 12 June 2021 to 9 September 2021. The day of the year (DOY) is from 163 to 252. The sampling interval is 5 min. The final ZTD data are used to simulate ZTD real-time or near real-time modeling. In K-RBF modeling, in t epoch, the data of 12 stations are used for modeling, and the remaining station data are used for accuracy verification. For R-LSTM modeling, for a station on the i-th day, when the epoch $t = 6$, the data of the first five epochs at the day are used for modeling, and the data of the current epoch t are used for accuracy verification. When $t > 6$, the data of epoch t-1 are used for modeling, and the data of the current epoch t are used for accuracy verification. KR-RBF-LSTM modeling is performed on the basis of the two aforementioned modeling methods. The modeling results of the first five epochs of each day are removed to compare the accuracy of different models. For 1 of the 13 stations, 283 epoch predicted data are involved in the statistical analysis of the model accuracy in a day, and 25,470 epochs are involved in the accuracy statistics for 90 consecutive days.

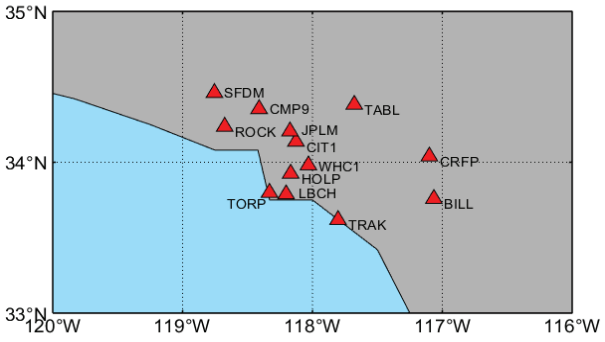

Figure 1. IGS monitoring station distribution map. Note: The station names are BILL, CIT1, CMP9, CRFP, HOLP, JPLM, LBCH, ROCK, SFDM, TAB1, TORP, TRAK, and WHC1, and their corresponding station numbers are 1, 2, . . . , 13.

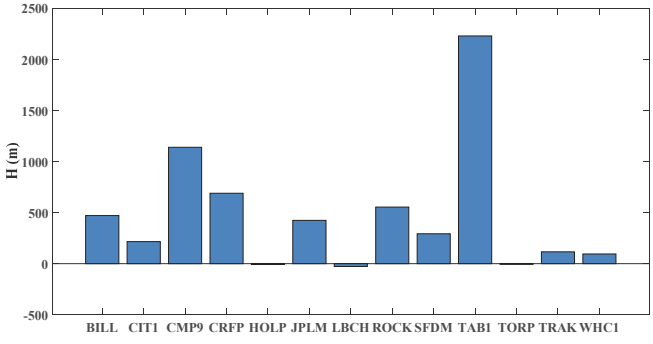

Figure 2. IGS monitoring station elevation distribution.

2.2. Methods

2.2.1. K-Means Clustering-Assisted RBF Neural Network Region ZTD Modeling

RBF neural network is a three-layer feedforward network with a single hidden layer. The first layer corresponds to the input layer, which is composed of signal source nodes. The second layer is the hidden layer, and the number of nodes in this layer depends on the needs of the problem. The conversion function of neurons in the hidden layer, namely, the RBF, is a non-negative linear function with radial symmetry and attenuation to the center point. The third layer is the output layer, which is the response to the input mode. The basic idea is to use RBF as the "base" of the hidden unit to form the hidden layer space. The hidden layer transforms the input vector and transforms the low-dimensional input data into the high-dimensional space so that the linear indivisible problem in the low-dimensional space can be linearly separable in the high-dimensional space.

For ZTD region modeling, the problems to be solved are presented as follows. Giving a dataset $D = \{\boldsymbol{x}_i, \overline{z_i}\}_{i=1}^{l}$ and assuming that the dataset is generated by an unknown function $z = f(\boldsymbol{x})$, a function as close to $z = f(\boldsymbol{x})$ as possible is learned by the dataset D. For any feasible kernel functions $K(\boldsymbol{x}_i, \boldsymbol{x}_j)$, the function of the required solution can be expressed as:

$$f(x) = \sum_{i=1}^{l} a_i K(\boldsymbol{x}_i, \boldsymbol{x}_j) + b, \tag{1}$$

where a is the parameter to be solved, and b is a constant.

From the sparse point of view, the RBF neural network adopts pruning ideas to achieve sparsity. First, an unsupervised learning process is performed on the input in the training

data. A set of center vectors is selected in advance, and the number is less than the number of the original data. Subsequently, all the training data are used to learn the weights in Equation (1). The methods for selecting the RBF neural network center vector include orthogonal least-squares method [34], clustering method [35], and K-SVD method [36]. In the clustering method, not only the center vector can be determined, but also the sample covariances that belong to a certain type of data can be used as the covariance of RBF. In this paper, the K-means clustering method is used to obtain the center vector and covariance matrix [37]. The following anisotropic covariance matrix is defined as the kernel function:

$$\mathrm{RBF}_j(\boldsymbol{x}) = \exp[-(\boldsymbol{x} - \boldsymbol{\xi}_j)^{\mathrm{T}} \boldsymbol{P}_j^{-1} (\boldsymbol{x} - \boldsymbol{\xi}_j)], \tag{2}$$

where ξ_j and P_j represent the center vector and covariance matrix of the j-th RBF, which are obtained by K-means clustering, respectively:

(1) Randomly select k objects, which indicate the initial centers of the k clusters to be divided. The number of k can be preferred by the k-fold cross-check or bootstrap method. In this paper, the value of k is selected as 1.
(2) Calculate the distance between each point and the center point and find the center with the shortest distance as the new center point of each cluster.
(3) Calculate the average value (centroid) of all objects in each cluster as the new center point of each cluster.
(4) Calculate the distance between all objects and the new k centers again and redistribute all objects to each cluster according to the nearest distance principle.
(5) Repeat the above steps until all cluster centers remain unchanged (the distance between the newly generated cluster and the previous cluster is less than a set threshold). This is the end of clustering.

After determining ξ_j and P_j, the function model to be established becomes:

$$\boldsymbol{z} = \sum_{j=1}^{k} \beta_j \mathrm{RBF}_j(\boldsymbol{x}) = \sum_{j=1}^{k} \beta_j \exp[-(\boldsymbol{x} - \boldsymbol{\xi}_j)^{\mathrm{T}} \boldsymbol{P}_j^{-1} (\boldsymbol{x} - \boldsymbol{\xi}_j)], \tag{3}$$

where β_j represents the weight vector.

It can be written in the form of the following observation equation:

$$\overline{\boldsymbol{z}} + \boldsymbol{e} = \boldsymbol{B}\boldsymbol{\beta}, \tag{4}$$

where $\overline{\boldsymbol{z}}$ represents the true value of ZTD, e denotes other unmodeled noises, and the $l \times m$ matrix $\boldsymbol{B}$ is expressed as follows:

$$[\boldsymbol{B}]_{i,j} = \exp[-(\boldsymbol{x}_i - \boldsymbol{\xi}_j)^{\mathrm{T}} \boldsymbol{P}_j^{-1} (\boldsymbol{x}_i - \boldsymbol{\xi}_j)]. \tag{5}$$

The $m \times 1$ weight vector β in Equation (5) is estimated by using the least-squares method [14]:

$$\boldsymbol{\beta} = (\boldsymbol{B}^{\mathrm{T}} \boldsymbol{B})^{-1} \boldsymbol{B}^{\mathrm{T}} \boldsymbol{z}. \tag{6}$$

The form of the observation equation can be seen as a trained estimator, that is, the regional ZTD model. In practical applications, the estimator is trained by using the ZTD data of the modeling station, and the corresponding ZTD can be estimated by inputting the coordinates and time of the prediction station inside or outside the area.

The ZTD region modeling flow chart is shown in Figure 3:

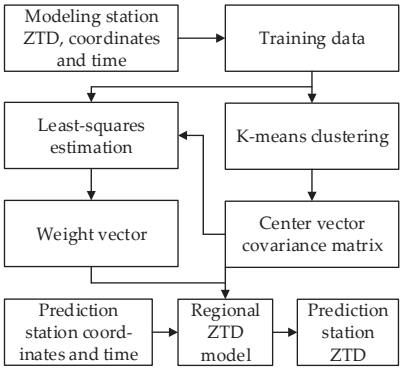

Figure 3. ZTD region modeling flow chart.

2.2.2. Real-Time Parameters Updating LSTM Single-Station ZTD Modeling

LSTM neural network is a variant of recursive neural network (RNN), and LSTM expands its memory ability [38]. This feature enables LSTM to make ZTD prediction in an environment where meteorological information with evident advantages, stronger feasibility, and higher stability than the traditional ZTD acquisition method, such as Hopfield model, cannot be obtained [21].

However, the traditional LSTM cannot reasonably use the online ZTD value derived from GNSS techniques, such as PPP-RTK and RT-PPP. From the perspective of real-time ZTD modeling, a single-station ZTD modeling method with R-LSTM is given. The LSTM network refers to an online update mechanism for LSTM learning that minimizes the cost function. It can establish a practical model with only a small number of non-full life cycle samples (seconds to hours). The modeling idea is that: first, the reasonable use of known historical data is necessary to establish the LSTM prediction model. Second, when the actual online data are obtained, the corresponding prediction value can be achieved using the selected prediction. The new data at the next epoch can be used as the actual value of the prediction value. The error between the predicted value and the true value is added to the overall error of the sample. Finally, the error minimization method is used to update the model parameters iteratively. With the increasing use of online data, the model's accuracy increases over time by updating the loop parameters. This modeling idea is more conducive to ZTD online modeling and prediction. The implementation steps of the R-LSTM prediction algorithm are presented as follows:

Assuming that the actual time series is $X(x_1, x_2, x_3 \ldots\ldots x_n)$, the improved LSTM calculation steps are presented as follows:

(1) The actual time series $X(x_1, x_2, \ldots, x_n)$ is extended to $X \begin{bmatrix} x_1 & x_2 & \cdots & x_{n-k+1} \\ x_2 & x_3 & \cdots & x_{n-k+2} \\ x_3 & x_4 & \cdots & x_{n-k+3} \\ & & \vdots & \\ x_k & x_{k+1} & \cdots & x_n \end{bmatrix}$,

where n is the time series length, k is the sample dimension, $n-k+1$ is the number of samples, and $y = (x_k, x_{k+1}, \cdots x_n)$ is the training data label. X is normalized:

$$X = \frac{x_i}{\sqrt{{x_i}^2 + {x_{i+1}}^2 + \cdots + {x_{k+1}}^2}} (i = 1, 2 \cdots, n-k+1), \tag{7}$$

(2) Initialize network parameters and set super parameters:

$$\begin{cases} W_f = rand(L, N) \\ b_f = rand(1, N) \\ \quad \vdots \\ Error\_Cost = M_1 \\ Max\_iter = M_2 \end{cases}, \tag{8}$$

where W_f and b_f represent the initial weight and bias of the forgetting gate, respectively. The symbol *rand* ( ) represents a random function; and L and N represent the number of LSTM cell units and the number of neuron layers, respectively. Similarly, the initial weights and biases of the input gate, the output gate, the cell state, W_i, b_i, W_c, b_c, W_o, b_o, and other parameters also need to be initialized. *Error_Cost* and *Max _ iter* represent the error threshold and the maximum number of hyperparameter iterations, respectively.

(3) Calculate what information needs to be forgotten from the cell state at time $t-1$.

$$\begin{cases} f_t = \sigma(W_f \cdot [h_{t-1}, x_t] + b_f) \\ \hat{f}_t = f_t \otimes C_{t-1} \end{cases}, \tag{9}$$

where f_t is the output of the forget gate. The symbol σ( ) represents a sigmoid activation function. h_{t-1} is the output value of the LSTM at the previous moment. x_t is the input value of the network at the current moment. C_{t-1} is the cell state at the previous moment. The symbol $\otimes$ represents the point multiplication operation of the two vectors.

(4) Calculate which input information can be left in the cell state at time t.

$$\begin{cases} i_t = \sigma(W_i \cdot [h_{t-1}, x_t] + b_i) \\ \widetilde{C}_t = \tanh(W_C \cdot [h_{t-1}, x_t] + b_C) \\ \hat{i}_t = i_t \otimes \widetilde{C}_t \end{cases}, \tag{10}$$

where i_t is the output of the input gate and determines what values will be updated. The symbol tanh ( ) represents a hyperbolic tangent activation function. $\widetilde{C}_t$ is a vector of new candidate values created by the tanh function.

(5) Calculate the cell state C_t at time t.

$$C_t = \hat{f}_t + \hat{i}_t, \tag{11}$$

where C_t is the result of the combined actions of the forget gate and the input gate on the cell states in Equations (9) and (10).

(6) Calculate the network output at time t.

$$\begin{cases} o_t = \sigma(W_o \cdot [h_{t-1}, x_t] + b_o) \\ h_t = o_t \otimes \tanh(C_t) \end{cases}, \tag{12}$$

where o_t is the output of the output gate. h_t is the predicted value at the current moment. Repeat Steps 3 to 6 to calculate the predicted values h of all training samples.

(7) Calculate the errors between the predicted values and the true values of all samples.

$$J_{(\theta)}(y, h; W, b) = \frac{1}{2}||y - h||^2, \tag{13}$$

where J ( ) represents the cost function. The minimum value of the function in Equation (13), namely, the optimal solution *error<Error_Cost*, or the current number of iterations *iter > Max_iter*, are considered. Thus, the training ends. Otherwise, the BPTT algorithm is used to update the network parameters, and one is added to the

number of iterations, and then the processing returns to Step 3 for circulation. It exits the loop until the error threshold or maximum number of iterations is reached. The following trained network parameters are saved:

$$\theta_0 = (W_f, W_i, W_C, W_o, C, h, b_f, b_i, b_C, b_o), \tag{14}$$

(8) Update parameters in real time according to online observation data. The new samples, $X_{n+1}(x_{n-k+2}, \cdots x_{n+1})$ and θ_0, perform the forward operation of the LSTM shown in Steps 3–6 to obtain the predicted value h_{n+1}. When the data $X_{n+2}(x_{n-k+3}, \cdots x_{n+2})$ are collected, they can be used as the true value label of the predicted value h_{n+1} to calculate the overall *error*:

$$error = error + \frac{1}{2}(h_{n+1} - x_{n+2})^2. \tag{15}$$

Then, the BPTT algorithm is used to update the model parameters to θ_1:

$$\theta_1 = (W_f - \lambda \times \Delta W_f, \cdots, b_f - \lambda \times \Delta b_f), \tag{16}$$

where λ is the learning rate; and ΔW_f and Δb_f are the gradient matrices and vectors of the weights and biases of each layer of neurons, respectively. The parameter initialization corresponds to the global optimal solution of the historical sample. Hence, when the new sample is added, the global optimal solution can be achieved again with only a few simple steps of updating.

The improved LSTM flow chart is shown in Figure 4:

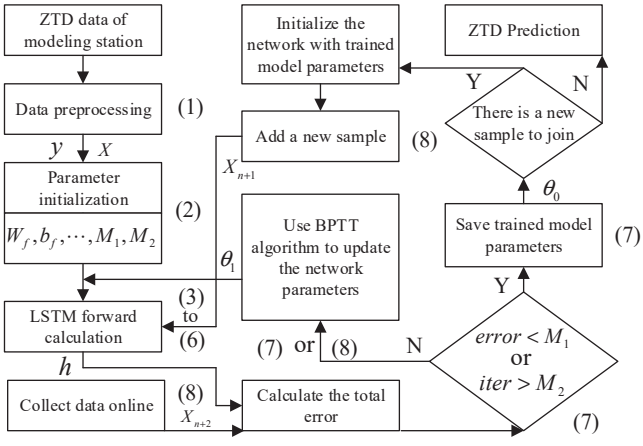

Figure 4. ZTD single station modeling flow chart. Note: The serial number refers to the corresponding calculation steps.

In addition, the model can be applied to the early warning of severe convective weather. In Steps 6–8, when the predicted value of ZTD at the next sampling time reaches the warning value of severe convective weather, the warning information is issued to make emergency response in time. As a result, the economic losses to industrial and agricultural production will be reduced, and the utilization rate of water resources will be improved [39].

2.2.3. Regional/Single Station ZTD Combination Model

Based on the regional and single station ZTD model above, the regional/single station ZTD combination model is obtained by weighting:

$$\begin{cases} Weight_R^i = a, Weight_S^i = b, (i = 1) \\ Weight_R^i = \frac{RMSE_S^{[1,i-1]}}{RMSE_R^{[1,i-1]} + RMSE_S^{[1,i-1]}}, (i = 2, 3, \ldots, N) \\ Weight_S^i = \frac{RMSE_R^{[1,i-1]}}{RMSE_R^{[1,i-1]} + RMSE_S^{[1,i-1]}}, (i = 2, 3, \ldots, N) \end{cases}, \quad (17)$$

where N is the total number of epochs. $Weight_R^i$ and $Weght_S^i$ represent the weights applied to the ZTD predicted by the regional and single station ZTD models in the i-th epoch, respectively. a and b represent the corresponding empirical weights, and $a + b = 1$. $RMSE_R^{[1,i-1]}$ and $RMSE_S^{[1,i-1]}$ represent the RMSE of the $i-1$ predicted values of the regional and single station ZTD models before the i-th epoch, respectively.

The weights are gradually updated by comprehensively considering the new predicted value weights of the two models in the prediction process and the error level of the predicted values of the previous stage. According to the weighting scheme in Equation (18), the ZTD that corresponds to the combined model in the i-th epoch is presented as:

$$ZTD_C^i = ZTD_R^i \times Weight_R^i + ZTD_S^i \times Weight_S^i, \quad (18)$$

where $ZTD_C^i, ZTD_R^i and ZTD_S^i$ represent the ZTD prediction values of the combined model, the regional model, and the single station model in the i-th epoch, respectively. ZTD_C^i is obtained by weighting the two other models.

2.2.4. Accuracy Evaluation Criteria

The RMSE, MAE, coefficient of determination (R2), and training time consumption (TTC) are used as the evaluation indexes of prediction model accuracy and efficiency. The computation is executed on a personal laptop with an Intel Core i7-10750H CPU at 2.60 GHz and with 16 GB of RAM. RMSE is used to measure the deviation between the predicted value and the true value of the model. MAE corresponds to the average of absolute error. No positive and negative offsets are observed because the deviation is absolute. Hence, the actual situation of the predicted value error can be reflected better. R2, also known as the goodness of fit in statistics, can measure the degree to which a variable is explained by another variable. Its value is between 0 and 1, which determines the degree of fitting among variables. The larger the value, the higher the correlation. TTC is used to measure the modeling efficiency of the model, which is particularly important for real-time modeling. The calculation formula of accuracy indicators, such as RMSE, MAE, and R2, are presented as follows:

$$RMSE = \sqrt{\frac{1}{N}\sum_{i=1}^{N}(P_i - M_i)^2}, \quad (19)$$

$$MAE = \frac{1}{N}\sum_{i=1}^{N}|P_i - M_i|, \quad (20)$$

$$R2 = \left(\frac{\sum_{i=1}^{N}(M_i - \overline{M})(P_i - \overline{P})}{\sqrt{\sum_{i=1}^{N}(M_i - \overline{M})^2 (P_i - \overline{P})^2}} \right)^2, \quad (21)$$

where M_i and P_i are the true and predicted values on the test set, respectively. $\overline{M}$ and $\overline{P}$ are the corresponding average values; and N is the number of predicted samples.

3. Results

3.1. Regional Modeling Results

To verify the modeling accuracy and efficiency in the regional modeling, the modeling effects of different amounts of modeling data are compared and analyzed. Two sets of experiments were carried out. The first set of experiments (K-RBF-0) did not use historical data in the modeling process. The second set of experiments (K-RBF-5) used the five nearest consecutive epoch historical data in the modeling process. Figure 5 shows the accuracy and efficiency statistics results of 13 stations of K-RBF model for 90 days.

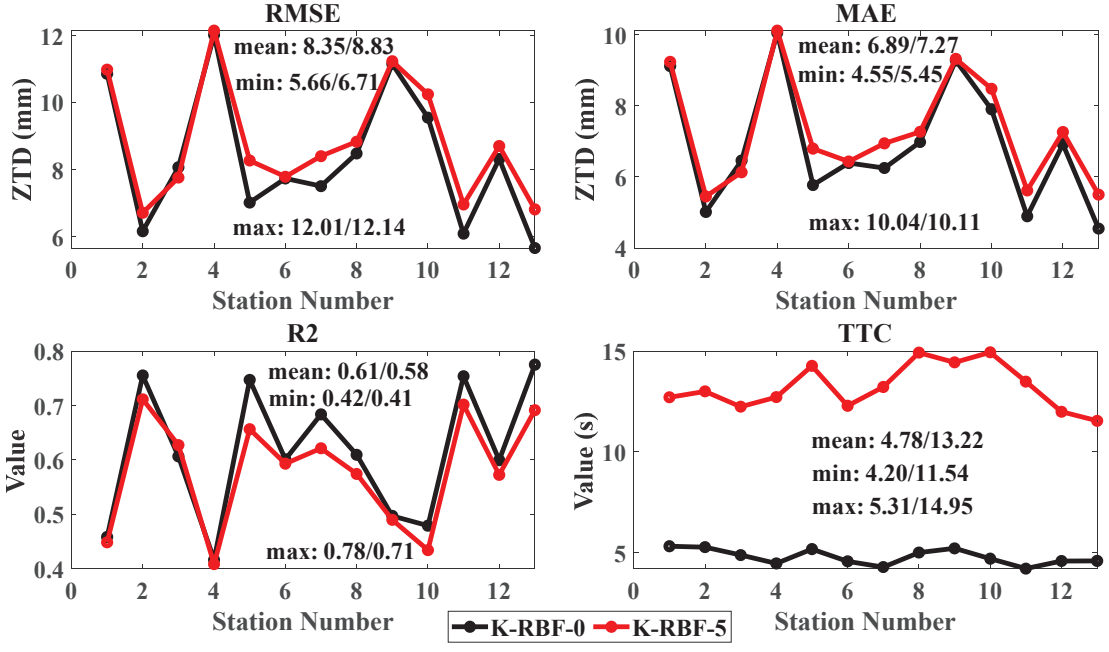

Figure 5. K-RBF model accuracy and efficiency statistics results of K-RBF-0, K-RBF-5 experiments.

3.2. Single Station Modeling Results

The relationship between the amount of historical data and the accuracy and efficiency of modeling is analyzed using the conventional LSTM model as a reference to verify the modeling accuracy and modeling efficiency for the single station modeling. Taking the WHC1 station as an example, the ZTD data of the first 5, $12 \times i$ ($i = 1,2, \ldots, 23$) epochs of each day are selected for modeling, and the ZTD of the current epoch is used for accuracy verification. A total of 24 sets of experiments are recorded as Group1, Group2, . . . , Group24. Figure 6 shows the accuracy statistics results of R-LSTM and LSTM models for the 24 groups of experiments for 90 consecutive days. Figure 7 shows the true values, predicted values, and the differences of both changes in the two models in the Group1 experiment.

3.3. Regional/Single Station Combination Modeling Results

To improve the real-time performance of modeling as much as possible, we select the K-RBF-0 group experimental method in the K-RBF regional modeling and the Group1 group experimental method in R-LSTM single station modeling for KR-RBF-STLM combined modeling. Table 1 and Figure 8 show the accuracy and efficiency statistics results of 13 stations for the three models for 90 days. The distribution of the modeling errors of various models is also compared and analyzed. Figure 9 shows the true values, predicted values, and the differences in the changes in the three models at the CIT1, JPLM, LBCH,

and TORP stations. Figure 10 shows the error distribution of the three models at 13 stations for 90 days.

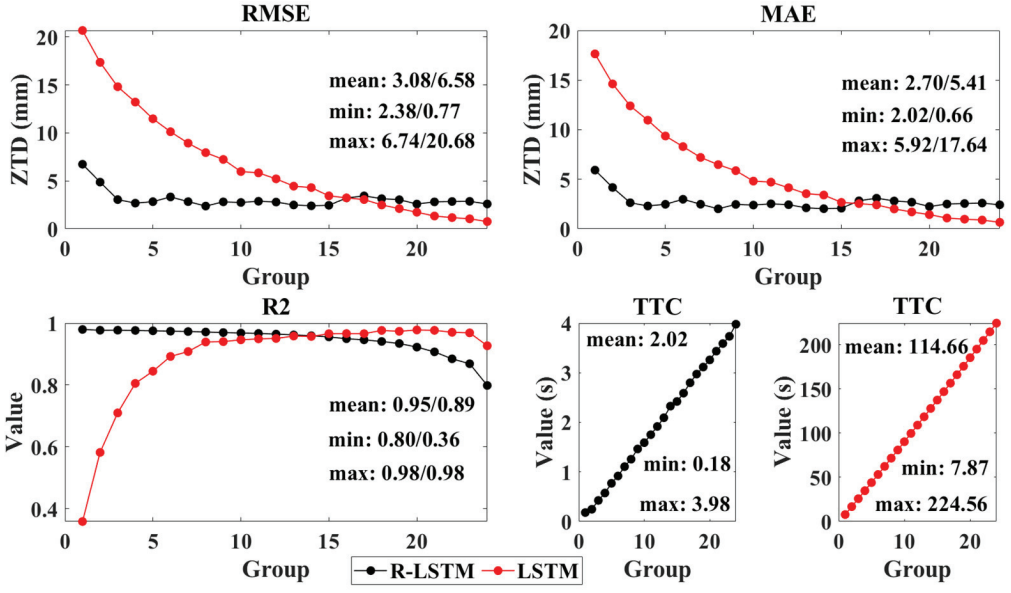

Figure 6. Accuracy and efficiency statistics results of 24 groups of experiments of R−LSTM and LSTM models.

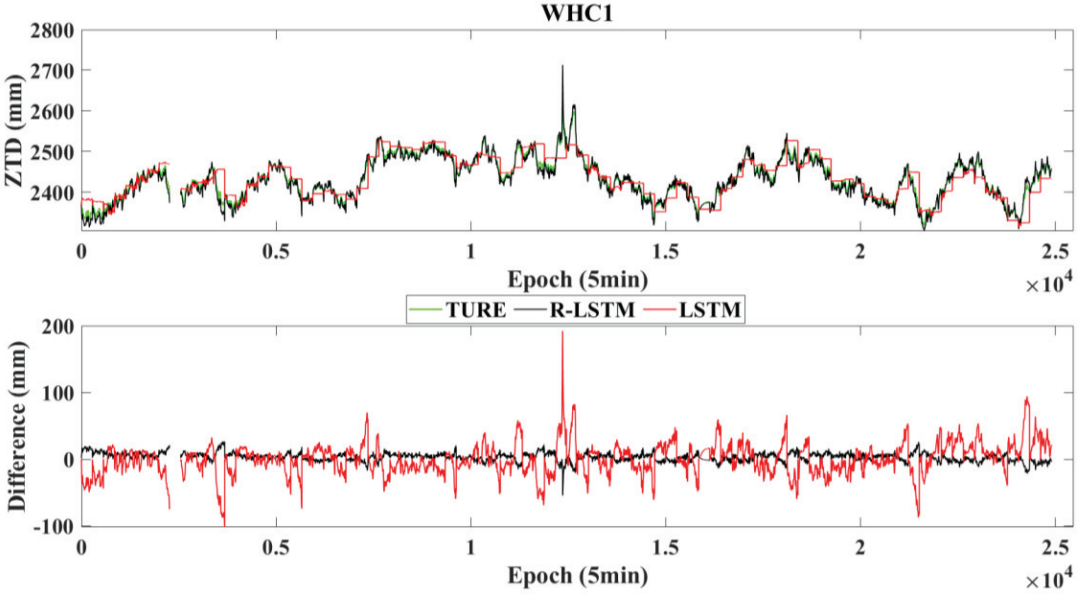

Figure 7. Variations in the true values, predicted values, and errors of the R-LSTM and LSTM modeling in the Group1 experiment of WHC1 Station. Note: The data−free period in the figure is caused by the absence of true value data in this period.

Table 1. Statistical results of prediction accuracy and efficiency of K-RBF, R-LSTM, and KR-RBF-STLM models.

Station Number	RMSE/mm	Increasing Rate/%	MAE/mm	Increasing Rate/%	R2	Increasing Rate/%	TTC/s	Increasing Rate/%
	K-RBF/R-LSTM/KR-RBF-LSTM	Imp1/Imp2	K-RBF/R-LSTM/KR-RBF-LSTM	Imp1/Imp2	K-RBF/R-LSTM/KR-RBF-LSTM	Imp1/Imp2	K-RBF/R-LSTM/KR-RBF-LSTM	Imp1/Imp2
1	**10.85/6.74/5.25**	51.63/22.09	9.11/5.92/4.38	51.94/26.10	0.46/0.98/0.90	49.05/−8.18	5.31/0.18/5.49	−3.30/−96.70
2	**6.16/6.18/3.95**	35.86/36.10	5.01/5.31/3.36	33.07/36.75	0.76/0.97/0.96	20.97/−1.80	5.26/0.18/5.44	−3.31/−96.69
3	**8.07/5.74/4.29**	46.83/25.28	6.46/4.98/3.49	45.95/29.85	0.61/0.98/0.92	33.72/−6.23	4.87/0.19/5.06	−3.70/−96.30
4	**12.01/6.83/5.26**	56.22/22.93	10.04/5.88/4.40	56.16/25.09	0.42/0.98/0.92	54.66/−6.00	4.46/0.18/4.63	−3.84/−96.16
5	**7.01/5.96/3.74**	46.72/37.35	5.77/5.09/3.13	45.80/38.59	0.75/0.98/0.96	22.02/−2.24	5.17/0.21/5.38	−3.88/−96.12
6	**7.73/6.28/4.62**	40.28/26.52	6.39/5.50/3.79	40.59/31.05	0.60/0.97/0.89	32.81/−8.05	4.56/0.18/4.74	−3.77/−96.23
7	**7.50/5.73/3.85**	48.65/32.82	6.25/4.92/3.23	48.28/34.33	0.68/0.98/0.95	27.86/−3.27	4.27/0.18/4.45	−4.05/−95.95
8	**8.48/5.85/4.23**	50.04/27.63	6.98/5.05/3.52	49.53/30.26	0.61/0.98/0.93	34.27/−5.03	4.99/0.18/5.18	−3.54/−96.46
9	**11.15/6.11/4.62**	58.56/24.37	9.27/5.22/3.86	58.36/26.05	0.50/0.98/0.93	46.79/−4.64	5.20/0.18/5.38	−3.30/−96.70
10	**9.55/6.23/5.15**	46.03/17.22	7.90/5.56/4.19	46.98/24.69	0.48/0.97/0.86	44.23/−11.73	4.69/0.18/4.87	−3.68/−96.32
11	**6.08/5.89/3.77**	38.02/35.98	4.89/5.13/3.16	35.51/38.48	0.75/0.98/0.94	20.18/−3.37	4.20/0.19/4.38	−4.28/−95.72
12	**8.31/5.70/4.23**	49.07/25.73	6.92/4.93/3.55	48.64/27.86	0.60/0.98/0.90	33.53/−7.74	4.58/0.19/4.76	−3.92/−96.08
13	**5.66/6.15/3.81**	32.57/37.98	4.55/5.32/3.22	29.19/39.51	0.78/0.97/0.95	18.46/−2.40	4.58/0.19/4.77	−3.90/−96.10
mean	**8.35/6.11/4.37**	47.70/28.48	6.89/5.29/3.64	47.20/31.29	0.61/0.98/0.92	33.51/−5.43	4.78/0.18/4.96	−3.71/−96.29
min	**5.66/5.70/3.74**	33.94/34.47	4.55/4.92/3.13	31.20/36.43	0.42/0.97/0.86	51.54/−11.73	4.20/0.18/4.38	−4.28/−95.94
max	**12.01/6.83/5.26**	56.22/22.93	10.04/5.92/4.40	56.16/25.68	0.78/0.98/0.96	19.10/−2.24	5.31/0.21/5.49	−3.30/−96.20

Note: (1) Imp1 and Imp2 refer to the modeling result increasing rate of KR−RBF−LSTM relative to K−RBF and R−LSTM, respectively; (2) The predicted time consumption of all prediction models is within 0.02 s, with no significant difference. Hence, it is not listed here.

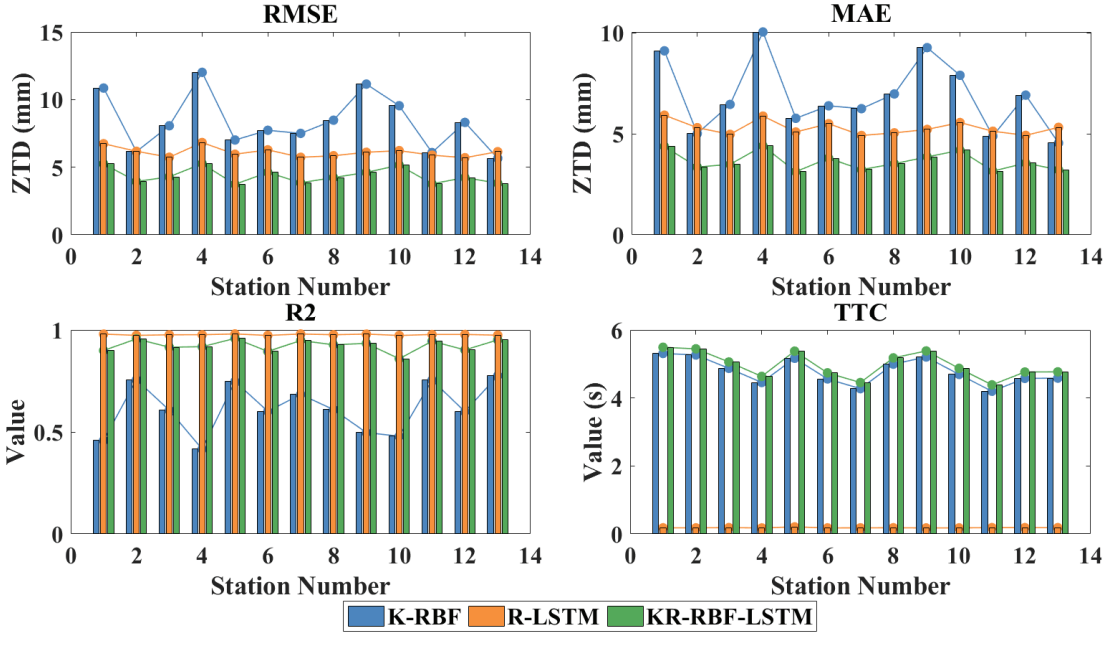

Figure 8. Accuracy and efficiency changes in K-RBF, R-LSTM, and KR-RBF-STLM models at different stations.

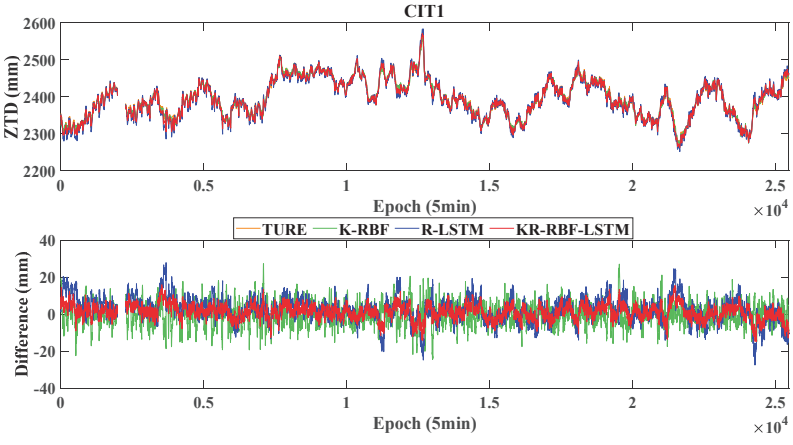

(**a**)

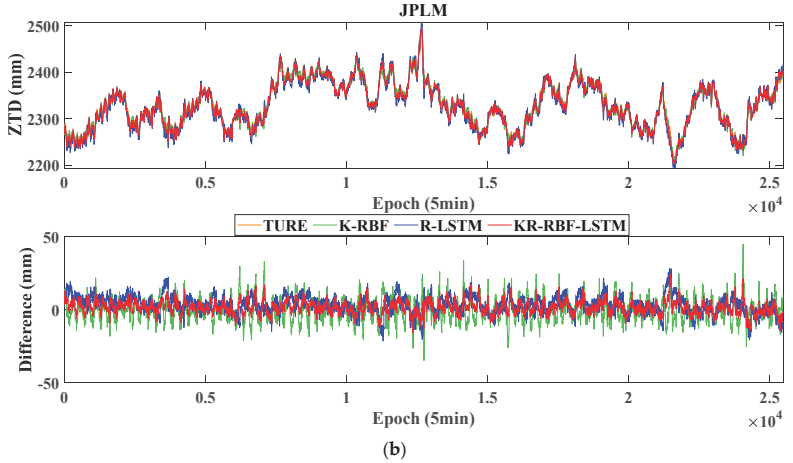

(**b**)

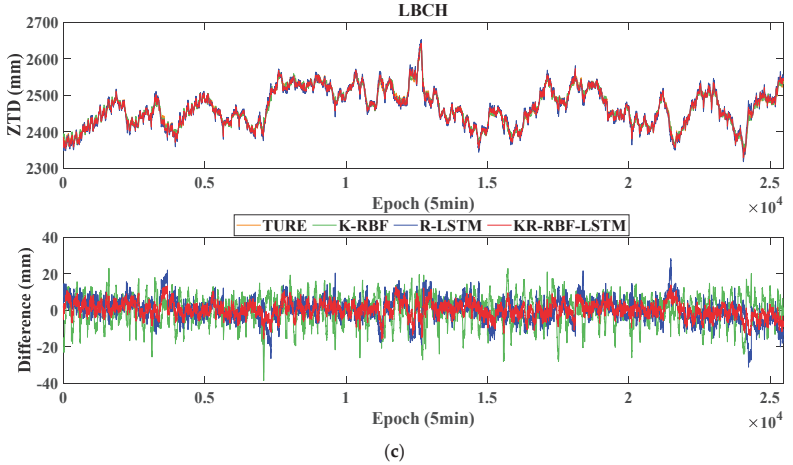

(**c**)

Figure 9. *Cont.*

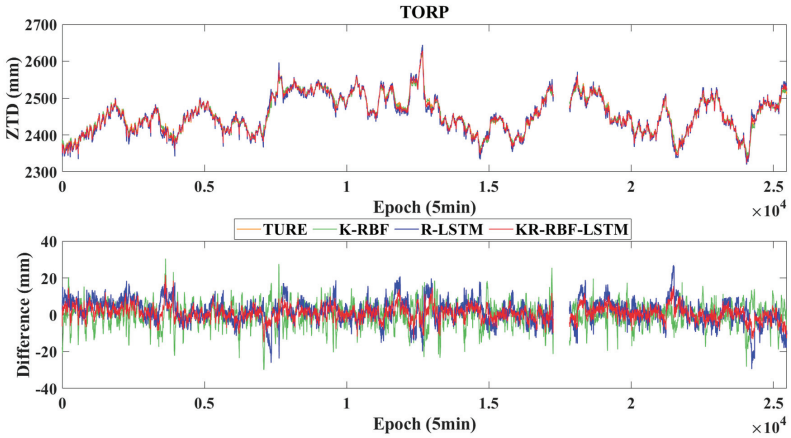

(**d**)

Figure 9. Variations in the true values, predicted values, and errors of the K-RBF, R-LSTM, and KR-RBF-LSTM. (**a**) CIT1, Station number 2.; (**b**) JPLM, Station number 6.; (**c**) LBCH, Station number 7; (**d**) TORP, Station number 11. Note: The data−free period in the figure is caused by the absence of the true value data in this period.

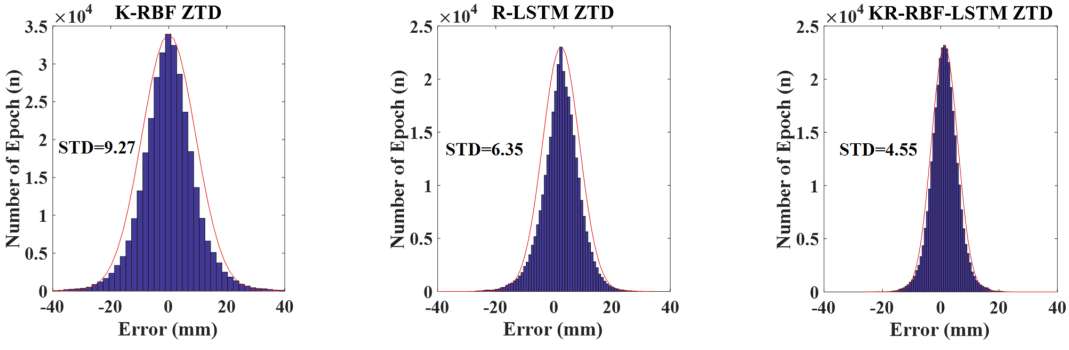

Figure 10. Error distribution of prediction results of K-RBF, R-LSTM, and KR-RBF-STLM models.

4. Discussion

4.1. Regional Modeling

Figures 1 and 5 suggest that:

(1) The mean, minimum (min), and maximum (max) of K-RBF-0 experiment are slightly higher than those of K-RBF-5. RMSE, MEA, and R2 are improved by 5.43%, 15.66%, 1.04%, 5.26%, 16.57%, 0.61%, 5.67%, 1.92%, and 8.22%. The mean, min, and max of TTC are greatly improved by 63.84%, 63.64%, and 64.49%, respectively. The main reason is that, with the increment in sample data, the total calculation time of the distance between each data and the center point in Equation (2) will increase. At the same time, the number of K-means clustering is not optimized and adjusted, thereby increasing time and slightly decreasing accuracy.

(2) The K-RBF-0 model has high accuracy and effectiveness. The means of RMSE, MAE, and R2 are 8.35 mm, 6.89 mm, and 0.61. Therefore, this model can meet the real-time forecasting needs for 4.78 s updates because the K-RBF model is simple, fast, robust, and highly accurate.

(3) For the K-RBF modeling, the accuracy of each station has certain differences. The distribution and density of the stations have a particular influence on the modeling accuracy.

The accuracy of the station in the modeling area is higher than that outside the modeling area. For example, the accuracies of CIT1 (2), CMP9 (3), HOLP (5), and JPLM (6) stations are better than those of BILL (1), CRFP (4), SFDM (9), and TAB1 (10). The accuracy of the station in the dense area of the modeling station is higher than that in the sparse areas, such as TROP (11), TRAK (12) and BILL (1), and CRFP (4). Although they are all outside the modeling area, the modeling accuracy of the first two stations is better than those of the two latter stations because of the dense stations around the former. The main reason is that ZTD has a certain correlation in space. The more uniform the distribution of stations is, the higher the density is, and the higher the modeling accuracy is [40].

4.2. Single Station Modeling

Figures 6 and 7 illustrate that:

(1) The RMSE and MAE of the R-LSTM model increase first and then stabilize with the increasing amounts of historical data. No significant increase was observed after the numbers of historical epochs exceeded 36. The mean values of the RMSE and MAE in Group3 to Group24 are 2.83 mm and 2.49 mm, respectively. R2 shows a slow downward trend, that is, from 0.98 to 0.80. TTC shows a gradual upward trend in mean, min, and max, which are equivalent to 2.02, 0.18, and 3.98 s, respectively.

(2) The RMSE, MAE, and TTC of the LSTM model show a gradual upward trend with increasing amounts of historical data, and R2 shows a gradual upward trend and a slow downward trend. When the number of historical epochs is 276, the RMSE and MAE are optimal at 0.77 mm and 0.66 mm, respectively. However, R2 is slightly lower than that of the previous group of experiment (Group23), and TTC is 56.44 times that of the R-LSTM model. When the number of historical epochs is 192, the accuracy of the two models is close, but the TTC difference is 56.81 times.

(3) When historical data are sufficient, the R-LSTM and LSTM prediction methods are effective. However, when the historical data are insufficient, the LSTM prediction effect is poor, and the R-LSTM method is still better. In the Group1 experiment (the experimental results are shown in Figure 8), the RMSE, MAE, R2, and TTC of the R-LSTM model are 6.74 mm, 5.92 mm, 0.98, and 0.18 s, respectively. Compared with those of the LSTM model, these values are improved by 67.43%, 66.42%, 63.33%, and 97.70%, respectively. The R-LSTM model can predict the trend of ZTD, whereas the prediction results of the LSTM model gradually changed linearly. For the epoch of dramatic changes in ZTD, such as the 3679th, 12,354th, and 21,489th epochs, the prediction results of R-LSTM are significantly better. The main reason is that the training samples of the LSTM model are insufficient in this case, and the parameters of the R-LSTM model can be updated in real time.

4.3. Regional/Single Station Combination Modeling

Table 1 and Figures 1, 2 and 8–10 show that:

(1) The mean, min, and max of the RMS, MAE, R2, and KR-RBF-LSTM relative to K-RBF are improved by 47.70%, 33.94%, 56.22%, 47.72%, 31.20%, 56.16%, 33.51%, 51.54%, and 19.10%; TTC is increased by 3.71%, 4.28%, and 3.30%. Compared with R-LSTM, the mean, min, and max of RMS and MAE are improved by 28.48%, 34.47%, and 22.93%, as well as 31.29%, 36.43%, and 25.68%, respectively. R2 is reduced by 5.43%, 11.73%, and 2.24%, and TTC is increased by 96.29%, 95.94%, and 96.20%. In general, the accuracy of the KR-RBF-LSTM model is the best mainly because the combination model relates the advantages of the two models. That is, K-RBF can consider the spatial correlation of the stations, and R-LSTM can consider the temporal correlation of the stations. When the two are combined, the spatial and temporal correlations can be considered. Specifically, this advantage is more obvious in the epoch where the ZTD changes greatly. The R-LSTM model has the best real-time performance. The main reason is that the parameters of the model can be updated in real time and can quickly reach the global optimal state. Its training samples are only five historical data of a certain station, whereas the training data of other models are 2.40 or 3.40 times greater than that. Compared with the BP neural network

model, the K-RBF model can avoid the problem of the unstable model and time-consuming training due to the lack of training samples. It exhibits a certain improvement in terms of accuracy and efficiency [24,41,42].

(2) The distribution of modeling stations will affect the K-RBF modeling effect to a certain extent, and the influence on the KR-RBF-LSTM model weakens. No significant difference is observed in the accuracy indicators of each R-LSTM station. The main reason is that the ZTD has spatial and temporal correlations. The strength of spatial correlation varies for the distribution of different stations. The regional model considers the spatial correlation of stations, and the combined model further considers the time correlation of stations. However, the influence of other stations is ignored in the single station model, which is only related to the small amount of historical data of the station and the physical change degree of the ZTD itself.

(3) The errors of the three models are subject to normal distribution, indicating that the models established in this paper are reasonable. At the same time, the error distribution of the KR-RBF-LSTM model is better than those of K-RBF and R-LSTM, and its standard deviation (STD) is improved by 50.98% and 28.43%, respectively.

(4) Although ZTD and station elevation are correlated [20] and the elevation of some stations in the study area fluctuates greatly, the prediction accuracy of the three models does not show a strong correlation with the station elevation. The main reason is that the K-RBF and KR-RBF-LSTM models consider the influence of elevation. The R-LSTM model can gradually optimize and update the established model parameters according to the ZTD data obtained at each epoch.

(5) The real-time/near real-time application of the three models can be selected according to the user's needs. Under the condition that no historical data are in the prediction station, the real-time ZTD data of the regional monitoring station exist around it, and the K-RBF model can be selected to provide high-precision ZTD enhancement products for RTK, PPP-RTK, and other positioning modes. Under the condition that the prediction station has a small amount of historical data (which can be obtained by empirical model), but no ZTD data of regional monitoring stations are around it, the R-LSTM model can be selected to improve the prediction accuracy of real-time PPP-based ZTD and serve the extreme weather forecast. KR-RBF-LSTM model can be used to meet the needs of RTK, real-time PPP, PPP-RTK, and other high-precision real-time positioning modes under the condition that the prediction station has a small amount of historical data and real-time ZTD data of regional monitoring station around it. Specifically, in a short time (such as within 2 min), the demand for mm-level positioning accuracy in the elevation direction, such as mining subsidence monitoring, is urgent.

5. Conclusions

A regional/single station ZTD combination prediction model is proposed, aiming at the problem that the traditional BP neural network modeling is inefficient and has local optimum and that the traditional LSTM modeling cannot effectively use the data of a non-full life cycle to establish an excellent ZTD prediction model and cannot reasonably use the online data. The model considers the ZTD spatiotemporal information and applies algorithms of the RBF neural network based on K-means clustering and LSTM with real-time parameter updating. The model mainly solves the problem of online modeling and model correction of small sample data in regional real-time/near real-time ZTD modeling. Taking the ZTD data of 13 IGS stations in Southern California for 90 consecutive days as an example (5 min sampling interval), the prediction performance of the proposed combined model in regional real-time ZTD modeling is verified. Compared with K-RBF, the RMSE, MAE, and STD of KR-RBF-LSTM are improved by 47.70%, 47.20%, and 50.98%, respectively. Compared with R-LSTM, the RMSE, MAE, and STD are improved by 24.48%, 31.29%, and 28.43%, respectively. Compared with the traditional BP model, the accuracy and efficiency of K-RBF exhibited a certain improvement. Compared with LSTM, the RMSE and MAE of R-LSTM are improved by 66.43% and 66.42%, respectively.

The research results of this paper have high reference values for PPP-RTK, RT-PPP, RTK, and extreme weather forecasting based on regional atmospheric enhancement products. Based on the current work, we can perform further research in the future. First, the ZTD prediction value of the model with better historical RMSE performance is weighted higher, and the ZTD prediction value of the combined model may not necessarily take the optimal value. If the weight in the combined model is adaptively adjusted by using the relevant optimization algorithm, then the prediction accuracy and stability of the model can be improved further. Second, the accuracy and efficiency of the regional and single station models are further improved by optimizing the K-means algorithm and by seeking more effective R-LSTM parameter optimization methods. Third, due to the lack of clear physical mechanism of artificial intelligence algorithms, such as that in this paper, the research on the dynamic change and formation mechanism of atmospheric water vapor is strengthened. From the perspective of meteorology, hydrology, geography, and other disciplines, the prediction model is established on the basis of strict physical causes. It is the focus of extreme weather forecast and climate change research to serve the response and feedback of carbon, nitrogen, and water cycle to climate change and other multidisciplinary scientific research.

Author Contributions: Conceptualization, X.Y. (Xu Yang) and Y.L.; methodology, X.Y. (Xu Yang) and X.Y. (Xuexiang Yu); software, X.Y. (Xu Yang) and X.Y. (Xuexiang Yu); validation, X.Y. (Xu Yang), Y.L. and X.Y. (Xuexiang Yu); formal analysis, X.Y. (Xu Yang) and Y.L.; investigation, X.Y. (Xu Yang) and H.T.; resources, X.Y. (Xu Yang) and J.Y.; data curation, X.Y. (Xu Yang) and M.Z.; writing—original draft preparation, X.Y. (Xu Yang); writing—review and editing, X.Y. (Xu Yang), Y.L., X.Y. (Xuexiang Yu), H.T., J.Y. and M.Z.; visualization, X.Y. (Xu Yang) and M.Z.; supervision, Y.L. and M.Z.; project administration, X.Y. (Xu Yang); funding acquisition, X.Y. (Xu Yang), Y.L., X.Y. (Xuexiang Yu) and J.Y. All authors have read and agreed to the published version of the manuscript.

Funding: This work was supported by the "Key Laboratory of Aviation-aerospace-ground Cooperative Monitoring and Early Warning of Coal Mining-induced Disasters of Anhui Higher Education Institutes (Anhui University of Science and Technology) (No.KLAHEI202204)", "Anhui Province Natural Science Foundation (No.2208085QD115, 2008085MD114)", "Major Special Projects of Science and Technology in Anhui Province (No.202103a05020026)", "Key Research and Development Projects of Anhui Province (No.202104a07020014)", "Open Foundation of the Key Laboratory of Universities in Anhui Province for Prevention of Mine Geological Disasters (No.2022-MGDP-08)", "Key Natural Science Projects of Anhui Provincial Department of Education (No.KJ2020A0311, 2022AH050820)", "Coal Industry Engineering Research Center of Mining Area Environmental And Disaster Cooperative Monitoring, Anhui University of Science and Technology (Anhui University of Science and Technology) (No.KSXTJC202005, KSXTJC202207)", and "Introduction of Talent Research Startup Fund Project of Anhui University of Science and Technology (No.2019, 13200458)".

Institutional Review Board Statement: Not applicable.

Informed Consent Statement: Not applicable.

Data Availability Statement: The data used to support the findings of this study are available from the corresponding author upon request.

Acknowledgments: The authors appreciate the International GNSS Service for providing relevant data and products.

Conflicts of Interest: The authors declare no conflict of interest.

Abbreviations

GNSS	Global navigation satellite system
GPS	Global positioning system
ZTD	Zenith tropospheric delay
ZHD	Zenith hydrostatic delay

ZWD	Zenith wet delay
BP	Back propagation
LSTM	Long short-term memory
LSTM E/D	Long short-term memory encoder decoder
RBF	Radial basis function
K-RBF	RBF neural network assisted by the K-means cluster algorithm
R-LSTM	LSTM of real-time parameter updating
KR-RBF-LSTM	K-RBF and R-LSTM
RMSE	Root-mean-square error
STD	Standard deviation
MAE	Mean absolute error
MAPE	Mean absolute percentage error
R2	Coefficient of determination
TTC	Training time consumption
PWV	Precipitable water vapor
NWP	Numerical weather prediction
ML	Machine learning
ANFIS	Adaptive network-based fuzzy inference system
ANN	Artificial neural network
LSSVM	Least-squares support vector machine
PCA	Principal component analysis
ICA	Independent component analysis
GGOS	Global geodetic observing system
CNN	Convolutional neural network
KNN	K-nearest neighbor
GP	Gaussian processes
ERA5	Fifth-generation European Center for Medium-range Weather Forecast reanalysis
PPP	Precision point positioning
RT-PPP	Real-time precision point positioning
RTK	Real-time kinematic positioning
CORS	Continuously-operating reference station
PPP-RTK	Integer ambiguity resolution-enabled precise point positioning
IGS	International GNSS Service
DOY	Day of the year

References

1. Van Baelen, J.; Aubagnac, J.P.; Dabas, A. Comparison of near-real time estimates of integrated water vapor derived with GPS, radiosondes, and microwave radiometer. *J. Atmos. Ocean. Technol.* **2005**, *22*, 201–210. [CrossRef]
2. Brenot, H.; Neméghaire, J.; Delobbe, L.; Clerbaux, N.; Meutter, P.D.; Deckmyn, A.; Delcloo, A.; Frappez, L.; Roozendael, M.V. Preliminary signs of the initiation of deep convection by GNSS. *Atmos. Chem. Phys.* **2013**, *13*, 5425–5449. [CrossRef]
3. Tunali, E. Water vapor monitoring with IGS RTS and GPT3/VMF3 functions over Turkey. *Adv. Space Res.* **2022**, *69*, 2376–2390. [CrossRef]
4. Troller, M.; Geiger, A.; Brockmann, E.; Bettems, J.M.; Bürkia, B.; Kahle, H.-G. Tomographic determination of the spatial distribution of water vapor using GPS observations. *Adv. Space Res.* **2006**, *37*, 2211–2217. [CrossRef]
5. Zangvil, A.; Portis, D.H.; Lamb, P.J. Investigation of the large-scale atmospheric moisture field over the midwestern United States in relation to summer precipitation. Part II: Recycling of local evapotranspiration and association with soil moisture and crop yields. *J. Clim.* **2004**, *17*, 3283–3301. [CrossRef]
6. Park, H.J.; Shin, D.B.; Yoo, J.M. Atmospheric water balance over oceanic regions as estimated from satellite, merged, and reanalysis data. *J. Geophys. Res.-Atmos.* **2013**, *118*, 3495–3505. [CrossRef]
7. National Research Council. *New Research Opportunities in the Earth Sciences*; National Academy Press: Washington, DC, USA, 2012. Available online: http://www.nap.edu/openbook.php?record_id=13236 (accessed on 31 October 2014).
8. Suni, T.; Guenther, A.; Hansson, H.C.; Kulmala, M.; Andreae, M.O.; Arneth, A.; Artaxo, P.; Blyth, E.; Brus, M.; Ganzeveld, L.; et al. The significance of land-atmosphere interactions in the Earth system—iLEAPS achievements and perspectives. *Anthropocene* **2015**, *12*, 69–84. [CrossRef]
9. Bevis, M.; Businger, S.; Herring, T.A.; Rocken, C.; Anthes, R.A.; Ware, R.H. GPS meteorology: Remote sensing of atmospheric water vapor using the Global Positioning System. *J. Geophys. Res.-Atmos.* **1992**, *97*, 15787–15801. [CrossRef]

10. Guerova, G.; Jones, J.; Douša, J.; Dick, G.; Haan, S.D.; Pottiaux, E.; Bock, O.; Pacione, R.; Elgered, G.; Vedel, H.; et al. Review of the state of the art and future prospects of the ground-based GNSS meteorology in Europe. *Atmos. Meas. Tech.* **2016**, *9*, 5385–5406. [CrossRef]
11. Zhang, K.; Manning, T.; Wu, S.; Rohm, W.; Silcock, D.; Choy, S. Capturing the Signature of Severe Weather Events in Australia Using GPS Measurements. *IEEE J. Sel. Top. Appl. Earth Obs. Remote Sens.* **2015**, *8*, 1839–1847. [CrossRef]
12. Liu, J.; Chang, Z.; Zheng, H. Analysis on the performances of the GNSS tropospheric delay correction models. *E3S Web Conf.* **2022**, *360*, 01043. [CrossRef]
13. Li, W.; Yuan, Y.; Ou, J.; He, Y. IGGtrop_SH and IGGtrop_rH: Two Improved Empirical Tropospheric Delay Models Based on Vertical Reduction Functions. *IEEE Trans. Geosci. Remote Sens.* **2018**, *56*, 5276–5288. [CrossRef]
14. Ghaderpour, E.; Pagiatakis, S.D.; Hassan, Q.K. A Survey on Change Detection and Time Series Analysis with Applications. *Appl. Sci.* **2021**, *11*, 6141. [CrossRef]
15. Ma, Y.; Liu, T.; Xu, G.; Lu, Z. Apparent Short-Period GNSS-ZTD Disturbance Correlated with Precipitation Events. *IEEE Geosci. Remote Sens.* **2022**, *19*, 1006305. [CrossRef]
16. Ghaderpour, E. Least-squares Wavelet and Cross-wavelet Analyses of VLBI Baseline Length and Temperature Time Series: Fortaleza–Hartebeesthoek–Westford–Wettzell. *Publ. Astron. Soc. Pac.* **2021**, *133*, 014502. [CrossRef]
17. Shamshiri, R.; Motagh, M.; Nahavandchi, H.; Haghighi, M.H.; Hoseini, M. Improving tropospheric corrections on large-scale Sentinel-1 interferograms using a machine learning approach for integration with GNSS-derived zenith total delay (ZTD). *Remote Sens. Environ* **2020**, *239*, 111608. [CrossRef]
18. Wilgan, K.; Geiger, A. High-resolution models of tropospheric delays and refractivity based on GNSS and numerical weather prediction data for alpine regions in Switzerland. *J. Geodesy* **2019**, *93*, 819–835. [CrossRef]
19. Chen, J.; Wang, J.; Wang, J.; Tan, W.; Observation, S.A. SHAtrop: Empirical ZTD Model Based on CMONOC GNSS Network. *Geomat. Inf. Sci. Wuhan Univ.* **2019**, *44*, 1588–1595.
20. Zhao, Q.; Su, J.; Xu, C.; Yao, Y.; Zhang, X.; Wu, J. High-precision ZTD model of altitude-related correction. *IEEE J. Sel. Top. Appl. Earth Obs. Remote Sens.* **2023**, *16*, 609–621. [CrossRef]
21. Chkeir, S.; Anesiadou, A.; Mascitelli, A.; Biondi, R. Nowcasting extreme rain and extreme wind speed with machine learning techniques applied to different input datasets. *Atmos. Res.* **2023**, *282*, 106548. [CrossRef]
22. Zhang, H.; Yao, Y.; Hu, M.; Xu, C.; Su, X.; Che, D.; Peng, W. A Tropospheric Zenith Delay Forecasting Model Based on a Long Short-Term Memory Neural Network and Its Impact on Precise Point Positioning. *Remote Sens.* **2022**, *14*, 5921. [CrossRef]
23. Xiao, X.; Lv, W.; Han, Y.; Lu, F.; Liu, J. Prediction of CORS Water Vapor Values Based on the CEEMDAN and ARIMA-LSTM Combination Model. *Atmosphere* **2022**, *13*, 1453. [CrossRef]
24. Xu, T.; Li, S.; Wang, S.; Jiang, N. Improved tropospheric delay model for China using RBF neural network and meteorological data. *Acta Geod. Cartogr. Sin.* **2022**, *51*, 1690–1707.
25. Wang, Y.; Zhang, L.; Yang, J. Study on prediction of zenith tropospheric delay by use of BP neural network. *J. Geod. Geodyn.* **2011**, *31*, 134–137.
26. Xiao, G.; Ou, J.; Liu, G.; Zhang, H. Construction of a regional precise tropospheric delay model based on improved BP neural network. *Chin. J. Geophys.* **2018**, *61*, 3139–3148. (In Chinese)
27. Li, S. *GNSS Tropospheric Delay Modeling and Prediction Based on Machine Learning*; Chang'an University: Xi'an, China, 2021.
28. Shi, Y.; Wu, F.; Zhu, H.; Han, X. Prediction of tropospheric delay based on the LSTM model of Keras platform. *GNSS World China* **2020**, *45*, 115–122.
29. Zhang, Q.; Li, F.; Zhang, S.; Li, W. Modeling and Forecasting the GPS Zenith Troposphere Delay in West Antarctica Based on Different Blind Source Separation Methods and Deep Learning. *Sensors* **2020**, *20*, 2343. [CrossRef] [PubMed]
30. Li, S.; Xu, T.; Xu, Y.; Jiang, N.; Bastos, L. Forecasting GNSS Zenith Troposphere Delay by Improving GPT3 Model with Machine Learning in Antarctica. *Atmosphere* **2022**, *13*, 78. [CrossRef]
31. Zhang, H.; Yao, Y.; Xu, C.; Xu, W.; Shi, J. Transformer-Based Global Zenith Tropospheric Delay Forecasting Model. *Remote Sens.* **2022**, *14*, 3335. [CrossRef]
32. Zheng, Y.; Lu, C.; Wu, Z.; Liao, J.; Zhang, Y.; Wang, Q. Machine learning-based model for real-time GNSS precipitable water vapor sensing. *Geophys. Res. Lett.* **2022**, *49*, e2021GL096408. [CrossRef]
33. Chen, B.; Liu, Z.; Wong, K.; Woo, W.C. Detecting Water Vapor Variability during Heavy Precipitation Events in Hong Kong Using the GPS Tomographic Technique. *J. Atmos. Ocean. Technol.* **2017**, *34*, 1001–1019. [CrossRef]
34. Chen, S.; Cowan, C.F.N.; Grant, P.M. Orthogonal least squares learning algorithm for radial basis function networks. *IEEE Trans. Neural Netw.* **1991**, *2*, 302–309. [CrossRef] [PubMed]
35. Moody, J.; Darken, C. Fast Learning in Networks of Locally-Tuned Processing Units. *Neural Comput.* **1989**, *1*, 281–294. [CrossRef]
36. Aharon, M.; Elad, M.; Bruckstein, A. K-SVD: An Algorithm for Designing Overcomplete Dictionaries for Sparse Representation. *IEEE Trans. Signal Process.* **2006**, *54*, 4310–4323. [CrossRef]
37. Jain, A.K. Data clustering: 50 years beyond K-means. *Pattern Recognit. Lett.* **2010**, *31*, 651–666. [CrossRef]
38. Yu, Y.; Si, X.; Hu, C.; Zhang, J. A Review of Recurrent Neural Networks: LSTM Cells and Network Architectures. *Neural Comput.* **2019**, *31*, 1235–1270. [CrossRef]
39. Li, L.; Kuang, C.; Zhu, J.; Chen, W.; Chen, Y.; Long, S.; Li, H. Rainstorm nowcasting based on GPS real-time precise point positioning technology. *Chin. J. Geophys.* **2012**, *55*, 1129–1136.

40. Wang, S.; Li, B.; Gao, Y.; Gao, Y.; Guo, H. A comprehensive assessment of interpolation methods for regional augmented PPP using reference networks with different scales and terrains. *Measurement* **2020**, *150*, 107067. [CrossRef]
41. Li, S.; Xu, T.; Jiang, N. Tropospheric Delay Modeling Based on Multi-source Data Fusion and Machine Learning Algorithms. In Proceedings of the China Satellite Navigation Conference (CSNC 2021), Nanchang, China, 26–28 May 2021; Lecture Notes in Electrical Engineering. Springer: Berlin/Heidelberg, Germany, 2021; Volume 772, pp. 145–158.
42. Qiao, X.; Chang, W.; Zhou, S.; Lu, X. A prediction model of hard landing based on RBF neural network with K-means clustering algorithm. In Proceedings of the 2016 IEEE International Conference on Industrial Engineering and Engineering Management (IEEM), Bali, Indonesia, 4−7 December 2016; pp. 462–465.

atmosphere

MDPI

Article

Study on Mapping and Identifying Risk Areas for Multiple Particulate Matter Pollution at the Block Scale Based on Local Climate Zones

Wen Wu, Ruihan Liu and Yu Tang *

Liaoning Provincial Key Laboratory of Urban and Architectural Digital Technology, JangHo Architecture College, Northeastern University, Shenyang 110819, China; wuwen@mail.neu.edu.cn (W.W.); 20207860@stu.neu.edu.cn (R.L.)

* Correspondence: tangyu@stumail.neu.edu.cn; Tel.: +86-13941713750

Abstract: As China's urbanization process accelerates, the issue of air pollution becomes increasingly prominent and urgently requires improvement, based on the fact that environmental conditions such as meteorology and topography are difficult to change. Therefore, relevant optimization studies from the perspective of architectural patterns are operable to mitigate pollution. This paper takes the Wenhua Road block in Shenyang, China, as the research object; obtains the concentration data of three kinds of particulate matter through fixed and mobile monitoring; and analyzes the spatial distribution characteristics of Local Climate Zones (LCZ) and particulate matter in the block based on the ArcGIS platform, identifies high-risk areas, and excavates the influence of LCZ on the concentrations of three kinds of particulate matter. The results show that the spatial distribution characteristics of PM_1, $PM_{2.5}$, and PM_{10} under the same pollution level are relatively similar, while the spatial heterogeneity of the distribution of the same particulate matter under different pollution levels is higher. The time-weighted results show that the PM_1 pollution level in the block ranges from 44 to 51 μg/m³, $PM_{2.5}$ ranges from 75 to 86 μg/m³, and PM_{10} ranges from 87 to 99 μg/m³. The pollution hot spots throughout the year are located in the central, eastern and western parts of the study area. In terms of the relationship between the LCZ and particulate matter, with the increase in the particulate matter diameter, the correlation between the three kinds of particulate matter and LCZ are all enhanced. The built-up LCZ always has a larger average concentration of particulate matter than that of the natural LCZ, and building height and building density are the main factors causing the difference. In the optimal design of the risk area, the proportion of natural vegetation or water surface should be increased and the building height should be properly controlled and the building density should be reduced in the renewal of the urban building form. This study will largely improve the spatial refinement of the optimization of urban architectural patterns oriented to mitigate particulate matter pollution.

Keywords: three-dimensional architectural forms; particulate matter; mobile monitoring; LCZ; hot spot analysis

Citation: Wu, W.; Liu, R.; Tang, Y. Study on Mapping and Identifying Risk Areas for Multiple Particulate Matter Pollution at the Block Scale Based on Local Climate Zones. *Atmosphere* **2024**, *15*, 794. https://doi.org/10.3390/atmos15070794

Academic Editors: Chaofan Xian, Yu-Sheng Shen, Cheng Gong and Kei Sato

Received: 28 May 2024
Revised: 25 June 2024
Accepted: 29 June 2024
Published: 30 June 2024

1. Introduction

In recent decades, China's rapid urbanization has changed the urban land use structure and building form characteristics [1], leading to ecological and air quality issues [2]. Among them, the influencing factors of air pollution are intricate and complex [3]. Under the premise that it is difficult to change the objective environmental factors such as topography and meteorology [4], mitigating the effect of particulate matter pollution from the urban design and architectural layout is a practical and feasible solution [5]. Atmospheric particulate matter is one of the main components of haze, and common atmospheric particulate matter is categorized into PM_1, $PM_{2.5}$, and PM_{10}, according to their aerodynamic diameters [6]. These particulate matters of different sizes are harmful to the healthy living

environment for people, and the smaller the diameter of the particulate matter, the more damaging it is to human health [7]. The influence of architectural forms on the dispersion of particulate matter has been confirmed [8]. Most of the existing studies are based on large-scale spatial simulation. Due to the high spatial heterogeneity of particulate matter distribution, it is necessary to carry out a small-scale study to obtain particulate matter pollution data at the block scale based on field monitoring. The introduction of the LCZ classification system can better distinguish the land use types in urban areas and better characterize the spatial features of the layout of architectural forms at the block scale [9,10], which is more closely related to the distribution of atmospheric particulate matter [11]. Therefore, it is necessary to explore the influence of 3D architectural forms on particulate matter dispersion from the LCZ perspective and realize the optimization of LCZ classes and architectural patterns based on particulate matter pollution mitigation. This study provides suggestions for the reduction of particulate matter pollution in urban design and building layout and for the regulation of urban construction and building layout. This has theoretical guiding significance for other urban blocks and even other urban construction and is of great significance for promoting the optimal control of neighborhood pollution exposure under the concept of a healthy city, the sustainable development of neighborhood construction, and the improvement of residents' quality of life and health and well-being.

The coupled research on three-dimensional urban morphology and air pollution needs to consider the issue of scale diversity, and the analytical methods differ for particulate matter pollution studies at different scales. In general, the dispersion of urban particulate pollution occurs in small-scale atmospheric environments but is inevitably affected by large-scale atmospheric motions [12]. On the regional scale, the study of pollutant dispersion mainly adopts the MODIS remote sensing image inversion method, and the data source is mainly from MODIS aerosol products, which covers a wide range and has economic benefits and can realize long-term monitoring, but the spatial resolution of the data is relatively low [13]. On the urban scale, the spatial interpolation methods are often used for simulation. Pollutant concentration data are obtained from urban air quality monitoring stations. This method is simple in principle, easy to operate, and relatively easy to obtain data. However, in underdeveloped cities, the density of its monitoring stations is insufficient, which limits research, and there are fewer factors to consider, which can easily amplify the changes in extreme pollutant concentration values [14]. On the block scale, by obtaining data on pollutant concentration, topography, and pollution emissions, atmospheric numerical simulation methods are often used to simulate pollutant dispersion. The advantages of this method are its simple structure, fast calculation speed, and low requirements for basic data, making it applicable to small- and medium-scale research. However, this small-scale model cannot simulate the composite air pollution process well, and its simulation accuracy needs further consideration [15].

Combining the above research methods, research scales, and data acquisition, the influence of urban morphology on particulate matter dispersion at the current stage mainly focuses on large-scale research, with the model simulation as a main method and the data sources mainly being publicly available data from weather monitoring stations. Lu et al. [16] focused on the Yangtze River Delta (YRD) region in China, acquired a global $PM_{2.5}$ concentration dataset, and analyzed the effects of different land use types and landscape pattern indicators on $PM_{2.5}$ concentrations. At the meso-scale, Leen et al. [17] used $PM_{2.5}$ sensors to collect air quality data in Hanoi, the capital of Vietnam, to assess the spatial distribution of $PM_{2.5}$ at the urban scale and to explore changes in $PM_{2.5}$ concentrations associated with urban morphology at the local climate zone scale. McCarty et al. [18] analyzed county-level data from 48 contiguous states in the contiguous U.S. mainland. By using available air quality monitoring data and remotely sensed land cover data, they explored the correlation between urban forms and air quality, particularly how urban morphology affects air quality in different types of county areas. On the micro scale, Jiang et al. [19] carried out a study of the relationship between urban morphology and air quality (wind speed, CO, and $PM_{2.5}$) in two residential districts in the central area of Beijing. They utilized Computational Fluid

Dynamics (CFD) [20] simulation technology to model the changes in microclimate and pollutant dispersion within the districts under different weather conditions and identified five main urban morphology parameters that affect pollutant dispersion and distribution. In summary, in today's research on particulate matter, the research scale methodology and data acquisition as a whole are seriously affected by the spatial resolution, and the insufficient level of spatial refinement leads to the lack of relevant research results at the block scale. However, field monitoring can solve the above problems, and in recent years, more and more scholars have tended to use mobile monitoring methods to investigate the spatial variations of urban air quality [21,22]. However, field measurements of particle concentrations require significant manpower, resources, and financial investment. As a result, research conducted through field measurements remains few. In view of this research background and its limitations, this study analyzed the correlation between block-scale particulate matter obtained by field measurement and urban morphology, which is of great significance to enrich the high-precision and refined research on block-scale particulate matter pollution prevention and control [23].

Based on the background mentioned above, the correlation between urban morphology and particulate matter has been confirmed in many studies, but the majority of these studies have primarily focused on the urban scale. Due to the high spatial heterogeneity of particulate matter distribution, the results from large-scale studies may not be applicable to small-scale optimization designs. There is a lack of quantitative research at the block scale. In terms of data acquisition, existing studies have mostly investigated the impact of architectural patterns on particulate matter through model simulations. The main reason for the limitation of small-scale studies is that it is difficult to obtain pollution data of high spatiotemporal resolution and high-precision spatial data of environmental factors. Therefore, there is an urgent need for studies that utilize field measurements to obtain particulate matter data at the block scale. In terms of innovation, in the existing studies of the block scale, the introduction of the local climate zones (LCZs) system is not frequent, while the LCZs can visually reflect the architectural differentiation characteristics, so it is necessary to introduce and establish a comprehensive analysis of the LCZs system at the block scale. In conclusion, conducting research on multiple particulate pollution mapping and risk zone identification based on field measurements of pollutants from the LCZ perspective, and elucidating the correlation between LCZ classification and pollutant concentrations, would greatly enhance the spatial refinement of architectural pattern optimization aimed at mitigating particulate pollution.

2. Study Area and Research Methods

2.1. Overview of the Study Area

The study area is located in Shenyang, capital city of Liaoning Province in China (41°11′51″ N–43°02′13″ N, 122°25′09″ E–123°48′24″ E) (Figure 1a), which has a temperate continental climate with an average annual temperature of 8.4 °C and annual precipitation of 510-680 mm. Shenyang serves as an important heavy industrial base with abundant natural resources and a solid industrial foundation [24]. As the largest central city in Northeast China and one of the most significant industrial bases in the country, the air pollution of Shenyang is mainly caused by vehicle exhaust, fossil fuel combustion, industrial production, and urban construction [25]. As the urbanization progresses quickly and the environmental pollution becomes increasingly serious, air pollution—particulate matter pollution, in particular—urgently needs to be addressed [26]. According to the data, through the kernel density estimation, the $PM_{2.5}$ in the Shenyang City area from 2000 to 2013 showed an increasing trend, with the annual average concentration up from 58.50 $\mu g/m^3$ to 72.49 $\mu g/m^3$; even though the $PM_{2.5}$ had been curbed to a certain extent in the area from 2013 to 2022 because of the implementation of policies such as the Air Pollution Prevention and Control Action Plan, the annual average concentration remained high, making the situation unfavorable (Figure 2).

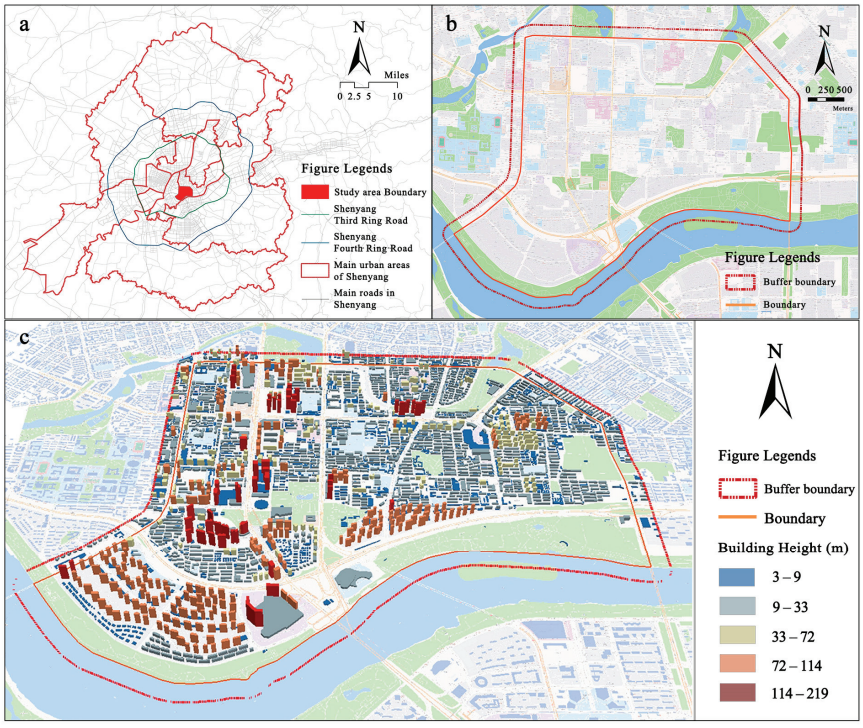

Figure 1. Schematic summary of the study area: (**a**) Location map of Shenyang City. (**b**) Wenhua Road block map. (**c**) Block three-dimensional architectural forms diagram.

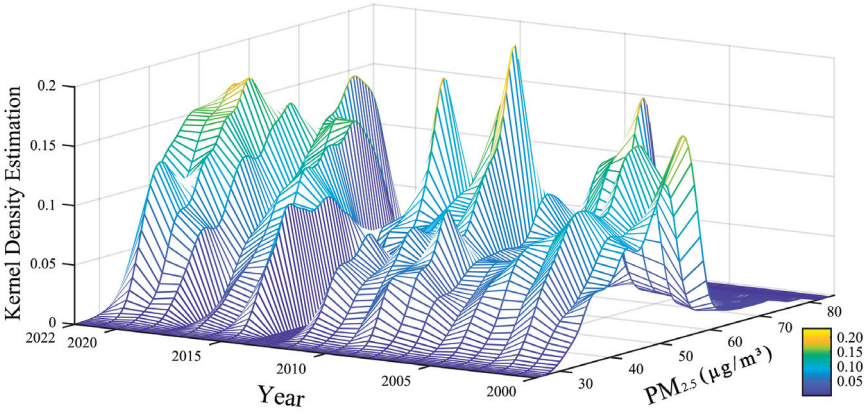

Figure 2. Change of $PM_{2.5}$ concentration in Shenyang City from 2000 to 2022.

The Wenhua Road block in Shenyang has serious particulate matter pollution, and its air pollution index has been continuously high over the years. The land use types of the block are diverse, which are mainly residential land and commercial land, with green space, rivers, and land for education. In addition, the mix of high-, medium-, and low-rise staggered buildings shows its rich three-dimensional architectural form. Boundary 1 of the block (Figure 1b) is delimited by the city's main roads, covering an area of 11.12 square kilometers. Considering the impact of the buildings on the periphery of Boundary 1 on the particulate matter in the block, existing studies have indicated that an architectural or urban

design project can strongly influence air quality within its 200-m radius [27]. Therefore, a 200-m buffer zone was created based on Boundary 1, which serves as the research boundary in this study, with 13.33 square kilometers of total area (as shown in Figure 1c).

2.2. Data Sources and Preprocessing

In this study, air pollution data from 11 air quality monitoring stations in Shenyang during 2000–2022 were used, including 6 kinds of conventional monitoring pollutants concentration data, such as fine particulate matter ($PM_{2.5}$), inhalable particulate matter (PM_{10}), ozone (O_3), nitrogen dioxide (NO_2), sulfur dioxide (SO_2), and carbon monoxide (CO). Rates are the daily mean values. Air pollution data were provided by the China National Environmental Monitoring Center (https://www.cnemc.cn, accessed on 1 March 2022), the U.S. Consulate General in Shenyang AQI (https://aqicn.org, accessed on 1 March 2022), and the Department of Ecological and Environment of Liaoning Province (https://sthj.ln.gov.cn, accessed on 1 March 2022). The land use data were obtained from the Land Use and Land-Cover Change (LUCC) dataset of Shenyang City in 2018 provided by the Resource and Environmental Science Data Platform (https://www.resdc.cn/, accessed on 1 May 2022). These data have a resolution of 30 m, which contains six main categories and eighteen subcategories.

The building vector data of Shenyang City in 2018 is sourced from the Baidu map (https://map.baidu.com/, accessed on 1 May 2022). The footprint data of buildings are represented in a polygonal vector, including the base outline and floors information. The building height is assumed to be 3 meters multiplied by the number of building floors. This data is verified by reference to Google Maps, supplemented by Baidu Maps panoramic imagery, and augmented by on-site and online research to add missing building footprints. In this case, the drawing of acquired building outlines and building floors is also refined so that more complete and accurate building information data in the study area is finally formed, with a total of 3171 individual buildings acquired.

2.3. Field Measurement

2.3.1. Monitoring Route Design

The data of the street-level particulate matter concentration are obtained by using fixed and mobile monitoring in the field. The monitoring activities were carried out for 7 days, including three typical particulate pollution situations in this area, to ensure the representativeness of the monitoring data. The specific monitoring steps are as follows:

(1) Instrument setting: The detection instrument is a Sniffer4D Lingxiu V2 atmospheric monitoring system (made by Kefei Technology Co., LTD., Shenzhen, China, purchased from the network official platform), which can record the concentration of PM_1, $PM_{2.5}$, and PM_{10} particles with a time resolution of 1 s.

(2) Layout of the monitoring points: Determine the layout of the monitoring points by combining field investigation and remote sensing. Considering the uniformity and representativeness of the distribution, 37 mobile monitoring stations are set up, which cover all LCZ types and are mainly located in the middle of intersections and roads for easy measurement.

(3) Make the mobile monitoring route: The mobile monitoring is carried out at time intervals. These routes are connected in a series with all the monitoring points. Considering the monitoring length and staffing, four monitoring routes are designed (Figure 3) to ensure that the monitoring data of the particulate matter concentration in different LCZ can be obtained in the same time period.

(4) Field measurement: The monitoring activity is from October 2022 to March 2023, and the times with good weather conditions are selected for actual measurement. The monitoring height is 1.5 m, and the time resolution is 1 s. The method of multi-cycle continuous repeated measurement is adopted, in which every 1.5 h is designated as a cycle, and the monitoring time is 8:00–11:00 in the morning and 14:00–17:00 in the afternoon, with four cycles measured every day. The specific implementation process

is as follows: after the instrument is turned on, let it stand for 5 min to start measuring activities. Fix the monitoring instrument at the front of the electric vehicle, drive on the route during the monitoring period, stay at each monitoring point for 1 min, and repeat the measurement in multiple periods after completing a closed route.

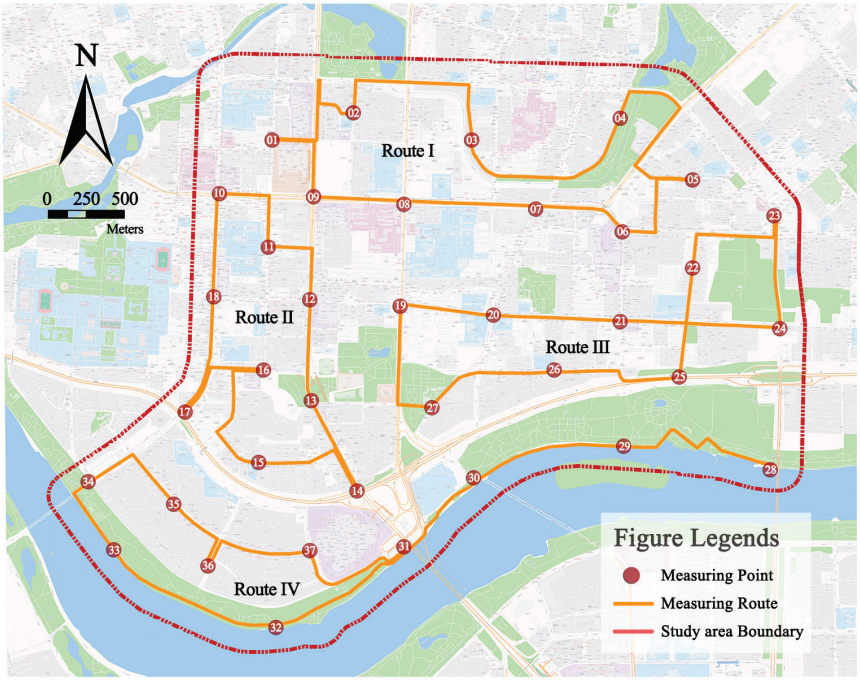

Figure 3. Design of the mobile monitoring route.

2.3.2. Quality Assurance and Quality Control of Particulate Matter Data

Before the monitoring activity begins, all instruments are placed in the same stable environment for three days for relative calibration. After the monitoring activities, all instruments were placed in the same stable environment for 3 days and absolutely calibrated with the public data of the Wenhua Road Meteorological Monitoring Station in the study area, and the obtained particulate matter concentration was fitted and corrected according to the calibration data. The collected data are visualized through a GIS platform, and the monitoring data within five minutes of startup are eliminated. At the same time, the abnormal high value and abnormal low value of each monitoring route in different time periods are eliminated, and the missing values are interpolated and replaced to ensure the integrity of the data. Overall, given these operations, the data in this study can be considered reliable and valid.

2.4. Research Methods

2.4.1. LCZ Construction in the Block

To map the LCZ for the Wenhua Road block, the study processed the acquired 30-m resolution land use data and building vector data of Shenyang City, referring to the LCZ mapping method based on ArcGIS [28] and combining the current status and research requirements of the study area. First, the collected data were integrated into the GIS platform for spatial extraction of the study area data. Second, considering the strongest correlation between the LCZ and PM pollution data at the 200-m grid scale revealed in the subsequent experimental calculations, the research scale was determined to be in a

200-m grid. At this scale, building indicators for the street block were calculated, including average building height and building density. Then, the land use data were categorized into construction land, green space, and water bodies and coupled with the building indicators for LCZ classification. Finally, the block LCZ was classified into six built-up environment types and two natural environment types.

2.4.2. Kriging Interpolation

This method was initially employed by Krige for locating gold resources, then was theorized and systematized by Matheron and was named the Kriging interpolation [29]. It needs to meet the second stationary assumption: (1) the average mean of random variables exists and is independent of the distance, and (2) when the distance between any two points is "h", the variance of the regional change increment exists and is independent of the coordinates [30]. Through the Kriging interpolation method, the relatively limited monitoring data in this study can be utilized to estimate the PM concentration at unmonitored points in the study area, thereby obtaining continuous spatial distribution maps of the three types of particulate matter concentrations.

2.4.3. Hot Spot Analysis

The Getis-Ord Gi* hot spot analysis model is a spatial analysis tool that detects and analyzes autocorrelation in a local space to identify regions characterized by significant high- or low-value clustering [31]. The model accurately determines where clustering of high- or low-value elements occurs in space by calculating the high-/low-clustering statistics for each data point in the region and determining whether the point belongs to the same class as its neighboring points [32]. The Getis-Ord Gi * statistic is calculated as follows using Equations (1)–(3) [33]:

$$G^* = \frac{\sum_{j=1}^{n} \omega_{ij} x_j - \overline{X} \sum_{j=1}^{n} \omega_{ij}}{S \sqrt{\frac{\left[n \sum_{j=1}^{n} \omega_{ij}^2 - \left(\sum_{j=1}^{n} \omega_{ij} \right)^2 \right]}{n-1}}} \tag{1}$$

$$\overline{X} = \frac{\sum_{j=1}^{n} x_j}{n} \tag{2}$$

$$S = \sqrt{\frac{\sum_{j=1}^{n} x_j}{n} - \overline{X}^2} \tag{3}$$

Among them, S is the standard deviation of the PM concentration in the block, and the G^* statistic obtained for each element in the dataset is the Z score. Higher G_i^* values indicate a tighter clustering of hot spots, while lower G_i^* values indicate a tighter clustering of cold spots.

2.4.4. Grid Spatial Data Integration

This study utilizes ArcGIS's Create Fishing Grid function to create a fishing grid matching the study area and integrates three-dimensional building morphology indicators and spatially interpolated particulate matter concentration distribution into the spatial grid through multiple grid units. This allows for the acquisition of the average building indicator values and interpolated particulate matter concentration values at different pollution levels within each grid unit, thus realizing grid-based spatial connectivity and facilitating subsequent spatial analysis tasks. Through iterative experimentation and the comparison of different grid scales concerning the correlation between building indicators and particulate matter concentration, it is found that the spatial correlation is highest at a 200-m grid scale. Hence, the optimal grid scale is established as 200 m × 200 m.

2.4.5. Correlation Analysis

The strength of a monotonic relationship between two variables can be determined using a nonparametric statistic called Spearman's correlation analysis, or Spearman's rho [34]. It does not require data to obey a normal distribution; in contrast, it is applied to data on a fixed-order scale—that is, the rank or order information of the categorical variables. It first transforms the data into ranks and then computes the Pearson's correlation coefficient between the ranks, as shown in Equation (4) below:

$$r_s = \frac{1 - \frac{6\sum d_i^2}{n(n^2-1)}}{n-1} \quad (4)$$

Among those, r_s is the Spearman's rank correlation coefficient, d_i is the difference in the rank order of the corresponding observations of the two variables, and n is the total number of observations.

2.5. Overall Research Approach

First, the block LCZs are described based on ArcGIS, and the spatial distribution characteristics of various types of LCZs are analyzed; second, in order to analyze the heterogeneity of the spatial distribution characteristics of the three kinds of particulate matter under different pollution levels, these data obtained from field monitoring are summarized and classified, and spatially continuous particulate matter pollution maps are drawn based on the Kriging interpolation. Then, annual particulate matter pollution exposure maps of the block are developed based on time weighting, and pollution risk zones of the block are identified through hot spot analysis. Finally, to analyze the correlation between LCZs and the three kinds of particulate matter concentrations, Spearman's rank correlation coefficient is used, and to analyze the results of the differences in the concentrations of particulate matter in the various types of LCZs and the reasons for the differences, the mean values of the three kinds of particulate matter concentrations of different LCZ classes are counted based on the correlation relationship.

3. Results and Discussion

3.1. Description and Analysis of Block LCZ

From the LCZ classification of the Wenhua Road block (Figure 4), it can be seen that the road block as a whole has a rich variety of architectural forms, including LCZ1–LCZ3 with a compact layout and LCZ4–LCZ6 with an open type, and there are also LCZP green areas and LCZG water areas with a natural environment type. The distribution of specific types of LCZs is characterized as follows: In terms of the built environment type, road block LCZ1 is mainly distributed on both sides of Qingnian Street and the commercial area on both sides of Wenhua Road; LCZ2 is mainly distributed on both sides of Wenhua Road, typically represented by dense mid-rise residential buildings; LCZ3 is mainly distributed on the north side of the Hunhe River, which consists of low-rise compact villas; LCZ4 is mainly distributed on both sides of Qingnian Street, which is a high-rise open residential area; LCZ5 is mainly distributed in the residential area on the north side of Nanta Street, which is an open mid-rise residential area; and LCZ6 is a relatively small distribution of open low-rise areas. As for the natural environment type, LCZG waters are represented by the Hunhe River, which appear as a zonal distribution on the south side of the study area; LCZP green spaces include Wulihe Park, Popular Science Park, and Nanta Park on the north side of the Hunhe River.

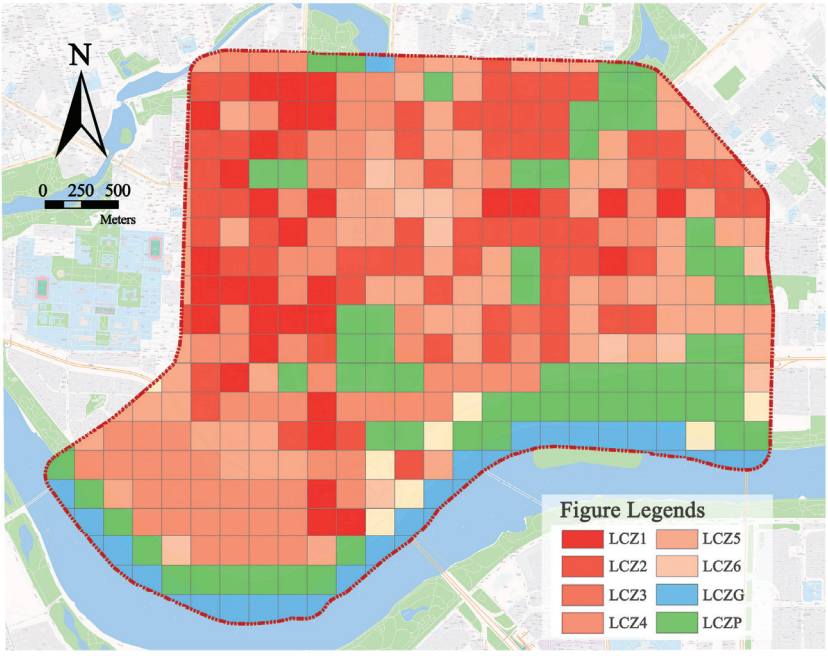

Figure 4. LCZ classification map of the Wenhua Road block.

3.2. Characterization of the Spatial Distribution of Particulate Matter Concentrations in the Block

3.2.1. Visualization of Measured Particulate Matter Concentrations in the Block

The particulate matter data obtained from field measurements were preprocessed, and all data within five minutes since startup and outliers were excluded, resulting in a total of more than 650,000 valid data for the three types of particulate matter concentrations obtained in this study. The effective data obtained were processed, and the four-cycle data of each route were superimposed on average to obtain the average daily concentration of three pollutants on the four routes, which was used as the daily average concentration of particulate matter. Combined with the air pollution data of Shenyang over the years, the China Ambient Air Quality Standard (GB3095-2012), and World Health Organization Air Quality Standard, the measured data are divided into pollution levels according to research needs:

PM_1, 0 μg/m³ < PM_1 pollution level 1 ≤ 20 μg/m³ < pollution level 2 ≤ 50 μg/m³ < pollution level 3;

$PM_{2.5}$, 0 μg/m³ < $PM_{2.5}$ pollution level 1 ≤ 50 μg/m³ < pollution level 2≤100 μg/m³ < pollution level 3;

PM_{10}, 0 μg/m³ < PM_{10} pollution level 1 ≤ 50 μg/m³ < pollution level 2 ≤ 100 μg/m³ < pollution level 3.

The data were combined according to pollution levels, in which the visualization of the measured data of the typical particle matter $PM_{2.5}$ concentration under three pollution levels is shown in Figure 5.

At the same time, we verified the accuracy of the measured data. By summarizing the hourly average data disclosed by the national monitoring stations, our research also counted the hourly average of the four monitoring routes under the seven-day measurement period. After fitting, it was found that the accuracy was 0.866 (Figure 6), and the fitting effect was good. The field measurement data studied were consistent with the trend of the national public data, and the measurement data had strong confidence. It could represent the concentration level of particulate matter in the study area.

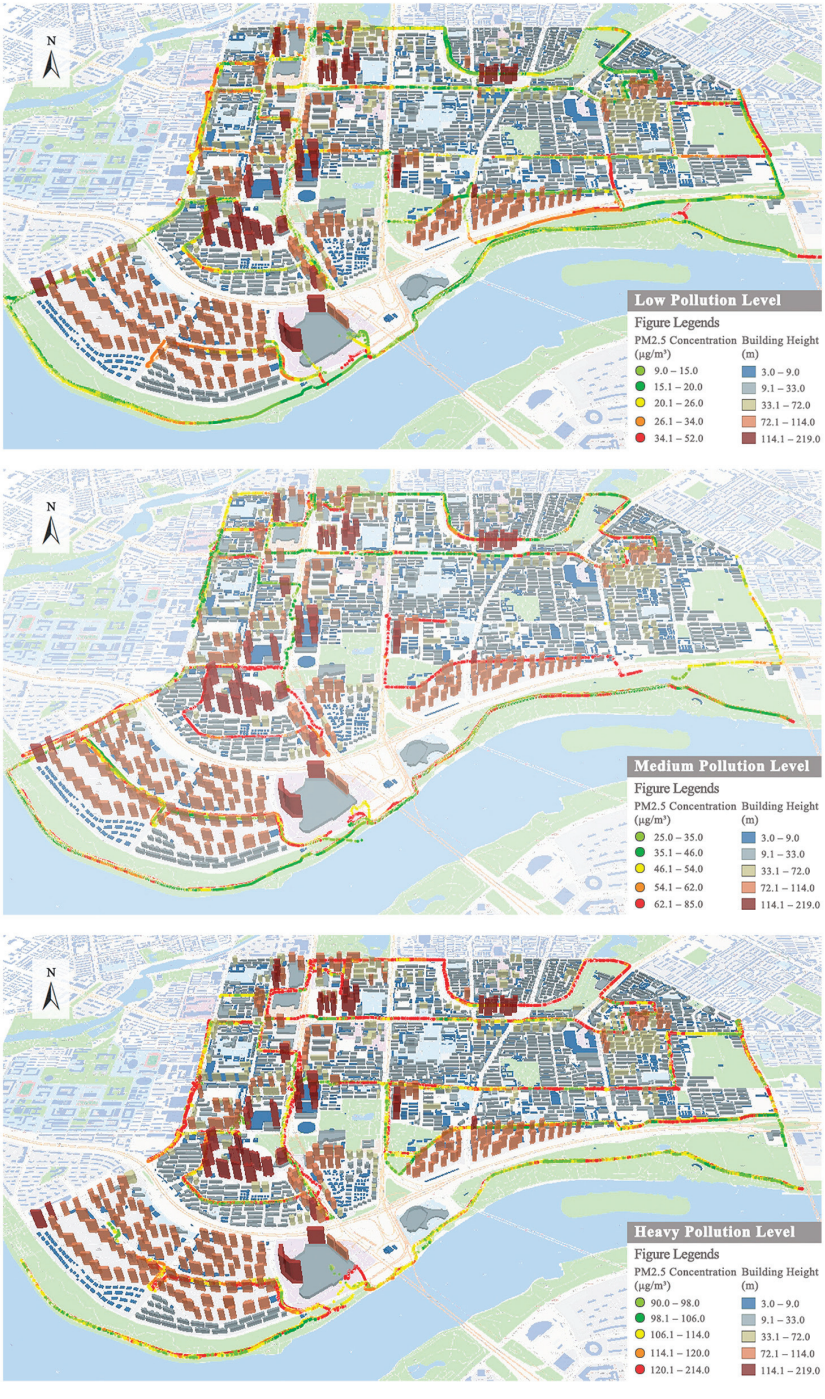

Figure 5. Visualization of $PM_{2.5}$ concentration data measurement in the blocks.

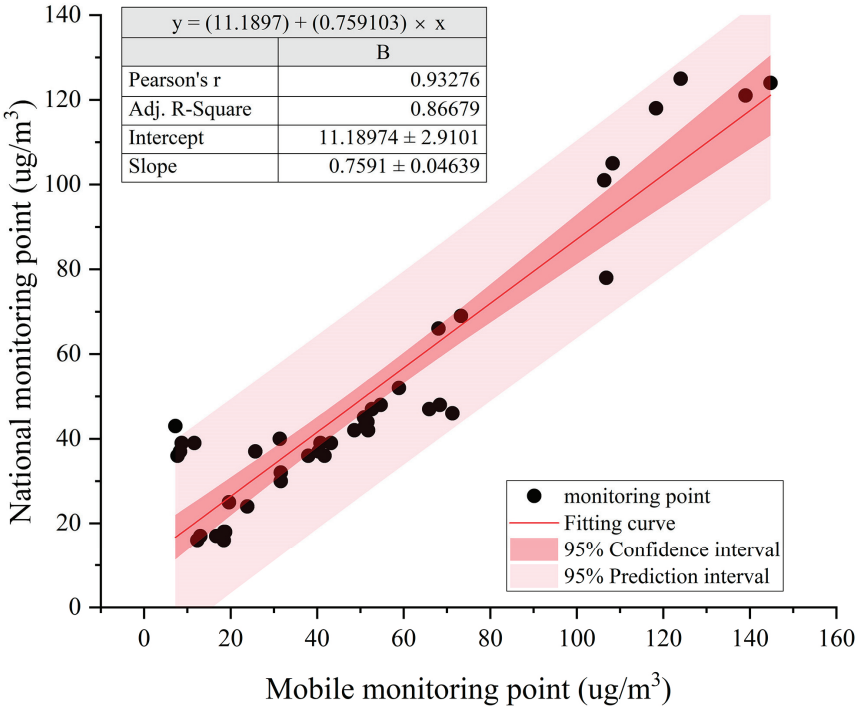

Figure 6. Verification of the measurement data accuracy.

The trend of the field measurement data in the study is consistent with that of the national public site data., and in view of the fact that the reliability of the national monitoring site data has been fully demonstrated in previous research work [35,36], and has been widely used in related studies [37,38], we believe that the mobile measurement data in this study verified with the officially released particulate matter detection data have sufficient confidence to represent the concentration level of particulate matter in the study area.

3.2.2. Spatial Interpolation Results of Particulate Matter in the Block

Due to the limited number of measuring points in the field, the acquired point data of three kinds of particulate matter concentrations were spatially interpolated, which generated spatially continuous distribution maps of average particulate matter mass concentrations under different pollution levels (Figure 7). The results showed that the spatial distribution characteristics of the three particulate matter concentrations under the same pollution level were relatively similar, while the spatial heterogeneity of the same particulate matter distribution under different pollution levels was high, but there were also local spatial similarities.

At pollution level 1 (Figure 7a), the concentration of PM_1 was in the range of 11–18 μg/m³, concentration of $PM_{2.5}$ was in the range of 17–28 μg/m³, and the concentration of PM_{10} was in the range of 21–33 μg/m³. The concentration values were enhanced with the increase in the diameter of particles, and the overall spatial distribution characteristics among the three particles were relatively similar, but the spatial distribution heterogeneity within each particle was high. The high pollution indices of the three pollutants are distributed on the west side of Qingnian Street and the east side of Shenshui District, Xinghuiyunjin District of the Yuexiu Group, and Yijingyuan District on the bank of South Canal, presumably related to the surrounding high-rise buildings shading, and the lower spatial openness leads to local deposition phenomenon. The low pollution index is distributed in the Mixc, Shenyang Pharmaceutical University, Popular Science Park, and

Nanta Park, places with better spatial openness, and the parks here are equipped with more greenery, smoothing the transmission of particulate matter.

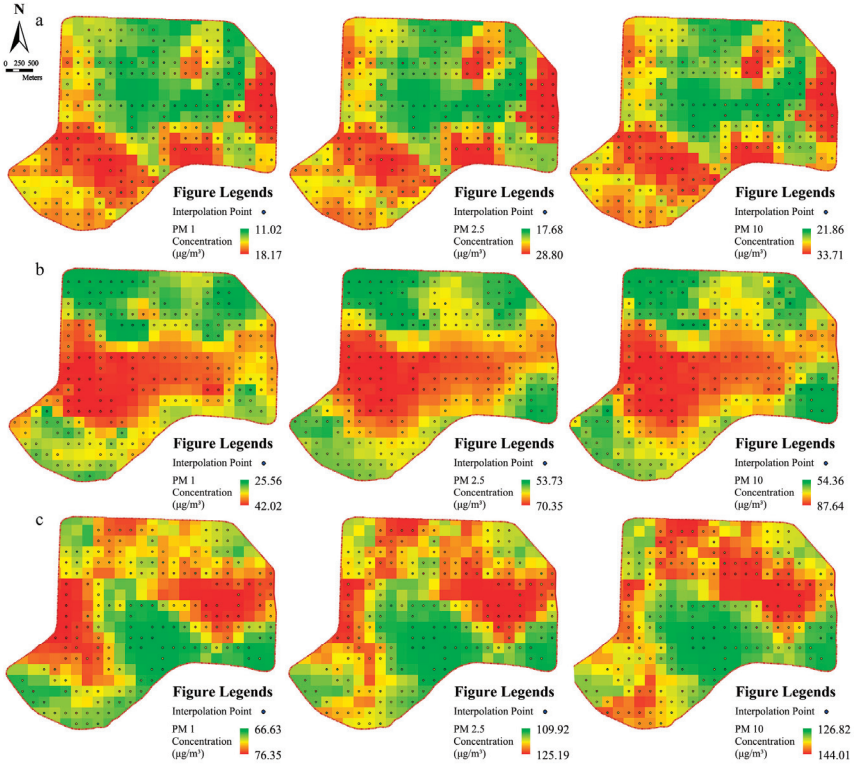

Figure 7. Spatial interpolation concentration distribution of three kinds of particulate matter at different pollution levels: (**a**) pollution level 1; (**b**) pollution level 2; (**c**) pollution level 3.

At pollution level 2 (Figure 7b), the concentration of PM_1 was in the range of 25–42 μg/m³, the concentration of $PM_{2.5}$ was in the range of 53–70 μg/m³, and the concentration of PM_{10} was in the range of 54–87 μg/m³. The high pollution indices of the three pollutants are located in the central areas of the block, including the Shenyang Conservatory of Music, Shimao Wulihe River Road block, Popular Science Park, and Nanta Road block. The central areas of the block as a whole show a high pollution phenomenon, mainly due to the influence of the Wulihe River Park of Hunhe River in the south and Qingnian Park and South Canal in the north, coupled with the dense construction in the central areas of the block, which makes it difficult for pollutants from the north and the south to be transported outward. The area with a low pollution index is distributed in the southern part of the study area, Wulihe River Park, the business district of the Mixc north of the study area, and the South Canal block; these two blocks are affected by the adsorption of pollutants from the park's greenery, and coupled with high spatial openness, the pollutants diffuse relatively quickly; thus, the pollution here is relatively low.

Under pollution level 3 (Figure 7c), the concentration of PM_1 is in the range of 66–76 μg/m³, the concentration of $PM_{2.5}$ is in the range of 109–125 μg/m³, and the concentration of PM_{10} is in the range of 126–144 μg/m³. The high pollution index area is located in the Shenyang Conservatory of Music, Shimao Wulihe block, the interchange of Wanliutang Road and Culture Road, Shenshui District, and the South Canal block. The main reason for this difference is the layout of the building. On the one hand, these areas are built environmental LCZs, often showing higher pollution than natural environmental

LCZs. On the other hand, a high building height or high building density in the region are the causes of high pollution, because a high building height and building density hinder the diffusion of particulate matter, making the local building layout not conducive to the diffusion and transmission of particulate matter. The low pollution index area is mainly distributed in the building complexes facing the Hun River and the vicinity of Popular Science Park, mainly due to the reduction and adsorption of particles by the green space and the relatively weak shading of the buildings, which makes the transmission of particles unaffected by the shading.

3.2.3. Identification of Particulate Matter Risk Areas Based on Time Weighting

Due to the high spatial heterogeneity of particulate matter distribution under different pollution levels, this study attempts to construct a time-weighted annual particulate matter pollution distribution map based on the proportion of different pollution levels throughout the year. By statistically categorizing the meteorological data of Shenyang, capital city of Liaoning Province, in 2022, it was found that pollution level 1 accounted for one-tenth of the year, pollution level 2 accounted for five-tenths of the year, and pollution level 3 accounted for four-tenths of the year. According to such a time-weighted ratio, the three kinds of particulate matter pollution data values were weighted and summarized in terms of time share, and the spatial distribution map of particulate matter in the study area for the whole year was obtained by the Kriging interpolation method. Then, the hot spot analysis method based on the GIS platform was used to identify the cold and hot spots analysis map of particulate matter in the study area for the whole year.

The results showed (Figure 8a) that the time-weighted pollution level of PM_1 in blocks was in the range of 44–51 $\mu g/m^3$, $PM_{2.5}$ was in the range of 75–86 $\mu g/m^3$, and PM_{10} was in the range of 87–99 $\mu g/m^3$, which all belonged to pollution level 2. The distribution of the year-round high-pollution areas for the three particulate matters is relatively similar, and they are all located in the middle of the block, from Culture Road in the north to Shenshui Road in the south. Low-pollution areas are located in the south and north of the block, including Wuli River Park along the Hunhe River, the Mixc near Qingnian Park, South Canal close to Wanliutang Park, and other places that are particulate matter low index areas, and the overall air quality is relatively good.

As can be seen from the three particulate matter cold and hot spots analysis map (Figure 8b), the overall cold and hot spots spatial distribution of the three particulate matters is relatively similar, and the spatial distribution of the high-risk and low-risk zones of particulate matter with different diameters is consistent, which is also consistent with the similarity of the spatial interpolation results. The hot and cold spots of the three kinds of particulate matter are all in a piecewise distribution, which is related to the spatial transmission distribution mode of the particulate matter. Specifically, the hot spots of particulate matter throughout the year are mainly distributed in two major areas: namely, the Dongbei Riza Market and the Shimao Wulihe area; the cold spots are mainly distributed in the Mixc near Qingnian Park, the South Canal, the Shengjing Grand Theater, and the Wulihe Ice and Snow Paradise area. From the difference between the hot and cold spots, it can be seen that the hot spot areas are urban construction land, and the buildings there are compact and dense with a large flow of people, while the cold spot areas are urban parks and the surrounding blocks.

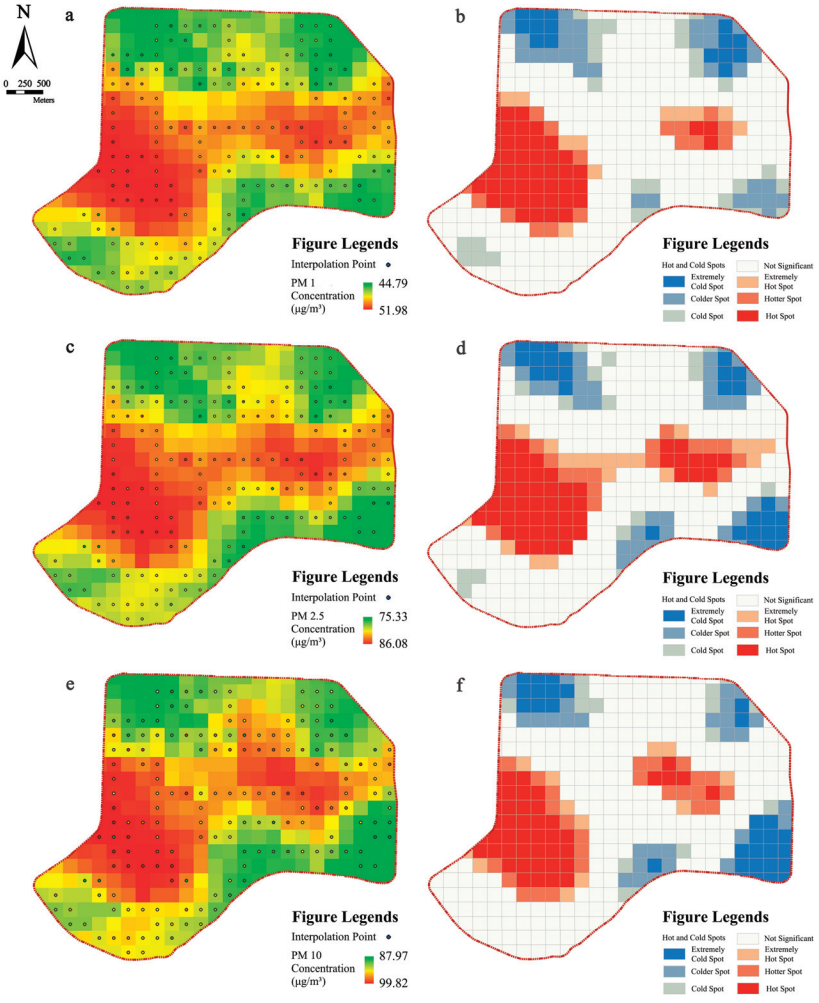

Figure 8. Particulate matter risk area identification map: (**a**,**c**,**e**) annual spatial interpolation results diagram of particulate matter; (**b**,**d**,**f**) particulate matter cold and hot spots analysis map.

3.3. Effect of LCZ on Particulate Dispersion

3.3.1. Correlation between LCZ and Particulate Matter

First, based on the data collection of the spatial grid and Spearman's correlation analysis, the LCZ calculation results and the particulate matter concentration calculation results were coupled on the block grid to calculate the correlation between the LCZ and the concentration of particulate matter of the three diameters. Then, the particulate matter concentrations of different LCZs were counted to excavate the differences in particulate matter concentrations caused by LCZ classification. From Table 1, it can be seen that there is a significant correlation between all three kinds of particulate matter concentrations and LCZs ($p < 0.01$), and this correlation is enhanced with the increase in particulate matter diameters, but the overall difference is not significant. This difference in correlation caused by the particle diameter is mainly due to the fact that large-diameter particles are more responsive to changes in the LCZ, thus showing a greater correlation between the LCZ and large-diameter particles. On the other hand, PM_1, a small-diameter particle, is less sensitive to changes in the LCZ than PM_{10} because of its smaller diameter compared to PM_{10}; thus, it

is affected to a weaker extent, and the overall correlation is lower than that between $PM_{2.5}$ and PM_{10}.

Table 1. Correlation analysis between the LCZ and particulate matter concentration in neighborhoods.

Variables of Analysis	LCZ	
	Spearman's Correlation Analysis	**Sig. (Two-Tailed)**
PM_1	−0.207 **	0.000
$PM_{2.5}$	−0.246 **	0.000
PM_{10}	−0.265 **	0.000

Note: ** is a significant correlation at the 0.01 level (two-tailed).

3.3.2. Correlation between LCZ and Particulate Matter

Based on the correlation between the LCZ and three kinds of particulate matter, the study statistic was the average value of particulate matter concentration under different LCZ land use classifications (Figure 9). The results show that, among the characteristic differences in particulate matter concentrations between LCZ classes, the built-up class always had a larger value of average particulate matter concentration than the natural class environment.

Further, the built environment class LCZs were divided into height-control and density-control groups. In the density-control group, first, the elevation of building heights under the dense building layout had a contributing effect on the concentration of particulate matter for different diameters. In the case of controlling the constant building density, there was LCZ1 > LCZ2 > LCZ3 in building height, and the corresponding particulate matter concentrations showed similar characteristics, which was because the obstruction effect of low-rise buildings on particulate matter transmission was weaker than the obstruction effect of high-rise buildings, and the higher spatial openness under the layout of low-rise buildings was favorable for particulate matter transmission and diffusion. Secondly, the effect of building height increase on particulate matters of different diameters under an open building layout was slightly different from that under a dense building layout. Similarly, in the case of controlling the building density unchanged, the building height was LCZ4 > LCZ5 > LCZ6, but the average particulate concentration showed the result of LCZ5 > LCZ4 > LCZ6, and the particulate concentration at LCZ4 produced a difference and showed a tendency to decrease, which might be due to the fact that the open high-rise building layout made the local wind speed accelerate, and the formation of local ventilation corridors was favorable for the diffusion and transmission of particulates, which, in turn, reduced their concentration. This may be due to the fact that the layout of open high-rise buildings accelerates the local wind speed and forms local ventilation corridors, which is favorable for the diffusion and transmission of particulate matter and thus reduces its concentration.

In the height control group, first, the increase in building density under the high-rise building layout has a contributing effect on the concentration of particulate matter of different diameters. In the case of controlling the constant building height, there is LCZ1 > LCZ4 on the building density, and its corresponding particulate matter concentration shows the same characteristics. Secondly, the building density under the middle- and low-rise building layouts of elevation showed a promoting effect on the concentration of particulate matter of different diameters, but none of these differential effects were significant. Under the condition of controlling the constant building height, there is LCZ2 > LCZ5 and LCZ3 > LCZ6 for the building density, the effect of density on particulate matter is weaker under the same conditions of mid-rise and low-rise building heights, and the difference in particulate matter concentrations under different densities at the same height is not significant.

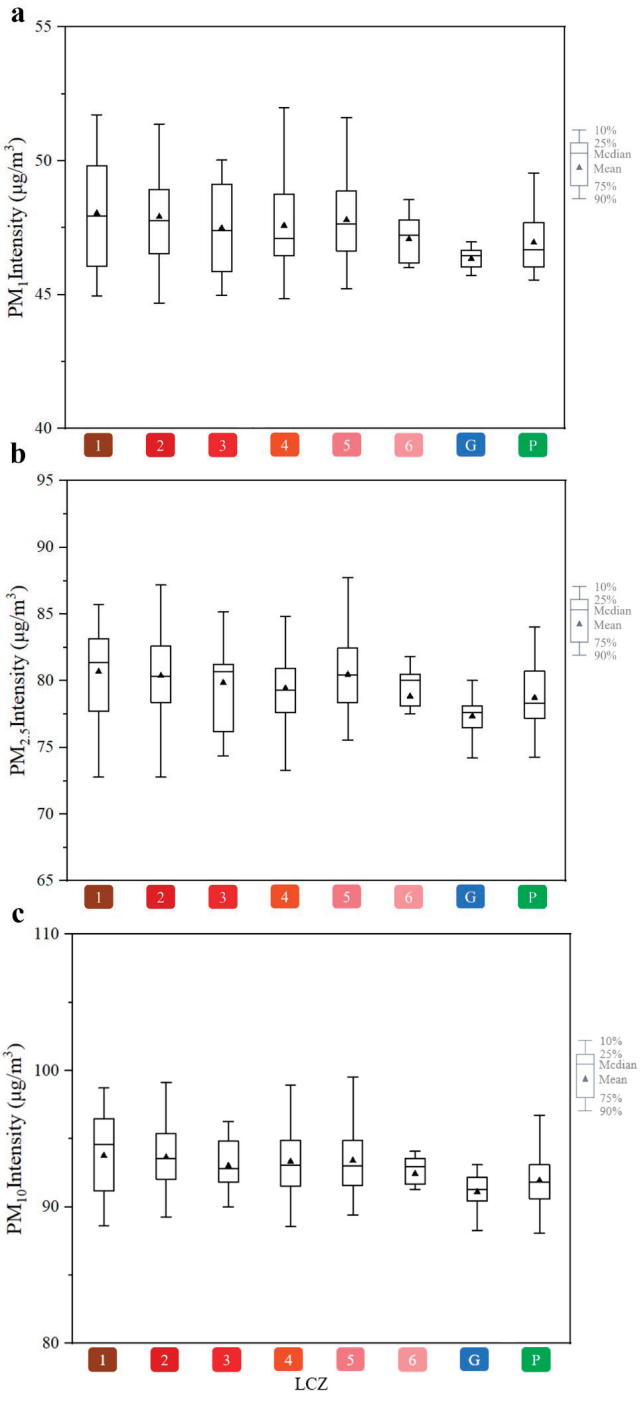

Figure 9. Statistical map particulate matter concentration under different LCZ land use classifications: (**a**) Statistical maps of PM_1 concentrations under different LCZ land use classifications; (**b**) Statistical Map of $PM_{2.5}$ Concentration under Different LCZ Land Use Classification; (**c**) Statistical maps of PM_{10} concentrations under different LCZ land use classifications.

4. Discussions

4.1. $PM_{2.5}$ Difference in LCZ Configuration

In the existing research on "urban form particulate matter", landscape indicators (such as PLAND, the NDVI, and the SEI) are usually used to express different landscape patterns [39,40], and the influence of different landscape configurations on the distribution of urban particulate matter is analyzed. However, landscape classification is often on a coarse-grained scale, and various architectural areas are regarded as a landscape type, often ignoring the change in architectural configuration [41]. The LCZ scheme includes the classification of architecture and landscape, and its research related to particulate matter has just arisen in recent years [42]. This study also supplemented relatively few pieces of literature, a further in-depth research scale, the block scale of three kinds of particles and LCZ scheme, and a comprehensive and intuitive discussion of the LCZ scheme on the impact of building configuration on particulate matter.

Referring to previous related studies, Gao et al. [43] assessed the changes in $PM_{2.5}$ concentrations in two representative communities in Shanghai by mobile measurements and found that $PM_{2.5}$ varied drastically at the community level and that this difference was mainly caused by the spatial pattern of $PM_{2.5}$ background levels and traffic volume. Li et al. [44] found that the Central and Causeway Bay areas in Hong Kong are pollution hot spots. Due to the street canyon effect, traffic intensity and mixing, and ambient meteorological conditions, these areas have high $PM_{2.5}$ concentrations. Ke et al. [45] conducted field measurements using fixed and mobile monitoring stations in the Xia Sha Economic and Technological Development Zone in Hangzhou, capital city of Zhejiang Province, and found that the spatial variability of the distribution of $PM_{2.5}$ was closely related to land use types, architectural layout, and building heights. Liu et al. [46] used mobile monitoring methods to collect $PM_{2.5}$ concentration data in Wuhan, capital city of Hubei Province, and found that the urban morphology factor was an important cause of high $PM_{2.5}$ concentrations. Combined with the results of established studies, it was found that there was little difference in the ambient meteorological conditions under the general background and industrial pollution emissions at the block level and that, controlling for such variables, the functional differences in the land use and the spatial differences in the way buildings are laid out between this study area, and other similar studies are the main reasons for the spatial heterogeneity of particulate matter in the study area, and thus, it is necessary to dig deeper into the effects of the block based on the LCZs of particulate matter pollution.

Among the differences in particulate matter concentrations caused by the LCZ configuration, it is found that a built environment always has a larger average particulate matter concentration than a natural environment. This is because natural species and built species represent emission sources and absorption/desorption sinks of pollutants, respectively, to a certain extent. In natural LCZs, trees and green spaces can absorb a large amount of air pollutants, thus reducing the concentration of particulate matter, which is consistent with previous research results [47,48]. At the same time, water can absorb particulate matter through evaporation [49,50] and reduce the local particulate matter deposition. In contrast, built-up LCZs often have high-rise, high-density buildings, which have the greatest impact on particulate matter concentrations by affecting the rate of particulate matter transport and diffusion, such as shading by buildings [51]. Similar laws have been found in the literature, for example, the $PM_{2.5}$ concentration is negatively correlated with the forest area ratio and positively correlated with the built-up area ratio [52,53].

In built-up LCZs, the building height and building density are the important factors causing the difference in particulate matter concentrations. Under the condition of controlling the building density being unchanged, it can be seen that the effect of building height on particulate matter concentrations is complex and may be influenced by a variety of factors, including pollutant emissions from ground-level sources, air flow and diffusion conditions, and the design of the building and the surrounding environment [54]. When the building height is controlled unchanged, the increase in the building density

can promote the particulate matter under the layout of high-rise buildings. It is because the low-density building layout facilitates the transport of particulate matter, while the high-density building layout brings about the deposition of localized pollutants, which is in line with the results of the study by Yang et al. This influence is weak under the layout of middle-level and low-rise buildings. This may be due to the fact that the buildings as a whole are low and have little hindering effect on the diffusion of particulate matter, so there is little overall change in the concentrations of the three kinds of particulate matter. Therefore, the building density is related to the density of the building and building size, which can affect the local accumulation of pollutants [55].

4.2. Suggestions for the Optimization of Risk Areas

LCZ interclass optimization strategy: A built environmental LCZ is the most typical feature of a high particulate matter concentration in the block risk area, which is significantly different from the low particulate matter concentration caused by a natural environment in the cold spot area. Therefore, in the optimization of risk areas, increasing the proportion of natural vegetation or water surface and reducing the impermeable surface as much as possible are feasible optimization means [56,57]. The construction area of green space in risk areas can be increased by an appropriate amount, and specific measures can be taken, including building miniature pocket parks, increasing roof greening and vertical greening, etc. [58]. To improve the green area of risk areas, optimize the air quality by using the adsorption effect of green plants on particulate matter, improve the high pollution exposure of risk areas, and promote the construction of healthy blocks in healthy cities. At the same time, small water landscapes can also be introduced in risk areas [59]. Make full use of the advantages of geographical resources adjacent to the Hunhe River in the block and through the connection of the groundwater system. Increase the water coverage area in risk areas, give full play to the evaporation of water bodies [60], and dilute or take away particulate matter with water vapor. Reducing the high-concentration pollution of particulate matter is of great significance for building a comfortable and livable block with fresh air.

However, the introduction and expansion of natural LCZ in risk areas cannot cover a large area, which may not be a sustainable optimization scheme. Facing the background of rapid urbanization, building a built-up LCZ configuration that is conducive to the diffusion of particulate pollution is the key point that should be considered in architectural design and urban planning layout [61]. Therefore, the LCZ build-up optimization strategy: According to the research results, a dense building layout and higher building height will lead to the increase in the particulate matter concentration. Therefore, the optimization of the risk area can start from two aspects: improving the building height and building layout density. Analyzing the characteristics of the building layout in risk areas, it is mainly the high concentration of particulate matter caused by the combination of high and dense, so, in the optimization design, we should consider reducing this high and dense building layout, which is not easy to diffuse pollutants, and adding a more low and scattered building layout design, so as to promote air circulation and diffusion and the transmission of particulate matter. By extension, in the urban construction, because it is impossible to arrange low and scattered buildings on a large scale in China's urban construction [62], the relationship between building height, building density, and $PM_{2.5}$ needs to be expanded, and the determination of a key height threshold will help urban and landscape planning achieve a cost-effective state in terms of air pollution [63].

4.3. Limitations

On the whole, the research has carried out a certain depth in spatial-scale and particulate matter species richness, but there are still the following shortcomings: First, the time period of field measurement is still short, so it is considered to increase the amount of field measurement work in the follow-up research to improve the data representativeness. Secondly, the influence of the LCZ on particulate matter has not been quantified, and the threshold of the building height and building density on particulate matter is still

unclear. In the follow-up study, we can consider building a relational model to quantify this influence relationship. The research has guiding significance for improving air pollution exposure and promoting the sustainable development of urban blocks.

5. Conclusions

This study conducted the mobile monitoring of three types of particulate pollutants at the block scale. By classifying building LCZ types, particulate pollution maps were generated. Subsequently, hot spot analysis was employed to identify particulate matter risk hot spots and cold spots within the neighborhoods, elucidating the correlation between pollutant distribution and the LCZ. The conclusion is as follows: Regarding the spatial distribution characteristics of the three types of particulate matter, under the same pollution level, the spatial distribution characteristics of the concentrations of the three types of particulate matter are relatively similar, while, under different pollution levels, there is higher spatial heterogeneity in the distribution of the same type of particulate matter. The time-weighted results show that the PM_1 pollution level in the block ranges from 44 to 51 $\mu g/m^3$, $PM_{2.5}$ ranges from 75 to 86 $\mu g/m^3$, and PM_{10} ranges from 87 to 99 $\mu g/m^3$. All three types of particulate matter pollution fall within pollution level 2. Regarding particulate matter risk areas, the spatial distribution of hot spots and cold spots for particles of different diameters is consistent. Throughout the year, particulate matter hot spots are mainly distributed in two areas: Dongbei Riza Market and the Shimao Wulihe area. There is a certain correlation between LCZs and the dispersion of particulate matter pollution. Built-up LCZs tend to have higher particulate matter concentrations than natural LCZs, while the building height and density are the key factors contributing to higher concentrations of particulate matter of different diameters in built-up LCZs. It is necessary to further investigate their specific mechanisms in subsequent research.

Author Contributions: Conceptualization, W.W. and Y.T.; methodology, Y.T.; software, Y.T.; formal analysis, Y.T.; investigation, R.L. and Y.T.; resources, W.W.; data curation, Y.T.; writing—original draft preparation, R.L. and Y.T.; writing—review and editing, W.W.; supervision, W.W. All authors have read and agreed to the published version of the manuscript.

Funding: This research was funded by the National Natural Science Foundation of China (No. 32101325), the Liaoning Provincial Natural Science Foundation of China (No. 2023-MS-084), and the Fundamental Research Funds for the Central Universities (No. N2211001).

Institutional Review Board Statement: Not applicable.

Informed Consent Statement: Not applicable.

Data Availability Statement: The data presented in this study are available on request from the corresponding author. The data are not publicly available due to privacy.

Conflicts of Interest: The authors declare no conflicts of interest.

References

1. Wu, D. Hazy weather research in China in the last decade: A review. *Acta Sci. Circumstantiae* **2012**, *32*, 257–269. [CrossRef]
2. Song, J.; Li, C.L.; Liu, M.; Hu, Y.M.; Wu, W. Spatiotemporal Distribution Patterns and Exposure Risks of $PM_{2.5}$ Pollution in China. *Remote Sens.* **2022**, *14*, 3173. [CrossRef]
3. Hrdličková, Z.; Michálek, J.; Kolář, M.; Veselý, V. Identification of factors affecting air pollution by dust aerosol PM_{10} in Brno City, Czech Republic. *Atmos. Environ.* **2008**, *42*, 8661–8673. [CrossRef]
4. Liu, H.M.; Fang, C.L.; Zhang, X.L.; Wang, Z.Y.; Bao, C.; Li, F.Z. The effect of natural and anthropogenic factors on haze pollution in Chinese cities: A spatial econometrics approach. *J. Cleaner Prod.* **2017**, *165*, 323–333. [CrossRef]
5. Fan, C.J.; Tian, L.; Li, J.W. Research Progress of lmpacts of Urban Form on Air Quality. *Urban Dev. Stud.* **2017**, *24*, 92–100. [CrossRef]
6. Gomišček, B.; Hauck, H.; Stopper, S.; Preining, O. Spatial and temporal variations of PM_1, $PM_{2.5}$, PM_{10} and particle number concentration during the AUPHEP—Project. *Atmos. Environ.* **2004**, *38*, 3917–3934. [CrossRef]
7. Wu, W.; Wang, Y.Q.; Liu, M.; Li, C.L. A Review on the Use of Landscape Indices to Study the Effects of Three-Dimensional Urban Landscape Patterns on Haze Pollution in China. *Pol. J. Environ. Stud.* **2021**, *30*, 2957–2967. [CrossRef]

8. Clark, P.L.; Millet, B.D.; Marshall, D.J. Air Quality and Urban Form in U.S. Urban Areas: Evidence from Regulatory Monitors. *Environ. Sci. Technol.* **2011**, *45*, 7028–7035. [CrossRef]
9. Abougendia, M.S. Investigating surface UHI using local climate zones (LCZs), the case study of Cairo's River Islands. *Alexandria Eng. J.* **2023**, *77*, 293–307. [CrossRef]
10. Lyu, T.; Buccolieri, R.; Gao, Z. A Numerical Study on the Correlation between Sky View Factor and Summer Microclimate of Local Climate Zones. *Atmosphere* **2019**, *10*, 438. [CrossRef]
11. Jiang, R.Y.; Xie, C.K.; Man, Z.H.; Afshari, A.; Che, S.Q. LCZ method is more effective than traditional LUCC method in interpreting the relationship between urban landscape and atmospheric particles. *Sci. Total Environ.* **2023**, *869*, 161677. [CrossRef] [PubMed]
12. Cui, G.X.; Zhang, Z.S.; Xu, C.X.; Huang, W.X. Research advances in large eddy simulation of urban atmospheric environment. *Adv. Mech.* **2013**, *43*, 295–328. [CrossRef]
13. Gong, J.; Hu, Y.; Liu, M.; Bu, R.; Chang, Y.; Bilal, M.; Li, C.; Wu, W.; Ren, B. Land use regression models using satellite aerosol optical depth observations and 3d building data from the central cities of Liaoning province, China. *Pol. J. Environ. Stud.* **2016**, *25*, 1015–1026. [CrossRef] [PubMed]
14. Gaines Wilson, J.; Zawar-Reza, P. Intraurban-scale dispersion modelling of particulate matter concentrations: Applications for exposure estimates in cohort studies. *Atmos. Environ.* **2006**, *40*, 1053–1063. [CrossRef]
15. Kim, C.H.; Meng, F.; Kajino, M.; Lim, J.; Tang, W.; Lee, J.J.; Kiriyama, Y.; Woo, J.H.; Sato, K.; Kitada, T.; et al. Comparative Numerical Study of $PM_{2.5}$ in Exit-and-Entrance Areas Associated with Transboundary Transport over China, Japan, and Korea. *Atmosphere* **2021**, *12*, 469. [CrossRef]
16. Lu, D.B.; Mao, W.L.; Yang, D.Y.; Zhao, J.N.; Xu, J.H. Effects of land use and landscape pattern on $PM_{2.5}$ in Yangtze River Delta, China. *Atmos. Pollut. Res.* **2018**, *9*, 705–713. [CrossRef]
17. Leen, B.; Vu, G.N.; Kim, C.V.; Han, H.D.; Ben, S.; Bruno, V. Assessment of the impact of local climate zones on fine dust concentrations: A case study from Hanoi, Vietnam. *Build. Sci.* **2023**, *242*, 110430. [CrossRef]
18. McCarty, J.; Kaza, N. Urban form and air quality in the United States. *Landsc. Urban Plan.* **2015**, *139*, 168–179. [CrossRef]
19. Jiang, Z.W.; Cheng, H.M.; Zhang, P.H.; Kang, T.F. Influence of urban morphological parameters on the distribution and diffusion of air pollutants: A case study in China. *J. Environ. Sci.* **2021**, *105*, 163–172. [CrossRef]
20. Zhu, G.; Chen, Y.; Wu, W.; Liu, R.H.; Tang, Y.; Li, P.C.; Xu, A.W. Coupling relationships between urban block spatial morphology and microclimate in severe cold regions. *iScience* **2023**, *26*, 108313. [CrossRef]
21. Shiva, N.S.; Pavan, R.Y.; Narayana, M.; Seema, K.; Pooja, R. Mobile monitoring of air pollution using low cost sensors to visualize spatio-temporal variation of pollutants at urban hotspots. *Sustain. Cities Soc.* **2019**, *44*, 520–535. [CrossRef]
22. Cummings, E.R.; Stewart, D.J.; Kremer, P.; Shakya, M.K. Predicting citywide distribution of air pollution using mobile monitoring and three-dimensional urban structure. *Sustain. Cities Soc.* **2022**, *76*, 103510. [CrossRef]
23. Messier, P.K.; Chambliss, E.S.; Gani, S.; Alvarez, R.; Brauer, M.; Choi, J.J.; Hamburg, P.S.; Kerckhoffs, J.; LaFranchi, B.; Lunden, M.M.; et al. Mapping Air Pollution with Google Street View Cars: Efficient Approaches with Mobile Monitoring and Land Use Regression. *Environ. Sci. Technol.* **2018**, *52*, 12563–12572. [CrossRef] [PubMed]
24. Li, P.C.; Chen, J.D.; Li, Y.X.; Wu, W. Using the InVEST-PLUS Model to Predict and Analyze the Pattern of Ecosystem Carbon storage in Liaoning Province, China. *Remote Sens.* **2023**, *15*, 4050. [CrossRef]
25. Li, C.L.; Xu, Y.Y.; Liu, M.; Hu, Y.M.; Huang, N.; Wu, W. Modeling the Impact of Urban Three-Dimensional Expansion on Atmospheric Environmental Conditions in an Old Industrial District: A Case Study in Shenyang, China. *Pol. J. Environ. Stud.* **2020**, *29*, 3171–3181. [CrossRef] [PubMed]
26. Li, K.M.; Li, C.L.; Liu, M.; Hu, Y.M.; Wang, H.; Wu, W. Multiscale analysis of the effects of urban green infrastructure landscape patterns on $PM_{2.5}$ concentrations in an area of rapid urbanization. *J. Cleaner Prod.* **2021**, *325*, 129324. [CrossRef]
27. Shi, Y.; Xie, X.L.; Fung, C.J.; Ng, E. Identifying critical building morphological design factors of street-level air pollution dispersion in high-density built environment using mobile monitoring. *Build. Sci.* **2018**, *128*, 248–259. [CrossRef]
28. Zhang, R.; Yang, J.; Ma, X.Y.; Xiao, X.M.; Xia, J.H. Optimal allocation of local climate zones based on heat vulnerability perspective. *Sustain. Cities Soc.* **2023**, *99*, 104981. [CrossRef]
29. Cressie, A.N. The origins of kriging. *Math. Geol.* **1990**, *22*, 239–252. [CrossRef]
30. Sampson, D.P.; Richards, M.; Szpiro, A.A.; Bergen, S.; Sheppard, L.; Larson, V.T.; Kaufman, D.J. A Regionalized National Universal Kriging Model Using Partial Least Squares Regression for Estimating Annual $PM_{2.5}$ Concentrations in Epidemiology. *Atmos. Environ.* **2013**, *75*, 383–392. [CrossRef]
31. Ord, J.K.; Getis, A. Local Spatial Autocorrelation Statistics: Distributional Issues and an Application. *Geogr. Anal.* **1995**, *27*, 286–306. [CrossRef]
32. Zhang, H.R.; Tripathi, N.K. Geospatial hot spot analysis of lung cancer patients correlated to fine particulate matter ($PM_{2.5}$) and industrial wind in Eastern Thailand. *J. Cleaner Prod.* **2018**, *170*, 407–424. [CrossRef]
33. Tadesse, S.; Enqueselassie, F.; Hagos, S. Spatial and Space-Time Clustering of Tuberculosis in Gurage Zone, Southern Ethiopia. *PLoS ONE* **2018**, *13*, 0198353. [CrossRef]
34. Md, F.K.; Yuichiro, S.; Koichiro, H.; Shigeki, M. Characterization of $PM_{2.5}$, $PM_{2.5–10}$ and $PM_{>10}$ in ambient air, Yokohama, Japan. *Atmos. Res.* **2010**, *96*, 159–172. [CrossRef]

35. Xie, Y.Y.; Zhao, B.; Zhang, L.; Luo, R. Spatiotemporal variations of $PM_{2.5}$ and PM_{10} concentrations between 31 Chinese cities and their relationships with SO_2, NO_2, CO and O_3. *Particuology* **2015**, *20*, 141–149. [CrossRef]
36. Kuerban, M.; Waili, Y.; Fan, F.; Liu, Y.; Qin, W.; Dore, J.A.; Peng, J.J.; Xu, W.; Zhang, F.S. Spatio-temporal patterns of air pollution in China from 2015 to 2018 and implications for health risks. *Environ Pollut.* **2020**, *258*, 113659. [CrossRef] [PubMed]
37. Zhang, A.Q.; Xia, C.; Li, W.F. Exploring the effects of 3D urban form on urban air quality: Evidence from fifteen megacities in China. *Sustain. Cities Soc.* **2022**, *78*, 103649. [CrossRef]
38. Luo, H.Y.; Tang, X.; Wu, H.J.; Kong, L.; Wu, Q.; Cao, Q.; Song, Y.T.; Luo, X.C.; Wang, Y.; Zhu, J.; et al. The Impact of the Numbers of Monitoring Stations on the National and Regional Air Quality Assessment in China During 2013–18. *Adv. Atmos. Sci.* **2022**, *39*, 1709–1720. [CrossRef] [PubMed]
39. Southworth, J.; Nagendra, H.; Tucker, M.C. Fragmentation of a landscape: Incorporating landscape metrics into satellite analyses of land-cover change. *Landscape. Res.* **2002**, *27*, 253–269. [CrossRef]
40. Kong, F.H.; Yin, H.W.; Nakagoshi, N. Using GIS and landscape metrics in the hedonic price modeling of the amenity value of urban green space: A case study in Jinan City, China. *Landsc Urban Plan.* **2007**, *79*, 240–252. [CrossRef]
41. Shi, Y.; Ren, C.; Lau, K.K.L.; Ng, E. Investigating the influence of urban land use and landscape pattern on $PM_{2.5}$ spatial variation using mobile monitoring and WUDAPT. *Landsc Urban Plan.* **2019**, *189*, 15–26. [CrossRef]
42. Yang, H.O.; Leng, Q.M.; Xiao, Y.F.; Chen, W.B. Investigating the impact of urban landscape composition and configuration on $PM_{2.5}$ concentration under the LCZ scheme: A case study in Nanchang, China. *Sustain. Cities Soc.* **2022**, *84*, 104006. [CrossRef]
43. Gao, Y.; Wang, Z.Y.; Liu, C.; Peng, Z.R. Assessing neighborhood air pollution exposure and its relationship with the urban form. *Build. Sci.* **2019**, *155*, 15–24. [CrossRef]
44. Li, Z.Y.; Fung, C.H.J.; Lau, K.H.A. High spatiotemporal characterization of on-road $PM_{2.5}$ concentrations in high-density urban areas using mobile monitoring. *Build. Sci.* **2018**, *143*, 196–205. [CrossRef]
45. Ke, B.; Hu, W.H.; Huang, D.M.; Zhang, J.; Lin, X.T.; Li, C.H.; Jin, X.J.; Chen, J. Three-dimensional building morphology impacts on $PM_{2.5}$ distribution in urban landscape settings in Zhejiang, China. *Sci. Total Environ.* **2022**, *826*, 154094. [CrossRef]
46. Liu, M.Y.; Chen, H.; Wei, D.; Wu, Y.N.; Li, C. Nonlinear relationship between urban form and street-level $PM_{2.5}$ and CO based on mobile measurements and gradient boosting decision tree models. *Build. Sci.* **2021**, *205*, 108265. [CrossRef]
47. Maleki, M.; Asadi, M.; Naghadehi, S.Z.; Khosravi, A.; Wang, J.Y.; Stewart, D.I.; Shakeryari, M. Detecting local climate zone change and its effects on PM_{10} distribution using fuzzy machine learning in Tehran, Iran. *Urban Clim.* **2023**, *49*, 101506. [CrossRef]
48. Deng, X.D.; Gao, F.; Liao, S.Y.; Li, S.Y. Unraveling the association between the built environment and air pollution from a geospatial perspective. *J. Cleaner Prod.* **2023**, *386*, 135768. [CrossRef]
49. Verma, V.; Fang, T.; Xu, L.; Peltier, E.R.; Russell, G.A.; Ng, L.N.; Weber, R. Organic aerosols associated with the generation of reactive oxygen species (ROS) by water-soluble $PM_{2.5}$. *Environ. Sci. Technol.* **2015**, *49*, 4646–4656. [CrossRef] [PubMed]
50. Liang, D.; Ma, C.; Wang, Y.Q.; Wang, Y.J.; Chen-Xi, Z. Quantifying $PM_{2.5}$ capture capability of greening trees based on leaf factors analyzing. *Environ. Sci. Pollut.* **2016**, *23*, 21176–21186. [CrossRef]
51. Yuan, M.; Song, Y.; Huang, Y.P.; Shen, H.F.; Li, T.W. Exploring the association between the built environment and remotely sensed $PM_{2.5}$ concentrations in urban areas. *J. Cleaner Prod.* **2019**, *220*, 1014–1023. [CrossRef]
52. Wu, J.S.; Li, J.; Peng, J.C.; Peng, J.; Li, W.F.; Xu, G.; Dong, C.C. Applying land use regression model to estimate spatial variation of $PM_{2.5}$ in Beijing, China. *Environ. Sci. Pollut.* **2015**, *9*, 7045–7061. [CrossRef] [PubMed]
53. Feng, H.H.; Zou, B.; Tang, Y.M. Scale-and region-dependence in landscape-$PM_{2.5}$ correlation: Implications for urban planning. *Remote Sens.* **2017**, *9*, 918. [CrossRef]
54. Azimi, P.; Zhao, H.R.; Fazli, T.; Zhao, D.; Faramarzi, A.; Leung, L.; Stephens, B. Pilot study of the vertical variations in outdoor pollutant concentrations and environmental conditions along the height of a tall building. *Build. Sci.* **2018**, *138*, 124–134. [CrossRef]
55. Huang, C.Y.; Hu, T.T.; Duan, Y.S.; Li, Q.Y.; Chen, N.; Wang, Q.; Zhou, M.G.; Rao, P.H. Effect of urban morphology on air pollution distribution in high-density urban blocks based on mobile monitoring and machine learning. *Build. Sci.* **2022**, *219*, 109173. [CrossRef]
56. Miao, C.P.; Yu, S.; Hu, Y.M.; Liu, M.; Yao, J.; Zhang, Y.; He, X.Y.; Chen, W. Seasonal effects of street trees on particulate matter concentration in an urban street canyon. *Sustain. Cities Soc.* **2021**, *73*, 103095. [CrossRef]
57. Bi, S.B.; Dai, F.; Chen, M.; Xu, S. A new framework for analysis of the morphological spatial patterns of urban green space to reduce $PM_{2.5}$ pollution: A case study in Wuhan, China. *Sustain. Cities Soc.* **2022**, *82*, 103900. [CrossRef]
58. Su, T.H.; Lin, C.S.; Lu, S.Y.; Lin, J.C.; Wang, H.H.; Liu, C.P. Effect of air quality improvement by urban parks on mitigating $PM_{2.5}$ and its associated heavy metals: A mobile-monitoring field study. *J. Environ. Man.* **2022**, *323*, 116283. [CrossRef] [PubMed]
59. Yang, S.; Wu, H.T.; Chen, J.; Lin, X.T.; Lu, T. Optimization of $PM_{2.5}$ Estimation Using Landscape Pattern Information and Land Use Regression Model in Zhejiang, China. *Atmosphere* **2018**, *9*, 47. [CrossRef]
60. Jones, A.B.; Fleck, J. Shrinking lakes, air pollution, and human health: Evidence from California's Salton Sea. *Sci. Total Environ.* **2020**, *712*, 136490. [CrossRef] [PubMed]
61. Cai, M.; Ren, C.; Xu, Y.; Dai, W.; Wang, X.M. Local Climate Zone Study for Sustainable Megacities Development by Using Improved WUDAPT Methodology—A Case Study in Guangzhou. *Procedia Environ. Sci.* **2016**, *36*, 82–89. [CrossRef]

62. Cao, Q.; Luan, Q.Z.; Liu, Y.P.; Wang, R.Q. The effects of 2D and 3D building morphology on urban environments: A multi-scale analysis in the Beijing metropolitan region. *Build Environ.* **2021**, *192*, 107635. [CrossRef]
63. Peng, J.; Chen, S.; Lü, H.L.; Liu, Y.X.; Wu, J.S. Spatiotemporal patterns of remotely sensed $PM_{2.5}$ concentration in China from 1999 to 2011. *Remote Sens. Environ.* **2016**, *174*, 109–121. [CrossRef]

atmosphere

MDPI

Article

Driving Forces on the Distribution of Urban Ecosystem's Non-Point Pollution Reduction Service

Chengji Shu [1,2], Kaiwei Du [3], Baolong Han [1,*], Zhiwen Chen [1,4], Haoqi Wang [1,5] and Zhiyun Ouyang [1]

[1] State Key Laboratory of Urban and Regional Ecology, Research Center for Eco-Environmental Sciences, Chinese Academy of Sciences, Beijing 100085, China; cjshu_st@rcees.ac.cn (C.S.); 15675809122@stu.hunau.edu.cn (Z.C.); swuwhq123@email.swu.edu.cn (H.W.); zyouyang@rcees.ac.cn (Z.O.)
[2] University of Chinese Academy of Sciences, Bejing 100049, China
[3] Department of Landscape Architecture and Horticulture, College of Architecture and Design, Chongqing College of Humanities, Science & Technology, Chongqing 401524, China; dkwyhy@126.com
[4] Laboratory of Ecosystem Services and Spatial Planning, College of Landscape Architecture and Art Design, Hunan Agricultural University, Changsha 410128, China
[5] Department of Landscape Architecture, College of Horticulture and Gardens, Southwest University, Chongqing 400100, China
* Correspondence: blhan@rcees.ac.cn

Abstract: In the context of increasing urbanization and worsening environmental pollution, nonpoint source pollution during high-frequency rainfall has become a major ecological problem that endangers residents in cities. This study takes Shenzhen as an example. On the basis of a large number of soil sample test data, and combined with relevant environmental variables, it has drawn the high-resolution, high-precision spatial distribution maps of soil attributes within the city. In addition, this paper combines the revised universal soil loss equation and the GeoDetector model to evaluate the supply capacity of nonpoint source reduction services in the city's ecological space and the main driving factors of spatial distribution characteristics for different types of land. The study found that increasing soil point density and combining environmental variables can help improve the accuracy of spatial mapping for soil attributes. The ME, MSE, ASE, RMSE, and RMSSE of spatial mapping all meet the accuracy evaluation criteria and are better than many existing studies; the spatial distribution characteristics of soil attributes and nonpoint source reduction services show significant differences among the whole city, secondary administrative regions, and different types of land; the GeoDetector results show that among the three main types of land use (forested land, industrial land, and street town residential land), topographic factors, habitat-quality factors, and ecosystem types have the greatest impact on the spatial differentiation characteristics of nonpoint source reduction services. Among climate factors, only precipitation factors have the greatest impact on the spatial differentiation characteristics of services. Facing the above factors, the *q*-values calculated by the GeoDetector are all higher than 10%. The results of this study can provide information for making better decisions on regional ecological system management and soil protection and on restoration work aimed at improving nonpoint source reduction services.

Keywords: Shenzhen; soil particle diameter; organic matter; soil contamination; GeoDetector; driving factor

Citation: Shu, C.; Du, K.; Han, B.; Chen, Z.; Wang, H.; Ouyang, Z. Driving Forces on the Distribution of Urban Ecosystem's Non-Point Pollution Reduction Service. *Atmosphere* **2023**, *14*, 873. https://doi.org/10.3390/atmos14050873

Academic Editor: Xuejun Liu

Received: 27 March 2023
Revised: 6 May 2023
Accepted: 10 May 2023
Published: 16 May 2023

1. Introduction

Since the Industrial Revolution, the global population has entered a period of rapid growth [1]. The United Nations predicts that by 2050, the global urban population will reach 68% of the world's total population [2]. Technological development has accelerated the expansion of cities around the world to accommodate housing and production needs. However, highly intensive land-use patterns have achieved economies of scale while severely altering local soil texture characteristics [3–6]. This has led to the destruction

of the soil environment and given rise to a series of ecological and environmental problems. For example, soil degradation can accelerate the degradation of local ecosystems and increase the risk of dust storm formation [7,8]. Some scholars have found through research that soil degradation can cause a reduction in the capacity of local ecosystem services and an increased risk of soil erosion [9]. In addition, while rapid technological development in agriculture has ensured global food security, the widespread application of chemical fertilizers and pesticides has also made the global soil environment increasingly polluted [10,11]. The excessive use of nutrients, such as nitrogen and phosphorus, has breached the soil environment's metabolic threshold, posing constant threats to human lives. For example, studies have found that nutrient enrichment in mangrove soils can accelerate CO_2 emissions, leading to an increase in global warming trends [12]. JunKang Guo et al. [13] have found by reviewing a large number of existing studies that using excessive fertilizer damages the integrity of soil characteristics.

Ecosystem services can effectively guarantee human ecological security and reduce environmental risks. Ecosystem services refer to all the benefits that humans obtain from ecosystems, including material supply services (such as providing food and water), regulation services (such as flood regulation, carbon fixation, water conservation, etc.), cultural services (such as landscape value enhancement, tourism, health care, etc.), and supporting services (such as biodiversity maintenance) [14–19]. Many studies have confirmed that ecosystem services can guarantee the ecological security of cities. Denis Maragno [20] and A. Rizzo [21] respectively took Dolo and Gorla Maggiore in Italy as case areas, and studied the positive effects of urban ecological space's flood reduction service on overall urban ecological security; in addition, Chae Yeon Park [22] also found that a reasonable urban green space planning scheme can play a more effective cooling role, so that residents can avoid the torment of extremely high temperatures. Among all ecosystem services, the reduction of nonpoint source pollution is crucial. It refers to the function of ecosystems to maintain soil while reducing the entry of substances such as nitrogen and phosphorus into downstream water bodies (including rivers, lakes, reservoirs, etc.), ultimately reducing nonpoint source pollution in the downstream basin. A stable supply of nonpoint source reduction services can improve the quality of the agricultural production environment and achieve source reduction for pollutants and systemic health for the production environment, laying the foundation for green agricultural development while ensuring the safety of urban residents' lives. However, it has been found that changes in soil texture characteristics and nutrient content can seriously affect the provision of local ecosystem services by altering the ecosystem's structure and function [23,24]. As research by Donghua Luo has found, inappropriate concentrations of soil pollutants can have negative effects on the growth, development, and forestation of vegetation [25] and on a larger scale can reduce the ability of trees to provide ecosystem services. Turlough F. Guerin [26] found in his research on industrial land soil that soil compaction can have negative effects on the germination, emergence, and early growth of the roots and stems of some plants. Addressing soil environmental problems in megacities with high land intensification and large populations poses a significant challenge for researchers and city managers, and developing strategies to alleviate urban surface pollution pressure and enhance ecosystem surface reduction services is a pressing issue.

The existing studies on the spatial mapping of the physicochemical properties of soil are mostly based on different ecosystems [27–29] or small and medium-size cities, and they rarely use megacities as research cases. Moreover, there are few studies on the influencing factors of the spatial distribution of nonpoint source pollution reduction services. In China, a megacity refers to a city with a population of over 10 million and is typically characterized by high levels of urbanization, industrialization, and economic development [30,31]. Megacities face many soil environmental issues, such as soil pollution [32], soil degradation [33,34], and soil erosion [35]. These issues not only affect the ecosystem services of the city but also threaten the health and quality of life of urban residents. This article takes Shenzhen as a case study and, on the basis of a large number of soil sample

data and environmental variables, draws high-resolution spatial distribution maps of soil particle size and soil pollutant (total phosphorus, total nitrogen) content for the entire city. Compared with existing research, this article has a higher density of points, considers more environmental variables, and has better mapping accuracy. Based on the spatial results of soil attributes, this article combines geospatial remote-sensing data, statistical data, and localized service function parameters to calculate and spatialize the nonpoint source pollution reduction services for the entire city. Finally, this article uses the geographic detector method to explore the main factors affecting the spatial distribution of nonpoint source pollution reduction services on different land types. The research results can provide a basis for decision-making for regional ecosystem management and soil protection and for restoration policies.

2. Materials and Methods

2.1. Study Area

Shenzhen, an important city along China's southern coast, is in the southern region of the Guangdong Province and on the east coast of the Pearl River Estuary, as shown in Figure 1. As one of the four central cities in the Guangdong-Hong Kong-Macao Greater Bay Area, Shenzhen was the first city in China to undergo reform and open up [36]. The city has a land area of 1997.47 km^2 [36], of which 1005.95 km^2 is built-up land, and has a year-end resident population of 17,681,600 (as of the end of 2021). In the context of continuous industrial development and transformation, the local soil environment has gradually deteriorated with the influx of population and the continuous reduction of nonecological space land; it has more-serious environmental problems, such as soil hardening and slabbing, soil acidification, soil salinization, and soil pollution [37,38]; and the supply base of ecosystem services has been challenged. Shenzhen is a southern subtropical monsoon climate zone characterized by high temperatures and rainfall in summer and mild winters, with high annual rainfall [39]. An overly fragile surface soil environment can cause serious erosion, surface runoff, and surface source pollution problems when washed by precipitation [40].

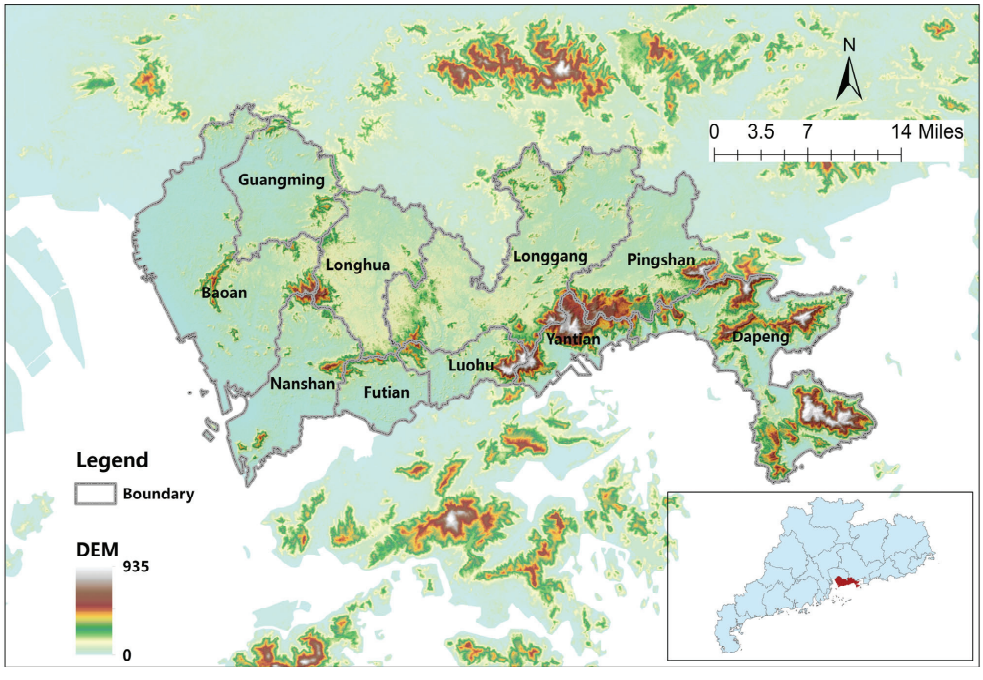

Figure 1. Location map of Shenzhen.

Shenzhen, as a demonstration area of China's economic development, is the first experimental place for many development policies in China. The development strategy adopted by Shenzhen is a reference and learning experience for other cities in China, but many of ecological and environmental problems faced by Shenzhen in the process of development are also possible problems faced by other cities in the process of development. Therefore, this paper takes Shenzhen, a megacity, as a case study, carries out spatial research on soil texture characteristics and pollutant content, and explores the main driving factors of the spatial distribution of nonpoint source pollution reduction services on different land-use types, providing a basis for regional ecosystem management and protection policy formulation for Shenzhen now and for other cities in the future.

2.2. Collection and Testing Methods of Soil Samples

At the city district scale, ArcGIS (Environmental Systems Research Institute, RedLands, CA, USA) was used to generate random points on different ecosystem types, considering the conditions of vegetation, topography, and climatic characteristics, as shown in Figure 2. Specifically, 451 points were selected for investigating and testing soil clay, silt, sand, and organic matter content, while 185 points were chosen for examining and testing the total soil phosphorus and nitrogen content, which is a significant increase in density compared with the traditional soil sampling point setup. To collect soil samples, the researchers removed topsoil weeds, then scooped up a 20 cm soil sample with a shovel, packaged it immediately, and sent it to the lab the same day for testing.

Soil particle composition/mechanical composition tests are carried out in accordance with the Forestry Industry Standard of the People's Republic of China for the Determination of Forest Soil Particle Composition (Mechanical Composition) LY/T 1225-1999 [41]. Soil organic matter is tested in accordance with "Soil Testing Part 6: Determination of Soil Organic Matter" NY/T 1121.6-2006 [42]. The determination of the total phosphorus in soils follows the "Determination of total phosphorus in soils: alkali fusion—molybdenum antimony anti-spectrophotometric method" HJ 632-2011 [43]. The detection of total soil nitrogen follows the "Kjeldahl method for the determination of total nitrogen by soil quality" HJ 717-2014 [44].

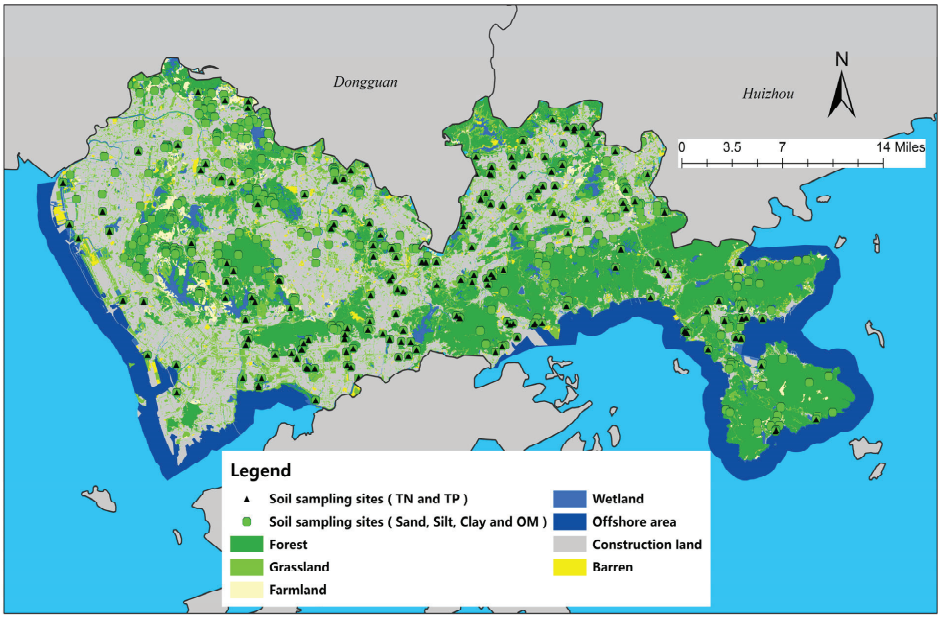

Figure 2. Ecosystem classification map and distribution of soil sampling sites in Shenzhen.

2.3. Methods for Mapping Soil Properties

Numerous methods exist for spatializing soil texture and contaminants. In this paper, the Kriging method of geostatistical methods in ArcGIS is employed for interpolation. Kriging is the most widely used and typical interpolation method in geostatistics and contains several types given that both ordinary Kriging (OK) and universal Kriging (UK) among them ignore the relationship between soil properties and their environmental components, whereas co-Kriging can combine soil predictor variables with environmental auxiliary variables for unbiased optimal estimation [45,46]. Consequently, this paper utilizes co-Kriging in combination with environmental variables for the interpolation of soil properties. In addition, log-ratio conversion methods, commonly used to address closure effects and the statistical analysis of component data during interpolation, are referenced in this study [47].

Environmental variables can directly or indirectly reflect geochemical cycling processes, such as soil occurrence, surface runoff, leaching, and vegetation distribution. These processes subsequently influence soil texture characteristics and nutrient spatial distribution, so combining auxiliary variables is one of the most important tools to improve the accuracy of interpolation, especially at the urban scale. This study uses both continuous and categorical variables to enhance the rationality of the spatial distribution in the mapping results. Continuous variables include elevation (Ele), slope (Slo), aspect (Asp), general curvature (GC), plan curvature (PLC), profile curvature (PRC), tangential curvature (TC), longitudinal curvature (LC), cross-sectional curvature (CSC), flow line curvature (FLC), LS factor (LSF), flow accumulation (FA), the topographic wetness index (TWI), the wind exposition index (WEI), and the normalized difference vegetation index (NDVI) [48–52]. All the continuous variables were extracted by using SAGA GIS software (Department of Physical Geography, University of Göttingen, Göttingen, Sachsen, Germany) that is based on DEM, and the categorical variables included the type of land use in which the monitoring sites were located.

2.4. Methods for the Assessment of Surface Source Pollution Reduction Services

The modified general soil loss equation proposed by Wischmeier et al. [53] was used to account for city-wide soil retention. Next, the soil retention was multiplied by the content factors of nutrients such as nitrogen and phosphorus in the soil [54] to calculate the physical quantity of surface source reduction services. The equation is shown below. See Equations (1) and (2):

$$Q_{dpbi} = Q_{sr} \times c_j \tag{1}$$

$$Q_{sr} = \sum_{i=1}^{n} \left[R_i \times K_i \times L_i \times S_i \times (1 - C_i) \times A_i \times 10^2 \right] \tag{2}$$

where Q_{dpbi} is the amount of type i surface source pollution reduced by the ecosystem (t/a); Q_{sr} is the soil retention (t/a); j is the number of nutrient species in the soil; c_j is the pure content of nitrogen and phosphorus in the soil (%); A_i is the area of ecosystem i (km^2); i is the ecosystem type, i = 1, 2, 3, . . . , n; n is the number of ecosystems; R_i is the rainfall erosivity factor for ecosystem i ($MJ \cdot mm \cdot hm^{-2} \cdot h^{-1} \cdot a^{-1}$); K_i is the soil erodibility factor of ecosystem i ($t \cdot hm^2 \cdot h \cdot hm^{-2} \cdot MJ^{-1} \cdot mm^{-1}$); L_i is the slope length factor of ecosystem i (dimensionless); S_i is the slope factor of ecosystem i (dimensionless); and C_i is the vegetation cover factor of ecosystem i (dimensionless).

2.5. Methods for the Study of Drivers for Surface Source Pollution Reduction Services

The GeoDetector (Institute of Geographical Sciences and Natural Resources, Chinese Academy of Sciences, Beijing, China) is a set of statistical methods designed to detect spatial heterogeneity and reveal the driving forces behind it. The core idea is based on the assumption that if an independent variable has a significant effect on a dependent variable, then the spatial distribution of the independent and dependent variables should be similar [55,56]. In this paper, we conducted a study on the drivers of the spatial distribution

of surface source reduction services in Shenzhen's ecological space by using GeoDetector, taking into account five major potential influences: climate, soil properties, topography, habitat quality, and ecosystem type (as shown in Table 1). Because GeoDetector requires categorical variables as inputs during operation, we have converted all the continuous input data into 5-level categorical input data by using the natural breakpoint method, before inputting the data.The GeoDetector consists of four components: (1) divergence and factor detection, (2) interaction detection, (3) risk zone detection, and (4) ecological detection, with detailed formulae taken from Dr. Jinfeng Wang's research paper [56]. This study uses the "divergence and factor detection" and "interaction detection" sections, as introduced below.

Table 1. Indicator system for potential drivers.

First-Level Indicators	Second-Level Indicators	General Information
Climate	X1: Annual precipitation	mm
	X2: Average annual temperature	°C
Soil properties	X3: Content of sand particles	g/kg
	X4: Content of clay particles	g/kg
	X5: Content of silt particles	g/kg
	X6: Content of organic matter	g/kg
Topography	X7: Elevation	m
	X8: Slope	Degree
Habitat quality	X9: Normalized difference vegetation index, NDVI	Dimensionless
	X10: Net primary productivity, NPP	t/hm^2
Ecosystem type	X11: Ecosystem type	Forests, grasslands, wetlands, impervious surfaces, farmlands, barren

(1) Divergence and factor detection are used to detect the spatial heterogeneity of the dependent variable and to detect the extent to which an independent variable explains the spatial divergence of the dependent variable.

(2) Interaction detection is used to assess the degree of influence from different driver factors combined on the dependent variable. There are five types of two-factor interactions. If the two-factor interaction q-value is less than any single-factor q-value, then it is nonlinearly attenuated; if the two-factor interaction q-value is between two single-factor q-values, then it is one-factor nonlinearly attenuated; if the two-factor interaction q-value is greater than any single-factor q-value, then it is two-factor enhanced; if the two-factor interaction q-value is equal to the sum of two single-factor q-values, then it is independent; and if the two-factor interaction q-value is greater than the sum of two single-factor q-values, then it is nonlinearly enhanced.

3. Results

3.1. Spatial Characteristics of Soil Properties

3.1.1. Accuracy Testing

Co-Kriging (CK) interpolation was evaluated by using a cross-validation method. Its valuation accuracy is assessed according to the following criteria: (1) the absolute value of the mean error (ME) is close to 0; (2) the standardized mean error (MSE) is close to 0; (3) the mean standard error (ASE) is closest to the root mean square error (RMSE); and (4) the standardized root mean square error (RMSSE) is closest to 1. As can be seen from Table 2, the relevant data all met the judgment criteria, indicating that all soil property indicators were interpolated well. The interpolation accuracy of this study is also better than that of previous research [57–60]. For example, Chen Lu et al. [57] obtained an ME of 0.09, an MSE of −0.04, and an RMSSE of 1.19 when interpolating soil particle size in the suburbs of Tianjin, China.

Table 2. Results of cross-validation.

Soil Properties	ME	MSE	ASE	RMSE	RMSSE
Silt particles	0.015	0.012	11.060	11.071	1.001
Clay particles	0.011	0.009	11.100	11.080	1.003
Sand particles	0.001	0.001	11.120	11.110	1.012
Organic matter	0.016	0.013	11.090	11.080	1.011
Total nitrogen	0.012	0.010	11.070	11.082	1.016
Total phosphorus	0.003	0.002	11.113	11.102	1.108

3.1.2. Spatial Distribution Characteristics of Soil Particle Size and Organic Matter

The areas with high silt content in Shenzhen are located in the central and eastern parts of the city, as shown in Figure 3a. The respective areas of high-content areas in Longgang District, Yantian District, Dapeng New District, and Longhua District are relatively large. The mean value of silt particle content was higher in the Yantian, Longgang, and Luohu districts, at 262.04 g/kg, 242.97 g/kg, and 238.15 g/kg, respectively, and lower in the Nanshan and Guangming districts (see Table S1). In terms of land types, the city's press and publication land, dry land, forested land, and railway land had higher mean values, of 231.02 g/kg, 230.22 g/kg, 226.96 g/kg and 224.72 g/kg, respectively, while pastureland, scenic facilities land, business and financial land, and airport land had lower mean values, as shown in Figure 4a and Table S2.

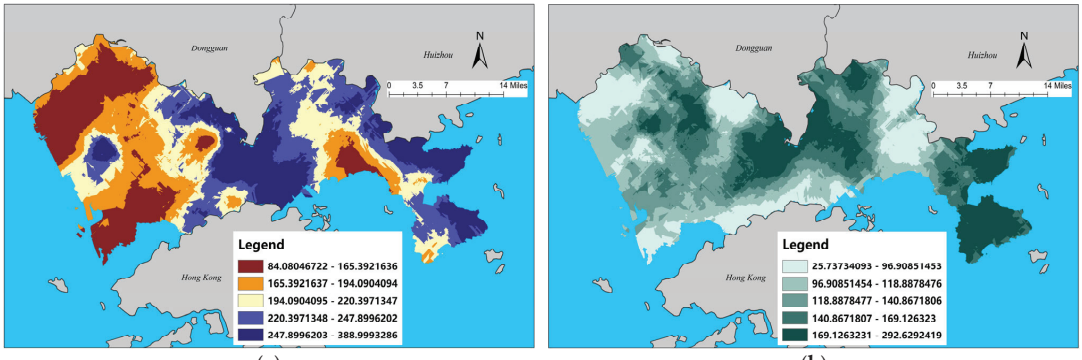

(**a**) (**b**)

Figure 3. (**a**) Spatial distribution characteristics of the content of silt; (**b**) spatial distribution characteristics of the content of clay.

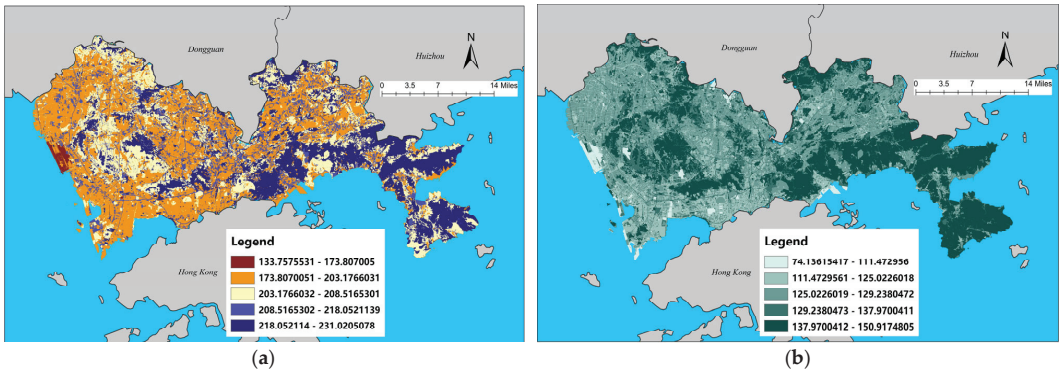

(**a**) (**b**)

Figure 4. (**a**) Spatial distribution characteristics of the mean silt content of each land type (g/kg); (**b**) spatial distribution characteristics of the mean clay content of each land type (g/kg).

The areas with high clay content in Shenzhen are in the central and southeastern parts of the city, as shown in Figure 3b. Longgang District, Dapeng New District, and Guangming District each have a relatively large area of high-content areas. The mean values of clay content were higher in the Dapeng and Longgang districts at 169.06 g/kg and 165.02 g/kg, respectively, and lower in the Nanshan and Guangming districts (see Table S1). In terms of land types, the city's paddy fields, agricultural land for facilities, shrublands, and forested land had higher mean values, of 150.92 g/kg, 150.91 g/kg, 148.59 g/kg, and 147.49 g/kg, respectively. The mean values for pastureland; port and terminal land; cultural, sports, and recreational land; and airport land were lower, as shown in Figure 4b and Table S2.

The areas with high sand content in Shenzhen are located in the west, southwest. and northwest of the city, as shown in Figure 5a. The respective areas of high-content areas in the Baoan, Nanshan, Guangming, and Futian districts are relatively large. The mean values of sand content were higher in Nanshan District and Baoan District, at 714.76 g/kg and 668.84 g/kg, respectively. On the other hand, the values were lower in Longgang District and Dapeng New District (see Supplementary Table S1). In terms of land types, the city's port and terminal land, natural grazing land, airport land, and business and financial land have higher mean values of sand content, at 722.98 g/kg, 721.28 g/kg, 707.71 g/kg, and 673.04 g/kg, respectively. Agricultural land for facilities, dry land, forested land, and railway land have lower mean values, as shown in Figure 6a and Table S2.

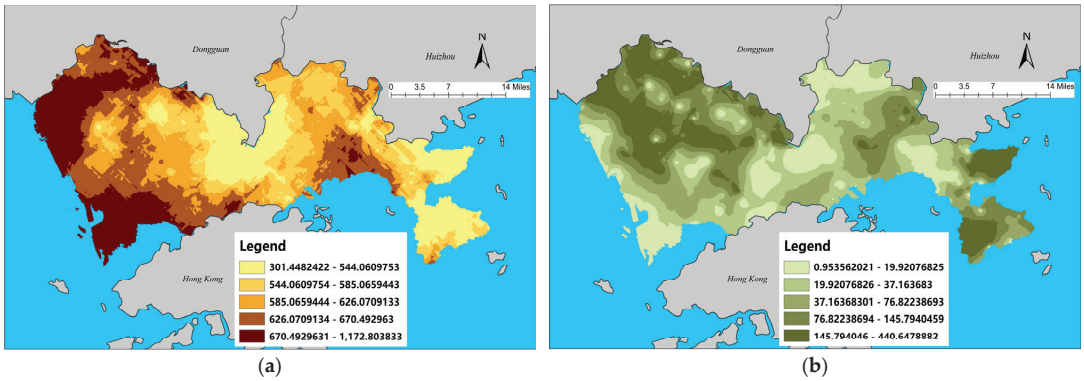

(**a**) (**b**)

Figure 5. (**a**) Spatial distribution characteristics of the content of sand; (**b**) spatial distribution characteristics of the content of organic matter.

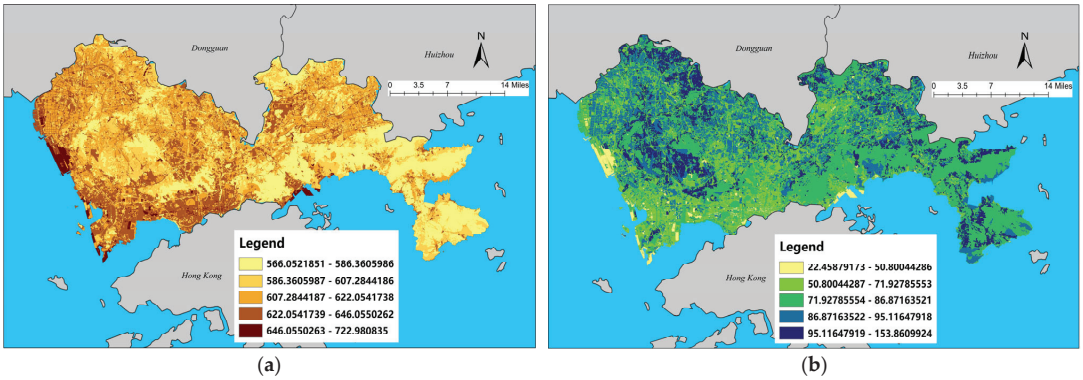

(**a**) (**b**)

Figure 6. (**a**) Spatial distribution characteristics of the mean sand content of each land type (g/kg); (**b**) spatial distribution characteristics of the mean organic matter content of each land type (g/kg).

The areas with high soil organic matter content in Shenzhen are in the northwest and southeast of the city, as shown in Figure 5b. Guangming District, Longhua District, Baoan District, Dapeng New District, and Pingshan District each have a relatively large area of high-content areas. The mean organic matter content was higher in Guangming District and Baoan District, at 139.81 g/kg and 122.83 g/kg, respectively. Meanwhile, the content was lower in Luohu District, Nanshan District, Futian District, and Longgang District (see Table S1). In terms of each land type, the city's artificial grazing land, watered land, paddy fields, and inland mudflats had higher mean values of organic matter, at 153.86 g/kg, 130.91 g/kg, 122.62 g/kg, and 117.53 g/kg, respectively. Port terminal land, airport land, tea plantations, and natural grazing land, however, had lower mean values, as shown in Figure 6b and Table S2.

3.1.3. Spatial Distribution Characteristics of Soil Contaminant Content

The areas with high total soil nitrogen content in Shenzhen are in the central and western parts of the city, as shown in Figure 7a. Futian District, Nanshan District, and Longhua District each have a relatively large area of high-content areas. The mean values of total soil nitrogen in Futian District and Longhua District were higher, at 737.90 mg/kg and 613.46 mg/kg, respectively, while Dapeng New District and Baoan District were lower (see Table S1). The mean values of the total soil nitrogen in the city were higher in natural pastureland and at correctional sites and scenic sites, at 604.59 mg/kg, 568.51 mg/kg, and 552.73 mg/kg, respectively. Lower values were found at airport sites and agricultural facilities and in tea gardens and artificial pastureland, as shown in Figure 8a and Table S2.

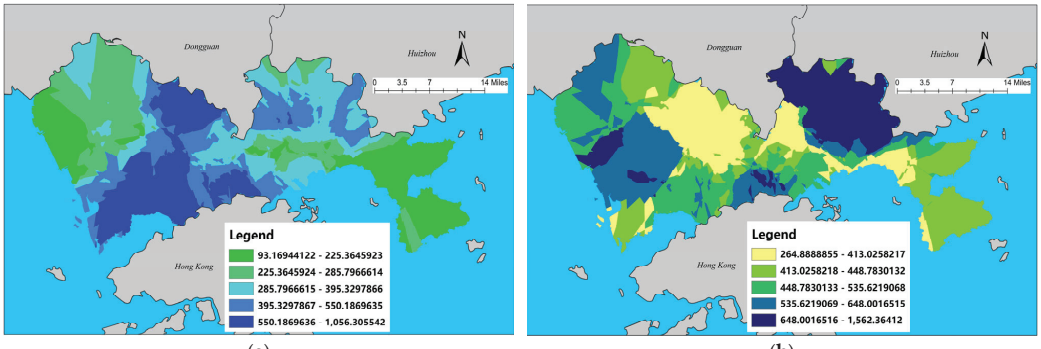

(**a**) (**b**)

Figure 7. (**a**) Spatial distribution characteristics of the content of TN; (**b**) spatial distribution characteristics of the content of TP.

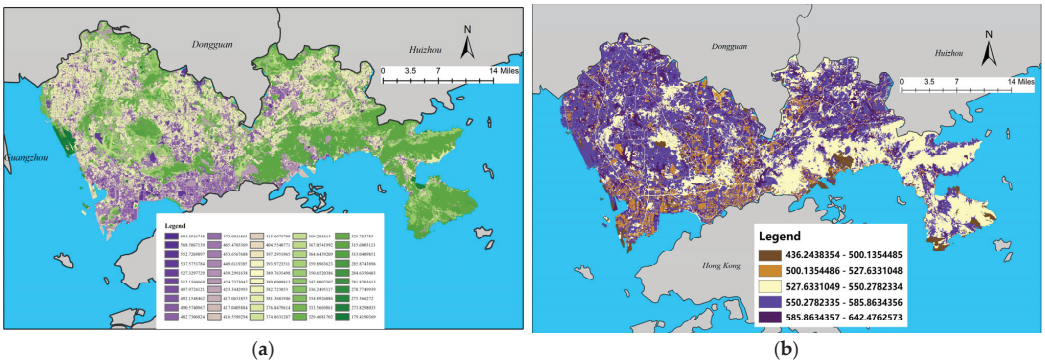

(**a**) (**b**)

Figure 8. (**a**) Spatial distribution characteristics of the mean TN content of each land type (mg/kg); (**b**) spatial distribution characteristics of the mean TP content of each land type (mg/kg).

The areas with high levels of total soil phosphorus in Shenzhen are in the northeast, as shown in Figure 7b. Longgang District and Pingshan District each have a relatively large area of high-content areas. The mean values of total phosphorus in Pingshan District and Longgang District were higher, at 967.57 mg/kg and 602.09 mg/kg, respectively. Lower values were observed in Longhua District, Dapeng New District, and Guangming District (see Table S1). The mean values of total soil phosphorus were higher in rivers, reservoirs, correctional sites, vacant land, and watered land, at 642.48 mg/kg, 635.21 mg/kg, 633.56 mg/kg, 610.28 mg/kg, and 603.78 mg/kg, respectively, while the mean values were lower in tea gardens, artificial pastureland, natural pastureland, and coastal mudflats, as shown in Figure 8b and Table S2.

3.2. Results of Surface Source Pollution Reduction Services

The areas with a higher supply of surface source reduction services in Shenzhen are distributed in the contiguous mountains with better vegetation cover conditions, along Dapeng New District–Pingshan District–Yantian District–Luohu District, followed by the Tanglang Mountain, Fenghuang Mountain, and Yangtai Mountain areas in the east (see Figure 9). Longgang District and Dapeng New District had higher physical quantities of TN service and TP service for surface source reduction, reaching 4399.80 t and 3247.69 t and reaching 7043.18 t and 7296.23 t, respectively, while Futian District and Guangming District had lower physical quantities of the two indicators (see Table S3). In terms of supply intensity, the Luohu, Yantian, and Futian districts have higher service averages for TN reduction from surface sources, at 0.26 t/hm^2, 0.20 t/hm^2, and 0.17 t/hm^2, respectively. The Pingshan, Yantian, and Luohu districts have higher service averages for TP reduction from surface sources, at 0.30 t/hm^2, 0.28 t/hm^2, and 0.28 t/hm^2, respectively.

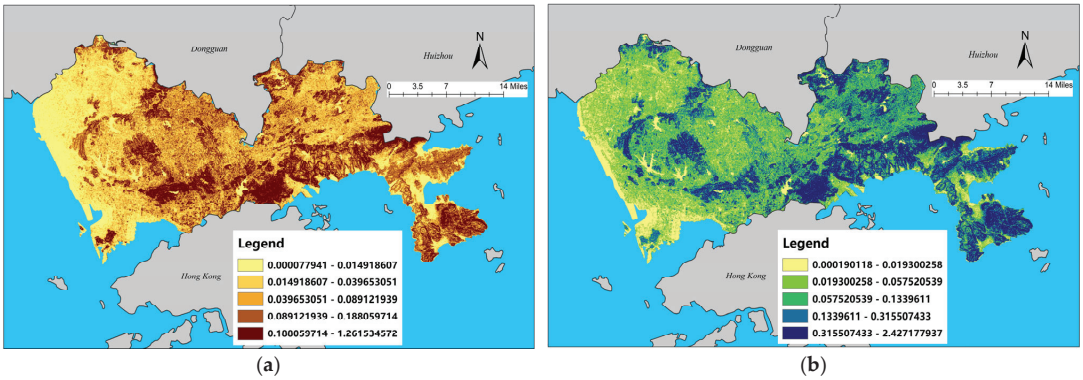

(**a**) (**b**)

Figure 9. (**a**) Spatial distribution characteristics of total nitrogen for city-wide surface source reduction services (t/hm^2); (**b**) spatial distribution characteristics of total phosphorus for city-wide surface source reduction services (t/hm^2).

3.3. Analysis of the Factors Influencing Surface Source Pollution Reduction Services

In this study, a driver analysis of surface source reduction services was carried out to determine the city's main land-use types of forest land, industrial land, and street town residential land (the cumulative land area accounts for 50.26% of the city's land area). The land-use classification data of Shenzhen City comes from the Shenzhen Land Ecological Survey Project. These data divide the city's land into 50 types of land use, and all types of land use can be seen in Table S2. The study fully considered five major factors, namely climate, soil properties, topography, habitat quality, and ecosystem type, with 11 potential drivers, and the results are shown in Table S4. The results of the study can provide guidance for environmental-management-oriented service enhancement measures for surface source reduction.

3.3.1. Forest Land

The spatial distribution of surface source TN reduction services on forested land is influenced mainly by the slope factor, vegetation normalization index, and elevation in the region. Table S4 shows that the *q*-statistics of each driver are ranked in descending order as the slope, vegetation normalization index, elevation, precipitation, net primary productivity, ecosystem type, sand content, organic matter content, sticky grain content, annual mean temperature, and silt content. In addition, some factors, such as precipitation, net primary productivity, ecosystem type, and sand content, also positively influence the formation of spatial variation in TN reduction services, while other factors with small *q*-values have little explanatory power (*q*-values below 10%) [61–65].

Similar to surface source TN reduction services, the spatial distribution of surface source TP reduction services on forested land is also influenced mainly by the slope factor, vegetation normalized index, and elevation within the area. As seen in Table S4, the *q*-statistics of the drivers are, in descending order, the slope, vegetation normalized index, elevation, precipitation, ecosystem type, net primary productivity, sand content, mean annual temperature, clay content, meal content, and organic matter content, and again, the slope factor, vegetation normalized index, and elevation have the greatest influence on the spatial variation of TP reduction services on forested land. Other influencing factors, such as precipitation, ecosystem type, net primary productivity, sand content, and annual mean temperature, also positively affect the formation of spatial differences in TN reduction services. Compared with the TN reduction services, the annual mean temperature also showed a greater influence, and the influence of ecosystem type was stronger than that of net primary productivity. Other factors with small *q*-values have less explanatory power (*q*-values below 10%) [61–65].

The results of the two-factor interaction detection of source reduction services (TN and TP) on forested land are shown in Figures S1 and S2, respectively. The interaction between the drivers showed a two-factor enhancement or nonlinear enhancement; i.e., the interaction of any two drivers on the spatial variance of the forested ground source reduction services (TN and TP) was greater than the effect of one driver alone, indicating that the spatial variance of the forested ground source reduction services (TN and TP) was affected by the joint effect of the drivers. There are more nonlinearly enhanced relationships between the factors of the TN reduction services than the TP reduction services, indicating that the joint effect between different factors has a greater impact on the spatial variation of the TN reduction services; the joint effect between the same pair of factors has a different impact on the TN reduction services and the TP reduction services.

3.3.2. Industrial Land

The main drivers of spatial distribution for both TN reduction services and TP reduction services on industrial land are the same: the vegetation normalized index, slope, and data elevation. As shown in Table S4, the *q*-statistics of the drivers of TN reduction services are ranked in descending order as the vegetation normalized index, slope, data elevation, precipitation, ecosystem type, net primary productivity, sand content, silt content, annual mean temperature, organic matter content, and clay content. Among them, the vegetation normalized index, slope, and data elevation have the greatest influence on the spatial variation of TN reduction services on industrial land. In addition, other influencing factors, such as precipitation, ecosystem type, net primary productivity, and sand content, positively affect the formation of spatial variation in TN reduction services from surface sources, while other factors with small *q*-values do not have strong explanatory power (*q*-values below 10%) [61–65].

The order of the *q*-statistics of the drivers of the TP reduction services is similar to that of the TN reduction services, with only silt content and mean annual temperature changing in order. Similarly, the vegetation normalized index, slope, and data elevation had the greatest influence on the spatial variation of TP reduction services on industrial land. Additionally, other factors, such as precipitation, ecosystem type, net primary productivity,

sand content, and mean annual temperature, positively influence the formation of spatial variation in TP reduction services, while other factors with small *q*-values have little explanatory power [61–65].

The results of the two-factor interaction detection for surface source reduction services (TN and TP) on industrial land are shown in Figures S3 and S4, respectively. The interaction between the drivers also shows a two-factor enhancement or nonlinear enhancement, and the spatial differentiation of surface source reduction services (TN and TP) on industrial land is affected by the combined effect of the drivers. There were more nonlinearly enhanced relationships between the factors for the TP reduction services service than for the TN reduction services, suggesting that the joint effect between different factors had a greater impact on the spatial variance of the TP reduction services. There are differences in the effects of the same pair of factors on the TN reduction services and the TP reduction services.

3.3.3. Street and Town Residential Land

The main drivers of the spatial distribution of TN reduction services and TP reduction services on street and town residential land are the same, both being the vegetation normalized index, slope, and elevation. As can be seen from Table S4, the *q*-statistics of the drivers of the TN service are, in descending order, the vegetation normalized index, slope, elevation, precipitation, ecosystem type, net primary productivity, sand content, mean annual temperature, organic matter content, silt content, and clay content. Among them, the vegetation normalization index, slope, and elevation have the greatest influence on the spatial variation of TN reduction services on street and town residential land. In addition, other factors, such as precipitation, ecosystem type, net primary productivity, sand content, and annual mean temperature, positively influence the formation of spatial variation in TN reduction services. Other factors with small *q*-values do not have strong explanatory power (*q*-values below 10%) [61–65].

Similar to the TN reduction services, the *q*-statistics of the drivers of the TP reduction services on street and town residential land are, in descending order, the vegetation normalized index, slope, elevation, ecosystem type, precipitation, net primary productivity, sand content, mean annual temperature, silt content, organic matter content, and clay content. Similarly, the vegetation normalized index, slope, and elevation had the greatest influence on the spatial variation of TP reduction services on street and town residential land. In addition, other influencing factors, such as precipitation, ecosystem type, net primary productivity, sand content, and annual mean temperature, positively affect the formation of spatial variation in TP reduction services. Other factors with small *q*-values do not have strong explanatory power (*q*-values below 10%) [61–65].

The results of the two-factor interaction detection for the surface source reduction services (TN and TP) on street and town residential land are shown in Figures S5 and S6, respectively. The interaction between the drivers shows a two-factor enhancement or nonlinear enhancement, indicating that the spatial variation of the surface source reduction services (TN and TP) on residential land in streets and lanes is affected by the joint action of the drivers. The nonlinearly enhanced relationship between the factors of the TP reduction services is comparable to the number of TN reduction services. There are also differences in the effects of the joint action between the same pair of factors on TN reduction services and TP reduction services; e.g., the joint action of the X1 and X2 factors is nonlinearly enhanced in relation to the spatial distribution of TN reduction services, while it is bifactorally enhanced in relation to the spatial distribution of TP reduction services.

4. Discussion

4.1. Soil Attribute Mapping Based on Multipoint Monitoring Data Provides Better Data Support for Relevant Research and Management Applications

The traditional accounting of surface source reduction services, which relies on the modified universal soil loss equation, primarily uses public data sets, such as the HWSD

global soil data [66–68], to determine the physical and chemical properties of soil. However, the public data sets have the disadvantages of low resolution and insufficient localization, making it difficult for them to reflect the actual spatial distribution of soil properties in the study area. In this study, 451 survey and testing points for soil clay, silt, sand, and organic matter content and 185 points for total phosphorus and total nitrogen content were selected across various ecosystem types within each administrative region of the city. This significantly increased density compared with traditional soil sampling points. At the same time, the co-Kriging spatial interpolation method, combined with a series of environmental auxiliary variables, has significantly improved the final spatial interpolation accuracy, and the interpolation results have passed cross-validation and are more accurate than the results of existing studies [57–60]. The highly localized, refined, and accurate spatial mapping results of soil properties also provide strong data support for relevant research and management application scenarios based on such data, guaranteeing the scientific soundness and rationality of subsequent results and applications.

4.2. The Distribution Characteristics of the Different Properties of the Soil Show Significant Differences across the City

The spatial distribution of soil sand, clay, silt, organic matter, and total phosphorus and nitrogen content in the city is significantly different thanks to the combined influence of soil parent material and external environmental factors. In terms of the overall distribution, the areas with high soil silt content are mainly in the eastern part of the city in the area of Qiniang Mountain and Paiya Mountain, in the central part of the city from Wutong Mountain to Qiushuiding, and in the western part of the city from Fenghuang Mountain to Tie Gang Reservoir. The areas with low soil silt content are mainly in the southern part of Nanshan District, the northwestern part of Bao'an District, the northern part of Guangming District, and the Maluan Mountain area in the western part of the city. Areas with high soil clay content are mainly in the Dapeng Peninsula, from Qiniang Mountain to Paiya Mountain, and from Qiushuiding to Shenxianling Reservoir, while areas with low content are distributed in the southern part of the city, in the northwestern part of Bao'an District, and in the northeastern part of Pingshan District. The areas with high sand content are mainly in the Western International Convention and Exhibition Centre area, the Nanshan Park area, and the Ma Luangshan area, while the lower content areas are in large areas of mountainous woodland on the Dapeng Peninsula and in a large area centered on Qiushui Ding in Longgang District. The areas with high soil organic matter content are mainly in the Paiya Mountain and Paogou Mountain areas on the Dapeng Peninsula, the woodland around the Jiulongkeng Reservoir, and the northeastern part of the Balcony Hill area. The areas with low soil organic matter content are mainly in the Nanshan Park area, a large area of mountain woodland from Tiantoushan to Guanyinshan Park, and a large area in Longgang District. Areas with high total soil phosphorus content are concentrated in the northeastern part of the city, from Shang Che Reservoir to a large area of woodland in Songzi Keng Forest Park, while the rest of the area has low total soil phosphorus content. Areas with high total soil nitrogen content are concentrated in large areas of the surrounding hills and woodlands centered on Tonglang Mountain, while the rest of the area has low total soil nitrogen content.

Soil properties also show a highly differentiated distribution across the different types of land uses. Among the 50 types of land in the city, the mean soil silt content is higher in the areas of press and publication land, dry land, wooded land, and railway land and lower in the areas of pastureland, scenic facilities, business and financial land, and airport land. The mean soil clay content values are higher in the range of paddy fields, agricultural facilities, shrublands, and forested land and lower in the range of pastureland; port and harbor land; cultural, sports, and recreational land; and airport land. The mean soil sand content is higher in the range of port and terminal land, natural grazing land, airport land, and business and financial land and lower in the range of agricultural land, dry land, forested land, and railway land. The mean soil organic matter content is higher in the range

of artificial grazing land, watered land, paddy fields, and inland mudflats and lower in the range of port terminal land, airport land, tea plantations, and natural grazing land. The mean value of total soil nitrogen is higher in the range of natural grazing land, correctional sites, and scenic sites and lower in the range of airport sites, agricultural facilities, tea gardens, and artificial grazing land. The mean value of total soil phosphorus is higher at correctional sites and in rivers, reservoirs, vacant land, and watered land and lower in tea gardens, artificial pastures, natural pasture, and coastal mudflats.

4.3. The Distribution Characteristics of Surface Source Pollution Reduction Services Show Significant Differences across the City

The distribution characteristics of the supply capacity of TN reduction services and TP reduction services in Shenzhen's ecological space are more consistent across the city. The areas with higher supply capacity are distributed mainly in the large mountain woodlands in the eastern part of the Dapeng Peninsula–Pingshan District–Yantian District–Luohu District contiguous area and in the Tanglang Mountain, Yangtai Mountain, and Fenghuang Mountain areas. On the other hand, urban green spaces with smaller slopes and lower-quality vegetation have lower supply capacity.

At the district scale, the mean value of TN reduction services was higher in Luohu District, Yantian District, and Futian District, while the mean value of TP reduction services was higher in Pingshan District, Yantian District, and Luohu District. At the scale of each land type, forested land, tea plantations, shrubland, and other forested land each have a high capacity to supply TN reduction services, while forested land, shrubland, tea plantations, pipeline transport land, and orchards each have a high capacity to supply TP reduction services. Paddy fields, reservoirs, port terminal land, natural grazing land, and airport land have a low capacity to reduce surface source pollution.

4.4. Spatial Distribution Characteristics of Surface Source Pollution Reduction Services Are Driven Mainly by Topography, Habitat Quality, and Ecosystem Type

The results of the GeoDetector show that topographic factors, habitat-quality factors, and the ecosystem type have the greatest influence on the spatial variability of the TN reduction services and the TP reduction services on the three types of sites. Among the climatic factors, precipitation is the only climatic factor that has a significant influence on the spatial variability of the services. Other than the sand content factor, which has a certain degree of influence, soil property factors do not have great influences on the spatial differentiation characteristics of the services. Additionally, the small q-value does not have strong explanatory power (as shown in Table S4).

An analysis from the perspective of the formation and reduction mechanism of surface source pollution found the following: (1) Different ecosystem types differ in their ability to reduce surface source pollutants under the same precipitation conditions owing to differences in their internal tree species composition, horizontal structure, vertical structure, biomass, and other factors. (2) Regions with higher topography and slopes, where precipitation has a stronger ability to scour the surface, form more-severe surface source pollution, increasing the amount of local surface source pollution reduction from the perspective of pollution volume production. Conversely, flat regions, where precipitation has a weaker ability to scour the surface, pose less of a risk for surface source pollution formation and to some extent weaken the amount of local surface source pollution reduction. (3) When other environmental factors remain unchanged, better vegetation conditions in a region imply a multilayered tree structure and high-quality plant growth conditions, which strengthen the surface source pollutant reduction capacity in the region. (4) Lastly, regions with higher precipitation experience more-severe surface soil washing by rainfall, leading to the formation of more surface source pollutants. This phenomenon to some extent strengthens the local capacity to reduce surface source pollution.

4.5. Based on the Results of the Interaction Detection between Different Factors, Service-Enhancement-Oriented Optimization Solutions Can Be Developed

In this study, the driving mechanisms of TN reduction services and TP reduction services were investigated for the city's major land types (forested land, industrial land, and street and residential land). The results show that the driving mechanisms of the three land types are similar, with elevation, slope, and the vegetation normalization index as the main drivers of the spatial distribution of the surface source reduction services. Net primary productivity, ecosystem type, precipitation, and mean annual temperature also play important roles in the spatial variation of the services. The interaction detection results of the factors on the three types of sites show that the interaction of each driver shows a two-factor enhancement or nonlinear enhancement, meaning that the interaction effect of any two drivers on the spatial variation of the surface source reduction service is greater than that of one driver alone. This finding suggests that the spatial variation of the surface source pollution reduction service is affected by the combined effect of the drivers. However, there are differences in the results of interaction detection between the factors on the three types of sites. On the same type of land, the interaction detection results of the TN reduction services and the TP reduction services are different, and the interaction detection results of the same service on different land types are also different. Therefore, the interaction and synergy between different driving factors should be considered when optimizing the ecosystem and controlling the risk of surface source pollution in the region. Targeted and differentiated treatment modes should be adopted to maximize the enhancement of surface source pollution reduction services and avoid the further reduction of service supply capacity due to unreasonable treatment. For example, in the process of urban old city reconstruction and reserve land development, in order to improve or maximize the ability of local ecosystems to reduce nonpoint source pollution service supply, urban managers can adjust different driving factors on the basis of the results of the geographic detector in this paper; in addition, facing the main nonpoint source pollution problems (total nitrogen pollution or total phosphorus pollution) that occur in different regions, urban managers can also transform the many environmental conditions of local ecosystems into the best combination to achieve the best nonpoint source pollution reduction effect.

4.6. The Innovations and Limitations of This Study

Cities face many ecological and environmental problems in the process of developing into megacities. Vegetation degradation and soil physicochemical property changes have great negative impacts on the ecosystem's service of reducing nonpoint source pollution. There are few studies on the spatial mapping of the physicochemical properties of soil for megacities with high degree of hardening and also few studies on the influencing factors of the spatial distribution of the service of reducing nonpoint source pollution. The novelty of this paper is reflected in the following aspects: (1) This study comprehensively considered various environmental variables and carried out a high-resolution spatial mapping of the physicochemical properties of soil for highly hardened megacities. (2) This study analyzed the spatial distribution influencing factors of the service of reducing nonpoint source pollution for the main three land-use types in the city, laying a foundation for urban ecological management applications. In addition, the research results of this paper can serve as the basis for future studies. High-quality physical and chemical property grid maps for soil can be used for the assessment and mapping of many ecosystem services (such as water conservation, flood reduction, soil conservation, etc.) in the whole city.

Although this paper has achieved some results in the spatial mapping of the physical and chemical properties of soil and the detection of driving factors for reducing nonpoint source pollution services, it has not quantified the joint driving effects of different environmental factors on reducing nonpoint source pollution services. In future studies, methods such as multiple regression, neural network training, random forest, etc. can be used to carry out such research.

5. Conclusions

Most megacities with high development intensity, fragile soil environments, and high precipitation are facing serious surface source pollution problems. In this study, the spatial distribution of soil particle size, organic matter, total phosphorus, and total nitrogen content was mapped with high accuracy by using a large number of soil field survey data and relevant environmental variables. Additionally, the spatial distribution characteristics of phosphorus and nitrogen pollutants in the city's soil were clarified. Furthermore, at the scale of each land type, this paper integrated a modified generic soil loss equation and a geographic probe to assess the current status and main drivers of spatial variation in the provision of surface reduction services in the city's ecosystems. The results of the study can serve as a foundation for decision-making on ecosystem management and soil conservation and restoration, ultimately enhancing surface reduction services in the region.

Supplementary Materials: The following supporting information can be downloaded at https://www.mdpi.com/article/10.3390/atmos14050873/s1, Table S1: Average content of soil properties and contaminants in each district; Table S2: Soil property detection results for various types of land use (mean); Table S3: Physical value of nonpoint source pollution reduction services in each district; Table S4: Drivers of nonpoint source pollution reduction services for major land-use types; Figure S1: Interaction detection results for nonpoint source pollution reduction service TN (forest land); Figure S2: Interaction detection results for nonpoint source pollution reduction service TP (forest land); Figure S3: Interaction detection results for nonpoint source pollution reduction service TN (industrial land); Figure S4: Interaction detection results for nonpoint source pollution reduction service TP (industrial land); Figure S5: Interaction detection results for nonpoint source pollution reduction service TN (street and town residential land); Figure S6: Interaction detection results for nonpoint source pollution reduction service TP (street and town residential land).

Author Contributions: Conceptualization, C.S. and B.H.; methodology, K.D.; software, K.D.; validation, Z.C. and H.W.; formal analysis, C.S.; investigation, K.D.; resources, K.D.; data curation, K.D.; writing—original draft preparation, C.S.; writing—review and editing, C.S.; visualization, C.S.; supervision, Z.O.; project administration, B.H.; funding acquisition, B.H. All authors have read and agreed to the published version of the manuscript.

Funding: This work was funded by the Technologies and Models for Optimizing Urban Ecological Spatial Patterns and Enhancing Functions with Multi-objective Synergy, grant number 2022YFF1301105; this work was also funded by the National Key Research and Development Program of China, grant number 2022YFB3903701.

Institutional Review Board Statement: Not applicable.

Informed Consent Statement: Not applicable.

Data Availability Statement: The data used to support the findings of this study are available from the corresponding author upon request.

Acknowledgments: The authors appreciate the Shenzhen Bureau of Ecology and Environment for providing relevant data and products.

Conflicts of Interest: The authors declare no conflict of interest.

References

1. Koomen, E.; van Bemmel, M.S.; van Huijstee, J.; Andrée, B.P.J.; Ferdinand, P.A.; van Rijn, F.J.A. An integrated global model of local urban development and population change. *Comput. Environ. Urban Syst.* **2023**, *100*, 101935. [CrossRef]
2. UN-Habitat. *World Cities Report 2022: Envisaging the Future of Cities*; UN-Habitat: Nairobi, Kenya, 2022.
3. Gui, H.; Yang, Q.; Lu, X.; Wang, H.; Gu, Q.; Martín, J.D. Spatial distribution, contamination characteristics and ecological-health risk assessment of toxic heavy metals in soils near a smelting area. *Environ. Res.* **2023**, *222*, 115328. [CrossRef] [PubMed]
4. Liu, S.; Yuan, R.; Wang, X.; Yan, Z. Soil tungsten contamination and health risk assessment of an abandoned tungsten mine site. *Sci. Total Environ.* **2022**, *852*, 158461. [CrossRef] [PubMed]
5. Perović, V.; Čakmak, D.; Srbinović, O.S.; Mrvić, V.; Simić, S.B.; Matić, M.; Pavlović, D.; Jaramaz, D.; Mitrović, M.; Pavlović, P. A conceptual modelling framework for assessment multiple soil degradation: A case study in the region of Šumadija and Western Serbia. *Ecol. Indic.* **2023**, *148*, 110096. [CrossRef]

6. Nascimento, C.M.; Demattê, J.A.M.; Mello, F.A.O.; Rosas, J.T.F.; Tayebi, M.; Bellinaso, H.; Greschuk, L.T.; Albarracín, H.S.R.; Ostovari, Y. Soil degradation detected by temporal satellite image in São Paulo state, Brazil. *J. S. Am. Earth Sci.* **2022**, *120*, 104036. [CrossRef]
7. Zucca, C.; Fleiner, R.; Bonaiuti, E.; Kang, U. Land degradation drivers of anthropogenic sand and dust storms. *Catena* **2022**, *219*, 106575. [CrossRef]
8. Zucca, C.; Middleton, N.; Kang, U.; Liniger, H. Shrinking water bodies as hotspots of sand and dust storms: The role of land degradation and sustainable soil and water management. *Catena* **2021**, *207*, 105669. [CrossRef]
9. Jiang, C.; Zhang, H.; Wang, X.; Feng, Y.; Labzovskii, L. Challenging the land degradation in China's Loess Plateau: Benefits, limitations, sustainability, and adaptive strategies of soil and water conservation. *Ecol. Eng.* **2019**, *127*, 135–150. [CrossRef]
10. Han, Y.; Gu, X. Enrichment, contamination, ecological and health risks of toxic metals in agricultural soils of an industrial city, northwestern China. *J. Trace Elem. Miner.* **2023**, *3*, 100043. [CrossRef]
11. Hu, W.; Wang, X.; Wang, X.; Xu, Y.; Li, R.; Zhao, L.; Ren, W.; Teng, Y. Enhancement of nitrogen fixation and diazotrophs by long-term polychlorinated biphenyl contamination in paddy soil. *J. Hazard. Mater.* **2023**, *446*, 130697. [CrossRef]
12. Barroso, G.C.; Abril, G.; Machado, W.; Abuchacra, R.C.; Peixoto, R.B.; Bernardes, M.; Marques, G.S.; Sanders, C.J.; Oliveira, G.B.; Oliveira Filho, S.R.; et al. Linking eutrophication to carbon dioxide and methane emissions from exposed mangrove soils along an urban gradient. *Sci. Total Environ.* **2022**, *850*, 157988. [CrossRef] [PubMed]
13. Guo, J.; Muhammad, H.; Lv, X.; Wei, T.; Ren, X.; Jia, H.; Atif, S.; Hua, L. Prospects and applications of plant growth promoting rhizobacteria to mitigate soil metal contamination: A review. *Chemosphere* **2020**, *246*, 125823. [CrossRef] [PubMed]
14. Brauman, K.A.; Garibaldi, L.A.; Polasky, S.; Aumeeruddy-Thomas, Y.; Brancalion, P.H.S.; DeClerck, F.; Jacob, U.; Mastrangelo, M.E.; Nkongolo, N.V.; Palang, H.; et al. Global trends in nature's contributions to people. *Proc. Natl. Acad. Sci. USA* **2020**, *117*, 32799–32805. [CrossRef] [PubMed]
15. Ouyang, Z.; Wang, X.; Miao, H. A primary study on Chinese terrestrial ecosystem services and their ecological-economic values. *Acta Ecol. Sin.* **1999**, *19*, 19–25.
16. Ouyang, Z.; Song, C.; Zheng, H.; Polasky, S.; Xiao, Y.; Bateman, I.J.; Liu, J.; Ruckelshaus, M.; Shi, F.; Xiao, Y.; et al. Using gross ecosystem product (GEP) to value nature in decision making. *Proc. Natl. Acad. Sci. USA* **2020**, *117*, 14593–14601. [CrossRef] [PubMed]
17. Ouyang, Z.; Zheng, H.; Xiao, Y.; Polasky, S.; Liu, J.; Xu, W.; Wang, Q.; Zhang, L.; Xiao, Y.; Rao, E.; et al. Improvements in ecosystem services from investments in natural capital. *Science* **2016**, *352*, 1455–1459. [CrossRef] [PubMed]
18. Daily, G.C.; Matson, P.A. Ecosystem services: From theory to implementation. *Proc. Natl. Acad. Sci. USA* **2008**, *105*, 9455–9456. [CrossRef]
19. Muhammad, S.; Wuyts, K.; Samson, R. Selection of Plant Species for Particulate Matter Removal in Urban Environments by Considering Multiple Ecosystem (Dis)Services and Environmental Suitability. *Atmosphere* **2022**, *13*, 1960. [CrossRef]
20. Maragno, D.; Gaglio, M.; Robbi, M.; Appiotti, F.; Fano, E.A.; Gissi, E. Fine-scale analysis of urban flooding reduction from green infrastructure: An ecosystem services approach for the management of water flows. *Ecol. Model.* **2018**, *386*, 1–10. [CrossRef]
21. Rizzo, A.; Bresciani, R.; Masi, F.; Boano, F.; Revelli, R.; Ridolfi, L. Flood reduction as an ecosystem service of constructed wetlands for combined sewer overflow. *J. Hydrol.* **2018**, *560*, 150–159. [CrossRef]
22. Park, C.Y.; Park, Y.S.; Kim, H.G.; Yun, S.H.; Kim, C.-K. Quantifying and mapping cooling services of multiple ecosystems. *Sustain. Cities Soc.* **2021**, *73*, 103123. [CrossRef]
23. Ferreira, C.S.S.; Seifollahi-Aghmiuni, S.; Destouni, G.; Ghajarnia, N.; Kalantari, Z. Soil degradation in the European Mediterranean region: Processes, status and consequences. *Sci. Total Environ.* **2022**, *805*, 150106. [CrossRef] [PubMed]
24. Wang, J.; Lu, P.; Valente, D.; Petrosillo, I.; Babu, S.; Xu, S.; Li, C.; Huang, D.; Liu, M. Analysis of soil erosion characteristics in small watershed of the loess tableland Plateau of China. *Ecol. Indic.* **2022**, *137*, 108765. [CrossRef]
25. Luo, D.; Wang, M.; Xu, Y. Research on the impact of soil pollution on plant growth. *J. Green Sci. Technol.* **2017**, *12*, 120–122.
26. Guerin, T.F. The effect of interactions between soil compaction and phenol contamination on plant growth characteristics: Implications for scaling bioremediation at industrial sites. *J. Environ. Manag.* **2022**, *302*, 114017. [CrossRef]
27. Wang, S.; Roland, B.; Adhikari, K.; Zhuang, Q.; Jin, X.; Han, C.; Qian, F. Spatial-temporal variations and driving factors of soil organic carbon in forest ecosystems of Northeast China. *For. Ecosyst.* **2023**, *10*, 100101. [CrossRef]
28. Hoeffner, K.; Santonja, M.; Monard, C.; Barbe, L.; Moing, M.L.E.; Cluzeau, D. Soil properties, grassland management, and landscape diversity drive the assembly of earthworm communities in temperate grasslands. *Pedosphere* **2021**, *31*, 375–383. [CrossRef]
29. Zeng, S.; Ma, J.; Yang, Y.; Zhang, S.; Liu, G.-J.; Chen, F. Spatial assessment of farmland soil pollution and its potential human health risks in China. *Sci. Total Environ.* **2019**, *687*, 642–653. [CrossRef]
30. Wang, W.; Wang, H.; Huang, J.; Yang, H.; Li, J.; Liu, Q.; Wang, Z. Causality and dynamic spillover effects of megacities on regional industrial pollution reduction. *Heliyon* **2023**, *9*, e14047. [CrossRef]
31. Li, H.; Huang, W.; Qian, Y.; Klemeš, J.J. Air pollution risk assessment related to fossil fuel-driven vehicles in megacities in China by employing the Bayesian network coupled with the Fault Tree method. *J. Clean. Prod.* **2023**, *383*, 135458. [CrossRef]
32. Huang, J.; Wu, Y.; Sun, J.; Li, X.; Geng, X.; Zhao, M.; Sun, T.; Fan, Z. Health risk assessment of heavy metal(loid)s in park soils of the largest megacity in China by using Monte Carlo simulation coupled with positive matrix factorization model. *J. Hazard. Mater.* **2021**, *415*, 125629. [CrossRef] [PubMed]

33. Xie, T.; Hou, Y.; Chen, W.P.; Wang, M.E.; Lv, S.T.; Li, X.Z. Impact of urbanization on the soil ecological environment: A review. *Acta Ecol. Sin.* **2019**, *39*, 1154–1164.
34. Chen, Q.; Su, Y.; Wang, S.; Zhao, L. Research and practice on the degradation and prevention technology of urban green space soil—Taking Tianjin Cultural Center as an example. *Tianjin Agric. Sci.* **2016**, *22*, 124–128.
35. Othman, A.; El-Saoud, W.A.; Habeebullah, T.; Shaaban, F.; Abotalib, A.Z. Risk assessment of flash flood and soil erosion impacts on electrical infrastructures in overcrowded mountainous urban areas under climate change. *Reliab. Eng. Syst. Saf.* **2023**, *236*, 109302. [CrossRef]
36. Xu, D.; Ouyang, Z.; Wu, T.; Han, B. Dynamic Trends of Urban Flooding Mitigation Services in Shenzhen, China. *Sustainability* **2020**, *12*, 4799. [CrossRef]
37. Yu, T. A brief analysis of the development of soil safety in Shenzhen since the 13th Five-Year Plan. *Guangdong Chem. Ind.* **2022**, *49*, 112–113, 126.
38. Sun, X.; Jia, L. Migration Characteristics of Heavy Metals in Rock-Soil-Plant System in Yangmeikeng Area, Shenzhen. *South China Geol.* **2020**, *36*, 270–279.
39. Shu, C.; Cai, W.; Du, K.; Jinag, N.; Lin, L.; Li, X. Study on the flora and risk distribution of dominant invasive plants in Shenzhen. *Acta Ecol. Sin.* **2023**, *43*, 1113–1125.
40. Zhang, X.; Chen, P.; Dai, S.; Han, Y. Analysis of non-point source nitrogen pollution in watersheds based on SWAT model. *Ecol. Indic.* **2022**, *138*, 108881. [CrossRef]
41. National Forestry and Grassland Administration of the People's Republic of China. *Measurement of Forest Soil Particle Composition (Mechanical Composition) in the Forestry Industry Standard of the People's Republic of China*; National Forestry and Grassland Administration of the People's Republic of China: Beijing, China, 1999.
42. Ministry of Agriculture and Rural Affairs of the People's Republic of China. *Soil Testing Part 6: Determination of Soil Organic Matter*; Ministry of Agriculture and Rural Affairs of the People's Republic of China: Beijing, China, 2006.
43. Ministry of Ecology and Environment of the People's Republic of China. *Determination of Total Phosphorus in Soil by Alkali Fusion-Molybdenum Antimony Anti-Spectrophotometry*; Ministry of Ecology and Environment of the People's Republic of China: Beijing, China, 2011.
44. Ministry of Ecology and Environment of the People's Republic of China. *Determination of Total Nitrogen in Soil Quality by Kjeldahl Method*; Ministry of Ecology and Environment of the People's Republic of China: Beijing, China, 2014.
45. Agyeman, P.C.; Kingsley, J.; Kebonye, N.M.; Khosravi, V.; Borůvka, L.; Vašát, R. Prediction of the concentration of antimony in agricultural soil using data fusion, terrain attributes combined with regression Kriging. *Environ. Pollut.* **2023**, *316*, 120697. [CrossRef]
46. Chen, B.; Yang, X.; Xu, J. Spatio-Temporal Variation and Influencing Factors of Ozone Pollution in Beijing. *Atmosphere* **2022**, *13*, 359. [CrossRef]
47. Li, C.; Luo, Y.; Bao, A.; Zhang, Y.; Yang, C.; Cui, L. Study on Spatial Interpolation of Compositional Data Based on Log-Ratio Transformation. *Sci. Agric. Sin.* **2012**, *45*, 648–655.
48. Shen, Z. *Spatial Prediction of Topsoil Texture and Analysis of the Causes in Loess Region of Southern Ningxia at Different Scales*; Chinese Academy of Agricultural Sciences: Beijing, China, 2020.
49. Desmet, P.; Govers, G. A GIS procedure for automatically calculating the USLE LS factor on topographically complex landscape units. *J. Soil Water Conserv.* **1996**, *51*, 427–433.
50. Kirkby, M.J.; Beven, K.J. A physically based, variable contributing area model of basin hydrology. *Hydrol. Sci. J.* **1979**, *24*, 43–69.
51. Qin, C.-Z.; Zhu, A.X.; Pei, T.; Li, B.-L.; Scholten, T.; Behrens, T.; Zhou, C.-H. An approach to computing topographic wetness index based on maximum downslope gradient. *Precis. Agric.* **2011**, *12*, 32–43. [CrossRef]
52. Zevenbergen, L.W.; Thorne, C.R. Quantitative analysis of land surface topography. *Earth Surf. Process. Landf.* **1987**, *12*, 47–56. [CrossRef]
53. Wischmeier, W.H.; Smith, D.D. *Predicting Rainfall Erosion Losses: A Guide to Conservation Planning*; Department of Agriculture, Science and Education Administration: Washington, DC, USA, 1978.
54. Shu, C.; Meng, H.; Han, B.; Yang, H.; Pan, X.; Lin, L.; Ouyang, Z. Impact of precipitation factors on gross ecosystem product. *Acta Ecol. Sin.* **2023**, *43*, 1054–1063.
55. Wang, J.-F.; Li, X.-H.; Christakos, G.; Liao, Y.-L.; Zhang, T.; Gu, X.; Zheng, X.-Y. Geographical Detectors-Based Health Risk Assessment and its Application in the Neural Tube Defects Study of the Heshun Region, China. *Int. J. Geogr. Inf. Sci.* **2010**, *24*, 107–127. [CrossRef]
56. Wang, J.; Xu, C. Geodetector: Principle and prospective. *Acta Geogr. Sin.* **2017**, *72*, 116–134.
57. Chen, L.; Chen, L.; Shi, M. Spatial Distribution and Variability of Soil Fine Diameter in Suburbs of Tianjin. *Environ. Sci. Technol.* **2013**, *36*, 29–34, 63.
58. Wan, H.; Qin, H.; Shang, S. Ordinary Kriging Interpolation and Smoothing Effect Correction for Soil Texture Mapping in Hetao Irrigation District. *Trans. Chin. Soc. Agric. Mach.* **2023**, *54*, 339–350.
59. Zhang, H.; Zhu, G.; Wu, J.; Wu, X. Simulation of spatial distribution simulation of soil organic matter based on BP neural network and Kriging interpolation—Taking Hua'an County, Fujian Province as an example. *Subtrop. Agric. Res.* **2021**, *17*, 40–47.
60. Tang, J.; Wang, C.; Li, Q.; Li, B.; YI, Y. Spatial variability of organic matter and total nitrogen in tobacco growing soil in the north part of Sichuan province. *Acta Table Sin.* **2014**, *20*, 66–72.

61. Wang, Y.; Yang, X.; Hao, L. *Spatio-Temporal Pattern and Influencing Factors of Vegetation NDVI in Western Sichuanplateau from 2001 to 2021*; Remote Sensing for Natural Resources: Beijing, China, 2023; pp. 1–9.
62. Chen, K.; Ding, Y.; Zhang, X. Analysis of Spatio-Temporal Dynamics and Driving Forces of Vegetation Cover in the Fuyang River Basin Based on the Geographic Detector. *Front. Earth Sci.* **2022**, 1–15.
63. Hang, L.; Chen, Q.; Feng, J.; Liu, R. Spatial-Temporal Characteristics and Driving Mechanisms Analysis of Habitat Quality in Shenfu Mining Area Based on Geodetector. *J. Xi'an Univ. Technol.* **2023**, 1–14.
64. Xue, L.; Li, H.; Shen, W.; Zhao, X.; Liu, Z.; Zheng, Z.; Hu, J.; Meng, S. Applying GeoDetector to disentangle the contributions of the 4-As evaluation indicators to the spatial differentiation of coal resource security. *Energy Policy* **2023**, *173*, 113418. [CrossRef]
65. Qiao, Y.; Wang, X.; Han, Z.; Tian, M.; Wang, Q.; Wu, H.; Liu, F. GeoDetector based identification of influencing factors on spatial distribution patterns of heavy metals in soil: A case in the upper reaches of the Yangtze River, China. *Appl. Geochem.* **2022**, *146*, 105459. [CrossRef]
66. Hao, Z.; Wu, D. Data Preprocessing of Soil Attributes for Ecohydrological Applications Using SWAT Model at Xin'anjiang Upstream Watershed, China. *Ecohydrol. Hydrobiol.* **2023**, *23*, 198–210. [CrossRef]
67. Bouslihim, Y.; Rochdi, A.; El Amrani Paaza, N.; Liuzzo, L. Understanding the effects of soil data quality on SWAT model performance and hydrological processes in Tamedroust watershed (Morocco). *J. Afr. Earth Sci.* **2019**, *160*, 103616. [CrossRef]
68. Deng, X.; Chen, X.; Ma, W.; Ren, Z.; Zhang, M.; Grieneisen, M.L.; Long, W.; Ni, Z.; Zhan, Y.; Lv, X. Baseline map of organic carbon stock in farmland topsoil in East China. *Agric. Ecosyst. Environ.* **2018**, *254*, 213–223. [CrossRef]

atmosphere

MDPI

Article

Does Atmospheric Nitrogen Deposition Confer a Competitive Advantage to Invasive *Bidens pilosa* L. over Native *Pterocypsela laciniata* (Houtt.) Shih?

Chuang Li [1], Yue Li [1], Yingsheng Liu [1], Shanshan Zhong [1], Huanshi Zhang [2,*], Zhelun Xu [1,3], Zhongyi Xu [1], Daolin Du [4] and Congyan Wang [1,5,6,*]

1 School of Environment and Safety Engineering, Jiangsu University, Zhenjiang 212013, China; 2222209081@stmail.ujs.edu.cn (C.L.); 2222209050@stmail.ujs.edu.cn (Y.L.); 3202202017@stmail.ujs.edu.cn (Y.L.); 2222109045@stmail.ujs.edu.cn (S.Z.); 2222109089@stmail.ujs.edu.cn (Z.X.); 3202202022@stmail.ujs.edu.cn (Z.X.)
2 College of Horticulture, Jinling Institute of Technology, Nanjing 210038, China
3 Weed Research Laboratory, College of Life Sciences, Nanjing Agricultural University, Nanjing 210095, China
4 Jingjiang College, Jiangsu University, Zhenjiang 212013, China; ddl@ujs.edu.cn
5 Jiangsu Collaborative Innovation Center of Technology and Material of Water Treatment, Suzhou University of Science and Technology, Suzhou 215009, China
6 Key Laboratory of Forest Plant Ecology, Ministry of Education, Northeast Forestry University, Harbin 150040, China
* Correspondence: zhanghuanshi@jit.edu.cn (H.Z.); liuyuexue623@ujs.edu.cn (C.W.)

Abstract: One of the key reasons for the success of invasive plants is the functional differences between invasive plants and native plants. However, atmospheric nitrogen deposition may disrupt the level of available nitrogen in soil and the functional differences between invasive plants and native plants, which may alter the colonization of invasive plants. Thus, there is a pressing necessity to examine the effects of atmospheric nitrogen deposition containing different nitrogen components on the functional differences between invasive plants and native plants. However, the progress made thus far in this field is not sufficiently detailed. This study aimed to elucidate the effects of artificially simulated nitrogen deposition containing different nitrogen components (i.e., nitrate, ammonium, urea, and mixed nitrogen) on the functional differences between the Asteraceae invasive plant *Bidens pilosa* L. and the Asteraceae native plant *Pterocypsela laciniata* (Houtt.) Shih. The study was conducted over a four-month period using a pot-competitive co-culture experiment. The growth performance of *P. laciniata*, in particular with regard to the sunlight capture capacity (55.12% lower), plant supporting capacity (45.92% lower), leaf photosynthetic area (51.24% lower), and plant growth competitiveness (79.92% lower), may be significantly inhibited under co-cultivation condition in comparison to monoculture condition. *Bidens pilosa* exhibited a more pronounced competitive advantage over *P. laciniata*, particularly in terms of the sunlight capture capacity (129.43% higher), leaf photosynthetic capacity (40.06% higher), and enzymatic defense capacity under stress to oxidative stress (956.44% higher). The application of artificially simulated nitrogen deposition was found to facilitate the growth performance of monocultural *P. laciniata*, particularly in terms of the sunlight capture capacity and leaf photosynthetic area. *Bidens pilosa* exhibited a more pronounced competitive advantage (the average value of the relative dominance index of *B. pilosa* is ≈ 0.8995) than *P. laciniata* under artificially simulated nitrogen deposition containing different nitrogen components, especially when treated with ammonium (the relative dominance index of *B. pilosa* is ≈ 0.9363) and mixed nitrogen (the relative dominance index of *B. pilosa* is ≈ 0.9328). Consequently, atmospheric nitrogen deposition, especially the increased relative proportion of ammonium in atmospheric nitrogen deposition, may facilitate the colonization of *B. pilosa* via a stronger competitive advantage.

Keywords: ammonium; co-cultivation condition; functional difference; growth performance; relative dominance

Citation: Li, C.; Li, Y.; Liu, Y.; Zhong, S.; Zhang, H.; Xu, Z.; Xu, Z.; Du, D.; Wang, C. Does Atmospheric Nitrogen Deposition Confer a Competitive Advantage to Invasive *Bidens pilosa* L. over Native *Pterocypsela laciniata* (Houtt.) Shih? *Atmosphere* **2024**, *15*, 825. https://doi.org/10.3390/atmos15070825

Academic Editors: Chaofan Xian, Yu-Sheng Shen, Cheng Gong and László Bencs

Received: 23 May 2024
Revised: 20 June 2024
Accepted: 9 July 2024
Published: 10 July 2024

1. Introduction

Invasive plants (IPs) can have a profound impact on environmental health and ecological security. In particular, IPs can affect the structure and ecological function of native ecosystems, which can result in the loss of native biodiversity [1–4]. At present, there are in excess of 500 IPs distributed throughout China [5,6]. In particular, the Asteraceae family has the highest species number of IPs at the family classification level, with a total of 92 IPs in the family Asteraceae [5,6]. Thus, the investigation of the mechanisms underlying the success of IPs, particularly those belonging to the Asteraceae family, represents a pivotal area of research within the field of invasion ecology in recent years [7–9].

One of the key reasons for the success of IPs is the functional differences between IPs and native plants. In particular, both IPs and native plants are subject to similar, if not identical, selection pressures, exerted by the environment [10–13]. More importantly, IPs generally exhibit higher values for the key functional traits, including plant height, leaf area, photosynthetic capacity, nutrient use efficiency, and environmental tolerance, etc. Consequently, they exhibit higher growth performance compared to native plants, even under stressful environments [14–17]. It is therefore essential to illuminate the functional differences and differences in growth performance-related functional traits between IPs and native plants to identify the intrinsic mechanisms that determine whether an IP is successfully invaded.

In general, nitrogen (N) is the main nutrient limiting plant growth in several terrestrial ecosystems [18–21]. Therefore, the capacity of IPs to obtain N is a pivotal element in determining their success in colonizing diverse habitats. More importantly, it is evident that IPs exhibit a greater capacity for N acquisition compared to native plants, due to their high availability and utilization of N [22–25]. In addition, the invasiveness and invasion intensity of numerous IPs are significantly related to the level of available N in soil [26–29]. Nevertheless, atmospheric N deposition may significantly disrupt the level of available N in soil and the interactions between IPs and native plants, which may influence the colonization of IPs.

In recent years, there has been a notable increase in atmospheric N deposition, which is largely attributed to the release of N-containing compositions into the atmosphere as a consequence of the excessive combustion of fossil fuels, unreasonable and/or unsuitable production and consumption of N-containing fertilizers, and the fast expansion of animal husbandry and cultivation [30–33]. Presently, East Asia (predominantly China) has one of the three maximum rates of atmospheric N deposition globally [31,34–36]. In addition, other parts of the globe are also experiencing more serious atmospheric N deposition problems, such as Europe and the United States [33,37–39]. Nevertheless, it has been demonstrated that atmospheric N deposition may promote the invasiveness of several IPs, which in turn leads to the acceleration of the colonization of IPs by increasing the level of available N in soil [40–43]. However, atmospheric N deposition encompasses a multitude of different N components, including nitrate (NO_3-N), ammonium (NH_4-N), urea ($CO(NH_2)_2$-N), etc., and that the relative proportions of these N components in atmospheric N deposition may also be subject to change contingent on the alterations in energy policy and the composition of energy sources employed [31,34–36]. Nevertheless, atmospheric N deposition containing different N components can result in alterations in the level of available N in soil and the interactions between IPs and native plants. Such variations may result in differences in the functional differences between IPs and native plants. This could have a significant impact on the colonization of IPs. Therefore, there is a compelling rationale for investigating the effects of atmospheric N deposition containing different N components on the functional differences between IPs and native plants, with the aim of elucidating the mechanisms that facilitate the success of IPs in the context of atmospheric N deposition, particularly in the context of different N components. Nevertheless, the current state of knowledge in this field is not sufficiently detailed.

This study aimed to elucidate the effects of artificially simulated N deposition containing different N components (including nitrate (NO_3-N), ammonium (NH_4-N), urea

($CO(NH_2)_2$-N), and mixed N with NO_3-N:NH_4-N:$CO(NH_2)_2$-N = 1:1:1) on the functional differences between the Asteraceae IPs *Bidens pilosa* L. and the Asteraceae native plant *Pterocypsela laciniata* (Houtt.) Shih. The study was conducted over a four-month period using a pot-competitive co-culture experiment. *Bidens pilosa* is a member of the Asteraceae family, and the species number of IPs belonging to this family that have been introduced to China is higher than that of any other family at the family level [5,6]. *Bidens pilosa* is native to tropical America and was introduced to China in ~1857 with imported crops and vegetables. In particular, the species number of IPs sourced from America is higher than that sourced from other countries and/or districts in China [5,6]. However, *B. pilosa* has been identified as a significant threat to ecosystem structure and function, particularly in terms of the loss of native biodiversity in China, and *B. pilosa* has been classified as a harmful IP in China [2,44–46]. The two Asteraceae plants occupy similar habitats, including agroecosystems, wasteland, and areas adjacent to the main road in China. Additionally, the two Asteraceae plants also share similar lifestyles, with erect herbs being a common feature. Furthermore, they exhibit comparable plant heights, reaching up to ≈2–3 m. More importantly, the two Asteraceae plants frequently co-occur in the same habitats, such as agroecosystems, wasteland, and areas adjacent to the main road, etc. Furthermore, the distributions of the two Asteraceae plants in China are among the areas most affected by atmospheric N deposition [31,34–36].

The following questions were proposed for this study: (1) Does *B. pilosa* exhibit higher values of the key functional traits (e.g., plant height, leaf area, and leaf nitrogen and chlorophyll contents) compared to *P. laciniata*? (2) Does artificially simulated N deposition confer a competitive advantage to *B. pilosa* over *P. laciniata*? (3) Which component of artificially simulated N deposition exerts the greatest influence on the competitive advantage of *B. pilosa*?

2. Materials and Methods

2.1. Experimental Design

Bidens pilosa (Figure S1) was designated as the target IP. *Pterocypsela laciniata* (Figure S2) was proposed as the native species. Seeds of both plants were collected in October 2022 from Zhenjiang, Jiangsu, China (32.15–32.16° N; 119.52–119.53° E). The selected ecosystems were classified as wastelands. *Bidens pilosa* was the only invasive plant species in the sampled communities. It is likely that the selected *B. pilosa* individuals were naturally dispersed in the sampled communities. The native plant species in the sampled communities are dominated by herbaceous plants, such as *Setaria viridis* (L.) P. Beauv., *Echinochloa crus-galli* (L.) P. Beauv., *Arthraxon hispidus* (Trin.) Makino, and *Artemisia argyi* H. Lév. and Vaniot. The geographical location of the sampling area is provided in Figure S3. Zhenjiang has a humid subtropical monsoon climate, and in 2022 the average annual temperature in Zhenjiang was ~17.1 °C, and an average monthly temperature reached a maximum of ~28.1 °C in July and a minimum of ~3.7 °C in January [47]. In 2022, the annual sunshine hours in Zhenjiang were ~1909.0 h, and the monthly average sunshine hours reached a maximum value of ~208.2 h in December, and a minimum value of ~125.9 h in August [47]. The annual precipitation in Zhenjiang in 2022 was ~1164.1 mm, and the average monthly precipitation reached a maximum value of ~432.1 mm in July, and a minimum value of ~2.7 mm in December [47].

A pot competitive co-culture experiment was conducted to examine the growth of *B. pilosa* and *P. laciniata* (Figure S4). Pasture yellow soil (manufacturer: Shenzhibei Sci. & Technol. Co., Ltd., Baishan, China; pH value: ~6.3; soil electrical conductivity: ≤3 ms/cm; organic content: ≥30%; ~3 kg/planting basin) was used as culture substrate. The reason for using pasture yellow soil as a culture substrate was to minimize the potential for previous introduction of IPs, as well as to reduce the risk of contamination from atmospheric N deposition in natural soils. The seeds of both plants were placed in garden pots (top diameter 25 cm; height 16.5 cm). Six uniformly sized, vigorous of *B. pilosa* and/or *P. laciniata* seedlings were cultivated in each garden pot. The following treatments were employed:

(1) six *B. pilosa* seedlings were planted in each garden pot, representing a monoculture of *B. pilosa*; (2) three *B. pilosa* seedlings and three *P. laciniata* seedlings were planted in each garden pot, representing a co-culture of *B. pilosa* and *P. laciniata*; (3) six *P. laciniata* seedlings were planted in each garden pot, representing a monoculture of *P. laciniata*. All garden pots were treated with artificially simulated N deposition, specifically (1) nitrate (potassium nitrate (KNO_3, AR, ≥99%; Aladdin®, Shanghai, China); inorganic nitrogen); (2) ammonium (ammonium chloride (NH_4Cl, GR, ≥99.8%; Sinopharm Chemical Reagent Co., Ltd., Shanghai, China); inorganic nitrogen); (3) urea ($CO(NH_2)_2$, BC, ≥99.5%; Sangon Biotech Co., Ltd., Shanghai, China; organic nitrogen); (4) mixed N (nitrate:ammonium:urea = 1:1:1), at 5 g N m^{-2} yr^{-1}. Sterile distilled water was used as the control (0 g N L^{-1}). The content of artificially simulated N deposition, which contained different N components, replicated the actual content of natural atmospheric N deposition (i.e., 5 g N m^{-2} yr^{-1}) in the southern Jiangsu, China [34,35,48,49]. The proportions of the three monomers in the N mixture were designed to simulate the actual proportions of natural atmospheric N deposition (i.e., equal mixing) in the southern Jiangsu, China [50–52]. The present study tested a range of planting type combinations (i.e., monocultural *B. pilosa*, co-cultivated *B. pilosa* and *P. laciniata*, and monocultural *P. laciniata*) and N component combinations (i.e., nitrate, ammonium, urea, and mixed N). Three replicates were arranged for each treatment. Seedlings of both plants were cultivated in the greenhouse at Jiangsu University, Zhenjiang, Jiangsu, China (32.2061° N, 119.5128° E) under natural light from April to July 2023 for ~4 months. The design of this experiment is shown in Figure 1.

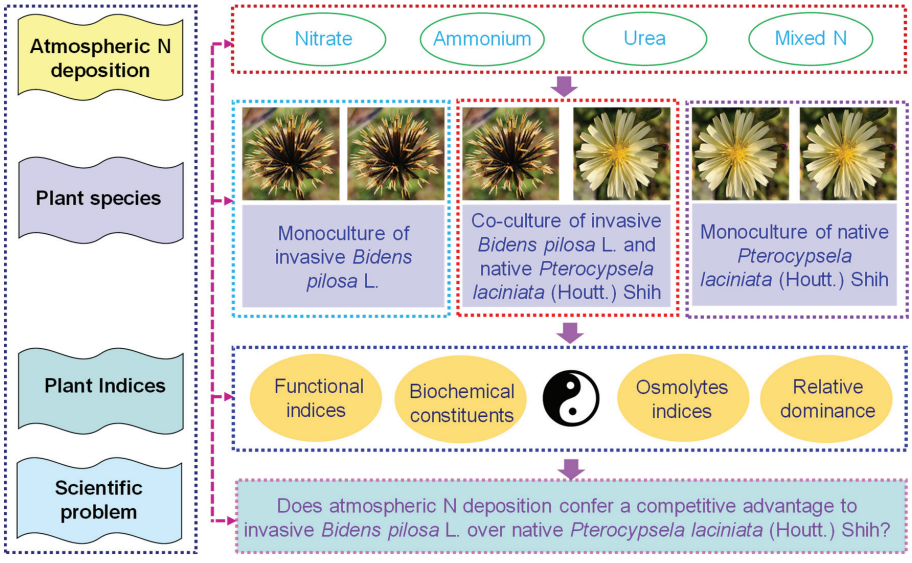

Figure 1. The chart of the experimental design in this study.

Following ~4 months of pot competitive co-culture experimentation, all individuals of *B. pilosa* and *P. laciniata* were collected to determine their functional indices, biochemical constituents, and osmolytes indices of *B. pilosa* and *P. laciniata*, as well as the relative dominance index of *B. pilosa*.

2.2. Determination of Plant Indices

The functional traits closely related to the growth performance of *B. pilosa* and *P. laciniata*, including plant height, ground diameter, leaf dimensions, green leaf area, specific leaf area, leaf chlorophyll and N contents, and biomass, were determined. The biomass stability index of both plants and the relative dominance index of *B. pilosa* were also quantified.

Similarly, biochemical constituents, and osmolytes indices of both plants were determined. The ecological significance, measuring method, and the corresponding references of the analyzed indices in this study are presented in Table S1.

2.3. Statistical Analysis

Shapiro–Wilk's test and Bartlett's test were employed to determine the extent of departure from the normality and the homogeneity of the examined variances, respectively. The statistical analysis of the differences in the values of the functional indices, biochemical constituents, and osmolytes indices of *B. pilosa* and *P. laciniata*, as well as the relative dominance index of *B. pilosa* among different treatments was conducted using the one-way analysis of variance (ANOVA) with the Duncan's test. Two-way ANOVA was employed to evaluate the effects of plant species and N component on the functional indices, biochemical constituents, and osmolytes indices of *B. pilosa* and *P. laciniata*. The effect size of each factor was also evaluated using Partial Eta Squared (η^2), which were calculated to be used in a two-way ANOVA. $p \leq 0.05$ was considered to represent a statistically significant difference. Statistical analyses were conducted using IBM SPSS Statistics 26.0 (IBM, Inc., Armonk, NY, USA).

3. Results and Discussion

Plant height, ground diameter, leaf width, green leaf area, and biomass of co-cultivated *P. laciniata* were significantly lower than those of monocultural *P. laciniata* ($p < 0.05$; Figures 2–4). Thus, the sunlight capture capacity, plant supporting capacity, leaf photosynthetic area, and plant growth competitiveness of co-cultivated *P. laciniata* were found to be significantly lower than those of monocultural *P. laciniata*. Hence, the growth performance of *P. laciniata* may be significantly reduced under co-cultivation conditions compared to monoculture condition. The diminished growth performance of *P. laciniata* under co-cultivation conditions may be attributed to the decreased availability of nutrients (especially N) resulting from the intensified interspecific competition under co-cultivation conditions. Our previous studies have also provided evidence to support this conclusion [53–56]. More importantly, no significant differences were detected in the growth performance of *B. pilosa* between the monoculture and co-cultivation conditions in the majority of cases ($p > 0.05$; Figures 2–5). Accordingly, the competitive advantage of *B. pilosa* is not affected by cultivation type. Consequently, *B. pilosa* exhibited a more pronounced competitive advantage compared to *P. laciniata*, especially under co-cultivation conditions.

The functional differences between IPs and native plants may be of critical importance in determining the success of IPs. More importantly, the results demonstrated that IPs exhibited a more pronounced competitive advantage over native plants, which were recruited by the higher values of key functional traits, such as plant height, leaf area, photosynthetic capacity, nutrient use efficiency, and environmental tolerance, etc. Consequently, Ips demonstrated superior growth performance than native plants, even under stressful environments [11,14–16]. Similarly, the plant height, leaf chlorophyll and N contents, and plant peroxidase activity of *B. pilosa* were significantly higher than those of *P. laciniata* under both monoculture and co-cultivation conditions ($p < 0.05$; Figures 2, 3 and 6). More importantly, plant species significantly affected all functional indices (except ground diameter) ($p < 0.00001$; Table S2). Thus, *B. pilosa* exhibited a more pronounced competitive advantage in comparison to *P. laciniata*. The pronounced competitive advantage of *B. pilosa* is likely attributable to its stronger sunlight capture capacity, leaf photosynthetic capacity, and enzymatic defense capacity under stress to oxidative stress compared to *P. laciniata*. However, leaf length of *B. pilosa* was found to be significantly shorter than that of *P. laciniata* under both monoculture and co-cultivation conditions ($p < 0.05$; Figure 3). Thus, the leaf photosynthetic area of *B. pilosa* was found to be significantly smaller than that of *P. laciniata* under both monoculture and co-cultivation conditions. Accordingly, the leaf photosynthetic area does not appear to be a determining factor in the strong competitive advantage exhibited by *B. pilosa*. In other words, *B. pilosa* can obtain a strong competitive advantage

mainly by means of partial key functional traits, e.g., stronger sunlight capture capacity, leaf photosynthetic capacity, and enzymatic defense capacity under stress to oxidative stress. The significantly functional differences between *B. pilosa* and *P. laciniata* permit *B. pilosa* to gain a stronger competitive advantage and to occupy more ecological niches in the habitats, which support the niche differentiation hypothesis (i.e., invasive and native species tend to exhibit functional divergence, resulting in invasive species exhibiting distinct functional traits compared to native species, thereby enabling the former to successfully invade new habitats via the higher growth competitiveness) [57–60] and the Darwin's naturalization hypothesis (i.e., invasive species that are phylogenetically unrelated to native species should be more successful, as they can exploit the unoccupied ecological niches in the invaded communities) [61–64]. Accordingly, the "Master-of-some" strategy (i.e., invasive species are more competitive in favorable habitat, such as the increased resource availability), in contrast to the "Jack-of-all" strategy (i.e., invasive species are more competitive in stressful habitats, such as the decreased resource availability) or "Jack and master" strategy (i.e., invasive species are more competitive in both unfavorable and favorable habitats) [65–67], serves to enhance the competitive advantage of *B. pilosa*, especially under atmospheric nitrogen deposition.

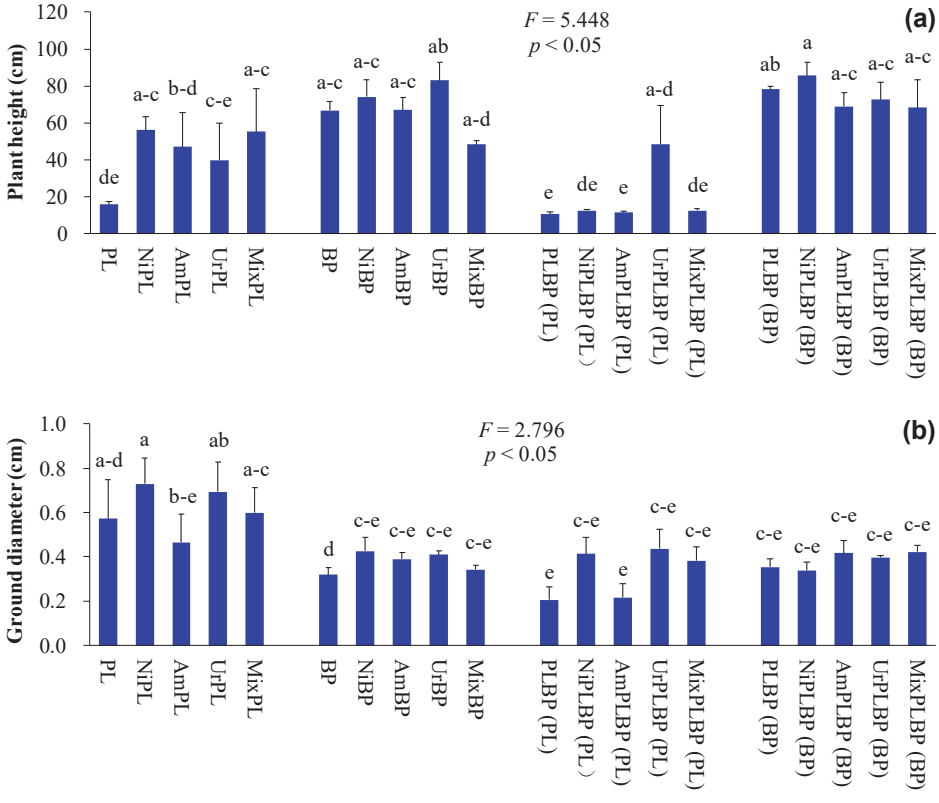

Figure 2. Plant height and ground diameter of *B. pilosa* and *P. laciniata* under monoculture and co-cultivation conditions, respectively ((**a**), plant height; (**b**), ground diameter). Bars (mean and standard error, $n = 3$) with different lowercase letters representing statistically significant differences ($p \leq 0.05$). Abbreviations: PL, monocultural *P. laciniata*; NiPL, monocultural *P. laciniata* treated with nitrate; AmPL, monocultural *P. laciniata* treated with ammonium; UrPL, monocultural *P. laciniata* treated with urea; MixPL, monocultural *P. laciniata* treated with mixed N; BP, monocultural *B. pilosa*; NiBP, monocultural *B. pilosa* treated with nitrate; AmBP, monocultural *B. pilosa* treated with ammonium;

UrBP, monocultural *B. pilosa* treated with urea; MixBP, monocultural *B. pilosa* treated with mixed N; PLBP(PL), co-cultivated *P. laciniata*; NiPLBP(PL), co-cultivated *P. laciniata* treated with nitrate; AmPLBP(PL), co-cultivated *P. laciniata* treated with ammonium; UrPLBP(PL), co-cultivated *P. laciniata* treated with urea; MixPLBP(PL), co-cultivated *P. laciniata* treated with mixed N; PLBP(BP), co-cultivated *B. pilosa*; NiPLBP(BP), co-cultivated *B. pilosa* treated with nitrate; AmPLBP(BP), co-cultivated *B. pilosa* treated with ammonium; UrPLBP(BP), co-cultivated *B. pilosa* treated with urea; Mix AmPLBP(BP), co-cultivated *B. pilosa* treated with mixed N.

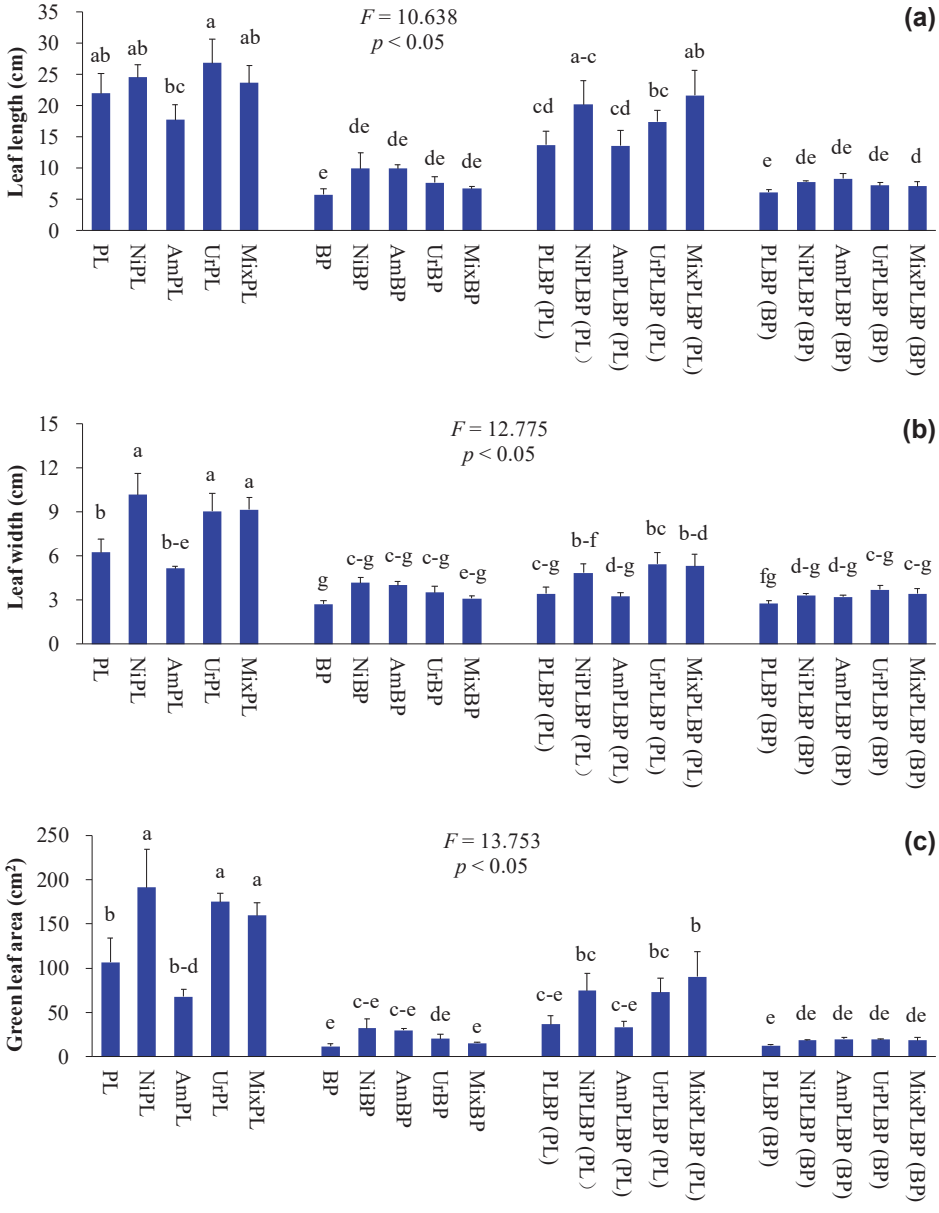

Figure 3. *Cont.*

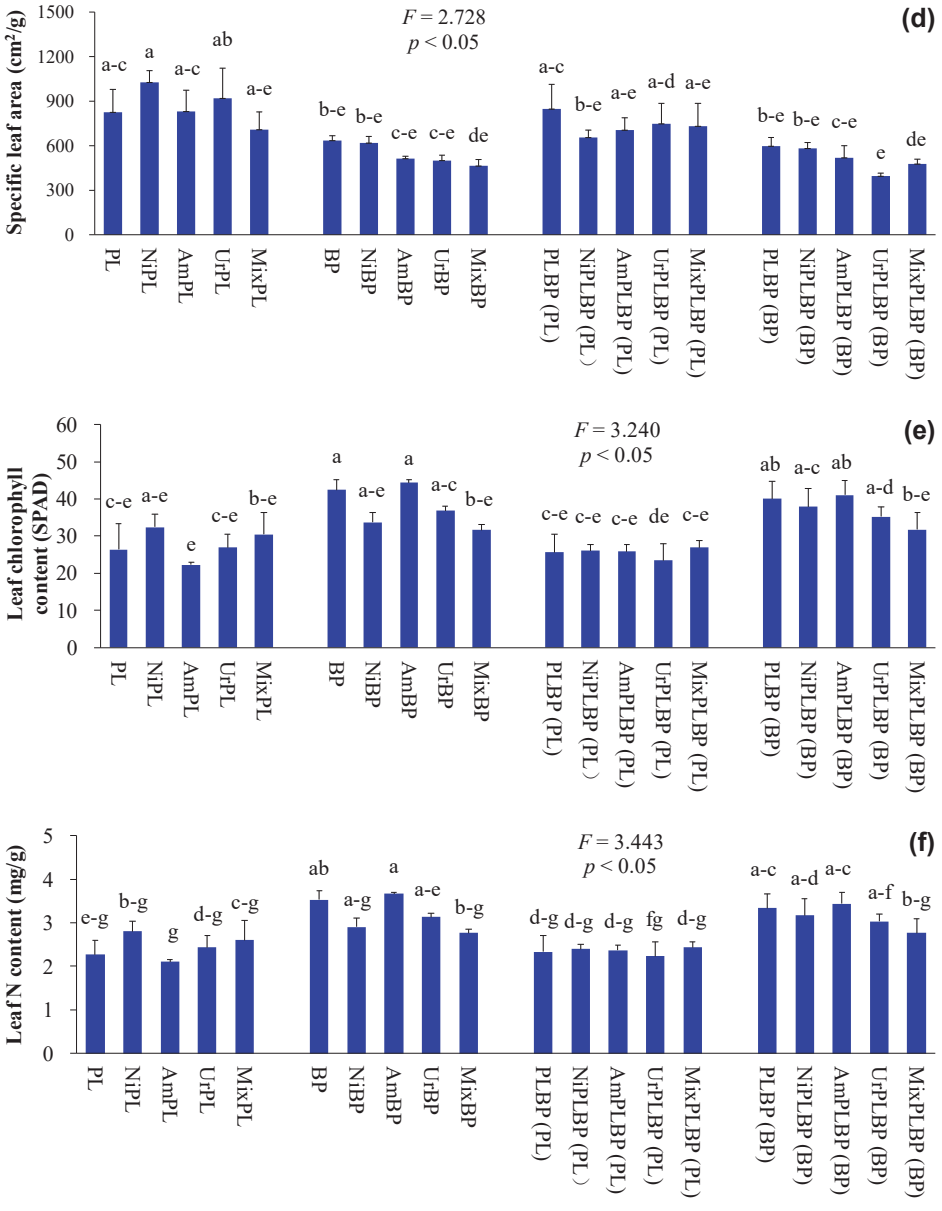

Figure 3. Leaf functional traits of *B. pilosa* and *P. laciniata* under monoculture and co-cultivation conditions, respectively ((**a**), leaf length; (**b**), leaf width; (**c**), green leaf area, (**d**), specific leaf area, (**e**), leaf chlorophyll content; (**f**), leaf N content). Bars (mean and standard error, $n = 3$) with different lowercase letters representing statistically significant differences ($p \leq 0.05$). Abbreviations have the same meanings as described in Figure 2.

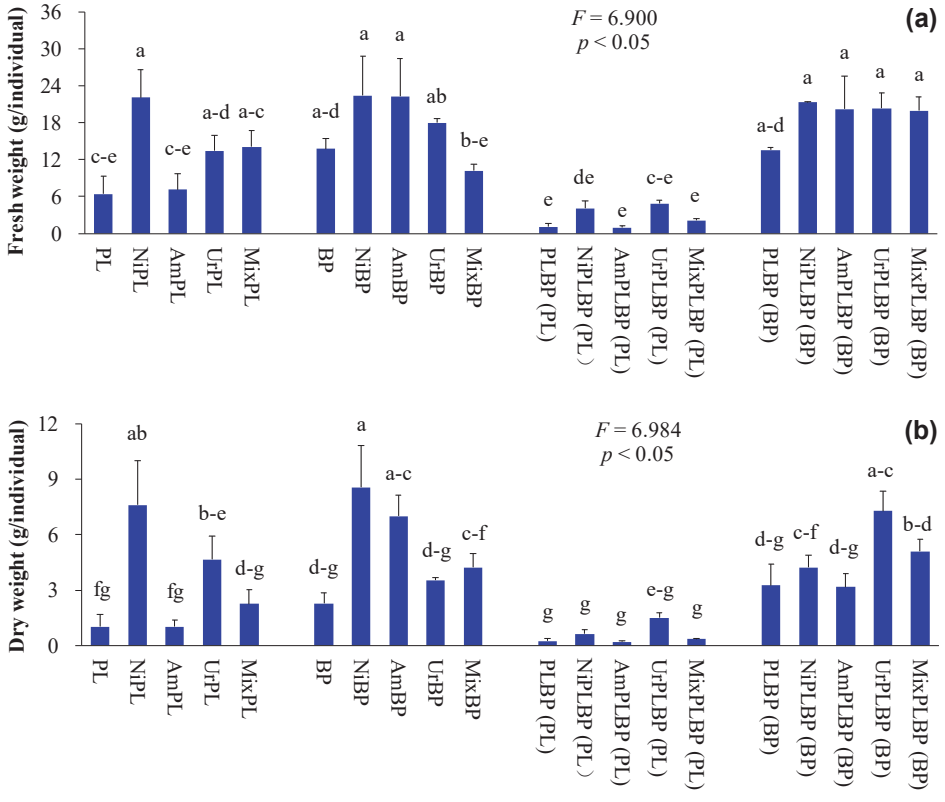

Figure 4. Biomass of *B. pilosa* and *P. laciniata* under monoculture and co-cultivation conditions, respectively ((**a**), fresh weight; (**b**), dry weight). Bars (mean and standard error, $n = 3$) with different lowercase letters representing statistically significant differences ($p \leq 0.05$). Abbreviations have the same meanings as described in Figure 2.

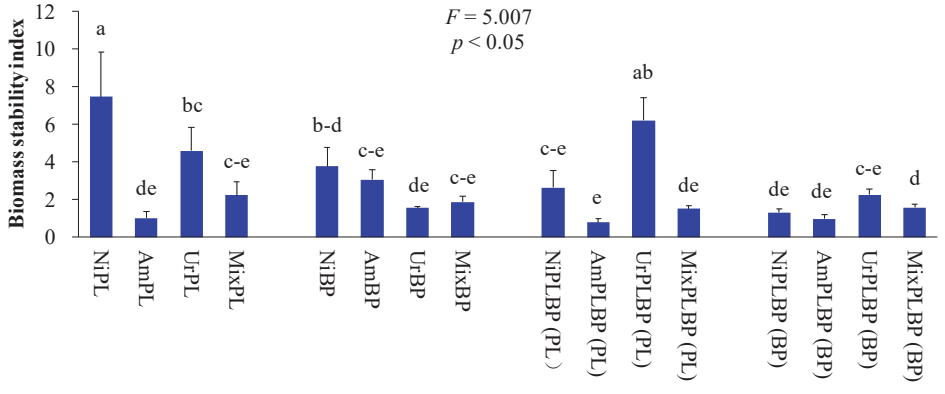

Figure 5. The biomass stability index of *B. pilosa* and *P. laciniata* under monoculture and co-cultivation conditions, respectively. Bars (mean and standard error, $n = 3$) with different lowercase letters representing statistically significant differences ($p \leq 0.05$). Abbreviations have the same meanings as described in Figure 2.

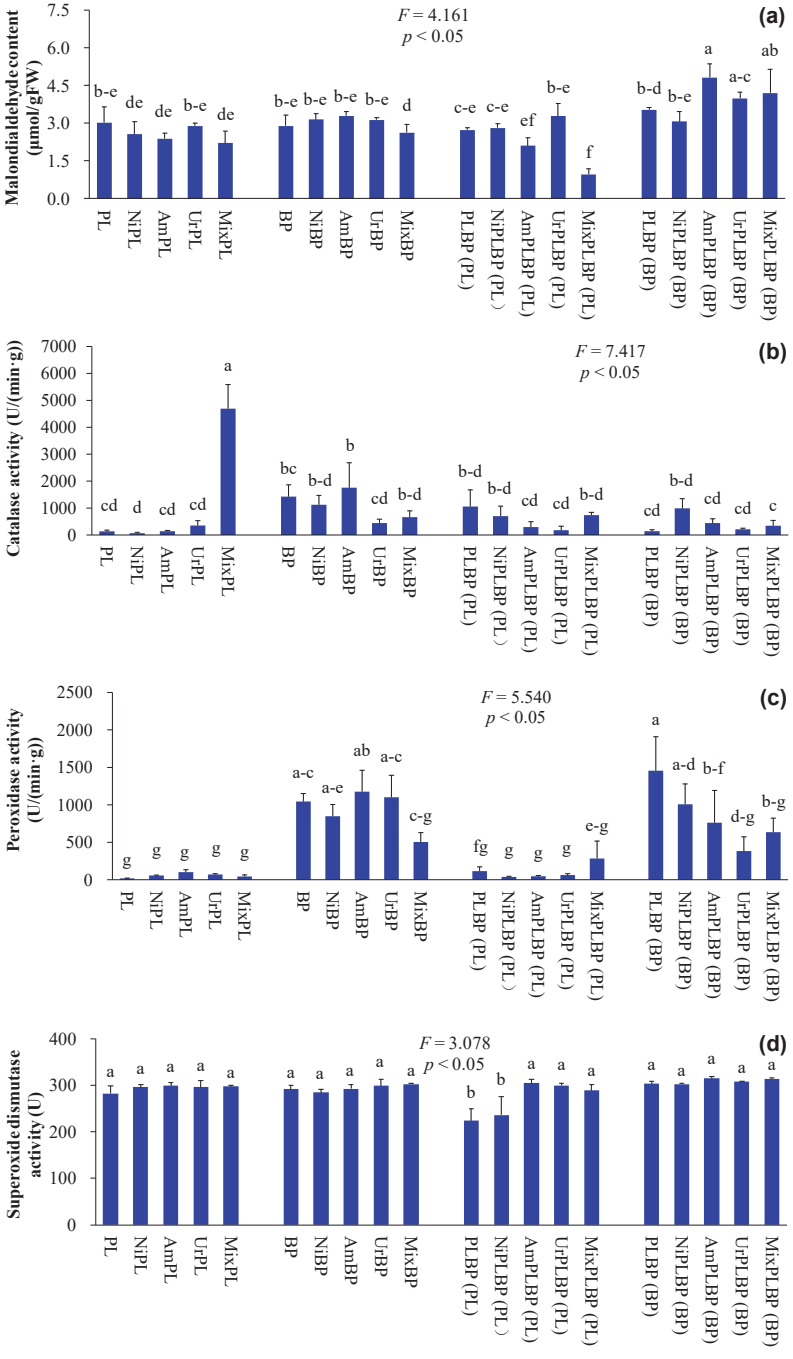

Figure 6. Biochemical constituents and osmolytes indices of *B. pilosa* and *P. laciniata* under monoculture and co-cultivation conditions, respectively ((**a**), malondialdehyde content; (**b**), catalase activity; (**c**), peroxidase activity; (**d**), superoxide dismutase activity). Bars (mean and standard error, $n = 3$) with different lowercase letters represent statistically significant differences ($p \leq 0.05$). Abbreviations have the same meanings as described in Figure 2.

As one of the essential nutrients required by plants, the application of exogenous N generally results in the enhanced growth performance of plants, attributed to the increased level of available N in soil. This is evidenced by numerous studies [68–71]. Similarly, the application of artificially simulated N deposition led to a significant increase in plant height, leaf width, and green leaf area of monocultural *P. laciniata* in the majority of cases ($p < 0.05$; Figures 2 and 3). Thus, the application of artificially simulated N deposition may be beneficial to the growth performance of monocultural *P. laciniata*, particularly in terms of the sunlight capture capacity and leaf photosynthetic area.

It can be generally observed that N acquisition and utilization capacity is a crucial factor in the success of IPs [22–25]. Hence, the application of exogenous N can facilitate the invasiveness of IPs. In this study, the values of the relative dominance index of *B. pilosa* (average value is ≈0.8995) was found to be obviously greater than 0.5 when exposed to artificially simulated N deposition containing different N components, especially when exposed to ammonium (the relative dominance index of *B. pilosa* is ≈0.9363) and mixed nitrogen (the relative dominance index of *B. pilosa* is ≈0.9328) (Figure 7). Consequently, *B. pilosa* demonstrated a more pronounced competitive advantage than *P. laciniata* under the application of artificially simulated N deposition containing different N components, especially when treated with ammonium and mixed N. Accordingly, artificially simulated N deposition, regardless of N component, may be conducive to the success of *P. laciniata*, especially under the deposition of ammonium and mixed N. This finding may be attributed to the fact that *B. pilosa* exhibits a proclivity for ammonium uptake and utilization. In particular, previous studies have demonstrated that other IPs also displays a preference for ammonium uptake and utilization over other N components [42,72–74]. It is noteworthy that the relative proportion of ammonium in atmospheric N deposition is increasing in certain countries and regions, including China [75–77] and the United States of America [78–80]. Accordingly, the augmented relative proportion of ammonium in atmospheric N deposition may further facilitate the colonization of *B. pilosa* via a more pronounced competitive advantage.

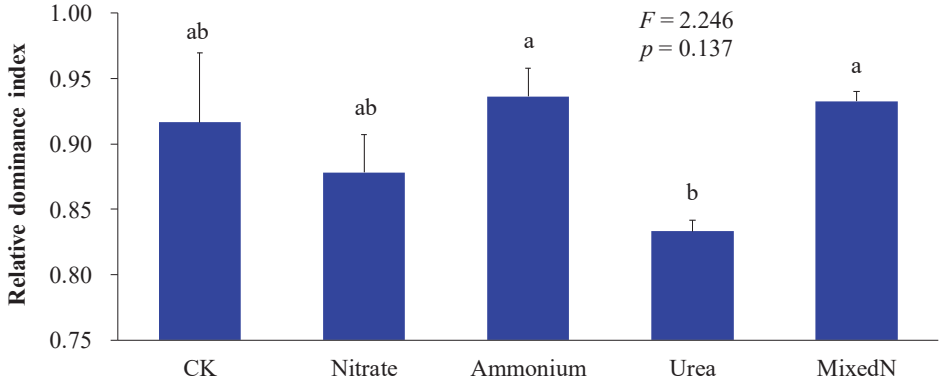

Figure 7. The relative dominance index of *B. pilosa* under co-cultivation condition. Bars (mean and standard error, $n = 3$) with different lowercase letters represent statistically significant differences ($p \leq 0.05$). Abbreviations have the same meanings as described in Figure 2.

In essence, there is a pressing need to impede or even halt the colonization of *B. pilosa*, especially under co-cultivation conditions and when exposed to atmospheric N deposition, particularly when there is an increase in the relative proportion of ammonium in atmospheric N deposition. The findings of this study also provide a substantial practical basis for the environmental management of IPs, including effective early warning prevention and control of IPs, especially when exposed to atmospheric N deposition. In particular, it is of great importance to reduce the level of atmospheric N deposition, in particular

the proportion of ammonium, via the alterations in energy policy and the composition of energy sources employed. This is to minimize the competitive advantage of *B. pilosa* under atmospheric N deposition, especially with an increase in the relative proportion of ammonium in atmospheric N deposition.

4. Conclusions

In conclusion, this study aims to elucidate the functional differences between *B. pilosa* and *P. laciniata* in the context of atmospheric N deposition containing different N components. The principal findings are as follows: (1) The sunlight capture capacity, plant supporting capacity, leaf photosynthetic area, and plant growth competitiveness of co-cultivated *P. laciniata* were found to be significantly lower than those of monocultural *P. laciniata*. (2) The sunlight capture capacity, leaf photosynthetic capacity, and enzymatic defense capacity under stress to oxidative stress of *B. pilosa* were meaningfully greater than those of *P. laciniata* under both monoculture and co-cultivation conditions. (3) The results of the artificially simulated N deposition demonstrated a significant increase in plant height, leaf width, and green leaf area of monocultural *P. laciniata* in the majority of cases. (4) The values of the relative dominance index of *B. pilosa* were found to be significantly greater than 0.5 in response to artificially simulated N deposition containing different N components, especially when exposed to ammonium and mixed N. In summary, atmospheric N deposition, especially the increased relative proportion of ammonium in atmospheric N deposition, may facilitate the colonization of *B. pilosa* via a stronger competitive advantage.

Supplementary Materials: The following supporting information can be downloaded at: https://www.mdpi.com/article/10.3390/atmos15070825/s1, Table S1 [81–96]: The ecological significances, determination methods, and the corresponding references for the determined indices; Table S2: Two-way ANOVA on the effects of plant species and nitrogen component on the functional indices, biochemical constituents, and osmolytes indices of *B. pilosa* and *P. laciniata*. *p* values equal to or less than 0.05 are shown in bold; Figure S1: *Bidens pilosa* L.; Figure S2: *Pterocypsela laciniata* (Houtt.) Shih; Figure S3: The geographical location (Zhenjiang, Jiangsu, China) of the sampling area (square with red) in this study (Map number: GS(2022)4317; produced by the Ministry of Natural Resources of China; http://bzdt.ch.mnr.gov.cn/ (accessed on 6 June 2024)); Figure S4: The picture of some of the garden pots used in this study.

Author Contributions: C.L.: data curation; investigation; methodology; writing—review and editing; Y.L. (Yue Li): data curation; investigation; methodology; writing—review and editing; Y.L. (Yingsheng Liu): data curation; investigation; methodology; writing—review and editing; S.Z.: data curation; investigation; methodology; writing—review and editing; H.Z.: funding acquisition; project administration; writing—review and editing; Z.X. (Zhelun Xu): data curation; investigation; methodology; writing—review and editing; Z.X. (Zhongyi Xu): data curation; formal analysis; writing—review and editing; D.D.: funding acquisition; project administration; writing—review and editing; C.W.: conceptualization; formal analysis; funding acquisition; project administration; supervision; writing—original draft. All authors have read and agreed to the published version of the manuscript.

Funding: This study was funded by Scientific Research Start-up Fund for High-level Talents of Jinling Institute of Technology (jit-rcyj-202302), Open Science Research Fund of Key Laboratory of Forest Plant Ecology, Ministry of Education (Northeast Forestry University), China (K2020B02), Special Research Project of School of Emergency Management, Jiangsu University (KY-C-01), National Natural Science Foundation of China (32071521), Research project on the application of invasive plants in soil ecological restoration in Jiangsu (20240110), Carbon Peak and Carbon Neutrality Technology Innovation Foundation of Jiangsu Province (BK20220030), and Jiangsu Collaborative Innovation Center of Technology and Material of Water Treatment (no grant number).

Institutional Review Board Statement: Not applicable.

Informed Consent Statement: Informed consent was obtained from all subjects involved in the study.

Data Availability Statement: All data generated or analyzed during this study are included in this article.

Acknowledgments: We greatly appreciate the anonymous reviewers for the insightful comments that greatly improved this manuscript.

Conflicts of Interest: The authors declare no conflicts of interest.

Abbreviations

IPs	invasive plants
N	nitrogen
PL	monocultural *P. laciniata*
NiPL	monocultural *P. laciniata* treated with nitrate
AmPL	monocultural *P. laciniata* treated with ammonium
UrPL	monocultural *P. laciniata* treated with urea
MixPL	monocultural *P. laciniata* treated with mixed N
BP	monocultural *B. pilosa*
NiBP	monocultural *B. pilosa* treated with nitrate
AmBP	monocultural *B. pilosa* treated with ammonium
UrBP	monocultural *B. pilosa* treated with urea
MixBP	monocultural *B. pilosa* treated with mixed N
PLBP(PL)	co-cultivated *P. laciniata*
NiPLBP(PL)	co-cultivated *P. laciniata* treated with nitrate
AmPLBP(PL)	co-cultivated *P. laciniata* treated with ammonium
UrPLBP(PL)	co-cultivated *P. laciniata* treated with urea
MixPLBP(PL)	co-cultivated *P. laciniata* treated with mixed N
PLBP(BP)	co-cultivated *B. pilosa*
NiPLBP(BP)	co-cultivated *B. pilosa* treated with nitrate
AmPLBP(BP)	co-cultivated *B. pilosa* treated with ammonium
UrPLBP(BP)	co-cultivated *B. pilosa* treated with urea
Mix AmPLBP(BP)	co-cultivated *B. pilosa* treated with mixed N

References

1. Beshai, R.A.; Truong, D.A.; Henry, A.K.; Sorte, C.J.B. Biotic resistance or invasional meltdown? Diversity reduces invasibility but not exotic dominance in southern *California epibenthic* communities. *Biol. Invasions* **2023**, *25*, 533–549. [CrossRef]
2. Sharma, A.; Kaur, A.; Kohli, R.K.; Singh, H.P.; Batish, D.R. *Bidens pilosa* (Asteraceae) invasion reshapes the pattern of plant communities and edaphic properties across the north-western Himalayan landscape. *Ecol. Inform.* **2023**, *77*, 102281. [CrossRef]
3. Savage, C.; Savage, K.; Keller, K.R. Effect of *Carpobrotus edulis* invasion history on plant communities. *West. N. Am. Nat.* **2023**, *83*, 484–497. [CrossRef]
4. Ettinger, C.L.; LaForgia, M.L. Invasive plant species interact with drought to shift key functions and families in the native rhizosphere. *Plant Soil* **2024**, *494*, 567–588. [CrossRef]
5. Yan, X.L.; Liu, Q.R.; Shou, H.Y.; Zeng, X.F.; Zhang, Y.; Chen, L.; Liu, Y.; Ma, H.Y.; Qi, S.Y.; Ma, J.S. The categorization and analysis on the geographic distribution patterns of Chinese alien invasive plants. *Biodivers. Sci.* **2014**, *22*, 667–676.
6. Wang, C.Y.; Liu, J.; Xiao, H.G.; Zhou, J.W.; Du, D.L. Floristic characteristics of alien invasive seed plant species in China. *An. Acad. Bras. Ciênc.* **2016**, *88*, 1791–1797. [CrossRef] [PubMed]
7. Brandt, A.J.; Png, G.K.; Jo, I.; McGrannachan, C.; Allen, K.; Peltzer, D.A.; D'Antonio, C.; Dickie, I.A.; French, K.; Leishman, M.R.; et al. Managing multi-species plant invasions when interactions influence their impact. *Front. Ecol. Environ.* **2023**, *21*, 370–379. [CrossRef]
8. Guo, X.; Ma, J.Y.; Liu, L.L.; Li, M.Y.; Wang, H.; Sun, Y.K.; Wang, T.; Wang, K.L.; Meyerson, L.A. Effects of salt stress on interspecific competition between an invasive alien plant *Oenothera biennis* and three native species. *Front. Plant Sci.* **2023**, *14*, 1144511. [CrossRef] [PubMed]
9. Ahmad Dar, M.; Ahmad, M.; Singh, R.; Kumar Kohli, R.; Singh, H.P.; Batish, D.R. Invasive plants alter soil properties and nutrient dynamics: A case study of *Anthemis cotula* invasion in Kashmir Himalaya. *Catena* **2023**, *226*, 107069. [CrossRef]
10. Minden, V.; Verhoeven, K.; Olde Venterink, H. Adaptive plasticity and fitness costs of endangered, nonendangered, and invasive plants in response to variation in nitrogen and phosphorus availabilities. *Ecol. Evol.* **2023**, *13*, e10075. [CrossRef]
11. Khatri, K.; Negi, B.; Bargali, K.; Bargali, S.S. Trait variability in co-occurring invasive and native plant species in road side population of Kumaun Himalaya. *Braz. J. Bot.* **2022**, *45*, 1099–1110. [CrossRef]
12. Petruzzellis, F.; Tordoni, E.; Tomasella, M.; Savi, T.; Tonet, V.; Palandrani, C.; Castello, M.; Nardini, A.; Bacaro, G. Functional differentiation of invasive and native plants along a leaf efficiency/safety trade-off. *Environ. Exp. Bot.* **2021**, *188*, 104518. [CrossRef]

13. Kumar, M.; Garkoti, S.C. Functional traits, growth patterns, and litter dynamics of invasive alien and co-occurring native shrub species of chir pine forest in the central Himalaya, India. *Plant Ecol.* **2021**, *222*, 723–735. [CrossRef]
14. Hibit, J.; Daehler, C.C. Plant functional, biogeographical and phylogenetic diversity are related to native and non-native plant abundance in invaded Hawaiian forests. *Biol. Invasions* **2024**, *26*, 705–717. [CrossRef]
15. Grotkopp, E.; Erskine-Ogden, J.; Rejmánek, M. Assessing potential invasiveness of woody horticultural plant species using seedling growth rate traits. *J. Appl. Ecol.* **2010**, *47*, 1320–1328. [CrossRef]
16. Yu, Y.L.; Cheng, H.Y.; Wang, S.; Wei, M.; Wang, C.Y.; Du, D.L. Drought may be beneficial to the competitive advantage of *Amaranthus spinosus*. *J. Plant Ecol.* **2022**, *15*, 494–508. [CrossRef]
17. Lenda, M.; Steudel, B.; Skórka, P.; Zagrodzka, Z.B.; Moroń, D.; Bączek-Kwinta, R.; Janowiak, F.; Baran, A.; Possingham, H.P.; Knops, J.M.H. Multiple invasive species affect germination, growth, and photosynthesis of native weeds and crops in experiments. *Sci. Rep.* **2023**, *13*, 22146. [CrossRef]
18. Kuypers, M.M.M.; Marchant, H.K.; Kartal, B. The microbial nitrogen-cycling network. *Nat. Rev. Microbiol.* **2018**, *16*, 263–276. [CrossRef] [PubMed]
19. Yu, H.X.; Le Roux, J.J.; Jiang, Z.Y.; Sun, F.; Peng, C.L.; Li, W.H. Soil nitrogen dynamics and competition during plant invasion: Insights from *Mikania micrantha* invasions in China. *New Phytol.* **2021**, *229*, 3440–3452. [CrossRef]
20. Francis, C.A.; Beman, J.M.; Kuypers, M.M.M. New processes and players in the nitrogen cycle: The microbial ecology of anaerobic and archaeal ammonia oxidation. *ISME J.* **2007**, *1*, 19–27. [CrossRef]
21. van den Elzen, E.; van den Berg, L.J.L.; van der Weijden, B.; Fritz, C.; Sheppard, L.J.; Lamers, L.P.M. Effects of airborne ammonium and nitrate pollution strongly differ in peat bogs, but symbiotic nitrogen fixation remains unaffected. *Sci. Total Environ.* **2018**, *610–611*, 732–740. [CrossRef] [PubMed]
22. Geng, X.Y.; Jiang, S.; Li, B.; Pan, X.Y. Higher resource capture ability and utilization efficiency facilitate the successful invasion of exotic plant? A case study of *Alternanthera philoxeroides*. *Am. J. Plant Sci.* **2013**, *4*, 1839–1845. [CrossRef]
23. Osunkoya, O.O.; Bayliss, D.; Panetta, F.D.; Vivian-Smith, G. Leaf trait co-ordination in relation to construction cost, carbon gain and resource-use efficiency in exotic invasive and native woody vine species. *Ann. Bot.* **2010**, *106*, 371–380. [CrossRef] [PubMed]
24. Feng, Y.L.; Lei, Y.B.; Wang, R.F.; Callaway, R.M.; Alfonso, V.B.; Inderjit; Li, Y.P.; Zheng, Y.L. Evolutionary tradeoffs for nitrogen allocation to photosynthesis versus cell walls in an invasive plant. *Proc. Natl. Acad. Sci. USA* **2009**, *106*, 1853–1856. [CrossRef] [PubMed]
25. Li, Q.W.; Zhang, X.Y.; Liang, J.F.; Gao, J.Q.; Xu, X.L.; Yu, F.H. High nitrogen uptake and utilization contribute to the dominance of invasive *Spartina alterniflora* over native *Phragmites australis*. *Biol. Fertil. Soils* **2021**, *57*, 1007–1013. [CrossRef]
26. Davidson, A.M.; Jennions, M.; Nicotra, A.B. Do invasive species show higher phenotypic plasticity than native species and, if so, is it adaptive? A meta-analysis. *Ecol. Lett.* **2011**, *14*, 419–431. [CrossRef] [PubMed]
27. Kamutando, C.N.; Vikram, S.; Kamgan-Nkuekam, G.; Makhalanyane, T.P.; Greve, M.; Le Roux, J.J.; Richardson, D.M.; Cowan, D.; Valverde, A. Soil nutritional status and biogeography influence rhizosphere microbial communities associated with the invasive tree *Acacia dealbata*. *Sci. Rep.* **2017**, *7*, 6472. [CrossRef] [PubMed]
28. Xu, C.W.; Yang, M.Z.; Chen, Y.J.; Chen, L.M.; Zhang, D.Z.; Mei, L.; Shi, Y.T.; Zhang, H.B. Changes in non-symbiotic nitrogen-fixing bacteria inhabiting rhizosphere soils of an invasive plant *Ageratina adenophora*. *Appl. Soil Ecol.* **2012**, *54*, 32–38. [CrossRef]
29. Li, J.; He, J.Z.; Liu, M.; Yan, Z.Q.; Xu, X.L.; Kuzyakov, Y. Invasive plant competitivity is mediated by nitrogen use strategies and rhizosphere microbiome. *Soil Biol. Biochem.* **2024**, *192*, 109361. [CrossRef]
30. Chen, H.Y.; Huang, S.Z. Composition and supply of inorganic and organic nitrogen species in dry and wet atmospheric deposition: Use of organic nitrogen composition to calculate the Ocean's external nitrogen flux from the atmosphere. *Cont. Shelf Res.* **2021**, *213*, 104316. [CrossRef]
31. Yang, Y.; Liu, L.; Zhang, F.; Zhang, X.; Xu, W.; Liu, X.; Li, Y.; Wang, Z.; Xie, Y. Enhanced nitrous oxide emissions caused by atmospheric nitrogen deposition in agroecosystems over China. *Environ. Sci. Pollut. Res.* **2021**, *28*, 15350–15360. [CrossRef] [PubMed]
32. Yang, Y.; Liu, L.; Zhang, F.; Zhang, X.; Xu, W.; Liu, X.; Wang, Z.; Xie, Y. Soil Nitrous Oxide Emissions by Atmospheric Nitrogen Deposition over Global Agricultural Systems. *Environ. Sci. Technol.* **2021**, *55*, 4420–4429. [CrossRef] [PubMed]
33. Dentener, F.; Drevet, J.; Lamarque, J.F.; Bey, I.; Eickhout, B.; Fiore, A.M.; Hauglustaine, D.; Horowitz, L.W.; Krol, M.; Kulshrestha, U.C.; et al. Nitrogen and sulfur deposition on regional and global scales: A multimodel evaluation. *Glob. Biogeochem. Cycles* **2006**, *20*, GB4003. [CrossRef]
34. Fu, Y.D.; Xu, W.; Wen, Z.; Han, M.J.; Sun, J.H.; Tang, A.H.; Liu, X. Enhanced atmospheric nitrogen deposition at a rural site in northwest China from 2011 to 2018. *Atmos. Res.* **2020**, *245*, 105071. [CrossRef]
35. Zhu, J.X.; Chen, Z.; Wang, Q.F.; Xu, L.; He, N.P.; Jia, Y.L.; Zhang, Q.Y.; Yu, G.R. Potential transition in the effects of atmospheric nitrogen deposition in China. *Environ. Pollut.* **2020**, *258*, 113739. [CrossRef] [PubMed]
36. Xu, W.; Zhang, L.; Liu, X.J. A database of atmospheric nitrogen concentration and deposition from the nationwide monitoring network in China. *Sci. Data* **2019**, *6*, 51. [CrossRef] [PubMed]
37. Holland, E.A.; Braswell, B.H.; Sulzman, J.; Lamarque, J.F. Nitrogen deposition onto the United States and Western Europe: Synthesis of observations and models. *Ecol. Appl.* **2005**, *15*, 38–57. [CrossRef]
38. Vishwakarma, S.; Zhang, X.; Dobermann, A.; Heffer, P.; Zhou, F. Global nitrogen deposition inputs to cropland at national scale from 1961 to 2020. *Sci. Data* **2023**, *10*, 488. [CrossRef] [PubMed]

39. White, C.; Ussher, S.J.; Fitzsimons, M.F.; Atkinson, S.; Woodward, E.M.S.; Yang, M.; Bell, T.G. Inorganic nitrogen and phosphorus in Western European aerosol and the significance of dry deposition flux into stratified shelf waters. *Atmos. Environ.* **2021**, *261*, 118391. [CrossRef]
40. Ren, G.Q.; Yang, B.; Cui, M.M.; Dai, Z.C.; Xiang, Y.; Zhang, H.Y.; Li, G.L.; Li, J.; Javed, Q.; Du, D.L. Warming and elevated nitrogen deposition accelerate the invasion process of *Solidago canadensis* L. *Ecol. Process.* **2022**, *11*, 62. [CrossRef]
41. Ding, W.L.; Xu, W.Z.; Gao, Z.J.; Xu, B.C. Effects of water and nitrogen on growth and relative competitive ability of introduced versus native C-4 grass species in the semi-arid Loess Plateau of China. *J. Arid Land* **2021**, *13*, 730–743. [CrossRef]
42. Zhong, S.S.; Xu, Z.L.; Yu, Y.L.; Liu, J.; Wang, Y.Y.; Guo, E.; Wang, C.Y. *Rhus typhina* decreased soil nitrogen contents and peroxidase activity following the addition of nitrogen. *Int. J. Environ. Sci. Technol.* **2023**, *111*, 17–22. [CrossRef]
43. Sparrius, L.B.; Kooijman, A.M. Invasiveness of *Campylopus introflexus* in drift sands depends on nitrogen deposition and soil organic matter. *Appl. Veg. Sci.* **2011**, *14*, 221–229. [CrossRef]
44. Mircea, D.M.; Calone, R.; Estrelles, E.; Soriano, P.; Sestras, R.E.; Boscaiu, M.; Sestras, A.F.; Vicente, O. Responses of different invasive and non-invasive ornamental plants to water stress during seed germination and vegetative growth. *Sci. Rep.* **2023**, *13*, 13281. [CrossRef] [PubMed]
45. Gao, F.L.; He, Q.S.; Xie, R.Q.; Hou, J.H.; Shi, C.L.; Li, J.M.; Yu, F.H. Interactive effects of nutrient availability, fluctuating supply, and plant parasitism on the post-invasion success of *Bidens pilosa*. *Biol. Invasions* **2021**, *23*, 3035–3046. [CrossRef]
46. Li, C.; Li, Y.; Zhong, S.S.; Xu, Z.L.; Xu, Z.Y.; Zhu, M.W.; Wei, Y.Q.; Wang, C.Y.; Du, D.L. Do the leaves of multiple invasive plants decompose more easily than a native plant's under nitrogen deposition with different forms? *Nitrogen* **2024**, *5*, 202–218. [CrossRef]
47. Zhejiang Provincial Bureau of Statistics. *Zhenjiang Statistical Yearbook 2022*; China Statistics Press: Beijing, China, 2022.
48. Luo, X.S.; Liu, X.J.; Pan, Y.P.; Wen, Z.; Xu, W.; Zhang, L.; Kou, C.L.; Lv, J.L.; Goulding, K. Atmospheric reactive nitrogen concentration and deposition trends from 2011 to 2018 at an urban site in north China. *Atmos. Environ.* **2020**, *224*, 117298. [CrossRef]
49. Zhang, Y.; Song, L.; Liu, X.J.; Li, W.Q.; Lu, S.H.; Zheng, L.X.; Bai, Z.C.; Cai, G.Y.; Zhang, F.S. Atmospheric organic nitrogen deposition in China. *Atmos. Environ.* **2012**, *49*, 422. [CrossRef]
50. Cornell, S.E. Atmospheric nitrogen deposition: Revisiting the question of the importance of the organic component. *Environ. Pollut.* **2011**, *159*, 2214–2222. [CrossRef] [PubMed]
51. Cornell, S.E.; Jickells, T.D.; Cape, J.N.; Rowland, A.P.; Duce, R.A. Organic nitrogen deposition on land and coastal environments: A review of methods and data. *Atmos. Environ.* **2003**, *37*, 2173–2191. [CrossRef]
52. Galloway, J.N.; Townsend, A.R.; Erisman, J.W.; Bekunda, M.; Cai, Z.; Freney, J.R.; Martinelli, L.A.; Seitzinger, S.P.; Sutton, M.A. Transformation of the nitrogen cycle: Recent trends, questions, and potential solutions. *Science* **2008**, *320*, 889–892. [CrossRef] [PubMed]
53. Wu, B.D.; Zhang, H.S.; Jiang, K.; Zhou, J.W.; Wang, C.Y. *Erigeron canadensis* affects the taxonomic and functional diversity of plant communities in two climate zones in the North of China. *Ecol. Res.* **2019**, *34*, 535–547. [CrossRef]
54. Wang, C.Y.; Cheng, H.Y.; Wu, B.D.; Jiang, K.; Wang, S.; Wei, M.; Du, D.L. The functional diversity of native ecosystems increases during the major invasion by the invasive alien species, *Conyza canadensis*. *Ecol. Eng.* **2021**, *159*, 106093. [CrossRef]
55. Wang, C.Y.; Wu, B.D.; Jiang, K.; Zhou, J.W. Differences in functional traits between invasive and native *Amaranthus* species under simulated acid deposition with a gradient of pH levels. *Acta Oecol.* **2018**, *89*, 32–37. [CrossRef]
56. Li, Y.; Li, C.; Zhong, S.S.; Xu, Z.L.; Liu, J.; Xu, Z.Y.; Zhu, M.W.; Wang, C.Y.; Du, D.L. Is the invasive plant *Amaranthus spinosus* L. more competitive than the native Plant *A. tricolor* L. when exposed to acid deposition with different sulfur-nitrogen ratios? *Atmosphere* **2024**, *15*, 29. [CrossRef]
57. Ordonez, A.; Wright, I.J.; Olff, H. Functional differences between native and alien species: A global-scale comparison. *Funct. Ecol.* **2010**, *24*, 1353–1361. [CrossRef]
58. Maire, V.; Gross, N.; Boerger, L.; Proulx, R.; Wirth, C.; Pontes, L.d.S.; Soussana, J.-F.; Louault, F. Habitat filtering and niche differentiation jointly explain species relative abundance within grassland communities along fertility and disturbance gradients. *New Phytol.* **2012**, *196*, 497–509. [CrossRef] [PubMed]
59. Gross, N.; Boerger, L.; Duncan, R.P.; Hulme, P.E. Functional differences between alien and native species: Do biotic interactions determine the functional structure of highly invaded grasslands? *Funct. Ecol.* **2013**, *27*, 1262–1272. [CrossRef]
60. Silveira, S.D.; Guimaraes, M. The enemy within: Consequences of the invasive bullfrog on native anuran populations. *Biol. Invasions* **2021**, *23*, 373–378. [CrossRef]
61. Pinto-Ledezma, J.N.; Villalobos, F.; Reich, P.B.; Catford, J.A.; Larkin, D.J.; Cavender-Bares, J. Testing Darwin's naturalization conundrum based on taxonomic, phylogenetic, and functional dimensions of vascular plants. *Ecol. Monogr.* **2020**, *90*, e01420. [CrossRef]
62. Thuiller, W.; Gallien, L.; Boulangeat, I.; De Bello, F.; Münkemüller, T.; Roquet, C.; Lavergne, S. Resolving Darwin's naturalization conundrum: A quest for evidence. *Divers. Distrib.* **2010**, *16*, 461–475. [CrossRef]
63. Fan, S.Y.; Yang, Q.; Li, S.P.; Fristoe, T.S.; Cadotte, M.W.; Essl, F.; Kreft, H.; Pergl, J.; Pyšek, P.; Weigelt, P.; et al. A latitudinal gradient in Darwin's naturalization conundrum at the global scale for flowering plants. *Nat. Commun.* **2023**, *14*, 6244. [CrossRef]
64. Omer, A.; Fristoe, T.; Yang, Q.; Razanajatovo, M.; Weigelt, P.; Kreft, H.; Dawson, W.; Dullinger, S.; Essl, F.; Pergl, J.; et al. The role of phylogenetic relatedness on alien plant success depends on the stage of invasion. *Nat. Plants* **2022**, *8*, 906–914. [CrossRef]

65. Richards, C.L.; Bossdorf, O.; Muth, N.Z.; Gurevitch, J.; Pigliucci, M. Jack of all trades, master of some? On the role of phenotypic plasticity in plant invasions. *Ecol. Lett.* **2006**, *9*, 981–993. [CrossRef]
66. Funk, J.L. Differences in plasticity between invasive and native plants from a low resource environment. *J. Ecol.* **2008**, *96*, 1162–1173. [CrossRef]
67. Matzek, V. Trait values, not trait plasticity, best explain invasive species' performance in a changing environment. *PLoS ONE* **2012**, *7*, e48821. [CrossRef] [PubMed]
68. Amanullah; Marwat, K.B.; Shah, P.; Maula, N.; Arifullah, S. Nitrogen levels and its time of application influence leaf area, height and biomass of maize planted at low and high density. *Pak. J. Bot.* **2009**, *41*, 761–768.
69. Cheng, H.Y.; Wei, M.; Wang, S.; Wu, B.D.; Wang, C.Y. Atmospheric N deposition alleviates the unfavorable effects of drought on wheat growth. *Braz. J. Bot.* **2020**, *43*, 229–238. [CrossRef]
70. Bai, T.; Liu, Y.Y.; Muhammad, I.; Yang, X.; Yin, X.J.; Bai, L.; Wang, Y.J. Mixed nitrogen form addition facilitates the growth adaptation of legume plant to heavy metal contamination in degraded mining areas. *Glob. Ecol. Conserv.* **2020**, *24*, e01387. [CrossRef]
71. Villar-Salvador, P.; Peñuelas, J.L.; Nicolás-Peragón, J.L.; Benito, L.F.; Domínguez-Lerena, S. Is nitrogen fertilization in the nursery a suitable tool for enhancing the performance of Mediterranean oak plantations? *New For.* **2013**, *44*, 733–751. [CrossRef]
72. Huang, Q.Q.; Xu, H.; Fan, Z.W.; Hou, Y.P. Effects of *Rhus typhina* invasion into young *Pinus thunbergii* forests on soil chemical properties. *Ecol. Environ. Sci.* **2013**, *22*, 1119–1123.
73. Hou, Y.P.; Liu, L.; Chu, H.; Ma, S.J.; Zhao, D.; Liang, R.R. Effects of exotic plant *Rhus typhina* invasion on soil properties in different forest types. *Acta Ecol. Sin.* **2015**, *35*, 5324–5330.
74. Huangfu, C.H.; Li, H.Y.; Chen, X.W.; Liu, H.M.; Wang, H.; Yang, D.L. Response of an invasive plant, *Flaveria bidentis*, to nitrogen addition: A test of form-preference uptake. *Biol. Invasions* **2016**, *18*, 3365–3380. [CrossRef]
75. Chen, S.L.; Chen, B.; Wang, S.Q.; Sun, L.G.; Shi, H.; Liu, Z.H.; Wang, Q.Y.; Li, H.; Zhu, T.T.; Li, D.H.; et al. Spatiotemporal variations of atmospheric nitrogen deposition in China during 2008–2020. *Atmos. Environ.* **2023**, *315*, 120120. [CrossRef]
76. Dong, J.; Li, B.; Li, Y.; Zhou, R.; Gan, C.; Zhao, Y.; Liu, R.; Yang, Y.; Wang, T.; Liao, H. Atmospheric ammonia in China: Long-term spatiotemporal variation, urban-rural gradient, and influencing factors. *Sci. Total Environ.* **2023**, *883*, 163733. [CrossRef] [PubMed]
77. Xue, J.; Xing, C.; Li, Q.; Wang, S.; Hu, Q.; Zhu, Y.; Liu, T.; Zhang, C.; Liu, C. Long-term spatiotemporal variations of ammonia in the Yangtze River Delta region of China and its driving factors. *J. Environ. Sci.* **2025**, *150*, 202–217. [CrossRef]
78. Gilliam, F.S.; Burns, D.A.; Driscoll, C.T.; Frey, S.D.; Lovett, G.M.; Watmough, S.A. Decreased atmospheric nitrogen deposition in eastern North America: Predicted responses of forest ecosystems. *Environ. Pollut.* **2019**, *244*, 560–574. [CrossRef]
79. Conrad-Rooney, E.; Gewirtzman, J.; Pappas, Y.; Pasquarella, V.J.; Hutyra, L.R.; Templer, P.H. Atmospheric wet deposition in urban and suburban sites across the United States. *Atmos. Environ.* **2023**, *305*, 119783. [CrossRef]
80. Johansen, A.M.; Duncan, C.; Reddy, A.; Swain, N.; Sorey, M.; Nieber, A.; Agren, J.; Lenington, M.; Bolstad, D.; Samora, B.; et al. Precipitation chemistry and deposition at a high-elevation site in the Pacific Northwest United States (1989–2015). *Atmos. Environ.* **2019**, *212*, 221–230. [CrossRef]
81. Wang, S.; Wei, M.; Cheng, H.Y.; Wu, B.D.; Du, D.L.; Wang, C.Y. Indigenous plant species and invasive alien species tend to diverge functionally under heavy metal pollution and drought stress. *Ecotox. Environ. Safe.* **2020**, *205*, 111160. [CrossRef]
82. Jiang, K.; Wu, B.D.; Wang, C.Y.; Ran, Q. Ecotoxicological effects of metals with different concentrations and types on the morphological and physiological performance of wheat. *Ecotox. Environ. Safe.* **2019**, *167*, 345–353. [CrossRef] [PubMed]
83. Rybiński, W.; Garczyński, S. Influence of laser light on leaf area and parameters of photosynthetic activity in DH lines of spring barley (*Hordeum vulgare* L.). *Int. Agrophys.* **2004**, *18*, 261–267.
84. Xia, T.T.; Miao, Y.X.; Wu, D.L.; Shao, H.; Khosla, R.; Mi, G.H. Active optical sensing of spring maize for in-season diagnosis of nitrogen status based on nitrogen nutrition index. *Remote Sens.* **2016**, *8*, 605. [CrossRef]
85. Huang, S.S.; Sun, L.Q.; Hu, X.; Wang, Y.H.; Zhang, Y.J.; Nevo, E.; Peng, J.H.; Sun, D.F. Associations of canopy leaf traits with SNP markers in durum wheat (*Triticum turgidum* L. durum (Desf.)). *PLoS ONE* **2018**, *13*, e0206226. [CrossRef] [PubMed]
86. Anwar, J.; Subhani, G.M.; Hussain, M.; Ahmad, J.; Hussain, M.; Munir, M. Drought tolerance indices and their correlation with yield in exotic wheat genotypes. *Pak. J. Bot.* **2011**, *43*, 1527–1530.
87. Farshadfar, E.; Elyasi, P. Screening quantitative indicators of drought tolerance in bread wheat (*Triticum aestivum* L.) landraces. *Eur. J. Exp. Biol.* **2012**, *2*, 577–584.
88. Sánchez-Reinoso, A.D.; Ligarreto-Moreno, G.; Restrepo-Díaz, H. Evaluation of drought indices to identify tolerant genotypes in common bean bush (*Phaseolus vulgaris* L.). *J. Integr. Agric.* **2020**, *19*, 99–107. [CrossRef]
89. Darkwa, K.; Ambachew, D.; Mohammed, H.; Asfaw, A.; Blair, M.W. Evaluation of common bean (*Phaseolus vulgaris* L.) genotypes for drought stress adaptation in Ethiopia. *Crop J.* **2016**, *4*, 367–376. [CrossRef]
90. Niu, H.B.; Liu, W.X.; Wan, F.H.; Liu, B. An invasive aster (*Ageratina adenophora*) invades and dominates forest understories in China: Altered soil microbial communities facilitate the invader and inhibit natives. *Plant Soil* **2007**, *294*, 73–85. [CrossRef]
91. Ding, W.; Wang, R.; Yuan, Y.; Liang, X.; Liu, J. Effects of nitrogen deposition on growth and relationship of *Robinia pseudoacacia* and *Quercus acutissima* seedlings. *Dendrobiology* **2012**, *67*, 3–13.
92. Yuan, Y.F.; Guo, W.H.; Ding, W.J.; Du, N.; Luo, Y.J.; Liu, J.; Xu, F.; Wang, R.Q. Competitive interaction between the exotic plant *Rhus typhina* L. and the native tree *Quercus acutissima* Carr. in Northern China under different soil N:P ratios. *Plant Soil* **2013**, *372*, 389–400. [CrossRef]

93. Li, L. *Experimental Guidance of Plant Physiology Module*, 1st ed.; Science Press: Beijing, China, 2009.
94. Zhang, J.E. *Experimental Methods and Techniques Commonly Used in Ecology*; Chemical Industry Press: Beijing, China, 2006.
95. Hodges, D.M.; DeLong, J.M.; Forney, C.F.; Prange, R.K. Improving the thiobarbituric acid-reactive-substances assay for estimating lipid peroxidation in plant tissues containing anthocyanin and other interfering compounds. *Planta* **1999**, *207*, 604–611. [CrossRef]
96. Cao, Y.; Luo, Q.X.; Tian, Y.; Meng, F.J. Physiological and proteomic analyses of the drought stress response in *Amygdalus Mira (Koehne) Yü et Lu* roots. *BMC Plant Biol.* **2017**, *17*, 53. [CrossRef] [PubMed]

atmosphere

MDPI

Communication

Is the Invasive Plant *Amaranthus spinosus* L. More Competitive than the Native Plant *A. tricolor* L. When Exposed to Acid Deposition with Different Sulfur–Nitrogen Ratios?

Yue Li [1], Chuang Li [1], Shanshan Zhong [1], Zhelun Xu [1], Jun Liu [2], Zhongyi Xu [1], Mawei Zhu [1], Congyan Wang [1,3,4,*] and Daolin Du [5,*]

[1] Institute of Environment and Ecology, School of Environment and Safety Engineering, Jiangsu University, Zhenjiang 212013, China; 2222209050@stmail.ujs.edu.cn (Y.L.); 2222209081@stmail.ujs.edu.cn (C.L.); 2222109045@stmail.ujs.edu.cn (S.Z.); 2222109089@stmail.ujs.edu.cn (Z.X.); 3202202022@stmail.ujs.edu.cn (Z.X.); 3212202003@stmail.ujs.edu.cn (M.Z.)
[2] Zhenjiang Environmental Monitoring Center of Jiangsu Province, Zhenjiang 212009, China; liujunq8@163.com
[3] Jiangsu Collaborative Innovation Center of Technology and Material of Water Treatment, Suzhou University of Science and Technology, Suzhou 215009, China
[4] Key Laboratory of Forest Plant Ecology, Ministry of Education, Northeast Forestry University, Harbin 150040, China
[5] Jingjiang College, Jiangsu University, Zhenjiang 212013, China
* Correspondence: liuyuexue623@ujs.edu.cn (C.W.); ddl@ujs.edu.cn (D.D.)

Abstract: The functional differences between invasive plants and coexisting native plants can affect the invasion process of the former because invasive plants and coexisting native plants are exposed to similar or even identical environmental pressures. Acid deposition is an important component of atmospheric pollution, and acid deposition with different sulfur–nitrogen ratios may affect the invasion process of invasive plants by shifting the functional differences and differences in the growth performance between the invasive and coexisting native plants. It is crucial to analyze the functional indices and growth performance of these plants when exposed to acid deposition with different chemical compositions to assess the ecological impacts of atmospheric pollution on the growth performance of invasive plants. This study aimed to evaluate the functional differences and growth performance between the invasive plant *Amaranthus spinosus* L. and the native plant *A. tricolor* L. in mono- and mixed culture when exposed to an acid deposition with different sulfur–nitrogen ratios, including sulfur-rich acid deposition (sulfur–nitrogen ratio = 5:1), nitrogen-rich acid deposition (sulfur–nitrogen ratio = 1:5), and mixed acid deposition (sulfur–nitrogen ratio = 1:1). The acidity of the three types of simulated acid deposition was set at pH = 5.6 and pH = 4.5, respectively, with distilled water as a control (pH = 7.0). The competition experiment between *A. spinosus* and *A. tricolor* was conducted in the greenhouse. *Amaranthus spinosus* exhibited a strong growth performance over *A. tricolor* in the mixed culture, mainly via the increased leaf photosynthetic capacity. The competitiveness for light acquisition, leaf photosynthetic capacity, and enzymatic defense capacity under stress of *A. spinosus* may be vital to its growth performance. The lower pH acid deposition had imposed a greater reduction in the growth performance of both *Amaranthus* species than the higher pH acid deposition. Sulfur-rich acid deposition was more toxic to the growth performance of both *Amaranthus* species than nitrogen-rich acid deposition. *Amaranthus spinosus* was more competitive than *A. tricolor*, especially when exposed to acid deposition, compared with just distilled water. Thus, acid deposition, regardless of the sulfur–nitrogen ratio, may facilitate the invasion process of *A. spinosus* via the stronger growth performance.

Keywords: functional difference; growth performance; invasion process; nitrogen-rich acid deposition; sulfur-rich acid deposition

Citation: Li, Y.; Li, C.; Zhong, S.; Xu, Z.; Liu, J.; Xu, Z.; Zhu, M.; Wang, C.; Du, D. Is the Invasive Plant *Amaranthus spinosus* L. More Competitive than the Native Plant *A. tricolor* L. When Exposed to Acid Deposition with Different Sulfur–Nitrogen Ratios?. *Atmosphere* **2024**, *15*, 29. https://doi.org/10.3390/atmos15010029

Academic Editor: Xuejun Liu

Received: 24 November 2023
Revised: 22 December 2023
Accepted: 23 December 2023
Published: 26 December 2023

1. Introduction

Invasive plants pose a significant threat to ecological stability because they can lead to changes in community function and biodiversity loss [1–3]. Therefore, the study of the mechanism by which invasion occurs is one of the hot topics in invasion ecology research in recent years [4–6].

The functional differences between invasive plants and coexisting native plants regulate whether the former can successfully invade, as invasive and coexisting native plants both suffer from similar or even the same selection pressures imposed by their environment [7–9]. In general, invasive plants have a higher growth performance than coexisting native plants due to higher values of key functional traits [7,8,10]. Therefore, it is imperative to elucidate the functional differences and differences in the growth performance-related traits between invasive and coexisting native plants to shed light on the mechanisms underlying the successful invasion of invasive plants.

Acid deposition is an important component of atmospheric pollution and can significantly affect ecological functions, such as the growth performance of plant species [11–13]. Acid deposition can also affect the invasion process of invasive plants, especially by altering their growth performance and allelopathic intensity [11,14,15]. China is one of the three regions in the world most severely affected by acid deposition [16–18], and the type of acid deposition in China has changed from sulfur-rich acid deposition to mixed sulfur and nitrogen acid deposition and, more recently, to nitrogen-rich acid deposition [14,19,20]. In other words, the sulfur–nitrogen ratio in the rain in China is gradually decreasing, mainly due to the recent adjustments in the energy structure and energy-related policies [14,19,20]. Changes in the composition of acid deposition may alter the ability of invasive plants to invade new habitats. Therefore, it is crucial to improve our understanding of the functional differences and differences in the growth performance between invasive and coexisting native plants when exposed to different compositions of acid deposition to explain the mechanisms driving the successful habitat invasion by invasive plants under various acid deposition scenarios. However, little progress has been made in this area so far.

This study aimed to estimate the functional differences and differences in the growth performance between the invasive plant *Amaranthus spinosus* L. (spiny amaranth) and the native plant *A. tricolor* L. (red amaranth) in mono- and mixed culture and when exposed to acid deposition composed of different sulfur–nitrogen ratios, including sulfur-rich acid deposition (sulfur–nitrogen ratio = 5:1), nitrogen-rich acid deposition (sulfur–nitrogen ratio = 1:5), and mixed acid deposition (sulfur–nitrogen ratio = 1:1). Both *Amaranthus* species can coexist in the same habitat, such as wasteland and farmland, in East China [10,21]. In East China, the number of invasive *Amaranthus* species is significantly higher than among other genera, and there are currently 16 species of invasive plants belonging to *Amaranthus*, which accounts for about 5.35% of the total number of invasive plant species in the region [22]. As a spiny annual or perennial herb, *A. spinosus* is native to tropical America and has had a significant impact on non-native ecosystems [23–25]. The area in China where *A. spinosus* has invaded (including East China) and is currently also experiencing severe acid deposition [14,19,20].

This study tested the following hypotheses: (I) acid deposition can reduce the growth performance of both *Amaranthus* species, and the effects of acid deposition vary with different sulfur–nitrogen ratios, and (II) *A. spinosus* may be more competitive than *A. tricolor* when exposed to acid deposition regardless of the sulfur–nitrogen ratios.

2. Materials and Methods

2.1. Experimental Design

The competition experiment between *A. spinosus* (seeds collected at 32.113° N, 119.532° E, Zhenjiang, Jiangsu, East China) and *A. tricolor* cv. xinbai (manufacturer: Qingxian Chunfeng Vegetable Cultivars Breeding Base, Hebei, China) was conducted in planting pots. The culture matrix was composed of pre-sterilized store-bought pasture soil (pH value: ≈6.5; organic content: ≥40%; produced by Jiangsu Zhongfang Agriculture and Pastoral Hus-

bandry Co. LTD) to avoid using soil collected from the field, which may be infested with invasive plants or contaminated by acid rain.

Six vigorous seedlings with uniform height belonging to the two *Amaranthus* species were planted in each planting pot (upper diameter: ≈25 cm). The planting pattern was as follows: (I) monoculture of *A. spinosus* with six seedlings, (II) monoculture of *A. tricolor* with six seedlings, and (III) mixed culture of *A. spinosus* and *A. tricolor* with three seedlings per species.

The seedlings were exposed to three types of acid deposition: (I) sulfur-rich acid deposition (sulfur–nitrogen ratio = 5:1), (II) nitrogen-rich acid deposition (sulfur–nitrogen ratio = 1:5), and (III) mixed acid deposition (sulfur–nitrogen ratio = 1:1). The three acid deposition scenarios were created by mixing 0.5 M L^{-1} H_2SO_4 and 0.5 M L^{-1} HNO_3 at different ratios. The acidity of the three acid deposition types was set to pH = 5.6 and pH = 4.5, respectively. In particular, (I) SO_4^{2-} and NO_3^- are the main components of natural acid precipitation in the study area, (II) the acidity of normal unpolluted precipitation is almost 5.6, (III) the acidity of natural acid precipitation in the study area is about 4.5, and (IV) the sulfur–nitrogen ratio of natural acid precipitation in the study area is about 5:1 [14,19,20]. Distilled water was used as a control (pH = 7.0). Three planting pots were used per treatment.

The seedlings were grown in a greenhouse at Jiangsu University, Zhenjiang, Jiangsu, East China (located at 32.206° N, 119.512° E) under natural light conditions for 50 d. The climate type of the study area is a subtropical monsoon wet climate (mean annual hours of sunshine ≈ 1996.8 h; mean annual precipitation ≈ 1101.4 mm, and mean annual temperature ≈ 15.9 °C) [26].

After 50 d of experimental treatment, all individuals of the two *Amaranthus* species were collected to estimate their functional indices, biochemical constituents, and osmolytes indices.

2.2. Determination of the Functional Indices, and Biochemical Constituents and Osmolytes Indices of the Two Amaranthus Species

The functional indices of the two *Amaranthus* species included (I) plant height (representing the competitiveness for sunlight acquisition), (II) ground diameter (representing plant supporting ability), (III) leaf size (characterized as leaf length and width, representing leaf photosynthetic area), (IV) green leaf area (representing leaf photosynthetic area), (V) leaf thickness (representing leaf supporting ability), (VI) single-leaf wet and dry weights (representing leaf growing competitiveness), (VII) leaf water content (representing leaf moisture content), (VIII) specific leaf area (representing leaf resource use efficiency and acquisition capacity), (IX) leaf chlorophyll and nitrogen concentrations (representing leaf photosynthetic capacity), (X) plant aboveground wet and dry weights (representing aboveground growing competitiveness), and (XI) plant aboveground water content (representing aboveground moisture content). The procedures used to determine the functional indices are described in our previous study [27,28].

The biochemical constituents and osmolytes indices of the two *Amaranthus* species included (I) plant malondialdehyde content (representing the level of peroxidation of the cytoplasm membrane under stress; measured using the thiobarbituric acid method with spectrophotometry (model: uv-2450; manufacturer: Shimadzu, Kyoto, Japan; the same as below) at 532 nm), (II) plant proline content (representing the level of osmotic adjustment capacity under stress; measured using the acidic ninhydrin method with spectrophotometry at 520 nm), (III) plant soluble sugar content (representing the level of osmotic adjustment capacity under stress; measured using the thiobarbituric acid method with spectrophotometry at 450 nm), (IV) plant catalase activity (EC 1.11.1.6; representing enzymatic defense capacity under stress specifically to oxidative stress; measured using the H_2O_2 method with spectrophotometry at 240 nm), (V) plant peroxidase activity (EC 1.11.1.7; representing enzymatic defense capacity under stress specifically to oxidative stress; measured using the guaiacol method with spectrophotometry at 470 nm), and

(VI) plant superoxide dismutase activity (EC 1.15.1.1; representing enzymatic defense capacity under stress specifically to oxidative stress; measured using the nitro-blue tetrazolium method with spectrophotometry at 560 nm) [29–32].

The growth performance of *A. spinosus* was evaluated using the relative dominance index. The value of the relative dominance index was evaluated using the ratio of *A. spinosus*' biomass in the mixed culture to the sum of *A. spinosus*' biomass and *A. tricolor*'s biomass in the mixed culture [6,33,34].

2.3. Statistical Analysis

The differences among the treatments were assessed using the one-way analysis of variance (ANOVA) and Tukey HSD. Four-way ANOVA was used to assess the effects of planting pattern, plant species, acid deposition acidity, acid deposition type, and their interactions on the evaluated variances. Partial Eta-squared (η^2) was also estimated to assess the effect size of each factor used in the four-way ANOVA. $p \leq 0.05$ was considered to represent a statistically significant difference. Statistical analyses were performed using IBM SPSS Statistics 26.0.

3. Results and Discussion

The growth performance of the two *Amaranthus* species may be reduced in the mixed culture compared with the monoculture mainly due to the limited resources available resulting from the increased interspecific competition in the mixed culture [11,35,36]. As expected, the leaf photosynthetic capacity of *A. tricolor* in the mixed culture was 20.59% lower than that in the monoculture when exposed to the mixed acid deposition at pH 4.5 ($p < 0.05$; Figure 1). Thus, the growth performance of *A. tricolor* in the mixed culture may be reduced largely via the decreased leaf photosynthetic capacity. However, the leaf photosynthetic capacity of *A. spinosus* in the mixed culture was ≈10.87% higher than that in the monoculture in all treatments (except nitrogen-rich acid at pH 5.6) ($p < 0.05$; Figure 1). Thus, the growth performance of *A. spinosus* may be increased in the mixed culture chiefly via the increased leaf photosynthetic capacity. Moreover, the leaf photosynthetic capacity of *A. spinosus* was ≈34.99% higher than that of *A. tricolor* in all treatments regardless of planting pattern ($p < 0.05$; Figure 1). Thus, *A. spinosus* exhibited a strong growth performance over *A. tricolor* in the mixed culture mainly due to the enhanced leaf photosynthetic capacity [11,28,37]. Hence, the leaf photosynthetic capacity of *A. spinosus* may be vital to its growth performance, especially in the mixed culture. In addition, the four-way ANOVA results also showed that the planting pattern significantly affected the leaf photosynthetic capacity of the two *Amaranthus* species ($p < 0.05$; Table S1).

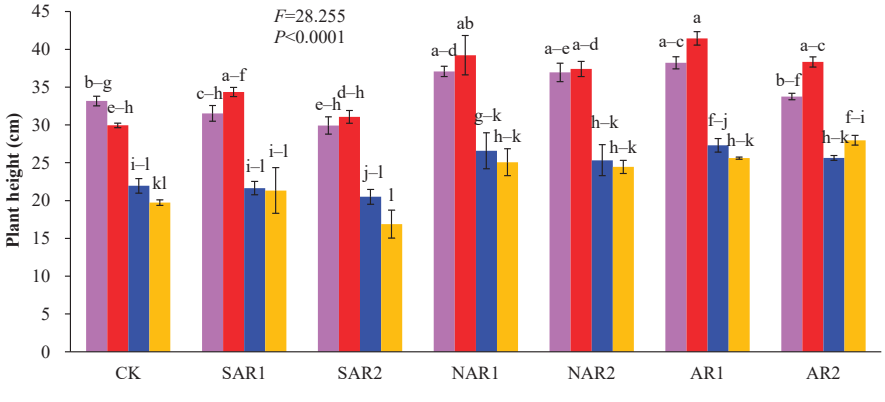

Figure 1. *Cont.*

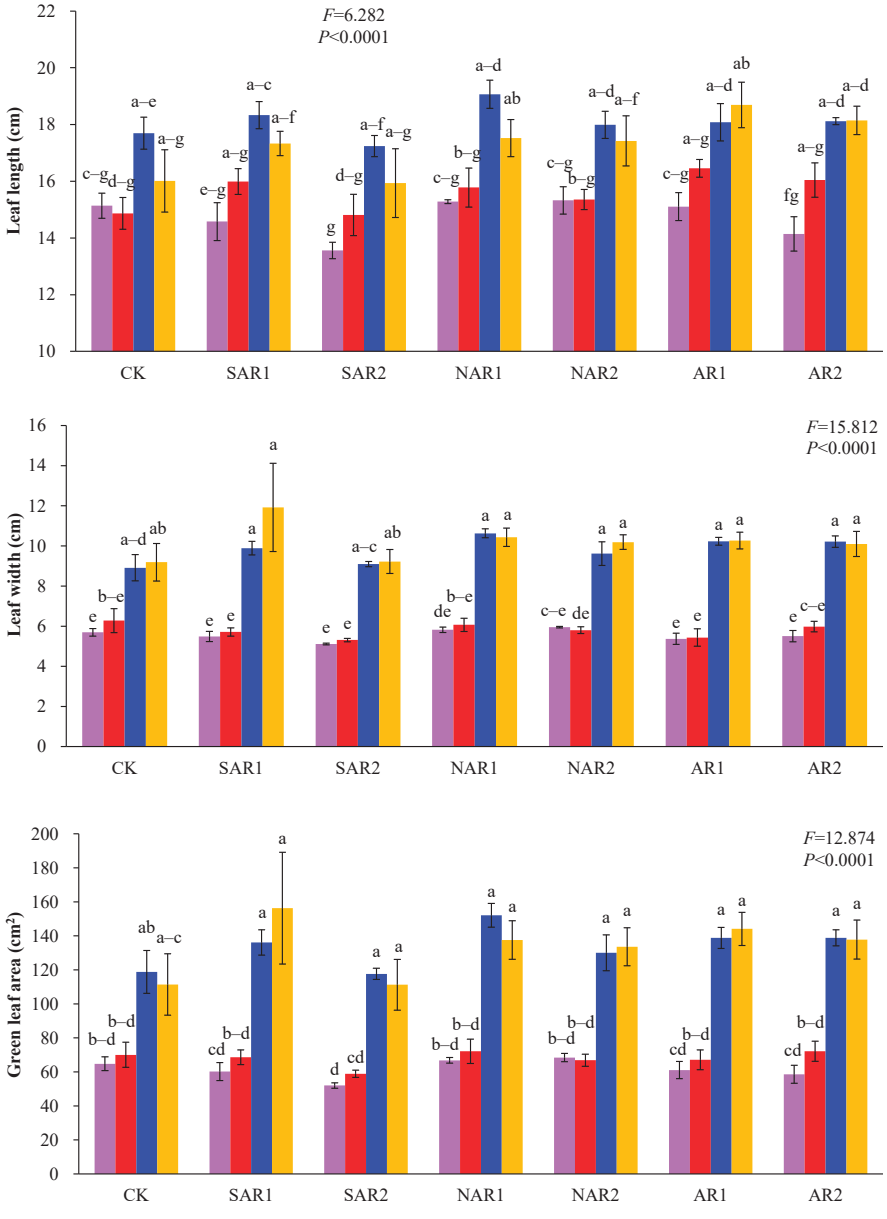

Figure 1. *Cont.*

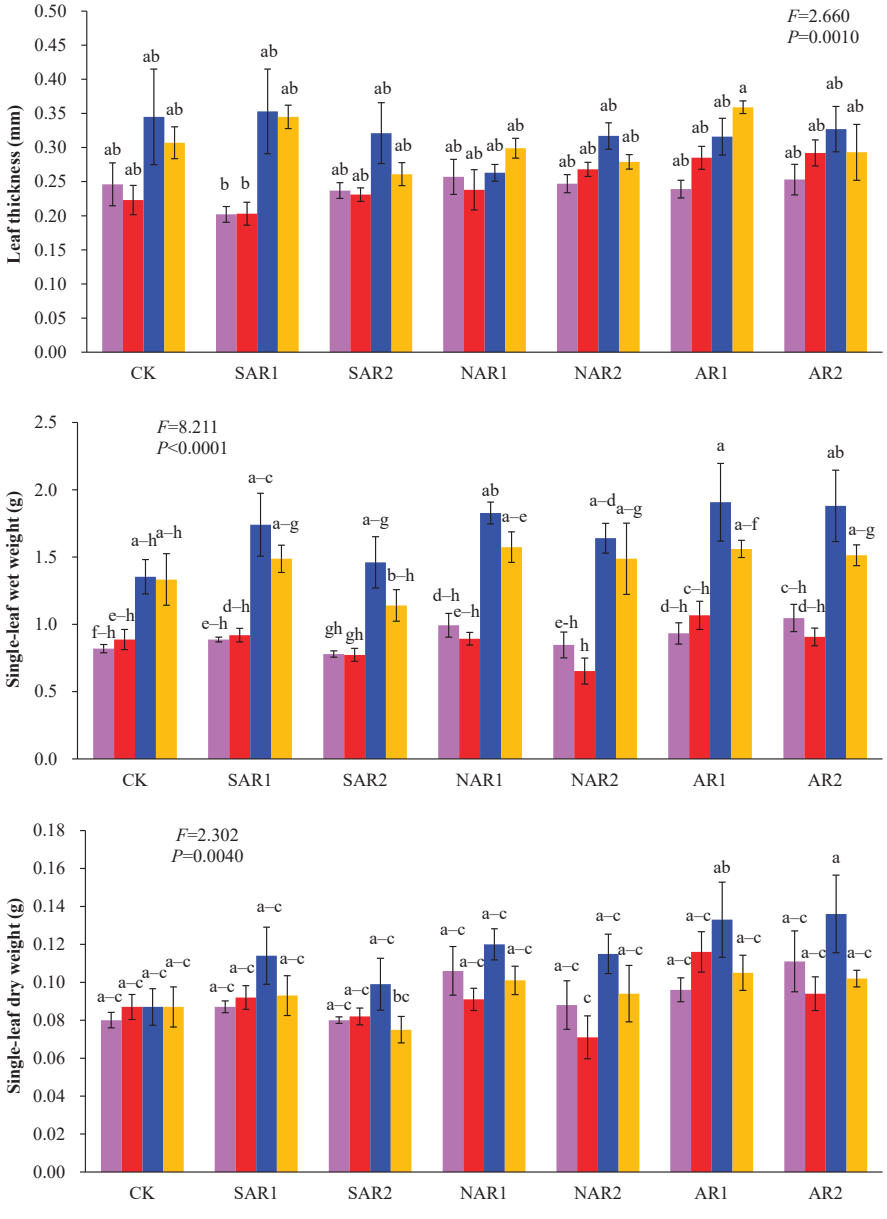

Figure 1. *Cont.*

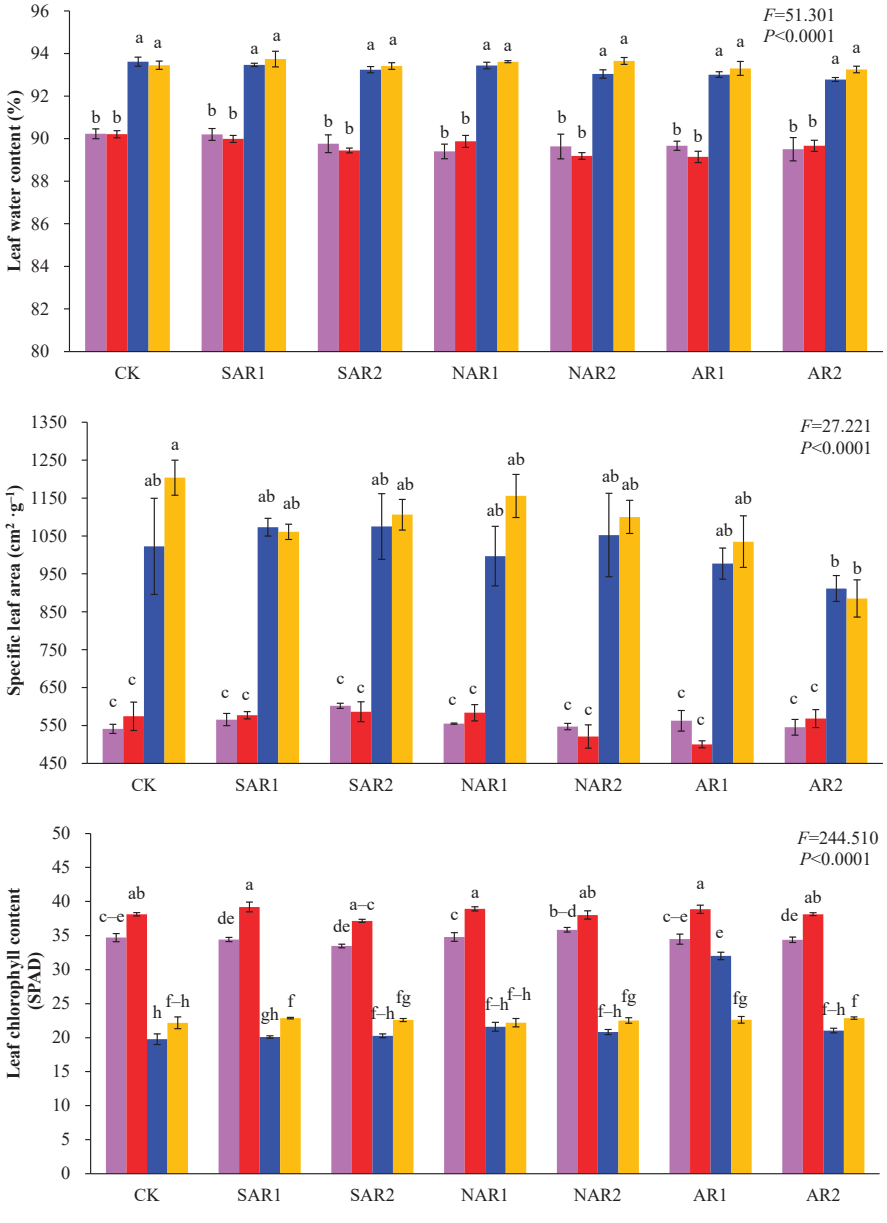

Figure 1. *Cont.*

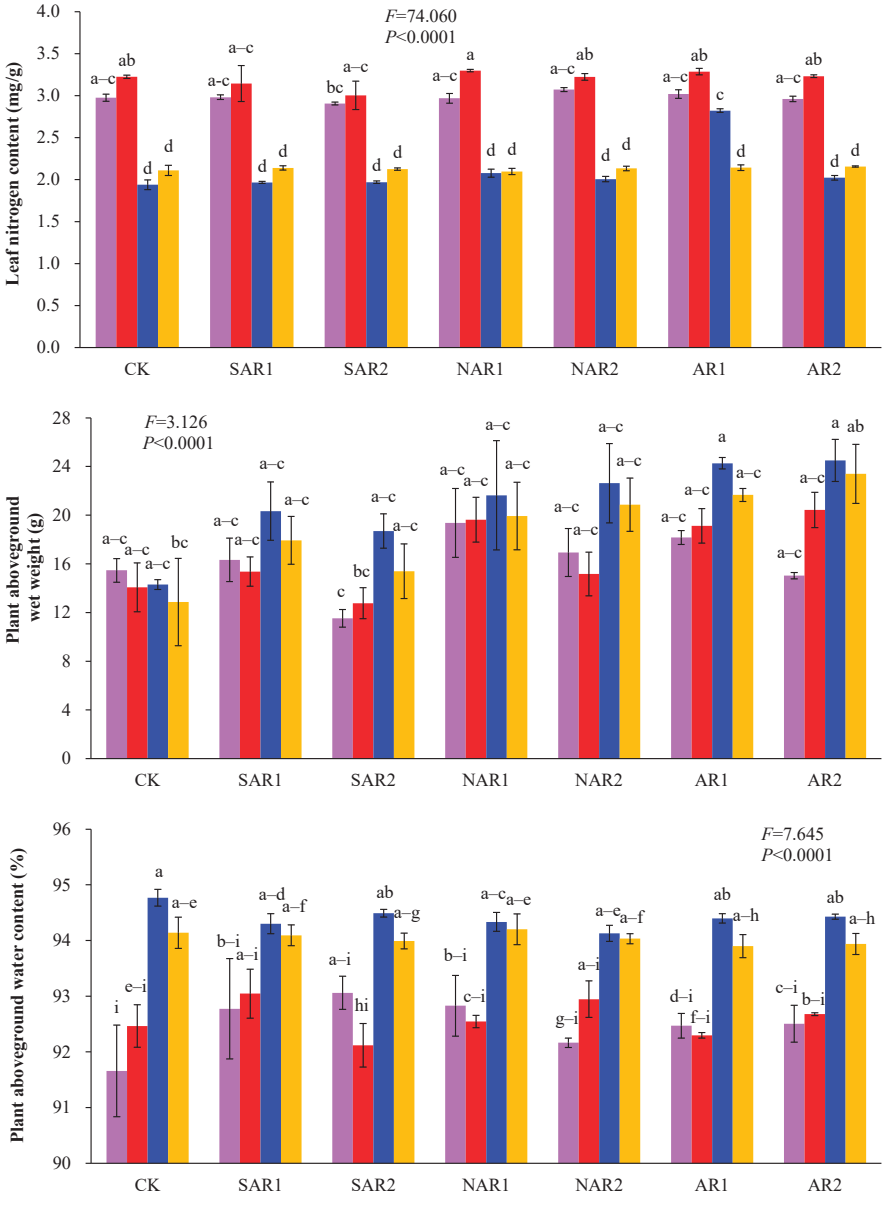

Figure 1. Morphological and physiological indices of *Amaranthus spinosus* and *A. tricolor* in mono- and mixed culture (monoculture *A. spinosus*, purple bars; mixed culture *A. spinosus*, red bars; monoculture *A. tricolor*, blue bars; mixed culture *A. tricolor*, orange bars). Bars (mean with standard error, $n = 3$) with different lowercase letters indicate statistically significant differences ($p \leq 0.05$). The two indices (i.e., ground diameter and plant aboveground dry weight) with no statistically significant difference ($p > 0.05$) among all treatments are not shown in this figure. Abbreviations: CK, control (distilled water; pH = 7.0); SAR1, sulfur-rich acid deposition (sulfur–nitrogen = 5:1; pH = 4.5); SAR2, sulfur-rich acid deposition (sulfur–nitrogen = 5:1; pH = 5.6); NAR1, nitrogen-rich acid deposition (sulfur–nitrogen = 1:5; pH = 4.5); NAR2, nitrogen-rich acid deposition (sulfur–nitrogen = 1:5; pH = 5.6); AR1, mixed acid deposition (sulfur–nitrogen = 1:1; pH = 4.5); AR2, mixed acid deposition (sulfur–nitrogen = 1:1; pH = 5.6).

Usually, the values of the key functional traits of invasive plants are higher than those of the coexisting native plants [8,10,11]. In this study, the competitiveness for light acquisition and leaf photosynthetic capacity of *A. spinosus* were ≈32.98% and ≈34.99% higher than those of *A. tricolor* in all treatments, respectively ($p < 0.05$; Figure 1). The enzymatic defense capacity under stress of *A. spinosus* was also higher than in *A. tricolor* when exposed to nitrogen-rich acid deposition ($p < 0.05$; Figure 2). Therefore, the competitiveness for light acquisition, leaf photosynthetic capacity, and enzymatic defense capacity under stress in *A. spinosus* may be critical to its growth performance, especially when exposed to acid deposition. In addition, the four-way ANOVA results showed that the plant species significantly affected the competitiveness for light acquisition, leaf photosynthetic capacity, and enzymatic defense capacity under stress of the two *Amaranthus* species ($p < 0.05$; Table S1). However, the leaf photosynthetic area, leaf growing competitiveness, leaf moisture content, leaf resource use efficiency, and acquisition capacity, and aboveground moisture content of *A. spinosus* were lower than those of *A. tricolor* under partial treatments ($p < 0.05$; Figures 1 and 2), which suggests that this latter list of functional indices may not be important to the growth performance of *A. spinosus*. Thus, *A. spinosus* may be gaining a higher growth performance by enhancing certain key ecological functions, such as the competitiveness for light acquisition, leaf photosynthetic capacity, and enzymatic defense capacity under stress.

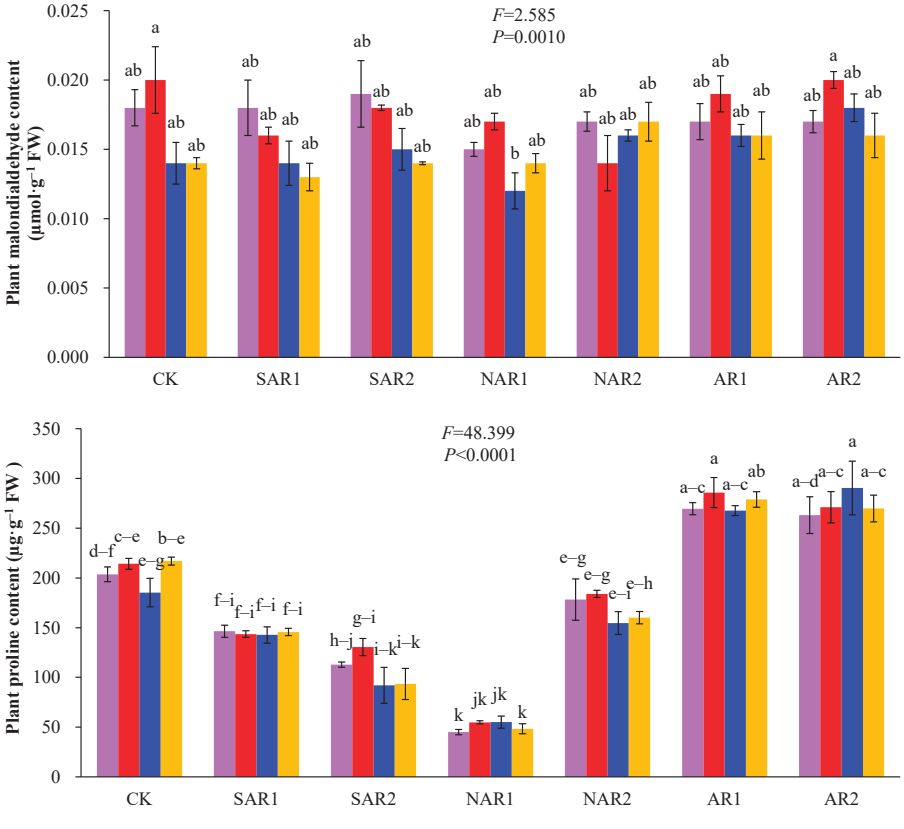

Figure 2. *Cont.*

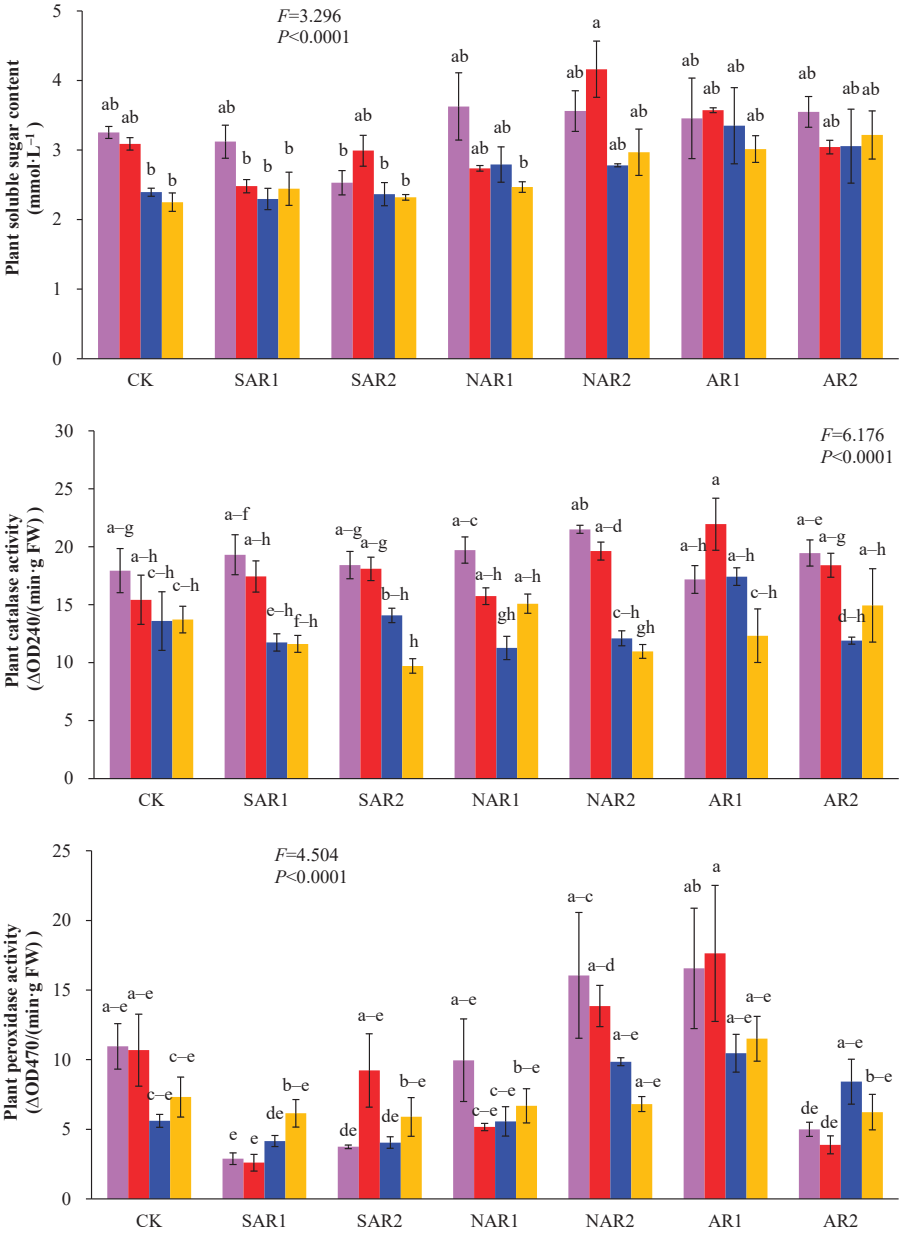

Figure 2. Biochemical constituents and osmolytes indices of *Amaranthus spinosus* and *A. tricolor* in mono- and mixed culture (monoculture *A. spinosus*, purple bars; mixed culture *A. spinosus*, red bars; monoculture *A. tricolor*, blue bars; mixed culture *A. tricolor*, orange bars). Bars (mean with standard error, $n = 3$) with different lowercase letters indicate statistically significant differences ($p \leq 0.05$). The index (i.e., plant superoxide dismutase activity) with no statistically significant difference ($p > 0.05$) across all treatments is not shown in this figure. Abbreviations have the same meanings as presented in Figure 1.

Acid deposition can reduce the growth performance of plant species [11–13]. In this study, the acidity and composition of the acid deposition were two major factors

affecting the growth performance of the two *Amaranthus* species (Figures 1 and 2; Table S1). The osmotic adjustment capacity under stress of the two *Amaranthus* species exposed to nitrogen-rich acid deposition at pH 4.5 was lower than when exposed to nitrogen-rich acid deposition at pH 5.6 ($p < 0.05$; Figure 2). Thus, the lower pH acid deposition may be more toxic to the growth performance of both *Amaranthus* species than the higher pH acid deposition because the lower pH acid deposition, especially given that more hydrogen ions may be released, may induce a more intense stress response potentially through enhanced nutrient leaching [11,14,38]. In addition, four-way ANOVA results showed that the acid deposition acidity significantly affected the osmotic adjustment capacity under stress of the two *Amaranthus* species ($p < 0.05$; Table S1).

The main components of acid deposition are SO_4^{2-} and NO_3^-, and acid deposition with different sulfur–nitrogen ratios can affect the growth performance of plant species [14,38,39]. In this study, sulfur-rich acid deposition caused a greater reduction in the competitiveness for light acquisition and leaf photosynthetic capacity of the two *Amaranthus* species than nitrogen-rich acid deposition ($p < 0.05$; Figure 1). This phenomenon may be due to the higher nitrogen content in nitrogen-rich acid deposition than in sulfur-rich acid deposition. Since nitrogen is one of the essential nutrients required for the growth performance of plants (i.e., fertilization effect), a nitrogen-rich deposition may actually provide some nutrient relief, albeit at the expense of soil acidification [14,38,39]. The two *Amaranthus* species also exhibited a higher level of osmotic adjustment capacity when exposed to sulfur-rich acid deposition than when exposed to nitrogen-rich acid deposition ($p < 0.05$; Figure 2). Thus, sulfur-rich acid deposition exerted a greater negative impact on the growth performance of the two *Amaranthus* species than nitrogen-rich acid deposition [14,40,41], and this result supports the first hypothesis. In addition, four-way ANOVA results showed that the acid deposition composition significantly affected the competitiveness for light acquisition, the leaf photosynthetic capacity, and the osmotic adjustment capacity of the two *Amaranthus* species ($p < 0.05$; Table S1).

The relative dominance index of *A. spinosus* in this study was higher than 0.5 in all acid deposition treatments (average: 0.5286) except in the nitrogen-rich acid deposition treatment at pH 5.6 (Figure 3). Thus, *A. spinosus* exhibited a higher growth performance than *A. tricolor*, especially when exposed to acid deposition with different sulfur–nitrogen ratios. Therefore, acid deposition, regardless of the sulfur–nitrogen ratio, may accelerate the invasion process of *A. spinosus* by allowing the plant to have a higher growth performance. Accordingly, the higher growth performance of *A. spinosus* can be attributed to an extremophilic strategy (being more competitive in a stressful environment) rather than either a specialist strategy (being more competitive in a favorable environment) or a generalist strategy (being more competitive in both stressful and favorable environments) [42–44]. Therefore, our results support the second hypothesis.

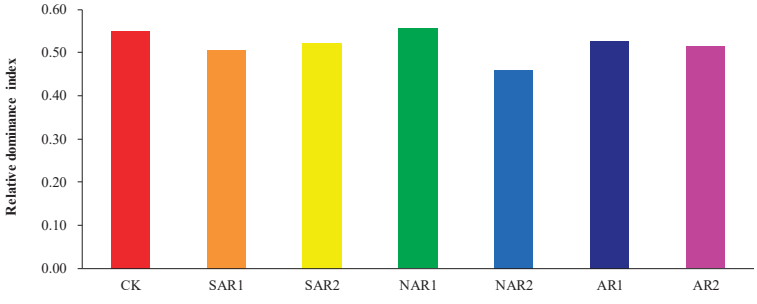

Figure 3. The relative dominance index of *Amaranthus spinosus* in mixed culture under acid deposition with different sulfur–nitrogen ratios. The value of the relative dominance index ranges from 0 to 1, and it means strong growth performance when the value of this index is higher than 0.5, while poor growth performance when the value of this index is less than 0.5. Abbreviations have the same meanings as presented in Figure 1.

Based on the results of this study, there is a great need to slow down, if not stop, the invasion process of *A. spinosus*, especially in mixed culture settings and when exposed to atmospheric pollution, notably acid deposition. Therefore, early warning and preventive control of this invasive plant is essential to maintain ecosystem stability and local biodiversity, especially in wastelands and farmland in East China.

4. Conclusions

In summary, this study is the first to attempt to elucidate the ecological effects of atmospheric pollution, represented by acid deposition with different sulfur–nitrogen ratios, on the functional differences and differences in the growth performance between the invasive and native plant species.

The main findings are as follows: (1) *Amaranthus spinosus* exhibited a strong growth performance over *A. tricolor* in the mixed culture, mainly via the increased leaf photosynthetic capacity. (2) The competitiveness for light acquisition, leaf photosynthetic capacity, and enzymatic defense capacity under stress of *A. spinosus* may be crucial to its growth performance. (3) The lower pH acid deposition exerted a greater negative impact on the growth performance of both *Amaranthus* species than the higher pH acid deposition. (4) Sulfur-rich acid deposition resulted in a greater reduction in the growth performance of both *Amaranthus* species than nitrogen-rich acid deposition. (5) The invasive plant *A. spinosus* was more competitive than the native plant *A. tricolor*, especially when exposed to acid deposition, regardless of the sulfur–nitrogen ratios. Accordingly, acid deposition, regardless of the sulfur–nitrogen ratio, may facilitate the invasion process of *A. spinosus* by enhancing its growth performance.

However, in this study, only six individuals of the same plant species were used per planting pattern to determine the functional differences and differences in the growth performance between *A. spinosus* and *A. tricolor* in mono- and mixed cultures when exposed to acid deposition with different sulfur–nitrogen ratios. In addition, the nitrogen and sulfur contents in the soil and plants were not measured. Thus, future studies will include more plant individuals so as to gain more insights into the differences in the functional traits between invasive and native plants, especially when exposed to acid deposition with different chemical compositions.

Supplementary Materials: The following supporting information can be downloaded at: https://www.mdpi.com/article/10.3390/atmos15010029/s1, Table S1: Four-way ANOVA on the effects of planting pattern, plant species, acid deposition acidity, acid deposition type, and their interactions on the evaluated variances. $p \leq 0.05$ is presented in bold.

Author Contributions: Y.L.: Data curation; Investigation; Methodology; Writing—review and editing; C.L.: Data curation; Investigation; Methodology; Writing—review and editing; S.Z.: Data curation; Investigation; Methodology; Writing—review and editing; Z.X. (Zhelun Xu): Data curation; Investigation; Methodology; Writing—review and editing; J.L.: Data curation; Formal analysis; Writing—review and editing; Z.X. (Zhongyi Xu): Data curation; Formal analysis; Writing—review and editing; M.Z.: Data curation; Formal analysis; Writing—review and editing; C.W.: Conceptualization; Formal analysis; Funding acquisition; Project administration; Supervision; Writing—original draft; D.D.: Funding acquisition; Project administration; Writing—review and editing. All authors have read and agreed to the published version of the manuscript.

Funding: This study was funded by the Open Science Research Fund of Key Laboratory of Forest Plant Ecology, Ministry of Education, Northeast Forestry University, China (Grant No.: K2020B02), Special Research Project of School of Emergency Management, Jiangsu University (Grant No.: KYC-01), National Natural Science Foundation of China (Grant No.: 32071521), Carbon Peak and Carbon Neutrality Technology Innovation Foundation of Jiangsu Province (Grant No.: BK20220030), and Jiangsu Collaborative Innovation Center of Technology and Material of Water Treatment (no grant number).

Institutional Review Board Statement: Not applicable.

Informed Consent Statement: Not applicable.

Data Availability Statement: All data generated or analyzed during this study are included in this article.

Acknowledgments: We greatly appreciate the anonymous reviewers for the insightful comments that greatly improved this manuscript.

Conflicts of Interest: The authors declare no conflicts of interest.

References

1. Williams, R.J.; Dunn, A.M.; da Costa, L.M.; Hassall, C. Climate and habitat configuration limit range expansion and patterns of dispersal in a non-native lizard. *Ecol. Evol.* **2021**, *11*, 3332–3346. [CrossRef] [PubMed]
2. Cowie, B.W.; Byrne, M.J.; Witkowski, E.T.F. Small-scale insights into the above- and below-ground invasion dynamics of *Parthenium hysterophorus* in a South African savanna: The potential role of stocking rate. *S. Afr. J. Bot.* **2022**, *144*, 229–237. [CrossRef]
3. Wang, C.Y.; Cheng, H.Y.; Wang, S.; Wei, M.; Du, D.L. Plant community and the influence of plant taxonomic diversity on community stability and invasibility: A case study based on *Solidago canadensis* L. *Sci. Total Environ.* **2021**, *768*, 144518. [CrossRef]
4. Beshai, R.A.; Truong, D.A.; Henry, A.K.; Sorte, C.J.B. Biotic resistance or invasional meltdown? Diversity reduces invasibility but not exotic dominance in southern *California epibenthic* communities. *Biol. Invasions* **2023**, *25*, 533–549. [CrossRef]
5. Czortek, P.; Królak, E.; Borkowska, L.; Bielecka, A. Effects of surrounding landscape on the performance of *Solidago canadensis* L. and plant functional diversity on heavily invaded post-agricultural wastelands. *Biol. Invasions* **2023**, *25*, 2477–2494. [CrossRef]
6. Niu, H.B.; Liu, W.X.; Wan, F.H.; Liu, B. An invasive aster (*Ageratina adenophora*) invades and dominates forest understories in China: Altered soil microbial communities facilitate the invader and inhibit natives. *Plant Soil* **2007**, *294*, 73–85. [CrossRef]
7. Diaz, J.G.; de la Riva, E.G.; Funk, J.L.; Vila, M. Functional segregation of resource-use strategies of native and invasive plants across Mediterranean biome communities. *Biol. Invasions* **2021**, *23*, 253–266. [CrossRef]
8. Sheppard, C.S. Relative performance of co-occurring alien plant invaders depends on traits related to competitive ability more than niche differences. *Biol. Invasions* **2019**, *21*, 1101–1114. [CrossRef]
9. Helsen, K.; Matsushima, H.; Somers, B.; Honnay, O. A trait-based approach across the native and invaded range to understand plant invasiveness and community impact. *Oikos* **2021**, *130*, 1001–1013. [CrossRef]
10. Yu, Y.L.; Cheng, H.Y.; Wang, S.; Wei, M.; Wang, C.Y.; Du, D.L. Drought may be beneficial to the competitive advantage of *Amaranthus spinosus*. *J. Plant Ecol.* **2022**, *15*, 494–508. [CrossRef]
11. Wang, C.Y.; Wu, B.D.; Jiang, K.; Zhou, J.W. Differences in functional traits between invasive and native *Amaranthus* species under simulated acid deposition with a gradient of pH levels. *Acta Oecol.* **2018**, *89*, 32–37. [CrossRef]
12. Ljubojevic, M.; Tomic, M.; Simikic, M.; Savin, L.; Narandzic, T.; Pusic, M.; Grubac, M.; Vejnovic, S.; Marinkovic, M. *Koelreuteria paniculata* invasiveness, yielding capacity and harvest date influence on biodiesel feedstock properties. *J. Environ. Manag.* **2021**, *295*, 113102. [CrossRef] [PubMed]
13. Liu, X.; Fu, Z.H.; Zhang, B.; Zhai, L.; Meng, M.J.; Lin, J.; Zhuang, J.Y.; Wang, G.G.; Zhang, J.C. Effects of sulfuric, nitric, and mixed acid rain on Chinese fir sapling growth in Southern China. *Ecotoxicol. Environ. Saf.* **2018**, *160*, 154–161. [CrossRef] [PubMed]
14. Zhong, S.S.; Xu, Z.L.; Li, Y.; Li, C.; Yu, Y.L.; Wang, C.Y.; Du, D.L. What modulates the impacts of acid rain on the allelopathy of the two Asteraceae invasives? *Ecotoxicology* **2023**, *32*, 114–126. [CrossRef] [PubMed]
15. Cheng, H.Y.; Wang, S.; Wei, M.; Yu, Y.L.; Wang, C.Y. Effect of leaf water extracts of four Asteraceae alien invasive plants on germination performance of *Lactuca sativa* L. under acid deposition. *Plant Ecol.* **2021**, *222*, 433–443. [CrossRef]
16. Dentener, F.; Drevet, J.; Lamarque, J.F.; Bey, I.; Eickhout, B.; Fiore, A.M.; Hauglustaine, D.; Horowitz, L.W.; Krol, M.; Kulshrestha, U.C.; et al. Nitrogen and sulfur deposition on regional and global scales: A multimodel evaluation. *GBioC* **2006**, *20*, GB4003. [CrossRef]
17. Yu, H.L.; He, N.P.; Wang, Q.F.; Zhu, J.X.; Gao, Y.; Zhang, Y.H.; Jia, Y.L.; Yu, G.R. Development of atmospheric acid deposition in China from the 1990s to the 2010s. *Environ. Pollut.* **2017**, *231*, 182–190. [CrossRef] [PubMed]
18. Xu, W.; Zhao, Y.H.; Liu, X.J.; Dore, A.J.; Zhang, L.; Liu, L.; Cheng, M.M. Atmospheric nitrogen deposition in the Yangtze River basin: Spatial pattern and source attribution. *Environ. Pollut.* **2018**, *232*, 546–555. [CrossRef]
19. Du, J.J.; Qv, M.X.; Zhang, Y.Y.; Cui, M.H.; Zhang, H.Z. Simulated sulfuric and nitric acid rain inhibits leaf breakdown in streams: A microcosm study with artificial reconstituted fresh water. *Ecotoxicol. Environ. Saf.* **2020**, *196*, 110535. [CrossRef]
20. Liu, X.; Zhang, B.; Zhao, W.R.; Wang, L.; Xie, D.J.; Huo, W.T.; Wu, Y.W.; Zhang, J.C. Comparative effects of sulfuric and nitric acid rain on litter decomposition and soil microbial community in subtropical plantation of Yangtze River Delta region. *Sci. Total Environ.* **2017**, *601–602*, 669–678. [CrossRef]
21. Cheng, H.Y.; Wang, S.; Wei, M.; Yu, Y.L.; Wang, C.Y. Alien invasive plant *Amaranthus spinosus* mainly altered the community structure instead of the α diversity of soil N-fixing bacteria under drought. *Acta Oecol.* **2021**, *113*, 103788. [CrossRef]
22. Yan, J.; Yan, X.L.; Li, H.R.; Du, C.; Ma, J.S. Composition, time of introduction and spatial-temporal distribution of naturalized plants in East China. *Biodivers. Sci.* **2021**, *29*, 428–438. [CrossRef]
23. Rajesh, V. Evaluation of analgesic activity of *Amaranthus spinosus* Linn. leaves in mice. *J. Pharm. Res.* **2010**, *3*, 3088.
24. Prajitha, V.; Thoppil, J. Genotoxic and antigenotoxic potential of the aqueous leaf extracts of *Amaranthus spinosus* Linn. using Allium cepa assay. *S. Afr. J. Bot.* **2016**, *102*, 18–25. [CrossRef]

25. Odero, D.C.; Wright, A.L. Preemergence and postemergence spiny amaranth (*Amaranthus spinosus*) and common lambsquarters (*Chenopodium album*) control in lettuce on organic soils. *Weed Technol.* **2022**, *36*, 531–536. [CrossRef]
26. Jia, S.; Wu, H.P. *Zhenjiang Yearbook: Overview of Zhenjiang*; Organized by Zhenjiang Municipal People's Government & Written by Zhenjiang Local Records Office; Yu, W., Ye, Z.G., Sun, W.Y., Yang, Z.H., Zong, C.J., Qian, J.J., Pan, Y., Eds.; Publishing House of Local Records: Beijing, China, 2020; pp. 14–15.
27. Cheng, H.Y.; Wei, M.; Wang, S.; Wu, B.D.; Wang, C.Y. Atmospheric N deposition alleviates the unfavorable effects of drought on wheat growth. *Braz. J. Bot.* **2020**, *43*, 229–238. [CrossRef]
28. Wang, S.; Wei, M.; Cheng, H.Y.; Wu, B.D.; Du, D.L.; Wang, C.Y. Indigenous plant species and invasive alien species tend to diverge functionally under heavy metal pollution and drought stress. *Ecotoxicol. Environ. Saf.* **2020**, *205*, 111160. [CrossRef]
29. Li, L. *Experimental Guidance of Plant Physiology Module*, 1st ed.; Science Press: Beijing, China, 2009.
30. Zhang, J.E. *Experimental Methods and Techniques Commonly Used in Ecology*; Chemical Industry Press: Beijing, China, 2006.
31. Hodges, D.M.; DeLong, J.M.; Forney, C.F.; Prange, R.K. Improving the thiobarbituric acid-reactive-substances assay for estimating lipid peroxidation in plant tissues containing anthocyanin and other interfering compounds. *Planta* **1999**, *207*, 604–611. [CrossRef]
32. Cao, Y.; Luo, Q.X.; Tian, Y.; Meng, F.J. Physiological and proteomic analyses of the drought stress response in *Amygdalus Mira (Koehne) Yü et Lu* roots. *BMC Plant Biol.* **2017**, *17*, 53. [CrossRef]
33. Yuan, Y.F.; Guo, W.H.; Ding, W.J.; Du, N.; Luo, Y.J.; Liu, J.; Xu, F.; Wang, R.Q. Competitive interaction between the exotic plant *Rhus typhina* L. and the native tree *Quercus acutissima* Carr. in Northern China under different soil N:P ratios. *Plant Soil* **2013**, *372*, 389–400. [CrossRef]
34. Ding, W.; Wang, R.; Yuan, Y.; Liang, X.; Liu, J. Effects of nitrogen deposition on growth and relationship of *Robinia pseudoacacia* and *Quercus acutissima* seedlings. *Dendrobiology* **2012**, *67*, 3–13.
35. Wu, B.D.; Zhang, H.S.; Jiang, K.; Zhou, J.W.; Wang, C.Y. *Erigeron canadensis* affects the taxonomic and functional diversity of plant communities in two climate zones in the North of China. *Ecol. Res.* **2019**, *34*, 535–547. [CrossRef]
36. Wang, C.Y.; Cheng, H.Y.; Wu, B.D.; Jiang, K.; Wang, S.; Wei, M.; Du, D.L. The functional diversity of native ecosystems increases during the major invasion by the invasive alien species, *Conyza canadensis*. *Ecol. Eng.* **2021**, *159*, 106093. [CrossRef]
37. He, C.; Li, Y.; Li, C.; Wang, Y.; Xu, Z.; Zhong, S.; Xu, Z.; Yu, Y.; Du, D.; Wang, C. Photosynthetic capacity of *Erigeron canadensis* L. may be more critical to its growth performance than photosynthetic area. *Biologia* **2023**, *78*, 1315–1321. [CrossRef]
38. Huang, J.; Wang, H.Y.; Zhong, Y.D.; Huang, J.G.; Fu, X.F.; Wang, L.H.; Teng, W.C. Growth and physiological response of an endangered tree, *Horsfieldia hainanensis* merr., to simulated sulfuric and nitric acid rain in southern China. *Plant Physiol. Biochem.* **2019**, *144*, 118–126. [CrossRef] [PubMed]
39. Liu, X.; Zhao, W.; Meng, M.; Fu, Z.; Xu, L.; Zha, Y.; Yue, J.; Zhang, S.; Zhang, J. Comparative effects of simulated acid rain of different ratios of SO_4^{2-} to NO_3^- on fine root in subtropical plantation of China. *Sci. Total Environ.* **2018**, *618*, 336–346. [CrossRef] [PubMed]
40. Wang, C.Y.; Xiao, H.G.; Zhao, L.L.; Liu, J.; Wang, L.; Zhang, F.; Shi, Y.C.; Du, D.L. The allelopathic effects of invasive plant *Solidago canadensis* on seed germination and growth of *Lactuca sativa* enhanced by different types of acid deposition. *Ecotoxicology* **2016**, *25*, 555–562. [CrossRef]
41. Chen, J.; Wang, W.H.; Liu, T.W.; Wu, F.H.; Zheng, H.L. Photosynthetic and antioxidant responses of *Liquidambar formosana* and *Schima superba* seedlings to sulfuric-rich and nitric-rich simulated acid rain. *Plant Physiol. Biochem.* **2013**, *64*, 41–51. [CrossRef]
42. Richards, C.L.; Bossdorf, O.; Muth, N.Z.; Gurevitch, J.; Pigliucci, M. Jack of all trades, master of some? On the role of phenotypic plasticity in plant invasions. *Ecol. Lett.* **2006**, *9*, 981–993. [CrossRef]
43. Davidson, A.M.; Jennions, M.; Nicotra, A.B. Do invasive species show higher phenotypic plasticity than native species and, if so, is it adaptive? A meta-analysis. *Ecol. Lett.* **2011**, *14*, 419–431. [CrossRef]
44. Matzek, V. Trait values, not trait plasticity, best explain invasive species' performance in a changing environment. *PLoS ONE* **2012**, *7*, e48821. [CrossRef] [PubMed]

atmosphere

MDPI

Article

Litter Mass Loss of the Invasive *Rhus typhina* L. and Native *Koelreuteria paniculata* Laxm. Trees Alters Soil N-Fixing Bacterial Community Composition under Different N Forms

Yue Li [1], Chuang Li [1], Huiyuan Cheng [1,2], Zhelun Xu [1], Shanshan Zhong [1], Mawei Zhu [1], Yuqing Wei [1], Zhongyi Xu [1], Daolin Du [3], Congyan Wang [1,4,5,*] and Huanshi Zhang [6,*]

1 School of Environment and Safety Engineering, Jiangsu University, Zhenjiang 212013, China; 2222209050@stmail.ujs.edu.cn (Y.L.); 2222209081@stmail.ujs.edu.cn (C.L.); 2022203067@stu.njau.edu.cn (H.C.); 2222109089@stmail.ujs.edu.cn (Z.X.); 2222109045@stmail.ujs.edu.cn (S.Z.); 3212202003@stmail.ujs.edu.cn (M.Z.); 3212202011@stmail.ujs.edu.cn (Y.W.); 3202202022@stmail.ujs.edu.cn (Z.X.)
2 College of Resources and Environmental Sciences, Nanjing Agricultural University, Nanjing 210095, China
3 Jingjiang College, Jiangsu University, Zhenjiang 212013, China; ddl@ujs.edu.cn
4 Jiangsu Collaborative Innovation Center of Technology and Material of Water Treatment, Suzhou University of Science and Technology, Suzhou 215009, China
5 Key Laboratory of Forest Plant Ecology, Ministry of Education, Northeast Forestry University, Harbin 150040, China
6 College of Horticulture, Jinling Institute of Technology, Nanjing 210038, China
* Correspondence: liuyuexue623@ujs.edu.cn or liuyuexue623@163.com (C.W.); zhanghuanshi@jit.edu.cn (H.Z.)

Abstract: Soil N-fixing bacterial (NFB) community may facilitate the successful establishment and invasion of exotic non-nitrogen (N) fixing plants. Invasive plants can negatively affect the NFB community by releasing N during litter decomposition, especially where N input from atmospheric N deposition is high. This study aimed to quantitatively compare the effects of the invasive *Rhus typhina* L. and native *Koelreuteria paniculata* Laxm. trees on the litter mass loss, soil physicochemical properties, soil enzyme activities, and the NFB. Following N supplementation at 5 g N m^{-2} yr^{-1} in four forms (including ammonium, nitrate, urea, and mixed N with an equal mixture of the three individual N forms), a litterbag-experiment was conducted indoors to simulate the litter decomposition of the two trees. After four months of decomposition, the litter cumulative mass losses of *R. typhina* under the control, ammonium chloride, potassium nitrate, urea, and mixed N were 57.93%, 57.38%, 58.69%, 63.66%, and 57.57%, respectively. The litter cumulative mass losses of *K. paniculata* under the control, ammonium chloride, potassium nitrate, urea, and mixed N were 54.98%, 57.99%, 48.14%, 49.02%, and 56.83%, respectively. The litter cumulative mass losses of equally mixed litter from both trees under the control, ammonium chloride, potassium nitrate, urea, and mixed N were 42.95%, 42.29%, 50.42%, 46.18%, and 43.71%, respectively. There were antagonistic responses to the co-decomposition of the two trees. The litter mass loss of the two trees was mainly associated with the taxonomic richness of NFB. The form of N was not significantly associated with the litter mass loss in either species, the mixing effect intensity of the litter co-decomposition of the two species, and NFB alpha diversity. Litter mass loss of *R. typhina* was significantly higher than that of *K. paniculata* under urea. The litter mass loss of the two trees under the control and N in four forms mainly affected the relative abundance of numerous NFB taxa, rather than NFB alpha diversity.

Keywords: antagonistic responses; atmospheric N deposition; co-decomposition; invasive plant; litter decomposition

Citation: Li, Y.; Li, C.; Cheng, H.; Xu, Z.; Zhong, S.; Zhu, M.; Wei, Y.; Xu, Z.; Du, D.; Wang, C.; et al. Litter Mass Loss of the Invasive *Rhus typhina* L. and Native *Koelreuteria paniculata* Laxm. Trees Alters Soil N-Fixing Bacterial Community Composition under Different N Forms. *Atmosphere* **2024**, *15*, 424. https://doi.org/10.3390/atmos15040424

Academic Editors: Chaofan Xian, Yu-Sheng Shen and Cheng Gong

Received: 10 March 2024
Revised: 26 March 2024
Accepted: 28 March 2024
Published: 29 March 2024

1. Introduction

Invasive plants can establish successfully if they can acquire soil nitrogen (N) more efficiently than native plants [1–4]. The invasiveness and the invasion intensity of several invasive plants are also significantly associated with the level of soil N available [5–8]. The abun-

dance and diversity of the nitrogenase reductase gene *nifH* (encoding the nitrogenase reductase subunit) are closely related to the level of soil N available [9–12]. Numerous invasive plants, such as *Trifolium* spp. [13], *Ageratina adenophora* [7], and *Amaranthus retroflexus* [14], *Cenchrus spinifex* [15], and multiple invasive plants (including *Paspalum notatum*, *Sphagneticola trilobata*, *Alternanthera philoxeroides*, and *Hydrocotyle vulgaris*) [8] can significantly increase the abundance and diversity of the *nifH* gene. Therefore, the soil N-fixing bacterial community (NFB) may be an important contributor to the successful invasion of invasive plants [6,7,16,17]. In addition, invasive plants can produce more litter and decompose more effectively and rapidly than native plants [18–21]. More importantly, invasive plants can also affect the NFB community via the decomposition process [7,22]. Thus, assessing the key mechanisms that govern the interactions between invasive plants-NFB via the decomposition process is crucial for elucidating the mechanisms that drive the successful invasion of invasive plants.

Atmospheric N deposition consists of several N components globally, including nitrate, ammonium, urea, and a mixture of several individual N forms. Additionally, the proportion of these different N components is dynamic and is expected to change as the frequency and intensity of human activities increase in the future [23–26]. In general, the positive effects of the mixture of several individual N forms on the ecological functions (e.g., the plant litter decomposition, soil enzyme activities, and the soil bacterial community metabolic activities) appear to be greater than those of the individual N forms [27,28]. More importantly, invasive plants may be more competitive than native plants under atmospheric N deposition via the altered NFB [14,29,30] or litter decomposition [28,31–33]. Consequently, it is essential to further elucidate the soil micro-ecological mechanisms underlying the invasion process of invasive plants from the perspective of the interactions between invasive plants and NFB, especially under different forms of atmospheric N deposition.

This study aimed to assess the effects of the invasive *Rhus typhina* L. and native *Koelreuteria paniculata* Laxm. trees on the litter mass loss, soil physicochemical properties, soil enzyme activities, and the NFB community in combination with N addition at 5 g N m^{-2} yr^{-1} in four forms (including ammonium, nitrate, urea, and an equal mixture of the three individual N forms) in southern Jiangsu, China. As two Sapindales trees, *R. typhina* and *K. paniculata* can coexist in the same habitat, the two trees have similar growing seasons (e.g., the growing season is usually from ~April to ~August in southern Jiangsu, China), growing environments (e.g., the parks, urban green spaces, and the areas near major roads in southern Jiangsu, China, etc.), and lifestyles (i.e., deciduous broadleaf trees). The two trees have similar stem heights and there is no significant difference in the space occupied by healthy mature individuals. In addition, both trees are commonly used in urban ornamentation in China. *Rhus typhina* originated from the Americas and was introduced to China in 1959 as an ornamental and landscape plant species [34,35]. However, *R. typhina* has caused biodiversity loss in China, especially in northern China, and has been classified as a destructive invasive tree [34,36]. The geographical range where *R. typhina* and *K. paniculata* are found in China is one of the most affected by atmospheric N deposition [24,37–39].

This study tested the following hypotheses: (1) *Rhus typhina* litter decomposes more easily than *K. paniculata* litter. (2) A synergistic effect might exist between the two trees' co-decomposition. (3) *Rhus typhina* increases soil enzyme activities and NFB alpha diversity compared to *K. paniculata*. (4) N addition increases the litter mass loss of the two trees and NFB alpha diversity. (5) The magnitude of influence of N addition on the litter mass loss of *R. typhina* may be greater than that of *K. paniculata*. (6) The magnitude of influence of the addition of mixed N forms on the litter mass loss of the two trees and NFB alpha diversity may be greater compared to the addition of the three individual N forms, individually.

2. Materials and Methods

2.1. Experimental Design

Leaf litter from *R. typhina* and *K. paniculata* was randomly collected from an urban ecosystem of Zhenjiang (32.21 °N, 119.51 °E), southern Jiangsu, China. Figure 1 defines the geographical location of the sampled area in this study. Figure S1 defines the image of the environment in which the two trees grow. The annual mean temperature of Zhenjiang was ~17.1 °C, and the monthly mean temperature reached a maximum of ~28.1 °C in July and decreased to a minimum of ~3.7 °C in January [40]. The annual precipitation of Zhenjiang was ~1164.1 mm, and the monthly mean precipitation reached a maximum of ~432.1 mm in July and decreased to a minimum of ~2.7 mm in December [40]. The annual sunshine duration of Zhenjiang was ~1909.0 h, and the monthly mean sunshine duration reached a maximum of ~208.2 h in December and decreased to a minimum of ~125.9 h in August [40].

Figure 1. The geographical location of the sampled area (square with red) in this study (Map number: GS(2022)4317; produced by the Ministry of Natural Resources of China, http://bzdt.ch.mnr.gov.cn/).

The litterbag experiment was conducted indoors from 15 April to 15 August 2021 (experimental period: ~4 months) to simulate the litter decomposition process. The air-dried leaf litter of the two trees was loaded into litterbags (10 × 15 cm; mesh size: 0.425 mm). Specifically, 6 g of *R. typhina* leaf litter, 6 g of *K. paniculata* leaf litter, or 6 g equally mixed *R. typhina* and *K. paniculata* leaf litter, were used per litterbag. The litterbags were then buried into the store-bought pasture soil (pH: ~6.3), at a depth of approximately 2 cm in planting pots (height: ~16.5 cm; top diameter: ~25 cm) with one litterbag per planting pot. The pasture yellow soil (pH value: ≈6.3; organic content: ≥30%; soil electrical conductivity: ≤3 ms/cm) was purchased from Zhong-Fang Agriculture & Livestock Co. Ltd., Taizhou, Jiangsu, China. The reason for using the pasture yellow soil as the culture medium was

to minimize or even eliminate the possibility of the presence of invasive plants and the possible previous N deposition in the natural soil. The pasture yellow soil was not sterilized to ensure the natural occurrence of soil microorganisms. N was added to the litterbags in four forms: ammonium (ammonium chloride), nitrate (potassium nitrate), urea, and mixed N (an equal mixture of the three individual N forms). The ratio of the three individual N forms in mixed N was set at 1:1:1 to match the actual proportion of the different N forms deposited in the soil through the natural atmospheric N deposition in the region (viz., southern Jiangsu, China) [23,26,41,42]. All four forms of N were added at 5 g N m^{-2} yr^{-1}, with sterile distilled water as the control (0 g N L^{-1}). The levels of the four N forms were similar to the actual concentration of N forms naturally deposited in the study area (viz., southern Jiangsu, China) [24,37–39].

The litterbag-experiment included 20 treatments: (1) Control (distilled water). (2) Ammonium, ammonium chloride. (3) Nitrate, potassium nitrate. (4) Urea, urea. (5) MixN, mixed N. (6) Rt, *R. typhina* litter under the control. (7) RtAmmonium, *R. typhina* litter under ammonium chloride. (8) RtNitrate, *R. typhina* litter under potassium nitrate. (9) RtUrea, *R. typhina* litter under urea. (10) RtMixN, *R. typhina* litter under mixed N. (11) Kp, *K. paniculata* litter under the control. (12) KpAmmonium, *K. paniculata* litter under ammonium chloride. (13) KpNitrate, *K. paniculata* litter under potassium nitrate. (14) KpUrea, *K. paniculata* litter under urea. (15) KpMixN, *K. paniculata* litter under mixed N. (16) RK, equally mixed litter from both trees under the control. (17) RKAmmonium, equally mixed litter from both trees under ammonium chloride. (18) RKNitrate, equally mixed litter from both trees under potassium nitrate. (19) RKUrea, equally mixed litter from both trees under urea. (20) RKMixN, equally mixed litter from both trees under mixed N. Each treatment was performed in three planting pots.

Litterbags were collected after ~120 d. Litter samples of the two trees in the litterbags were moderately cleaned and completely air-dried to a constant weight to evaluate the decomposition variables. Soil samples within 1 cm around the litterbags were also collected and passed through a 2 mm sieve and were used to estimate soil physicochemical properties, soil enzyme activities, and NFB.

2.2. Determination of the Decomposition Variables

The litter mass loss of the two trees was calculated as the ratio between the initial litter dry weight and the dry weight after time t to the initial litter dry weight [20,43,44].

The expected litter decomposition coefficient of the equally mixed litter from the two trees was calculated as follows [45,46]:

$$\text{Expected decomposition coefficient} = \frac{x + y}{2}$$

where x and y correspond to the observed litter decomposition coefficient of *R. typhina* and that of *K. paniculata*, respectively. The litter decomposition coefficient (k) of the two trees was determined as follows [47]:

$$X_t = X_o \times e^{-kt}$$

where X_o and X_t correspond to the initial litter dry weight and the litter dry weight after time t, respectively.

The mixing effect intensity of the litter co-decomposition of the two trees was calculated as follows [20,45,46]:

$$\text{Mixing effect intensity of the litter co} - \text{decomposition} = \frac{O}{E} - 1$$

where O and E correspond to the observed litter decomposition coefficient and the expected litter decomposition coefficient of equally mixed litter from both trees, respectively. A stronger response corresponds to a greater deviation from zero. In the presence of synergistic effects, the intensity is greater than zero, while the intensity is lower than zero in the presence of antagonistic effects.

2.3. Determination of Soil Physicochemical Properties and Soil Enzyme Activities

Soil pH and moisture were determined in situ using a digital soil acidity-moisture meter (ZD-06; ZD Instrument Co., Ltd., Taizhou, China) [28,48,49].

Soil enzyme activities, closely related to the soil nutrient cycles, were estimated: (1) urease (E.C. 3.5.1.5) activity was assessed using the sodium phenolate–sodium hypochlorite method with a colorimetric assay at 578 nm [50,51]; (2) protease (E.C. 3.4.11.4) activity was measured using the tyrosine method with a colorimetric assay at 700 nm [52]; (3) polyphenol oxidase (E.C. 1.10.3.1) activity was measured using the pyrocatechol method with a colorimetric assay at 410 nm [53]; (4) catalase (E.C. 1.11.1.6) activity was measured using the pyrogallol method with a colorimetric assay at 430 nm [51].

2.4. Determination of NFB

To estimate the composition and structure of the NFB community in this study, DNA sequences of the nifH gene were amplified. The nifH gene is highly conserved among NFB taxa and is widely used as a marker for phylogenetic analyses of NFB [12,54–57]. The primers for the amplification of the nifH gene are PolF and PolR [57]. The methods for subsequent sequencing data analysis can be found in earlier studies [14]. The sequence data of NFB did not submit to the NCBI database.

2.5. Statistical Analysis

Shapiro–Wilk's test and Bartlett's test were used to assess the deviations from normality and the homogeneity of the assessed variances, respectively. Differences in the values of the decomposition variables, soil physicochemical properties, soil enzyme activities, and NFB alpha diversity among different treatments were evaluated using a one-way analysis of variance (ANOVA; Tukey's test). Path analysis was used to assess the contribution intensity of soil physicochemical properties, soil enzyme activities, and NFB alpha diversity to the litter mass loss of the two trees, according to the absolute values of the direct path coefficients. Statistical analyses were performed using IBM SPSS Statistics 26.0 (IBM, Inc., Armonk, NY, USA).

3. Results

3.1. Differences in the Decomposition Variables

After four months of decomposition, the litter cumulative mass losses of *R. typhina* under the control, ammonium chloride, potassium nitrate, urea, and mixed N were 57.93%, 57.38%, 58.69%, 63.66%, and 57.57%, respectively. The litter cumulative mass losses of *K. paniculata* under the control, ammonium chloride, potassium nitrate, urea, and mixed N were 54.98%, 57.99%, 48.14%, 49.02%, and 56.83%, respectively. The litter cumulative mass losses of equally mixed litter from both trees under the control, ammonium chloride, potassium nitrate, urea, and mixed N were 42.95%, 42.29%, 50.42%, 46.18%, and 43.71%, respectively (Figure 2). The litter mass loss of equally mixed litter from both trees was lower than that of *R. typhina* under the control ($p < 0.05$; Figure 2). The litter mass loss of equally mixed litter from both trees was lower than that of *R. typhina* and *K. paniculata* under ammonium chloride ($p < 0.05$; Figure 2). The litter mass loss of equally mixed litter from both trees and that of *K. paniculata* was lower than that of *R. typhina* under urea ($p < 0.05$; Figure 2). The litter mass loss of equally mixed litter from both trees was also lower than that of *R. typhina* under mixed N ($p < 0.05$; Figure 2). There was no significant difference in the litter mass loss of *R. typhina* and that of *K. paniculata* under the control ($p > 0.05$; Figure 2). The form of N did not significantly affect the litter mass loss of the two trees ($p > 0.05$; Figure 2).

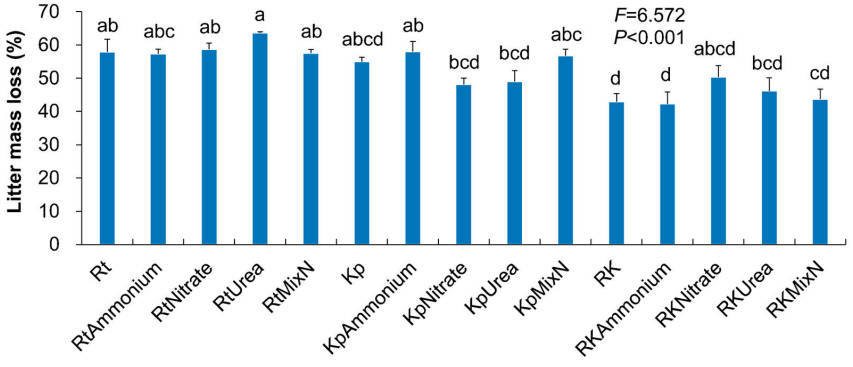

Figure 2. Differences in the litter mass loss of the two trees. Bars (means ± SE; $n = 3$) with different letters indicate significant differences ($p < 0.05$). Abbreviations: Control, the control; ammonium, ammonium chloride; nitrate, potassium nitrate; urea, urea; MixN, mixed N; Rt, *Rhus typhina* L. litter under the control; RtAmmonium, *R. typhina* litter under ammonium chloride; RtNitrate, *R. typhina* litter under potassium nitrate; RtUrea, *R. typhina* litter under urea; RtMixN *R. typhina* litter under mixed N; Kp, *Koelreuteria paniculata* Laxm. litter under the control; KpAmmonium, *K. paniculata* litter under ammonium chloride; KpNitrate, *K. paniculata* litter under potassium nitrate; KpUrea, *K. paniculata* litter under urea; KpMixN, *K. paniculata* litter under mixed N; RK, equally mixed litter from both trees under the control; RKAmmonium, equally mixed litter from both trees under ammonium chloride; RKNitrate, equally mixed litter from both trees under potassium nitrate; RKUrea, equally mixed litter from both trees under urea; RKMixN, equally mixed litter from both trees under mixed N.

The observed decomposition coefficient of equally mixed litter from both trees was lower than its expected decomposition coefficient under the control, ammonium chloride, and mixed N ($p < 0.05$; Figure 3a). The mixing effect intensity of the litter co-decomposition of the two trees was less than zero under all treatments (Figure 3b). The form of N did not significantly affect the mixing effect intensity of the litter co-decomposition of the two trees ($p > 0.05$; Figure 3b).

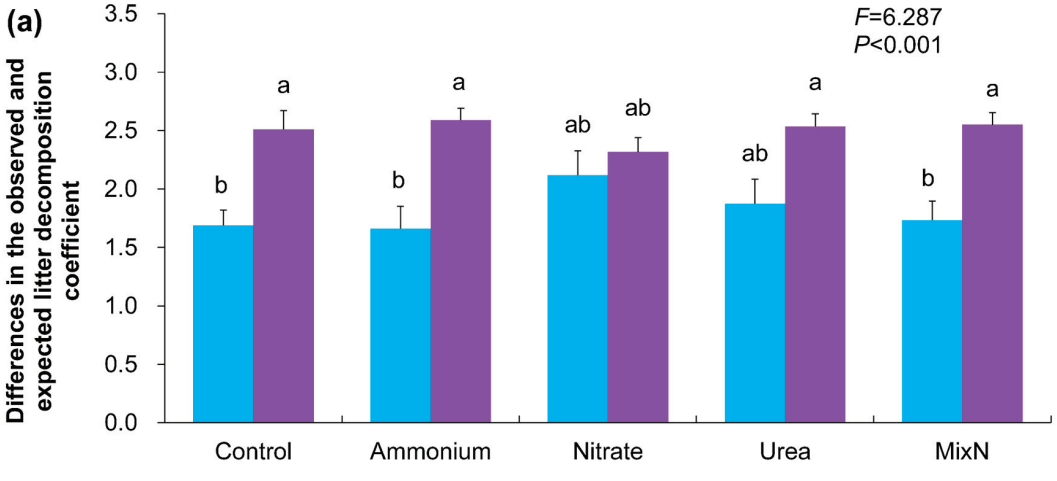

Figure 3. *Cont.*

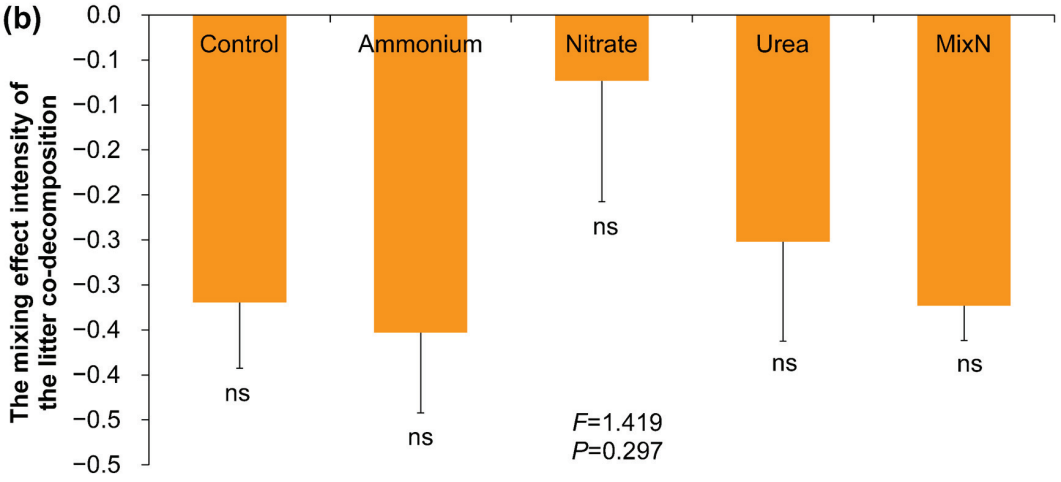

Figure 3. Differences in the observed (blue bars) and expected (purple bars) litter decomposition coefficients (**a**), and the mixing effect intensity of the litter co-decomposition (**b**) of the two trees. Bars (means ± SE; $n = 3$) with different letters indicate significant differences ($p < 0.05$); "ns" means no significant difference ($p > 0.05$). Abbreviations have the same meanings as presented in Figure 2.

3.2. Differences in Soil Physicochemical Properties and Soil Enzyme Activities

Urea and mixed N decreased soil pH and polyphenol oxidase activity, but increased soil total N content compared to the control ($p < 0.05$; Table 1). Ammonium chloride increased soil protease activity compared to the control ($p < 0.05$; Table 1).

Table 1. Soil physicochemical properties and soil enzyme activities. Data (means ± SE; $n = 3$) with different letters in a vertical column indicate significant differences ($p < 0.05$). Data (including soil moisture and soil catalase activity) without significant differences ($p > 0.05$) did not show in this table. Abbreviations have the same meanings as presented in Figure 2.

	Soil pH	Soil Total N Content (g/kg)	Soil Urease Activity (μg/g soil/d)	Soil Protease Activity (μg/g soil/d)	Soil Polyphenol Oxidase Activity (μmol/g soil/h)
Control	6.54 ± 0.03 a–c	8.31 ± 0.41 de	76.67 ± 5.48 b	486.78 ± 53.12 b–e	79.91 ± 6.96 ab
Ammonium	6.53 ± 0.07 a–c	8.94 ± 0.41 de	73.28 ± 2.64 b	838.24 ± 66.48 a	86.67 ± 7.22 a
Nitrate	6.47 ± 0.03 a–d	9.33 ± 0.44 de	98.08 ± 15.08 b	251.47 ± 13.20 e–h	50.21 ± 4.05 b–d
Urea	6.13 ± 0.09 de	15.92 ± 0.37 c	95.50 ± 25.05 b	501.94 ± 41.44 b–e	30.30 ± 2.79 d
MixN	6.10 ± 0.06 e	15.42 ± 0.50 c	78.59 ± 21.97 b	731.19 ± 76.38 ab	31.79 ± 6.59 d
Rt	6.67 ± 0.07 ab	9.20 ± 0.33 de	86.16 ± 8.89 b	653.43 ± 48.04 a–c	36.37 ± 1.85 cd
RtAmmonium	6.33 ± 0.07 b–e	9.22 ± 0.20 de	85.36 ± 14.53 b	133.31 ± 36.15 gh	27.74 ± 2.24 d
RtNitrate	6.50 ± 0.10 a–c	9.40 ± 0.41 de	79.08 ± 21.52 b	553.44 ± 71.11 a–d	32.86 ± 6.22 d
RtUrea	6.40 ± 0.00 a–e	9.38 ± 0.27 de	82.78 ± 12.34 b	89.882 ± 11.91 h	45.06 ± 17.21 d
RtMixN	6.533 ± 0.07 a–c	9.39 ± 0.11 de	79.56 ± 10.38 b	430.23 ± 54.23 c–f	44.74 ± 5.0 cd
Kp	6.67 ± 0.07 ab	10.06 ± 0.40 d	87.45 ± 8.18 b	112.10 ± 24.30 gh	65.15 ± 2.61 a–c
KpAmmonium	6.60 ± 0.00 a–c	8.33 ± 0.52 de	85.84 ± 8.14 b	359.54 ± 23.23 d–h	50.30 ± 1.86 b–d
KpNitrate	6.27 ± 0.07 c–e	9.31 ± 0.34 de	207.76 ± 19.63 a	456.49 ± 67.90 b–f	50.14 ± 6.75 b–d
KpUrea	6.43 ± 0.03 a–e	9.25 ± 0.48 de	86.32 ± 14.70 b	248.44 ± 42.42 e–h	45.62 ± 1.39 cd
KpMixN	6.53 ± 0.03 a–c	9.23 ± 0.04 de	47.67 ± 7.91 b	199.972 ± 71.46 f–h	47.74 ± 1.53 cd
RK	6.40 ± 0.06 a–e	7.82 ± 0.62 e	76.02 ± 10.19 b	258.54 ± 47.60 e–h	51.47 ± 6.31 b–d
RKAmmonium	6.43 ± 0.09 a–e	8.35 ± 0.44 de	94.86 ± 9.13 b	274.70 ± 46.49 d–h	46.10 ± 7.40 cd
RKNitrate	6.630.12 ab	21.73 ± 0.23 a	64.90 ± 14.08 b	276.72 ± 86.13 d–h	29.26 ± 2.016 d
RKUrea	6.70 ± 0.06 a	19.30 ± 0.53 b	85.04 ± 5.32 b	483.76 ± 55.60 b–f	26.82 ± 2.58 d
RKMixN	6.60 ± 0.10 a–c	9.78 ± 0.52 de	87.45 ± 7.86 b	391.85 ± 51.37 c–g	41.23 ± 2.93 cd

The equally mixed litter from both trees under potassium nitrate and urea increased soil total N content compared to the control ($p < 0.05$; Table 1). *K. paniculata* litter under potassium nitrate increased soil urease activity compared to the control ($p < 0.05$; Table 1). *R. typhina* litter under ammonium chloride and urea, and *K. paniculata* litter under the control decreased soil protease activity compared to the control ($p < 0.05$; Table 1). The litter of the two trees, whether mixed or not under N, regardless of the form of N, decreased soil polyphenol oxidase activity compared to the control ($p < 0.05$; Table 1).

Soil pH treated with equally mixed litter from both trees was higher than that treated with *K. paniculata* litter under potassium nitrate ($p < 0.05$; Table 1). Soil pH treated with *K. paniculata* litter under the control was greater than that treated with *K. paniculata* litter under potassium nitrate ($p < 0.05$; Table 1). Soil total N content treated with *K. paniculata* litter was higher than that treated with equally mixed litter from both trees under the control ($p < 0.05$; Table 1). Soil total N content treated with *R. typhina* litter and that treated with *K. paniculata* litter was lower than that treated with equally mixed litter from both trees under potassium nitrate and urea ($p < 0.05$; Table 1). Soil total N content treated with equally mixed litter from both trees following the addition of N in four forms decreased in the following order: potassium nitrate > urea > ammonium chloride > MixN and the control ($p < 0.05$; Table 1). Soil urease activity treated with *R. typhina* litter, and that treated with equally mixed litter from both trees, was lower than that treated with *K. paniculata* litter under potassium nitrate ($p < 0.05$; Table 1). Soil urease activity treated with *K. paniculata* litter under potassium nitrate was greater than that treated with other forms of N ($p < 0.05$; Table 1). Soil protease activity treated with *R. typhina* litter was greater than that treated with *K. paniculata* litter under the control and that treated with equally mixed litter from both trees under the control ($p < 0.05$; Table 1). Soil protease activity treated with *R. typhina* litter was lower than that treated with equally mixed litter from both trees under urea ($p < 0.05$; Table 1).

3.3. Differences in NFB Alpha Diversity

The form of N did not significantly affect NFB alpha diversity ($p > 0.05$; Table 2).

Table 2. Alpha diversity of soil N-fixing bacterial communities. Data (means ± SE; $n = 3$) with different letters in a vertical column indicate significant differences ($p < 0.05$). Data (i.e., Shannon's diversity index) without significant differences ($p > 0.05$) did not show in this table. Abbreviations have the same meanings as presented in Figure 2.

	OTU's Species Index	Simpson's Dominance Index	Chao1's Richness Index	ACE's Richness Index
Control	941.67 ± 25.56 a	0.81 ± 0.01 a–c	1597.13 ± 52.36 a	1591.61 ± 33.56 a–d
Ammonium	897.33 ± 19.62 ab	0.79 ± 0.00 a–c	1489.10 ± 3.04 ab	1534.02 ± 44.11 a–e
Nitrate	941.00 ± 35.57 a	0.83 ± 0.02 a–c	1588.74 ± 62.94 a	1619.08 ± 68.79 ab
Urea	904.33 ± 22.81 ab	0.85 ± 0.02 ab	1583.79 ± 57.64 a	1656.02 ± 38.10 a
MixN	823.67 ± 21.17 a–c	0.86 ± 0.02 a	1435.62 ± 107.20 ab	1487.79 ± 59.44 a–f
Rt	819.67 ± 0.67 a–c	0.81 ± 0.01 a–c	1385.54 ± 37.03 ab	1417.76 ± 32.54 b–f
RtAmmonium	921.00 ± 20.31 ab	0.79 ± 0.01 a–c	1560.81 ± 22.94 ab	1603.92 ± 17.34 a–c
RtNitrate	895.00 ± 9.45 ab	0.79 ± 0.01 a–c	1486.11 ± 25.69 ab	1530.61 ± 20.43 a–e
RtUrea	755.33 ± 31.57 c	0.81 ± 0.01 a–c	1325.73 ± 23.99 ab	1396.96 ± 35.28 c–f
RtMixN	861.67 ± 37.24 a–c	0.77 ± 0.00 a–c	1370.22 ± 24.60 ab	1444.76 ± 35.28 a–f
Kp	856.33 ± 19.70 a–c	0.75 ± 0.02 a–c	1383.04 ± 73.72 ab	1362.96 ± 54.94 ef
KpAmmonium	849.00 ± 15.72 a–c	0.74 ± 0.02 bc	1385.36 ± 21.76 ab	1375.59 ± 24.04 ef
KpNitrate	834.67 ± 56.16 a–c	0.73 ± 0.03 c	1368.83 ± 130.51 ab	1379.77 ± 72.14 d–f
KpUrea	876.67 ± 13.25 a–c	0.74 ± 0.02 a–c	1430.61 ± 25.78 ab	1428.08 ± 12.92 b–f
KpMixN	844.67 ± 21.94 a–c	0.79 ± 0.04 a–c	1288.93 ± 55.25 b	1341.60 ± 39.35 ef
RK	821.67 ± 12.17 a–c	0.76 ± 0.02 a–c	1312.43 ± 32.68 ab	1323.73 ± 26.17 ef
RKAmmonium	875.00 ± 20.11 a–c	0.78 ± 0.04 a–c	1443.83 ± 34.18 ab	1448.28 ± 29.61 a–f
RKNitrate	806.67 ± 8.41 bc	0.78 ± 0.03 a–c	1317.81 ± 14.34 ab	1306.66 ± 7.45 f
RKUrea	795.00 ± 28.43 bc	0.74 ± 0.03 bc	1412.85 ± 40.51 ab	1350.84 ± 38.09 ef
RKMixN	832.00 ± 15.63 a–c	0.73 ± 0.03 c	1383.86 ± 44.21 ab	1356.12 ± 25.61 ef

R. typhina litter under urea, and equally mixed litter from both trees under potassium nitrate and urea, decreased OTU's species index of NFB compared to the control ($p < 0.05$; Table 2). *K. paniculata* litter under mixed N decreased Chao1's richness index of NFB compared to the control ($p < 0.05$; Table 2). *K. paniculata* litter under the control, ammonium chloride, and mixed N, and equally mixed litter from both trees under the control, potassium nitrate, urea, and mixed N, decreased ACE's richness index of NFB compared to the control ($p < 0.05$; Table 2).

The OTU's species index of NFB treated with *R. typhina* litter under ammonium chloride and potassium nitrate was greater than that treated with *R. typhina* litter under urea ($p < 0.05$; Table 2). The ACE's richness index of NFB treated with *R. typhina* litter under potassium nitrate was greater than that treated with equally mixed litter from both trees under potassium nitrate ($p < 0.05$; Table 2).

3.4. The Contribution Intensity of Soil Physicochemical Properties, Soil Enzyme Activities, and NFB Alpha Diversity to the Litter Mass Loss of the Two Trees

The absolute values of the direct path coefficient of Simpson's dominance index (~0.6358), Chao1's richness index (~0.5922), and ACE's richness index (~0.8369) of NFB on the litter mass loss of the two trees were significantly higher than those of other variables (<0.400) (Figure 4).

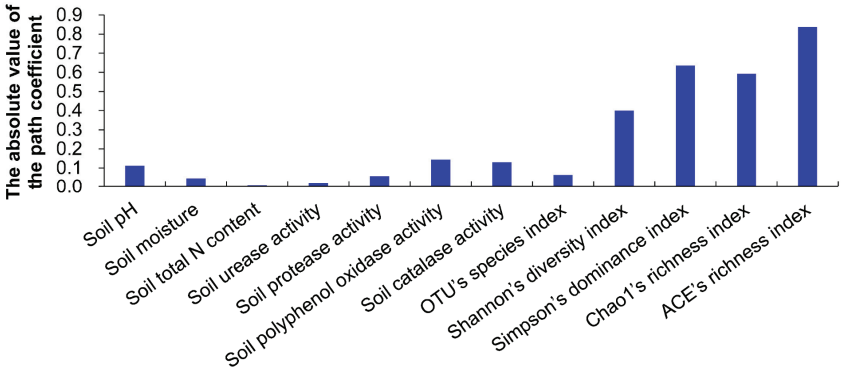

Figure 4. The contribution intensity of soil physicochemical properties, soil enzyme activities, and alpha diversity of soil N-fixing bacterial communities to the litter mass loss of the two trees using the path analysis based on the absolute value of the path coefficient.

3.5. Differences in the NFB Community Structure among Different Treatments

Based on the results of LEfSe analyses, Desulfovibrio and Methylomonas methanica were primarily changed for NFB treated with the control and mixed N, respectively (Figure 5a). Rhodocyclales and Thioploca were primarily changed for NFB treated with *R. typhina* litter under the control (Figure 5b). Thiohalocapsa and Chromatiaceae were primarily changed for NFB treated with *K. paniculata* litter under the control (Figure 5b). Xanthobacter_sp_91 was primarily changed for NFB treated with equally mixed litter from both trees under ammonium chloride (Figure 5c). Desulfotomaculum arcticum was primarily changed for NFB treated with *R. typhina* litter under potassium nitrate (Figure 5d). Desulfovibrio longus, Thioalbus denitrificans, and Methylomicrobium were primarily changed for NFB treated with *K. paniculata* litter under potassium nitrate (Figure 5d). Propionibacterium, Propionibacteriaceae, Propionibacteriales, Actinobacteria, Niveispirillum, and Geoalkalibacter were primarily changed for NFB treated with equally mixed litter from both trees under potassium nitrate (Figure 5d). Marinospirillum, Oceanospirillaceae, and Oceanospirillales were primarily changed for NFB treated with *R. typhina* litter under urea (Figure 5e). Sphingomonadaceae, Sphingomonadales, and Geopsychrobacter were primarily changed for NFB treated with *K. paniculata* litter under urea (Figure 5e). Geother-

mobacter, Methylomonas, Thioflexothrix, Thiotrichales, and unclassified Thiotrichales were primarily changed for NFB treated with equally mixed litter from both trees under urea (Figure 5e). Celerinatantimonas diazotrophica, Celerinatantimonas, Celerinatantimonadaceae, and unclassified Gammaproteobacteria were primarily changed for NFB treated with *R. typhina* litter under mixed N (Figure 5f). Azoarcus communis was primarily changed for NFB treated with equally mixed litter from both trees under mixed N (Figure 5f).

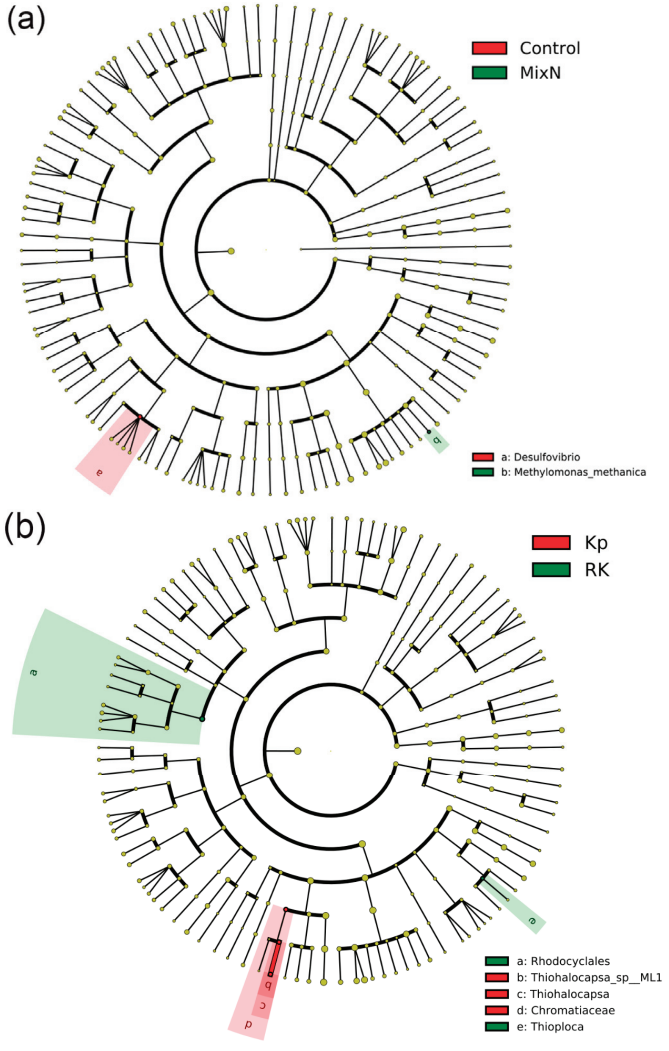

Figure 5. *Cont.*

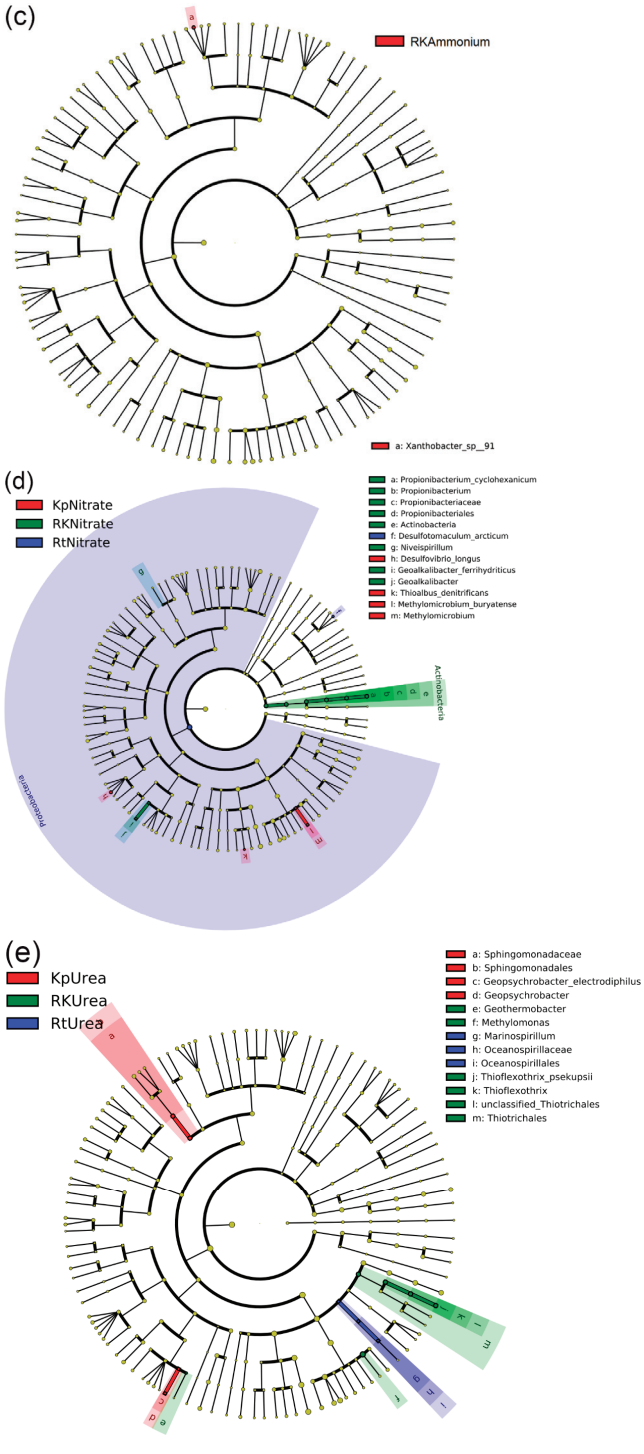

Figure 5. *Cont.*

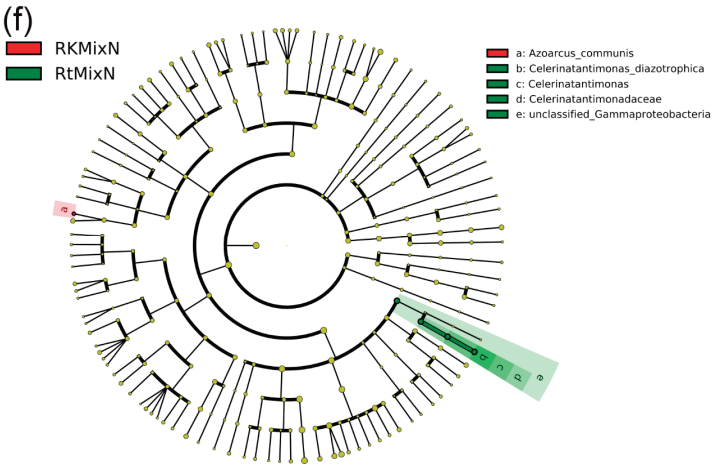

Figure 5. LEfSe evolutionary branch diagram of soil N-fixing bacterial communities. (**a**) The addition of N in four forms; (**b**) the litter of the two trees under the control; (**c**) the litter of the two trees under ammonium chloride; (**d**) the litter of the two trees under potassium nitrate; (**e**) the litter of the two trees under urea; (**f**) the litter of the two trees under mixed N. The taxa with significantly different abundances among treatments are signified by colored dots, and from the center outward, they mean the kingdom, phylum, class, order, family, genus, and species levels, respectively. The colored shadows mean trends of the significantly differed taxa. Only taxa meeting an LDA significance threshold of >2 are displayed. Abbreviations have the same meanings as presented in Figure 2.

4. Discussion

The litter mass loss of *R. typhina* was similar to that of *K. paniculata* (Figure 2). Thus, contrary to the first hypothesis, *R. typhina* litter did not degrade more easily than *K. paniculata* litter. These observations are also inconsistent with the results of previous research which has shown that invasive plants either degrade more rapidly [18–21], or significantly more slowly than native plants [58–60]. This phenomenon may be due to the similar proportions of soluble and recalcitrant components in the litter of the two trees [28]. In other words, the two trees had similar litter quality, probably because they coexist in the same habitat and have similar growing seasons, growing environments, and lifestyles. This phenomenon may also be attributed to the relatively short time frame of this study, in which the rapid decomposition of *R. typhina* could not be manifested.

In nature, the two trees typically co-exist [21,42]. As a result, the litter decomposition may be altered when the litter from the two trees is mixed. Non-additive responses in the litter co-decomposition of invasive plants and native plants are often observed, and generally, the litter decomposition of invasive plants can accelerate that of native plants [21,49,61,62]. In this study, the decomposition of the mixed litter from both trees was slower than that of the individual litter of either species (Figure 2). In addition, the observed decomposition rate for equally mixed litter from both trees was also significantly lower than its expected decomposition rate (Figure 3a). More importantly, the mixing effect intensity of the litter co-decomposition of the two trees was less than zero (Figure 3b). Thus, contrary to the second hypothesis, antagonistic responses were observed in the litter co-decomposition of the two trees. Accordingly, there may be an interspecific interference during the litter co-decomposition process for the co-decomposition of the two trees. In addition, some recalcitrant components (difficult to decompose) may be formed during the litter co-decomposition process for the co-decomposition of the two trees. Studies on the non-additive responses for the co-decomposition of two plant species have shown that only 30% additive, 50% synergistic, and 50% antagonistic responses were observed [63]. The reason for these differences may be closely related to the differences in the relatedness of

plant species, the initial quality and quantity of plant litter, the type of culture medium, the initial soil physicochemical properties, the initial (decomposer) microbial communities in culture medium, the ratio of the two plant litters mixed, and the duration of the experiment.

Invasive plants can mediate changes in soil enzyme activity [64–67] by releasing nutrients, such as carbon- and N-containing substances, during the litter co-decomposition process. Surprisingly, *R. typhina* litter significantly increased soil protease activity under the control, but significantly decreased soil urease activity under potassium nitrate compared to that of *K. paniculata* in this study (Table 1). Hence, *R. typhina* can increase the level of urea hydrolysis but decrease the level of protein hydrolysis. Previous studies also showed that invasive plants can increase [65,66,68,69] or decrease soil enzyme activities [48,70–72], or have no significant on soil enzyme activities [67,73–75]. Thus, the effects of invasive plants on soil enzyme activities may be species-dependent [28,76] and N-form-dependent [48,77], mainly due to the differences in soil physicochemical properties and the level of available soil nutrients under different plant species and/or different forms of N.

ACE's richness of NFB under *K. paniculata* litter and equally mixed litter from both trees was lower than that under the control (Table 2). Thus, the litter decomposition of *K. paniculata* and that of equally mixed litter from both trees under the control may be slower, mainly due to the reduced richness of NFB. Previous studies have shown that the abundance and diversity of the nifH gene are strongly associated with the soil available N levels [9–12]. At the same time, the contribution intensity of the richness of NFB to the litter mass loss was obviously greater than other variables based on the results of path analysis (Figure 4). However, contrary to the third hypothesis, the litter decomposition of *R. typhina* under the control did not significantly affect NFB alpha diversity (Table 2). Interestingly, the litter mass loss of the two trees under the control appeared to result in significant variations in the relative abundance of various NFB taxa, i.e., Rhodocyclales and Thioploca were abundant during the litter decomposition of *R. typhina* under the control, and Thiohalocapsa and Chromatiaceae were abundant during the litter decomposition of *K. paniculata* under the control (Figure 5). Thus, the litter decomposition of the two trees under the control results in the presence of numerous dominant biomarkers of NFB. The main reason may be that there is still some difference in the litter quality between the two trees, leading to the species differentiation of NFB. Accordingly, the litter decomposition of the two trees under the control mainly affected the composition of NFB, rather than their alpha diversity. Earlier studies have also verified that plant species, particularly the invasive plants, mainly affected the composition of soil microbial communities rather than NFB alpha diversity [78,79].

Generally, N addition can trigger soil acidification mainly due to the release and accumulation of free H^+ via nitrification [14,80,81]. The same results were observed in this study (Table 1). In addition, ammonium chloride increased soil protease activity, but urea and mixed N decreased soil polyphenol oxidase activity (Table 1). Thus, the impacts of N addition on soil enzyme activities could vary and depend on the form of N. However, the form of N did not significantly affect the litter mass loss of the two trees and NFB alpha diversity (Figure 2 and Table 2). Thus, the fourth hypothesis could not be supported based on this finding. Nonetheless, mixed N triggered a significant variation in the abundance of Methylomonas methanica (Figure 5). Thus, Methylomonas methanica may be used as a dominant biomarker under mixed N.

In addition, contrary to the fifth and sixth hypotheses, the form of N did not significantly affect the litter mass loss of the two trees (Figure 2), the mixing effect intensity of the litter co-decomposition of the two trees (Figure 3b), or NFB alpha diversity (Table 2). Thus, the degree of influence of N addition on the litter mass loss of *R. typhina* and NFB alpha diversity was similar to that of *K. paniculata*. However, the litter mass loss of *R. typhina* was significantly higher than that of *K. paniculata* under urea (Figure 2). Thus, *R. typhina* litter may decompose more effectively and rapidly than *K. paniculate* litter under urea. This finding is consistent with the previous studies, i.e., invasive plants decompose more easily and rapidly than native plants [18–21]. This phenomenon may be due to the higher

percentage of soluble components and lower percentage of recalcitrant components in *R. typhina* litter compared to those of *K. paniculate* litter, and/or the compounds contained in *R. typhina* litter may be more readily released into the soil in the presence of urea. This may also be due to the fact that the limitation of the level of N utilization for the metabolic activity of soil bacterial community in relation to the decomposition process is alleviated to a greater extent in *R. typhina* litter, compared to *K. paniculate* litter under urea [14,82]. In this study, soil total N content under urea was significantly higher than that under ammonium chloride and potassium nitrate (Table 1). Previous studies also showed that soil bacterial community is more likely to utilize organic N than inorganic N [14,83]. Thus, the nutrient cycling rate during the decomposition process of *R. typhina* may be obviously higher than that of *K. paniculate* under urea. Consequently, an increase in the relative proportion of urea in the atmospheric N deposition may be beneficial to the invasion of *R. typhina* via the increased nutrient cycling rate mediated by the accelerated litter mass loss.

The LEfSe analysis revealed that the litter decomposition of the two trees following the addition of N in four forms resulted in significant variations in the relative abundance of various NFB taxa, i.e., Xanthobacter_sp_91 under the litter decomposition of equally mixed litter from both trees treated with: ammonium chloride; Desulfotomaculum arcticum under the litter decomposition of *R. typhina* treated with potassium nitrate; Desulfovibrio longus, Thioalbus denitrificans, and Methylomicrobium under the litter decomposition of *K. paniculata* treated with potassium nitrate; Propionibacterium, Propionibacteriaceae, Propionibacteriales, Actinobacteria, Niveispirillum, and Geoalkalibacter under the litter decomposition of equally mixed litter from both trees treated with potassium nitrate; Marinospirillum, Oceanospirillaceae, and Oceanospirillales under the litter decomposition of *R. typhina* treated with urea; Sphingomonadaceae, Sphingomonadales, and Geopsychrobacter under the litter decomposition of *K. paniculata* treated with urea; Geothermobacter, Methylomonas, Thioflexothrix, Thiotrichales, and unclassified Thiotrichales under the litter decomposition of equally mixed litter from both trees treated with urea; Celerinatantimonas diazotrophica, Celerinatantimonas, Celerinatantimonadaceae, and unclassified Gammaproteobacteria under the litter decomposition of *R. typhina* treated with mixed N; Azoarcus communis under the litter decomposition of equally mixed litter from both trees treated with mixed N (Figure 5). Thus, the litter decomposition of the two trees following the addition of N in four forms causes a substantial effect on certain NFB taxa. The differential shifts in NFB composition in response to the litter decomposition of the two trees following the addition of N in four forms could be primarily due to the differences in the level of nitrogenophilic ability of those NFB taxa. Thus, the addition of N in different forms can exert different intensities of selective pressure on different NFB taxa, leading to increases (e.g., the nitrogenophilic NFB taxa) or decreases (e.g., the NFB taxa that are poorly tolerant to N addition) in the proportion of specific NFB taxa.

5. Conclusions

This study is the first attempt to elucidate the effects of the invasive *R. typhina* and native *K. paniculata* trees on the litter mass loss, soil physicochemical properties, soil enzyme activities, and the NFB community under different forms of N deposition. The main conclusions are that: (1) There were antagonistic responses to the litter co-decomposition of the two trees based on the values of the mixing effect intensity of the litter co-decomposition of the two trees; (2) the litter mass loss of the two trees was mainly affected by the richness of NFB based on the results of path analysis; (3) the form of N did not significantly affect the litter mass loss of the two trees, the mixing effect intensity of the litter co-decomposition of the two trees, or NFB alpha diversity based on the results of one-way ANOVA; (4) the litter mass loss of *R. typhina* was significantly higher than that of *K. paniculata* under urea based on the results of one-way ANOVA; (5) The litter decomposition of the two trees under the control, and following the addition of N in four forms, mainly affected the composition of NFB, i.e., resulted in significant variations in the relative abundance of various NFB taxa, rather than NFB alpha diversity, based on the results of LEfSe analyses.

Supplementary Materials: The following supporting information can be downloaded at: https://www.mdpi.com/article/10.3390/atmos15040424/s1, Figure S1. The photo of the environment in which the two trees grow (a), *Rhus typhina* L.; (b), *Koelreuteria paniculata* Laxm.).

Author Contributions: Y.L.: Data curation; Investigation; Methodology; Writing—review and editing; C.L.: Data curation; Investigation; Methodology; Writing—review and editing; H.C.: Data curation; Investigation; Methodology; Writing—review and editing; Z.X. (Zhelun Xu): Data curation; Methodology; Writing—review and editing; S.Z.: Data curation; Methodology; Writing—review and editing; M.Z.: Data curation; Formal analysis; Writing—review and editing; Y.W.: Data curation; Formal analysis; Writing—review and editing; Z.X. (Zhongyi Xu): Data curation; Formal analysis; Writing—review and editing; D.D.: Funding acquisition; Project administration; Writing—review and editing; C.W.: Conceptualization; Formal analysis; Funding acquisition; Project administration; Supervision; Writing—original draft; H.Z.: Conceptualization; Formal analysis; Funding acquisition; Project administration; Supervision; Writing—review and editing. All authors have read and agreed to the published version of the manuscript.

Funding: This study was funded by Scientific Research Start-up Fund for High-level Talents of Jinling Institute of Technology (jit-rcyj-202302), Open Science Research Fund of Key Laboratory of Forest Plant Ecology, Ministry of Education (Northeast Forestry University), China (Grant No.: K2020B02), National Natural Science Foundation of China (Grant No.: 32071521), Special Research Project of School of Emergency Management, Jiangsu University (Grant No.: KY-C-01), Carbon Peak and Carbon Neutrality Technology Innovation Foundation of Jiangsu Province (Grant No.: BK20220030), and Jiangsu Collaborative Innovation Center of Technology and Material of Water Treatment (no grant number).

Institutional Review Board Statement: Not applicable.

Informed Consent Statement: Not applicable.

Data Availability Statement: The datasets generated during and/or analyzed during the current study are available from the corresponding author on reasonable request due to non-commercial academic research.

Acknowledgments: We are extremely grateful to the anonymous reviewers for their most insightful and constructive comments and valuable editorial efforts, which have enabled us to improve the manuscript significantly.

Conflicts of Interest: The authors declare no conflicts of interest.

References

1. Li, Q.W.; Zhang, X.Y.; Liang, J.F.; Gao, J.Q.; Xu, X.L.; Yu, F.H. High nitrogen uptake and utilization contribute to the dominance of invasive *Spartina alterniflora* over native *Phragmites australis*. *Biol. Fertil. Soils* **2021**, *57*, 1007–1013. [CrossRef]
2. Parepa, M.; Fischer, M.; Bossdorf, O. Environmental variability promotes plant invasion. *Nat. Commun.* **2013**, *4*, 1604. [CrossRef] [PubMed]
3. Feng, Y.L.; Lei, Y.B.; Wang, R.F.; Callaway, R.M.; Alfonso, V.B.; Inderjit; Li, Y.P.; Zheng, Y.L. Evolutionary tradeoffs for nitrogen allocation to photosynthesis versus cell walls in an invasive plant. *Proc. Natl. Acad. Sci. USA* **2009**, *106*, 1853–1856. [CrossRef] [PubMed]
4. Mantoani, M.C.; Gonzalez, A.B.; Sancho, L.G.; Osborne, B.A. Growth, phenology and N-utilization by invasive populations of *Gunnera tinctoria*. *J. Plant Ecol.* **2020**, *13*, 589–600. [CrossRef]
5. Davidson, A.M.; Jennions, M.; Nicotra, A.B. Do invasive species show higher phenotypic plasticity than native species and, if so, is it adaptive? A meta-analysis. *Ecol. Lett.* **2011**, *14*, 419–431. [CrossRef] [PubMed]
6. Kamutando, C.N.; Vikram, S.; Kamgan-Nkuekam, G.; Makhalanyane, T.P.; Greve, M.; Le Roux, J.J.; Richardson, D.M.; Cowan, D.; Valverde, A. Soil nutritional status and biogeography influence rhizosphere microbial communities associated with the invasive tree *Acacia dealbata*. *Sci. Rep.* **2017**, *7*, 6472. [CrossRef] [PubMed]
7. Xu, C.W.; Yang, M.Z.; Chen, Y.J.; Chen, L.M.; Zhang, D.Z.; Mei, L.; Shi, Y.T.; Zhang, H.B. Changes in non-symbiotic nitrogen-fixing bacteria inhabiting rhizosphere soils of an invasive plant *Ageratina adenophora*. *Appl. Soil Ecol.* **2012**, *54*, 32–38. [CrossRef]
8. Li, J.; He, J.Z.; Liu, M.; Yan, Z.Q.; Xu, X.L.; Kuzyakov, Y. Invasive plant competitivity is mediated by nitrogen use strategies and rhizosphere microbiome. *Soil Biol. Biochem.* **2024**, *192*, 109361. [CrossRef]
9. Reed, S.C.; Townsend, A.R.; Cleveland, C.C.; Nemergut, D.R. Microbial community shifts influence patterns in tropical forest nitrogen fixation. *Oecologia* **2010**, *164*, 521–531. [CrossRef] [PubMed]

10. Chinnadurai, C.; Gopalaswamy, G.; Balachandar, D. Long term effects of nutrient management regimes on abundance of bacterial genes and soil biochemical processes for fertility sustainability in a semi-arid tropical Alfisol. *Geoderma* **2014**, *232*, 563–572. [CrossRef]
11. Huhe; Borjigin, S.; Buhebaoyin; Wu, Y.P.; Li, M.Q.; Cheng, Y.X. Microbial nitrogen-cycle gene abundance in soil of cropland abandoned for different periods. *PLoS ONE* **2016**, *11*, e0154697. [CrossRef] [PubMed]
12. Silva, M.; Schloter-Hai, B.; Schloter, M.; van Elsas, J.D.; Salles, J.F. Temporal dynamics of abundance and composition of nitrogen-fixing communities across agricultural soils. *PLoS ONE* **2013**, *8*, e74500.
13. Lindsay, E.A.; Colloff, M.J.; Gibb, N.L.; Wakelin, S.A. The abundance of microbial functional genes in grassy woodlands is influenced more by soil nutrient enrichment than by recent weed invasion or livestock exclusion. *Appl. Environ. Microbiol.* **2010**, *76*, 5547–5555. [CrossRef] [PubMed]
14. Wang, C.Y.; Zhou, J.W.; Liu, J.; Jiang, K.; Du, D.L. Responses of soil N-fixing bacteria communities to *Amaranthus retroflexus* invasion under different forms of N deposition. *Agric. Ecosyst. Environ.* **2017**, *247*, 329–336. [CrossRef]
15. Ren, B.H.; Meng, M.; Yu, J.X.; Ma, X.W.; Li, D.Y.; Li, J.H.; Yang, J.Y.; Bai, L.; Feng, Y.L. Invasion by *Cenchrus spinifex* changes the soil microbial community structure in a sandy grassland ecosystem. *Heliyon* **2023**, *9*, e20860. [CrossRef] [PubMed]
16. Lau, J.A.; Suwa, T. The changing nature of plant-microbe interactions during a biological invasion. *Biol. Invasions* **2016**, *18*, 3527–3534. [CrossRef]
17. Wang, Z.J.; Li, X.; Wang, J.H.; Qi, S.S.; Dai, Z.C.; Du, D.L. Effect of nitrogen-fixing bacteria on resource investment of the root system in an invasive clonal plant under low nutritional environment. *Flora* **2022**, *297*, 152166. [CrossRef]
18. Cuassolo, F.; Diaz Villanueva, V.; Modenutti, B. Litter decomposition of the invasive *Potentilla anserina* in an invaded and non-invaded freshwater environment of North Patagonia. *Biol. Invasions* **2020**, *22*, 1055–1065. [CrossRef]
19. Liao, C.Z.; Peng, R.H.; Luo, Y.Q.; Zhou, X.H.; Wu, X.W.; Fang, C.M.; Chen, J.K.; Li, B. Altered ecosystem carbon and nitrogen cycles by plant invasion: A meta-analysis. *New Phytol.* **2008**, *177*, 706–714. [CrossRef] [PubMed]
20. Hu, X.; Arif, M.; Ding, D.D.; Li, J.J.; He, X.R.; Li, C.X. Invasive plants and species richness impact litter decomposition in Riparian Zones. *Front. Plant Sci.* **2022**, *13*, 955656. [CrossRef] [PubMed]
21. Xu, Z.L.; Zhong, S.S.; Yu, Y.L.; Li, Y.; Li, C.; Xu, Z.Y.; Liu, J.; Wang, C.Y.; Du, D.L. Heavy metal contamination alters the co-decomposition of leaves of the invasive tree *Rhus typhina* L. and the native tree *Koelreuteria paniculata* Laxm. *Plants* **2023**, *12*, 2523. [CrossRef] [PubMed]
22. Marchante, E.; Marchante, H.; Freitas, H.; Kjøller, A.; Struwe, S. Decomposition of an N-fixing invasive plant compared with a native species: Consequences for ecosystem. *Appl. Soil Ecol.* **2019**, *138*, 19–31. [CrossRef]
23. Galloway, J.N.; Townsend, A.R.; Erisman, J.W.; Bekunda, M.; Cai, Z.; Freney, J.R.; Martinelli, L.A.; Seitzinger, S.P.; Sutton, M.A. Transformation of the nitrogen cycle: Recent trends, questions, and potential solutions. *Science* **2008**, *320*, 889–892. [CrossRef] [PubMed]
24. Zhang, Y.; Song, L.; Liu, X.J.; Li, W.Q.; Lu, S.H.; Zheng, L.X.; Bai, Z.C.; Cai, G.Y.; Zhang, F.S. Atmospheric organic nitrogen deposition in China. *Atmos. Environ.* **2012**, *49*, 422. [CrossRef]
25. Gao, Y.; Wang, L.; Guo, X.; Xu, Y.; Luo, L. Atmospheric wet and dry deposition of dissolved inorganic nitrogen to the South China Sea. *Sci. China-Earth Sci.* **2020**, *63*, 1339–1352. [CrossRef]
26. Cornell, S.E. Atmospheric nitrogen deposition: Revisiting the question of the importance of the organic component. *Environ. Pollut.* **2011**, *159*, 2214–2222. [CrossRef] [PubMed]
27. Sinsabaugh, R.L.; Carreiro, M.M.; Repert, D.A. Allocation of extracellular enzymatic activity in relation to litter composition, N deposition, and mass loss. *Biogeochemistry* **2002**, *60*, 1–24. [CrossRef]
28. Li, C.; Li, Y.; Zhong, S.S.; Xu, Z.L.; Xu, Z.Y.; Zhu, M.W.; Wei, Y.Q.; Wang, C.Y.; Du, D.L. Do the leaves of multiple invasive plants decompose more easily than a native plant's under nitrogen deposition with different forms? *Nitrogen* **2024**, *5*, 202–218. [CrossRef]
29. Saiz, E.; Sgouridis, F.; Drijfhout, F.P.; Peichl, M.; Nilsson, M.B.; Ullah, S. Chronic atmospheric reactive nitrogen deposition suppresses biological nitrogen fixation in Peatlands. *Environ. Sci. Technol.* **2021**, *55*, 1310–1318. [CrossRef] [PubMed]
30. Berthrong, S.T.; Yeager, C.M.; Gallegos-Graves, L.; Steven, B.; Eichorst, S.A.; Jackson, R.B.; Kuske, C.R. Nitrogen fertilization has a stronger effect on soil nitrogen-fixing bacterial communities than elevated atmospheric CO_2. *Appl. Environ. Microbiol.* **2014**, *80*, 3103–3112. [CrossRef] [PubMed]
31. Huang, X.L.; Chen, J.Z.; Wang, D.; Deng, M.M.; Wu, M.Y.; Tong, B.L.; Liu, J.M. Simulated atmospheric nitrogen deposition inhibited the leaf litter decomposition of *Cinnamomum migao* H. W. Li in Southwest China. *Sci. Rep.* **2021**, *11*, 1748. [CrossRef]
32. Whalen, E.D.; Smith, R.G.; Grandy, A.S.; Frey, S.D. Manganese limitation as a mechanism for reduced decomposition in soils under atmospheric nitrogen deposition. *Soil Biol. Biochem.* **2018**, *127*, 252–263. [CrossRef]
33. Zhang, Z.L.; Suseela, V. Nitrogen availability modulates the impacts of plant invasion on the chemical composition of soil organic matter. *Soil Biol. Biochem.* **2021**, *156*, 108195. [CrossRef]
34. Zhang, Z.J.; Jiang, C.D.; Zhang, J.Z.; Zhang, H.J.; Shi, L. Ecophysiological evaluation of the potential invasiveness of *Rhus typhina* in its non-native habitats. *Tree Physiol.* **2009**, *29*, 1307–1316. [CrossRef] [PubMed]
35. Kossah, R.; Zhang, H.; Chen, W. Antimicrobial and antioxidant activities of Chinese sumac (*Rhus typhina* L.) fruit extract. *Food Control* **2011**, *22*, 128–132. [CrossRef]
36. Tan, X.F.; Guo, X.; Guo, W.H.; Liu, S.N.; Du, N. Invasive *Rhus typhina* invests more in height growth and traits associated with light acquisition than do native and non-invasive alien shrub species. *Trees* **2018**, *32*, 1103–1112. [CrossRef]

37. Fu, Y.D.; Xu, W.; Wen, Z.; Han, M.J.; Sun, J.H.; Tang, A.H.; Liu, X. Enhanced atmospheric nitrogen deposition at a rural site in northwest China from 2011 to 2018. *Atmos. Res.* **2020**, *245*, 105071. [CrossRef]
38. Luo, X.S.; Liu, X.J.; Pan, Y.P.; Wen, Z.; Xu, W.; Zhang, L.; Kou, C.L.; Lv, J.L.; Goulding, K. Atmospheric reactive nitrogen concentration and deposition trends from 2011 to 2018 at an urban site in north China. *Atmos. Environ.* **2020**, *224*, 117298. [CrossRef]
39. Zhu, J.X.; Chen, Z.; Wang, Q.F.; Xu, L.; He, N.P.; Jia, Y.L.; Zhang, Q.Y.; Yu, G.R. Potential transition in the effects of atmospheric nitrogen deposition in China. *Environ. Pollut.* **2020**, *258*, 113739. [CrossRef] [PubMed]
40. National Bureau of Statistics. *Zhenjiang Statistical Yearbook 2022*; China Statistics Press: Beijing, China, 2022.
41. Cornell, S.E.; Jickells, T.D.; Cape, J.N.; Rowland, A.P.; Duce, R.A. Organic nitrogen deposition on land and coastal environments: A review of methods and data. *Atmos. Environ.* **2003**, *37*, 2173–2191. [CrossRef]
42. Xu, Z.L.; Zhong, S.S.; Yu, Y.L.; Wang, Y.Y.; Cheng, H.Y.; Du, D.L.; Wang, C.Y. *Rhus typhina* L. triggered greater allelopathic effects than *Koelreuteria paniculata* Laxm under ammonium fertilization. *Sci. Hortic.* **2023**, *309*, 111703. [CrossRef]
43. Voříšková, J.; Baldrian, P. Fungal community on decomposing leaf litter undergoes rapid successional changes. *ISME J.* **2013**, *7*, 477–486. [CrossRef] [PubMed]
44. Li, H.; Wei, Z.; Huangfu, C.; Chen, X.; Yang, D. Litter mixture dominated by leaf litter of the invasive species, *Flaveria bidentis*, accelerates decomposition and favors nitrogen release. *J. Plant Res.* **2017**, *130*, 167–180. [CrossRef] [PubMed]
45. Hoorens, B.; Aerts, R.; Stroetenga, M. Does initial litter chemistry explain litter mixture effects on decomposition. *Oecologia* **2003**, *137*, 578–586. [CrossRef] [PubMed]
46. Jones, G.L.; Scullion, J.; Worgan, H.; Gwynn-Jones, D. Litter of the invasive shrub *Rhododendron ponticum* (Ericaceae) modifies the decomposition rate of native UK woodland litter. *Ecol. Indic.* **2019**, *107*, 105597. [CrossRef]
47. Olson, J.S. Energy storage and the balance of producers and decomposers in ecological systems. *Ecology* **1963**, *44*, 322–331. [CrossRef]
48. Zhong, S.S.; Xu, Z.L.; Yu, Y.L.; Liu, J.; Wang, Y.Y.; Guo, E.; Wang, C.Y. *Rhus typhina* decreased soil nitrogen contents and peroxidase activity following the addition of nitrogen. *Int. J. Environ. Sci. Technol.* **2023**, *111*, 17–22. [CrossRef]
49. Yu, Y.L.; Cheng, H.Y.; Wang, C.Y.; Du, D.L. Heavy drought reduces the decomposition rate of the mixed litters of two composite invasive alien plants. *J. Plant Ecol.* **2023**, *16*, rtac047. [CrossRef]
50. Nannipieri, P.; Ceccanti, B.; Cervelli, S.; Matarese, E. Extraction of phosphatase, urease, proteases, organic-carbon, and nitrogen from soil. *Soil Sci. Soc. Am. J.* **1980**, *44*, 1011–1016. [CrossRef]
51. Guan, S.Y. *Soil Enzyme and Its Research Methods*; Agricultural Press: Beijing, China, 1986.
52. Zhang, J.E. *Experimental Methods and Techniques Commonly Used in Ecology*; Chemical Industry Press: Beijing, China, 2006.
53. Perucci, P.; Casucci, C.; Dumontet, S. An improved method to evaluate the *o*-diphenol oxidase activity of soil. *Soil Biol. Biochem.* **2000**, *32*, 1927–1933. [CrossRef]
54. Gaby, J.C.; Buckley, D.H. A comprehensive aligned *nifH* gene database: A multipurpose tool for studies of nitrogen-fixing bacteria. *Database* **2014**, *2014*, bau001. [CrossRef] [PubMed]
55. Liu, J.Y.; Peng, M.J.; Li, Y.G. Phylogenetic diversity of nitrogen-fixing bacteria and the *nifH* gene from mangrove rhizosphere soil. *Can. J. Microbiol.* **2012**, *58*, 531–539. [CrossRef] [PubMed]
56. Liu, Y.J.; Hu, B.; Zhu, J.B.; Shen, S.J.; Yu, G.Q. *nifH* promoter activity is regulated by DNA supercoiling in *Sinorhizobium meliloti*. *Acta Biochim. Biophys. Sin.* **2005**, *37*, 221–226. [CrossRef] [PubMed]
57. Poly, F.; Ranjard, L.; Nazaret, S.; Gourbière, F.; Monrozier, L.J. Comparison of *nifH* gene pools in soils and soil microenvironments with contrasting properties. *Appl. Environ. Microbiol.* **2001**, *67*, 2255–2262. [CrossRef] [PubMed]
58. Norris, M.D.; Blair, J.M.; Johnson, L.C. Land cover change in eastern Kansas: Litter dynamics of closed-canopy eastern redcedar forests in tallgrass prairie. *Can. J. Bot. Rev. Can. Bot.* **2001**, *79*, 214–222. [CrossRef]
59. Ehrenfeld, J.G. Ecosystem consequences of biological invasions. *Annu. Rev. Ecol. Evol. Syst.* **2010**, *41*, 59–80. [CrossRef]
60. Vila, M.; Espinar, J.L.; Hejda, M.; Hulme, P.E.; Jarosik, V.; Maron, J.L.; Pergl, J.; Schaffner, U.; Sun, Y.; Pysek, P. Ecological impacts of invasive alien plants: A meta-analysis of their effects on species, communities and ecosystems. *Ecol. Lett.* **2011**, *14*, 702–708. [CrossRef] [PubMed]
61. Mitchell, J.D.; Lockaby, B.G.; Brantley, E.F. Influence of Chinese Privet (*Ligustrum sinense*) on decomposition and nutrient availability in riparian forests. *Invasive Plant Sci. Manag.* **2011**, *4*, 437–447. [CrossRef]
62. Schuster, M.J.; Dukes, J.S. Non-additive effects of invasive tree litter shift seasonal N release: A potential invasion feedback. *Oikos* **2014**, *123*, 1101–1111. [CrossRef]
63. Gartner, T.B.; Cardon, Z.G. Decomposition dynamics in mixed species leaf litter. *Oikos* **2004**, *104*, 230–246. [CrossRef]
64. Torres, N.; Herrera, I.; Fajardo, L.; Bustamante, R.O. Meta-analysis of the impact of plant invasions on soil microbial communities. *BMC Ecol. Evol.* **2021**, *21*, 172. [CrossRef] [PubMed]
65. Zhou, Y.; Staver, A.C. Enhanced activity of soil nutrient-releasing enzymes after plant invasion: A meta-analysis. *Ecology* **2019**, *100*, e02830. [CrossRef] [PubMed]
66. Keet, J.H.; Ellis, A.G.; Hui, C.; Novoa, A.; Le Roux, J.J. Impacts of invasive Australian acacias on soil bacterial community composition, microbial enzymatic activities, and nutrient availability in fynbos soils. *Microb. Ecol.* **2021**, *82*, 704–721. [CrossRef] [PubMed]

67. Wei, H.; Yan, W.B.; Quan, G.M.; Zhang, J.E.; Liang, K.M. Soil microbial carbon utilization, enzyme activities and nutrient availability responses to *Bidens pilosa* and a non-invasive congener under different irradiances. *Sci. Rep.* **2017**, *7*, 11309. [CrossRef] [PubMed]
68. Allison, S.D.; Nielsen, C.; Hughes, R.F. Elevated enzyme activities in soils under the invasive nitrogen-fixing tree *Falcataria moluccana*. *Soil Biol. Biochem.* **2006**, *38*, 1537–1544. [CrossRef]
69. Xu, H.W.; Liu, Q.; Wang, S.Y.; Yang, G.S.; Xue, S. A global meta-analysis of the impacts of exotic plant species invasion on plant diversity and soil properties. *Sci. Total Environ.* **2022**, *810*, 152286. [CrossRef] [PubMed]
70. Wang, L.; Yuan, J.H.; Wang, Y.; Butterly, C.R.; Tong, D.L.; Zhou, B.; Li, X.Z.; Zhang, H.B. Effects of exotic *Spartina alterniflora* invasion on soil phosphorus and carbon pools and associated soil microbial community composition in coastal wetlands. *ACS Omega* **2021**, *6*, 5730–5738. [CrossRef] [PubMed]
71. Stefanowicz, A.M.; Stanek, M.; Nobis, M.; Zubek, S. Species–specific effects of plant invasions on activity, biomass, and composition of soil microbial communities. *Biol. Fertil. Soils* **2016**, *52*, 841–852. [CrossRef]
72. Zubek, S.; Majewska, M.L.; Błaszkowski, J.; Stefanowicz, A.M.; Nobis, M.; Kapusta, P. Invasive plants affect arbuscularmycorrhizal fungi abundance and species richness as well as the performance of native plants grown in invaded soils. *Biol. Fertil. Soils* **2016**, *52*, 879–893. [CrossRef]
73. Sun, X.; Gao, C.; Guo, L. Changes in soil microbial community and enzyme activity along an exotic plant *Eupatorium adenophorum* invasion in a Chinese secondary forest. *Chin. Sci. Bull.* **2013**, *58*, 4101–4108. [CrossRef]
74. Scharfy, D.; Güsewell, S.; Gessner, M.O.; Venterink, H.O. Invasion of *Solidago gigantea* in contrasting experimental plant communities: Effects on soil microbes, nutrients and plant–soil feedbacks. *J. Ecol.* **2010**, *98*, 1379–1388. [CrossRef]
75. Stanek, M.; Zubek, S.; Stefanowicz, A.M. Differences in phenolics produced by invasive *Quercus rubra* and native plant communities induced changes in soil microbial properties and enzymatic activity. *For. Ecol. Manag.* **2021**, *482*, 118901. [CrossRef]
76. Yu, Y.L.; Xu, Z.L.; Zhong, S.S.; Cheng, H.Y.; Guo, E.R.; Wang, C.Y. The co-invasion of the three Asteraceae invasive plants can synergistically increase soil phenol oxidase activity. *Biol. Bull.* **2023**, *50*, 467–473.
77. Li, Y.; Wang, C.M.; Gao, S.J.; Wang, P.; Qiu, J.C.; Shang, S.H. Impacts of simulated nitrogen deposition on soil enzyme activity in a northern temperate forest ecosystem depend on the form and level of added nitrogen. *Eur. J. Soil Biol.* **2021**, *103*, 103287. [CrossRef]
78. Cheng, H.Y.; Wang, S.; Wei, M.; Yu, Y.L.; Wang, C.Y. Alien invasive plant *Amaranthus spinosus* mainly altered the community structure instead of the α diversity of soil N-fixing bacteria under drought. *Acta Oecol.* **2021**, *113*, 103788. [CrossRef]
79. Wang, C.Y.; Jiang, K.; Zhou, J.W.; Wu, B.D. *Solidago canadensis* invasion affects soil N-fixing bacterial communities in heterogeneous landscapes in urban ecosystems in East China. *Sci. Total Environ.* **2018**, *631–632*, 702–713. [CrossRef] [PubMed]
80. Chang, C.T.; Yang, C.J.; Huang, K.H.; Huang, J.C.; Lin, T.C. Changes of precipitation acidity related to sulfur and nitrogen deposition in forests across three continents in north hemisphere over last two decades. *Sci. Total Environ.* **2022**, *806*, 150552. [CrossRef] [PubMed]
81. Matocha, C.J.; Grove, J.H.; Karathanasis, T.D.; Vandiviere, M. Changes in soil mineralogy due to nitrogen fertilization in an agroecosystem. *Geoderma* **2016**, *263*, 176–184. [CrossRef]
82. Craine, J.M.; Morrow, C.; Fierer, N. Microbial nitrogen limitation increases decomposition. *Ecology* **2007**, *88*, 2105–2113. [CrossRef] [PubMed]
83. Thirukkumaran, C.M.; Parkinson, D. Microbial respiration, biomass, metabolic quotient and litter decomposition in a lodgepole pine forest floor amended with nitrogen and phosphorous fertilizers. *Soil Biol. Biochem.* **2000**, *32*, 59–66. [CrossRef]

atmosphere

MDPI

Article

Insight into Municipal Reactive Nitrogen Emissions and Their Influencing Factors: A Case Study of Xiamen City, China

Yanmin Li [1,*], Xu Yang [1], Shihang Wang [1] and Shenghui Cui [2,3,4]

[1] School of Spatial Informatics and Geomatics Engineering, Anhui University of Science and Technology, Huainan 232001, China
[2] Key Lab of Urban Environment and Health, Institute of Urban Environment, Chinese Academy of Sciences, Xiamen 361021, China
[3] Xiamen Key Lab of Urban Metabolism, Institute of Urban Environment, Chinese Academy of Sciences, Xiamen 361021, China
[4] University of Chinese Academy of Sciences, Beijing 101408, China
* Correspondence: yanminli@aust.edu.cn

Abstract: Reactive nitrogen (Nr) has been confirmed as an indispensable nutrient for the city ecosystem, but high-intensity human activities have led to nitrogen pollution in cities, especially in coastal cities, jeopardizing ecosystem services and human health. Despite this, the characteristics and influencing factors of Nr remain unclear in coastal cities, particularly in the context of rapid urbanization. This study used the material flow analysis method to estimate Nr emissions in Xiamen from 1995 to 2018 and evaluated the characteristics of excessive Nr emissions. The STIRPAT model was used to identify and explore factors contributing to observed Nr levels in coastal cities. As indicated by the results, (1) the quantity of Nr generated by human activities increased 3.5 times from 1995 to 2018. Specifically, the total Nr entering the water environment showed a general increase with fluctuations, exhibiting an average annual growth rate of 3.1%, increasing from 17.2 Gg to 35.1 Gg. (2) Nr loads in the nearby sea increased notably from 8.1 Gg in 1995 to 25.4 Gg in 2018, suggesting a threefold augmentation compared with surface waters and groundwater. (3) NO_x was the gaseous Nr with the greatest effect on the atmosphere in Xiamen, which was primarily due to fossil fuel consumption. (4) Population and per capita GDP were major factors contributing to Nr load in the water environment, while Nr emission to the atmosphere was influenced by population and energy consumption. These findings provide valuable insights for tailored approaches to sustainable nitrogen management in coastal cities.

Keywords: reactive nitrogen; coastal city; Xiamen; STIRPAT model

Citation: Li, Y.; Yang, X.; Wang, S.; Cui, S. Insight into Municipal Reactive Nitrogen Emissions and Their Influencing Factors: A Case Study of Xiamen City, China. *Atmosphere* **2023**, *14*, 1549. https://doi.org/10.3390/atmos14101549

Academic Editors: Peter Wiesen and László Bencs

Received: 25 June 2023
Revised: 1 September 2023
Accepted: 21 September 2023
Published: 11 October 2023

1. Introduction

Nitrogen (N) is a fundamental component of proteins, nucleic acids, and other vital living substances [1,2]. However, the excessive use of chemical fertilizers and fossil fuels as well as high food consumption have resulted in the release of large amounts of reactive nitrogen (Nr: all species of nitrogen (N) except N_2) into the environment, which has led to environmental pollution such as water eutrophication, atmospheric pollution, and acid rain [3,4]. Research has suggested that 75% of Nr production on land arises from human activities [5]. The 2030 Sustainable Development Goals (SDGs) formulated by the United Nations aim to achieve various goals, including food security, protection of the environment, and social development. The realization of many of the above-mentioned goals is closely tied to the responsible use of nitrogen [6].

In cities, Nr emissions are influenced by a wide range of factors (e.g., population, technology, and other socioeconomic factors). The rapid population growth, industrialization, and socioeconomic development that accompany urbanization can have various consequences for the environment. Urbanization and agglomeration have led to increased

levels of nitrogen (Nr) emissions [7]. The anthropogenic sources of Nr in cities mainly comes from human consumption, croplands, energy consumption, and livestock processing, while N deposition is the main natural source. China continues to prioritize urbanization, particularly in the highly developed, high-income eastern coastal cities. This area encompasses 53 cities and account for almost 20% of the total Chinese population and over 40% of China's gross regional product [8]. The increasing urbanization of coastal cities is boosting nitrogen production and emissions; thus, these cities have already become the largest anthropogenic nitrogen source worldwide [9,10]. It is essential to investigate the characteristics of Nr emission as well as its control mechanisms and influencing factors and change trends in coastal cities to address the increasingly serious problem of Nr pollution in coastal cities. This investigation is of critical significance both theoretically and practically to managing nitrogen emissions and protecting the environment.

To address the rising pollution caused by Nr, research has been conducted worldwide to explore the characteristics of Nr emissions in various cities. It has focused on several aspects such as the characteristics of Nr emissions, the effect of Nr emissions, and Nr management [11–13]. For example, a study conducted in Paris suggested that emissions from food consumption had tripled between 1801 and 1914 [14]. In a study on Nr emissions in Phoenix, Arizona, researchers considered the residential consumption system and specific industries in the city (e.g., the dairy and livestock sectors) [15]. In addition, domestic scholars have also conducted several studies on Nr emissions in cities such as Beijing, Shanghai, Hangzhou, and Guangzhou, analyzing Nr emissions and their driving factors [16–19]. Nevertheless, the above-mentioned studies have typically quantified Nr emissions from food consumption, while the environmental effects of Nr on air, water, and soil have not been fully determined. Therefore, further research is necessary to determine the extent of the impact of Nr emissions on the environment and to develop effective measures for Nr management.

Most researchers have focused on identifying the factors that stimulate carbon emissions using the STIRPAT model, whereas limited research has been conducted on the trend of Nr emissions. Liu and Nie [20] analyzed China's per capita food nitrogen footprint and the effect of a wide range of socioeconomic factors on the footprint using the STIRPAT model. Furthermore, Cui et al. [21] employed the STIRPAT model to investigate the factors stimulating agricultural carbon emissions in China's Hebei province. The STIRPAT model is effective in analyzing the driving forces behind environmental effects [22] and can help comprehensively evaluate the dynamic interplay of contributing factors and highlight the characteristic features of the macrosocial "complex coupling system" with respect to environmental effects. Previous studies on Nr emissions and their factors have generally considered urbanization, population size, per capita GDP, production structure, energy efficiency, as well as technological improvements [23–27]. However, the geographic and socioeconomic conditions of different cities can lead to significant variations in the factors driving Nr emissions. Understanding the changes in Nr emissions and their influencing factors is crucial, and further research is needed to account for city-specific factors.

Xiamen, a typical coastal city, is facing increasingly serious air pollution, particularly regarding Nr emissions, whose environmental effects and influencing factors remain unclear. This study aimed to achieve several objectives. First, the characteristics of Nr emission in Xiamen were analyzed. Second, we discussed the variation characteristics of Nr loads in the atmosphere and water bodies. Third, this study attempted to gain insights into the critical socioeconomic factors of Nr emissions to provide decision-makers with a more scientific basis for formulating N management policies. Furthermore, this study can contribute to sustainable city development.

2. Materials and Methods

2.1. Study Area

Xiamen (117°53′–118°26′ E, 24°23′–24°54′ N) is located in the southeast of China, covering a total area of 1699.39 km^2. The altitude is 63.2 m (Figure 1). Xiamen has a subtrop-

ical maritime monsoon climate with concentrated precipitation and warm temperatures. The resident population of Xiamen has increased from 1.89 million in 1995 to 4.29 million in 2020. Xiamen is characterized by a high degree of intensive human activities that consume considerable amounts of food and energy. With excessive nitrogen inputs, nitrogen pollution has grown more serious. Xiamen's booming economy and rapid urbanization have changed its land use distribution. In 2020, the urban residential land, industrial land, and transportation land accounted for 37.2% and were concentrated on the island; the most of forest land, agricultural land, and other land took up 62.8% of Xiamen, and these lands were extensively distributed in the surrounding areas. With the continuous acceleration of urbanization in Xiamen, the urbanization rate was elevated from 62.7% in 2005 to 89.4% in 2020. According to the results of monitoring surface water nitrogen concentration from 2004 to 2016, provided by the monitoring station of the Xiamen Environmental Protection Bureau, it was found that major rivers in the area had excessive levels of nitrite and ammonia nitrogen. Furthermore, from 1995 to 2015, the concentration of inorganic nitrogen in the nearby sea of Xiamen increased from 0.35 mg L^{-1} to 1.34 mg L^{-1} [28].

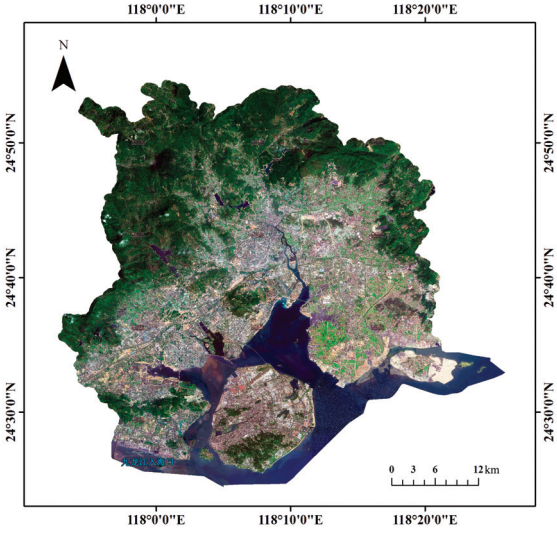

Figure 1. Map of the study area.

2.2. Data Sources

In this study, socioeconomic data on Xiamen from 1995 to 2018 were collected from several published government sources (e.g., the Yearbook of the Xiamen Special Economic Zone (1997–2019) and the Xiamen Ecological Environmental Quality Bulletin). The parameters of Nr emission primarily originated from the published literature, government departments, and experiments. The detailed parameters of this study are elucidated in the Supplementary Materials (Tables S1–S30).

2.3. Reactive Nitrogen (Nr) Calculations

Different systems can generate varying levels of nitrogen that affect the environment in different ways. The systems that primarily affect water bodies include croplands, livestock, aquaculture, greenbelts, industry, sewage treatment, and garbage disposal (Figure 2). Moreover, Nr emissions from the above-mentioned systems also have a certain negative effect on the atmospheric environment. Nitrogen oxide emissions are increasing, notably in economically developed areas. In this study, NO_x, NH_3, and N_2O emissions were considered the main gaseous Nr forms in the atmosphere. In general, systems that exerted a certain effect on the atmosphere comprised croplands, livestock, aquaculture, greenbelts, sewage treatment,

and garbage disposal. The calculation formulas for the nitrogen flow and Nr emissions of each system are detailed in the Supplementary Materials (Equations (S1.1)–(S11.2)).

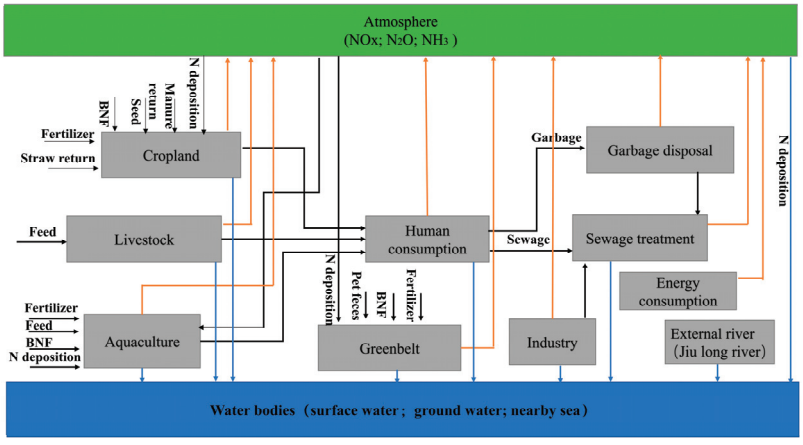

Figure 2. Framework of Nr emissions to the environment (blue arrows represent Nr emission to water environments; red arrows represent Nr emission to the atmosphere; black arrows represent nitrogen flow between different systems; BNF: Biological nitrogen fixation).

2.4. Influencing Factor Analysis Model

2.4.1. STIRPAT Model

The effects of demographic (P), economic (A), and technological (T) factors on the environment are mainly postulated in the IPAT model [29]. The IPAT model is reformulated into a stochastic model (STRIPAT), so that the nonmonotonic or nonproportional effects of driving forces on the environment can be statistically evaluated [30]. The STRIPAT model has been successfully adopted to analyze the effects of driving forces on a variety of environmental effects [31,32], which is expressed as:

$$I_{it} = \alpha P_{it}^{b} A_{it}^{c} T_{it}^{d} \varepsilon_{it} \quad (1)$$

After taking logarithms, the model takes the following form:

$$Ln(I_{it}) = a + bLn(P_{it}) + cLn(A_{it}) + dLn(T_{it}) + \varepsilon_i \quad (2)$$

where suffixes i and t denote country and years, respectively; P expresses population size; A is real GDP per capita; T represents technology; the dependent variable I denotes pollutant emissions; ε_i is the error term, a is the constant term; and b, c, and d are the coefficients of P, A, and T, respectively.

The STRIPAT model refers to a nonlinear model with multiple dependent variables. By implementing an index, the model is capable of analyzing the nonproportional effects of factors on the environment. Besides the three variables already covered in the model, any other detrimental factor that affects the environment can be introduced for in-depth examination. The coefficients of the STRIPAT model represent the elasticity relationship between the independent and dependent variables. For instance, an environmental effect will result in changes of a%, b%, and c%, respectively, if a 1% change exists in the driver (PAT). a, b, and c equal to 1 indicate a proportional change in the environmental effect and the driver (PAT) at a constant ratio. A coefficient greater than 1 reveal that an increase in socioeconomic factors leads to a higher rate of environmental change. A coefficient over 0 and less than 1 reveals that increasing socioeconomic factors leads to a rise in the rate of environmental change but at a slower pace than the driving force. However, a coefficient less than 0 implies that increasing socioeconomic factors is conducive to reducing the

environmental effect. Based on the STIRPAT model, this paper utilizes the ridge regression analysis method to fit independent variables and dependent variables through regression. This method is deemed more compatible and stable compared to the least-squares method employed in previous research studies.

2.4.2. Model Indicator Selection

In this paper's STIRPAT model, the "I" variable representing environmental factors is the total amount of Nr emissions. The wealth factor (A) is represented by the per capita GDP index. The variable P is further broken down into two indicators: Xiamen residents (P_1), and urbanization level (P_2) (the percentage of built-up areas in the entire region). The technical indicator T is also separated into two indicators: energy consumption (T_1) and industrial structure (T_2). Energy consumption is defined as the amount of standard coal consumed per unit of GDP production, while industrial structure refers to the percentage of secondary industry. This paper utilizes ridge regression analysis to fit the STIRPAT model and comprehensively explores the factors affecting Nr emissions in the water and atmospheric environment.

2.4.3. Mann–Kendall Test and Theil–Sen's Slope Estimator

The Mann–Kendall test is typically used to detect the presence of a temporal trend when analyzing environmental data. Thus, the test can be viewed as a nonparametric test for zero slope of the linear regression of time-ordered data versus time. The calculation of the Mann–Kendall test statistic can be found in previous research [33,34]. As for the results, when the Z value is negative, a falling trend is recognized, and when the Z value is positive, a rising trend is discerned. At a significance level of 0.05 (0.01, 0.001), $Z > 1.96$ (2.58) and $Z < -1.96$ (-2.58) indicate significant increasing and decreasing trends, respectively [35].

Theil–Sen is a nonparametric alternative to ordinary least-squares regression. Sen's slope has an advantage compared to linear regression, in that the test is not affected by the number of outliers and data errors [35]. The Sen's slope equation is written as follows:

$$\beta = Median(\frac{x_j - x_i}{i - j}) \quad (3)$$

where x_i and x_j are the data values at time i and j ($i > j$), respectively. When β is greater than zero, it indicates a growth trend, while the opposite indicates a decreasing trend.

3. Results

3.1. The Characteristics of Reactive Nitrogen (Nr) Emissions

Human activities have a considerable impact on the water and air environments of a city, with varying effects depending on the amount of Nr produced. Analysis of time series data reveals that the release of Nr into water bodies and the atmosphere undergoes unique changes with the process of urbanization (Figure 3). By estimating the Mann–Kendall test and Theil–Sen's slope estimation at a 99% confidence level ($Z > 2.58$, $p < 0.001$) (Table 1), we found that the total of Nr emissions from anthropogenic activities tended to increase significantly, going from 42.6 Gg in 1995 to 149.2 Gg in 2018. Moreover, the amount of Nr released into the atmosphere far exceeded that released into water bodies. Nr loads released into water bodies tended to fluctuate, increasing from 17.2 Gg in 1995 to 35.1 Gg in 2018, with an average annual increase rate of 3.1%. On the other hand, Nr loads released into the atmosphere increased from 25.4 Gg in 1995 to 114.2 Gg in 2018, with an average annual increase rate of 6.7%. The Nr released into the atmosphere accounts for over half of the total Nr emissions resulting from anthropogenic activities.

Table 1. Theil–Sen median slope estimation and Mann–Kendall trend test.

Item	Sen's Slope	Mann–Kendall Statistic	The Z Value of the Mann–Kendall Test	The *p*-Value of the Mann–Kendall Test
Total Nr emission	4.834	250.000	6.176	0.000
Nr emission to water bodies	0.945	178.000	4.390	0.000
Nr emission to atmosphere	3.793	252.000	6.226	0.000
Nr emission to surface water	0.033	82.000	2.009	0.045
Nr emission to groundwater	0.001	6.000	0.124	0.901
Nr emission to nearby sea	0.880	182.000	4.490	0.000
NH_3 emission	0.375	244.000	6.027	0.000
NO_x emission	3.436	238.000	5.879	0.000
N_2O emission	−0.026	−198.000	−4.886	0.000

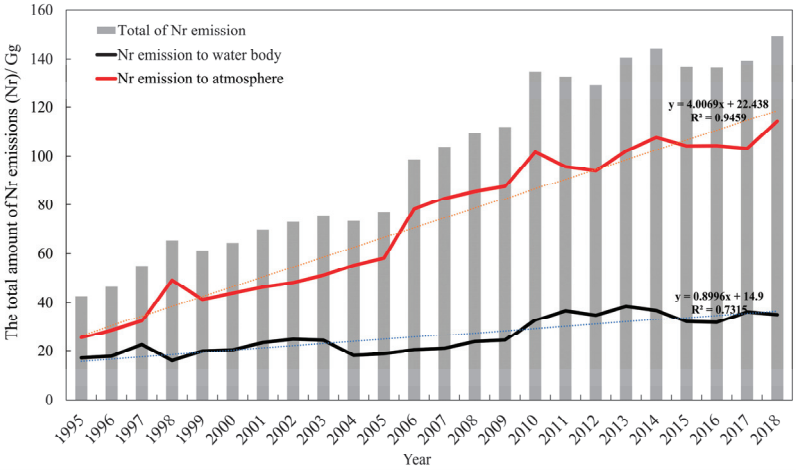

Figure 3. Total amount of Nr emissions.

3.1.1. Characteristics of Nr Emission to Water Bodies

In general, the water bodies in this study comprised surface water, groundwater, and the nearby sea. All types of water bodies were affected by Nr emissions from different systems in the city, and the trends of Nr loads differed between the above-mentioned water body types from 1995 to 2018 (Figure 4). During urbanization, anthropogenic nitrogen (Nr) discharges exceeded those from natural sources, leading to severe effects on water body quality. By estimating the Mann–Kendall test and Theil–Sen's slope estimation at a 99% confidence level ($Z > 2.58$, $p < 0.001$) (Table 1), the total Nr loads in Xiamen's water bodies showed a fluctuating increasing trend between 1995 and 2018, with an average annual growth rate of 3.2%, increasing from 17 Gg to 35 Gg. While Nr loads in surface water bodies showed no significant changes during the period from 1995 to 2018, Nr loads in surface water bodies increased from 6.9 Gg to 8.1 Gg during 1995–2012 and decreased from 7.7 Gg to 7.4 Gg from 2013 to 2018. However, as Xiamen is a typical coastal city, Nr pollution in nearby seas became more serious. As the river upstream carried considerable Nr into Xiamen's nearby sea, the Nr loads in nearby seas increased, from 8.1 Gg in 1995 to 25.4 Gg in 2018—three times higher than the Nr in surface waters and groundwater in this 23 year-period. Furthermore, most Nr pollutants originated from the upstream of the external river (Jiulong River).

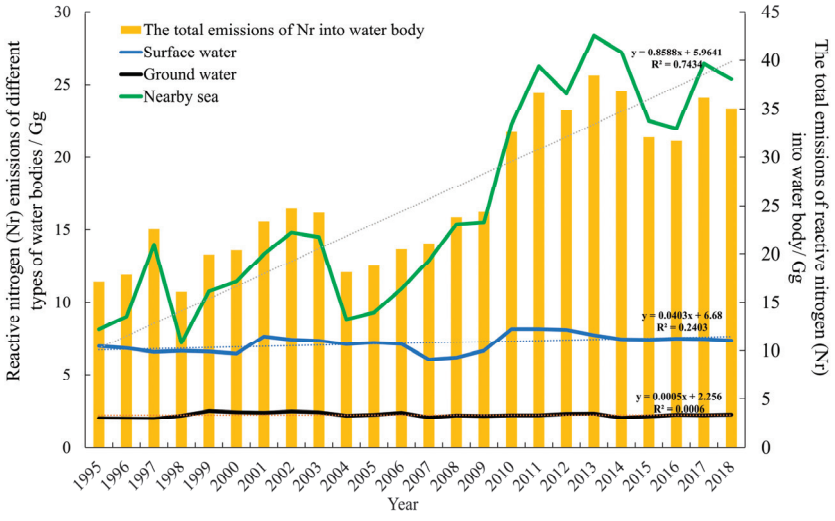

Figure 4. Characteristics of Nr load in different water bodies in Xiamen.

The results of this study revealed differences in the contribution ratios of various systems to the Nr loads in water bodies in the city; different water bodies were affected by Nr emissions from the respective systems. In addition, different characteristics and trends were displayed from 1995 to 2018 (Figure 5). Surface water bodies in the city were affected by various systems (Figure 5a). To be specific, the contribution of Nr emissions to surface waters from cropland systems decreased, from 20.2% in 1995 to 6.3% in 2018, marking a threefold decrease. Moreover, industrial systems contributed to 37.5% of Nr loads in surface water in 1995, which declined to 1.6% in 2018, with an average annual decrease of 4.5%. Furthermore, the contribution of livestock systems to Nr loads in surface water showed a gradual decline, with an average annual decrease of 3.6%. However, the contribution of N deposition to surface water progressively increased, and it emerged as a major source of Nr pollution in surface water. From a contribution ratio of 15% in 1995, N deposition in surface water rose to 65% in 2018, marking a 4.3-fold increase over the following 23 years.

The nearby sea environment of Xiamen, a typical coastal city located at the mouth of the Jiulong River, is affected by Nr inputs from a wide variety of inland subsystems and Nr inputs from external rivers, like the Jiulong River (Figure 5b). As revealed by this study, external rivers were the primary source of Nr loads in the nearby sea, contributing to an average annual ratio of 60% from 1995 to 2018. Sewage treatment and surface water served as the main inland sources of Nr loads. The contribution ratio of Nr emissions from sewage treatment systems in the nearby sea was elevated from 6.1% in 1995 to 12.7% in 2018.

The discharge of Nr from different systems in the city can substantially affect groundwater bodies (Figure 5c). The reduction in cropland area led to a decrease in N fertilizer leaching to groundwater over the past few years. Moreover, the percentage of N fertilizer in groundwater declined from 88% in 1995 to just 10% in 2018, marking an overall decrease of approximately eight times. However, the impact of sewage treatment systems on groundwater was found to have grown. On average, there was an annual increase of 10.9% in Nr loads. The increasing workload of the sewage treatment system and aging sewer pipes were the primary causes of Nr leakage from the sewage treatment system into groundwater bodies. Furthermore, there was an increase in Nr contaminants that leach into groundwater from the greenbelt system, whose contribution to the overall Nr load was elevated from 2.7% in 1995 to 26.3% in 2018. The reason for the above result is the development of Xiamen as an ecological city, leading to an average annual increase of 12.1% in greenbelt area, as well as an increase in pet feces.

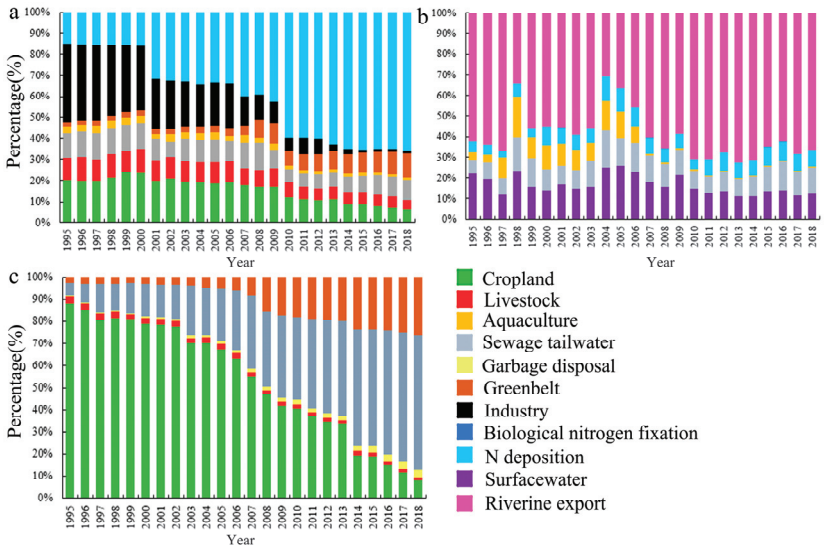

Figure 5. Characteristics of variations in Nr load contributions to different water bodies ((**a**): surface water; (**b**): nearby sea; (**c**): groundwater).

3.1.2. Characteristics of Nr Emission to the Atmosphere

Anthropogenic Nr emissions change the nitrogen cycle in cities, adversely impacting not only water bodies but also the atmosphere, and this issue is becoming more severe. The atmospheric Nr forms primarily responsible for the damage comprised NH_3, NO_x, and N_2O. By estimating the Mann–Kendall test and Theil–Sen's slope estimation at a 99% confidence level (Table 1), we found that NO_x presented a significant increasing trend, while N_2O presented a decreasing trend. NO_x emissions exerted the greatest effect, accounting for nearly 80% of the city's overall Nr emissions (Figure 6a). The second-greatest emission was NH_3, primarily originating from ammonia volatilization in croplands and livestock systems. Although N_2O accounted for a relatively small proportion, it is the third most critical greenhouse gas after CO_2 and CH_4, with a warming potential 298 times that of CO_2 and contributing to 8% of greenhouse gas emissions [36].

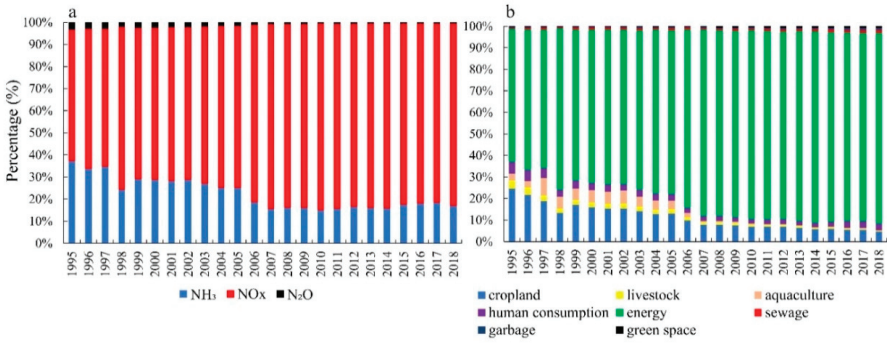

Figure 6. Trends and contributions of gaseous Nr emissions from 1995 to 2018 ((**a**): emission ratio of different forms of gaseous Nr; (**b**): gaseous Nr emission of each subsystem).

Additionally, there were substantial variations in gaseous Nr emissions among different systems (Figure 6b). From 1995 to 2018, Nr emissions from energy consumption tended to increase, becoming the primary contributor to Nr emissions in city ecosystems.

Furthermore, Nr emissions from human consumption, sewage treatment, and garbage disposal systems also increased, although this increase was at a slower rate. In contrast, the aggregate amount of Nr produced by cropland systems tended to decline over the same period.

3.2. Analysis of Influencing Factors on Nr Emission

3.2.1. Analysis of Influencing Factors on Nr Emission into Water Bodies

According to the STRIPAT model and ridge analysis, the goodness of fit (R^2 value) of the model was 0.752 and the model met the requirements. This indicated that the independent variable explained 75.2% of the variation in the dependent variable (Table 2). Moreover, the equation's F value was 8.6, and it was statistically significant at 0.001 level, indicating that the ridge regression equation could withstand the 99% significance test. This result indicated that population size, wealth, and urbanization had a positive impact on environmental Nr load, with both linear and elastic effects. Environmental pressure increased with the rise in population size, which was found to determine the amplitude of the environmental Nr load. An increase in population size increased environmental pressure. The elasticity coefficient, which ranged from 0 to 1, suggested that an increase in these factors could lead to environmental changes worsening faster than the driving force. Specifically, for every 1% increase in population, Nr load in water bodies increased by 0.17%, making population explosion a potential factor for the Nr load in Xiamen's water bodies. Similarly, per capita GDP had a positive linear effect on water environmental pressure, with a 1% increase resulting in a 0.16% increase in liquid Nr emissions. However, in comparison to population and GDP, industrial structure showed a negative correlation with Nr emissions. The primary reason for this result is the decline of traditional industries and the rise of tertiary and high-tech industries. Improving industrial structure could have a positive impact on reducing Nr emissions into the water environment.

Table 2. Ridge regression of various socioeconomic factors affecting Nr load in water bodies.

	Standardization Coefficient	t	*p*	R^2	F
Constants	-	0	1		
Population (P_1)	0.170	5.019	0.000 **		F = 8.604
Urbanization (P_2)	0.153	5.732	0.000 **	0.752	p = 0.001
Industrial structure (T_2)	−0.117	2.334	0.032 *		
Per capita GDP (A)	0.160	6.652	0.000 **		

* $p < 0.05$, ** $p < 0.01$.

3.2.2. Analysis of Influencing Factors on Nr Emission to the Atmosphere

A ridge analysis was conducted according to the STRIPAT model using population, industrial structure, energy consumption, and GDP per capita as independent variables and gaseous Nr emissions as the dependent variable. The results indicated an R^2 value of 0.932 and the model met the requirements. This indicated that the independent variable explained 93.2% of the variation in the dependent variable (Table 3). The primary factor driving this increase was the growing population. Moreover, the city's energy consumption rose at a rate of 2.9% per year, which had a direct impact on gaseous Nr emissions. In fact, for every 1% increase in energy consumption, there was a corresponding 0.91% increase in emissions. Additionally, per capita GDP had a linear positive effect on the environment, with a 1% increase in per capita GDP resulting in a 0.31% increase in gaseous Nr emissions. In comparison to the aforementioned factors, Xiamen's industrial structure had a suppressing effect on gaseous Nr emissions. Over the years, the proportion of the secondary industry in Xiamen declined by an average of 4.6% annually. Furthermore, the secondary industry transitioned into high-tech industries, which can help reduce the nitrogen pollution caused by heavy industries in the region.

Table 3. Ridge regression of socioeconomic factors affecting Nr load in the atmosphere.

	Standardization Coefficient	t	*p*	R^2	F
Constants	-	0	1		
Population (P_1)	1.091	2.075	0.000 **		F (6,7) =15.897
Industrial structure (T_2)	−0.468	−1.201	0.027 *	0.932	$p = 0.001$
Energy consumption (T_1)	0.911	2.081	0.000 **		
Per capita GDP (A)	0.310	0.993	0.035 *		

* $p < 0.05$, ** $p < 0.01$.

4. Discussion

Nr emissions have increased significantly due to anthropogenic activities over the past few decades, particularly in coastal cities, which is expected to adversely affect the environment of the above-described cities. Accordingly, the sources of Nr emissions and the factors that contribute to their increase in coastal areas should be explored. This study aimed to conduct a systematic analysis of the effect of human activities on Nr emissions and examine the environmental effects arising from such emissions to more effectively curb and manage nitrogen pollution. The results suggested an increase in Nr emissions from coastal cities in recent years, with gaseous Nr emissions outweighing the amount entering the water environment, thus triggering a growing problem of Nr pollution in the atmosphere. Most Nr emissions have originated from energy systems, cropland systems, and human consumption systems. Moreover, socioeconomic factors (e.g., population) have affected Nr emissions. The above-mentioned findings reveal the importance of identifying the key systems and critical factors of Nr emission to effectively reduce nitrogen pollution in cities. In brief, a substantial difference was found between the environmental effects of Nr emissions from different systems in cities, and action should be taken to alleviate this issue.

In Xiamen, the level of Nr entering water bodies tended to fluctuate and increase. This result is in good agreement with the actual change in nitrogen concentration in surface water. Previous studies found that according to the results of monitoring nitrogen concentration in surface water in Xiamen from 2004 to 2016, nitrite and ammonia nitrogen in major streams and surface water in the territory seriously exceeded the standard. The average nitrogen concentration in surface water showed a fluctuating increasing trend, and the nitrogen concentration in surface water showed a significant linear positive correlation with Nr load [37]. The variation in Nr load in surface water bodies is influenced by multiple systems. Among them, the agricultural system made the largest contribution during the period from 1995 to 2012, resulting in an increasing trend of Nr load in surface water bodies due to the extensive use of nitrogen fertilizers. However, from 2013 to 2018, the urbanization process accelerated and the area of grain cultivation decreased. As a result, there was a reduction in wastewater discharge from the agricultural system. Furthermore, policies had an impact on the livestock and aquaculture systems in Xiamen, leading to a continuous decrease in Nr emissions from 2013 to 2018. This ultimately resulted in a decrease in wastewater discharge and subsequent fluctuations in Nr load in surface water bodies. In addition, in our study, we also found severe levels of Nr pollution in the nearby sea. The coastal city's nearby sea is affected by outside rivers. In the upstream of the Jiulong River, the development of industries (e.g., pig breeding and crop cultivation) led to the elevation of pollution levels [38]. Existing research has suggested that Nr pollutants from the Jiulong River have resulted in elevated pollution levels in the sea near Xiamen since the 1990s. Human activities (e.g., fertilizer application and pig breeding) in the upstream of the Jiulong River have disrupted the biogeochemical processes expediting N cycling [39,40]. The above result is confirmed by the frequent occurrence of red tides in the waters of Xiamen over the past few years. Thus, local sources of pollution should be controlled and inter-regional cooperation should be developed in the future management of pollutants in the nearby sea.

The source of Nr pollution that exerts the greatest effect on surface water has changed from the cropland system to N deposition. Consequently, the contribution of N deposition to Nr loads in surface water in Xiamen increased by 4.3 times over the 23 years analyzed

in this study. The increased deposition of atmospheric nitrogen was closely correlated with the large number of nitrogen oxides generated by energy consumption processes in the local region, as well as the dispersion of N pollutants attributed to the socioeconomic development of the surrounding region [41]. The above-described nitrogen oxides primarily originate from fossil fuel combustion in cities while accounting for a larger share of anthropogenic Nr emissions [42]. In addition, given that, as indicated by statistics, energy consumption in Xiamen has increased by 2.5 times over the last decade, it is concerning that half of the nitrogen oxide and ammonia nitrogen emissions eventually return to the land and water bodies of the city's ecosystems in the form of a deposition. This N deposition has contributed to eutrophication in surface water bodies. It can break the material cycle and energy flow of the surface water ecosystem, so that the stability of surface water ecosystems can be seriously affected [43]. As revealed by this study, sewage treatment and greenbelt systems in city ecosystems more notably affect groundwater. The overloading of the sewage treatment process and the aging of sewage pipes have been confirmed as the main reasons for the leakage of N pollutants into groundwater bodies [44]. Moreover, since Xiamen strives to become an ecological and green city, the greenbelt area has achieved an annual average growth of 12.1%. However, the extensive use of artificial fertilizers on the greenbelt, coupled with the rising amount of pet waste being discarded in the area, can trigger an escalation of N pollutants seeping into groundwater [45].

The release of significant amounts of Nr adversely affected the water bodies and the air environment. This study suggested that Nr emissions resulting from energy consumption tended to increase and turned out to be the most critical contributor to Xiamen's Nr emissions into the atmosphere from 1995 to 2018. This result is consistent with existing research, which states that energy consumption has become the most important source of gaseous Nr emissions in cities [46,47]. NO_x has accounted for the production of most gaseous Nr resulting from energy consumption, notably in cities. The total emissions of NO_x at the city level have been substantially greater than those at the global and national levels [48–50]. On that basis, the regulation of sectors that emit higher NO_x levels (e.g., transportation services) should be prioritized in the future. Cities should develop effective NOx control mechanisms that primarily target reducing motor vehicle emissions in the future [51].

In the atmosphere, NH_3 has been reported as a critical nitrogen-containing gas and also an alkaline gas. As revealed by previous studies, the majority of NH_3 present in the atmosphere arises as a result of the livestock system and the application of N fertilizers, accounting for 39% and 17% of the total Nr, respectively, on the global scale [42–53]. It is noteworthy that China is a large agricultural producer, and nitrogen fertilizer application remains the largest contributor to NH_3 emissions on the national scale [54]. Unlike on the global or national scale, in Xiamen, a typical coastal city, NH_3 emissions primarily originate from croplands and energy consumption systems. NH_3 can be employed as a catalyst for secondary aerosols, and it takes on critical significance in atmospheric physicochemical reactions. Additionally, it can neutralize acidic gases, so that the acidity of clouds and aerosols can be affected [55]. Accordingly, it is imperative to adopt a more reasonable and scientific farming method that is capable of increasing the utilization rate of nitrogen fertilizer and the rate of straw return.

N_2O is a critical greenhouse gas, and although it is the least emitted compared with other forms of gaseous nitrogen (NH_3, N_2O), it is still not negligible in city ecosystems. Globally, N_2O emissions from soils contribute the most to N_2O in the atmosphere [56]. In contrast, this study suggested that N_2O emissions from the cropland system accounted for two-thirds of the total gaseous Nr emissions in Xiamen. Subsequently, the sewage treatment system followed. N_2O emissions in the sewage treatment system were attributed to the biochemical actions of nitrifying and denitrifying bacteria. The above-mentioned N_2O emissions increase during the sewage treatment process [57]. Thus, in the future, the focus should be placed on updating sewage treatment technologies to increase N removal rates while reducing greenhouse gas emissions in Xiamen.

The influencing factors for Nr loads in water bodies, i.e., population and urbanization levels, are crucial in Xiamen. However, as for Nr loads in the atmosphere, population and energy consumption are the main factors. This finding further confirms that global population growth is one of the critical drivers of long-term changes in nutrient cycling [58]. As revealed by existing research, population, economic development, urbanization, agricultural patterns, and per capita GDP are the main factors for Nr emission to the environment [59–61]. The variations in environmental Nr loads identified in this study were likely the result of social factors, economic development, and population changes. In particular, as a developed coastal city, the local industries and energy consumption were identified as crucial factors for the environmental effects of Nr emissions. As revealed by the analyses of this study, the driving forces of increased Nr emissions due to population growth shifted progressively from changes in energy consumption to satisfy the city's development needs. Consequently, there still exists a significant burden of Nr pollution in the coastal city. Accordingly, the way energy is produced and exploited should be actively facilitated by increasing energy efficiency and transitioning from smokestack industries to high-tech ones. The above-described measures promise to substantially mitigate nitrogen pollution in Xiamen.

5. Limitations

Although this study presents an expansion of our understanding of the characteristics and influencing factors of Nr emissions in coastal cities, it is limited in several ways that future research must address. (1) Future analyses should consider the nitrogen concentrations and chemical composition of N deposition when analyzing ecological effects. (2) The critical impact of Nr emissions on the soil environment was not taken into account in this study. (3) Two types of variables—activity data and N parameters—are needed to estimate the various kinds of Nr emissions in this paper. Based on previous studies in the field of uncertainty analysis, activity data are mainly derived from official statistics which are widely considered as a reliable data source for analysis. Nr emissions in Xiamen are simply assumed to have uncertainty ranges of 10% to 30% [62]. Based on previous research, this study will further refine the analysis of uncertainty in future research. Despite these limitations, this study provided a comprehensive analysis of Nr in coastal cities. Nevertheless, future research needs to address these limitations to create more sophisticated and perfected works.

6. Conclusions

The emission of Nr in Xiamen from 1995 to 2018 was estimated using the method of material flow analysis. In this study, an increase in Nr emissions was revealed over the 23-year period. Moreover, a quantitative analysis of the key factors driving the above-mentioned long-term changes was conducted. The main findings of this study are elucidated as follows:

First, as urbanization leapt forward in Xiamen, the effects of Nr emissions to water bodies increased, particularly in surface water and the nearby sea. Nr load in the nearby sea was notably higher than that in surface waters and groundwater, and it increased incrementally from 8.1 Gg in 1995 to 25.4 Gg in 2018, marking an increase of 3.1 times in these 23 years. The majority of the Nr originated from the upstream of the external river, Jiulong River. Second, the emission of Nr from various subsystems into the water bodies tended to vary from 2005 to 2018. In terms of surface water, the effect of N deposition and greenbelt subsystems increased as urbanization accelerated. On the other hand, the cropland, sewage treatment, and greenbelt subsystems had a greater impact on groundwater bodies. Since Xiamen is a typical coastal city, the issue of Nr pollution in the nearby sea aroused more attention. The sea near Xiamen was primarily affected by external rivers (Jiulong River) and the direct discharge of tailwater from sewage treatment facilities. Third, the gaseous Nr with the greatest impact on the atmosphere in Xiamen was NO_X, which mainly resulted from fossil fuel consumption. Fourth, the STRIPAT model was adopted to analyze the socioeconomic drivers impacting Nr emissions in Xiamen. As revealed by

the findings, population and per capita GDP were the major factors for Nr load in water bodies, while population and energy consumption affected Nr loads in the atmosphere. Several potential solutions were proposed (e.g., cooperation between adjacent cities and upstream areas of the river, improvements in energy utilization technology, and appropriate N fertilizer application). Subsequent research should emphasize analyzing N management strategies for coastal cities in different scenarios.

Supplementary Materials: The following supporting information can be downloaded at: https://www.mdpi.com/article/10.3390/atmos14101549/s1, Table S1: Input and output items in processes of cropland system; Table S2. The parameter of cropland system; Table S3. the activity data of cropland system; Table S4. Input and output items in processes of human consumption system; Table S5. The parameter of human consumption system; Table S6. The activity data of human consumption system; Table S7. Input and output items in processes of livestock system; Table S8. The parameters of livestock system; Table S9. The activity data of livestock system; Table S10. Input and output items in processes of sewage treatment system; Table S11. The parameters of sewage treatment system; Table S12. The activity data of sewage treatment system; Table S13. Input and output items in processes of garbage treatment system; Table S14. The parameters of garbage treatment system; Table S15. The activity data of garbage treatment system; Table S16. Input and output items in processes of aquaculture system; Table S17. The parameter of aquaculture system; Table S18. The activity data of aquaculture system; Table S19. Input and output items in processes of green space system; Table S20. The parameter of green space system; Table S21. The activity data of green space system; Table S22. Input and output items in processes of green space system; Table S23. The parameter of energy system; Table S24. The activity data of energy system; Table S25. Input and output items in processes of pet; Table S26. The parameter of pet system; Table S27. Input and output items in processes of industry system; Table S28. Input and output items in processes of coastal system; Table S29. The parameter of coastal system; Table S30. The activity data of coastal system. References [63–86] are cited in Supplementary file.

Author Contributions: Conceptualization, Y.L. and S.C.; methodology, Y.L.; software, X.Y.; validation, S.W.; formal analysis, S.W.; investigation, Y.L.; resources, Y.L.; data curation, S.C.; writing—original draft preparation, Y.L.; writing—review and editing, Y.L.; visualization, S.C.; supervision, S.C.; project administration, S.C.; funding acquisition, Y.L. and X.Y. All authors have read and agreed to the published version of the manuscript.

Funding: This research was funded by Natural Science Research Project of Anhui Educational Committee (GrantNo.2022AH050820); Scientific Research Foundation for High-level Talents of Anhui University of Science and Technology (GrantNo.13200458); Anhui Provincial Natural Science Foundation (GrantNo.2208085QD115); the Open Foundation of the Key Laboratory of Universities in Anhui Province for Prevention of Mine Geological Disasters (GrantNo.2022-MGDP-08); the Key Laboratory of Aviation–Aerospace–Ground Cooperative Monitoring and Early Warning of Coal Mining-Induced Disasters of Anhui Higher Education Institutes (Anhui University of Science and Technology) (GrantNo.KLAHEI202204).

Institutional Review Board Statement: Not applicable.

Informed Consent Statement: Not applicable.

Data Availability Statement: The data used to support the findings of this study are available from the corresponding author upon request.

Acknowledgments: We would like to thank all the authors and reviewers for their great guidance and help in writing this manuscript.

Conflicts of Interest: The authors declare that they have no known competing financial interests or personal relationships that could have appeared to influence the work reported in this paper.

References

1. Galloway, J.N.; Dentener, F.J.; Capone, D.G.; Boyer, E.W.; Howarth, R.W.; Seitzinger, S.P.; Asner, G.P.; Cleveland, C.C.; Green, P.A.; Holland, E.A.; et al. N cycles: Past, present, and future. *Biogeochemistry* **2004**, *70*, 153–226. [CrossRef]
2. Stevens, C.J. Nitrogen in the environment. *Science* **2019**, *363*, 578–580. [CrossRef] [PubMed]
3. Schlesinger, W.H. On the fate of anthropogenic nitrogen. *Proc. Natl. Acad. Sci. USA* **2009**, *106*, 203–208. [CrossRef]

4. Shibata, H.; Galloway, J.N.; Leach, A.M.; Cattaneo, L.R.; Cattell, N.L.; Erisman, J.W.; Gu, B.J.; Xiao, L.; Hayashi, K.; Ma, L.; et al. Nitrogen footprints: Regional realities and options to reduce nitrogen loss to the environment. *Ambio* **2017**, *46*, 129–142. [CrossRef] [PubMed]
5. Galloway, J.N.; Winiwarter, W.; Leip, A.; Leach, A.M.; Bleeker, A.; Erisman, J.W. Nitrogen footprints: Past, present and future. *Environ. Res. Lett.* **2014**, *9*, 115003. [CrossRef]
6. Wiedmann, T.; Lenzen, M. Environmental and social footprints of international trade. *Nat. Geosci.* **2018**, *11*, 314–321. [CrossRef]
7. Chen, C.; Wen, Z.G.; Wang, Y.H. Nitrogen flow patterns in the food system among cities within urban agglomeration: A case study of the Pearl River Deltal region. *Sci. Total Environ.* **2020**, *703*, 135506. [CrossRef] [PubMed]
8. National Bureau of Statistics of China (NBSC). *2004–2018 China Statistical Yearbook*; China Statistics Press: Beijing, China. Available online: http://www.stats.gov.cn (accessed on 14 May 2023).
9. Shi, L.; Zhang, M.; Zhang, Y.; Yang, B.; Sun, H.; Xu, T. Comprehensive analysis of nitrogen deposition in urban ecosystem: A case study of Xiamen city, China. *Sustainability* **2018**, *10*, 4673. [CrossRef]
10. Xian, C.; Wu, T.; Lu, F.; Zhang, J.; Gong, C.; Ouyang, Z. The nitrogen footprints of China's major urban agglomerations: Understanding regional challenges to advance sustainable development. *Environ. Res. Lett.* **2022**, *17*, 045020. [CrossRef]
11. Xu, W.; Du, E.Z.; Tang, A.H.; Zhang, Y.; Zhang, Y.Y.; Wen, Z.; Hao, T.X.; Pan, Y.P.; Zhang, L.; Gu, B.J.; et al. Environmental impacts of nitrogen emissions in China and the role of policies in emission reduction. *Philos. Trans. R. Soc. A* **2020**, *378*, 20190324.
12. Kanter, D.R.; Winiwarter, W.; Bodirsky, B.L.; Bouwman, L.; Boyer, E.; Buckle, S.; Compton, J.E.; Dalgaard, T.; Vries, d.W.; Leclère, D.; et al. A framework for nitrogen futures in the shared socioeconomic pathways. *Glob. Environ. Chang.* **2020**, *61*, 102029. [CrossRef] [PubMed]
13. Ma, S. High-resolution assessment of ammonia emissions in China: Inventories, driving forces and mitigation. *Atmos. Environ.* **2020**, *229*, 117458. [CrossRef]
14. Barles, S. Feeding the city: Food consumption and flow of N, Paris, 1801–1914. *Sci. Total Environ.* **2007**, *375*, 48–58. [CrossRef] [PubMed]
15. Baker, L.A.; Hope, D.; Xu, Y.; Edmonds, J.; Lauver, L. Nitrogen balance for the Central Arizona–Phoenix (CAP) ecosystem. *Ecosystems* **2001**, *4*, 582–602. [CrossRef]
16. Gu, B.; Chang, J.; Ge, Y.; Ge, H.; Yuan, C.; Peng, C.; Jiang, H. Anthropogenic modification of the nitrogen cycling within the Greater Hangzhou Area system, China. *Ecol. Appl.* **2009**, *19*, 974–988. [CrossRef]
17. Gu, B.; Dong, X.; Peng, C.; Luo, W.; Chang, J.; Ge, Y. The long-term impact of urbanization on nitrogen patterns and dynamics in Shanghai, China. *Environ. Pollut.* **2012**, *171*, 30–37. [CrossRef]
18. Dong, Y.; Xu, L. Aggregate risk of reactive nitrogen under anthropogenic disturbance in the Pearl River Delta urban agglomeration. *J. Clean. Prod.* **2019**, *211*, 490–502. [CrossRef]
19. Zhang, Y.; Lu, H.; Fath, B.D.; Zheng, H. Modelling urban nitrogen metabolic processes based on ecological network analysis: A case of study in Beijing, China. *Ecol. Model.* **2016**, *337*, 29–38. [CrossRef]
20. Liu, C.; Nie, G.H. Identifying the driving factors of food nitrogen footprint in China, 2000–2018, econometric analysis of provincial spatial panel data by the STIRPAT Model. *Sustainability* **2021**, *13*, 6147. [CrossRef]
21. Cui, H.; Zhao, T.; Shi, H. STIRPAT-Based Driving Factor Decomposition Analysis of Agricultural Carbon Emissions in Hebei, China. *Pol. J. Environ. Stud.* **2018**, *27*, 1449–1496. [CrossRef]
22. York, R.; Rosa, E.A.; Dietz, T. STIRPAT, IPAT, and ImPACT: Analytic tools for unpacking the driving forces of environmental impacts. *Ecol. Econ.* **2003**, *46*, 351–365. [CrossRef]
23. Xu, S.C.; Miao, Y.M.; Gao, C.; Long, R.Y.; Chen, H.; Zhao, B.; Wang, S.X. Regional differences in impacts of economic growth and urbanization on air pollutants in China based on provincial panel estimation. *J. Clean. Prod.* **2019**, *208*, 340–352. [CrossRef]
24. Ge, X.; Zhou, Z.; Zhou, Y.; Ye, X.; Liu, S. A spatial panel data analysis of economic growth, urbanization, and NOx emissions in China. *Int. J. Environ. Res. Public Health* **2018**, *15*, 725. [CrossRef] [PubMed]
25. Jiang, L.; Chen, Y.; Zhou, H.; He, S. NOx emissions in China: Temporal variations, spatial patterns and reduction potentials. *Atmos. Pollut. Res.* **2020**, *11*, 1473–1480. [CrossRef]
26. Zhang, X.; Zhang, Y.; Fath, B.D. Analysis of anthropogenic nitrogen and its influencing factors in Beijing. *J. Clean. Prod.* **2020**, *244*, 118780. [CrossRef]
27. Zeng, Y.; Xu, C.; Wang, Q.; Li, Y.; Hou, S. Basin-scale estimation of nitrogen footprint and corresponding dynamic change characteristics: A case study. *Environ. Dev.* **2019**, *29*, 81–93. [CrossRef]
28. Huang, L.H.; Jiang, Y.; Lin, Q.; Li, T.W.; Chen, F.; Wang, W.Y. Research on the coupling coordination relationship between Xiamen port development and coastal eco-environment evolution. *Environ. Pollut. Prev.* **2020**, *42*, 890–900. (In Chinese)
29. Sadorsky, P. The effect of urbanization on CO_2 emissions in emerging economies. *Energy Econ.* **2014**, *41*, 147–153. [CrossRef]
30. Chikaraishi, M.; Fujiwara, A.; Kaneko, S.; Poumanyvong, P.; Komatsu, S.; Kalugin, A. The moderating effects of urbanization on carbon dioxide emissions: A latent class modeling approach. *Technol. Forecast. Soc. Chang.* **2015**, *90*, 302–317. [CrossRef]
31. Salim, R.A.; Shafiei, S. Urbanization and renewable and non-renewable energy consumption in OECD countries: An empirical analysis. *Econ. Model.* **2014**, *38*, 581–591. [CrossRef]
32. Zhao, C.S.; Niu, S.W.; Zhang, X. Effects of household energy consumption on environment and its influence factors in rural and urban areas. *Energy Procedia* **2012**, *14*, 805–811.
33. Agbo, E.P.; Nkajoe, U.; Edet, C.O. Comparison of Mann–Kendall and Şen's innovative trend method for climatic parameters over Nigeria's climatic zones. *Clim. Dyn.* **2023**, *60*, 3385–3401. [CrossRef]

34. Chu, T.; Guo, X.; Takeda, K. Remote sensing approach to detect post-fire vegetation regrowth in Siberian boreal larch forest. *Ecol. Indic.* **2016**, *62*, 32–46. [CrossRef]
35. Guo, A.; He, L. Correlations between Summer Discharge and South Asian Summer Monsoon Subsystems in Mekong River Basin. *Atmosphere* **2023**, *14*, 958. [CrossRef]
36. IPCC. *Intergovernmental Panel on Climate Change: Greenhouse Gas Inventory Reference Manual*; Cambridge University Press: Cambridge, UK, 2007.
37. Li, Y.M.; Gao, B.; Tang, J.X.; Huang, W.; Cui, S.H. The evolution characteristics of nitrogen flow and water environment load in Xiamen. *Acta Sci. Circumstantiae* **2019**, *39*, 610–623. (In Chinese)
38. Huang, W.; Gao, B.; Huang, Y.; Zhang, Z.; Xu, S.; Xu, L.; Cui, S. Transforming nitrogen management of the urban food system in a food-sink city. *J. Environ. Manag.* **2019**, *249*, 109180. [CrossRef]
39. Chen, B.; Ji, W.; Chen, J.; Lin, C.; Huang, H.; Huo, Y.; Ji, X. Characteristics of nutrients in the Jiulong River and its impact on Xiamen Water, China. *Chin. J. Oceanol. Limnol.* **2013**, *31*, 1055–1063. [CrossRef]
40. Chen, N.W.; Hong, H.S.; Zhang, L.P. Preliminary results concerning the spatio-temporal pattern and mechanism of nitrogen sources and exports in the Jiulong River watershed. *Acta Sci. Circumstantiae* **2009**, *29*, 830–839. (In Chinese)
41. Liu, C.; Wang, Q.X.; Zou, C.J. Recent trends in N flows with urbanization in Shanghai megacity and the effects on the water environment. *Environ. Sci. Pollut. Res.* **2015**, *22*, 3431–3440. [CrossRef]
42. Elliott, E.M.; Kendall, C.; Wankel, S.D.; Burns, D.A.; Boyer, E.W.; Harlin, K.; Bain, D.J.; Butler, T.J. N isotopes as indicators of NOx source contributions to atmospheric nitrate deposition across the midwestern and northeastern United States. *Environ. Sci. Technol.* **2007**, *41*, 7661–7667. [CrossRef]
43. Gao, Y.; Zhou, F.; Ciais, P.; Miao, C.Y.; Yang, T.; Jia, Y.L.; Zhou, X.D.; Klaus, B.B.; Yang, T.T.; Yu, G.R. Human activities aggravate nitrogen-deposition pollution to inland water over China. *Natl. Sci. Rev.* **2020**, *7*, 430–440. [CrossRef] [PubMed]
44. Dey, C.S.; Bhunia, P. Simultaneous carbon and nitrogen removal from domestic wastewater using high rate vermifilter. *Indian J. Microbiol.* **2021**, *61*, 218–228.
45. Li, Y.; Tang, J.; Cui, S. Dynamic Changes of Nitrogen Loads in Source–Sink Landscapes under Urbanization. *Land* **2022**, *11*, 1371. [CrossRef]
46. Chen, J. Mitigating nitrogen dioxide air pollution: The roles and effect of national smart city pilots in China. *Energy* **2023**, *263*, 125652. [CrossRef]
47. Gu, B.; Leach, A.M.; Ma, L.; Galloway, J.N.; Chang, S.X.; Ge, Y.; Chang, J. Nitrogen footprint in China: Food, energy, and nonfood goods. *Environ. Sci. Technol.* **2013**, *47*, 9217–9224. [CrossRef]
48. Winiwarter, W.; Höglund-Isaksson, L.; Klimont, Z.; Schöpp, W.; Amann, M. Technical opportunities to reduce global anthropogenic emissions of nitrous oxide. *Environ. Res. Lett.* **2018**, *13*, 014011. [CrossRef]
49. Jaeglé, L.; Steinberger, L.; Martin, R.V.; Chance, K. Global partitioning of NO_x sources using satellite observations: Relative roles of fossil fuel combustion, biomass burning and soil emissions. *Faraday Discuss.* **2005**, *130*, 407–423. [CrossRef]
50. Shi, Y.L.; Cui, S.H.; Xu, S.; Lin, J.Y.; Huang, W. Nitrogen oxide emission in energy consumption in China from a consumption-based perspective. *Acta Sci. Circumstantiae* **2014**, *34*, 2684–2692. (In Chinese)
51. Clark, L.P.; Millet, D.B.; Marshall, J.D. Changes in transportation-related air pollution exposures by race-ethnicity and socioeconomic status: Outdoor nitrogen dioxide in the United States in 2000 and 2010. *Environ. Health Perspect.* **2017**, *125*, 097012. [CrossRef] [PubMed]
52. Warner, J.X.; Dickerson, R.R.; Wei, Z.; Strow, L.L.; Wang, Y.; Liang, Q. Increased atmospheric ammonia over the world's major agricultural areas detected from space. *Geophys. Res. Lett.* **2017**, *44*, 2875–2884. [CrossRef]
53. Clarisse, L.; Clerbaux, C.; Dentener, F.; Hurtmans, D.; Coheur, P.F. Global ammonia distribution derived from infrared satellite observations. *Nat. Geosci.* **2009**, *2*, 479–483. [CrossRef]
54. Kang, Y.; Liu, M.; Song, Y.; Huang, X.; Huang, X.; Yao, H.; Cai, X.H.; Zhang, H.S.; Kang, L.; Liu, X.J.; et al. High-resolution ammonia emissions inventories in China from 1980 to 2012. *Atmos. Chem. Phys.* **2016**, *16*, 2043–2058. [CrossRef]
55. Behera, S.N.; Sharma, M.; Aneja, V.P.; Balasubramanian, R. Ammonia in the atmosphere: A review on emission sources, atmospheric chemistry and deposition on terrestrial bodies. *Environ. Sci. Pollut. Res.* **2013**, *20*, 8092–8131. [CrossRef]
56. Wang, C.; Amon, B.; Schulz, K.; Mehdi, B. Factors that influence nitrous oxide emissions from agricultural soils as well as their representation in simulation models: A review. *Agronomy* **2021**, *11*, 770. [CrossRef]
57. Masuda, S.; Otomo, S.; Maruo, C.; Nishimura, O. Contribution of dissolved N_2O in total N_2O emission from sewage treatment plant. *Chemosphere* **2018**, *212*, 821–827. [CrossRef]
58. Hou, Y.; Ma, L.; Gao, Z.L.; Wang, F.H.; Sims, J.T.; Ma, W.Q.; Zhang, F.S. The driving forces for nitrogen and phosphorus flows in the food chain of China, 1980 to 2010. *J. Environ. Qual.* **2013**, *42*, 962–971. [CrossRef]
59. Gao, B.; Huang, W.; Wang, L.; Huang, Y.; Ding, S.; Cui, S. Driving forces of nitrogen flows and nitrogen use efficiency of food systems in seven Chinese cities, 1990 to 2015. *Sci. Total Environ.* **2019**, *676*, 144–154. [CrossRef]
60. Gu, B.; Zhang, X.; Bai, X.; Fu, B.; Chen, D. Four steps to food security for swelling cities. *Nature* **2019**, *566*, 31–33. [CrossRef]
61. Wang, F.; Wang, Y.; Cai, Z.; Chen, X. Environmental losses and driving forces of nitrogen flow in two agricultural towns of Hebei province during 1997–2017. *Environ. Pollut.* **2020**, *264*, 114636. [CrossRef]
62. Li, Y.; Cui, S.; Gao, B.; Tang, J.X.; Huang, W. Modeling nitrogen flow in a coastal city—A case study of Xiamen in 2015. *Sci. Total Environ.* **2020**, *735*, 139294. [CrossRef]

63. Ti, C.; Pan, J.; Xia, Y.; Yan, X. A nitrogen budget of mainland China with spatial and temporal variation. *Biogeochemistry* **2012**, *108*, 381–394. [CrossRef]
64. Yan, W.; Yin, C.; Zhang, S. Nutrient budgets and biogeochemistry in an experimental agricultural watershed in Southeastern China. *Biogeochemistry.* **1999**, *45*, 1–19. [CrossRef]
65. Chen, N.W.; Hong, H.S.; Huang, Q.J.; Wu, J.Z. Atmospheric nitrogen deposition and its long-term dynamics in a southeast China coastal area. *J. Environ. Manag.* **2011**, *92*, 1663–1667. [CrossRef] [PubMed]
66. Zhou, T.; Wang, Y.; Wang, F.; Feng, Y. Analysis of the nitrogen footprint of agriculture in Guangdong. *China Environ. Sci.* **2014**, *34*, 2430–2438.
67. Wang, M.; Ma, L.; Strokal, M.; Ma, W.Q.; Liu, X.J.; Kroeze, C. Hotspots for nitrogen and phosphorus losses from food production in China: A county-scale analysis. *Environ. Sci. Technol.* **2018**, *52*, 5782–5791. [CrossRef]
68. Cui, S.; Shi, Y.; Groffman, P.M.; Schlesinger, W.H.; Zhu, Y.G. Centennial-scale analysis of the creation and fate of reactive nitrogen in China (1910–2010). *Proc. Natl. Acad. Sci. USA* **2013**, *110*, 2052–2057. [CrossRef]
69. Ma, L.; Velthof, G.L.; Wang, F.H.; Qin, W.; Zhang, W.F.; Zhang, F.S.; Oenema, C. Nitrogen and phosphorus use efficiencies and losses in the food chain in China at reginal scales in 1980 and 2005. *Sci. Total Environ.* **2012**, *434*, 51–61. [CrossRef]
70. Zheng, X.; Han, S.; Huang, Y.; Wang, Y.; Wang, M. Re-quantifying the emission factors based on field measurements and estimating the direct N_2O emission from Chinese croplands. *Glob. Biogeochem. Cycles* **2004**, *18*, GB2018. [CrossRef]
71. Möller, D.; Schieferdecker, H. Ammonia emission and deposition of NHx in the GDR. *Atmos. Environ.* **1989**, *23*, 1187–1193. [CrossRef]
72. Cai, B.F. *City's Greenhouse Gas (GHG) Emission Inventory Research*; Chemical Industry Press: Beijing, China, 2009. (In Chinese)
73. Ma, L.; Ma, W.Q.; Velthof, G.L.; Wang, F.H.; Qin, W.; Zhang, F.S.; Oenema, O. Modeling nutrient flows in the food chain of China. *J. Environ. Qual.* **2010**, *39*, 1279–1289. [CrossRef]
74. Min, J.; Shi, W. Nitrogen discharge pathways in vegetable production as non-point sources of pollution and measures to control it. *Sci. Total Environ.* **2018**, *613*, 123–130. [CrossRef] [PubMed]
75. NBS. *Xiamen Statistic Yearbook*; Xiamen Bureau of Statistics of China: Xiamen, China, 2015. (In Chinese)
76. Liao, C.; Xia, Y.; Wu, D. Nitrogen flows associated with food production and consumption system of Shanghai. *Environ. Pollut.* **2021**, *279*, 116906. [CrossRef] [PubMed]
77. Gu, B.; Ju, X.; Chang, J.; Ge, Y.; Vitousek, P.M. Integrated reactive nitrogen budgets and future trends in China. *Proc. Natl. Acad. Sci. USA* **2015**, *112*, 8792–8797. [CrossRef] [PubMed]
78. Huang, X.; Song, Y.; Li, M.; Li, J.; Huo, Q.; Cai, X.; Zhang, H. A high-resolution ammonia emission inventory in China. *Glob. Biogeochem. Cycles.* **2012**, *26*, 1030. [CrossRef]
79. Xian, C.; Ouyang, Z.; Lu, F.; Xiao, Y.; Li, Y. Quantitative evaluation of reactive nitrogen emissions with urbanization: A case study in Beijing megacity, China. *Environ. Sci. Pollut. Res.* **2016**, *23*, 17689–17701. [CrossRef]
80. Crab, R.; Avnimelech, Y.; Defoirdt, T.; Bossier, P.; Verstraete, W. Nitrogen removal techniques in aquaculture for a sustainable production. *Aquaculture* **2007**, *270*, 1–14. [CrossRef]
81. Shu, T.F.; Wen, Y.M.; Tang, Y.T. Cycle and budget balance of nitrogen in the cultivated water. *Fish. Sci.* **2002**, *21*, 30–34. (In Chinese)
82. Zhang, R.L. Research advances on fertilizer application to lawn. *Chin. J. Trop. Agric.* **2002**, *22*, 77–81. (In Chinese)
83. Xu, J.R.; Wang, Y.S.; Sun, S. The characteristics of nitrogen fixation, ammonification, nitrification and denitrification in coastal zones. *Acta Ecol. Sin.* **2004**, *24*, 2907–2914. (In Chinese)
84. Hu, W.; Huaiyang, Z.; Xiaotong, P.; Qunhui, Y.; Chaomei, Q.; Xijie, Y.; Guangqian, C. Denitrification in Qi'ao Island coastal zone, the Zhujiang Estuary in China. *Acta Oceanol. Sin.* **2009**, *28*, 37–46. (In Chinese)
85. Yan, W.; Yang, L.; Wang, F.; Wang, J.; Ma, P. Riverine N_2O concentrations, exports to estuary and emissions to atmosphere from the Changjiang River in response to increasing nitrogen loads. *Glob. Biogeochem. Cycles* **2012**, *26*, 4006. [CrossRef]
86. Yu, Y.; Song, J.; Li, X.; Yuan, H.; Li, N. Distribution, sources and budgets of particulate phosphorus and nitrogen in the East China Sea. *Cont. Shelf Res.* **2012**, *43*, 142–155. [CrossRef]

MDPI AG
Grosspeteranlage 5
4052 Basel
Switzerland
Tel.: +41 61 683 77 34

Atmosphere Editorial Office
E-mail: atmosphere@mdpi.com
www.mdpi.com/journal/atmosphere

Academic Open
Access Publishing

mdpi.com

ISBN 978-3-7258-3696-3